

*Studies in Chemistry of Some Novel Copper
Complexes*

THESIS SUBMITTED
TO
JADAVPUR UNIVERSITY

FOR THE DEGREE OF
DOCTOR OF PHILOSOPHY (SCIENCE)
IN
CHEMISTRY

BY
Naba Kr Mandal
M.Sc.



DEPARTMENT OF CHEMISTRY
JADAVPUR UNIVERSITY
JADAVPUR, KOLKATA 700 032
INDIA
July, 2024

Prof. Jnan Prakash Naskar
Professor
Department of Chemistry
Inorganic Chemistry Section



JADAVPUR UNIVERSITY
KOLKATA – 700 032, INDIA
Telephone: 91-033-2414-6666
Facsimile: 91-033-2414-6584
E-mail: ipnaskar@rediffmail.com
inanp.naskar@jadavpuruniversity.in

CERTIFICATE FROM THE SUPERVISOR

This is to certify that the thesis entitled “*Studies in Chemistry of Some Novel Copper Complexes*” submitted by *Sri Naba Kr Mandal* who got his name registered on 06.09.2019 for the award of Ph.D. (Science) Degree of Jadavpur University, is absolutely based upon his own work under the supervision of Prof. Jnan Prakash Naskar, Jadavpur University and that neither this thesis nor any part of it has been submitted for either any degree/diploma or any other academic award anywhere before.

Jnan Prakash Naskar 29.7.24
(Prof. Jnan Prakash Naskar)

(Signature of the Supervisor
& date with official seal)

DR. JNAN PRAKASH NASKAR
Professor of Chemistry
Jadavpur University
Kolkata-700 032

Declaration

*I hereby declare that the thesis entitled “**Studies in Chemistry of Some Novel Copper Complexes**” submitted for the degree of Doctor of Philosophy (Science) of Jadavpur University is based on the original work done by me under the guidance of Dr. Jnan Prakash Naskar, Professor, Department of Chemistry, Jadavpur University, Kolkata-700 032 and this work has not been included in any other thesis submitted previously for the award of any other degree.*

Jadavpur University

Naba Kr Mandal
29/07/24

(Naba Kr Mandal)

Department of Chemistry

Jadavpur University

Kolkata 700 032



Acknowledgement

It is my great pleasure to express deepest gratitude to my Ph.D. thesis supervisor, Dr. Jnan Prakash Naskar, Professor, Department of Chemistry, Jadavpur University, Kolkata for his constant guidance during the hard time. I am greatly indebted to him for his constant support, untiring guidance, encouragement, motivation and valuable suggestions throughout my research work.

I wish to express my deep sense of gratitude to the Vice-Chancellor, Pro Vice-Chancellor and Registrar of Jadavpur University for the infrastructural and instrumental facilities.

I solicit to extend my sincere thanks to Prof. Kajal Krishna Rajak, Head, Department of Chemistry and Prof. Ashis Kumar Sarkar, Dean, Faculty of Science, Jadavpur University for providing me the necessary infrastructural facilities to carry out this work.

I would like to express my heartfelt gratitude to Dr. B. B. Show, Prof. M. Ali, Prof C. R. Sinha and Prof. S. Baitalik for providing me the necessary instrumental facilities.

I am thankful to all the teaching and non-teaching staff members of the Department of Chemistry, Jadavpur University for their gesture, help and cordial support to carry out my research work.

I would like to express my heartfelt gratitude to Dr. Shubhamoy Chowdhury, Professor, Department of Chemistry, University of Gour Banga, Malda for theoretical calculations.

I am thankful to Prof. Neera Raghav, Department of Chemistry, Kurukshetra University, Haryana for biological studies.

I am extremely grateful to Prof. Carlos J. Gómez-García, Professor, Department of Chemistry, University of Valencia, Spain for magnetic studies.

I gratefully acknowledge Prof. Krishnendu Acharya and Dr. Sudeshna Nandi, University of Calcutta, Ballygunge Science College for studies on anticancer properties.

I am grateful to Dr. Chandra Shekhar Purohit, School of Chemical Sciences, National Institute of Science Education and Research, Bhubaneswar, India for X-ray crystal structure determination.

I am also thankful to Dr. Pritha Basu and Dr. Priyanka Arya for their kind help and cooperation.

I sincerely thank for support and encouragement of my seniors Dr. Bhargab Guhathakurta, Dr. Nirmalya Bandyopadhyay and Dr. Mihir Sasmal at different stages of my work.

I am grateful to acknowledge the services received from IACS, Kolkata.

Financial assistance received from the University Grants Commission (UGC), New Delhi, India is gratefully acknowledged.

Most importantly, I invariably express my respect, love and gratitude to my beloved parents, Mr. Sushil Mandal and Mrs. Pratima Mandal.

Finally, I would like to thank all my family members and everyone who was behind the fulfilment of my work.

Jadavpur University

Naba Kr Mandal 29/07/24

(Naba Kr Mandal)

Department of Chemistry

Jadavpur University

Kolkata 700 032

Preface

The work embodied in the thesis entitled “*Studies in Chemistry of Some Novel Copper Complexes*” have been carried out in the Department of Chemistry, Jadavpur University. The thesis consists of seven chapters.

Chapter I contains salient aspects of chemistry pertinent to copper in its oxidation states of +I and +II. The aim, objective and scope of the present work is delineated herewith.

Chapter II demonstrates the DNA and RNA binding efficacies of a bromo-bridged copper(II) dimer stabilized from a Schiff base ligand. The mode of binding has also been evaluated through molecular docking.

Chapter III deals with a naphthaldehyde based Schiff base ligand and its mononuclear copper(II) complex. The complex has been studied for its possible inhibition of various digestive enzymes. The ligand has also been employed for its efficacy of copper(II) sensing.

Chapter IV illustrates the preparation and thorough characterization of a morpholine based Schiff base ligand and its two 1D coordination polymers. The magnetic aspect of both the coordination polymers have also been investigated.

Chapter V highlights two mononuclear copper(II) complexes stabilized from a morpholine based Schiff base ligand. Both the ligand and complexes have also been screened against human lung cancer cell lines (A549).

Chapter VI embodies the chemistry of an oxime based Schiff base ligand and its trinuclear copper(II) complex. The complex has been screened against human lung cancer cell lines (A549). The magnetic properties of this complex has also been studied.

Chapter VII delineates two air-stable mononuclear copper(I) complexes stabilized from a quinoxaline based ligand. The modified electrode based on these complexes has been demonstrated for electrochemical sensing of melanin.

Jadavpur University

Naba Kr Mandal
29/07/24

(Naba Kr Mandal)

Department of Chemistry

Jadavpur University

Kolkata 700 032

List of abbreviations and symbols

NMR	:	nuclear magnetic resonance
CV	:	cyclic voltammetry
GC	:	glassy carbon
TBAP	:	tetrabutylammonium perchlorate
ESI-MS	:	electrospray ionization mass spectroscopy
FT-IR	:	Fourier transform infrared spectroscopy
Fc/Fc ⁺	:	ferrocene-ferrocenium
UV-Vis	:	ultraviolet-visible
BVS	:	bond-valence sum
CT	:	calf-thymus
DNA	:	deoxy-ribonucleic acid
RNA	:	ribonucleic acid
°C	:	degree Celsius
h	:	hour
min	:	minute
mL	:	milliliter
mmol	:	millimole
mm	:	millimeter
Å	:	angstrom
CP	:	citrate-phosphate
ppm	:	parts per million
DFT	:	density functional theory
VDW	:	van der Waals
HB	:	hydrogen bond
J	:	coupling constant
m.p	:	melting point
g	:	gram
mg	:	milligram
nm	:	nanometer
MHz	:	megahertz

CH ₃ OH	:	methanol
CH ₃ CN	:	acetonitrile
DMF	:	N,N-dimethylformamide
DMSO	:	dimethyl sulfoxide
DCM	:	dichloromethane
THF	:	tetrahydrofuran
TMS	:	tetramethylsilane
CaCl ₂	:	calcium chloride
WST	:	water soluble tetrazolium salt
NSCLC	:	non-small cell lung cancer
TGA	:	thermo-gravimetric analysis
PXRD	:	powder X-ray diffraction
DAPI	:	4,6-diamidno phenyl indole
AO/EtBr	:	acridine orange/ethidium bromide
ILCT	:	intra-ligand charge transfer
LMCT	:	ligand to metal charge transfer
τ	:	tau
SQUID	:	superconducting quantum interference device
PBS	:	phosphate buffered saline

Contents

	Page No.
<i>Acknowledgement</i>	<i>i</i>
<i>Preface</i>	<i>iii</i>
<i>List of abbreviations and symbols</i>	<i>iv</i>
<i>Contents</i>	<i>vi</i>
CHAPTER-I	
A brief overview of copper chemistry & Purpose of the present work	1-27
<i>Graphical Abstract</i>	<i>2</i>
<i>Abstract</i>	<i>3</i>
<i>1. Introduction</i>	<i>4</i>
<i>2. Schiff base ligands</i>	<i>4</i>
<i>2.1. Morpholine</i>	<i>6</i>
<i>2.2. Oxime</i>	<i>7</i>
<i>3. Copper chemistry</i>	<i>8</i>
<i>3.1 Oxidation states of copper</i>	<i>9</i>
<i>3.2 Coordination chemistry of copper</i>	<i>9</i>
<i>4. Application of copper-Schiff base complexes</i>	<i>11</i>
<i>4.1. Cu(II) complexes: Bio-macromolecular interaction study</i>	<i>11</i>
<i>4.1.1. Interaction with DNA</i>	<i>11</i>
<i>4.1.2. Interaction with RNA</i>	<i>12</i>
<i>4.2. Cu(II) complexes: Digestive enzymes</i>	<i>12</i>
<i>4.3. Cu(II) complexes: Sensing properties</i>	<i>13</i>
<i>4.4. Cu(II) complexes: Magnetic properties</i>	<i>14</i>
<i>4.5. Cu(II) complexes: Anti-cancer properties</i>	<i>17</i>
<i>5. An overview of Cu(I) chemistry: Melanin sensing</i>	<i>19</i>
<i>6. Objectives of present studies</i>	<i>20</i>
<i>7. References</i>	<i>21</i>
CHAPTER-II	
DNA and RNA binding studies on a novel bromo-bridged dimeric copper(II) complex stabilized from a Schiff base ligand	28-58

<i>Graphical Abstract</i>	29
<i>Abstract</i>	30
<i>1. Introduction</i>	31
<i>2. Experimental section</i>	32
<i>2.1. Materials</i>	32
<i>2.2. Nucleic acids and buffer</i>	32
<i>2.3. Physical measurements</i>	32
<i>2.4. Computational details</i>	33
<i>2.5. Methods for DNA and RNA binding</i>	33
<i>2.5.1. Spectrophotometric study</i>	33
<i>2.5.2. Fluorescence spectroscopic and</i> <i>Ethidium Bromide displacement studies</i>	34
<i>2.5.3. Thermodynamic studies: temperature</i> <i>dependent spectrofluorimetry</i>	34
<i>2.5.4. Circular dichroism studies</i>	35
<i>2.5.5. Molecular docking study</i>	35
<i>2.6. Syntheses</i>	36
<i>2.6.1. Preparation of ligand (LH)</i>	36
<i>2.6.2. Preparation of [Cu₂(μ-Br)₂(L)₂] (I)</i>	36
<i>2.7. Crystal structure determination</i>	36
<i>3. Results and discussion</i>	38
<i>3.1. Synthesis and formulation</i>	38
<i>3.2. Electronic spectra of LH and I</i>	41
<i>3.3. Molecular structure of [Cu₂(μ-Br)₂(L)₂] (I)</i>	43
<i>3.4. Electrochemistry</i>	44
<i>3.5. DNA and RNA binding aspect</i>	45
<i>3.5.1. Spectrophotometric study</i>	45
<i>3.5.2. Spectrofluorimetric study</i>	47
<i>3.5.3. Ethidium bromide displacement assay</i>	49
<i>3.5.4. Thermodynamics of the interaction</i>	51
<i>3.5.5. Circular dichroism studies</i>	52
<i>3.6. Molecular docking</i>	53
<i>4. Conclusions</i>	54
<i>5. References</i>	55

CHAPTER-III

Synthesis, characterization, structure, *in vitro* enzymatic activity and sensing aspects of a copper(II) complex stabilized from a naphthaldehyde based Schiff base ligand 59-89

<i>Graphical Abstract</i>	60
<i>Abstract</i>	61
<i>1. Introduction</i>	62
<i>2. Experimental section</i>	63
<i>2.1. Materials and Measurements</i>	63
<i>2.2. Synthesis</i>	64
<i>2.2.1. Synthesis of 1-(benzothiazol-2-yl-hydrazonomethyl)-naphthalen-2-ol (LH)</i>	64
<i>2.2.2. Synthesis of [CuL(ClO₄)(H₂O)].THF (1)</i>	64
<i>2.3. X-ray data collection and structure determination</i>	65
<i>2.4. Trypsin Assay</i>	67
<i>2.5. Amylase Assay</i>	67
<i>2.6. Lipase Assay</i>	67
<i>2.7. Molecular Docking studies</i>	68
<i>2.8. Sensing experiments</i>	68
<i>3. Results and discussion</i>	68
<i>3.1 Synthesis and general characterization</i>	68
<i>3.2. Molecular structure of [CuL(ClO₄)(H₂O)].THF (1)</i>	72
<i>3.3. Enzymes assay</i>	73
<i>3.4. Docking analysis</i>	74
<i>3.5. Absorption studies</i>	76
<i>3.6. Cu²⁺ ion sensing by fluorescence studies</i>	77
<i>3.7. Limit of detection (LOD) determination</i>	79
<i>3.8. Sensing mechanism</i>	81
<i>3.9. DFT calculations</i>	82
<i>3.10. Powder X-ray diffraction</i>	84
<i>4. Conclusions</i>	85
<i>5. References</i>	86

CHAPTER-IV

Syntheses of two copper(II) coordination polymers from a novel morpholine-based tridentate Schiff base ligand: Crystal structures and magnetic properties 90-114

<i>Graphical Abstract</i>	91
<i>Abstract</i>	92
<i>1. Introduction</i>	93
<i>2. Experimental section</i>	94
<i>2.1. Reagents and instruments</i>	94
<i>2.2. Synthesis of (1-methyl-1H-imidazol-2-yl)-N-[2-(morpholin-4-yl)ethyl]methanimine (L)</i>	95
<i>2.3. Synthesis of [Cu(L)(μ-1,3-N_3)]_n(ClO₄)_n (1)</i>	95
<i>2.4. Synthesis of [Cu(L)(μ-1,3-SCN)]_n(ClO₄)_n (2)</i>	96
<i>2.5. Crystallographic data collection and refinement</i>	97
<i>3. Results and discussion</i>	99
<i>3.1. Syntheses of the complexes</i>	99
<i>3.2. Infrared spectra</i>	100
<i>3.3. Electronic spectra</i>	102
<i>3.4. Powder X-ray diffraction</i>	103
<i>3.5. Crystal structures of compounds 1 and 2</i>	103
<i>3.6. Magnetic properties</i>	106
<i>3.7. Coupling mechanism</i>	107
<i>3.8. EPR spectra</i>	109
<i>4. Conclusions</i>	110
<i>5. References</i>	111

CHAPTER-V

Synthesis, characterization, crystal structure, thermal and redox behavior and antiproliferative studies of morpholine-based two copper(II) compounds 115-151

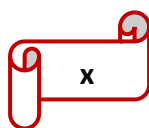
<i>Graphical Abstract</i>	116
<i>Abstract</i>	117
<i>1. Introduction</i>	118
<i>2. Experimental section</i>	119
<i>2.1. Materials and methods/ Chemicals</i>	119
<i>2.2. Synthesis of the ligand (L)</i>	121

2.3. Synthesis of $[\text{CuL}(\text{Cl})_2]\cdot\text{H}_2\text{O}$ (1)	121
2.4. Synthesis of $[\text{CuL}(\text{N}_3)_2]$ (2)	122
2.5. Cell culture	123
2.6. Cell proliferation assay	123
2.7. Assay of cell viability with Trypan Blue Exclusion assay	123
2.8. Colony formation assay	124
2.9. Morphological evaluation	124
2.10. Cell cycle assay	124
2.11. Morphological observation of nuclear change	124
2.12. Assessment of apoptosis by AO/EtBr staining	124
2.13. X-ray crystallography	125
3. Results and discussion	128
3.1. Synthesis and characterisation	128
3.2. Description of the crystal structures of 1 and 2	132
3.3. In vitro cell growth inhibition	134
3.4. Compounds, 1 and 2 impede colony formation of A549 cells	136
3.5. Compounds, 1 and 2 induce arrest in cell-cycle progression	137
3.6. Compounds 1 and 2 induce morphological changes in cultured human adenocarcinoma cells A549	138
3.7. Compounds 1 and 2 compelled apoptotic induction in A549 cells	139
3.8. Cytotoxic mechanistic action and structure-activity relationship	142
3.9. Cyclic voltammetry	142
3.10. TGA analysis	143
3.11. PXRD	144
4. Conclusions	145
5. References	146

CHAPTER-VI

Design, synthesis and structure of a trinuclear copper(II) complex having a Cu_3OH core with regard to aspects of antiproliferative activity and magnetic properties 152-191

Graphical Abstract	153
Abstract	154
1. Introduction	155
2. Experimental section	157



2.1. Materials	157
2.2. Physical measurements	158
2.3. Solution Preparation for Spectroscopic Studies	158
2.4. DNA Binding Studies	158
2.5. Cell culture	159
2.5.1. Cell viability assay using WST-1	159
2.5.2. Evaluation of A549 cell count and viability by trypan blue assay	159
2.5.3. Colony formation assay	160
2.5.4. Cytomorphological observation of A549 cells by bright field microscopy/fluorescence microscopy	160
2.5.5. In vitro cell wound repair assay	160
2.5.6. Nuclear morphology by DAPI staining under inverted fluorescent microscope	160
2.5.7. Direct fluorescence microscopic analysis for apoptosis induction	160
2.5.8. Data analysis and statistics	161
2.6. Synthesis of the ligand (HL)	161
2.7. Synthesis of complex $[(\text{CuL})_3(\mu_3\text{-OH})(\text{ClO}_4)_2]\cdot\text{CH}_3\text{OH}\cdot\text{H}_2\text{O}$ (1)	161
2.8. Crystallographic data collection and refinement	163
3. Results and discussion	165
3.1. Synthesis and IR spectroscopy	165
3.2. Electronic spectra	168
3.3 Description of the crystal structure of $[(\text{CuL})_3(\mu_3\text{-OH})(\text{ClO}_4)_2]\cdot\text{CH}_3\text{OH}\cdot\text{H}_2\text{O}$ (1)	168
3.4. DNA binding	171
3.5. CD spectra	172
3.6. Biological study	173
3.6.1. Complex induced potent cytotoxic effects and inhibition of cell colony forming tendency	173
3.6.2. Morphological changes induced by complex 1	175
3.6.3. Apoptotic cell death in A549 cells induced by complex 1	176
3.6.4. Effect of complex (1) on the migration of A549 cells	177
3.6.5. Cell death mechanism	178
3.7. Magnetic properties	179

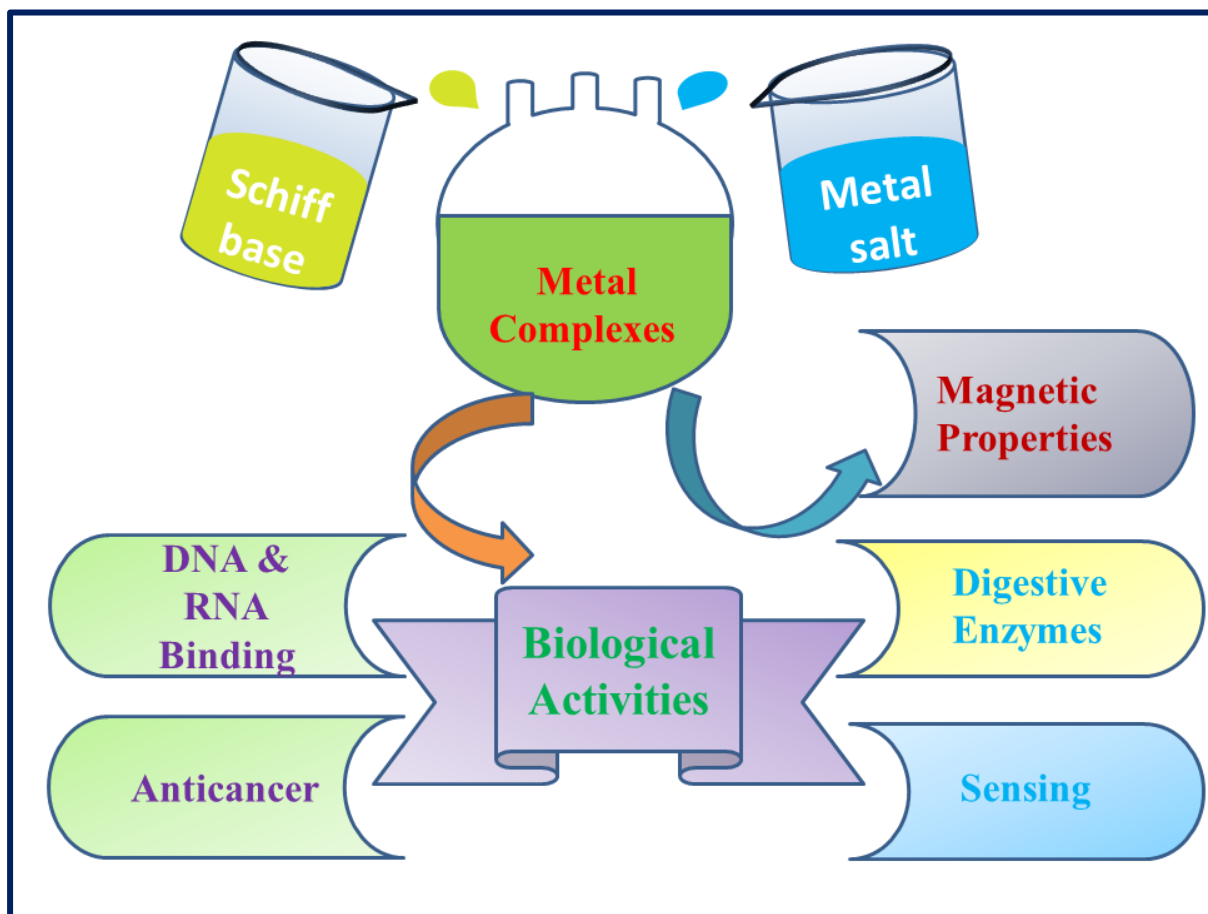
3.8. Magneto-structural correlation	180
3.9. EPR spectroscopy	182
4. Conclusions	183
5. References	184
CHAPTER-VII	
Syntheses, crystal structures and spectroscopic properties of copper(I) complexes stabilized from a quinoxaline based ligand: Enzyme-less electrochemical sensing of melanin	192-216
Graphical Abstract	193
Abstract	194
1. Introduction	195
2. Experimental section	197
2.1 Materials and method	197
2.2. Physical measurements	197
2.3. Fabrication of GCE/ 1 Electrode	198
2.4. Sample preparation	198
2.5. Synthetic procedure of [Cu(bpq) ₂ (ClO ₄)] (1)	198
2.6. Synthetic procedure of [(Cu(bpq) ₂)]BF ₄ (2)	199
2.7. X-ray Crystallography	200
3. Results and discussion	201
3.1 Synthesis and IR Spectroscopy of complexes 1 and 2	201
3.2. Electronic spectra	203
3.3. Structural description of 1 and 2	203
3.4. Cyclic voltammetry	205
3.5. Melanin sensing	206
3.5.1. Interference and selectivity studies	208
3.5.2. Reproducibility and stability	209
3.5.3. pH effect	210
3.5.4. Real sample analysis	211
3.6. PXRD	211
4. Conclusions	212
5. References	213
List of Publications	217



CHAPTER-I

A brief overview of copper chemistry
&
Purpose of the present work

Graphical Abstract



Highlights

- An overview of the chemistry of Schiff bases
- A brief overview of copper chemistry
- Salient aspects of nucleic acids (DNA and RNA) and sensing properties
- An overview of digestive enzymes and magnetic properties
- Short review of anti-cancer properties
- A brief discussion on melanin sensing

Keywords

Coordination chemistry; copper; Schiff base; morpholine; oxime; nucleic acids; digestive enzymes; magnetic properties; anticancer properties; modified electrodes and melanin sensing

Abstract

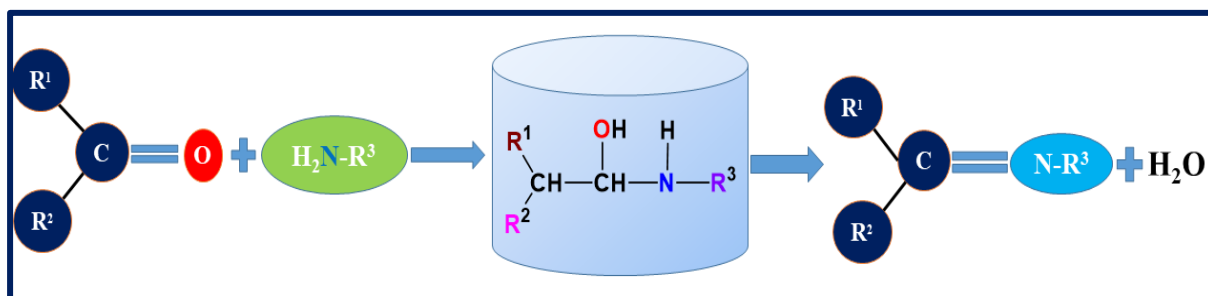
An overview of Schiff bases has vividly been outlined with pertinent literature survey. The general chemistry of copper, relevant in the context of present investigation, has comprehensively been reviewed. The salient aspects of copper(I) chemistry having relevance with current work have been forwarded. In this perspective; the aim, objective and scope of the present work have been delineated.

1. Introduction

Copper, the last of the first-row transition elements in Group 11, is the prime focus of this research work. The term ‘copper’ is originated from the Latin word ‘cuprum’. Copper, a ductile and soft metal, has high thermal and electrical conductivity. The electronic configuration of copper in its zero oxidation state is $[\text{Ar}]4s^13d^{10}$. The atomic and covalent radii of it are respectively of 1.96 and 1.28 Å. The relative abundance of two important isotopes of copper, ^{63}Cu and ^{65}Cu , are 69.15 and 30.85% respectively. Copper is ubiquitous and plays unique role in coordination chemistry. It forms a wide range of coordination complexes. The common geometries of copper coordination complexes are octahedral, tetrahedral and square planar.

2. Schiff base ligands

Schiff bases, an important class of ligands, have drawn unabated keen interest. They offer structural versatilities and have implications in diverse fields of application. Our present work encompasses various types of Schiff base ligands. These ligands have been designed, synthesized and subsequently been employed to enrich the significant aspects of copper(II) chemistry. The preparation of Schiff base condensate was first reported by Hugo Schiff in 1864 [1]. The general synthetic route of a Schiff base is shown in [scheme I.1](#).



Scheme I.1. Synthetic scheme of Schiff base formation [R^1 , R^2 and R^3 are alkyl groups].

Jacobsen described the Schiff base ligands as “privileged ligands” [2]. In a Schiff base ligand, the nitrogen atom of azomethine group can anchor a metal ion. Schiff bases, adorned with one or more donor centers in addition to azomethine group, can serve as polydentate ligands. The lone pair of electron on the nitrogen atom in a sp^2 hybrid orbital of the azomethine group is of remarkable biological and chemical importance as had been demonstrated in several studies [3-5]. The chemistry of Schiff base ligands has been fleshed out by the seminal work of Sprung [6], Sollenberger and Martin [7]. This class of ligands is versatile indeed due to their different coordination sites, different shapes, functionalities and sensitivity. Taken together, all these factors make them an interesting class of ligands in coordination chemistry. Fig. I.1 depicts some Schiff base ligands [8-11].

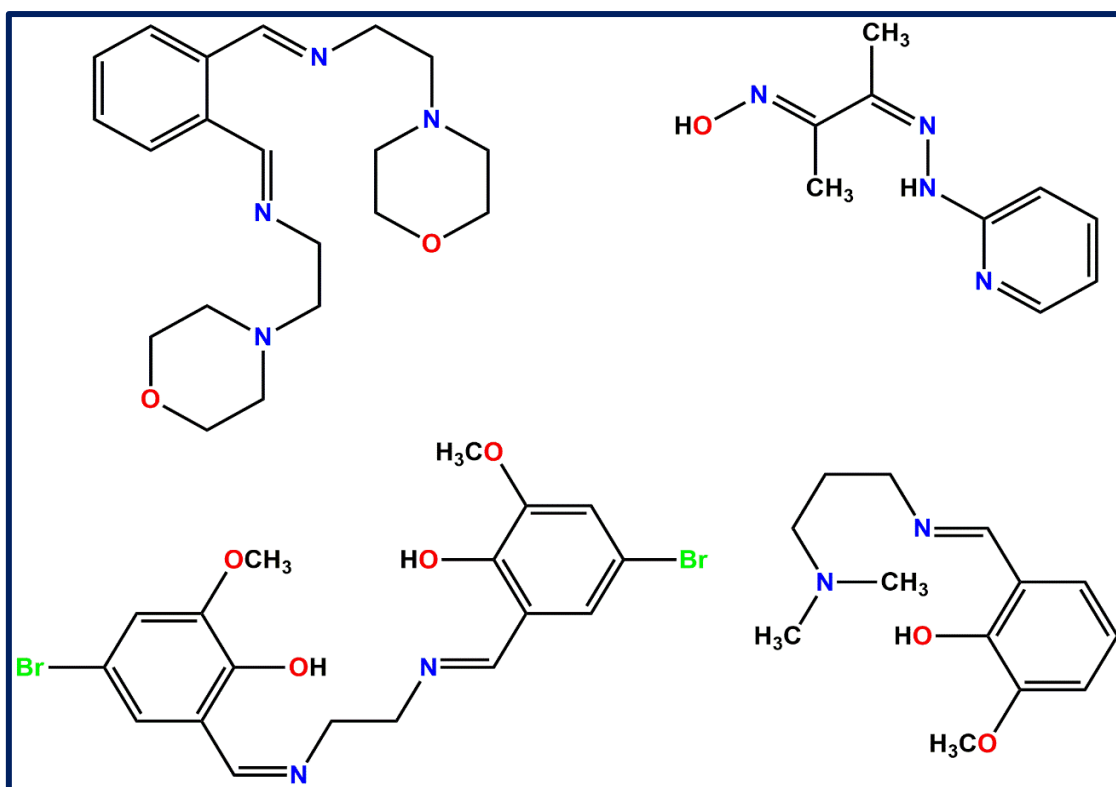


Fig. I.1. Examples of some Schiff base ligands.

Again, they bear structural closeness to several naturally existing biological substances [12]. In fact, the azomethine ($-\text{CH}=\text{N}$) linkage, present in a Schiff base, plays a pivotal role for commendable anti-microbial activities [13].

Some notable examples of Schiff base ligands with varying donor capabilities are illustrated in Fig. I.2.

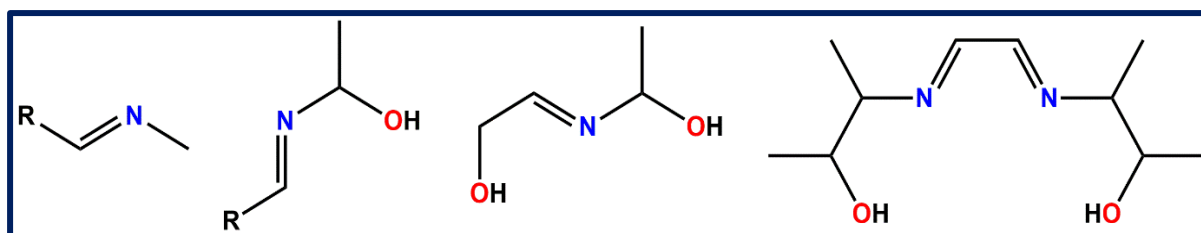


Fig. I.2. Some Schiff bases with varying denticity.

On the other hand, the basicity of Schiff bases also offers a key role in the development and stabilization of complexes. Oxygen is a ‘hard’ donor, whereas imine nitrogen is a ‘borderline’ one. ‘Hard’ donor centers stabilise the higher oxidation state of a metal ion; while the ‘soft’ donor sites stabilise the lower oxidation state of a metal ion [14]. Schiff base ligands may contain multiple donor sites like O, N and S. As a result, they can manifest beneficial binding interaction [15]. The $-\text{OH}$ group present in a Schiff base may undergo keto-enol tautomerism. Patra *et al.*, in 2016, reported a Schiff base ligand, 1,2-diphenyl-2-(2-(pyridin-2-

yl)hydrazineylidene)ethan-1-one, that manifests keto-enol tautomerism as shown in Fig. I.3 [16].

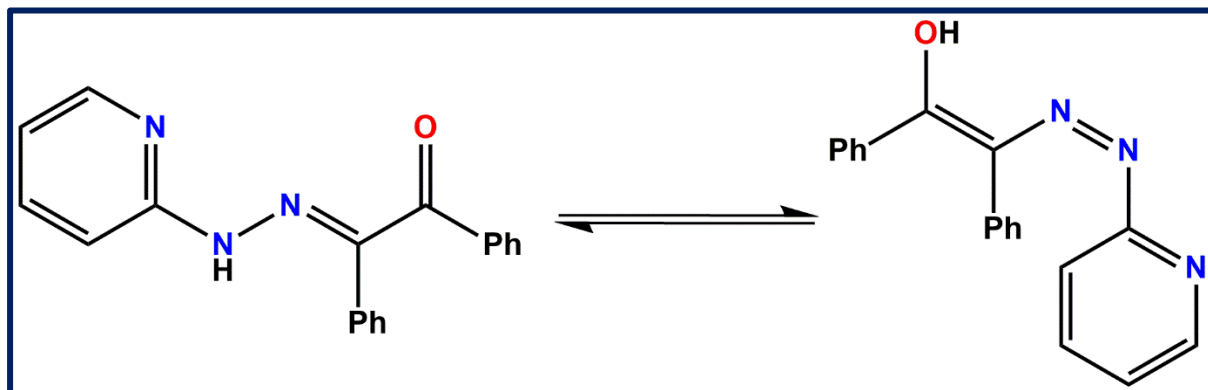


Fig. I.3. Tautomers of 1,2-diphenyl-2-(2-(pyridin-2-yl)hydrazineylidene)ethan-1-one.

Apart from these factors, ligand flexibility is one of the important factors that may have sufficient impact in coordination chemistry. The condensing amine chiefly favours to yield such kind of flexible Schiff bases [17]. In this context, piperazine based Schiff bases are noteworthy [18]. Morpholine based Schiff bases are also well-known in this perspective [19]. Fig. I.4. depicts the chair-boat conformations of amino ethyl morpholine moiety.

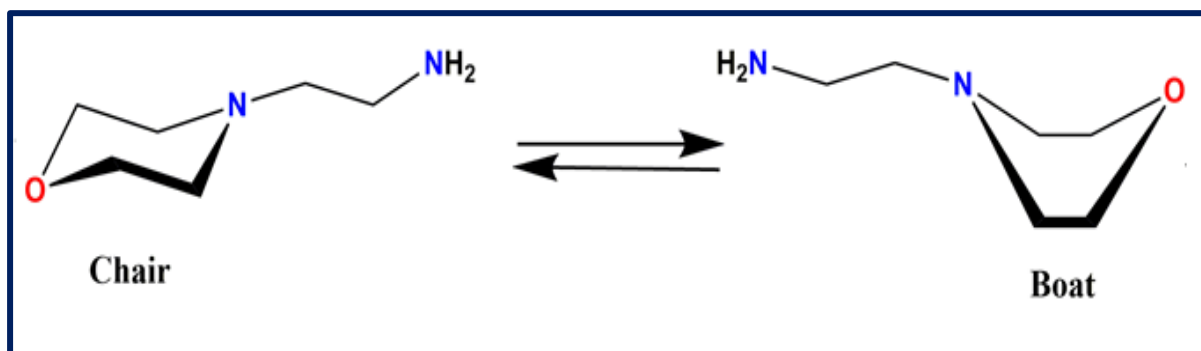


Fig. I.4. Chair-boat conformations of amino ethyl morpholine moiety.

2.1. Morpholine

Morpholine based Schiff base ligands are of contemporary interest. The reasons are myriad. Morpholine is a six-membered heterocyclic moiety that possesses both amine and ether functional groups (Fig. I.5) [20]. It plays a pivotal role to form reaction intermediates in many organic syntheses [21,22]. It is a point to note that in this present research endeavour, we are concerned with morpholine appended Schiff base ligands. Over the past few decades, such heterocyclic derivatives containing N and O atoms had drawn significant attention because of their high therapeutic values [23].

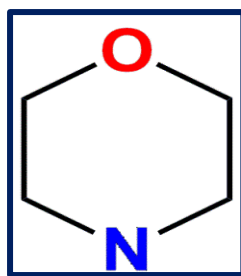


Fig. I.5. Six-membered morpholine moiety.

They offer significant therapeutic usages [24]. Morpholine based compounds are of contemporary interest for manifesting promising cytotoxic activity [25-27]. In medicinal chemistry, such types of assemblies are considered as ‘auspicious’ building blocks. In such cases, the oxygen atom plays an important key role for its bioactivity. Such entity also facilitates to form strong complexes with its target(s) through host-guest interaction mode [28,29]. Morpholine tagged Schiff bases are satisfactorily stable in biological systems. They offer long-term implications as they take part in radical redesign of DNA [30,31]. All these promising factors kindled us to design and synthesize new morpholine-tagged Schiff base ligands. Two Schiff base ligands, pertinent to our work, are shown in Fig. I.6.

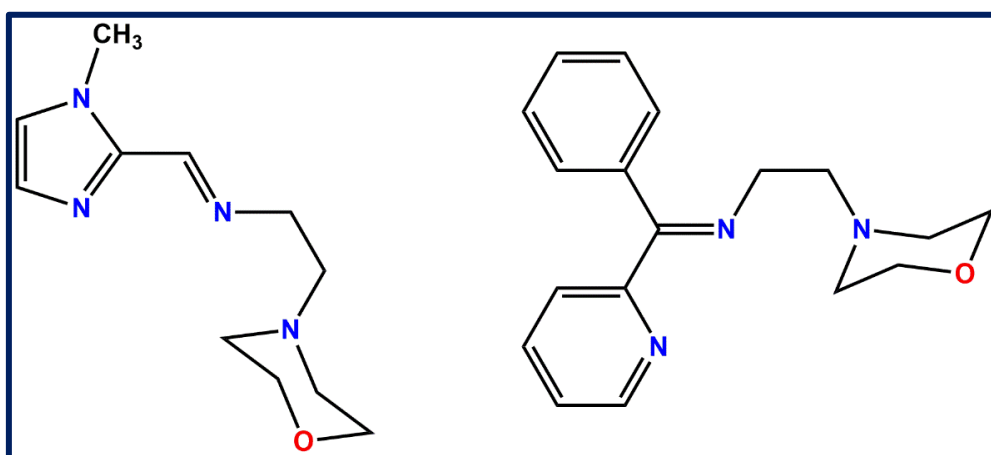
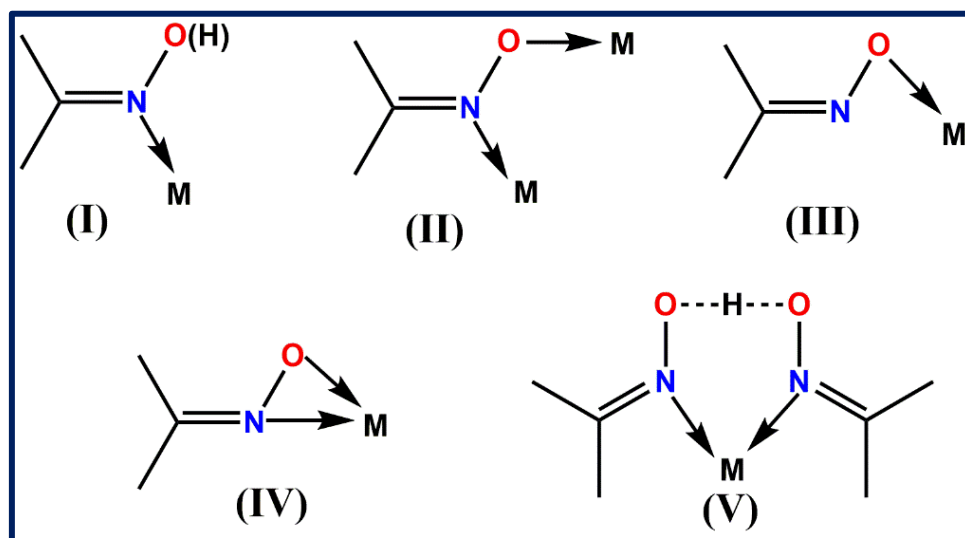


Fig. I.6. Two morpholine-based Schiff base ligands having relevance with present work.

2.2. Oxime

Oxime based ligands are the most important bioactive ligands. It has widely been used in coordination chemistry because of their versatile modes of binding ability [32-33]. The condensation of hydroxylamine with aldehydes or ketones yields oximes. A. Werner was the first to isolate the two isomeric forms of aldoximes that exist in the *-syn* and *-anti* geometric forms [34]. Two German chemists, Victor Meyer and Alois Janny, synthesised oxime for the first time in 1882, naming it "acetoxim" [35]. The presence of nitrogen atom in an oxime renders it weakly basic; while the hydroxyl group (-OH) group turns it slightly acidic. The combined effect of these two opposing factors makes it amphoteric [36-38]. The functional

groups, ($-\text{CH}=\text{N}$ and $-\text{OH}$), and additional donor atom(s) offer promising binding sites for an oxime based ligand to form stable complexes [39,40]. The varying modes of binding in metal oxime structures are provided in scheme I.2.



Scheme I.2. Different modes of binding of oximes and oximato species with metal centers.

Oxime based ligands form a wide range of complexes with diverse metal ions. Oxime based transition metal complexes are being employed in different research areas like catalysis, drug discovery, biological applications and sensing [41,42]. These complexes also display remarkable medicinal properties [43,44].

Many binuclear and polynuclear copper(II) complexes based on oxime based Schiff base ligands are of contemporary interest. Magnetic aspects of many of them are rich indeed [45,46]. From industrial viewpoint, oximes are also important. In the course of present research work, we have employed oxime based Schiff base ligand for the synthesis of a trinuclear copper(II) complex.

3. Copper chemistry

Copper, an essential trace element, is the most abundant element after iron and zinc in human body [47,48]. The concentration of copper in Earth's crust and in human blood are respectively of 50 and 1.0 ppm. Many enzymes containing copper ions act as cofactors and maintain various biological functions such as cellular activities and metabolism [49,50]. In human metabolism, copper plays a vital role for essential enzymes. In medicinal chemistry, copper offers remarkable and significant contribution. This owes to the strong affinity of blood plasma (biological fluid in human) to bind copper ions [51,52]. Deficiency of copper causes several ailments such as Parkinson's disease, cardiovascular diseases, anaemia, Menke's disease [53-56]. Again, excessive intake of it makes human body toxic. This also

causes various diseases like Wilson's disease and Alzheimer's disease [56,57]. Thus, sensing and monitoring of copper preferably at physiological p^H is crucial. Our present work also encompasses copper sensing.

3.1. Oxidation states of copper

Copper exists in five oxidation states: 0, +I, +II, +III and +IV. The most common oxidation state is +II, followed by +I. Copper(II) complexes are prone to Jahn-Teller distortion. With closed-shell d^{10} electronic-configuration, copper(I) complexes are diamagnetic. Structurally characterised copper(III) complexes are truly rare [58,59]. Stable copper(IV) complexes are scarcely known. To the best of our knowledge, such assemblies are found to be stable in macrocyclic systems [60]. According to R. G. Pearson's 'Hard-Soft' classification [61], copper(I) and copper(III) are respectively classified as "soft" and "hard"; while copper(II) is a "borderline" case. As a result, copper(I) tends to form stable complexes conveniently with "soft" donor centers. On the contrary, Cu(III) is susceptible to yield stable compounds only with 'hard' donor centers like fluoride, amide nitrogen etc. Copper(II) can be stabilised with a broad range of donor centers, "hard" as well as "soft".

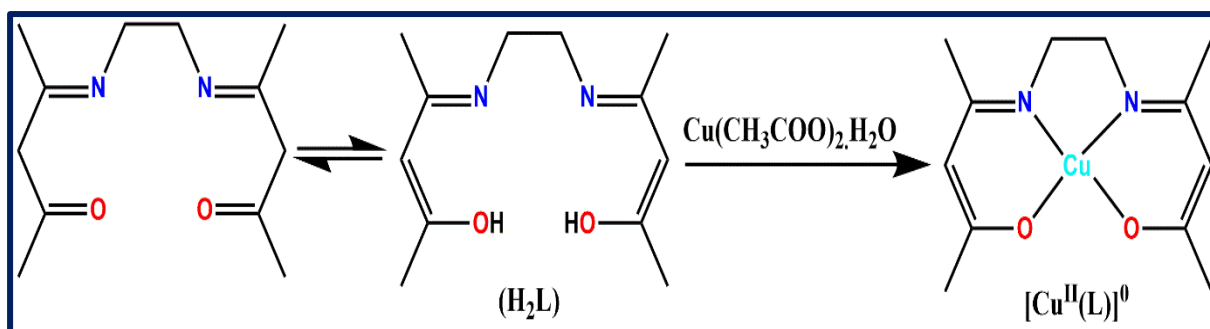
In aqueous milieu, simple Cu^{2+} ion is stable than free Cu^+ ion. Cu(I) easily undergoes disproportionation in water to give rise Cu(II) and Cu(0) as shown in Table I.1 [62]. The stability of copper ions can be discerned from the following redox potential values as have been forwarded vs NHE (normal hydrogen electrode).

Table I.1. Redox behaviour of copper ions in aqueous medium

$Cu^+_{(aq)}$	+	e^-	\longrightarrow	$Cu^0_{(s)}$	$E^0 = 0.52V$
$Cu^{2+}_{(aq)}$	+	e^-	\longrightarrow	$Cu^+_{(aq)}$	$E^0 = 0.153V$
$2Cu^+_{(aq)}$	\rightleftharpoons			$Cu^{2+}_{(aq)} + Cu^0_{(s)}$	$E^0 = 0.37V \quad K_{eq} = 10^6$

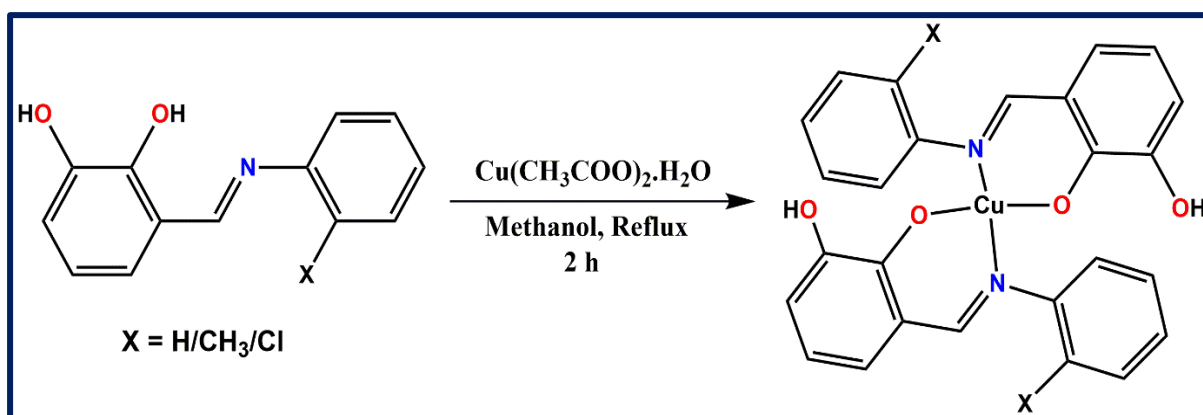
3.2. Coordination chemistry of copper

Schiff bases form stable chelate rings with Cu^{2+} ions through varying donor sites [63,64]. The first metal complex, ever stabilised by a Schiff base ligand, had been synthesized by Alphonse Combes in 1889 [65]. Combes designed and prepared a Schiff base ligand through the condensation of ethylenediamine and acetylacetone in 1:2 stoichiometric proportion. Most likely this Schiff base ligand was the first that had ever been used to yield a coordination complex. The synthetic scheme of the copper(II) complex, as had been proposed by Combes, is shown in scheme I.3 [66].



Scheme I.3. Structure of copper(II) complex proposed by Combes obtained through the reaction of Schiff base ligand with copper(II) acetate.

Copper(II) ion manifests various stereochemistry in its coordination complexes [67]. It has the ability to coordinate with various types of ligands and also shows interesting redox features due to its varying oxidation states [68]. These attributes are important and hence give rise distinguishable features of this coinage metal. Of late, N. Mabuba *et al.* has outlined the synthetic route for the preparation of Schiff base copper(II) complexes (scheme I.4) [69].



Scheme I.4. Synthetic route for the preparation of Schiff base copper(II) complexes.

The preferred coordination numbers of copper(II) in its Schiff base complexes are 4, 5 and 6. With 6 coordination number, the most common geometry of the central copper(II) ion of Schiff base copper(II) complexes is Jahn-Teller distorted octahedron. B. S. Parajon-Costa *et al.* has recently reported mononuclear penta-dentate (N₂O₃ donor sites) copper(II) complexes stabilised by a Schiff base ligand with distorted square pyramidal geometry [70]. Such type of complexes has subsequently been demonstrated for cytotoxic studies.

Morpholine based copper(II) complexes are also noteworthy in the context of current search (Fig. I.7) [71,72].

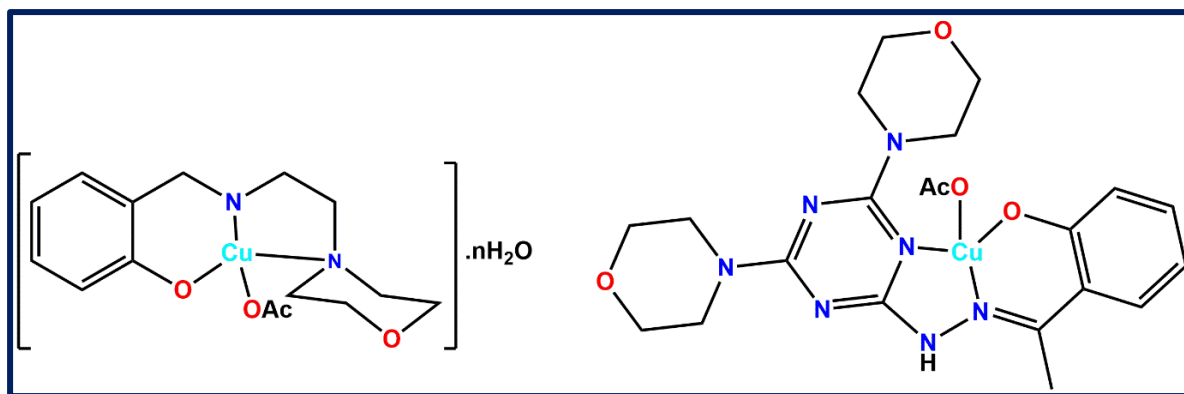


Fig. I.7. Examples of morpholine based copper(II) complexes.

4. Application of copper-Schiff base complexes

In coordination chemistry, copper-Schiff base complexes have encompassed a broadened area of research work in diverse fields like biological, analytical and medicinal. Some of the studies, having relevance in the context of present work, are highlighted below:

- Bio-macromolecular interaction (DNA and RNA)
- Inhibition of digestive enzymes
- Sensing of copper
- Magnetic properties
- Anti-cancer activity

4.1. Cu(II) complexes: Bio-macromolecular interaction study

Studies on the bio-macromolecular interactions with small molecules are of contemporary interest. This phenomenon aids to comprehend the underlying mechanism of binding interactions [73]. Among various types of bio-macromolecules, we have focused only on DNA and RNA to put our exercise into context.

4.1.1. Interaction with DNA

Deoxyribonucleic acid (DNA), one of the most important nucleic acids, regulates many biochemical processes in the cellular system. Friedrich Miescher, young Swiss biochemist, was the first to isolate it in 1869 [74]. DNA is comprised of the purine derivatives, adenine (A) and guanine (G), and the pyrimidine derivatives, cytosine (C) and thymine (T). Watson and Crick [75] proposed the right-handed double helix structure of DNA. Many transition metal complexes have been studied to demonstrate potential binding and cleaving aspects of DNA [76,77]. However, such type of activity is rich indeed for Schiff base copper(II) complexes [78]. In this context, studies on the interaction of DNA with copper(II) complexes are crucial from the perspective of drug design. Such interactions may either be covalent or non-covalent. Covalent type DNA interactions occur mainly through the replacement of the

labile part of the complexes by nitrogen bases. On the contrary, non-covalent DNA interactions include intercalative, electrostatic, and major- and minor groove bindings. Different binding modes are shown in Fig. I.8 [79].

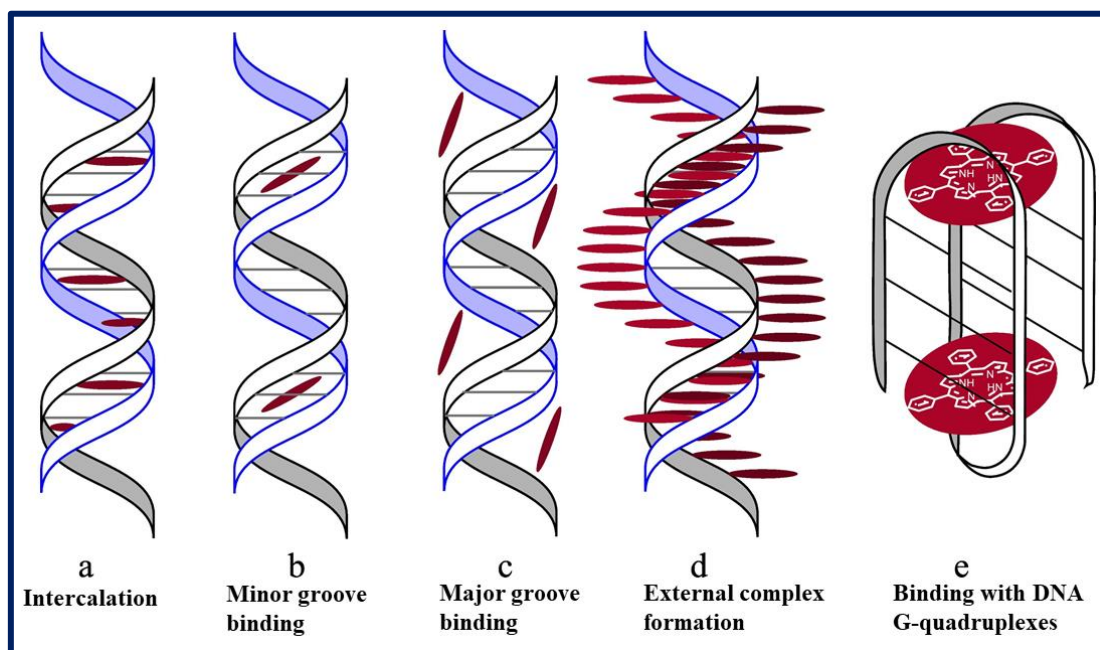


Fig. I.8. Different modes of binding in DNA.

Studies on the DNA binding interaction of copper(II) complexes have been the topic of interest in the course of present research work.

4.1.2. Interaction with RNA

Ribonucleic acid (RNA) is a single stranded molecule. It offers greater structural versatility than DNA in terms of conformation and chemical reactivity [80]. Like double helical DNA, RNAs are also comprised of ribose sugar, base and phosphate [81]. Herein, purine bases are adenine (A) and guanine (G) while cytosine (C) and uracil (U) are pyrimidine bases.

To know the molecular recognition process, studies on the RNA interactions with small molecules are crucial. In this work, we are concerned with the DNA/RNA binding aspects of a novel copper(II) dimer, stabilised with a Schiff base ligand.

4.2. Cu(II) complexes: Digestive enzymes

Digestive enzymes, naturally occurring proteins, are involved in the digestion process. Most of these enzymes are secreted by various parts of the body (digestive glands). The primary task of such entities is to break down both nutrients and non-nutrients. Among the various digestive enzymes, here we mainly focus on trypsin, amylase and lipase.

Inhibition of digestive enzymes is of much need for the treatment of several health problems [82,83]. Our literature survey reveals that Schiff bases along with their transition metal

complexes suppress enzymatic activity [84,85]. Amylase enzymes [86] aid to the hydrolysis of polysaccharide starch molecules. Long chain triglycerides are hydrolysed by lipase enzymes, which are useful in biotechnological applications [87]. The prime function of pancreatic lipase enzyme is the breaking down of lipid molecules [88]. Pancreatic lipase catalyses the hydrolysis of triacylglycerol. It plays a crucial role in dietary triacylglycerol absorption so much so that it is of judicious choice for the treatment of obesity [89]. Proper inhibition of pancreatic lipase is much needed to regulate obesity and to control some other allied health issues [90].

A. J. Muller *et al.*, in 2023, reported a Schiff base ligand, 2-(((2-bromo-4-chlorophenyl)amino)methyl)chlorophenyl)amino)methyl)phenol (HL1). Its copper(II) complex, Cu(L1)₂ (Fig. I.9) shows promising amylase inhibitory activity [91].

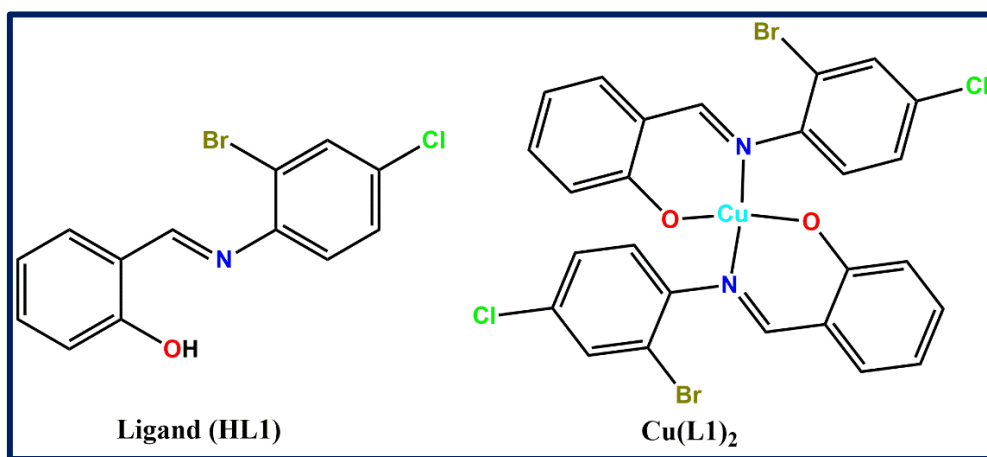


Fig. I.9. Schiff base ligand (HL1) and its copper(II) complex, Cu(L1)₂.

To the best of our knowledge, inhibition of digestive enzymes by Schiff base copper(II) complexes is rare indeed. In the course of our present investigation, we have employed a mononuclear copper(II) complex towards inhibition of amylase, trypsin and lipase.

4.3. Cu(II) complexes: Sensing properties

Chemosensors offer simple yet reliable and sensitive method for the detection of analytes in solution [92-94]. Chemo-sensing is one of the basic analytical methods. Detection of copper(II) ion is important from many perspectives. Imbalance of copper may lead to many diseases including metabolic abnormalities [95,96]. Sensing of copper(II) ion, based on a Schiff base probe, has become a point of interest in the course of present work. Techniques based on atomic absorption spectroscopy (AAS), inductively coupled plasma (ICP), atomic emission spectrometry (IES) and many others are in vogue for the sensing of Cu²⁺ ions [97]. Based on instruments, these methods are naturally expensive [98]. Other reliable techniques are colorimetry and fluorometry [99].

Tsien first demonstrated the idea of chemical sensing in 1980 during the synthesis of fluorescent calcium indicators [100,101]. Depending on the binding ability with the ions of interest, their fluorescence behaviour also undergoes concomitant changes. This change in signal may occur through enhancing (turn-on), quenching (turn-off) or shifting of the signal. Fig. I.10 depicts the pictorial representation of “turn-on” and “turn-off” type fluorescent sensors.

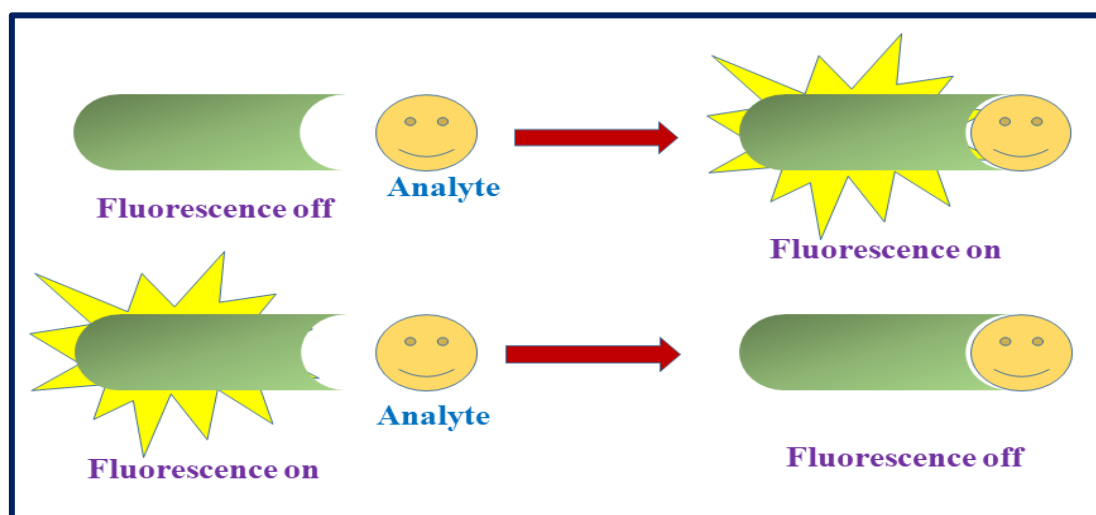


Fig. I.10. Pictorial view of “turn-on” and “turn-off” type sensors.

Recently M. Sankarganesh *et al.* reported a fluorine-substituted Schiff base ligand, 2-[N-(fluorophenyl)-4-hydroxy-4-phenyl]3-butene (FHPB), as a highly sensitive and selective sensor for the detection of copper(II) ion through spectroscopic techniques (Fig. I.11) [102].

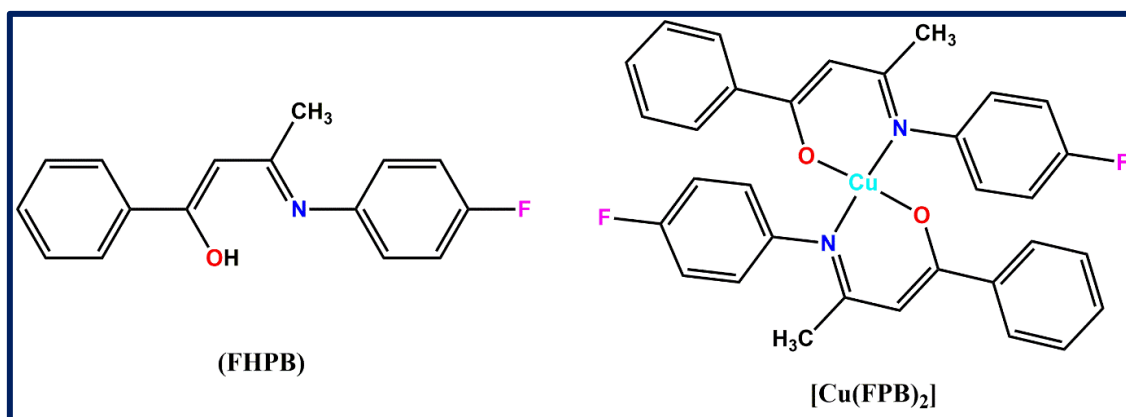


Fig. I.11. Schiff base ligand (FHPB) and the proposed structure of its Cu(II) complex.

4.4. Cu(II) complexes: Magnetic properties

Multinuclear copper(II) complexes are of contemporary interest. The reasons are myriad. Notable among them are their manifested structural diversities and significant prospects in the realm of molecular magnetism [103-107]. They have often been designed and synthesized from appropriate ligands with compatible donor atoms. The effective magnetic moment of

the copper(II) core in multinuclear copper(II) complexes may decrease or increase depending on variation in temperature. These occur due to cooperative magnetic interactions of the local spin centers. On lowering temperature if $\chi_M T$ increases, the interaction is ferromagnetic. On the other hand, the interaction is anti-ferromagnetic when $\chi_M T$ decreases on lowering the temperature. The exact mode of interaction is governed by total spin states instead of local spin states. The schematic representation of magnetic interactions is shown in Fig. I.12.

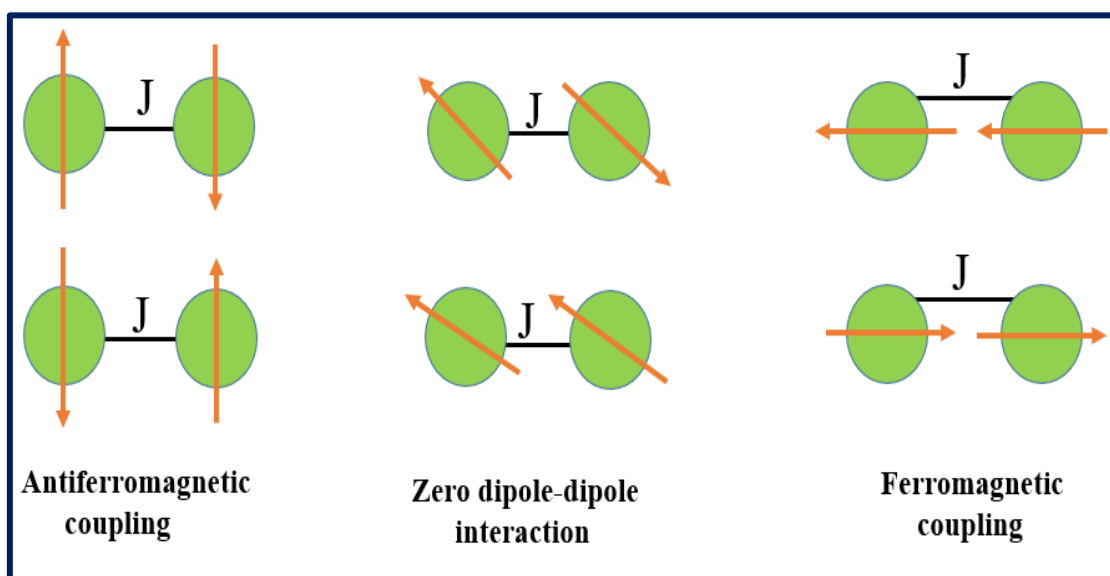


Fig. I.12. Pictorial view of spin orientation of coupling interaction.

Design and synthesis of copper(II) coordination polymers have evoked significant attention over the last decade in synthetic inorganic chemistry and crystal engineering [108,109]. Due to their impressive structural diversity, copper(II) coordination polymers show interesting magnetic dimensionality [110,111]. Suitable bridging groups play a crucial role in the making of magnetic coordination polymers [112]. In this context, the nature of the bridging groups has determined the extent of magnetic exchange interaction amongst the copper(II) ions [113].

A. Ghosh and his research group recently reported a Cu(II)-azido coordination polymer, $[\text{Cu}_4(\text{L}^1)_2(\text{N}_3)_6]_\infty$, using a Schiff base ligand (HL^1 : 2-[(2-ethylamino-ethylamino)-methyl]phenol). This shows anti-ferromagnetic exchange interaction between the Cu(II) centers (Fig. I.13a) [114]. Single end-to-end thiocyanate bridged copper(II) polymer, $[\text{CuL}(\mu_{1,3}\text{-NCS})]_n$, stabilised from a Schiff base ligand, $\text{HL} = 3-((2-(\text{dimethylamino})\text{ethyl})\text{imino})-1\text{-phenylbutan-1-one}$ and exhibiting weak anti-ferromagnetic coupling interaction with a J value -0.57 cm^{-1} had been reported by J. Ribas *et al.* (Fig. I.13b) [115].

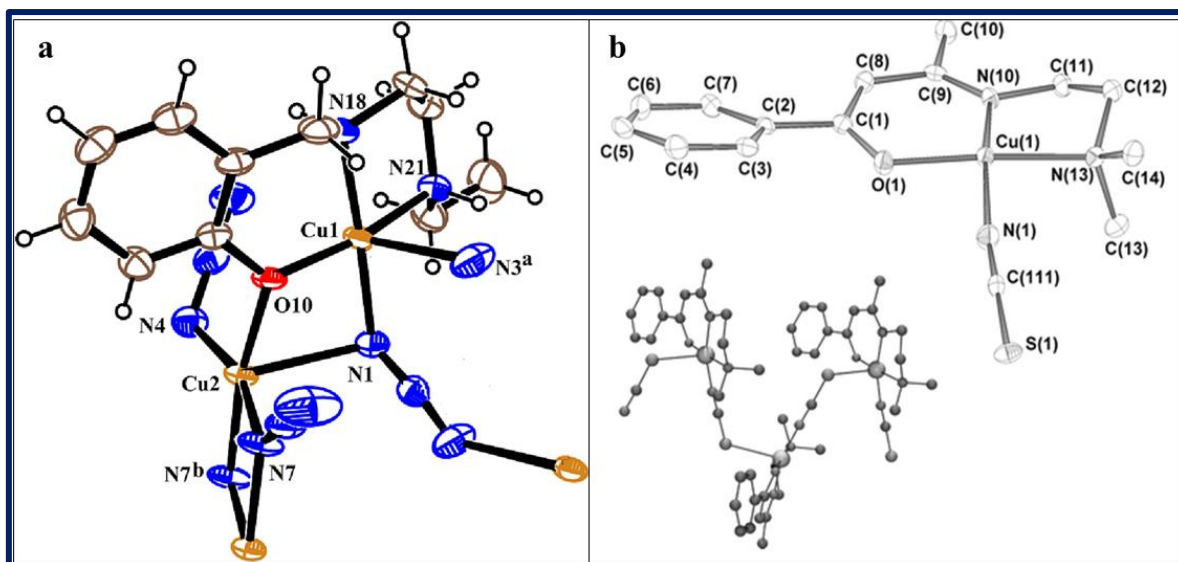


Fig. I.13. Molecular structures of azido bridged (a) and thiocyanato bridged (b) copper(II) coordination polymers.

Oxime based trinuclear copper(II) systems are well-known from magnetic point of view. T. K. Paine *et al.*, in 2010, reported an oxime based trinuclear copper(II) core, $[\text{Cu}^{\text{II}}_6(\mu_3\text{-O}\cdots\text{H}\cdots\text{O}-\mu_3)\text{L}_3(\text{H}_2\text{O})_6](\text{ClO}_4)_3$ (Fig. I.14). It dimerises through hydrogen bond [116].

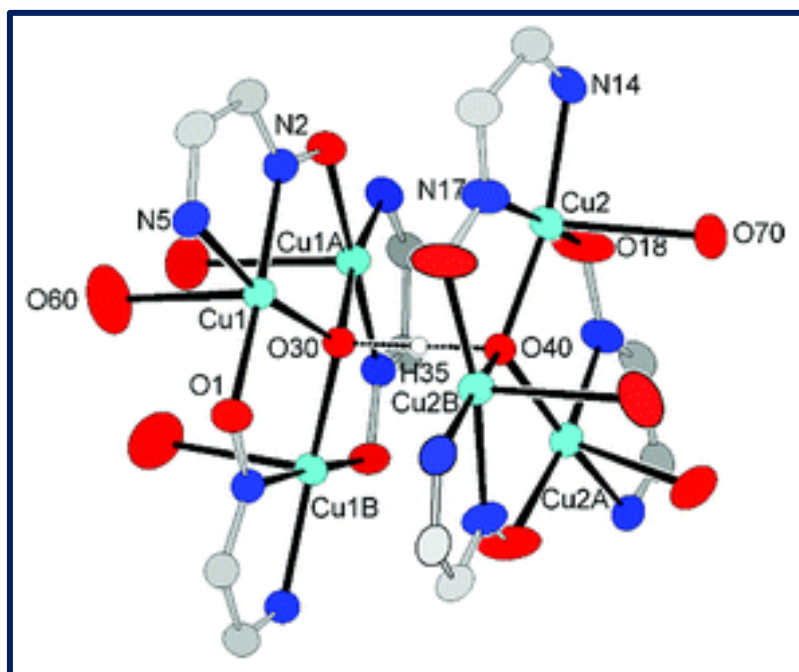


Fig. I.14. Hydrogen bonded dimer of two trinuclear copper(II) cores.

It is stabilized from an oxime based Schiff base ligand, (H_2L : 3,3'-((1,3-phenylenebis(methylene))bis(azaneylylidene))bis(butan-2-one)dioxime). Here two Cu_3O cores interact anti-ferromagnetically through hydrogen bonding.

4.5. Cu(II) complexes: Anti-cancer properties

Cancer, the second leading cause of death worldwide, is one of the most aggressive and deadly diseases [117]. This harmful disease arises from uncontrolled cell division (pathophysiological changes). This malady adversely affects global human well-being and also is accentuated by environmental conditions. Cisplatin, the most successful metallo-drug, has widely been used in chemotherapy over the past decade for cancer treatment [118,119]. However, this platinum based drug has some inherent serious side effects which limit its wide usage [120]. Thus, development of novel metallo-drugs, based on transition metals with fewer side effects, is the need of the hour [121,122]. A plethora of various transition metal-based metallo-drugs have been designed for anti-proliferative propensities. Copper based anti-cancer agent is of prime focus in the context of present work.

Being a biocompatible physiological metal, copper seems to be a remarkable choice in this regard. Copper complexes show promising cytotoxicity both in ‘*in vivo*’ and in ‘*in vitro*’ modes [123,124]. Copper complexes have drawn considerable attention due to their strong affinity for nucleobases and for their potential ability to crumble up mitochondrial function. The cell death mechanism of copper based system is different from that of platinum drugs (Fig. I.15).

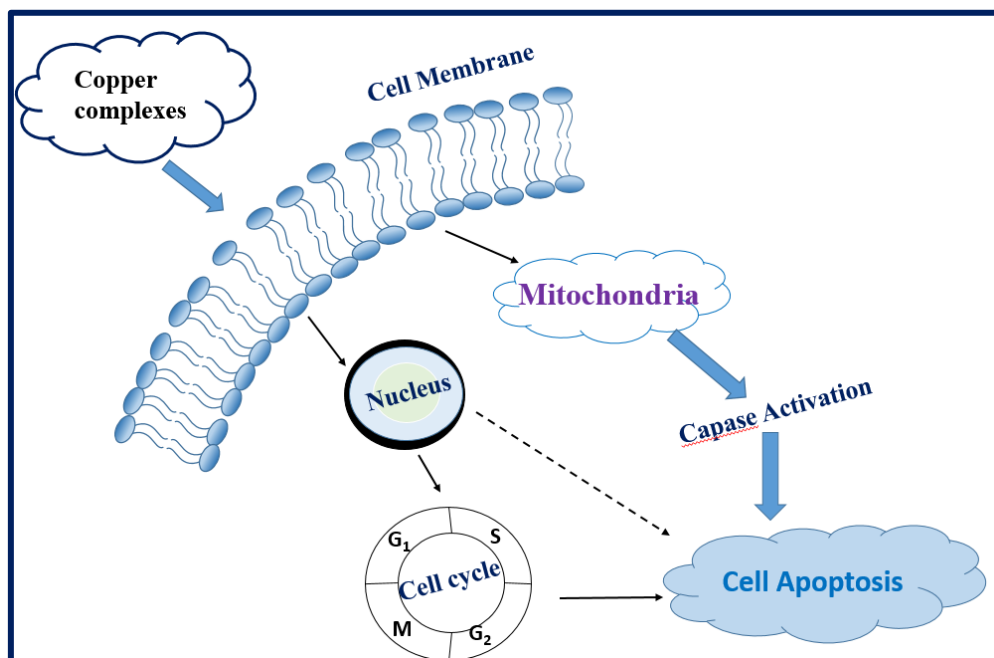


Fig. I.15. Proposed cell death mechanism.

L. Ruiz-Azuara and co-workers have reported copper(II) compounds with substituted diamine or phenanthroline (phen) group, calling it “Casiopinas group”, for promising anti-cancer activity. The general formula of such mixed chelates, Casiopinas group, is [Cu(N-

$N)(N-O)]^+$, and $[Cu(N-N)(O-O)]^+$, where N-N refers to primary ligand. Among several complexes with Casiopeinas group, two mononuclear Cu(II) complexes, $[Cu(4,4'$ -dimethyl-2,2'-bipyridine)(acetylacetonate)](NO_3) (Cas III-ia) and $[Cu(4,7$ -dimethyl-1,10-phenanthroline)(glycinate)](NO_3) (Cas II-gly), manifest promising cytotoxic and anti-tumour propensities (Fig. I.16). Both of them are in phase I (clinical trials) [125,126].

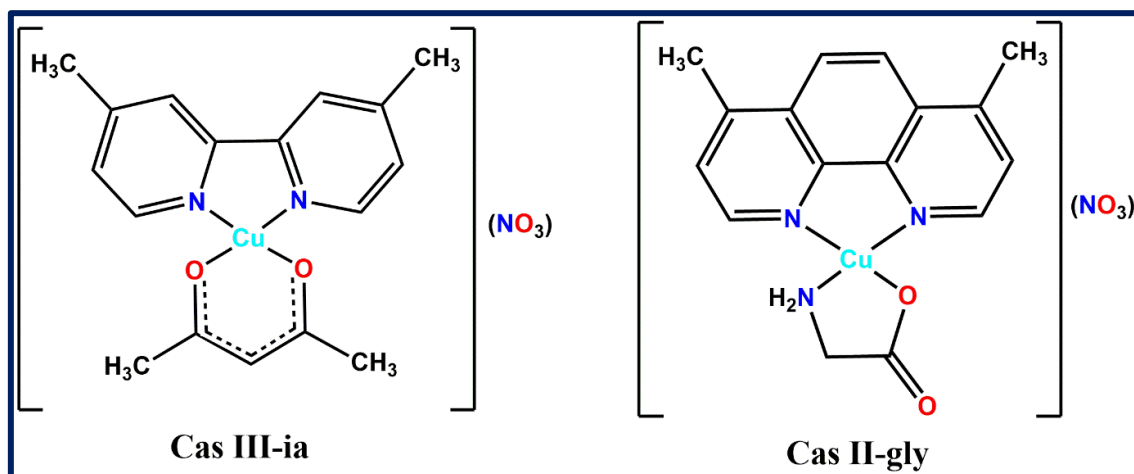


Fig. I.16. Structures of mononuclear copper(II) complexes with anti-cancer properties.

However, a five-coordinate mononuclear Cu(II) complex, $[Cu(tpy-tpp)Br_2]Br$, (abbreviated as CTB, tpy: 4'-(*p*-tolyl)-2,2':6',2''-terpyridine and tpp: triphenylphosphine) having a tri-phenyl-phosphine group effectively shows mitochondrial apoptosis against various kinds of tumour cells (Fig. I.17) [127]. Recently, linear trinuclear copper(II) complexes have been reported with limited cytotoxicity ($IC_{50} > 100 \mu M$) [128]. Generally, trinuclear copper(II) systems show lower cytotoxicity.

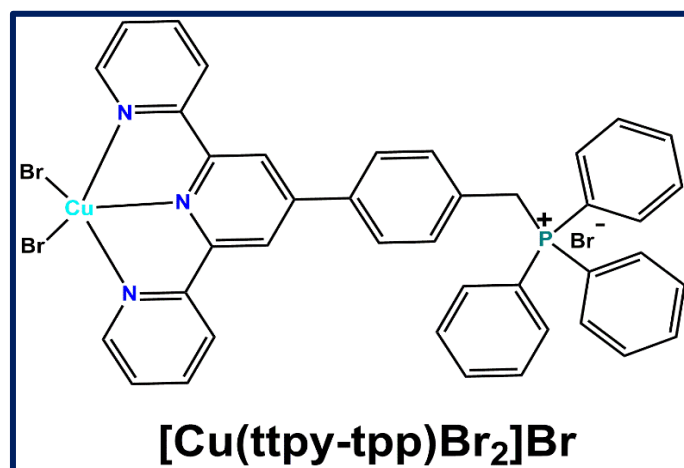


Fig. I.17. Structure of a five-coordinate mononuclear Cu(II) complex, $[Cu(tpy-tpp)Br_2]Br$.

This pertinent aspect prompts us to work along this line and to develop new anti-cancer agents based on copper(II) complexes. In this thesis, we have reported two mononuclear Cu(II) complexes with promising cytotoxic activity against non-small cell lung cancer

(NSCL) cell line, A549. The present work also embodies a novel trinuclear copper(II) complex having promising anti-proliferative propensities.

5. An overview of copper(I) chemistry: Melanin sensing

A German chemist, Rudolf Christian Böttger, first synthesized copper(I) compound, Cu_2C_2 , in 1859 [129]. Copper(I) systems display diverse structural motifs [130,131]. Such systems bear significance in the arena of catalysis [132]. Copper(I) complexes show moderate cytotoxicity against different human cell lines [133]. Besides, copper(I) complexes have been used in OLEDs and in gas sensing [134,135]. The photophysical aspect of copper(I) complexes is, however, well explored. McMillin's pioneering work is also noteworthy in this context [136]. However, electrochemical melanin sensing using any copper(I) complex is hitherto unprecedented. Herein we are concerned with the same.

Melanin is a kind of natural polymeric pigment. It is commonly present in biological systems [137]. The most studied melanin is eumelanin [138]. This is present in human hair and skin, in squid ink and in bird feathers [137]. The chemical structures of the monomeric units of eumelanin are summarised in Fig. I.18.

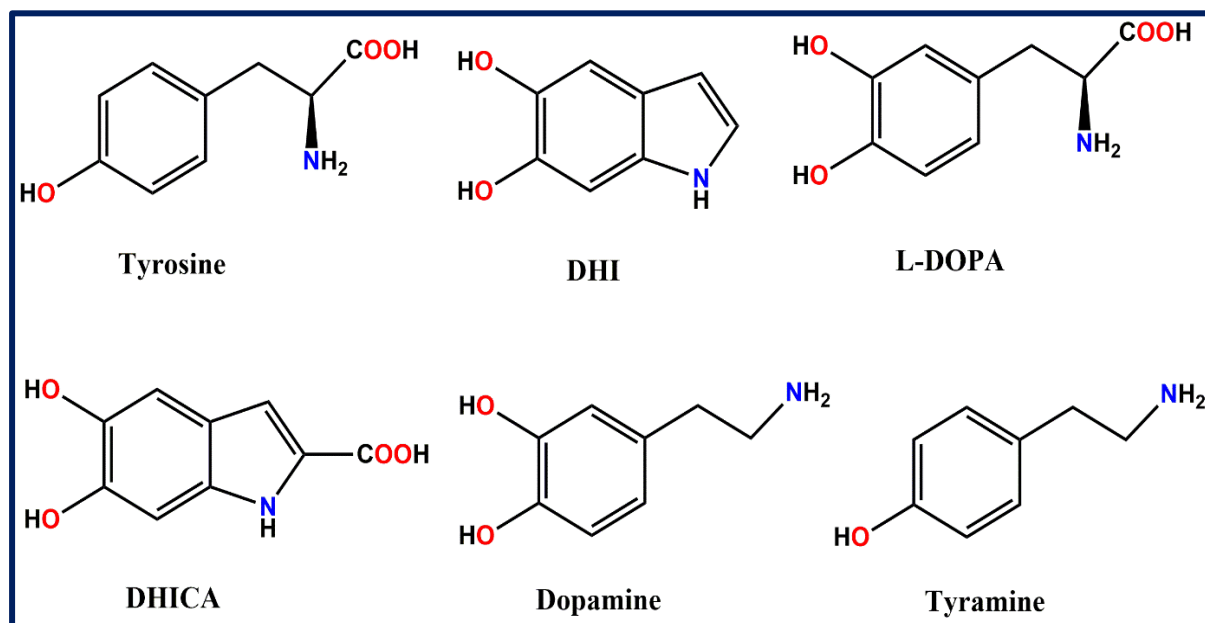


Fig. I.18. Chemical structures of eumelanin monomers.

Some heteroleptic copper(I) complexes, stabilised from quinoxaline based probes, have been reported. They have also been tested for their possible role in photo-redox catalysis [139]. López-Cortés *et al.* recently reported a well-defined dinuclear copper(I) complex to demonstrate its catalytic properties in 1,3 dipolar cycloaddition reactions [140] (Fig. I.19).

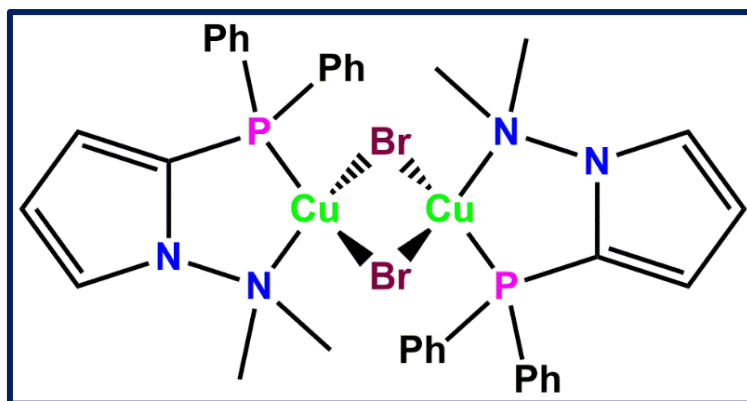


Fig. I.19. Structure of the dinuclear Cu(I) complex.

Electrochemical sensing of melanin has become an important topic in the context of present research endeavour. This sensing has been made a reality through modification of electrode with our novel copper(I) complexes.

6. Objectives of present studies

The aim of our present endeavour is to explore the chemistry of copper encompassing two of its main oxidation states, +I and +II. Specifically, the purpose here is to design, synthesise and comprehensively characterize some new copper(II) complexes with a view to expound their chemistry from biological perspectives like studies on bio-macromolecular interaction (DNA and RNA), inhibition of digestive enzymes and studies on anti-proliferative activity. Another objective is to examine the magnetic properties of some polynuclear copper(II) complexes. For the oxidation state of +I, the prime aim is to produce some stable copper(I) complexes at least in the solid state. Exploration of their possible application is also kept in mind. Modification of electrode(s) with these new copper(I) complexes for the electrochemical sensing of melanin has also been our prime objective. Herein also lies the future scope of this present research work.

7. References

1. H. Schiff, Communications from the University Laboratory at Pisa: A new series of organic bases. *Justus Liebigs Ann. Chem.* 131 (1864) 118-119.
2. T.P. Yoon, E.N. Jacobsen, *Science* 299 (2003) 1691-1693.
3. S. Patai, "The Chemistry of the Carbon-Nitrogen Double Bond". Interscience Publishers Inc., New York, 1970.
4. S.K. Raju, A. Settu, A. Thiagarajan, D. Rama, P. Sekar, S. Kumar, *GSC Biol. Pharm. Sci.* 21 (2022) 203-215.
5. S. Manzoor, R.A. Tahir, M.A. Younis, W.-L. Cao, Q. Tariq, A. Ali, N. Ahmad, C. Qiu, B. Tian, J.-G. Zhang, *Bioorg. Chem.* 140 (2023) 106822.
6. M.M. Sprung, *Chem. Rev.* 26 (1940) 297-338.
7. P.Y. Sollenberger, R.B. Martin, *J. Am. Chem. Soc.* 94 (1970) 4261-4270.
8. K. Ghosh, A. Banerjee, A. Bauzá, A. Frontera, S. Chattopadhyay, *RSC Adv.* 8 (2018) 28216-28237.
9. S. Kumar, M. Choudhary, *J. Biomol. Struct. Dyn.* 41 (2023) 4957-4980.
10. S.S. Saleem, M. Sankarganesh, P.A. Jose, J.D. Raja, *Inorg. Chem. Commun.* 124 (2021) 108396.
11. F.A. El-Saied, T.A. Salem, M.M.E. Shakhdofta, A.N. Al-Hakimi, A.S. Radwan, *J. Basic Appl. Sci.* 7 (2018) 420-429.
12. E. Jungreis, S. Thabet, *Analytical applications of Schiff bases*, Marcell Dekker, New York (1969).
13. A.M. Hassan, A.O. Said, B.H. Heakal, A. Younis, W.M. Aboulthana, M.F. Mady, *ACS Omega* 7 (2022) 32418-32431.
14. A.D. Garnovskii, B.I. Kharisov, Marcel Dekker, Inc. New York (2003).
15. A.M.S. Hossain, J.M. Méndez-Arriaga, C. Xia, J. Xie, S. Gómez-Ruiz, *Polyhedron* 217 (2022) 115692.
16. S.G. Patra, N.K. Shee, M.G.B. Drew, D. Datta, *New J. Chem.* 40 (2016) 3238-3243.
17. S. Mukhopadhyay, D. Mandal, D. Ghosh, I. Goldberg, M. Chaudhury, *Inorg. Chem.* 42 (2003) 8439-8445.
18. H. Keypour, M. Rezaeivala, L. Valencia, P. Pérez-Lourido, H.R. Khavasi, *Polyhedron* 28 (2009) 3755-3758.
19. I.R. Laskar, T.K. Maji, D. Das, T.-H. Lu, W.-T. Wong, K.-I. Okamoto, N.R. Chaudhuri, *Polyhedron* 20 (2001) 2073-2082.
20. K. Rupak, S.R. Vulichi, K. Suman, *Int. J. Chem. Sci.* 14 (2016) 1777-1788.

21. M.J. Naim, O. Alam, M.J. Alam, P. Alam, N. Shrivastava, *Int. J. Pharmacol. Pharm. Sci.* 3 (2015) 40-51.
22. F. Arshad, M.F. Khan, W. Akhtar, M.M. Alam, L.M. Nainwal, S.K. Kaushik, M. Akhter, S. Parvez, S.M. Hasan, M. Shaquiquzzaman, *Eur. J. Med. Chem.* 167 (2019) 324-356.
23. D.W. Young, *Heterocyclic Chemistry*, Longman Group Ltd., London, 1975.
24. J.W.F. Oliveira, H.A.O. Rocha, W.M.T.Q. Medeiros, M.S. Silva, *Molecules* 24 (2019) 2806.
25. K. Ohui, E. Afanasenko, F. Bacher, R.L.X. Ting, A. Zafar, N. Blanco-Cabra, E. Torrents, O. Dömötör, N.V. May, D. Darvasiova, É.A. Enyedy, A. Popović-Bijelić, J. Reynisson, P. Rapta, M.V. Babak, G. Pastorin, V.B. Arion, *J. Med. Chem.* 62 (2019) 512-530.
26. K. Dhahagani, S.M. Kumar, G. Chakkaravarthi, K. Anitha, J. Rajesh, A. Ramu, G. Rajagopal, *Spectrochim. Acta Part A: Mol. Biol. Spectros.* 117 (2014) 87-94.
27. N.S. Gwaram, P.J. Hassandarvish, *J. Appl. Pharm. Sci.* 4 (2014) 075-080.
28. M. Hosseini-Kharat, R. Rahimi, D. Zargarian, Z.M. Lighvan, A.A. Momtazi-Borojeni, T. Sharifi, E. Abdollahi, H. Tavakol, T. Mohammadi, *J. Biomol. Struct. Dyn.* 37 (2019) 3788-3802.
29. J.A. War, S.K. Srivastava, S.D. Srivastava, *Spectrochim. Acta Part A: Mol. Biomol. Spectrosc.* 173 (2017) 270-278.
30. J.E. Summerton, *Curr. Top. Med. Chem.* 7 (2007) 651-660.
31. D.P. Gouvea, F.A. Vasconcellos, G.A. Berwaldt, A.C.P.S. Neto, G. Fischer, R.P. Sakata, W.P. Almeida, W. Cunico, *Eur. J. Med. Chem.* 118 (2016) 259-265.
32. Ü. Korkmaz, B.T. Findik, B. Dede, F. Karipcin, *Bioorg. Chem.* 121 (2022) 105685.
33. J.P. Naskar, C. Biswas, L. Lu, M. Zhu, *J. Chem. Crystallogr.* 41 (2011) 502-507.
34. A. Hantzsch, A. Werner, *Chem. Ber.* 23 (1890) 1
35. V. Meyer, A. Janny, *Eur. J. Inorg. Chem.* 15 (1882) 1164.
36. M.A. Motaleb, A.A. Selim, *Bioorg. Chem.* 82 (2019) 145-155.
37. D.S. Bolotin, N.A. Bokach, M.Y. Demakova, V.Y. Kukushkin, *Chem. Rev.* 117 (2017) 13039-13122.
38. I. Belkhattab, S. Boutamine, H. Slaouti, M.F. Zid, H. Boughzala, Z. Hank, *J. Mol. Struct.* 1206 (2020) 127597.
39. R. Kose, S.A. Gungor, S.E. Kariper, M. Kose, M. Kurtoglu, *Inorg. Chim. Acta.* 462 (2017) 130-141.
40. C.J. Milios, T.C. Stamatatos, S.P. Perlepes, *Polyhedron* 25 (2006) 134-194.

41. B. Ren, C. Guo, R.-Z. Liu, Z.-Y. Bian, R.-C. Liu, L.-F. Huang, J.J. Tang, *Eur. J. Med. Chem.* 228 (2022) 114031.
42. A. Kumar, D. Kumar, K. Kumari, Z. Mkhize, L.M.K. Seru, I. Bahadur, P. Singh, *J. Mol. Liq.* 322 (2021) 114872.
43. M. Erdem-Tunçmen, F. Karipcin, M. Atis, S. Perçin-Ozkorucuklu, *J. Organomet. Chem.* 756 (2014) 10-18.
44. Z.A. Siddiqi, M. Khalid, S. Kumar, M. Shahid, S. Noor, *Eur. J. Med. Chem.* 45 (2010) 264-269.
45. D. Premužić, M. Korabik, M. Hołyńska, *J. Mol. Struct.* 1059 (2014) 265-270.
46. Y.-B. Jiang, H.-Z. Kou, R.-J. Wang, A.-L. Cui, J. Ribas, *Inorg. Chem.* 44 (2005) 709-715.
47. R.M. Roat-Malone, *Bioinorganic Chemistry: A Short Course*; Wiley, 2003.
48. S.K. Mustafa, M.A. AlSharif, *Am. J. Anal. Chem.* 9 (2018) 15-26.
49. J.E. Weder, C.T. Dillon, T.W. Hambley, B.J. Kennedy, P.A. Lay, J.R. Biffin, H.L. Regtop, N.M. Davies, *Coord. Chem. Rev.* 232 (2002) 95-126.
50. P. Zatta, A. Frank, *Brain Res. Rev.* 54 (2007) 19-33.
51. N.E. Hellman, J.D. Gitlin, *Annu. Rev. Nutr.* 22 (2002) 439-458.
52. H. Tapiero, D.M. Townsend, K.D. Tew, *Biomed. Pharmacother.* 57 (2003) 386-398.
53. J.-P. Bach, N. Kumar, C. Depboylu, C. Noelker, T. Klockgether, M. Bacher, M. Balzer-Geldsetzer, R. Dodel, *J. Neurol. Sci.* 291 (2010) 95-97.
54. G. Forte, A. Alimonti, N. Violante, M.D. Gregorio, O. Senofonte, F. Petrucci, G. Sancesario, B. Bocca, *J. Trace Elem. Med. Biol.* 19 (2005) 195-201.
55. T. Kaido, H. Hashimoto, H. Okamura, K. Tsukaguchi, *J. Clin. Neurosci.* 12 (2005) 205-206.
56. G.J. Brewer, *Chem. Res. Toxicol.* 23 (2010) 319-326.
57. J.M. Walshe, In *Advances in Clinical Chemistry*; G.S. Makowski, Ed.; Elsevier, Vol. 50 (2010).
58. X. Ribas, J.C. Dias, J. Morgado, K. Wurst, E. Molins, E. Ruiz, M. Almeida, J. Veciana, C. Rovira, *Chem. Eur. J.* 10 (2004) 1691-1704.
59. F.C. Anson, T.J. Collins, T.G. Richmond, B.D. Santarsiero, J.E. Toth, B.G.R.T. Treco, *J. Am. Chem. Soc.* 109 (1987) 2974-2979.
60. O.V. Mikhailiv, D.V. Chachkov, *Materials* 13 (2020) 3162.
61. R.G. Pearson, *J. Am. Chem. Soc.* 85 (1963) 3533-3539.
62. R.L. Peterson, S. Kim, K.D. Karlin. In *Comprehensive Inorganic Chemistry II* (2nd Eds.); J. Reedijk, K. Poeppelmeier, Eds.; Elsevier: Amsterdam, 2013.

63. X. Liu, C. Manzur, N. Novoa, S. Celedón, D. Carillo, J.-R. Hamon, *Coord. Chem. Rev.* 357 (2018) 144-172.
64. H.H. El-Shalakany, R.M. Ramadan, M.A. Sayed, *Inorg. Chem. Commun.* 159 (2024) 111826.
65. A. Combes, *C. R. Acad. Sci.* 108 (1889) 1252-1255.
66. L. Fabbrizzi, *J. Org. Chem.* 85 (2020) 12212-12226.
67. A.A.G. Tomlinson, B.J. Hathaway, *J. Chem. Soc. (A)*, (1968) 2578-2583.
68. T. Malcomson, P. Repiščák, S. Erhardt, M.J. Paterson, *ACS Omega* 7 (2022) 45057-45066.
69. T.L. Yusuf, S.D. Oladipo, S. Zamisa, H.M. Kumalo, I.A. Lawal, M.M. Lawal, N. Mabuba, *ACS Omega* 6 (2021) 13704-13718.
70. Y. Burgos-López, L.M. Balsa, O.E. Piro, I.E. León, J. García-Tojal, G.A. Echeverría, A.C. González-Baró, B.S. Parajón-Costa, *Polyhedron* 213 (2022) 115621.
71. K. Sakthikumar, J.D. Raja, M. Sankarganesh, J. Rajesh, *Ind. J. Pharm. Sci.* 80 (2018) 727-738.
72. T.E. Khalil, K.A. Dahlous, S.M. Soliman, N.A. Khalil, A. El-Faham, A. El-Dissouky, *Molecules* 27 (2022) 2989.
73. G.M. Blackburn, M.J. Gait, D. Loakes, D.M. Williams, *Nucleic Acids in Chemistry and Biology*, 3rd ed., The Royal Society of Chemistry, Cambridge (2006).
74. R. Dahm, *Develop. Biol.* 278 (2005) 274-288.
75. J.D. Watson, F.H.C. Crick, *Nature* 171 (1953) 737-738.
76. P. Krishnamoorthy, P. Sathyadevi, A.H. Cowley, R.R. Butorac, N. Dharmaraj, *Eur. J. Med. Chem.* 46 (2011) 3376-3387.
77. D. Mukherjee, R.K. Das, *Int. J. Pharm. Biol. Sci.* 9 (2019) 1089-1106.
78. D. Zhao, Y. Wu, W. Huang, S. Gong, Z. Chen, *New J. Chem.* 46 (2022) 15219-15226.
79. N.S. Lebedeva, E.S. Yurina, Y.A. Gubarev, S.A. Syrbu, *Spectrochim. Acta A: Mol. Biomol. Spectrosc.* 199 (2018) 235-241.
80. A.B. Pradhan, S. Bhuiya, L. Haque, S. Das, *Int. J. Biol. Macromol.* 95 (2017) 340-347.
81. G.M. Blackburn, M.J. Gait, D. Loakes, D.M. Williams, *Nucleic Acids in Chemistry and Biology*, 3rd ed., The Royal Society of Chemistry, Cambridge (2006).
82. K.J. Kilpin, P.J. Dyson, *Chem. Sci.* 4 (2013) 1410-1419.
83. A.Y. Louie, T.J. Meade, *Chem. Rev.* 99 (1999) 2711-2734.

84. K. Buldurun, N. Turan, A. Aras, A. Mantarci, F. Turkan, E. Bursal, *Chem. Biodivers.* 16 (2019) e1900243.
85. G.A. Krishna, T.M. Dhanya, A.A. Shanty, K.G. Raghu, P.V. Mohanan, *J. Mol. Struct.* 1274 (2023) 134384.
86. N.S. Reddy, A. Nimmagadda, K.R.S.S. Rao, *African J. Biotech.* 2 (2003) 645-648.
87. K.-E. Jaeger, T. Eggert, *Curr. Opin. Biotechnol.* 13 (2002) 390-397.
88. A. Kumar, S. Chauhan, *Life Sci.* 271 (2021) 119115.
89. J. Zhang, Y. Yang, X.-K. Qian, P.-F. Song, Y.-S. Zhao, X.-Q. Guan, L.-W. Zou, X. Bao, H. Wang, *ChemMedChem.* 16 (2021) 1600-1604.
90. S.N.C. Sridhar, G. George, A. Verma, A.T. Paul, *Springer* (2019) 149-191.
91. T.L. Yusuf, I. Waziri, K.A. Olofinisan, E.O. Akintemi, E.C. Hosten, A.J. Muller, *J. Mol. Liq.* 389 (2023) 122845.
92. A. Kundu, P.S. Hariharan, K. Prabakaran, S.P. Anthony, *Sens. Actuators B: Chem.* 206 (2015) 524-530.
93. S. Liu, Y.-M. Wang, J. Han, *J. Photochem. Photobiol. C: Photochem. Rev.* 32 (2017) 78-103.
94. S. Kumar, B. Lal, R.K. Tittal, G. Singh, J. Singh, V.D. Ghule, R. Sharma, J.K. Sabane, *Sens. Diagn.* 2 (2023) 1267-1276.
95. H.S. Jung, P.S. Kwon, J.W. Lee, J.I. Kim, C.S. Hong, J.W. Kim, S. Yan, J.Y. Lee, J.H. Lee, T. Joo, J.S. Kim, *J. Am. Chem. Soc.* 131 (2009) 2008-2012.
96. J.-J. Xiong, P.-C. Huang, C.-Y. Zhang and F.-Y. Wu, *Sens. Actuators B: Chem.* 226 (2016) 30-36.
97. D. Harvey, *Modern analytical chemistry*, Boston: McGraw-Hill Companies, Inc., 2000.
98. J.C. Yu, J.M. Lo, C.M. Wai, *Analyt. Chim. Acta* 154 (1983) 307-312.
99. N. Mergu, V.K. Gupta, *Sens. Actuators B: Chem.* 210 (2015) 408-417.
100. R.Y. Tsien, *Biochem.* 19 (1980) 2396-2404.
101. G. Gryniewicz, M. Poenie, R.Y. Tsien, *J. Biol. Chem.* 260 (1985) 3440-3450.
102. C. Kanagavalli, M. Kalanithi, S. Gurusamy, R.N. Asha, N.M. Megtalin, M. Sankarganesh, *Chem. Phys. Imp.* 8 (2024) 100582.
103. M.S. Jana, S. Dey, J.L. Priego, R. Jiménez-Aparicio, T.K. Mondal, P. Roy, *Polyhedron* 59 (2013) 101-106.
104. F. Klongdee, Y. Sasada, M. Nakano, K. Chainok, S. Youngmea, J. Boonmak, *New J. Chem.* 47 (2023) 9669-9680.
105. P. Roy, M. Nandi, M. Manassero, M. Riccò, M. Mazzani, A. Bhaumik, P. Banerjee,

- Dalton Trans. (2009) 9543-9554.
106. Q. Zhu, C. Tian, C. Shen, T. Sheng, S. Hu, X. Wu, CrystEngComm 15 (2013) 2120-2126.
107. J. Gregoliński, K. Ślepokura, J. Kłak, M. Witwicki, Dalton Trans. 51 (2022) 9735-9747.
108. H.M. Tay, N. Kyratzis, S. Thoonen, S.A. Boer, D.R. Turner, C. Hua, Coord. Chem. Rev. 435 (2021) 213763.
109. I.B. Vírveda, S.A. Siddiqui, A. Prado-Roller, M. Eistererd, H. Shiozawa, RSC Adv. 11 (2021) 23943-23947.
110. Q. Liu, X. Liu, C. Shi, Y. Zhang, X. Feng, M.-L. Cheng, S. Sua, J. Gu, Dalton Trans. 44 (2015) 19175-19184.
111. X.-F. Yang, M. Liu, H.-B. Zhu, C. Hang, Y. Zhao, Dalton Trans. 46 (2017) 17025-17031.
112. M. Du, C.-P. Li, C.-S. Liu, S.-M. Fang, Coord. Chem. Rev. 257 (2013) 1282-1305.
113. R. Bikas, M. Korabik, J. Sanchiz, N. Noshiranzadeh, P. Mirzakhani, A. Gałkowska, D. Szeliga, A. Kozakiewicz-Piekarz, J. Solid State Chem. 303 (2021) 122484.
114. M. Mondal, J. Mayans, A. Escuer, A. Ghosh, Inorg. Chim. Acta 557 (2023) 121696.
115. P. Talukder, A. Datta, S. Mitra, G. Rosair, M.S.E. Fallah, J. Ribas, Dalton Trans. 2004, 4161-4167.
116. S. Karmakar, O. Das, S. Ghosh, E. Zangrando, M. Johann, E. Rentschler, T. Weyhermüller, S. Khanra, T.K. Paine, Dalton Trans. 39 (2010) 10920-10927.
117. L.A. Torre, F. Bray, R.L. Siegel, J. Ferlay, J. Lortet-Tieulent, A. Jemal, CA-Cancer J. Clin. 65 (2015) 87-108.
118. B. Rosenberg, L. Vancamp, Nature 222 (1969) 385-386.
119. L. Kelland, Nat. Rev. Cancer 7 (2007) 573-584.
120. D. Ding, B.L. Allman, R. Salvi, Anat. Rec. 295 (2012) 1851-1867.
121. S. Ray, R. Mohan, J.K. Singh, M.K. Samantaray, M.M. Shaikh, D. Panda, P. Ghosh, J. Am. Chem. Soc. 129 (2007) 15042-15053.
122. C. Marzano, M. Pellei, F. Tisato, C. Santini, Anti-Cancer Agents Med. Chem. 9 (2009) 185-211.
123. R. Alemón-Medina, M. Breña-Valle, J.L. Muñoz-Sánchez, M.I. Gracia-Mora, L. Ruiz-Azuara, Cancer Chemother. Pharmacol. 60 (2007) 219-228.
124. Q. Peña, G. Sciortino, J.-D. Maréchal, S. Bertaina, A.J. Simaan, J. Lorenzo, M. Capdevila, P. Bayón, O. Iranzo, Ò. Palacios, Inorg. Chem. 60 (2021) 2939-2952.
125. J. Serment-Guerrero, P. Cano-Sanchez, E. Reyes-Perez, F. Velazquez-Gracia, M.E. Bravo-Gomez, L. Ruiz-Azuara, In Vitro Toxicol. 25 (2011) 1376-1384.
126. L. Becco, A. Rodriguez, M.E. Bravo, M.J. Prieto, L. Ruiz-Azuara, B. Garat, V. Moreno,

- D. Gambino, J. Inorg. Biochem. 109 (2012) 49-56.
127. W. Zhou, X. Wang, M. Hu, C. Zhu, Z. Guo, Chem. Sci. 5 (2014) 2761-2770.
128. H.H. Nguyen, T.T. Pham, N.O. Pham-Thi, V.H. Tran, C.D. Le, B.V. Hoi, T.N. Trieu, C.T. Pham, J. Mol. Struct. 1249 (2022) 131680.
129. R.C. Böttger, Ann. Chem. 109 (1859) 351-362.
130. Y.-H. Chen, T.T.Y. Lin, H.-Y. Chen, C.-L. Kao, H.-Y. Chen, S.C.N. Hsu, J.R. Carey, M.Y. Chiang, J. Inorg. Biochem. 120 (2013) 24-31.
131. B.K. Najafabadi, J.F. Corrigan, Dalton Trans. 43 (2014) 2104-2111.
132. E. Sperotto, G.P.M. van Klink, J.G. de Vries, G. van Koten, Tetrahedron 66 (2010) 9009-9020.
133. M. Porchia, F. Benetollo, F. Refosco, F. Tisato, C. Marzano, V. Gandin, J. Inorg. Biochem. 103 (2009) 1644-1651.
134. B. Wolpert, O.S. Wolfbeis, V.M. Mirsky, Sens. Actuators B: Chem. 142 (2009) 446-450.
135. N. Kandasamy, N. Keerthi, J. Jeyasekaran, ACS Appl. Electron. Mater. 5 (2023) 4805-4815.
136. K.A. Meadows, F. Liu, J. Sou, B.P. Hudson, D.R. McMillin, Inorg. Chem. 32 (1993) 2919-2923.
137. L. D'Alba, M.D. Shawkey, Physiol. Rev. 99 (2019) 1-19.
138. M. d'Ischia, A. Napolitano, A. Pezzella, P. Meredith, M.J. Buehler, Angew. Chem. Int. Ed. 59 (2020) 11196-11205.
139. C. Bruschi, X. Gui, N. Salaeh-arae, T. Barchi, O. Fuhr, S. Lebedkin, W. Kloppe, C. Bizzarri, Eur. J. Inorg. Chem. (2021) 4074-4084.
140. M.A. Alvarado-Castillo, S. Cortés-Mendoza, J.E. Barquera-Lozada, F. Delgado, R.A. Toscano, M.C. Ortega-Alfaro, J.G. López-Cortés, Dalton Trans. 53 (2024) 2231-2241.

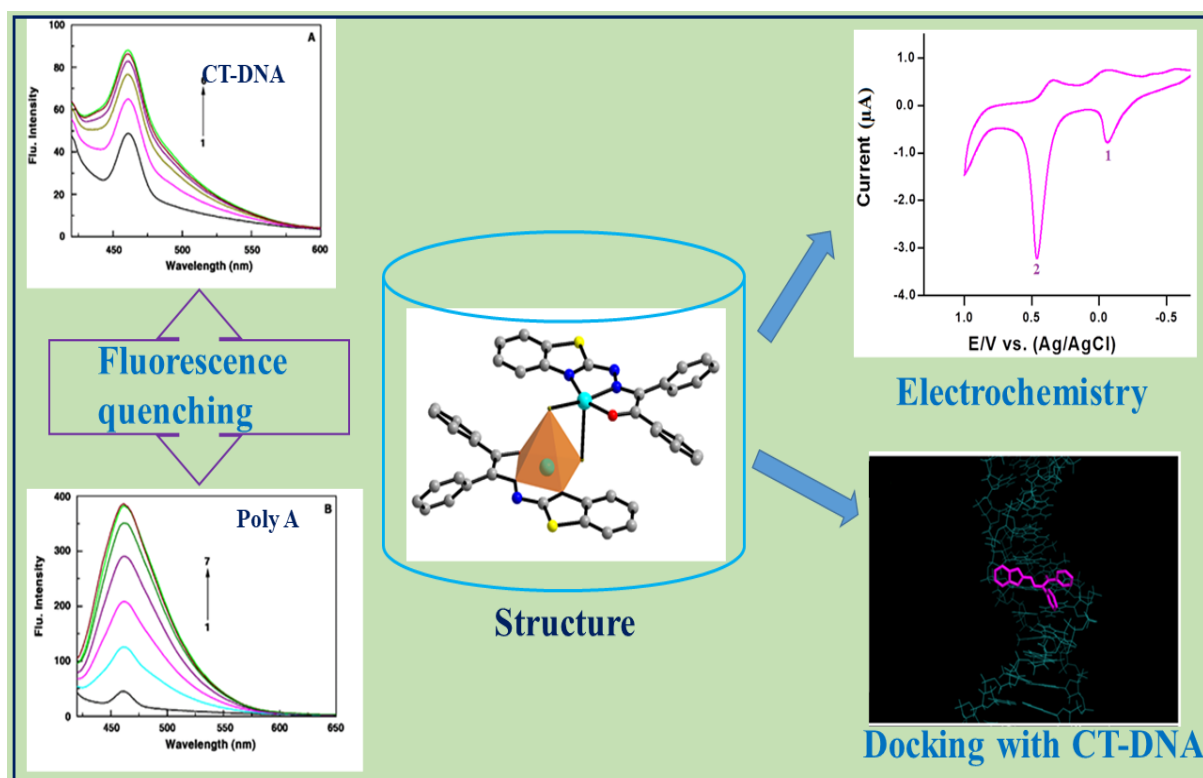


CHAPTER-II

DNA and RNA binding studies on a novel bromo-bridged dimeric copper(II) complex stabilized from a Schiff base ligand

This work has been published in
Journal of Coordination Chemistry
72 (2019) 3625–3644

Graphical Abstract



Highlights

- Synthesis, characterization and structure of a red copper(II) dimer with a rare mode of bromo bridge.
- The compound displays two step one electron copper based oxidation.
- The compound is a good binder of DNA and poly riboadenylic acid.
- Docked conformer of the compound manifests minor DNA groove binding.
- Thermodynamic parameters of the binding have been evaluated.

Key words

Schiff base; copper; structure; DNA and docking

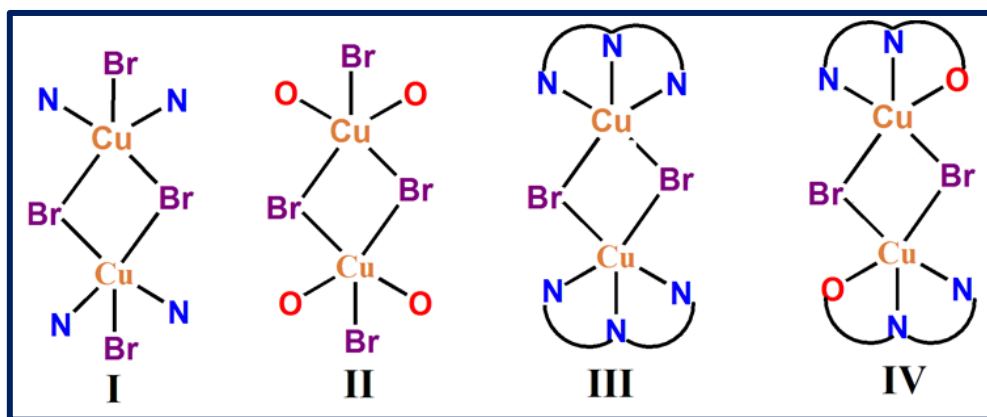
Abstract

A novel red copper(II) compound, bis(μ -bromo)bis(2-(benzothiazol-2-yl-hydrazono)-1,2-diphenyl-ethanone)-dicopper(II) (**1**), has been fostered by equimolar reaction of a Schiff base ligand, 2-(benzothiazol-2-yl-hydrazono)-1,2-diphenyl-ethanone (**LH**) with copper(II) bromide in satisfactory yield. **1** has thoroughly been characterized by C, H and N elemental analyses, FT-IR, UV-Vis (both in solid state and in solution) and room temperature magnetic susceptibility and conductivity measurements. Dimeric **1** bears symmetric rare bromo bridges in its crystal structure. **1** retains its solid-state identity even in a protic solvent like methanol. **1** in methanol displays two step one electron redox response. Theoretical calculations based on DFT were executed to probe the electronic structure of **1** and to augment its colour. DNA and RNA binding aspects of both **LH** and **1** have been explored. Thermodynamic binding parameters have been determined. **LH** is a major groove binder to DNA; while **1** manifests itself as a minor groove binder. This binding has been corroborated through molecular docking. Nucleic acid binding aspect of such type of rare bromo bridged red copper(II) dimer is unprecedented.

1. Introduction

Binuclear copper(II) complexes are of contemporary interest. The reasons are myriad. Such assemblies encompass a special echelon in copper coordination chemistry. Binuclear copper(II) compounds are the probing systems for different theories and models in magnetochemistry [1,2]. From biological viewpoint, they serve as DNA molecular probes [3]. For the development of novel anticancer drugs with less toxicity but with pronounced potentiality, copper(II) dimers are of ideal choice for their commendable anti-proliferative efficacies [4]. These assemblies even perform excellent DNA strand scission [5,6]. Accordingly, they are the optimum candidates from the viewpoint of genetic engineering. Again, such systems are important in enzymatic catalytic reaction [7,8]. A plethora of copper(II) dimers with varying bridging entities are known to exist. For ready reckoning, end-on azido [9], end-to-end azido [10], end-to-end thiocyanate [11], bis(μ -sulphato) [12], alkoxo [13,14], hydroxo [15,16] and imidazolate [17] bridged dinuclear copper(II) compounds have been reported. In the halo-bridged family, chloro bridged copper(II) dimers are comfortably common; while bromo bridged systems are really lesser known. Copper(II) dimers having bis(μ -iodo) [18,19] and bis(μ -fluoro) entities are also known [20]. Our literature search reveals that N,O donor Schiff base ligand has been employed to foster dimeric chloro bridged copper(II) compound [21]. This prompted us to generate bromo bridged system using this type of ligand. It is a point to note that symmetric bromo bridged dimeric copper(II) compound, generated from N,O donor Schiff base ligand, is unprecedented. Here, we are concerned with such type of a bromo bridged copper(II) dimer.

For bis(μ -bromo) bridged copper(II) complexes, various bridging modes have been known to exist (scheme II.1).



Scheme II.1. Different modes of bromo bridges as observed in copper(II) dimers.

Among the bridging modes, as shown in scheme II.1, I is the most common. This mode is rampant in a multitude of copper(II) complexes [22-25]. Compounds bearing other modes, II

[26] and III [27-29], have also been known along with their magnetic studies. Ours is the rare IV mode. Prior to this work, only one example of such mode is known in a copper(II) dimer. This has been stabilized from a L-leucine based ligand [30]. Halo bridged dinuclear copper(II) complexes with 'N₂Cl₃' coordination environment having pyridine based ligand show chromotropic behavior. These properties have been attributed to structural changes accentuated in different solvents [31]. Of late, monomeric copper(II) complexes, stabilized from a Schiff base ligand, have been studied to show DNA and RNA binding efficacies [32]. Again, chromone based monomeric copper(II) complexes with N,N donor ligand have been shown to manifest DNA/RNA binding interaction with remarkable cytotoxic propensities [33]. It is pertinent to note that DNA and RNA binding studies on bromo bridged copper(II) dimer evaded earlier attention. Herein, for the first time we have taken initiative to study the DNA/RNA binding interaction of a symmetric rare bromo bridged binuclear copper(II) complex. In this work, synthesis, characterization, structure, spectroscopic and redox aspects of a novel red dimeric bis(μ -bromo) bridged Cu(II) complex (**1**) having a rare 'CuN₂OBr₂' chromophore have been reported along with its DNA/RNA binding studies.

2. Experimental section

2.1. Materials

2-hydrazino benzothiazole and benzil were procured from Aldrich, USA and Loba Chemie, India respectively. Copper(II) bromide was purchased from Sigma-Aldrich. All other chemicals and solvents were of analytical reagent grade and were used as received.

2.2. Nucleic acids and buffer

Polyriboadenylic acid [Poly(A)] as potassium salt and calf thymus (CT) DNA (Type I, 42 mol% GC) were both purchased from Sigma-Aldrich Corporation (St. Louis, Mo, USA). 10 mM citrate-phosphate (CP) buffer in presence of 2% DMSO at pH 7.0 was employed for all biophysical studies. Nucleic acid solutions were also prepared in the same buffer. The buffer solution was filtered through Millipore membrane filters (0.22 μ M pore size). The Millipore membrane filters had been procured from Millipore, India Pvt. Ltd., Bangalore, India. The concentrations of the CT DNA and Poly(A) were determined spectrophotometrically by considering the molar absorption coefficient value of 13 200 M⁻¹ cm⁻¹ (base pairs) [34] and 10 000 M⁻¹ cm⁻¹ [35] respectively.

2.3. Physical measurements

To determine the melting point of **1**, an electro-thermal digital melting point apparatus was used. The value is not corrected. FT-IR spectrum (KBr disc) [ν = sharp] of **1** was recorded in

the range 400-4000 cm^{-1} on a Shimadzu FTIR 8400S spectrophotometer. To have the C, H and N micro-analytical data, a Perkin Elmer 2400 II elemental analyzer was employed. On a Shimadzu UV-160A spectrophotometer, UV-Vis spectrum of the compound was recorded in methanol. UV-Vis spectrum of **1** in solid state was run on a Perkin Elmer LAMBDA 35 UV-Vis spectrophotometer. The magnetic susceptibility of **1** was measured with a PAR 155 vibrating sample magnetometer at 298 K. For the calibration of the magnetometer, $\text{Hg}[\text{Co}(\text{SCN})_4]$ was used as the calibrant. Following Pascal's constants, the magnetic susceptibility data were corrected for requisite diamagnetism. The electrochemical redox behavior of our title compound was investigated employing a conventional three-electrode configuration on a BAS Epsilon Electrochemical workstation (Model: CV-50) in methanol at 298 K. A glassy carbon working electrode, a platinum-wire auxiliary electrode and a Ag/AgCl reference electrode completed the conventional three-electrode assembly. 0.1 M tetra-*n*-butyl ammonium perchlorate (TBAP) was used as the indifferent electrolyte. Dry and degassed nitrogen gas was purged for 10 minutes to maintain an inert atmosphere during our CV data acquisition. The cell was blanketed with pure nitrogen during scanning. The electrical conductivity was measured in methanol on a Systronics (India) direct reading conductivity meter (Model: 304) at room temperature. To calibrate the meter, 0.1 M KCl solution in water was employed.

2.4. Computational details

The GAUSSIAN-09 Revision C.01 program package was employed for all theoretical calculations [36]. The gas phase geometries of the molecules, **LH** and its bromo bridged copper(II) dimer (**1**), were optimized fully without any restrictions of symmetry in singlet ground states with the gradient-corrected DFT level coupled with the level of three parameter-fit of the exchange and correlation functional of Becke B3LYP [37] which includes the correlation functional of Lee *et al.* (LYP) [38]. The basis set LANL2DZ with effective core potential (ECP) was employed for Cu and bromine following the associated valence double zeta basis set of Hay and Wadt [39-41]. This is in combination with the 6-31+G(d) basis set selected for hydrogen, carbon, nitrogen and oxygen [42,43].

2.5. Methods for DNA and RNA binding

2.5.1. Spectrophotometric study

All the spectrophotometric studies were executed on a Jasco V 660 double beam monochromatic spectrophotometer (Jasco International Co. Ltd., Hachioji, Japan) at room temperature. The spectrophotometer was connected with a thermoelectrically controlled cell

holder with a temperature controller to keep the temperature steady during the experiment. The spectrophotometric measurements were carried out in matched quartz cuvettes of 1 cm path length (Hellma, Germany). Following our earlier protocol, we performed the experiment as described herein [27]. In each set of scanning, the self-absorption values of DNA and Poly(A) were eliminated.

The binding constants (K) for the anchoring of both ligand (**LH**) and **1** with DNA and Poly(A) were determined in the spirit of Benesi-Hildebrand (BH) equation [44]

$$A_0/\Delta A = A_0/\Delta A_{\max} + (A_0/\Delta A_{\max}) \times 1/K \times 1/L_t \quad (1)$$

Where, $\Delta A = A_0 - A$, ΔA_{\max} = maximum reduced absorbance, A_0 = maximum absorbance at λ_{\max} , A = reduced absorbance and L_t = nucleotide concentration.

2.5.2. Fluorescence spectroscopic and Ethidium Bromide displacement studies

Spectrofluorimetric studies were performed on a PTI QM-400 spectrofluorimeter. Here we have explored the binding propensities of **LH** and **1** with the nucleotides by fluorescence titrimetric methods. Three different temperatures were considered employing a temperature controller unit in fluorescence free quartz cuvettes of 1 cm path length following earlier methods [45]. The binding constants of **1** and **LH** with DNA and Poly(A) were evaluated by Benesi-Hildebrand (BH) equation. Ethidium bromide (EB) displacement assay was performed for **1** and **LH** with DNA and Poly(A) in 50 mM Tris-HCl buffer (pH = 7.0) in presence of 2% DMSO in fluorescence free quartz cuvettes of 1 cm path length at 25 °C. Initially, the fluorescence intensity of a pre-equilibrated mixture of CT DNA and Poly(A) (50 μ M) and EB (7 μ M) was recorded at 590 nm. Then **1** and **LH** were added to the earlier complex and the change in fluorescence intensity was monitored carefully [46]. IC₅₀ values for the complexes have subsequently been determined following the protocol described earlier [47]. The same experiment was repeated for **LH** following similar methodology.

2.5.3. Thermodynamic studies: temperature dependent spectrofluorimetry

Temperature dependent fluorescence titration experiments, both for **1** and **LH**, were carried out on a PTI QM-400 spectrofluorimeter at three different temperatures — 15, 25 and 35 °C. The instrument was accentuated with thermometric cell temperature programmer and temperature controller. The binding constant for each case was evaluated by the BH plot as alluded in Section 2.5.1.

From van't Hoff plot ($\ln K'$ vs $1/T$), different thermodynamic parameters were determined. The binding enthalpy change (ΔH°) has been ascertained from the slope of the plot

$$\partial \ln(K') / \partial (1/T) = -\frac{\Delta H^{\circ}}{R} \quad (2)$$

Employing the following equation, Gibbs free energy change (ΔG°) was determined at a definite temperature.

$$\Delta G^{\circ} = -RT \ln(K') \quad (3)$$

Finally, entropy change (ΔS°) during binding was ascertained following the thermodynamic Eq. 4,

$$\Delta S^{\circ} = (\Delta H^{\circ} - \Delta G^{\circ} / T) \quad (4)$$

2.5.4. Circular dichroism studies

The conformational changes of DNA and RNA due to the binding of **1** and **LH** were monitored by a JASCO J815 unit equipped with a temperature programmer (model PFD 425L/15) at 298 K.

The CD spectra of fixed concentration of DNA/RNA were first monitored and then with increasing concentration of the ligand and complex in a rectangular strain free quartz cuvette of 1 cm path length. The CD spectra were recorded in the range 400-230 nm at a scan speed of 100 nm min⁻¹ keeping a band width of 1.0 nm at a sensitivity of 100 milli degrees. During each measurement of the CD spectrum, we performed the requisite base line correction, smoothening and normalization to nucleotide concentration. The calibration of the CD unit was routinely checked employing an aqueous solution of d-10 ammonium camphor sulphonate.

2.5.5. Molecular docking study

Molecular docking study was employed to have an idea about the possible binding location of the ligand and complex with protein. The native structure of calf thymus (CT) DNA was taken from RSC Protein Data Bank having PDB ID: BDL001. Docking studies were performed with the AutoDock 4.2 software, which utilizes the Lamarckian Genetic Algorithm (LGA). For the docking of the ligand (**LH**) and complex (**1**) with CT DNA, the required file for **LH** and **1** were generated through the combined use of the Gaussian 09W and AutoDock 4.2 software packages. The optimized geometries of **LH** and **1** were obtained from DFT//B3LYP/6-31G level of theory using Gaussian 09W suite of programs and the resulting geometries were read in the Gauss view 5 software in a compatible file format. From this, the requisite file was generated in AutoDock 4.2. The grid box was set to 110, 110 and 110 Å respectively along X, Y and Z axes with a grid spacing of 0.37 Å in order to recognize the binding site of both **LH** and **1** in CT DNA. The employed AutoDocking parameters were as follows: GA population size = 150; maximum number of energy evaluations = 250 000; GA crossover mode = two

points. The lowest binding energy conformer was selected from 10 different conformations for each docking simulation and the resulting minimum energy conformation was chosen for further analyses. The PyMOL software package was used for better visualization of the docked conformations.

2.6. Syntheses

2.6.1. Preparation of ligand (**LH**)

LH was generated following a reported method that had been modified by us [21]. Herein, it was synthesized by the condensation reaction of 0.040 g (0.24 mmol) of 2-hydrazino benzothiazole and 0.052 g (0.24 mmol) of benzil in methanol. A yellow crystalline compound was obtained thereby with satisfactory yield (85%). The ligand was used for the preparation of **1**.

2.6.2. Preparation of $[Cu_2(\mu\text{-Br})_2(L)_2]$ (**1**)

0.017 g (0.05 mmol) of the ligand was dissolved in 20 mL of methanol to have a straw yellow solution. 0.015 g (0.05 mmol) of solid $CuBr_2$ was added all at a time to the ligand solution with constant stirring. Immediately the color of the solution turned pinkish red. The stirring was continued for 2 h. After stirring, the resulting reaction mixture was left for aerial evaporation. After 3 days, wine red crystalline compound was harvested. The separated compound was filtered and washed thoroughly with chilled diethyl ether. Subsequently it was dried in a vacuum desiccator over anhydrous fused $CaCl_2$.

Yield: 0.018 g (75%). m.p. >200 °C. Elemental analyses for $C_{42}H_{28}Br_2Cu_2N_6O_2S_2$ (999.476): Found (%): C, 50.40; H, 2.85; N, 8.37; Anal. Calcd. (%) for $C_{42}H_{28}Br_2Cu_2N_6O_2S_2$: C, 50.42; H, 2.82; N, 8.40. FT-IR (KBr): $\nu[cm^{-1}]$: 1559s [$\nu(C=N)$], 1537s, 1462s [$\nu(C=C)$ of phenyl ring skeletal]. UV-Vis (MeOH): λ_{max}/nm ($\epsilon/M^{-1} cm^{-1}$) 203 (26,310), 252 (12,960), 290 (7,749) and 535 (5,794). UV-Vis (Solid state): λ_{max}/nm 250, 295 and 531. Λ_M (MeOH): 22 $ohm^{-1}cm^2mol^{-1}$ (non-electrolyte). μ_{eff}/μ_B : 1.94 (at 298 K) per Cu atom.

Needle-shaped glittering single crystals, fit for X-ray structure determination, were developed by standing a dilute methanolic solution of the compound in a refrigerator for a fortnight. The compound is soluble in CH_3OH , C_2H_5OH , THF, DMSO, DMF and partly soluble in DCM. The compound is insoluble in CH_3CN , C_6H_6 , *n*-hexane and *n*-pentane.

2.7. Crystal structure determination

An appropriate shining red, needle-shaped single crystal of **1** was selected for X-ray crystallography under visualization through a microscope. Intensity data of **1** were collected on a Bruker-Kappa APEX II CCD diffractometer. The diffractometer was equipped with 1K

charge-coupled device (CCD) area detector employing graphite monochromated Mo-K α radiation ($\lambda = 0.71073$ Å) at 296(2) K. The cell parameters were determined using SMART software [48]. For the reduction and correction of the collected data, SAINTPlus was used [48]. Employing SADABS absorption corrections were done [49]. Finally, by the direct method with SHELXL-97 program package, the structure was solved [50]. The refinement by full-matrix least-squares method was executed on all F^2 data with SHELXL-97. For all non-hydrogen atoms, anisotropic refinement was performed. Subsequently the additional hydrogen atoms were positioned by riding model. The cycle of full-matrix least-squares methods for refinement was performed based on observed reflections and the variable parameters. The structural refinement data for **1** are shown in Table II.1.

Table II.1. Crystal data and structure refinement for **1**

CCDC NO.	1831458
Empirical formula	C ₄₂ H ₂₈ Br ₂ Cu ₂ N ₆ O ₂ S ₂
Formula weight	999.743
Temperature [K]	296(2)
Wavelength [Å]	0.71073
Crystal system and space group	Monoclinic and $P2_1/n$
a [Å], b [Å] and c [Å]	10.1790(5), 14.3499(7) and 13.0811(7)
α [°], β [°] and γ [°]	90, 95.615(3) and 90
Volume [Å ³]	1748.40 (2)
Z and ρ_{calcd} [mg/cm ³]	2 and 1.753
Absorption coefficient [mm ⁻¹]	3.377
F (000)	1004
Crystal size [mm]	0.7 × 0.51 × 0.24
θ range for data collection [deg]	2.112 to 26.321
Limiting indices	-12 < h < 12, -16 < k < 17, -16 < l < 14
Reflections collected/unique	9574/3841 [$R_{\text{int}} = 0.0327$]
Completeness of theta	99.9 % (25.242)
Data / restraints / parameters	3841/0/253
Goodness-of-fit on F^2	1.036

Final R indices [$I > 2\sigma(I)$]	$R_1 = 0.0340$, $wR_2 = 0.0801$
R indices (all data)	$R_1 = 0.0503$, $wR_2 = 0.0870$
Largest diff. peak and hole	0.586 and -0.479 e.Å ⁻³

Some selected bond lengths and angles of **1** are also tabulated in Table II.2.

Table II.2. Selected experimental and optimized bond distances (Å) and angles (°) for **1**

Bond/Angle	Experimental	Optimized	Bond/Angle	Experimental	Optimized
C(1)-N(1)	1.318(4)	1.3273	C(1)-N(2)	1.369(4)	1.3457
C(1)-S(1)	1.719(3)	1.7720	C(8)-N(3)	1.320(4)	1.3195
C(9)-O(1)	1.255(4)	1.2385	N(1)-Cu(1)	2.006(2)	2.0977
N(2)-N(3)	1.312(3)	1.3219	N(3)-Cu(1)	1.970(3)	2.0294
O(1)-Cu(1)	2.036(2)	2.1357	Br(1)-Cu(1)	2.381(5)	2.4526
			Cu(1)-Br(1)#1	2.772(5)	2.6847
N(3)-N(2)-C(1)	108.4(3)	111.1483	N(2)-N(3)-Cu(1)	119.2(2)	117.2636
C(8)-N(3)-Cu(1)	117.2(2)	120.1976	C(9)-O(1)-Cu(1)	112.7(19)	110.7791
C(1)-S(1)-C(2)	89.19(15)	88.6381	Cu(1)-Br(1)-Cu(1)#1	84.75(17)	79.8353
N(3)-Cu(1)-N(1)	78.99(10)	76.9908	N(3)-Cu(1)-O(1)	79.00(9)	74.6519
N(1)-Cu(1)-O(1)	156.22(10)	152.5391	N(3)-Cu(1)-Br(1)	165.22(8)	161.0387
N(1)-Cu(1)-Br(1)	105.27(7)	106.1297	O(1)-Cu(1)-Br(1)	93.98(6)	96.8459
N(3)-Cu(1)-Br(1)#1	97.70(8)	99.0054	N(1)-Cu(1)-Br(1)#1	101.94(7)	104.1297
O(1)-Cu(1)-Br(1)#1	89.82(7)	92.8459	Br(1)-Cu(1)-Br(1)#1	95.24(17)	98.1646

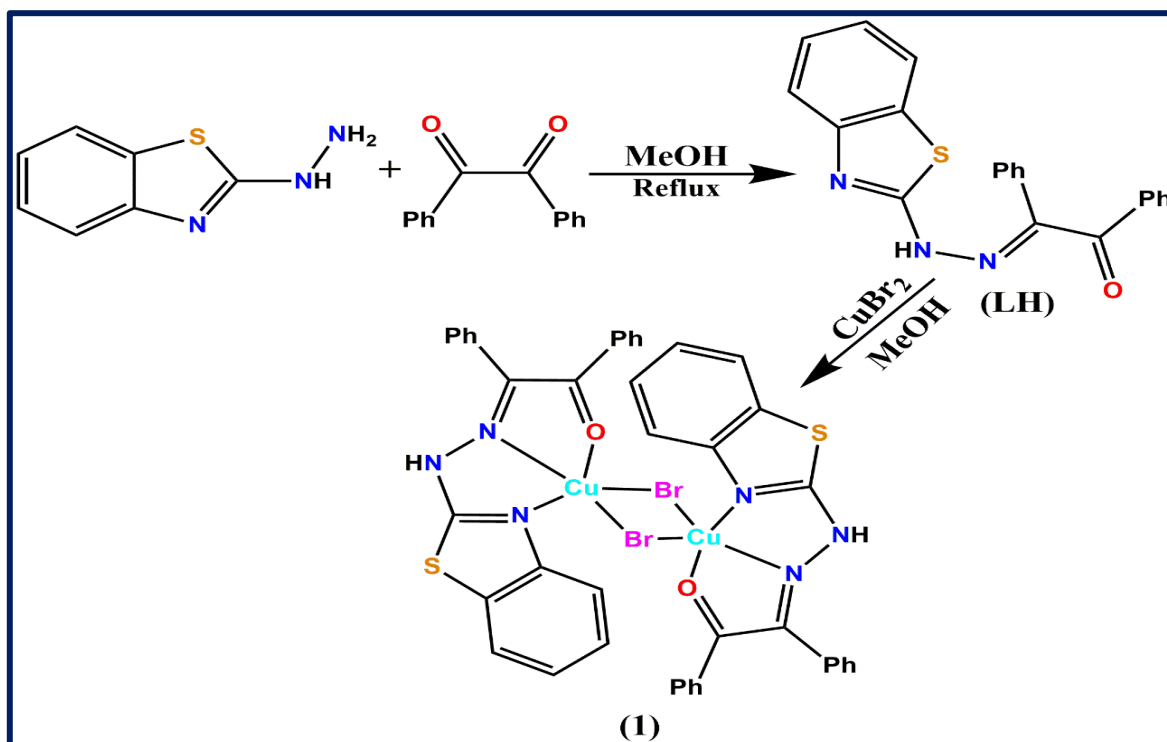
Symmetry transformations used to generate equivalent atoms: #1 -x+1, -y+1, -z+1

3. Results and discussion

3.1. Synthesis and formulation

LH has been synthesized by the 1:1 Schiff base condensation of 2-hydrazino benzothiazole and benzil in methanol. **LH** can exist in two forms — keto and enol. Thus, **LH** can undergo keto-enol tautomerism. However, during complex formation, the less stable enol form binds the metal ion [21]. Our subsequent reaction of **LH** with CuBr₂ in methanol afforded a red dimeric bis(μ -bromo) bridged Cu(II) complex in satisfactory yield.

The synthetic scheme of **LH** along with **1** has been outlined below: (scheme II.2).



Scheme II.2. Synthetic scheme of **LH** and **1**.

In the FT-IR spectrum of **LH**, three strong absorption bands have been observed (Fig. II.1). These have been reported earlier along with assignments [21]. The $\nu(\text{C}=\text{N})$ stretching frequency was observed at 1595 cm^{-1} for **1**. The aromatic $\text{C}=\text{C}$ ring vibrations were observed in the range of $1537\text{--}1462\text{ cm}^{-1}$ (Fig. II.2).

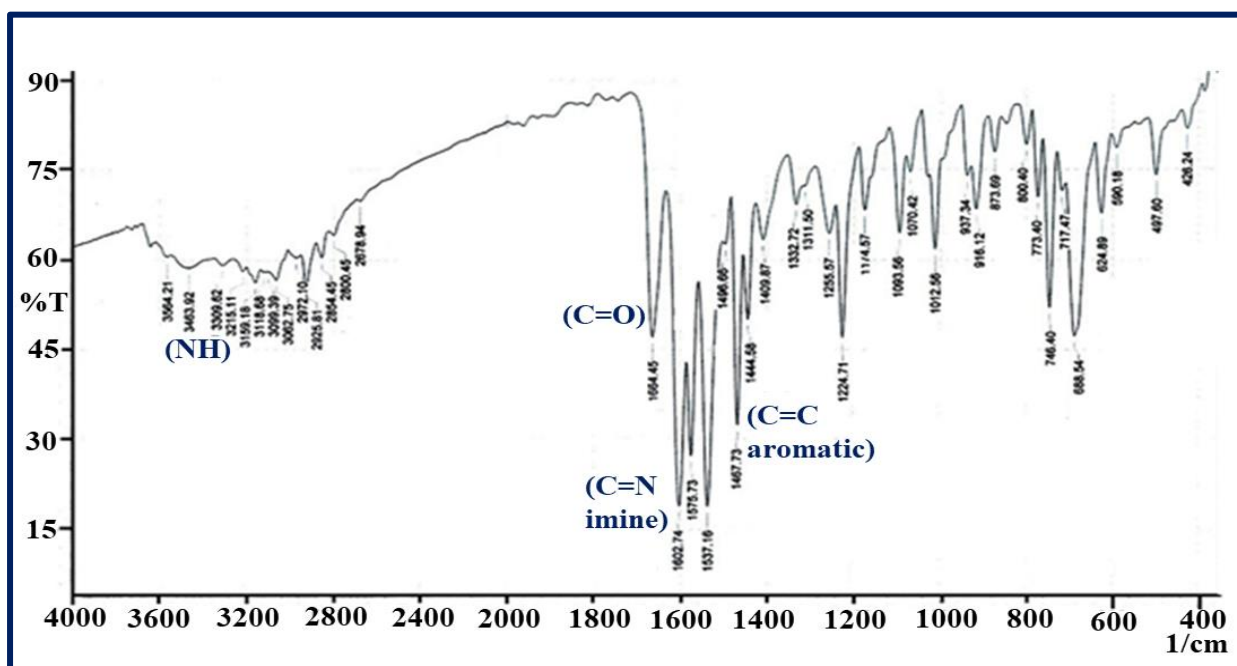


Fig. II.1. FT-IR spectrum of **LH**.

The Cu-Br stretching frequency is generally observed in the range 200-400 cm^{-1} . Red copper(II) compounds are scarce indeed. Nitrocyanin (NC), a brilliant red mononuclear copper(II) protein, is known to present in a chemoautotrophic bacterium, *Nitrosomonas europaea* [51]. This microorganism derives energy currency from the oxidation of ammonia to nitrite. In the perspective of global nitrogen cycle, this prokaryote offers ubiquitous role. One true example of the synthetic analogue of this red mononuclear copper(II) system has been published recently [52].

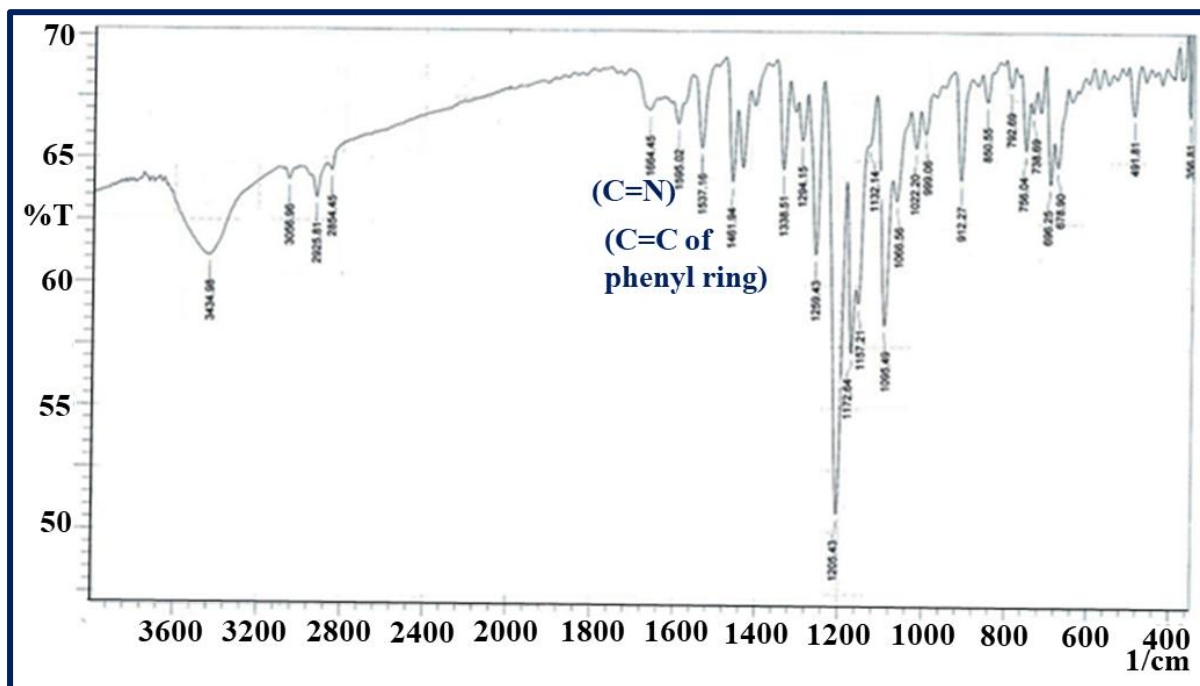


Fig. II.2. FT-IR spectrum of **1**.

To the best of our knowledge, such example is hitherto unknown for binuclear copper(II) system. **1** is red and shows an absorption band at 535 nm with ϵ value of $5794 \text{ M}^{-1} \text{ cm}^{-1}$. Accordingly, we have taken recourse to perform DFT calculations on **1** to delve into the electronic structure of it in comparison to its stabilizing ligand, **LH**.

The UV-Vis spectrum of **1** retains its identical identity, in terms of peak position, both in the solid state as well as in methanolic solution (Fig. II.3). This testifies that the compound retains its solid state dimeric identity even in a methanolic solution as well. Again, the compound is a non-electrolyte in methanol. **1** displays two well separated CV responses in solution. These data also corroborate that the dimeric core in **1** as observed in its solid state retains as such in solution phase.

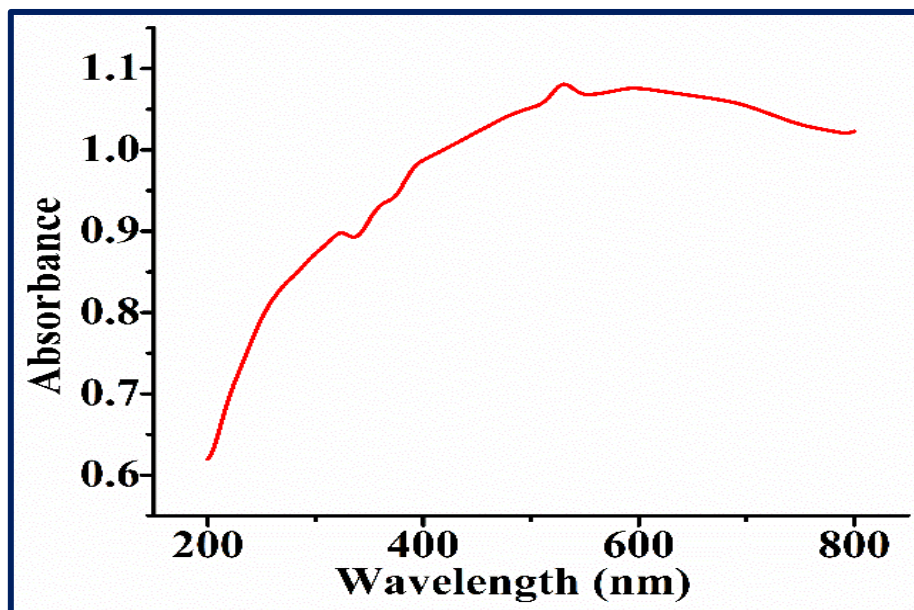


Fig. II.3. Solid state UV-Vis spectrum of **1**.

3.2. Electronic spectra of **LH** and **1**

LH shows an intra-ligand charge transfer band in methanol at 355 nm with an intensity ϵ of $19,070 \text{ M}^{-1} \text{ cm}^{-1}$ (Fig. II.4) [21].

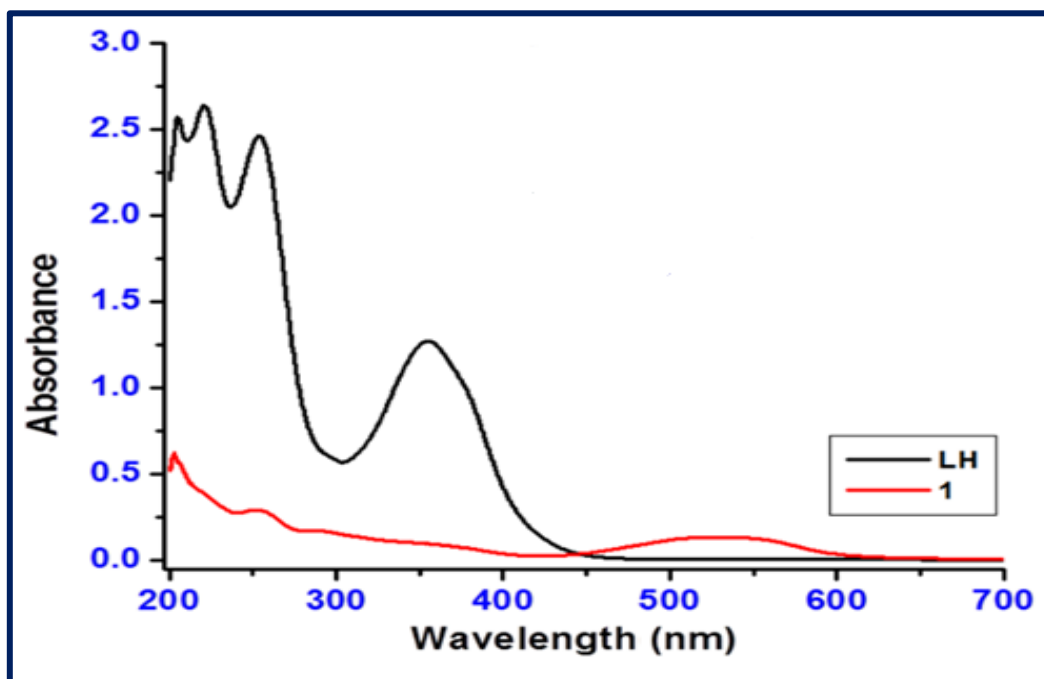


Fig. II.4. UV-Vis spectra of **LH** and **1** in methanol.

The CT band appears in **1** around 535 nm in methanol (Fig. II.4). In general, the extent of red shift depends on the charge on the central metal ion. The higher the charge on the metal ion, the lesser is its red shift. For the sake of comparison, here we have performed calculations on an analogous Zn(II) complex of **LH**. Being a d^{10} spherically symmetrical system, Zn(II) enjoys

no CFSE. Our Mulliken population analyses show that the residual charge on Zn center in the same geometry with analogous ligand environment is 1.08 and that on Cu is 0.23 in **1**. The HOMO-LUMO gap for **LH** is 2.893 eV. This gap is of 0.558 eV in **1** (Fig. II.5). Accordingly, the absorption band at 535 nm with a ϵ value of $5,794 \text{ M}^{-1} \text{ cm}^{-1}$ (Fig. II.4), brings about red colour in **1** in its methanolic solution. That way, **1** is akin to nitrocyanin.

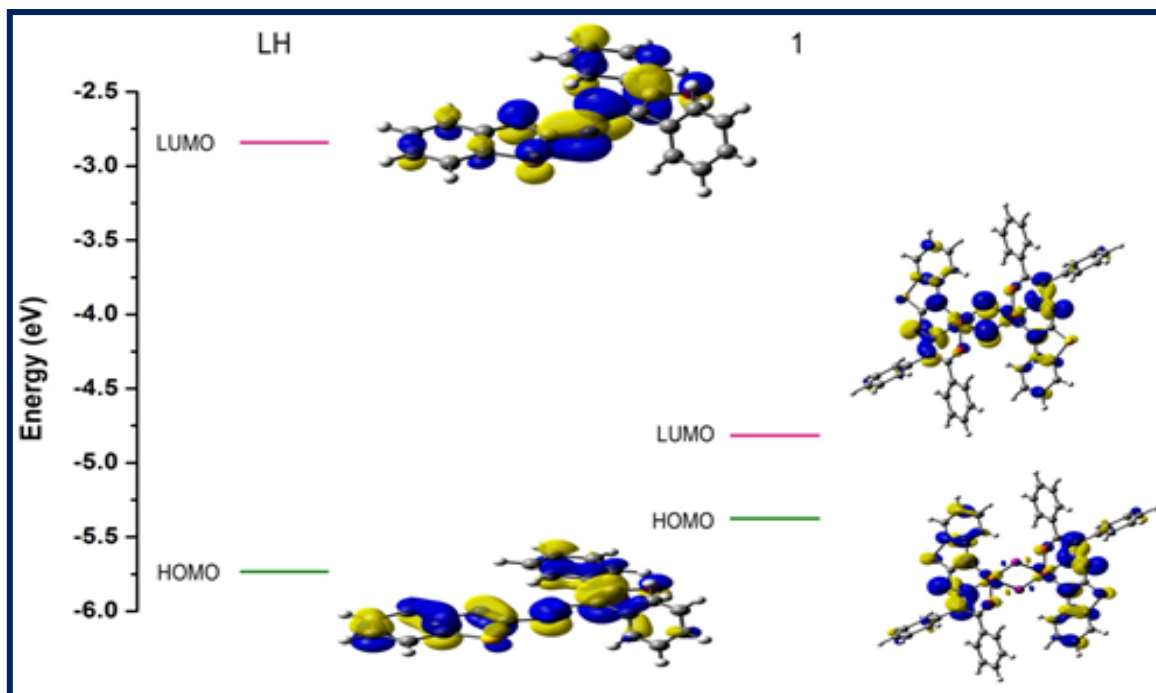


Fig. II.5. HOMO, LUMO energy and their contour diagram of orbitals of **LH** and **1**. The geometry optimized structures of **1** and zinc(II) compound at the same coordination environment are shown in Fig. II.6.

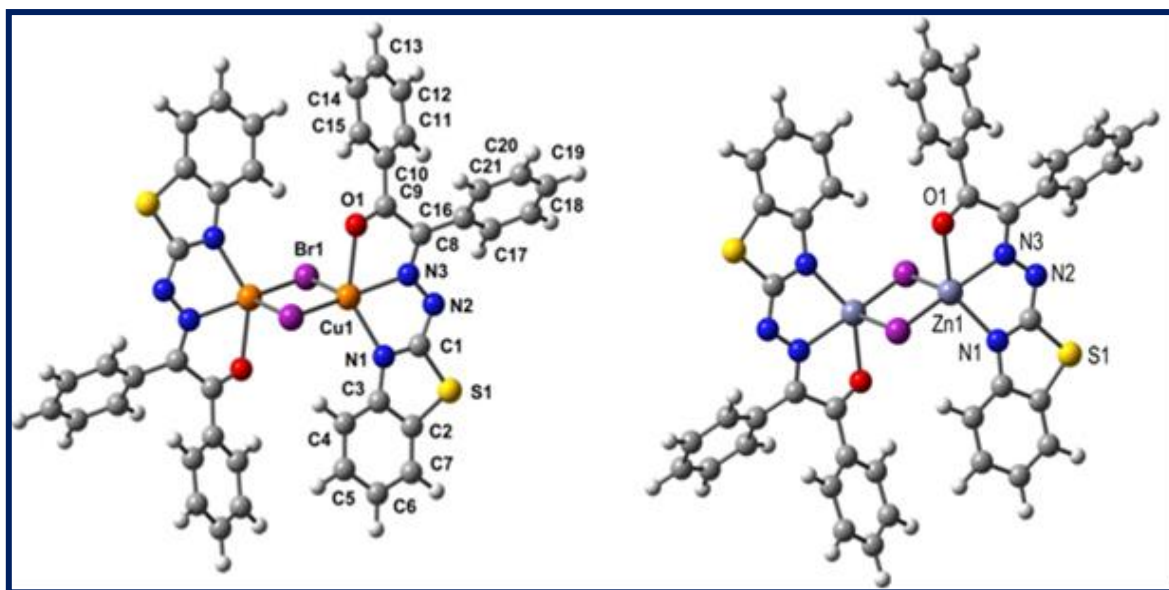


Fig. II.6. Geometry optimized structure of **1** (left) and $[\text{ZnLBr}]_2$ (right).

3.3. Molecular structure of $[Cu_2(\mu-Br)_2(L)_2]$ (**1**)

The X-ray crystal structure (Fig. II.7) of **1** has been determined. **1** is a bis(μ -bromo) bridged dimeric copper(II) complex. It is a centro symmetric copper(II) dimer with two CuLBr sub-units. Each penta-coordinated copper centre in **1** is in 'N₂OBr₂' coordination environment.

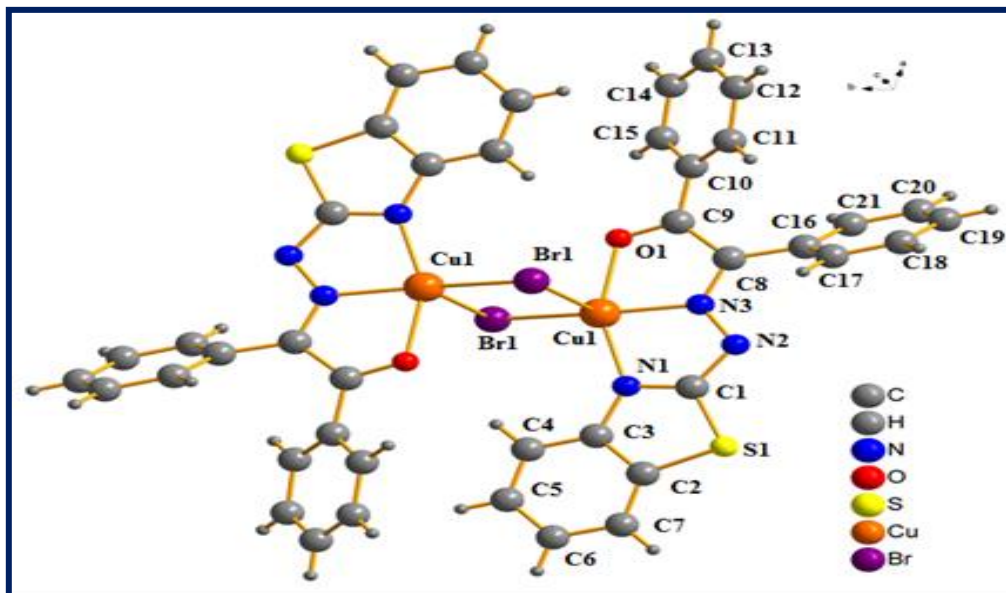


Fig. II.7. Molecular structure of **1** in ball and stick diagram.

Each copper center in **1** enjoys three donations from the approaching ligand moiety. One is oxygen (O1) from enol moiety and the two others are — one nitrogen (N1) from the benzothiazole ring and one imine nitrogen (N3) of Schiff base. This penta coordination around each copper center has been fulfilled by the additional donation of two symmetrically disposed doubly bridged bromide centers, (Br1) and (Br1#1) (Fig. II.8).

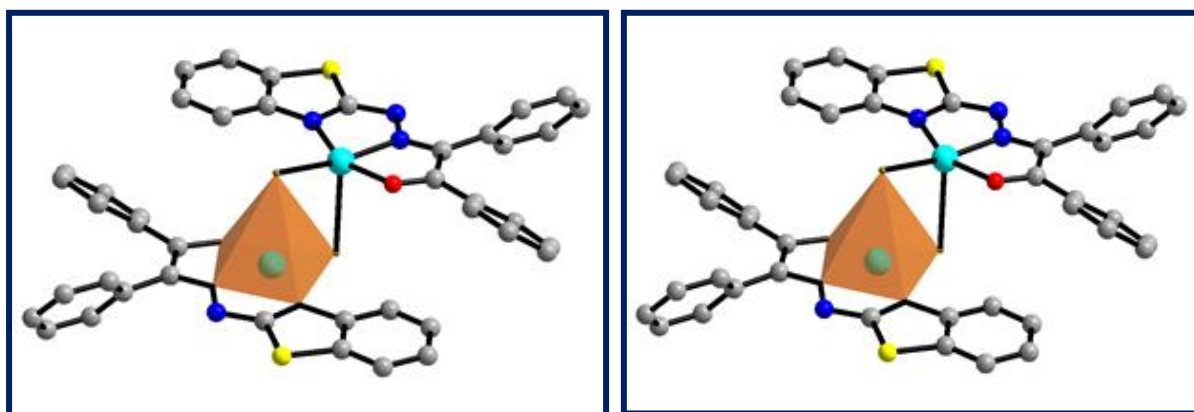


Fig. II.8. Penta coordination around each copper centre [colour code: blue = nitrogen, red = oxygen, cyan = copper]

Here, each metal center prefers to adopt the square pyramidal geometry rather than trigonal bipyramidal geometry. To augment the geometry around each copper center in **1**, we have

determined the geometry index or structural parameter(τ). In **1**, the τ_5 value comes out to be 0.15 [53-55]. Thus, the geometry around each copper center in **1** is square pyramidal with some degree of distortion in it. The structural core in **1** has also been characterized by the Cu-Cu distance of 3.486 Å and an acute angle of Cu1-Br1-Cu1#1, 84.76°. From the X-ray crystallographic data, it is revealed that the four basal bonds — Cu1-N3, Cu1-N1, Cu1-O1 and Cu1-Br1 are respectively of 1.970, 2.006, 2.036 and 2.381 Å. Collectively they form the square based basal plane around Cu1. The Cu1-Br1#1 bond is longer and Br1#1 occupies the apical site of the square based pyramid around Cu1. The Cu1-Br1#1 bond distance [2.773 Å] is longer in comparison to earlier report for analogous chloro bridged Cu(II) dimers [56,57]. For ready reckoning, Cu-Cu distance as found earlier for mode I (scheme II.1) is 3.626 Å and Cu1-Br1-Cu2 angle is of 87.00° [24]. For bridging modes II and III, the Cu-Cu distances are found respectively to be 3.714 and 3.803 Å; while Cu-Br-Cu angles respectively are of 85.51 and 92.14°. In **1**, copper to copper separation is 3.486 Å and the respective angle is of 84.76°. Thus, Cu-Cu bond distance in **1** is found to be shorter. However, the Cu1-Br1#1 bond distance [2.773 Å] is comparable with the respective bond distance value [2.706 Å] as observed previously for a bis(μ -bromo) bridged copper(II) dimer having 'N₂Br₃' donor sites [22]. In **1**, copper to copper bond distance [3.486 Å] is found to be longer when compared to analogous chloro bridged dimer with the same ligand [21].

3.4. Electrochemistry

The redox property of **1** was studied by CV in methanol (Fig. II.9) with a GC electrode at a scan rate 100 mVs⁻¹ under N₂ atmosphere. Two oxidative peaks were observed for **1** on the positive side of Ag/AgCl reference electrode. The corresponding reductive peaks were also found.

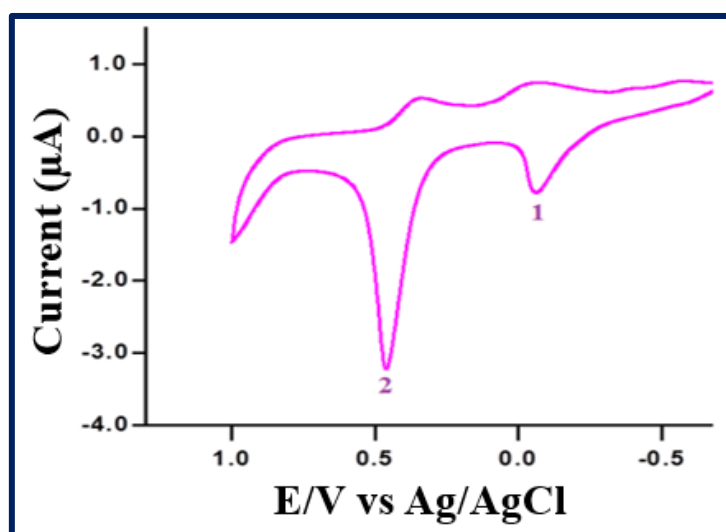


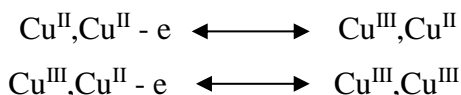
Fig. II.9. CV of **1** in methanol at a scan rate of 100 mVs⁻¹ (conc. 3.22×10^{-4} M).

The CV data for **1** is shown in Table II.3. **LH** was found to be potentially inert within our potential domain of interest. Thus, the observed redox response is truly metal centered. Comparing with the standard redox couple, Fc/Fc^+ , it can be inferred that each redox couple as observed here involves only one electron. Accordingly, the observed response can be assigned as one electron two-step process involving one electron in each step.

Couple 2 is irreversible, whereas couple 1 is almost quasi-reversible in nature. The i_{pc}/i_{pa} value for couple 2 is 6.679 in **1**. During CV experiment a mixed valence species, Cu(III)/Cu(II) , is formed in the intermediate redox step. For such type of mixed valence species, the extent of stability can be realized electrochemically by evaluating conproportionation constant (K_{con}). The conproportionation constant may be represented as —

$$K_{con} = \frac{[\text{Cu(III)Cu(II)}]^2}{[\text{Cu(III)Cu(III)}][\text{Cu(II)Cu(II)}]} = \exp\left[\frac{nF(\Delta E)}{RT}\right]$$

Where, $\Delta E = [E_{1/2}(\text{Ox2}) - E_{1/2}(\text{Ox1})]$. The greater is the stability of the mixed valence species, the higher is the value of K_{con} [58,59]. The magnitude of K_{con} was found to be 3.72×10^3 by taking ΔE for **1** as 0.378 V versus SCE (after reference conversion to SCE). The stability of the mixed valence species also depends on ligand unsaturation [60]. The redox response in **1** can be written as —



For dinuclear copper(II) system similar redox response is, however, known [21,61].

Table II.3. Cyclic voltammetric data for **1**

$E_{pa1}(i_{pa1})$	$E_{pc1}(i_{pc1})$	$E_{1/2}(1)$	$I_{pc}/I_{pa}(1)$	$E_{pa2}(i_{pa2})$	$E_{pc2}(i_{pc2})$	$E_{1/2}(2)$	$I_{pc}/I_{pa}(2)$
0.076 (7.49)	0.072 (7.55)	0.074	1.05	0.35 (5.072)	0.465 (33.88)	0.408	6.679

E_{pc1}, E_{pc2} = cathodic peak potential, V; E_{pa1}, E_{pa2} = anodic peak potential, V; i_{pc1}, i_{pc2} = cathodic peak current, μA ; i_{pa1}, i_{pa2} = anodic peak current, μA ; $E_{1/2} = 0.5(E_{pc} + E_{pa})$, V.

3.5. DNA and RNA binding aspect

3.5.1. Spectrophotometric study

Absorption spectroscopy is one of the powerful techniques commonly employed to characterize ligand and complex and their binding with nucleic acids. We have a characteristic spectrum of both **1** and **LH** in the wavelength of 300-600 nm range. **1** has a characteristic peak at 535 nm; while **LH** has a peak at 355 nm. The absorption intensity of **1** and **LH** decreases

gradually with increasing concentration of both CT DNA and Poly(A) but the magnitude of decrement is higher for ligand in comparison to the complex. Poly(A) shows much higher hypochromic effect with ligand than CT DNA (Figs. II.10 and II.11).

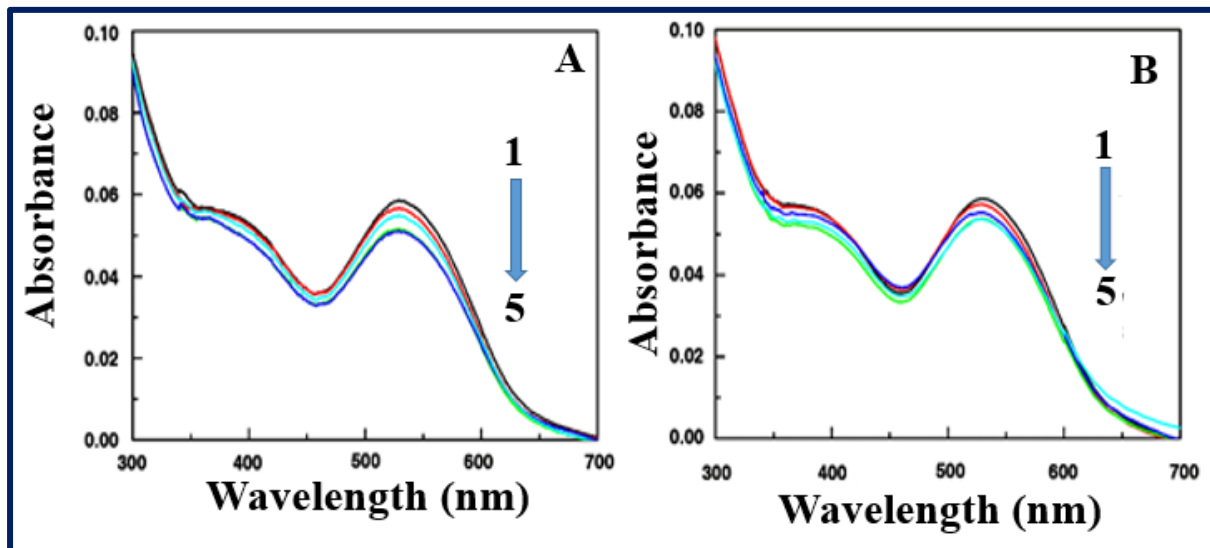


Fig. II.10. Change of absorption spectra of complex (curve 1) on increasing concentration of (A) CT DNA and (B) Poly(A) (curves 2-5).

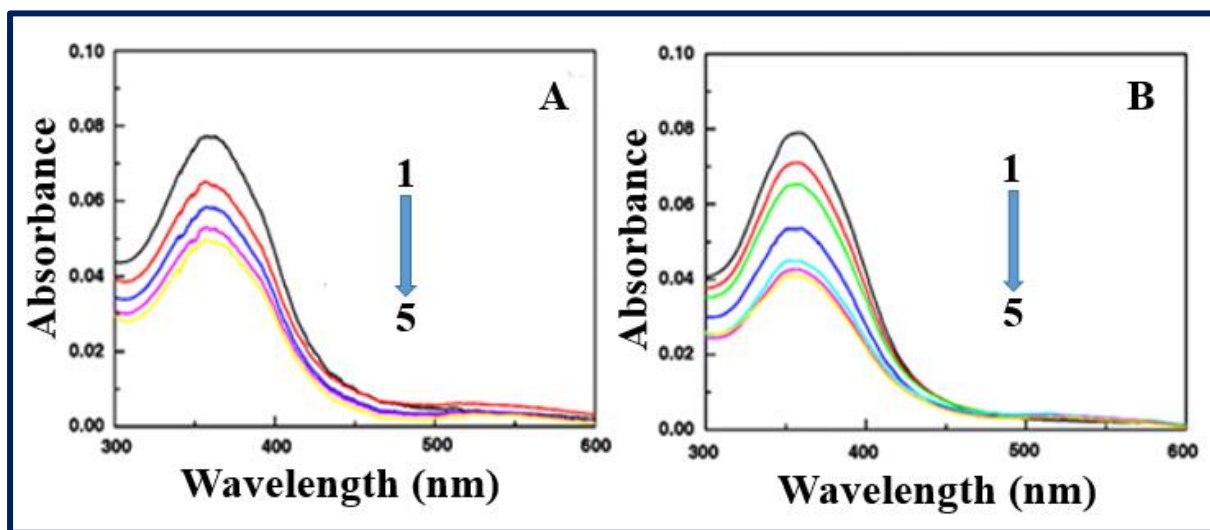


Fig. II.11. Change of absorption spectra of ligand (curve 1) on increasing concentration of (A) CT DNA and (B) Poly(A) (curves 2-5).

This hypochromic effect is indicative of strong intermolecular interaction involving effective overlap of the π electron cloud of **1** and **LH** with those base pairs of nucleic acids. The affinity constant values were calculated for each system with the B-H plots (Fig. II.12) and equation as described in section 2.5.1. The binding affinity(K) values follow the trend: Ligand-Poly(A) >

Ligand-CT DNA > Complex-Poly(A) > Complex-CT DNA. The observed values are shown in Table II.4.

Table II.4. Binding parameters as obtained from absorption spectroscopy

System	$K \times 10^{-4} \text{ M}^{-1}$
Ligand+DNA	1.013 ± 0.05
Ligand+Poly(A)	1.238 ± 0.02
Complex+DNA	0.779 ± 0.03
Complex+Poly(A)	0.912 ± 0.06

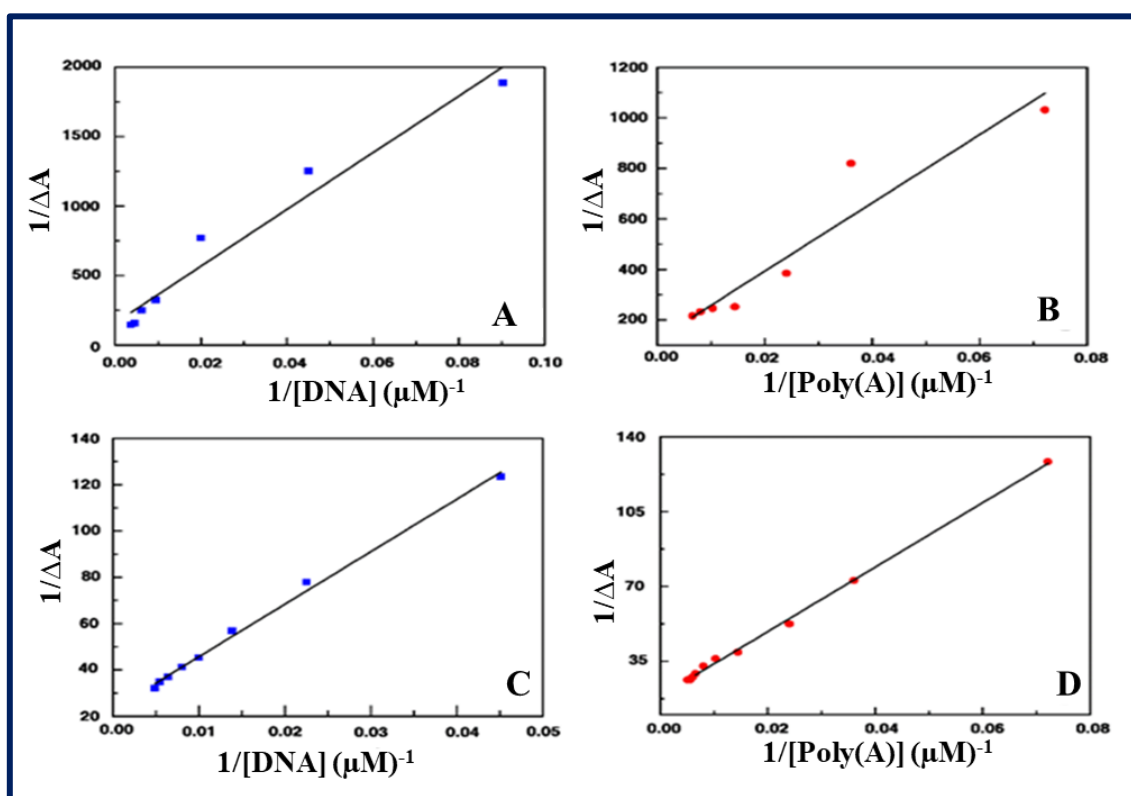


Fig. II.12. B-H plot for (A) complex with CT DNA (B) complex with Poly(A) (C) ligand with CT DNA and (D) ligand with Poly(A) as obtained from absorption titrimetric data.

3.5.2. Spectrofluorimetric study

The interaction of **1** and **LH** with CT DNA and Poly(A) was further characterized by spectrofluorimetric study. We have a characteristic fluorescence spectrum for **1** and **LH** in 400-650 nm wavelength range. Complex has a maxima value at 460 nm. The intensity was enhanced with gradual addition of both DNA and Poly(A) which indicates the strong association of nucleic acid with complex (Fig. II.13).

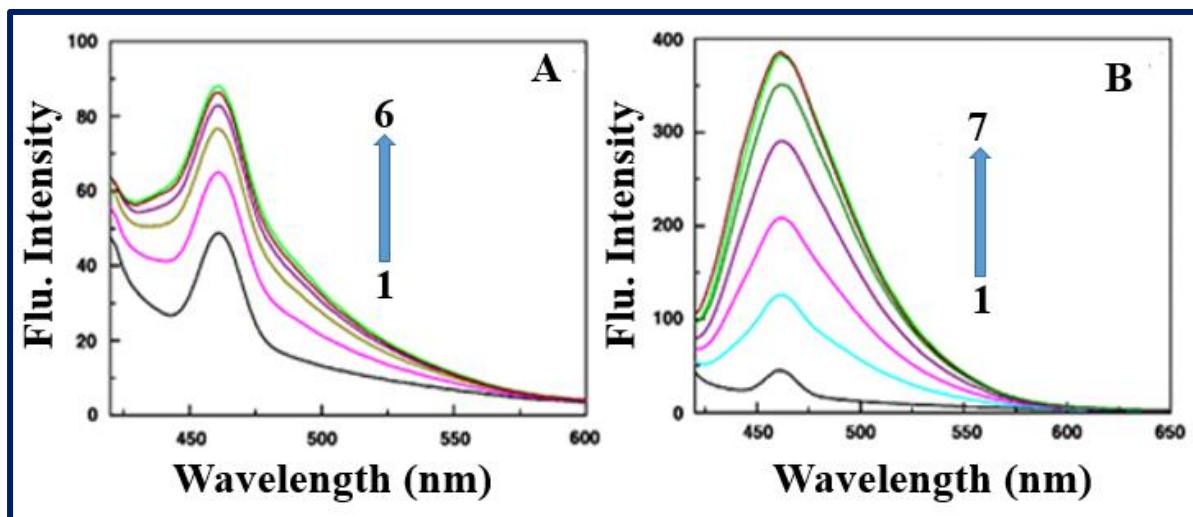


Fig. II.13. Fluorescence titration of complex (curve 1) with increasing concentration of (A) CT DNA (curves 2-6) and (B) Poly(A) (curves 2-7).

Bare **LH** displays a small peak at 403 nm; but on complexation with CT DNA, a new peak at 430 nm emerges (Fig. II.14). With Poly(A) this new peak comes out at 450 nm. This authenticates that **LH** undergoes strong binding both DNA and Poly(A) with concomitant emergence of new peaks with pronounced intensity. The observed magnitude of peak-intensity enhancement was maximum for Ligand-Poly(A) binding followed by Ligand-DNA, Complex-Poly(A) and the Complex-DNA.

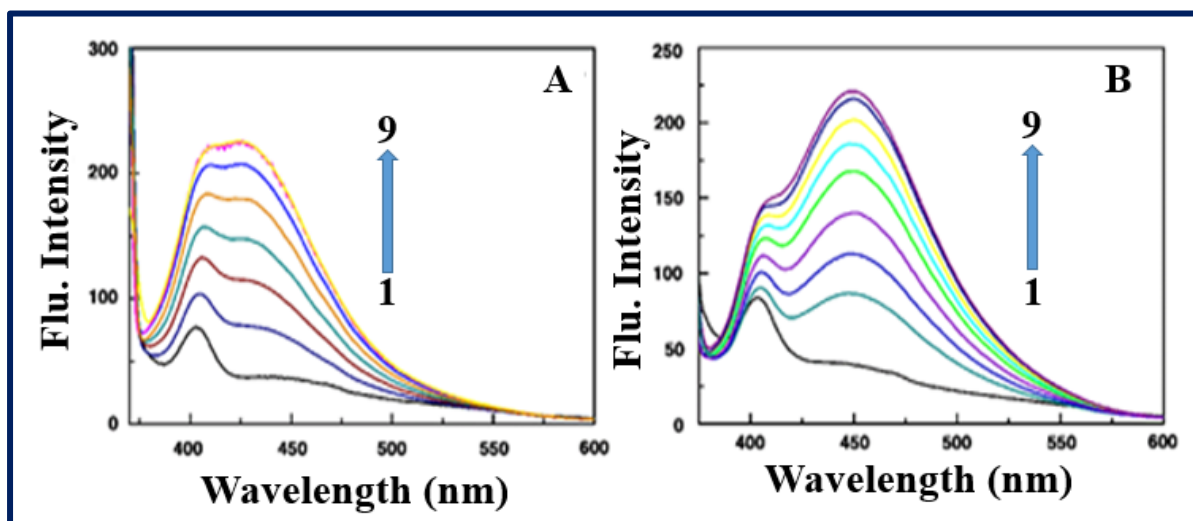


Fig. II.14. Fluorescence titration of ligand (curve 1) with increasing concentration of (A) CT DNA (curves 2-9) and (B) Poly(A) (curves 2-9).

The binding values as determined by us from UV-Vis titration also follow the same trend. The sequence runs as: Ligand-Poly(A) > Ligand-CT DNA > Complex-Poly(A) > Complex-CT

DNA. All the binding constants were calculated from the B-H plot and are listed in Table II.5 (Fig. II.15).

Table II.5. Binding parameters as observed from fluorescence spectroscopy

System	$K \times 10^{-4} \text{ M}^{-1}$
Ligand+DNA	1.010 ± 0.05
Ligand+Poly(A)	1.275 ± 0.03
Complex+DNA	0.987 ± 0.01
Complex+Poly(A)	1.064 ± 0.02

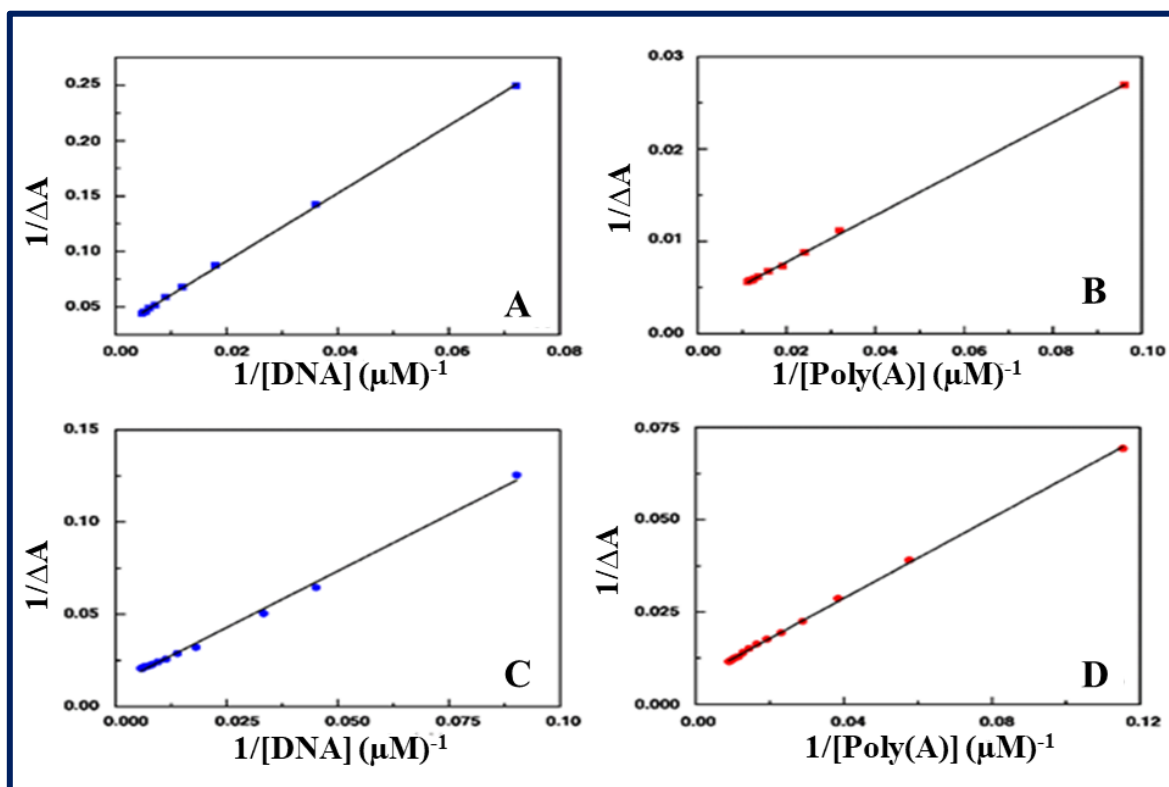


Fig. II.15. B-H plot for (A) complex with CT DNA (B) complex with Poly(A) (C) ligand with CT DNA and (D) ligand with Poly(A) as obtained from the fluorescence titrimetric data.

3.5.3. Ethidium bromide displacement assay

Ethidium bromide (EB) displacement assay was employed for the determination of mode of binding of complex and ligand with nucleic acids. EB is a well-known classical DNA intercalator commonly used as a fluorescent tag. On displacement of EB from its EB-DNA complex by a molecule, the fluorescence intensity lessens. This is suggestive of the intercalation of the molecule inside the helix. On addition of **1** to the EB-DNA and EB-Poly(A)

complex, we observed a quenching in fluorescence intensity and it reaches half of the initial value after addition of $21\mu\text{M}$ and $39\mu\text{M}$ concentration of **1** for EB-DNA and EB-Poly(A) respectively (Figs. II.16 and II.17). It indicates the intercalative nature of the binding of complex with DNA and partial intercalative binding or groove binding nature of complex with Poly(A) as the IC₅₀ value was high for Poly(A).

On gradual addition of **LH** to EB-DNA and EB-Poly(A) complex, no significant change was observed in fluorescence intensity although **LH** strongly binds both CT DNA and Poly(A) than complex. Thus, we can conclude that **LH** is unable to displace EB from its complex with DNA and Poly(A). This observation indicates possible groove binding or partial intercalative binding nature of ligand towards the nucleic acid.

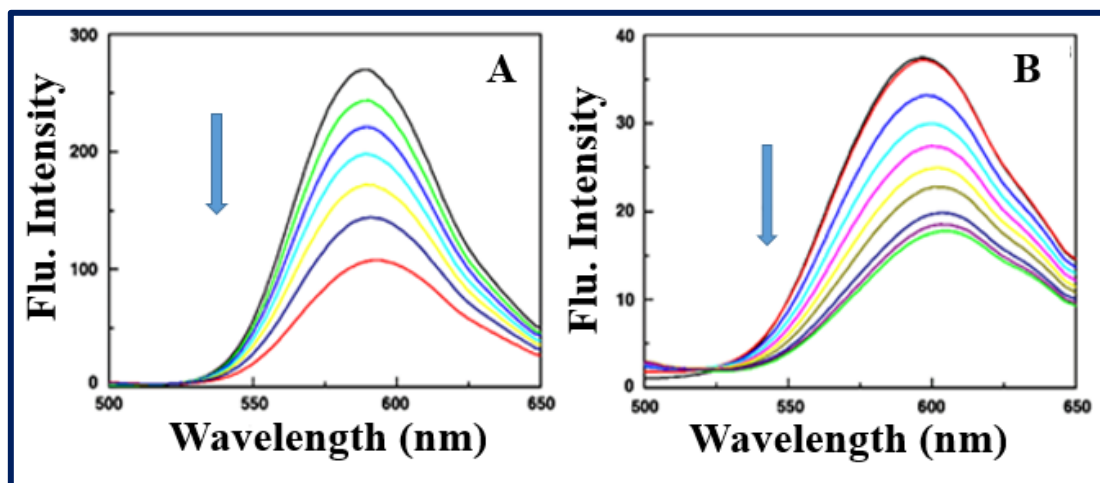


Fig. II.16. Quenching of fluorescence intensity of (A) EB-CT DNA and (B) EB-Poly(A) complex with addition of increasing concentration of **1**.

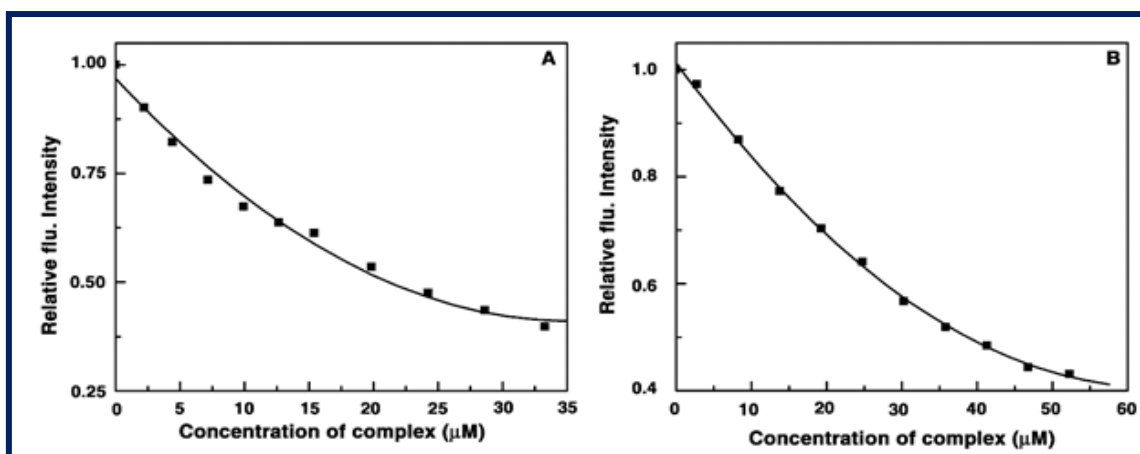


Fig. II.17. Relative fluorescence intensity decrement of (A) EB (7 μM)-CT DNA (50 μM) and (B) EB (7 μM)-Poly(A) (50 μM) (■) complex induced by the binding of complex.

3.5.4. Thermodynamics of the interaction

Temperature dependent fluorescence titration studies were carried out at three different temperatures and binding constant values were calculated as described in the material method section by B-H plots. This is also used to determine the thermodynamic parameters of the binding phenomenon of complex and ligand with DNA and Poly(A). The thermodynamic parameters were calculated by using van't Hoff plots. The values of the thermodynamic parameters for both the complex and ligand with CT DNA and Poly(A) are given in Table II.6. The van't Hoff plot for binding is presented in Fig. II.18.

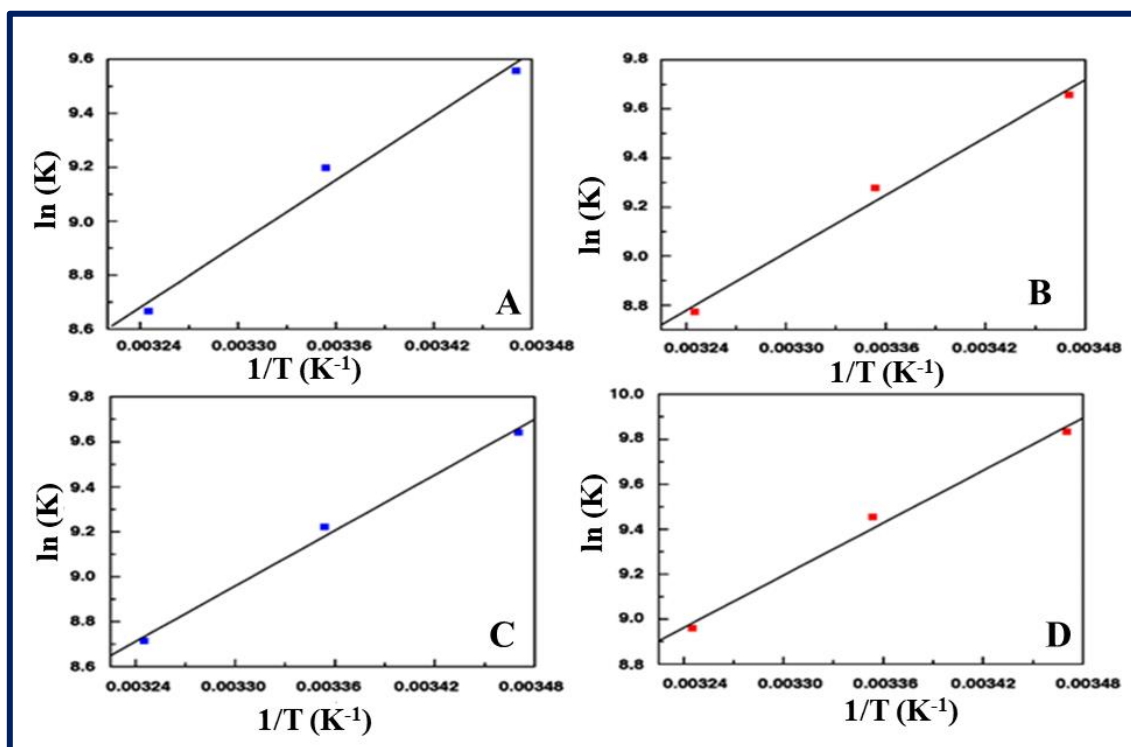


Fig. II.18. van't Hoff plot for binding of (A) complex with CT DNA, (B) complex with Poly(A), (C) ligand with CT DNA and (D) ligand with Poly(A).

Thermodynamic parameters, presented in Table II.6, show that the binding was driven by negative enthalpy and entropy change in every case.

Table II.6. Thermodynamic parameters as obtained from temperature dependent fluorescence study

System	ΔG^0 (Kcal/mol)	ΔH^0 (Kcal/mol)	$T\Delta S^0$ (Kcal/mol)
Ligand+DNA	-5.462	-8.187	-2.724
Ligand+Poly(A)	-5.600	-7.718	-2.118
Complex+DNA	-5.448	-7.829	-2.381
Complex+Poly(A)	-5.496	-7.787	-2.292

Common forms of interaction between small molecules and macromolecules are hydrogen bonding, van der Waals' force, hydrophobic and electrostatic interaction. From the underlying thermodynamic parameters, we can predict those binding modes. The values of positive enthalpy ($\Delta H > 0$) and entropy ($\Delta S > 0$) changes suggest a hydrophobic interaction; while van der Waals' force or hydrogen bond formation may occur when the enthalpy ($\Delta H < 0$) and entropy ($\Delta S < 0$) changes become negative [62] In our case, the negative enthalpy and entropy changes for the binding process indicates that the binding may occur via van der Waals' interaction or hydrogen bond formation.

3.5.5. Circular dichroism studies

Conformational changes of CT DNA and Poly(A) due to the interaction with the Cu complex and ligand were followed by circular dichroism studies. The CD spectra of DNA and Poly(A) have been shown in Fig. II.19.

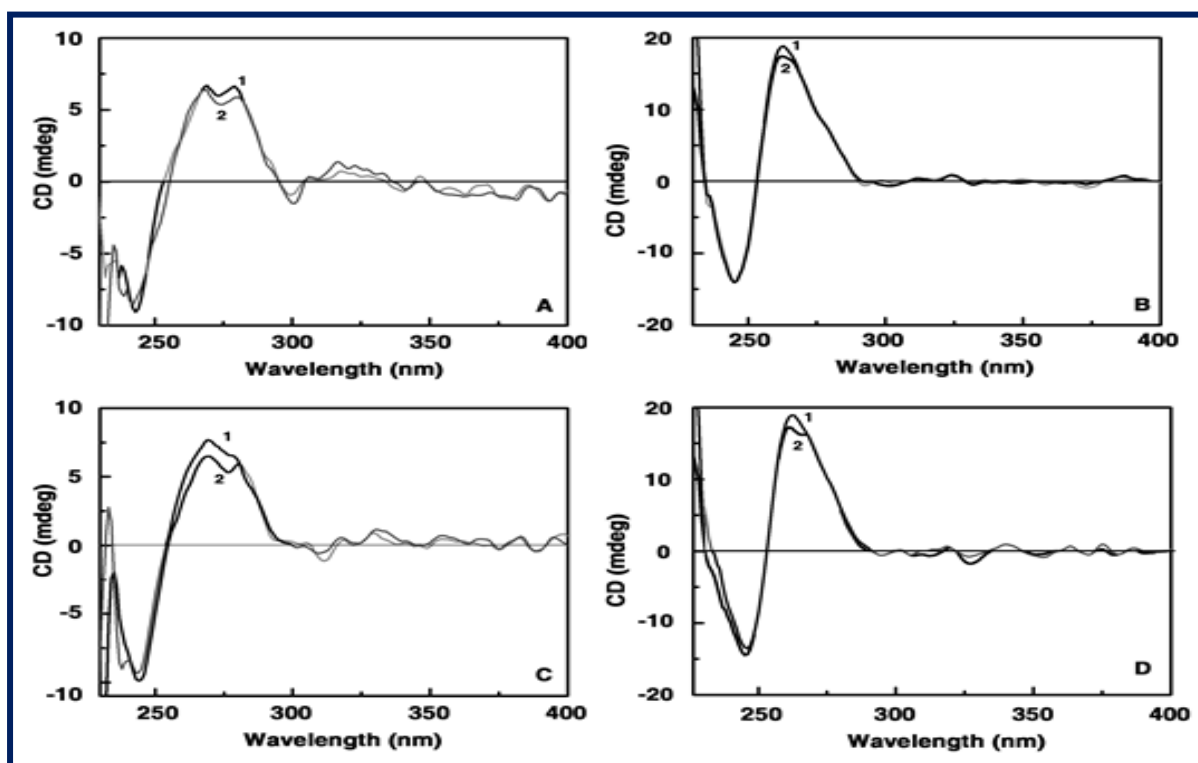


Fig. II.19. CD spectra of (A) free CT DNA (1) and CT DNA in presence of complex (2), (B) free poly(A) (1) and poly (A) in presence of complex (2), (C) free CT DNA (1) and CT DNA in presence of ligand (2) and (D) free poly(A) (1) and poly(A) in presence of ligand (2).

DNA has a characteristic positive peak at 275 nm and a negative peak at 245 nm in its CD spectrum respectively due to base stacking and polynucleotide helicity. Here we observed a distinct change in CD spectrum of CT DNA due to association with **1** and **LH** as represented in Fig. II.19 (A and C). Poly(A) shows characteristic positive and negative bands at 265 and

247 nm respectively. The spectral pattern of Poly(A) was also changed in presence of both the complex and ligand as shown in Fig. II.19 (B and D). Although the magnitude of the spectral changes of both DNA and Poly(A) were not very large but the nature of the spectral changes indicates that both the complex and ligand bind with DNA and Poly(A). **1** shows groove binding with CT-DNA as has been deciphered from our molecular docking studies. Secondary structure of DNA is perturbed markedly by the intercalative binding of DNA with small molecules [63,64]. However, groove binding imparts substantially low impact on the native CD spectra of nucleic acids. This situation has been demonstrated recently for copper(II) systems stabilized from Schiff base ligands [65]. **1**, a copper(II) dimer, generated out of a Schiff base ligand, also shows groove binding as evidenced from our CD spectra.

3.6. Molecular docking

To have an idea about the possible location of **LH** and **1** in the DNA environment, we have taken recourse to molecular modelling study. The details of the adopted method have been given in section 2.5.5. Fig. II.20 represents the docked conformation of **LH** and **1** with DNA.

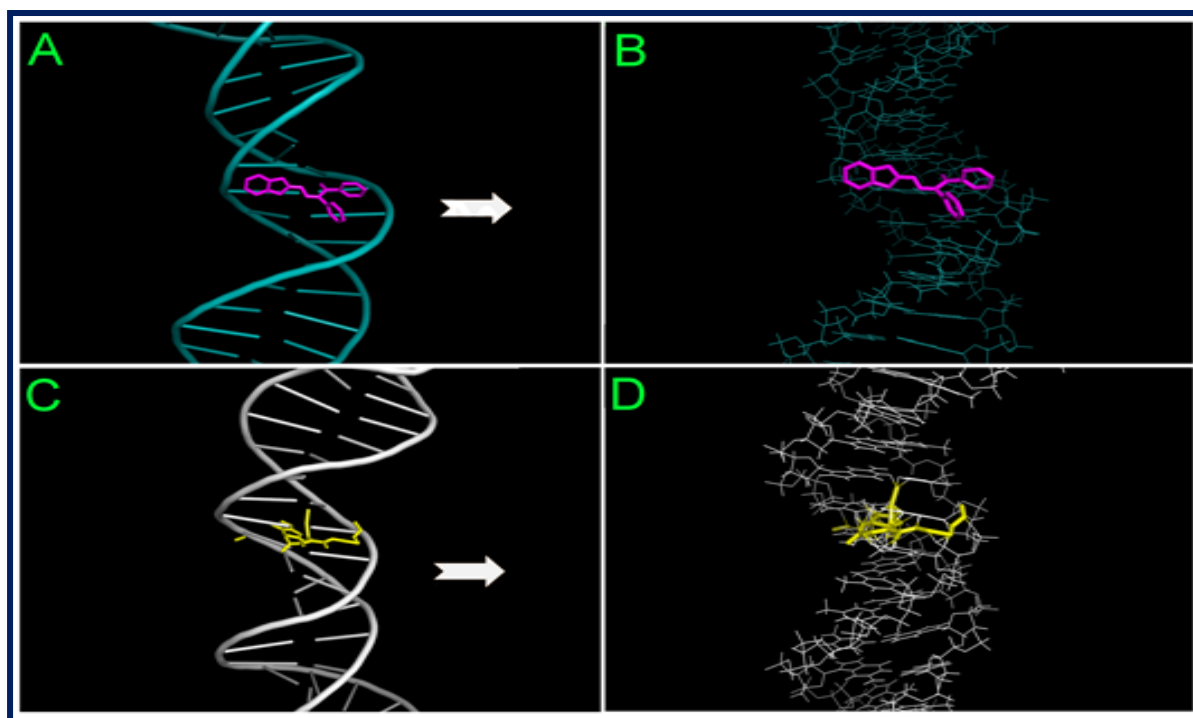


Fig. II.20. Stereo-view of the docked conformation of **LH** (A and B) and **1** (C and D) with CT DNA.

It is observed that major groove of DNA is the most suitable position for the binding in case of **LH**. However, for **1** minor groove is the most suitable position. The free energies of binding for **LH** and **1** with DNA were found to be -5.82 and -5.26 kcal mol⁻¹ respectively as revealed from molecular docking analyses. Respective binding constants as found from molecular

docking were 1.54×10^4 and $1.01 \times 10^4 \text{ M}^{-1}$ respectively for **LH** and **1**. The data as obtained from the molecular docking analyses are in good concordance with that obtained from UV-Vis and fluorescence titrimetric analyses. In both cases, the possible contribution of negative free energy change for the binding process may be attributed due to the van der Waals' stacking interactions, hydrophobic as well as weak electrostatic interactions. Hydrophobic interaction and van der Waals' contacts along with H-bonding by N or O atom may contribute to the stronger binding of ligand to CT DNA compared to **1**. The magnitude of binding constant is a useful parameter to assess the binding abilities of small molecules with nucleic acids. Here for **1**, the binding constant values with DNA and RNA are found respectively to be 0.779×10^4 and $0.912 \times 10^4 \text{ M}^{-1}$. These values are close to the respective values, 7.6×10^3 and $6.5 \times 10^3 \text{ M}^{-1}$, as have been reported for a mononuclear copper(II) complex [66]. **1** shows higher RNA binding abilities than DNA. This is indicative of the inherent hypochromic effect of RNA. Again, the binding constant value as obtained for azo bridged binuclear copper(II) complex with DNA was found to be $17.75 \times 10^4 \text{ M}^{-1}$ [67]. Most likely this higher value owes to the bridging azo moieties. The DNA binding constant values as obtained for a group of mononuclear copper(II) complexes, derived from a Schiff base ligand, were found to be 7.35×10^4 , 2.51×10^4 , 3.46×10^4 and $0.94 \times 10^4 \text{ M}^{-1}$ [68]. These values are akin to us.

4. Conclusions

Here, we have synthesized and characterized a novel centrosymmetric bis(μ -bromo) bridged red copper(II) dimer (**1**) from a Schiff base ligand, 2-(benzothiazol-2-yl-hydrazono)-1,2-diphenyl-ethanone (**LH**). The X-ray crystal structure of **1** has been determined. In CV, **1** generates a mixed valence species. The DNA and Poly(A) binding aspects of both **LH** and **1** have been demonstrated by several spectrophotometric and spectrofluorimetric methods. Docked conformer of **LH** reveals its major DNA groove binding; while **1** is a minor DNA groove binder. Comparing with the earlier report, it is evident that chloro bridged copper(II) dimer of **LH** is superior to its bromo counterpart (**1**) in terms of DNA binding. Most likely this is due to the presence of bulky bromide bridges. However, studies on DNA and RNA binding aspects of symmetric bromo bridged copper(II) dimer is hitherto unprecedented. In this perspective, the significance and prospect of the present work is apparent.

5. References

1. O. Kahn, *Acc. Chem. Res.* 33 (2000) 647-657.
2. E. Pardo, J. Faus, M. Julve, F. Lloret, M.C. Muñoz, J. Cano, X. Ottenwaelde, Y. Journaux, R. Carrasco, G. Blay, I. Fernández, R. Ruiz-García, *J. Am. Chem. Soc.* 125 (2003) 10770-10771.
3. X. Zhang, Y. Wang, Q. Zhang, Z. Yang, *Spectrochim. Acta Part A: Mol. Biomol. Spectrosc.* 77 (2010) 1-5.
4. L.M. López-Martínez, H. Santacruz-Ortega, R.E. Navarro, M. Inoue, R. Sugich-Miranda, J. Hernández-Paredes, I. Castillo, R.R. Sotelo-Mundo, *Polyhedron* 127 (2017) 438-448.
5. S. Das, C. Madhavaiah, S. Verma, P.K. Bharadwaj, *Inorg. Chim. Acta* 358 (2005) 3236-3240.
6. S. Thyagarajan, N.N. Murthy, A.A.N. Sarjeant, K.D. Karlin, S.E. Rokita, *J. Am. Chem. Soc.* 128 (2006) 7003-7008.
7. R.H. Holm, P. Kennepohl, E.I. Solomon, *Chem. Rev.* 96 (1996) 2239-2314.
8. R.L. Lieberman, A.C. Rosenzweig, *Nature* 434 (2005) 177-182.
9. S. Koner, S. Saha, T. Mallah, K.I. Okamoto, *Inorg. Chem.* 43 (2004) 840-842.
10. S. Shit, P. Talukder, J. Chakraborty, G. Pilet, M.S.E. Fallah, J. Ribas, S. Mitra, *Polyhedron* 26 (2007) 1357-1363.
11. J.A.R. Navarro, M.A. Romero, J.M. Salas, M. Quirós, E.R.T. Tiekink, *Inorg. Chem.* 36 (1997) 4988-4991.
12. H. Endres, D. Nothe, E. Rossato, W.E. Hatfield, *Inorg. Chem.* 23 (1984) 3467-3473.
13. M.G. Álvarez, G. Alzuet, J. Borrás, M. Pitié, B. Meunier, *J. Biol. Inorg. Chem.* 8 (2003) 644-652.
14. S.-C. Cheng, H.-H. Wei, *Inorg. Chim. Acta* 340 (2002) 105-113.
15. L.-P. Lu, M.-L. Zhu, P. Yang, *J. Inorg. Biochem.* 95 (2003) 31-36.
16. E. Ruiz, P. Alemany, S. Alvarez, J. Cano, *J. Am. Chem. Soc.* 119 (1997) 1297-1303.
17. D. Li, S. Li, D. Yang, J. Yu, J. Huang, Y. Li, W. Tang, *Inorg. Chem.* 42 (2003) 6071-6080.
18. T.S. Lobana, R.J. Rekha, Butcher, *Trans. Met. Chem.* 29 (2004) 291-295.
19. T.S. Lobana, S. Khanna, R.J. Butcher, A.D. Hunter, M. Zeller, *Inorg. Chem.* 46 (2007) 5826-5828.
20. F.J. Rietmeijer, R.A.G. De Graaff, J. Reedijk, *Inorg. Chem.* 23 (1984) 151-156.

21. B. Guhathakurta, P. Basu, C.S. Purohit, N. Bandyopadhyay, G.S. Kumar, S. Chowdhury, J.P. Naskar, *Polyhedron* 126 (2017) 195-204.
22. M.A. Romero, J.M. Salas, M. Quirós, M.P. Sánchez, J. Romero, D. Martín, *Inorg. Chem.* 33 (1994) 5477-5481.
23. P. Singh, D.Y. Jeter, W.E. Hatfield, D.J. Hodgson, *Inorg. Chem.* 11 (1972) 1657-1661.
24. W.E. Marsh, T.L. Bowman, W.E. Hatfield, D.J. Hodgson, *Inorg. Chim. Acta* 59 (1982) 19-24.
25. H. Endres, *Acta Cryst. B* 34 (1978) 3736-3739.
26. C.P. Landee, R.E. Greeney, *Inorg. Chem.* 25 (1986) 3771-3775.
27. S. Chakrabarty, P. Sarkhel, R.K. Poddar, *Inorg. Chem.* 61 (2008) 3260-3266.
28. R. Li, B. Moubaraki, K.S. Murray, S. Brooker, *Dalton Trans* 37 (2008) 6014-6022.
29. D.K. Towle, S.K. Hoffmann, W.E. Hatfield, P. Singh, P. Chaudhuri, K. Wieghardt, *Inorg. Chem.* 24 (1985) 4393-4397.
30. D. Žilić, B. Rakvin, D. Milić, D. Pajić, I. Đilović, M. Cametti, Z. Džolić, *Dalton Trans.* 43 (2014) 11877-11887.
31. A. Shirvan, H. Golchoubian, E. Bouwman, *J. Mol. Struct.* 1195 (2019) 769-777.
32. S. Zehra, T. Roisnel, F. Arjmand, *ACS Omega* 4 (2019) 7691-7705.
33. F. Arjmand, Z. Afsan, T. Roisnel, *RSC Adv.* 8 (2018) 37375-37390.
34. P. Basu, D. Bhowmik, G.S. Kumar, *J. Photochem. Photobiol. B: Biol.* 129 (2013) 57-68.
35. C. Ciatto, M.L. D'Amico, G. Natile, F. Secco, M. Venturini, *Biophys. J.* 77 (1999) 2717-2724.
36. M.J. Frisch, G.W. Trucks, H.B. Schlegel, G.E. Scuseria, M.A. Robb, J.R. Cheeseman, G. Scalmani, V. Barone, B. Mennucci, G. A. Petersson, H. Nakatsuji, M. Caricato, X. Li, H. P. Hratchian, A.F. Izmaylov, J. Bloino, G. Zheng, J.L. Sonnenberg, M. Hada, M. Ehara, K. Toyota, R. Fukuda, J. Hasegawa, M. Ishida, T. Nakajima, Y. Honda, O. Kitao, H. Nakai, T. Vreven, J.A. Montgomery Jr, J.E. Peralta, F. Ogliaro, M. Bearpark, J.J. Heyd, E. Brothers, K.N. Kudin, V.N. Staroverov, R. Kobayashi, J. Normand, K. Raghavachari, A. Rendell, J.C. Burant, S.S. Iyengar, J. Tomasi, M. Cossi, N. Rega, J.M. Millam, M. Klene, J.E. Knox, J.B. Cross, V. Bakken, C. Adamo, J. Jaramillo, R. Gomperts, R.E. Stratmann, O. Yazyev, A.J. Austin, R. Cammi, C. Pomelli, J.W. Ochterski, R.L. Martin, K. Morokuma, V.G. Zakrzewski, G.A. Voth, P. Salvador, J.J. Dannenberg, S. Dapprich, A. D. Daniels, "O. Farkas, J. B. Foresman, J.V. Ortiz, J. Cioslowski, D. J. Fox, *Gaussian 09, Revision C.01* Gaussian Inc., Wallingford, CT, 2009.

37. A.D. Becke, J. Chem. Phys. 98 (1993) 5648.
38. C. Lee, W. Yang, R.G. Parr, Phys. Rev. B 37 (1988) 785.
39. P.J. Hay, W.R. Wadt, J. Chem. Phys. 82 (1985) 299.
40. W.J. Hehre, R. Ditchfield, J.A. Pople, J. Chem. Phys. 56 (1972) 2257-2261.
41. J.D. Dill, J.A. Pople, J. Chem. Phys. 62 (1975) 2921-2923.
42. P.C. Hariharan, J.A. Pople, Theoret. Chim. Acta 28 (1973) 213-222.
43. T. Clark, J. Chandrasekhar, G.W. Spitznagel, P.V.R. Schleyer, J. Comp. Chem. 4 (1983) 294-301.
44. H.A. Benesi, J.H. Hildebrand, J. Am. Chem. Soc. 71 (1949) 2703-2707.
45. K. Bhadra, M. Maiti, G.S. Kumar, Biochim. Biophys. Acta 1770 (2007) 1071-1080.
46. P. Basu, G.S. Kumar, RSC Adv. 5 (2015) 29953-29964.
47. J.-H. Tan, Y.-J. Lu, Z.-S. Huang, L.-Q. Gu, J.-Y. Wu, Eur. J. Med. Chem. 42 (2007) 1169-1175.
48. Bruker, SMART (Version 5.0) and SAINT (Version 6.02). Bruker AXS Inc., Madison, Wisconsin, USA, 2000.
49. G.M. Sheldrick, SADABS, Program for Empirical Correction of Area Detector Data, University of Göttingen, Germany, 2000.
50. G.M. Sheldrick, SHELXS97 and SHELXL97, Program for Crystal Structure Refinement, University of Göttingen, Germany, 1997.
51. R.L. Lieberman, D.M. Arciero, A.B. Hooper, A.C. Rosenzweig, Biochemistry 40 (2001) 5674-5681.
52. N.K. Shee, S.G. Patra, M.G.B. Drew, D. Datta, J. Coord. Chem. 69 (2016) 3677-3691.
53. A.W. Addison, T.N. Rao, J. Reedijk, J.V. Rijn, G.C. Verschoor, Dalton Trans. (1984) 1349-1356.
54. K.P. Maresca, G.H. Bonavia, J.W. Babich, J. Zubieta, Inorg. Chim. Acta 284 (1999) 252-257.
55. M. Li, A. Ellern, J.H. Espenson, Inorg. Chem. 44 (2005) 3690-3699.
56. G.R. Desiraju, H.R. Luss, D.L. Smith, J. Am. Chem. Soc. 100 (1978) 6375-6382.
57. B. Guhathakurta, P. Basu, C.S. Purohit, N. Bandyopadhyay, G.S. Kumar, S. Chowdhury, J.P. Naskar, Polyhedron 126 (2017) 195-204.
58. S.K. Mondal, L.K. Thompson, K. Nag, J.P. Charland, E.J. Gabe, Inorg. Chem. 26 (1987) 1391-1395.
59. W. Zhang, S. Liu, C. Ma, D. Jiang, Polyhedron 17 (1998) 3835-3839.

60. J.P. Naskar, C. Biswas, B. Guhathakurta, N. Aliaga-Alcalde, L. Lu, M. Zhu, Polyhedron 30 (2011) 2310-2319.
61. J.P. Naskar, B. Guhathakurta, L. Lu, M. Zhu, Polyhedron 43 (2012) 89-96.
62. X.-B. Fu, G.-T. Weng, D.-D. Liu, X.-Y. Le, J. Photochem. Photobiol. A: Chem. 276 (2014) 83-95.
63. S.S. Jain, M. Polak, N.V. Hud, Nucleic Acids Res. 31 (2003) 4608-4615.
64. J.L. Mergny, G. Dubal-Valentin, C.H. Nguyen, L. Perrouault, B. Faucon, M. Rougee, T. Montenay-Garestier, E. Bisagni, C. Helene, Science 256 (1992) 1681-1684.
65. S. Banerjee, P. Ghorai, P. Brandao, D. Ghosh, S. Bhuiya, D. Chattopadhyay, S. Das, A. Saha, New J. Chem. 42 (2018) 246-259.
66. M. Tripathi, G.C. Giri, D. Das, R. Pande, S. Sarkar, S. Giri, G. Roymahapatra, A. Sarkar, NUCLEOSIDES, NUCLEOTIDES AND NUCLEIC ACIDS 37 (2018) 563.
67. A. Pradhan, S. Haldar, K.B. Mallik, M. Ghosh, M. Bera, N. Sepay, D. Schollmeyer, S.K. Ghatak, S. Roy, S. Saha, Inorg. Chim. Acta 484 (2019) 197-205.
68. S. Kathiresan, S. Mugesh, J. Annaraj, M. Murugan, New J. Chem. 41 (2017) 1267-1283.

CHAPTER-III

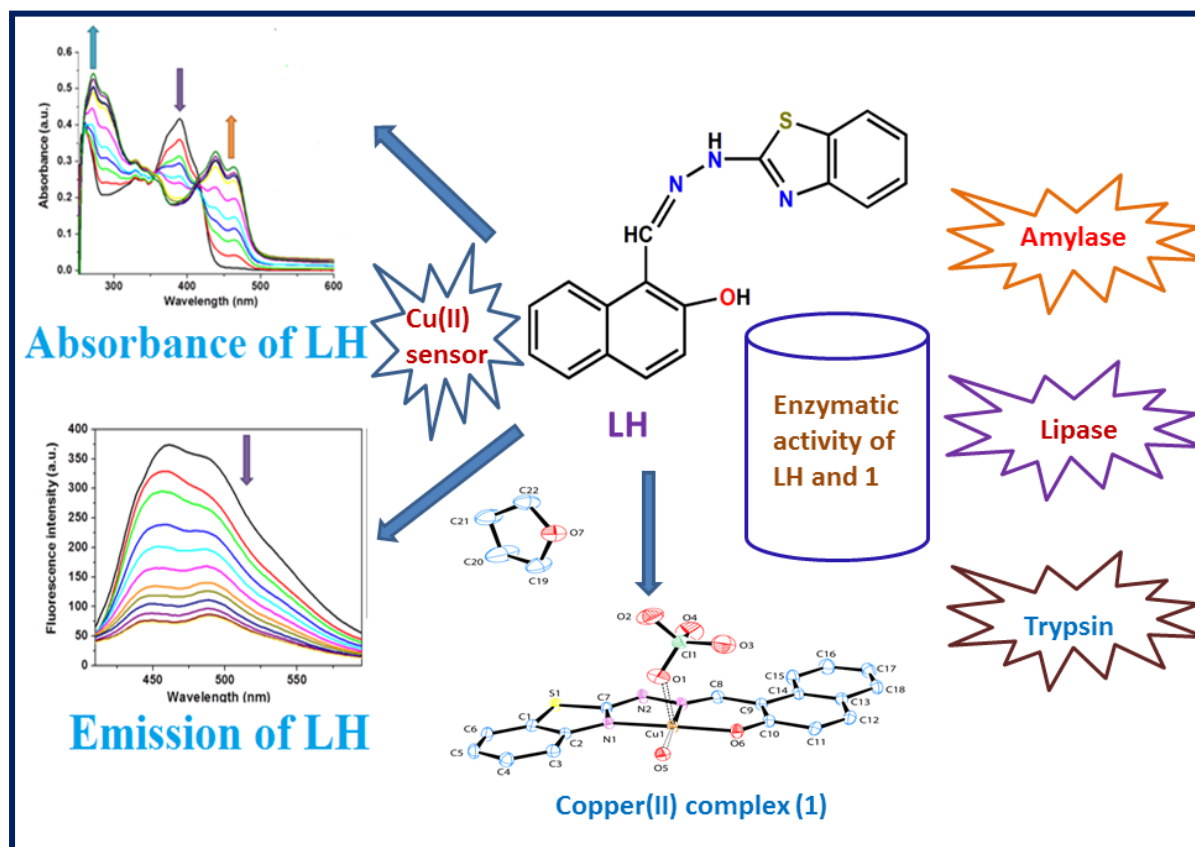
Synthesis, characterization, structure, *in vitro* enzymatic activity
and sensing aspects of a copper(II) complex stabilized from a
naphthaldehyde based Schiff base ligand

This work has been published in

Inorganica Chimica Acta

544 (2023) 121229

Graphical Abstract



Highlights

- *In vitro* enzymatic activity of **LH** and **1** on digestive enzymes like amylase, trypsin and lipase has been investigated.
- The probe **LH** is a highly sensitive and selective fluorescent chemosensor towards Cu^{2+} ion with low LOD value.
- The crystal structure of the copper(II) complex, employing the probe, has been determined.
- **LH** shows fluorescence quenching only upon addition of Cu^{2+} ion.
- Job's plot analysis indicates 1:1 complex formation of **LH** with Cu^{2+} ion.

Keywords

Schiff base; copper; structure; enzymatic activity; molecular docking and fluorescence quenching

Abstract

A mononuclear copper(II) complex, $[\text{CuL}(\text{ClO}_4)(\text{H}_2\text{O})]\cdot\text{THF}$ (**1**), from a naphthaldehyde based Schiff base probing ligand, 1-(benzothiazol-2-yl-hydrazonomethyl)-naphthalen-2-ol (**LH**), has been prepared and characterized by FT-IR, UV-Vis, EPR, CHN analysis, electrical conductivity and magnetic susceptibility measurements. The X-ray crystal structure of **1** has also been determined. *In vitro* enzymatic activity of **LH** and **1** on digestive enzymes like amylase, trypsin and lipase has been investigated. Molecular docking studies have also been performed to corroborate this bioactivity. **LH** displays quenching of fluorescence intensity only upon addition of a Cu^{2+} ion at 459 nm. Other metal ions under present study, however, offer no influence. The low limit of detection value, 0.35 μM , indicates that **LH** offers high selectivity towards Cu^{2+} . Calculations at the level of DFT were also undertaken to have an insight into the electronic environment of both **LH** and **1**.

1. Introduction

Digestive enzymes help in the digestion of food stuffs into proper simple subunits to be fit for subsequent absorption. Studies on digestive enzymes primarily help to monitor nutrient digestibility. Moreover, digestive enzymes are important from the point of view of medicinal research as well as industrial applications [1-3]. Digestive enzymes span from microscopic to macroscopic living organisms. For ready reckoning, the role of energy currency as required to assemble the different bacterial cell constituents can be mentioned. This requisite energy is derived from the breaking down of various organic substrates like starch, lipids and proteins aided by digestive enzymes [4,5]. Amylase enzymes help to hydrolyze polysaccharide starch molecules [6,7]. Lipase enzymes hydrolyze long chain triglycerides. They aid in biotechnological applications [8]. Schiff base metal complexes offer a plethora of pharmacological attributes leading to their prospective biomedical applications [9-11]. Schiff base metal complexes display anti-microbial, anti-viral, anti-fungal, anti-inflammatory and anti-cancer properties [12-14]. However, to the best of our knowledge, studies of Schiff base copper(II) complexes on digestive enzymes is rare indeed. Of late extracellular amylase production, accentuated by a tetra-dentate Schiff base copper(II) complex, has been reported [15]. Copper(II) complex from a Schiff base ligand towards trypsin inhibition is also known [16,17]. Strikingly, the lipase activity of any Schiff base copper(II) complex evaded earlier attention.

Chemosensors are compounds that selectively bind specific counterparts with noticeable changes in their optical signal, magnetic property, electrical property and many other attributes. Fluorescent chemosensors have drawn unabated contemporary interest because of their potential implications in environmental and medicinal research. Fluorescent sensors manifest ubiquitous advantages due to their convenient handling, high specificity coupled with pronounced sensitivity [18,19]. Copper, the third most abundant element in the human body after iron and zinc, plays a crucial role in diverse biological processes like oxygen transport activation, signal transduction and cellular energy generation [20-22]. However, owing to its inherent toxicity, copper is a significant pollutant to natural environment and habitat as well [23-25]. In this perspective, selective but sensitive sensing of copper is of utmost importance. Over the past several years, a good number of fluorescence based chemosensors have been reported emphasizing the detection of copper(II) ions [26-30]. The World Health Organization (WHO) recommends 10-12 mg/day of copper(II) intake for an adult human being. Again, the average concentration of blood copper under normal physiological conditions should not

exceed the limit of 100-150 $\mu\text{g/dL}$ (15.7-23.6 μM) [31,32]. Imbalance of Cu^{2+} poses serious health hazards like gastrointestinal catarrh, hypoglycemia, dyslexia Menke's and Wilson's [33-35] and Alzheimer's diseases [36]. Fluorescent molecular probes can even quantitatively sense metal ions in biological samples [37,38].

Here we wish to report the interaction of a naphthaldehyde based Schiff base probing ligand, 1-(benzothiazol-2-yl-hydrazonomethyl)-naphthalen-2-ol (**LH**) and its mononuclear copper(II) complex, $[\text{CuL}(\text{ClO}_4)(\text{H}_2\text{O})]\cdot\text{THF}$ (**1**), with amylase, trypsin and lipase. We also wish to report a simple yet convenient method for the selective detection of copper(II) ions employing **LH** with a commendable low LOD value. The binding mode of **LH** with Cu^{2+} has been confirmed by the single crystal X-ray structure of its copper(II) complex. For copper(II) systems, the crystal structures are, however, known with its sensing probes [39,40].

2. Experimental section

2.1. Materials and Measurements

All analytical reagent grade chemicals were procured from commercial suppliers and were used as received without further purification. 2-hydroxy-1-naphthaldehyde and 2-hydrazino benzothiazole were purchased from Aldrich, USA. (St. Louis, MO, USA). Melting point of the probe was determined with the aid of an electro-thermal digital melting point apparatus (SUMSIM India). C, H and N microanalytical data were acquired on a Perkin-Elmer 2400II elemental analyzer. FT-IR spectra (KBr pellets) of both **LH** and **1** were recorded on a Perkin Elmer spectrophotometer. UV-Vis absorption spectra were recorded on a Shimadzu UV-160A spectrophotometer. A Bruker DPX300 MHz spectrometer was used to run both ^1H NMR (300 MHz) and ^{13}C NMR (76 MHz) spectra (in DMSO-d_6 , reference: TMS) of **LH**. An ESI mass spectrum of **LH** was recorded on a Waters Q-TOF Micro YA263 spectrometer in acetonitrile in the positive ionization mode. Fluorescence emission spectra were run on a Perkin Elmer spectrophotometer (Model LS-55). Conductivity measurement of **1** was performed on a Systronics (India) direct reading conductivity meter (model 304) at room temperature. A PAR 155 vibrating sample magnetometer fitted with a walker scientific L75FBAL magnet, calibrated with $\text{Hg}[\text{Co}(\text{SCN})_4]$, was used to determine the magnetic susceptibility of **1** at room temperature. The magnetic susceptibility data were corrected for diamagnetism using Pascal's constants [41]. The program package GAUSSIAN-09 Revision C.01 was used for all calculations [42]. The gas phase geometries of the compounds were fully optimized with symmetry restrictions in the singlet ground state with the gradient-corrected DFT level coupled with B3LYP [43,44]. The LanL2DZ basis set was used for **LH** and **1** [45]. The HOMOs and

LUMOs of **LH** and **1** were calculated with the TD-DFT method, and the solvent effect (in methanol) was simulated using the polarizing continuum model with the integral equation formalism (C-PCM) [46,47]. Powder X-ray diffraction analysis of **1** was done on a Bruker D8 advance X-ray diffractometer with Cu K α radiation ($\lambda = 1.548 \text{ \AA}$) generated at 40 kV and 40 mA.

Caution: Perchlorate salts of metal complexes are potentially explosive [48]. It should be handled in small quantities with the utmost caution.

2.2. Synthesis

2.2.1. Synthesis of 1-(benzothiazol-2-yl-hydrazone)methyl-naphthalen-2-ol (**LH**)

The Schiff base ligand (**LH**) was synthesized following the method reported earlier [49] and modified by us. 0.016 g (0.1 mmol) of 2-hydrazinobenzothiazole and 0.017 g (0.1 mmol) of 2-hydroxy naphthaldehyde were dissolved in 40 mL of MeOH. Brown colored solution was obtained thereby. It was filtered to obtain a neat solution. The solution was heated under refluxing condition for 5 h. After refluxing, the resulting yellow solution was kept in air for slow evaporation. After 2 days, a fluffy yellow precipitate was obtained. It was filtered and thoroughly washed with diethyl ether. It was dried in a vacuum desiccator over fused CaCl₂.

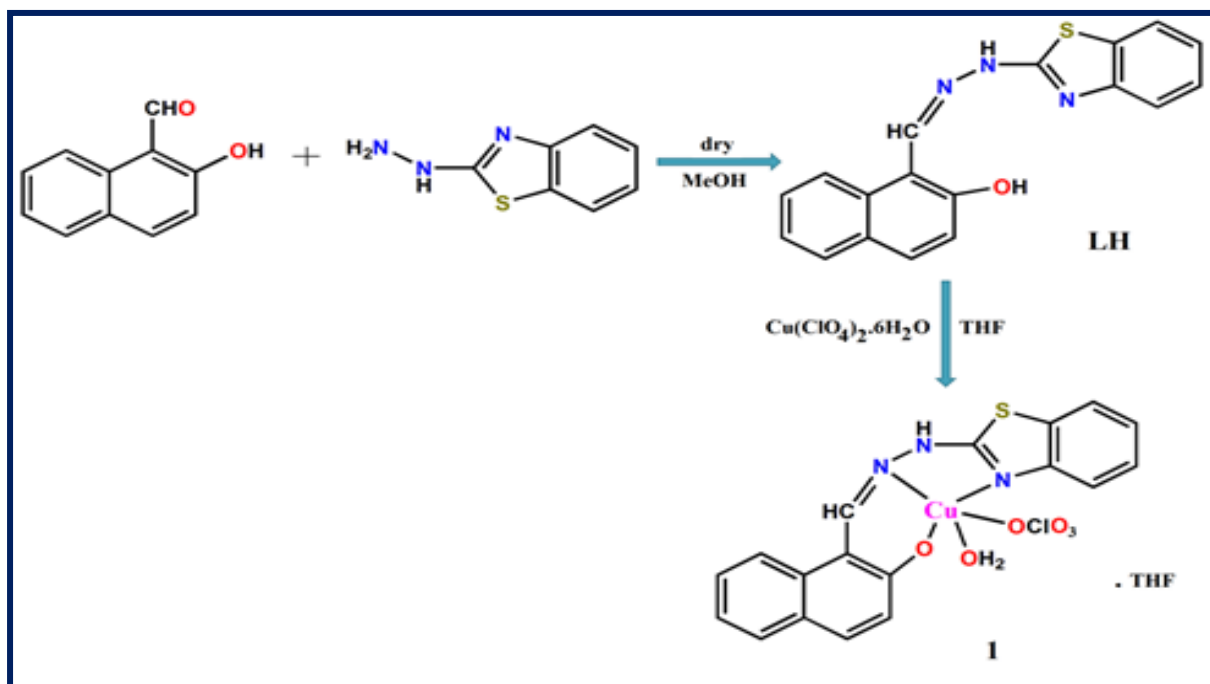
Yield: 0.028 g (89%); m.p. 243-245 °C (lit. 242-243 °C); Anal. Calcd. for C₁₈H₁₃N₃OS: C, 67.69; H, 4.11; N, 13.16. Found: C, 67.66; H, 4.13; N, 13.14; FT-IR (KBr, cm⁻¹): 3435(vb) [ν (O-H)], 2926(s) [ν (N-H)], 1624(s) [ν (C=N) of azomethine], 1587(w) [ν (C=N) of benzothiazole]; UV-Vis (THF): λ (ϵ , M⁻¹cm⁻¹) = 407 (12 000), 381 (16 000), 335 (99 000), 248 (16 000), 244 (28 599) nm; ¹H NMR (300 MHz, DMSO-d₆) δ (ppm): 9.17 (s, 1H), 8.61 (s, 1H), 7.09-7.89 (ring proton, 10H), 4.01 (s, 1H); ¹³C NMR (76 MHz, DMSO-d₆, TMS) δ [ppm]: 166.362, 157.788, 110.175 and 118.897- 132.723 (all aromatic carbons). ESI-MS (positive ion mode in CH₃CN) (m/z): 320.001 (calcd. 320.112) for [**LH**+H]⁺.

2.2.2. Synthesis of [CuL(ClO₄)(H₂O)].THF (**1**)

LH (0.012 g, 0.03 mmol) was dissolved in 10 mL THF to obtain a light yellow solution. 0.011 g (0.03 mmol) of Cu(ClO₄)₂.6H₂O, dissolved in 3 mL of THF, was added dropwise to the ligand solution with constant stirring. The resulting green solution was stirred for 15 min at room temperature. After stirring, the resulting reaction mixture was left for slow aerial evaporation. On slow evaporation, a green mass was obtained and it was thoroughly washed with diethyl ether and was vacuum dried over fused CaCl₂. The compound is soluble in DMF, THF, CH₃COCH₃, CH₃OH and CH₃CN. It is insoluble in *n*-hexane and *n*-pentane.

Yield: 0.014 g (62%); Anal. Calcd. for $C_{22}H_{22}ClCuN_3O_7S$: C, 46.23; H, 3.88; N, 7.35. Found: C, 46.19; H, 3.90; N, 7.33; FT-IR (KBr, cm^{-1}): 3470(vb) [$\nu(O-H)$], 2924(m) [$\nu(N-H)$], 1537(s) [$\nu(C=N)$ of azomethine], 1500(m) [$\nu(C=N)$ of benzothiazole]; 1121,1095,1045(s) [$\nu(ClO_4)$]; 625(s) [$\delta(ClO_4)$]; UV-Vis (MeOH): λ (ϵ , $M^{-1}cm^{-1}$) = 660 (153), 435 (15 000), 326 (16 168), 280 (22 204), 244 (28 599) nm; ESI-MS (positive ion mode in acetonitrile) (m/z): Found: 380.988 (Calc.: 381.006) for $[^{63}Cu(L) + H^+ - (THF+H_2O+ClO_4)]$ with 100% intensity and 382.990 (cal.: 383.006) for $[^{65}Cu(L) + H^+ - (THF+H_2O+ClO_4)]$ with 33% intensity; Λ_M (in MeOH): Non-electrolyte. $\mu_{eff} = 1.91$ B.M.

The synthetic scheme of **LH** and **1** is shown in [scheme III.1](#).



Scheme III.1. Synthetic route of **LH** and **1**.

2.3. X-ray data collection and structure determination

Shining needle shaped green single crystals of **1**, suitable for X-ray crystallography, were grown by direct diffusion of diethyl ether into a moderately concentrated mother liquor at room temperature. The crystals were chosen under visualization through an optical microscope. The data for **1** was collected with a Bruker-Kappa APEX II CCD diffractometer at 293(2) K. The diffractometer was equipped with a 1 K charge-coupled device area detector. Data collection had been performed using MoK α radiation (0.71073 Å). SMART software was used to determine the cell parameters [50]. The reduction and correction of the collected data was done by using the SAINTPlus software [50]. Using SADABS software, absorption corrections had been done [51]. Using the direct method with SHELXL-97 program suites, we solved the structure [52]. The refinement by full-matrix least-squares methods on all F^2 data was done by

the SHELXL-97 program. The cycle of full-matrix least square refinement had been performed on the basis of observed reflections and variable parameters. Crystal data and structure refinement parameters of the crystal have been summarized in Table III.1. The hydrogen bonding data are given in Table III.2.

Table III.1 Crystal data and structure refinement for **1**.

CCDC NO.	1900538
Empirical formula	C ₂₂ H ₂₂ N ₃ CuO ₇ SCl
Formula weight	571.47
Temperature [K]	293(2)
Wavelength [Å]	0.71073
Crystal system and Space group	Triclinic and <i>P</i> -1
a [Å], b [Å] and c [Å]	9.9550(2), 9.9777(2) and 13.7706(3)
α [°], β [°] and γ [°]	105.8940(10), 90.228(2) and 117.2250(10)
Volume [Å ³]	1156.34(4)
Z and ρ _{calcd} [mg/cm ³]	2 and 1.641
Absorption coefficient [mm ⁻¹] and F(000)	1.201 and 586
Crystal size [mm]	0.386 × 0.346 × 0.148
θ range for data collection [deg]	2.327 to 30.565
Limiting indices	-14 ≤ h ≤ 14, -14 ≤ k ≤ 14, -19 ≤ l ≤ 19
Reflections collected/unique	24728/7050 [R _{int} = 0.0396]
Completeness of theta	99.9 % (25.242)
Data / restraints / parameters	7050/0/324
Goodness-of-fit on F ²	1.040
Final R indices [I > 2σ(I)]	R ₁ = 0.0613, wR ₂ = 0.1095
R indices (all data)	R ₁ = 0.0403, wR ₂ = 0.0998
Largest diff. peak and hole	0.451 and -0.339 e.Å ⁻³

Table III.2 Hydrogen bonds (Å and °) for **1**.

D–H...A	<i>d</i> (D–H)	<i>d</i> (H...A)	<i>d</i> (D...A)	∠(D–H–A)	Symmetry
C(3)–H(3)...O(5)	0.93	2.46	3.194(3)	135.6	
N(2)–H(2)...O(7)	0.86	1.92	2.692(2)	148.4	x,y-1,z
O(5)–H(51)...O(3)	0.75(3)	2.06(4)	2.787(3)	166(4)	-x+2,-y+1,-z+1
O(5)–H(51)...Cl(1)	0.75(3)	2.99(3)	3.6579(19)	151(3)	-x+2,-y+1,-z+1
O(5)–H(52)...O(6)	0.81(4)	1.93(4)	2.705(2)	160(3)	-x+2,-y+1,-z+1

2.4. Trypsin Assay

Trypsin inhibition studies were carried out following the previously described assay [53] with slight modification. The experiment was performed for **LH** and **1** at varying concentrations. Trypsin stock solution (1mg per mL) was prepared in 0.1M phosphate buffer (pH 7.4). 150 enzyme units were incubated with 200 µL samples for half an hour and the 20 µL substrate (Bz-D, L-Arg-βNA) was added. The reaction was stopped by adding butanol and was read spectrophotometrically at 520 nm. The experiments were performed in triplicate and the % activity was determined from the average value. Curcumin was taken as a control at its respective concentration.

2.5. Amylase Assay

Amylase studies were performed as had been described earlier [53] using the DNS method. 10 mg/mL amylase stock solution was prepared in 0.1 M phosphate buffer at pH 7. 200 µL of samples at varying concentrations were incubated with 13 enzyme units for half an h. 1mL of 0.2% starch solution was added as substrate and the enzyme inhibition was estimated by adding 3,5-dinitrosalicylic acid (DNS). The reaction mixture was heated for 10 min after adding DNS and the absorbance was noted after dilution at 540 nm taking curcumin as a control for the synthesized compounds.

2.6. Lipase Assay

Lipase studies were performed colorimetrically using olive oil as substrate. 200 µL of samples were incubated with 1.65 mL of lipase solution (prepared 2 mg per mL in 0.2 M Tris buffer of pH 7.7). After 1 h, 1mL olive oil substrate was added to the reaction mixture and was kept for 24 h. The reaction was stopped after 24 h by adding 6 mL ethanol and was then titrated with 50 mM NaOH solution using phenolphthalein indicator. Orlistat, a known lipase inhibitor, was taken as a control.

% Inhibition was calculated using the following formula:

$$\% \text{ Inhibition} = [(A_C - A_S) / A_C] \times 100$$

where, A_C and A_S represent absorbance of control and sample respectively.

2.7. Molecular Docking studies

All the docking experiments were performed using iGEMDOCK that requires ligand and enzyme active sites. The structures of trypsin, amylase and lipase were retrieved from the Protein Data Bank (<http://www.rcsb.org/>) as Trypsin (1avw) [54], Amylase (1dhk) [55] and Lipase (1lbs) [56]. The structures of **LH** and **1** were drawn in Chem 3D and were saved after minimizing the energy as pdb file. After loading the prepared ligand and the binding site, slow docking parameters were set as: screening population size = 300, generations = 80, number of solutions = 10, radius = 8 Å. Finally, the output files obtained thereby as best pose were visualized by using DS visualizer and further the interactions with the enzymes were computed.

2.8. Sensing experiments

In DMSO solvent, the sensing study on **LH** was carried out with different metal ions (Al^{3+} , Na^+ , K^+ , Mg^{2+} , Ca^{2+} , Pb^{2+} , Hg^{2+} , Zn^{2+} , Cd^{2+} , Cr^{3+} , Mn^{2+} , Fe^{2+} , Fe^{3+} , Co^{2+} , Ni^{2+} and Cu^{2+}). For studies of absorption and emission titration experiments, **LH** and metal ions had been added in such a manner that the final concentration was consistently at 55 μM .

3. Results and discussion

3.1 Synthesis and general characterization

LH, 1-(benzothiazol-2-yl-hydrazonomethyl)-naphthalen-2-ol, was synthesized by an equimolar Schiff base condensation of 2-hydroxy-1-naphthaldehyde with 2-hydrazino benzothiazole in methanol. **LH** was characterized by ^1H and ^{13}C NMR, FT-IR and ESI mass spectroscopy. Our subsequent 1:1 stoichiometric reaction of **LH** and $\text{Cu}(\text{ClO}_4)_2 \cdot 6\text{H}_2\text{O}$ in THF enabled us to afford **1**. The mass spectra of **LH** and **1** are shown in Figs. III.1 and III.2, respectively.

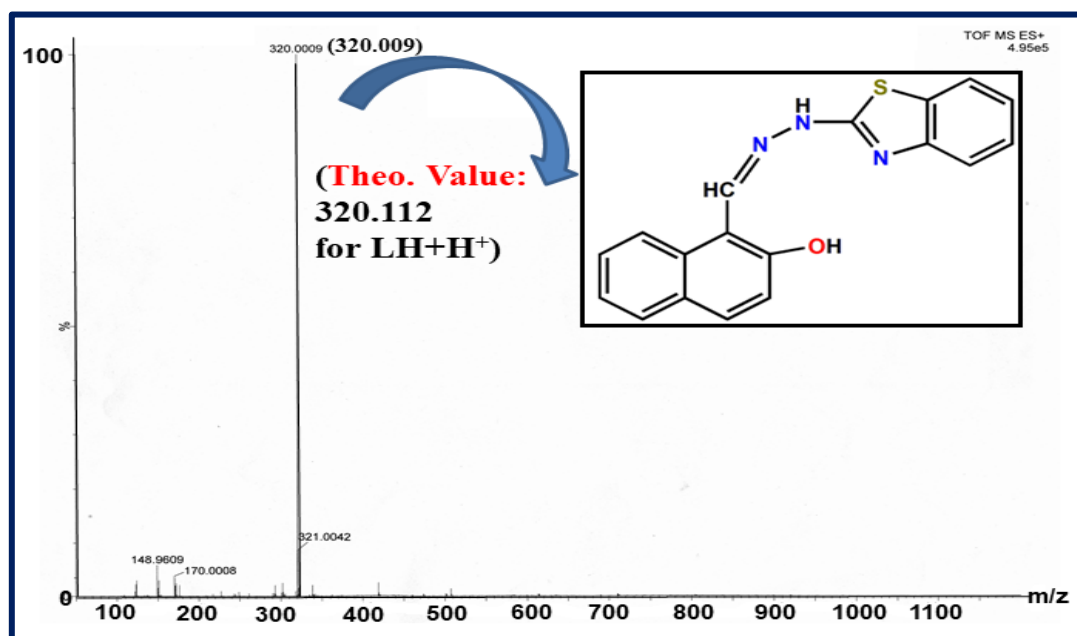


Fig. III.1. ESI-MS of **LH** in acetonitrile.

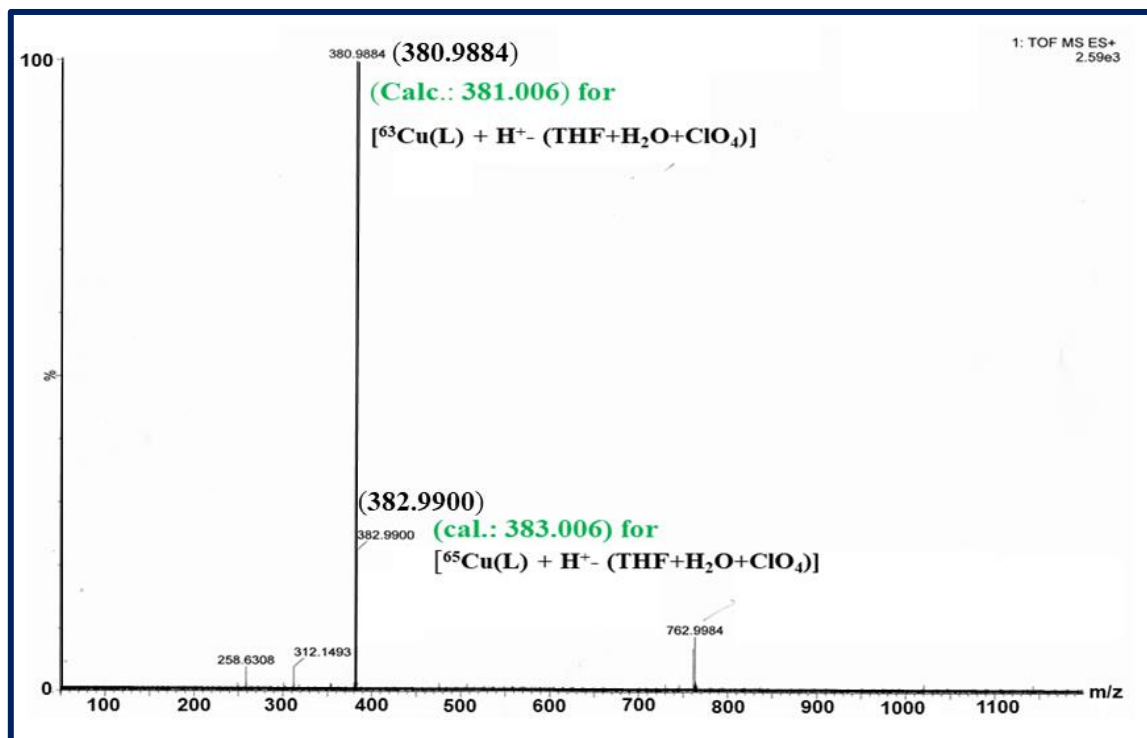


Fig. III.2. ESI-MS of **1** in acetonitrile.

The ^1H and ^{13}C NMR spectra of both **LH** and **1** are shown in Fig. III.3 and Fig. III.4, respectively.

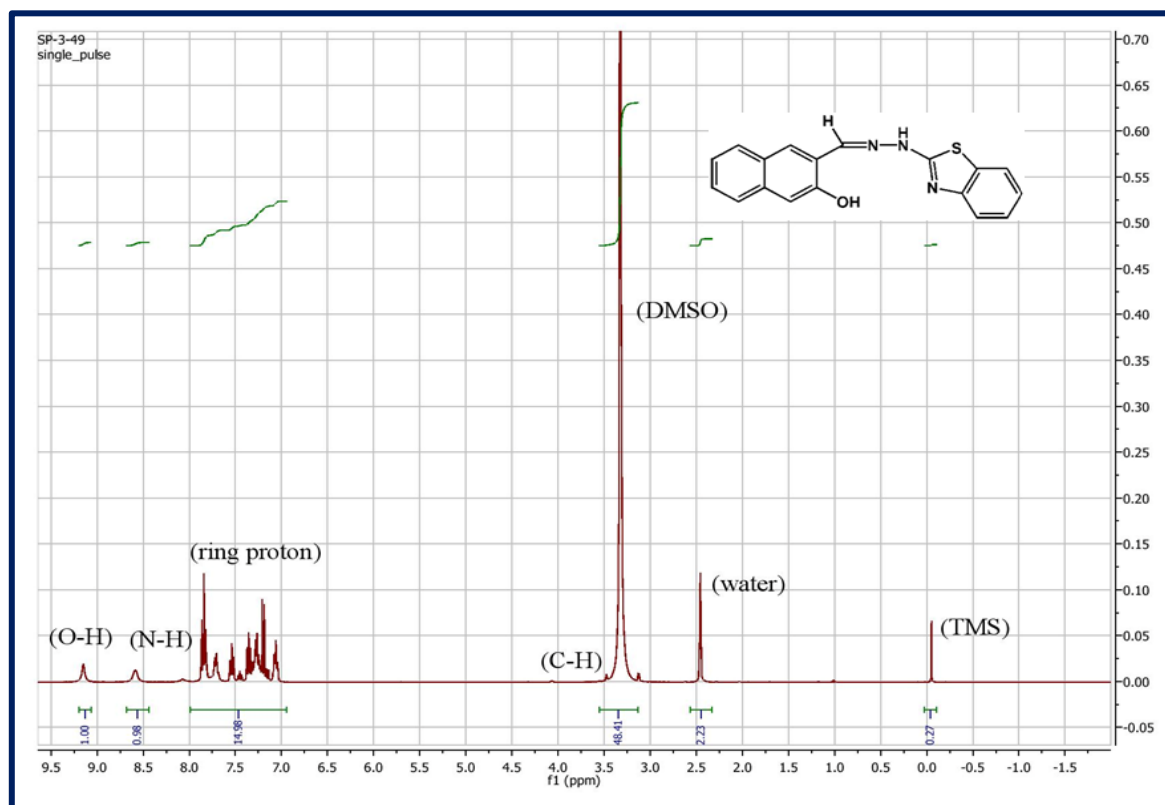


Fig. III.3. ^1H NMR spectrum of **LH** in DMSO-d_6 .

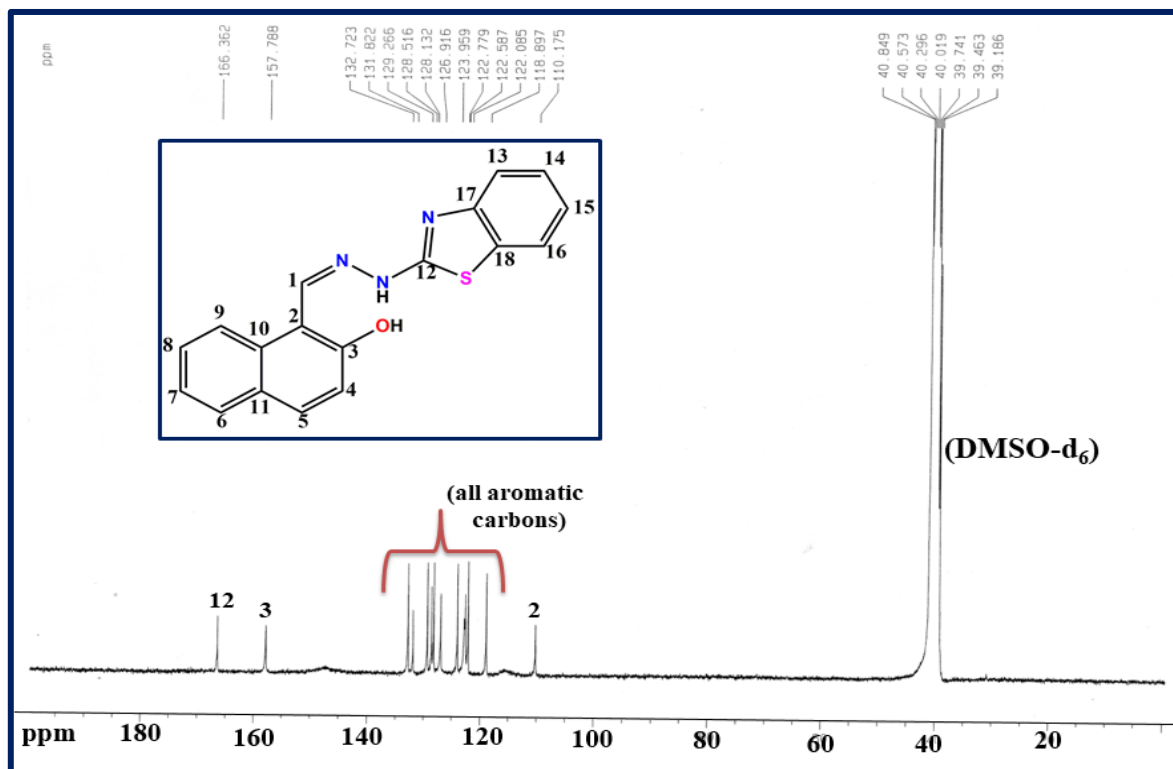


Fig. III.4. ^{13}C NMR spectrum of LH in DMSO-d_6 .

Free ligand exhibits FT-IR stretching vibrations at 3435(vb) [$\nu(\text{O-H})$], 2926(s) [$\nu(\text{N-H})$], 1624(s) [$\nu(\text{C=N})$ of azomethine] and 1587(w) cm^{-1} [$\nu(\text{C=N})$ of benzothiazole] (Fig. III.5).

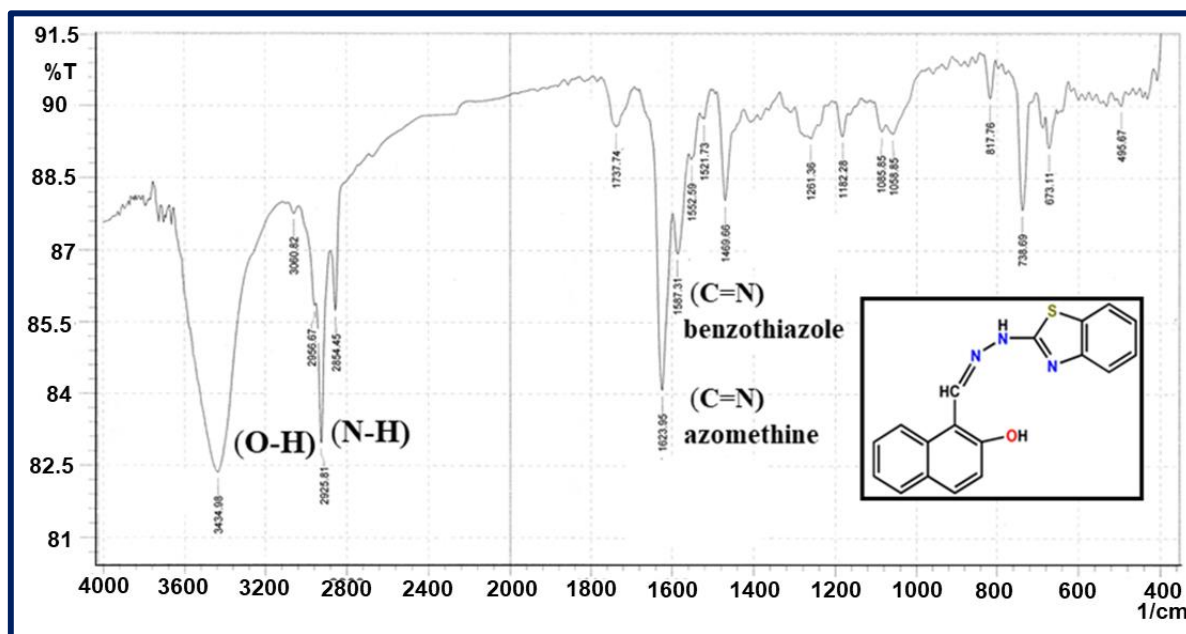


Fig. III.5. FT-IR spectrum of LH.

In the FT-IR spectrum of **1**, corresponding bands have been assigned at 3429 [$\nu(\text{O-H})$], 2923 [$\nu(\text{N-H})$], 1618-1600 [$\nu(\text{C=N})$ of azomethine] and 1577 cm^{-1} [$\nu(\text{C=N})$ of benzothiazole]. A

characteristic broad but split band at $1116\text{--}1045\text{ cm}^{-1}$ indicates that the perchlorate ion is directly coordinated to the central metal ion of **1** [57] (Fig. III.6).

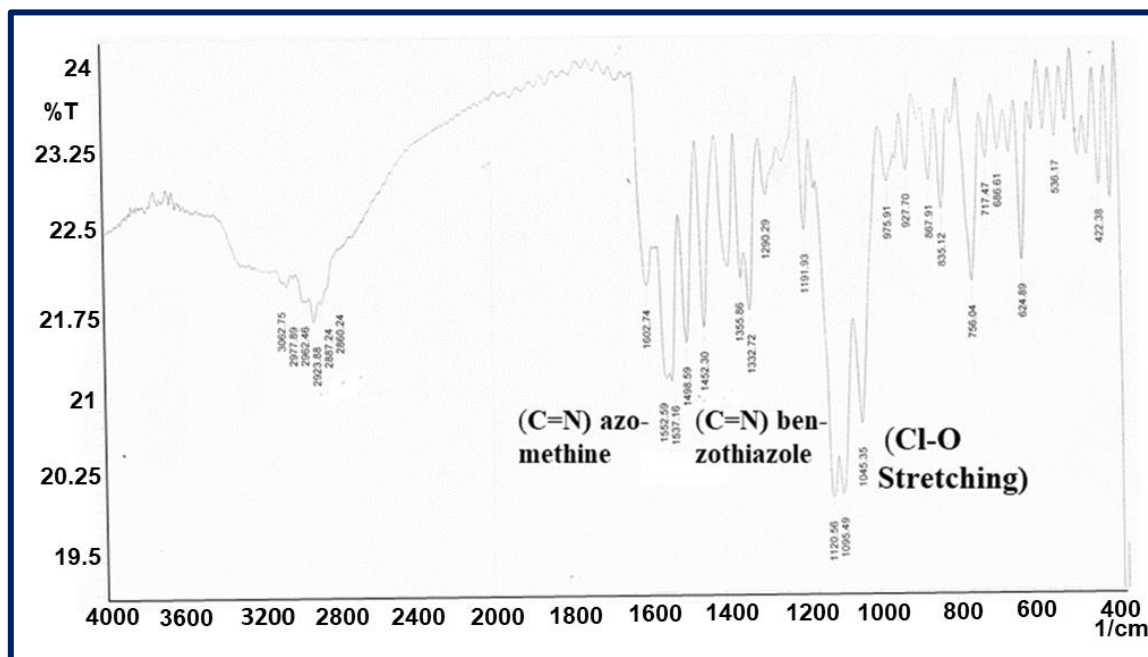


Fig. III.6. FT-IR spectrum of **1**.

The electronic absorption spectrum of **LH** in THF shows absorption bands at 407, 381, 335, 248 and 244 nm (Fig. III.7). These are due to $n\text{--}\pi^*$ and $\pi\text{--}\pi^*$ transitions, characteristic of a carbonyl group [58]. UV-Vis spectrum of **1** in methanol shows characteristic bands at 435, 326, 280 and 244 nm (Fig. III.7). The d-d transition band is observed at 660 nm which is indicative of a five coordinated square-pyramidal geometry [59].

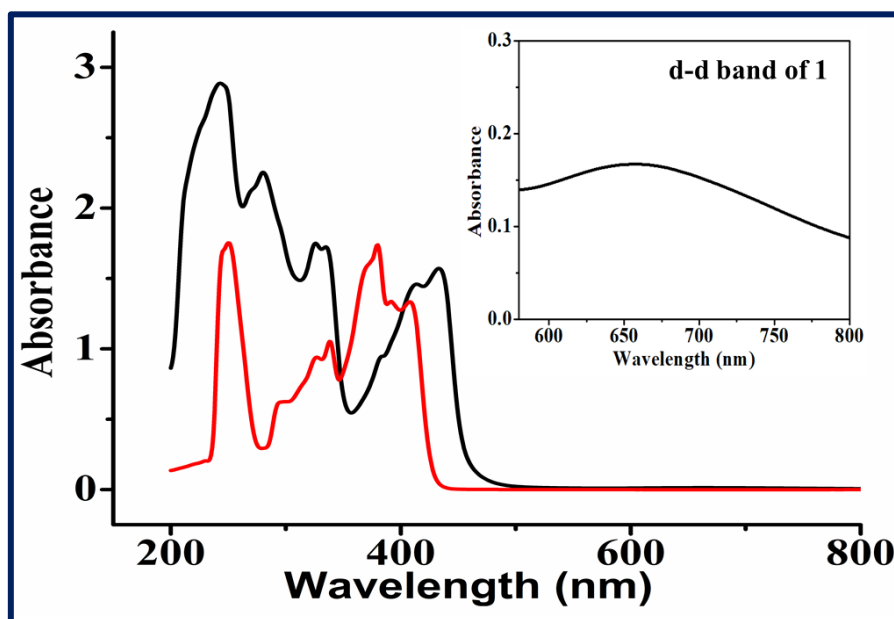


Fig. III.7. UV-Vis spectra of **LH** (red) and **1** (black) in THF. Concentration of **LH** and **1** are 1.06×10^{-3} and 1.07×10^{-3} M respectively.

The X-band EPR spectrum of solid **1** was recorded on a JEOLJES- FA200 EPR spectrometer at room temperature (Fig. III.8). The observed g value was 2.06. This g value is compatible with the Jahn-Teller distorted copper(II) compound in distorted square-pyramidal geometry [60].

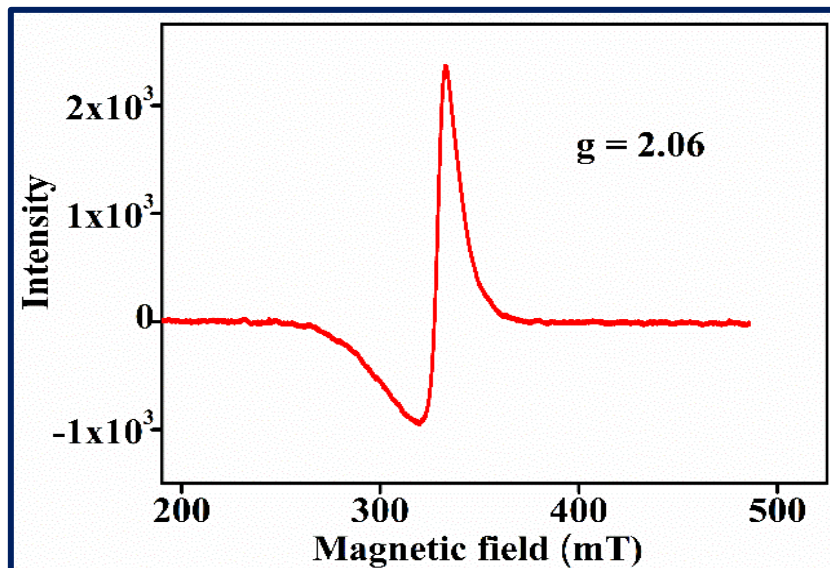


Fig. III.8. EPR spectrum of **1**.

3.2. Molecular structure of $[\text{CuL}(\text{ClO}_4)(\text{H}_2\text{O})]\cdot\text{THF}$ (**1**)

1 is a monomeric Cu(II) complex, $[\text{CuL}(\text{ClO}_4)(\text{H}_2\text{O})]\cdot\text{THF}$, with N,N,O donor Schiff base ligand as illustrated in Fig. III.9. The central copper atom is nested in a penta-coordinated environment involving two Cu-N bonds and three Cu-O bonds. **1** crystallizes in triclinic $P-1$ space group with two asymmetric units per unit cell. The geometry index (τ_5) has been determined to augment the geometry around the copper center in **1**.

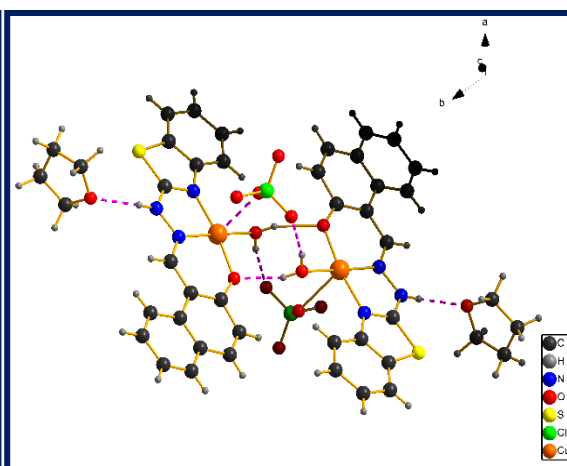
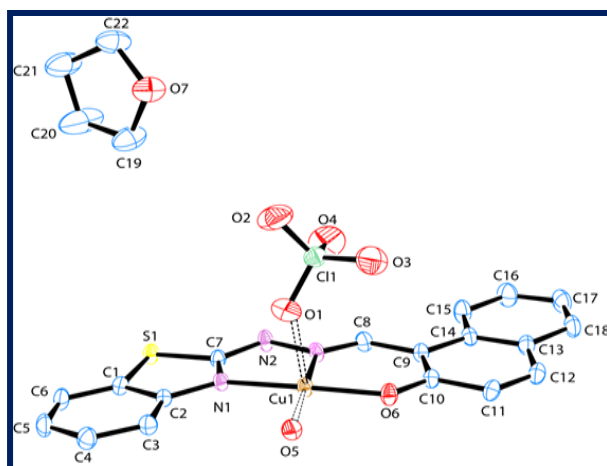


Fig. III.9. ORTEP of **1** (30% probability ellipsoid). Fig. III.10. H-bonded diagram of **1**.

By definition, $\tau_5 = (\alpha - \beta)/60^\circ$, where α and β are the largest and second largest bond angles in a complex. For a penta-coordinated complex, τ_5 may either be zero or unity. For a perfectly

square pyramidal geometry, τ_5 would be zero. This value is unity in a regular trigonal bipyramidal core [61-63]. Considering [N(3)-Cu(1)-O(5)=176.07(8)° and O(6)-Cu(1)-N(1)=170.88(7)°] respectively as α and β , τ_5 value here comes out to be 0.0865. This magnitude is indicative of a distorted square-pyramidal geometry around the copper center.

The four basal bonds, [Cu(1)-N(1), Cu(1)-N(3), Cu(1)-O(6) and Cu(1)-O(5)] are respectively of 1.9781(16), 1.9447(17), 1.8926(14) and 1.9793(14) Å. Collectively they form a square based basal plane around the copper centre in **1**. O(1) occupies the apical site of the square based pyramid. One perchlorato oxygen, O(1), is weakly bonded to the copper center. The crystal structure has been stabilized through THF solvent mediation. **1** undergoes dimerization through hydrogen bonding (Fig. III.10).

3.3. Enzymes assay

Digestive enzymes are the enzymes secreted by various parts of the body that primarily aim at breaking down food components. Out of the various enzymes, trypsin, amylase and lipase are the enzymes that significantly help in food digestion by breaking down proteins, carbohydrates and fats respectively. Amylase and trypsin inhibitors can be successfully used as anti-pancreatitis agents.

Trypsin is a serine protease found in the small intestine that helps in hydrolyzing proteins. This proteolytic enzyme is widely used as an anti-inflammatory agent and as a promoter in tissue repair. Although having much importance, if trypsin activation exceeds a certain limit, then it can damage cells and can lead to pancreatitis. Hence, trypsin activity needs to be regulated. **1** manifests appreciable inhibition towards trypsin at moderate concentrations.

Table III.3. *In vitro* analysis of **LH** and **1** towards extracellular digestive enzymes

Co nc.	% Trypsin Inhibition			% Amylase Inhibition			% Lipase Inhibition		
	Cur- cumin	Ligand	Complex	Cur- cumin	Ligand	Complex	Orlistat	Ligand	Complex
10 ⁻³ M	85.36± 1.29	51.29± 1.32	72.33± 0.98	55.70± 2.12	17.07± 1.23	21.39± 0.88	86.29± 1.26	63.52± 2.19	79.28± 1.28
10 ⁻⁴ M	69.88± 2.26	46.87± 1.68	65.94± 2.03	38.47 ± 1.25	12.23± 2.02	17.87± 1.38	80.38± 2.66	58.48± 1.98	75.31± 2.10
10 ⁻⁵ M	56.28± 2.45	30.16± 1.23	54.68± 1.56	25.05± 1.38	9.23± 1.13	12.42± 1.21	71.98± 2.93	50.87± 2.43	69.26± 1.85
10 ⁻⁶ M	48.76± 1.88	26.27± 1.73	19.94± 1.09	18.75 ± 2.17	4.06± 1.27	8.36± 1.25	67.52± 1.28	31.48± 1.87	64.19± 2.06
10 ⁻⁷ M	39.64± 2.04	19.94± 1.09	36.19± 1.63	14.02 ± 1.35	1.24± 1.42	5.96± 1.82	59.86± 2.27	26.32± 2.09	50.75± 1.98

Amylase is responsible for digestion of carbohydrates by breaking down of starch into sugars. High amylase levels can also lead to acute pancreatitis. Curcumin, taken as a control, is known to inhibit α -amylase appreciably. However, **1** exhibits little inhibition towards α -amylase. Lipases are responsible for the breaking down of fats into fatty acids and glycerol. Lipase inhibitors are primarily used as anti-obesity agents as they tend to decrease the gastrointestinal absorption of fats by preventing the hydrolysis of dietary triglycerides. **LH** and **1** inhibited lipase by almost 50% at a lower concentration i.e. 10^{-7} M. This demonstrates the potential of them to act as anti-obesity agents. The results of *in vitro* studies are shown in Table III.3.

3.4. Docking analysis

Molecular docking studies reveal that none of the compounds is directly attached to the amino acids of the catalytic triads of the enzymes — trypsin, amylase and lipase. However, the interaction with other active amino acids leads to conformational changes in enzymes, which directly affect their interaction with the substrate and hence result in decreased or increased activity of the enzyme. The total energy of a predicted pose of an inhibitor with an enzyme active site as a sum total of van der Waals (VDW), H-bonding (HB) and electrostatic energy is presented in Table III.4.

Table III.4. In silico analysis of the synthesized ligand (**LH**) and its complex (**1**) towards extracellular digestive enzymes

Docking parameters		Energy (kCal/mol)			Total no. of interactions (Ligand-Enz)	No. of H-bonds	No. of Hydrophobic bonds
		Total	VDW	HB			
Trypsin	Curcumin	-106.636	-86.6059	-20.03	6	5	1
	Ligand	-98.9765	-89.1898	-9.78667	8	2	6
	Complex	-104.24	-73.4211	-30.8194	11	10	1
Amylase	Curcumin	-95.3669	-71.4793	-23.8876	8	6	2
	Ligand	-82.5903	-71.3879	-11.2024	13	3	10
	Complex	-104.443	-76.4021	-28.0407	18	8	10
Lipase	Orlistat	-85.796	-63.4156	-22.3804	4	1	3
	Ligand	-84.7505	-73.7099	-11.0406	11	2	9
	Complex	-85.1988	-38.8634	-46.3354	5	1	4

Chapter III: Synthesis, characterization.....Schiff base ligand

2-D and 3-D figures of the respective enzymes are compiled in [Tables III.5](#) and [III.6](#), respectively. The colour code for different interactions is compiled in the figures itself.

Table III.5. 2D docking figures of ligand (**LH**) and complex (**1**) with extracellular digestive enzymes

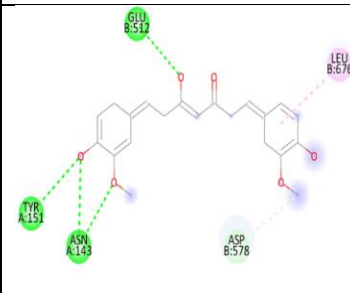
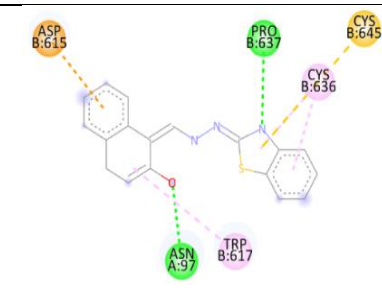
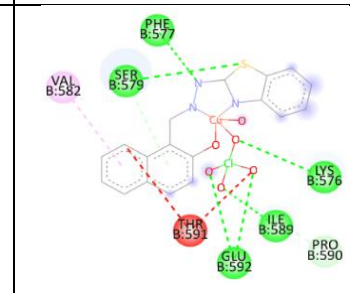
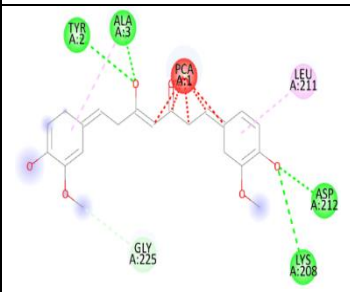
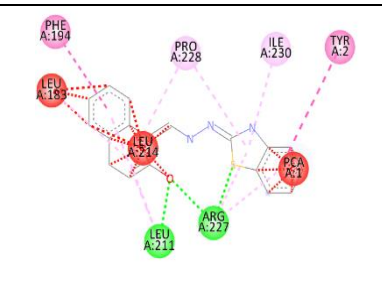
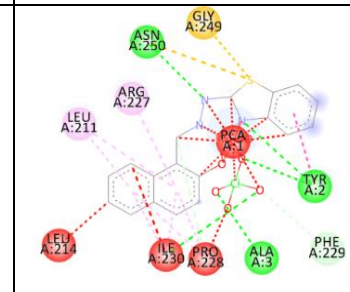
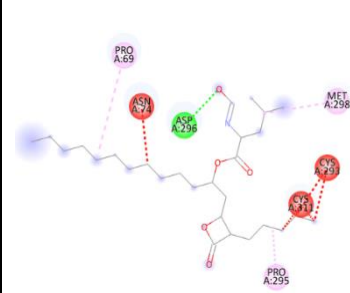
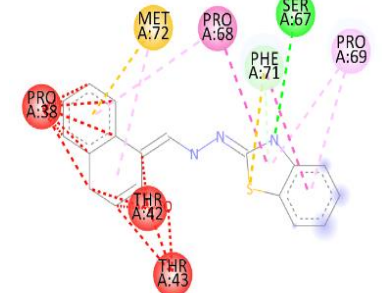
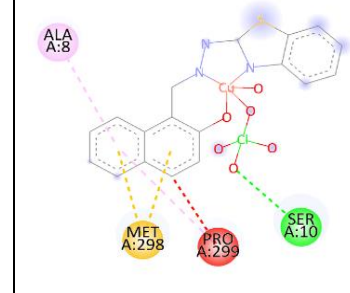
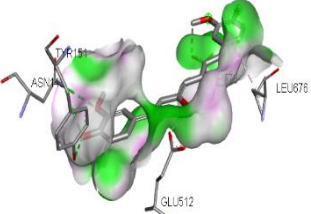

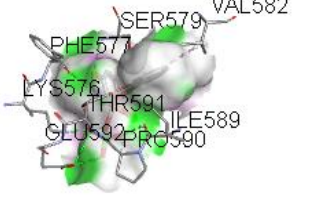
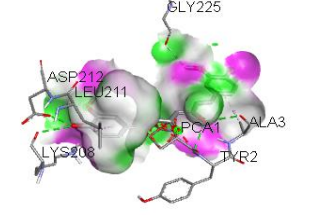
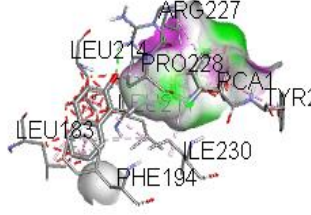
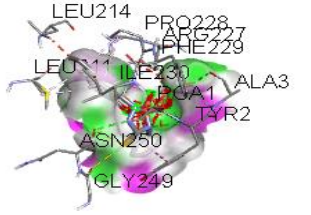
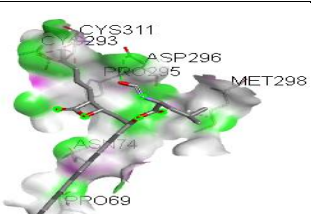
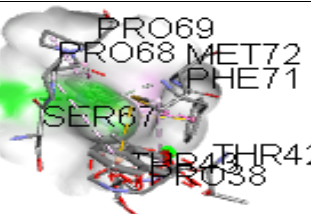
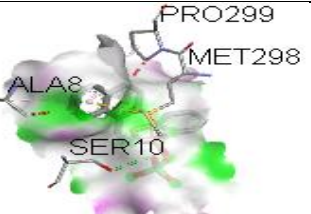
Enz.	Reference	Ligand	Complex
Trypsin			
Amylase			
Lipase			

Table III.6. 3D docking figures of **LH** and **1** with extracellular digestive enzymes.

Enz.	Reference	Ligand	Complex
Trypsin			
Amylase			
Lipase			

3.5. Absorption studies

By UV-visible absorption spectroscopy, the complex ion of Cu^{2+} with **LH** was investigated in DMSO solution. The absorption spectra of **LH** (20 μM) were recorded with different concentration of Cu^{2+} (0-22 μM) at room temperature (Fig. III.11).

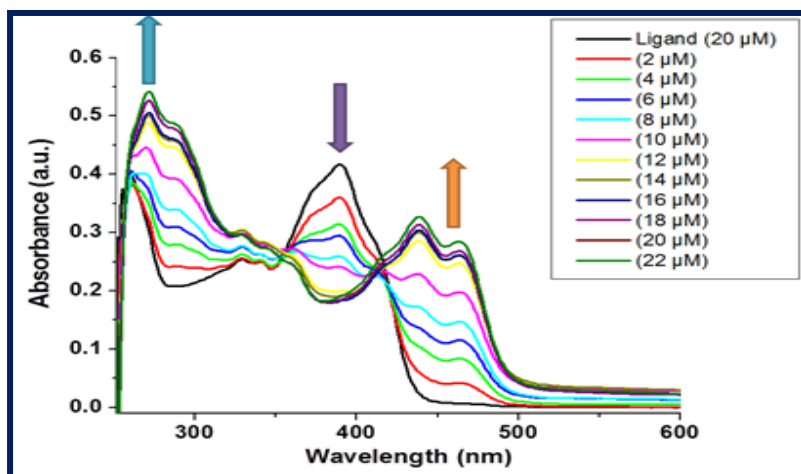


Fig. III.11. Absorption spectra of **LH** (20 μM) in presence of 0, 2, 4, 6, 8, 10, 12, 14, 16, 18, 20 and 22 μM of Cu^{2+} ion in DMSO at room temperature.

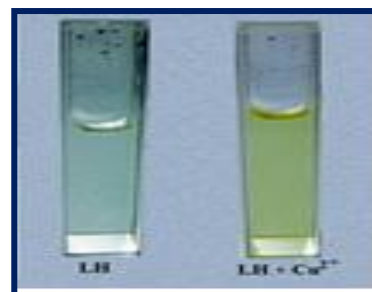


Fig. III.12. Color change of **LH** on addition of Cu^{2+} ion.

In the absence of copper ion, **LH** exhibited absorption bands at 271, 390 and 440 nm. On addition of different concentrations of copper ion, a significant change was observed in all absorption bands. With addition of Cu^{2+} , the band at 390 nm weakened and those at 270 and 440 nm intensified. This result clearly indicates that the probe (**LH**) anchors Cu^{2+} with remarkable selectivity towards Cu^{2+} . Fig. III.12 shows color change of **LH** on addition of Cu^{2+} ion.

3.6. Cu^{2+} ion sensing by fluorescence studies

To explore the photophysical properties of our probe **LH**, fluorescence emission studies were executed by various methods. On excitation at 390 nm, **LH** (20 μM) shows an emission band at 459 nm in DMSO solvent at room temperature.

The fluorescence emission intensity of **LH** noticeably diminishes on the addition of Cu^{2+} . The probe **LH** is thus a selective binder of Cu^{2+} . The fluorescence quenching occurred in emission band at 459 nm. A titration experiment was also performed with the gradual addition of Cu^{2+} to the solution of **LH**. When Cu^{2+} ions with varying concentrations (0-22 μM) were added to **LH**, a systematic fluorescence quenching was observed (Fig. III.13). With the addition of a small amount of Cu^{2+} , the quenching occurred with enhanced rapidity. However, this quenching of fluorescence intensity gradually weakened with the continuous addition of Cu^{2+} .

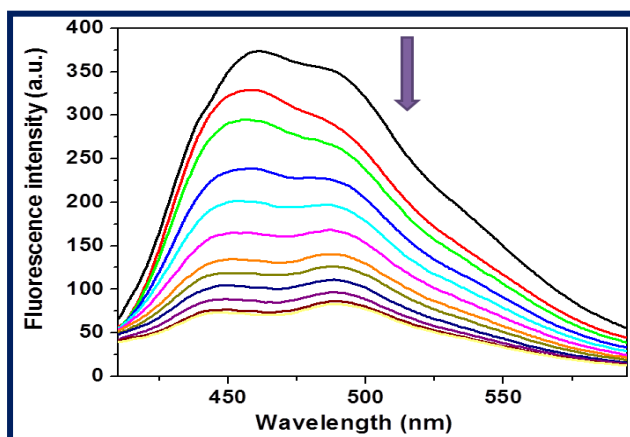


Fig. III.13. Emission spectra of **LH** (20 μM) in presence of 0, 2, 4, 6, 8, 10, 12, 14, 16, 18, 20 and 22 μM of Cu^{2+} ions in DMSO at room temperature ($\lambda_{\text{ex}} = 390 \text{ nm}$).

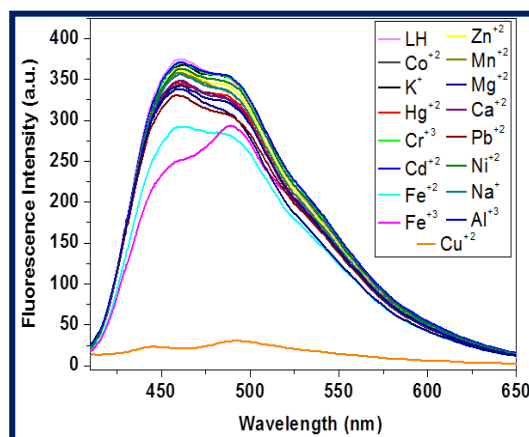


Fig. III.14. Change of fluorescence spectrum of **LH** (20 μM) in presence of different metal ions in DMSO solution. $\lambda_{\text{ex}} = 390 \text{ nm}$.

With 20 μM **LH** probe, the fluorescence efficacies were monitored towards different metal ions as shown in Fig. III.14. For selectivity determination, one equivalent amount of **LH** was exposed to one equivalent of various metal ion solution under current investigation (Al^{3+} , Na^+ , K^+ , Mg^{2+} , Ca^{2+} , Pb^{2+} , Hg^{2+} , Zn^{2+} , Cd^{2+} , Cr^{3+} , Mn^{2+} , Fe^{3+} , Fe^{2+} , Co^{2+} , Ni^{2+} and Cu^{2+}). However,

only on addition of Cu^{2+} , a significant change was noticed. Only Cu^{2+} ion showed fluorescence quenching with characteristic emission.

The selectivity of **LH** for Cu^{2+} had been checked in the presence of other metal ions (Fig. III.15). A DMSO solution of the fluorescence probe **LH** was exposed to 1.0 equivalent of Cu^{2+} in the presence of other metal ions in the equivalent concentration. Only Fe^{3+} ions were able to reduce the negligible amount of emission intensity. No other alkali or alkaline metal ion was able to quench the fluorescence intensity of **LH**. The relative changes in fluorescence intensity of **LH** with Cu^{2+} along with other relevant metal ions are shown in Fig. III.16.

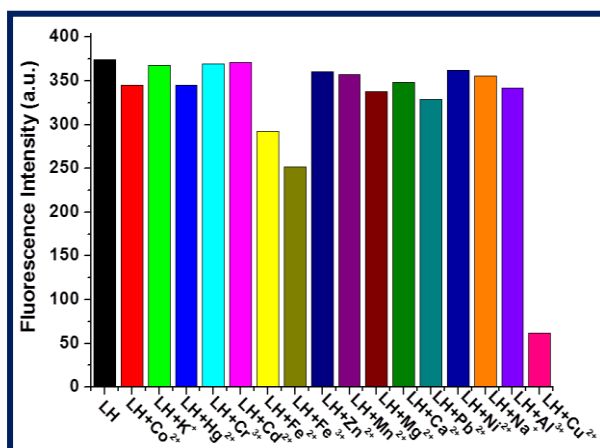


Fig. III.15. Relative fluorescence intensity changes of **LH** in presence of different metal ions in DMSO.

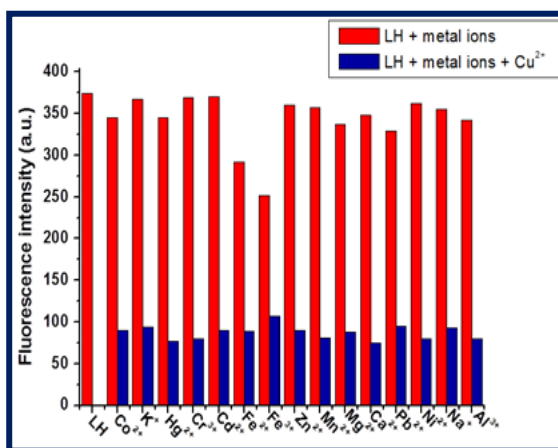


Fig. III.16. Relative fluorescence intensity changes of **LH** in presence of Cu^{2+} along with relevant other metal ions in DMSO.

Job's plot of the probe **LH** was done with Cu^{2+} varying different equivalent concentration of both by measuring fluorescence intensity (Fig. III.17).

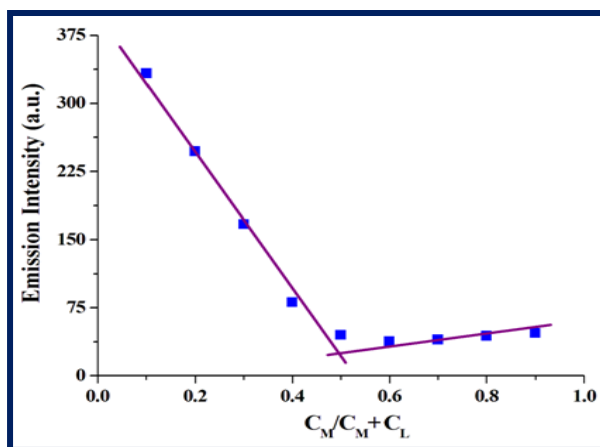


Fig. III.17. Job's plot indicating 1:1 complex formation of **LH** with Cu^{2+} ion.

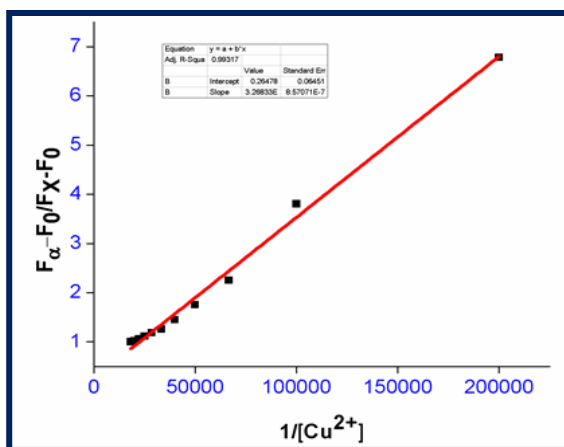


Fig. III.18. Benesi-Hildebrand plot for **LH** with Cu^{2+} .

At the same equivalent mixture condition, plot shows a significant break. This clearly indicates that the probe **LH** forms a complex with Cu^{2+} in a 1:1 molar proportion. It is pertinent to note that our crystal structure of the copper complex of **LH** also confirms this stoichiometric proportion (Fig. III.9). From the Benesi-Hildebrand plot, the binding constant value (K_a) was found to be $3.05 \times 10^4 \text{ M}^{-1}$ (Fig. III.18).

3.7. Limit of detection (LOD) determination

Following 3σ method, the limit of detection (LOD) value of the present probe for copper(II) ion had been evaluated [64]. The determined LOD value was $0.35 \mu\text{M}$. The World Health Organization has set the LOD value of $31.5 \mu\text{M}$ (maximum adoptable) [65]. In comparison, our LOD value is significantly lower (Fig. III.19). This low LOD value clearly indicates that the probe, **LH**, offers high sensitivity towards Cu^{2+} . We take recourse to comparing our present result with some recently published Cu^{2+} probes [66-71] (Table III.7). From this comparison, it is obvious that our present probe is superior to most of the currently reported probes. However, a recently published naphthaldehyde based sensor, akin to our probe, has been found to manifest the best efficacy [69]. Additionally, a good linear dynamic relationship at 459 nm was obtained between fluorescence intensity and Cu^{2+} ion concentration with an R value of 0.98732 . This obtained value suggests more accurate detection of Cu^{2+} ion (Fig. III.19).

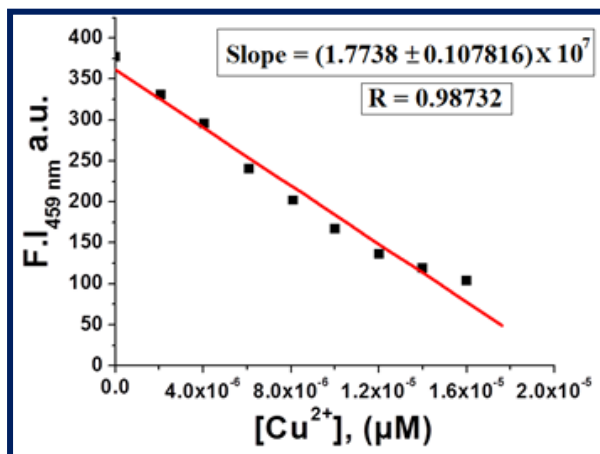


Fig. III.19. Linear plot of F.I. (459 nm) vs $[\text{Cu}^{2+}]$ for the determination of S (slope).

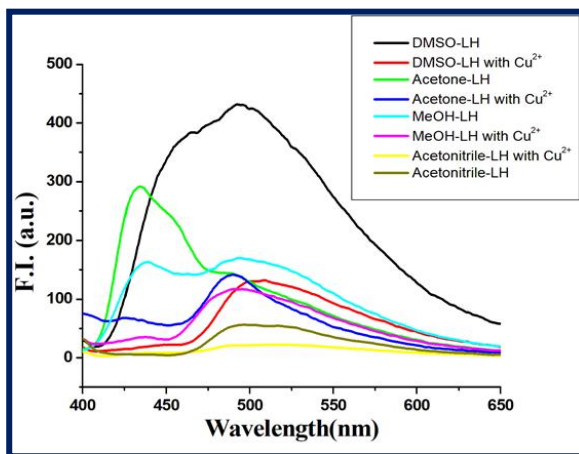
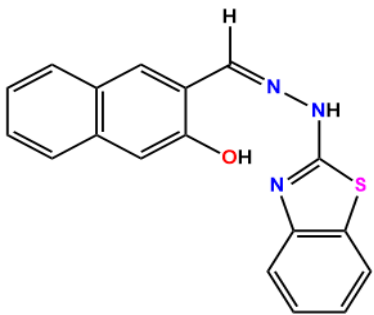
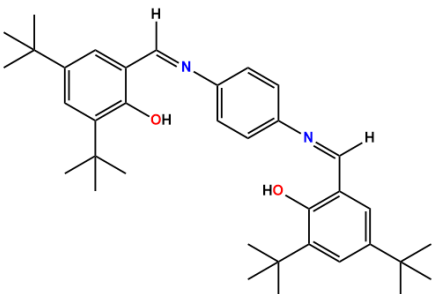
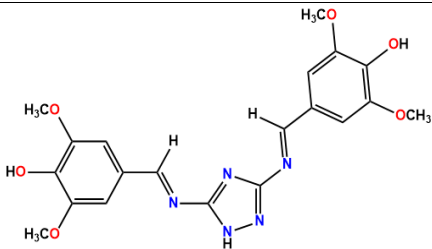
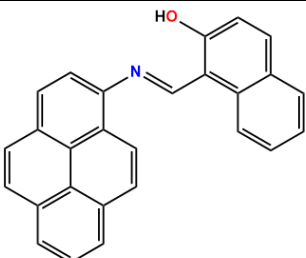


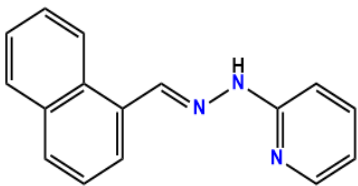
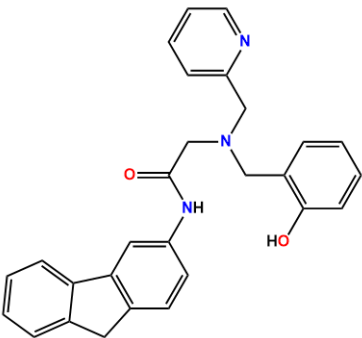
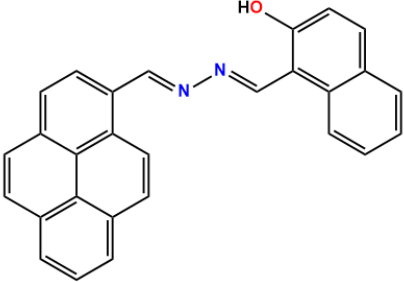
Fig. III.20. Plot of fluorescence intensity with different solvent for **LH** with Cu^{2+} .

We also checked the copper(II) sensing aspect of **LH** ($20 \mu\text{M}$) in methanol, acetone and acetonitrile along with DMSO. We observed promising changes in fluorescence intensity in DMSO. For the rest of the solvents, the response was poor (Fig. III.20).

Our present low LOD value has been compared with some other previously reported sensors and has been tabulated in Table III.7.

Table III.7. Comparison of some priorly published chemosensors for Cu²⁺ ion with present work

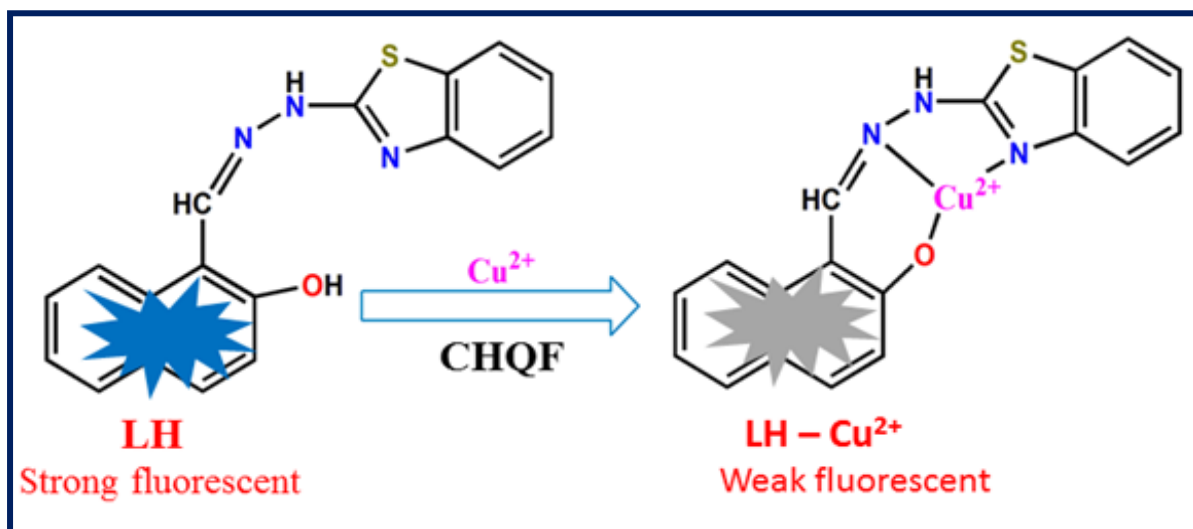
Sl. No	Structure of probe	Solvent	Sensing method	LOD (μM)	Reference
1		DMSO	Fluorescent sensor	0.35	Present work
2		DMF	Fluorescent sensor	0.35	66
3		CH ₃ OH-Tris buffer (1:1)	Colorimetric and fluorescent sensor	1.2	67
4		DMSO-H ₂ O (4:1)	Colorimetric and fluorescent sensor	2.17	68

5		Tris-HCl buffer	Fluorescent sensor	3.90×10^{-3}	69
6		DMF-Tris buffer (1:1)	Colorimetric and fluorescent sensor	2.9	70
7		MeOH-H ₂ O (7:3)	Colorimetric and fluorescent sensor	0.1	71

3.8. Sensing mechanism

To augment the proposed sensing mechanism of the present fluorescent probe **LH**, we had taken recourse to monitoring the fluorescence phenomenon of **LH** (20 μ M) in DMSO solution towards different metal ions. On excitation at 390 nm, a strong emission band was observed at 499 nm for the fluorescent sensor **LH** in DMSO solvent at room temperature. However, a distinct fluorescence quenching was observed only for the Cu^{2+} ion during our experiment over other tested metal ions. Most likely this can be attributed to the paramagnetic behaviour of Cu^{2+} ion. Due to the formation of the **LH**- Cu^{2+} complex, a photoinduced energy/charge transfer occurs from metal to fluorophore. This pathway, the chelation-quenched fluorescence (CHQF) sensing mechanism, caused by the complexation of **LH** with Cu^{2+} is most likely operative here [72]. Earlier, **LH** had been reported for time dependent selectivity for copper(II) ion through the turn-on mode. The authors proposed that the binding mode of **LH** with Cu^{2+} is either through N or S of the benzothiazole ring in an acetonitrile milieu. For the chelation of Cu^{2+} with a S donor atom, strong fluorescence was observed; while a non-fluorescence situation resulted for anchoring through a N atom [73]. Here, we have confirmed the unambiguous

binding mode of **LH** with Cu^{2+} solely through the N donor atom by single crystal X-ray structure as depicted in Fig. III.9. The fluorescence intensity was quenched upon the continuous addition of Cu^{2+} . Other tested metal ions under the present study, however, failed to quench fluorescence intensity. Possibly this may be attributed to the not so stable coordination geometry arising out of unfavourable anchoring of other metal ions other than copper with **LH** in DMSO. The proposed sensing mechanism is shown in scheme III.2.



Scheme III.2. Proposed sensing mechanism of **LH**.

3.9. DFT calculations

Calculated bond parameters as obtained by DFT are consistent with the crystallographic data of **1** (Table III.8). The calculated bond distances of Cu1–N1, Cu1–N3, Cu1–O3, Cu1–O5 and Cu1–O6 are a little bit longer than their respective crystallographic values. For **1**, the computed angles lie within $\pm 5^\circ$ deviation from their respective experimental values. The optimized bond parameters of free ligand (**LH**) and both optimized as well as experimental bond parameters of coordinated ligand are almost the same. Thus, our calculated bond lengths and bond angles are in fair agreement with the experimental data.

Table III.8. Selected experimental and optimized bond distances (Å) and angles ($^\circ$) for **LH** and **1**

Bond/Angle	Optimized	Bond/Angle	Optimized
LH			
C1-C2	1.42606	C8-N3	1.31519
C1-S1	1.82619	C8-C9	1.45362
C2-N1	1.40782	C9-C10	1.42012

C7-N1	1.30232		C10-O6	1.36735	
C7-N2	1.37891		N2-N3	1.38076	
N1-C7-N2	126.241		N2-N3-C8	119.491	
1					
Bond/Angle	Experiment	Optimized	Bond/Angle	Experiment	Optimized
C1-C2	1.399	1.41813	C8-N3	1.292	1.32196
C1-S1	1.743	1.83604	C8-C9	1.435	1.43057
C2-N1	1.405	1.41284	C9-C10	1.402	1.43869
C7-N1	1.310	1.32489	C10-O6	1.323	1.33051
C7-N2	1.348	1.36565	N2-N3	1.386	1.40444
Cu1-N1	1.9871(16)	2.06300	Cu1-O1	2.525	2.22314
Cu1-N3	1.9447(17)	1.96511	Cl1-O1	1.434(2)	1.83196
Cu1-O5	1.9793(16)	1.99710	Cl1-O2	1.402(2)	1.83196
Cu1-O6	1.8926(14)	1.91265	Cl1-O3	1.409(2)	1.70303
N1-C7-N2	120.69	120.463	N2-N3-C8	118.03	120.033
O6-Cu1-N3	90.57(7)	90.421	O2-Cl1-O4	109.04(16)	113.358
O6-Cu1-N1	170.88(7)	166.094	O2-Cl1-O3	110.74(19)	109.604
N3-Cu1-N1	82.05(7)	81.584	O4-Cl1-O3	110.00(19)	111.226
O6-Cu1-O5	89.70(7)	86.697	O2-Cl1-O1	109.86(15)	110.320
N3-Cu1-O5	176.07(8)	175.880	O4-Cl1-O1	108.84(16)	114.390
N1-Cu1-O5	97.29(7)	102.036	O3-Cl1-O1	108.35(14)	96.712

The manifested overall variations are reasonable since being carried out *in vacuo* at 0 K, theoretical optimization cannot match exactly with the experimental data set. Again, the deviation of the calculated bond parameters from the experimental data may arise due to conformational changes induced by the crystal field perturbation and temperature effect. This may be due to the basis sets chosen for calculations [74]. To get insight into the electronic absorption aspects of **LH** and **1**, TD-DFT calculations were carried out with the optimized

structures. The evaluated transition energies of **LH** and **1**, using the LanL2DZ basis set and TD-SCF calculation, are shown in Fig. III.21. The molecular orbitals (MOs) of **LH** at the first lower excited state were ascribed to the HOMO \rightarrow LUMO transition found at 388.58 nm against the experimental absorption at 390 nm. For free **LH**, the HOMO-LUMO energy gap was found to be 3.595 eV; while the HOMO-4 \rightarrow LUMO value for **1** was 2.821 eV. In **1**, comparatively less amount of energy is required to excite the electron due to decrease in energy gap as compared to free **LH**. This results in a bathochromic shift in the absorption spectrum. However, the main MO contributions of **1** at the third lower excited states were analyzed to be the HOMO-5 \rightarrow LUMO, HOMO-4 \rightarrow LUMO and HOMO \rightarrow LUMO+2 transitions found at 463.37 nm against the experimental λ_{max} value of 465 nm.

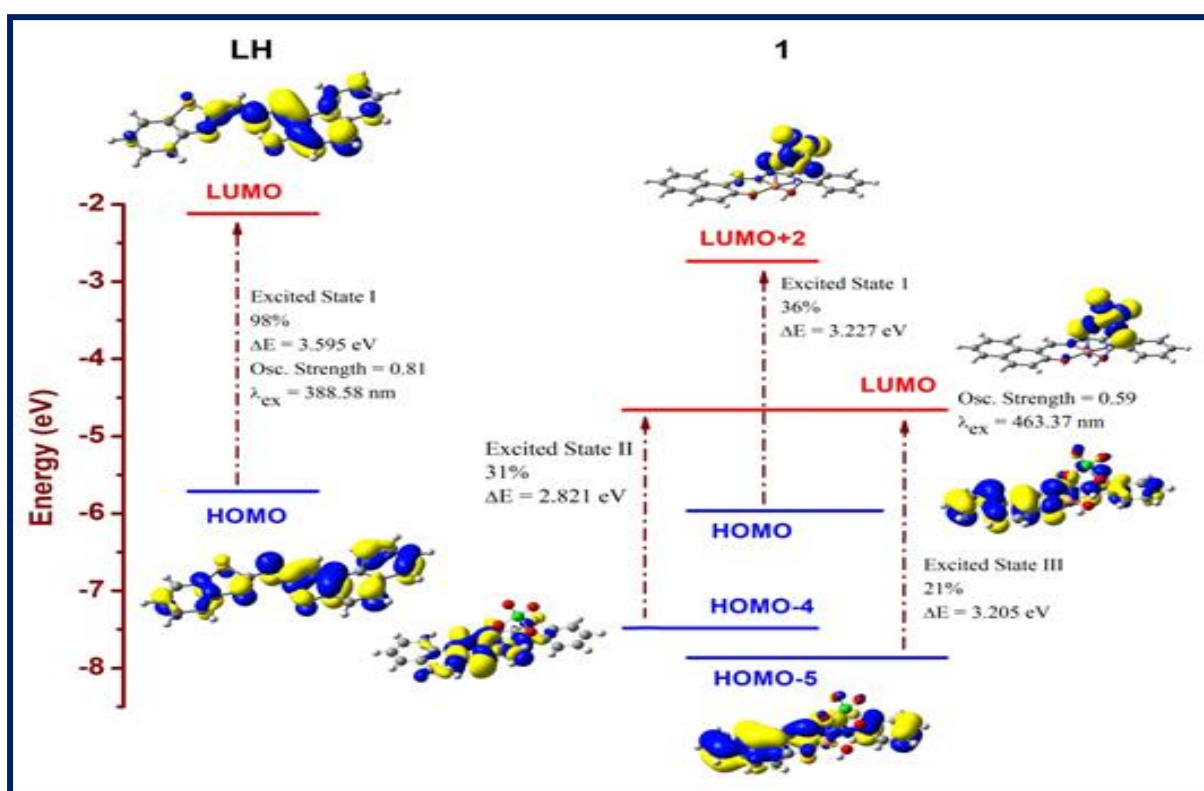


Fig. III.21. Molecular orbital diagram and excitation energies for **LH** and **1**.

3.10. Powder X-ray diffraction

Powder X-ray diffraction of **1** was done to check the phase purity of the bulk materials. Simulated patterns as obtained from SC-XRD are in good agreement with the powder pattern. This confirms the phase purity of the bulk materials of **1** (Fig. III.22).

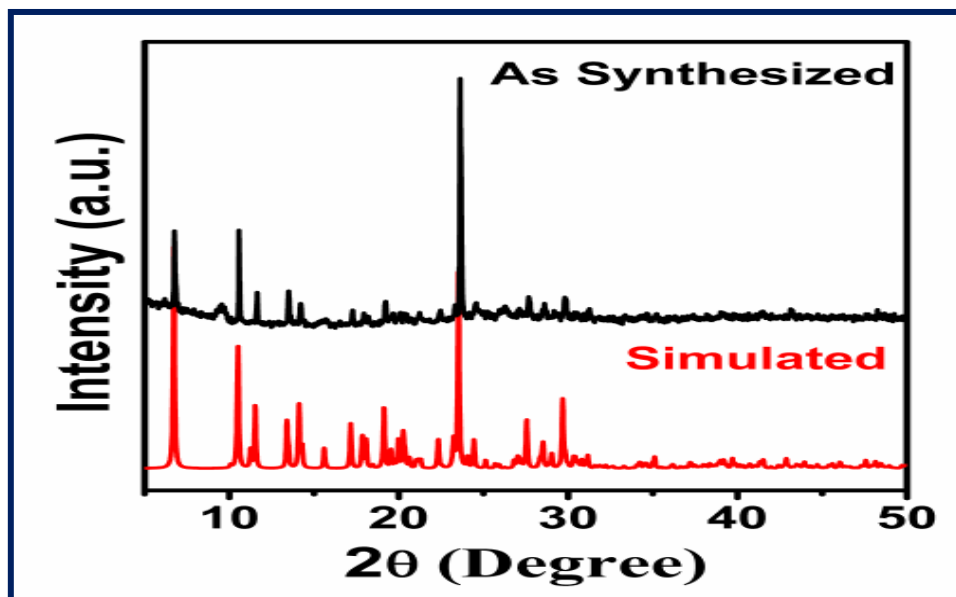


Fig. III.22. Powder X-ray diffraction pattern of complex **1**.

4. Conclusions

In summary, we have synthesized a novel mononuclear Cu(II) complex (**1**) from a naphthaldehyde based Schiff base ligand (**LH**) and was thoroughly characterized. The crystal structure of the copper(II) complex of **LH** has also been determined. *In vitro* enzymatic studies employing amylase, trypsin and lipase were carried out for both **LH** and **1**. *In silico* analysis of **LH** and **1** have also been carried out towards extracellular digestive enzymes. **1** shows inhibition towards the tested enzymes. This study reveals that both **LH** and **1** can be used as anti-obesity agents due to their strong inhibition towards lipase at lower concentrations. Accordingly, the present work may bear some significant biological perspective. In addition, the fluorescent probe (**LH**) shows selectivity towards the Cu²⁺ ion in organic milieu. In the absence of Cu²⁺ ions, the probe shows an emission band at 459 nm while on addition of the Cu²⁺, it shows significant fluorescence quenching. Our Job's plot analysis confirms a 1:1 binding stoichiometry of the probe with the Cu²⁺ ion. The present work demonstrates a rare situation where the solid state crystal structure of the probe-metal system has been deciphered. This probe offers high selectivity coupled with significant sensitivity towards Cu(II) ion with satisfactory low LOD value of 0.35 μM. Based on this outcome, the present contribution may draw attention at least to the monitoring of copper(II) ions in industrial and environmental samples.

5. References

1. M. Furne, M.C. Hidalgo, A. Lopez, M. Gracia-Gallego, A.E. Morales, A. Domezain, J. Domezaine, A. Sanz, *Aquaculture* 250 (2005) 391-398.
2. R.D. Schmid, R. Verger, *Angew. Chem. Int. Ed.* 37 (1998) 1608-1633.
3. M. Hirota, M. Ohmuraya, H. Baba, J. Gastro. 41 (2006) 832-836.
4. N.Y, Ensari, B. Otludil, M.C. Aytekin, *Starch/Stärke* 47 (1995) 315-321.
5. M.E. Fárez-Vidal, A. Fernandez-Vivas, J.M. Arias, *J. Appl. Bacterio.* 73 (1992) 148-156.
6. N.S. Reddy, A. Nimmagadda, K.R.S.S. Rao, *African J. Biotech.* 2 (2003) 645-648.
7. K. Yamane, B. Maruo, *J. Bact.* 120 (1974) 792-798.
8. F. Hasan, A.A. Shah, A. Hameed, *Enzyme Microb. Technol.* 39 (2006) 235-251.
9. W.A. Zoubi, A.A.S. Al-Hamdani, S.D. Ahmed, Y.G. Ko, *J. Phys. Org. Chem.* 31 (2018) e3752.
10. M.S. More, P.G. Joshi, Y.K. Mishra, P.K. Khanna, *Mater. Today Chem.* 14 (2019) 100195.
11. A. Kajal, S. Bala, S. Kamboj, N. Sharma, V. Saini, *J. Catalysts* (2013) 893512.
12. C. Biswas, A. Chatterjee, V. Vijayan, C.S. Purohit, M.S. Kiran, R. Ghosh, *Inorg. Chem. Commun.* 136 (2022) 109178-109183.
13. M.N. Uddin, S.S. Ahmed, S.M.R. Alam, *J. Coord. Chem.* 73 (2020) 3109-3149.
14. S. Patil, S.D. Jadhav, U.P. Patil, *Arch. Appl. Sci. Res.* 4 (2012) 1074-1078.
15. B. Otludil, B.A. Otludil, R. Demir, V. Tolan, H. Temel, *Biotechnol. Biotechnol. Equip.* 19 (2005) 105-110.
16. D. Iyaguchi, S. Kawano, K. Takada, E. Toyota, *Bioorganic & Medicinal Chemistry* 18 (2010) 2076-2080.
17. E. Toyota, K.K.S. Ng, H. Sekizaki, K. Itoh, K. Tanizawa, M.N.G. James, *J. Mol. Biol.* 305 (2001) 471-479.
18. Z. Liu, W. He, M. Pei, G. Zhang, *Chem. Commun.* 51 (2015) 14227-14230.
19. C.-Y. Lai, B.G. Trewyn, D.M. Jeftinija, K. Jeftinija, S. Xu, S. Jeftinija, V.S.-Y. Lin, *J. Am. Chem. Soc.* 125 (2003) 4451-4459.
20. B. Muthuraj, R. Deshmukh, V. Trivedi, P.K. Iyer, *ACS Appl. Mater. Interfaces* 6 (2014) 6562-6569.
21. A.M. Abu-Dief, L.A.E. Nassr, *J. Iran. Chem. Soc.* 12 (2015) 943- 955.
22. Y. Wang, S. Liu, H. Chen, Y. Liu, H. Li, *Dyes Pigm.* 142 (2017) 293-299.
23. E. Merian, *Analysis and Biological Relevance*, VCH, Weinheim, 1991, p. 893.

24. E. Merian, *Metals and Their Compounds in the Environment*, VCH, Weinheim, Germany, 1991.
25. D.W. Domaille, E.L. Que, C.J. Chang, *Nat. Chem. Biol.* 4 (2008) 168-175.
26. S.-P. Wu, T.-H. Wang, S.-R. Liu, *Tetrahedron* 66 (2010) 9655-9658.
27. T. Li, Z. Yang, Y. Li, Z. Liu, G. Qi, B. Wang, *Dyes Pigments* 88 (2011) 103-108.
28. H.S. Jung, P.S. Kwon, J.W. Lee, J.I. Kim, C.S. Hong, J.W. Kim, S. Yan, J.Y. Lee, J.H. Lee, T. Joo, J.S. Kim, *J. Am. Chem. Soc.* 131 (2009) 2008-2012.
29. A. Saravanan, G. Subashini, S. Shyamsivappan, T. Suresh, K. Kadirvelu, N. Bhuvanesh, R. Nandhakumar, P.S. Mohan, *J. Photochem. Photobiol. A: Chem.* 364 (2018) 424-432.
30. M. Sadia, R. Naz, J. Khan, R. Khan, *J. Fluoresc.* 18 (2018) 1281-1294.
31. J.R. Barrull, M. d'Halluin, E.L. Grogne, F.-X. Felpin, *Chem. Commun.* 52 (2016) 6569-6572.
32. X. Ma, Z. Tan, G. Wei, D. Wei, Y. Du, *Analyst* 137 (2012) 1436-1439.
33. D.J. Waggoner, T.B. Bartnikas, J.D. Gitlin, *Neurobiol. Dis.* 6 (1999) 221-230.
34. C. Vulpe, B. Levinson, S. Whitney, S. Packman, J. Gitschier, *Nat. Genet.* 3 (1993) 7-13.
35. P.C. Bull, G.R. Thomas, J.M. Rommens, J.R. Forbes, D.W. Cox, *Nat. Genet.* 5 (1993) 327-337.
36. Y.H. Hung, A.I. Bush, R.A. Cherny, *J. Biol. Inorg. Chem.* 15 (2010) 61-76.
37. P. Jiang, Z. Guo, *Coord. Chem. Rev.* 248 (2004) 205-229.
38. F. Pina, M.A. Bernardo, E. Garcia-Espana, *Eur. J. Inorg. Chem.* (2000) 2143-2157.
39. G.K. Patra, R. Chandra, A. Ghorai, K.K. Shrivastava, *Inorg. Chim. Acta* 462 (2017) 315-322.
40. M. Boiocchi, L. Fabbrizzi, M. Licchelli, D. Sacchi, M. Vázquez, C. Zampa, *Chem. Commun.* (2003) 1812-1813.
41. G.A. Bain, J.F. Berry, *J. Chem. Educ.* 85 (2008) 532-536.
42. M.J. Frisch, G.W. Trucks, H.B. Schlegel, G.E. Scuseria, M.A. Robb, J.R. Cheeseman, G. Scalmani, V. Barone, B. Mennucci, G.A. Petersson, H. Nakatsuji, M. Caricato, X. Li, H.P. Hratchian, A.F. Izmaylov, J. Bloino, G. Zheng, J.L. Sonnenberg, M. Hada, M. Ehara, K. Toyota, R. Fukuda, J. Hasegawa, M. Ishida, T. Nakajima, Y. Honda, O. Kitao, H. Nakai, T. Vreven, J.A. Montgomery Jr., J.E. Peralta, F. Ogliaro, M. Bearpark, J.J. Heyd, E. Brothers, K. N. Kudin, V.N. Staroverov, R. Kobayashi, J. Normand, K. Raghavachari, A. Rendell, J.C. Burant, S.S. Iyengar, J. Tomasi, M. Cossi, N. Rega, J.M. Millam, M. Klene, J.E. Knox, J.B. Cross, V. Bakken, C. Adamo, J. Jaramillo, R. Gomperts, R.E. Stratmann, O. Yazyev, A.J. Austin, R. Cammi, C. Pomelli, J.W. Ochterski, R.L. Martin, K. Morokuma, V.G.

- Zakrzewski, G.A. Voth, P. Salvador, J.J. Dannenberg, S. Dapprich, A.D. Daniels, Ö. Farkas, J.B. Foresman, J.V. Ortiz, J. Cioslowski, D.J. Fox, Gaussian 09, Revision C.01, GaussianInc., Wallingford, CT, 2009.
43. A.D. Becke, J. Chem. Phys. 98 (1993) 5648
 44. C. Lee, W. Yang, R.G. Parr, Phys. Rev. Sect. B 37 (1988) 785-789.
 45. P.J. Hay, W.R. Wadt, J. Chem. Phys. 82 (1985) 299-310.
 46. V. Barone, M. Cossi, J. Phys. Chem. A 102 (1998) 1995-2001
 47. J. Tomasi, B. Mennucci, R. Cammi, Chem. Rev. 105 (2005) 2999-3094.
 48. W.C. Wolsey, J. Chem. Educ. 50 (1973) A335-A337.
 49. S.R. Girish, V.K. Revankar, V.B. Mahale, Transit. Met. Chem. 21 (1996) 401-405.
 50. Bruker, SMART (Version 5.0) and SAINT (Version 6.02). Bruker AXS Inc., Madison, Wisconsin, USA, 2000.
 51. G.M. Sheldrick, SADABS, Program for Empirical Correction of Area Detector Data, University of Göttingen, Germany, 2000.
 52. G.M. Sheldrick, SHELXS97 and SHELXL97, Program for Crystal Structure Refinement, University of Göttingen, Germany, 1997.
 53. P. Arya, N. Raghav, J. Mol. Struct. 1228 (2021) 129774.
 54. L. Migliolo, A.S. de Oliveira, E.A. Santos, O.L. Franco, M.P. de Sales, J. Mol. Graph. Model. 29 (2010) 148-156.
 55. F. Xie, W. Zhang, S. Gong Z, X. Gu, X. Lan, J. Wu, Z. Wang, Food Chem. 271 (2019) 62-69.
 56. D.I. Habeych, P.B. Juhl, J. Pleiss, D. Vanegas, G. Eggink, C.G. Boeriu, J. Mol. Catal. B: Enzym. 71 (2011) 1-9.
 57. Y. Fukuda, A. Shimura, M. Mukaida, E. Fujita, K. Sone, J. Inorg. Nucl. Chem. 36 (1974) 1265-1270.
 58. M.H. Habibi, M. Mikhak, Spectrochim. Acta part A: Mol. Biomol. Spectrosc. 96 (2012) 501-505.
 59. B.J. Hathaway, R.J. Dudley, P. Nicholls, J. Chem. Soc. A (1969) 1845-1848.
 60. M. Kumar, S.U. Parsekar, N. Duraipandy, M.S. Kiran. A.P. Koley, Inorg. Chim. Acta 484 (2019) 219-226.
 61. A.W. Addison, T.N. Rao, J. Reedijk, J.V. Rijn, G.C. Verschoor, Dalton Trans. (1984) 1349-1356.
 62. M. Li, A. Ellern, J.H. Espenson, Inorg. Chem. 44 (2005) 3690-3699.

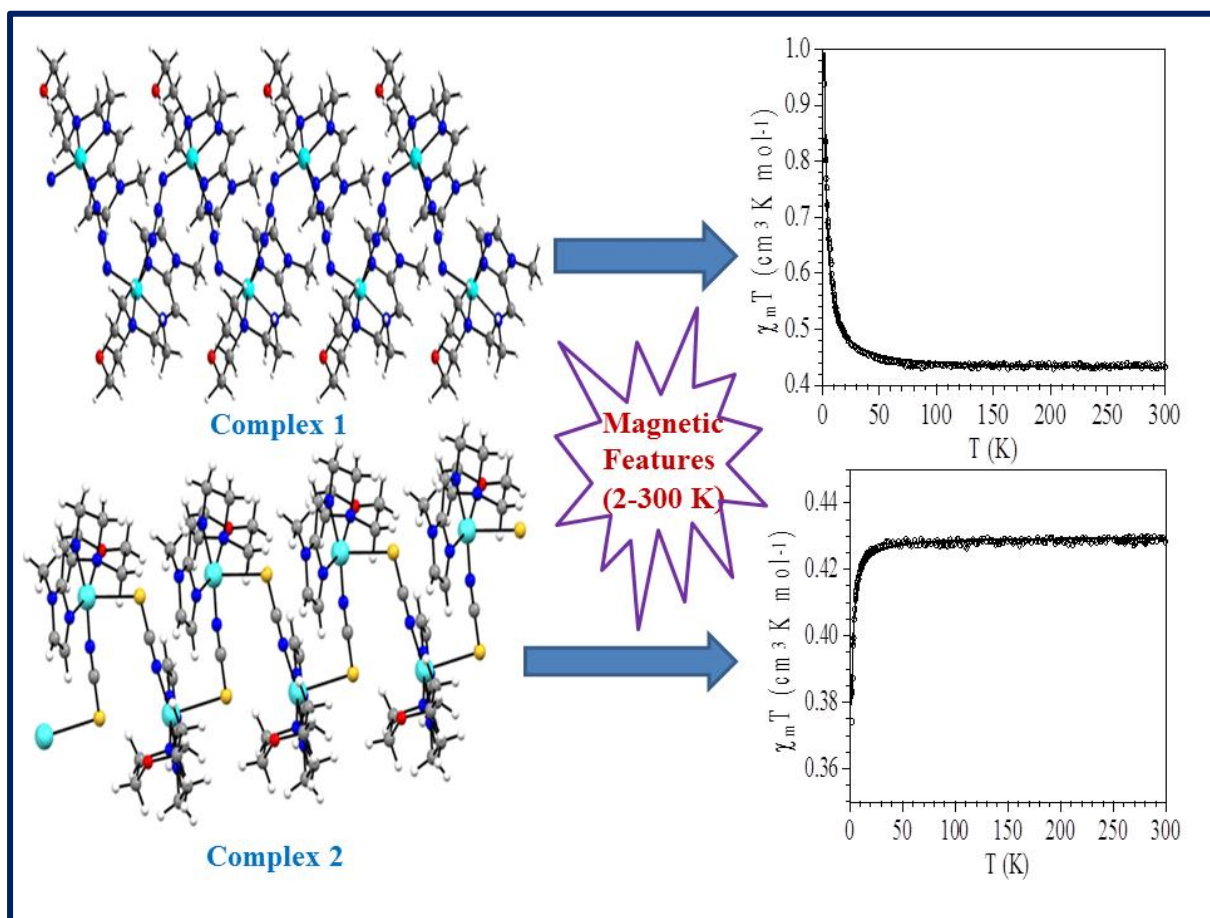
63. K.P. Maresca, G.H. Bonavia, J.W. Babich, J. Zubieta, *Inorg. Chim. Acta* 284 (1999) 252-257.
64. V. Thomsen, D. Schatzlein, D. Mercurio, *Spectros.* 18 (2003) 112-114.
65. J.H. Kang, S.Y. Lee, H.M. Ahn, C. Kim, *Inorg. Chem. Commun.* 74 (2016) 62-65.
66. P. Torawane, S.K. Sahoo, A. Borse, A. Kuwar, *Luminescence* 32 (2017) 1426-1430
67. K. Rout, A.K. Manna, M. Sahu, J. Mondal, S.K. Singh, G.K. Patra, *RSC Adv.* 9 (2019) 25919-25931.
68. Y.R. Bhorge, H.-T. Tsai, K.-F. Huang, A.J. Pape, S.N. Janaki, Y.-P. Yen, *Spectrochem. Acta Part A: Mol. Biomol. Spectrosc.* 130 (2014) 7-12.
69. N. Xiao, C. Zhang, *Inorg. Chem. Commun.* 107 (2019) 107467.
70. G.J. Park, G.R. You, Y.W. Choi, C. Kim, *Sens. Actuators B: Chem.* 229 (2016) 257-271.
71. S. Ghosh, A. Ganguly, M.R. Uddin, S. Mandal, M.A. Alam, N. Guchhait, *Dalton Trans.* 45 (2016) 11042-11051.
72. Z. Guo, Q. Niu, T. Li, T. Sun, H. Chi, *Spectrochim. Acta Part A: Mol. Biomol. Spectrosc.* 213 (2019) 97-103.
73. Z. Zhang, S. Yuan, E. Wang, *J. Fluoresc.* 28 (2018) 1115-1119.
74. A. Bhattacharya, J.P. Naskar, S. Majumder, R. Ganguly, P. Mitra, S. Chowdhury, *Inorg. Chim. Acta.* 425 (2015) 124-133.

CHAPTER-IV

Syntheses of two copper(II) coordination polymers from a novel morpholine-based tridentate Schiff base ligand: Crystal structures and magnetic properties

This work has been published in
Journal of Coordination Chemistry
76 (2023) 705–719

Graphical Abstract



Highlights

- Two polynuclear Cu(II) complexes were synthesized by using a new morpholine based Schiff base ligand.
- Both the complexes have been confirmed by X-ray single crystal structures.
- Spectroscopic properties of the ligand and complexes have been studied.
- Variable temperature magnetic studies were carried out on the copper(II) complexes.
- EPR measurements were also done at low temperature to corroborate the magnetic data.

Key words

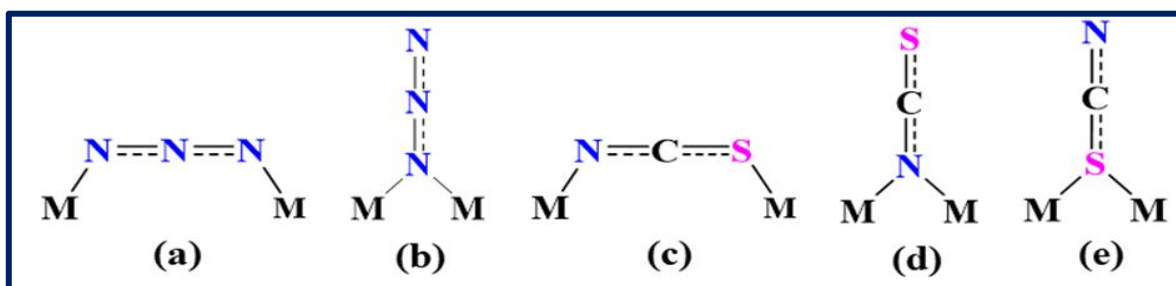
Copper; Schiff base; crystal structures and magnetic properties

Abstract

Two new one-dimensional (1D) end-to-end azido and thiocyanato bridged Cu(II) coordination polymers, $[\text{Cu}(\text{L})(\mu\text{-}1,3\text{-N}_3)]_n(\text{ClO}_4)_n$ (**1**) and $[\text{Cu}(\text{L})(\mu\text{-}1,3\text{-NCS})]_n(\text{ClO}_4)_n$ (**2**) with a morpholine based tridentate N,N,N-donor Schiff base ligand, (1-methyl-1H-imidazol-2-yl)-N-[2-(morpholin-4-yl)ethyl]methanimine, (**L**), have been synthesized. Compounds **1** and **2** have been characterised by elemental analyses and different spectroscopic techniques. The X-ray single crystal structures of **1** and **2** show the formation of regular zigzag chains with $\mu\text{-}1,3\text{-azido}$ and $\mu\text{-}1,3\text{-thiocyanate}$ bridges, respectively. Variable temperature (2-300 K) magnetic studies indicate that **1** shows a ferromagnetic intrachain exchange interaction with $g = 2.135(2)$ and $J = 2.13(2) \text{ cm}^{-1}$; while in **2** this interaction is antiferromagnetic with $g = 2.1412(3)$ and $J = -0.277(2) \text{ cm}^{-1}$. X-band EPR spectra of **1** and **2** in frozen (143 K) DMF solution corroborate our magnetic studies.

1. Introduction

Design and synthesis of discrete polynuclear molecules and/or coordination polymers with efficient mediators are of contemporary interest from the viewpoint of magnetochemistry [1-6]. With diverse bridging modes, pseudo-halides are ubiquitous in mediating effective magnetic coupling [7-10]. Consequently, pseudo-halide bridged metal ligand complexes are of contemporary interest in the area of magnetic studies [11-14]. Magneto-structural correlation on these systems is often sought. In this context, azido and thiocyanato bridged complexes are noteworthy [15-24]. Two common bridging modes, μ -1,3 or end-to-end (EE) and μ -1,1 or end-on (EO), for azide and thiocyanate are shown in scheme IV.1. Such complexes with remarkable structural diversities manifest appealing magnetic behaviours [25-27]. A remarkable example, reported by Liu *et al.* in 2004, is a 1D polymeric chain with azido linkers displaying spin-canted long range ferromagnetic exchange due to significant interchain magnetic interaction and strong axial magnetic anisotropy [28]. Additionally, azido based 1D Cu(II) coordination polymers may also show applications in opto-electronic devices [29]. Due to their different coordination modes, the azido ligand may give rise to various structural topologies [30,31]. Although there are some exceptions, magnetic coupling is generally ferromagnetic for the μ -1,1 mode and antiferromagnetic for the μ -1,3 mode [32-36]. The μ -1,3 thiocyanate bridges are generally found in binuclear compounds that show double μ -1,3 thiocyanate bridges. Copper(II) compounds with single thiocyanate bridges are quite scarce [37-39].



Scheme IV.1. μ -1,3 (a, c) and μ -1,1 (b, d, e) bridging modes of azido and thiocyanato ligands.

The prime aim of this present work is to synthesize new copper based coordination assemblies with promising magnetic behaviour mediated through pseudo-halides as co-ligands. Morpholine based tridentate homoleptic Schiff base ligand has been found to be promising in this perspective [34]. The three nitrogen donor atoms of such type of ligand may offer efficient binding to 'hard' copper(II) center simultaneously. The present Schiff base ligand has been selected as it can form stable chelate ring through endo-cyclic N atom to bring about the desired

degree of stability and plasticity around the copper(II) center facilitating magnetic interaction. Here we report the syntheses, X-ray structure, spectroscopic and magnetic properties of two new 1D copper(II) coordination polymers formulated as $[\text{Cu}(\text{L})(\mu\text{-}1,3\text{-N}_3)]_n(\text{ClO}_4)_n$ (**1**) and $[\text{Cu}(\text{L})(\mu\text{-}1,3\text{-NCS})]_n(\text{ClO}_4)_n$ (**2**), formed with the morpholine based Schiff base ligand $\text{L} = (1\text{-methyl-}1\text{H-imidazol-}2\text{-yl})\text{-N-[}2\text{-(morpholin-}4\text{-yl)ethyl]methanimine}$. Compound **1** contains single $\mu\text{-}1,3$ azido auxiliary ligand; while single $\mu\text{-}1,3$ ambidentate thiocyanate moiety serves as the ancillary bridging ligand in **2**. Variable temperature magnetic studies have been performed on them. The observed magnetic behaviours of them have been substantiated through low temperature EPR measurements.

2. Experimental section

2.1. Reagents and instruments

Reagent grade 1-methyl-2-imidazolecarboxaldehyde and 4-(2-aminoethyl)morpholine were obtained from Sigma Aldrich, USA and were used as received. Other chemicals like sodium azide and sodium thiocyanate were also purchased from Sigma Aldrich and were used as received. The solvents were of spectroscopic grade. Elemental analyses (C, H and N) were performed on a Perkin Elmer 2400 II elemental analyser. FT-Infrared spectra (KBr pellet) ($400\text{--}4000\text{ cm}^{-1}$) were recorded on a Shimadzu FTIR 8400 spectrophotometer. UV-Vis spectra were recorded in acetonitrile solutions using a Shimadzu UV-1900I spectrophotometer. Solid state electronic spectra of both **1** and **2** were recorded on a PerkinElmer UV/VIS spectrophotometer (LAMBDA 35). Powder X-ray diffraction (PXRD) patterns of **1** and **2** were recorded on a Bruker D8 Advance X-ray diffractometer with Cu $\text{K}\alpha$ radiation ($\lambda = 1.548\text{ \AA}$) generated at 40 kV and 40 mA. 300 MHz ^1H and ^{13}C NMR spectra of **L** in CD_3OD solvent were measured on a Bruker NMR spectrometer. The ESI-MS (positive ion mode) were measured on a Waters HRMS model XEVO-G2QTOF#YCA351 mass-spectrometer. Room temperature electrical conductivity measurements of **1** and **2** in solution were measured on a calibrated direct reading conductivity meter (Systronics, India, model 304). Low temperature (143 K) EPR spectra of **1** and **2** were recorded with a Magnetech GmbH MiniScope MS400 spectrometer. The spectrometer was equipped with a temperature controller, TC H03. The spin resonance spectrometer was equipped with an FC400 frequency detector. Simulations of the EPR spectra were done using the EasySpin software package [40]. Variable temperature magnetic measurements were performed on polycrystalline samples of compounds **1** and **2** (with masses of 25.043 and 28.912 mg, respectively) with a Quantum Design MPMS-XL-5 SQUID susceptometer in the temperature range 2–300 K and with an applied magnetic field of 100 mT.

The isothermal magnetization was measured with the same samples at 2 K with applied magnetic fields in the range 0 to 5 T. The susceptibility data were corrected for the sample holder previously measured using the same conditions and for the diamagnetic contribution of the samples as deduced by using Pascal's constant tables [41].

2.2. Synthesis of (1-methyl-1H-imidazol-2-yl)-N-[2-(morpholin-4-yl)ethyl]methanimine (**L**)

1-methyl-2-imidazolecarboxaldehyde (55 mg; 0.5 mmol) was dissolved in 10 mL of methanol. 4-(2-aminoethyl)morpholine (65 mg; 0.5 mmol), dissolved in 10 mL of methanol, was added dropwise to the previous solution with continuous stirring. It was stirred for half an h to obtain a colourless solution. The resulting solution was refluxed for 4 h in presence of pre-activated molecular sieves (4 Å x 5 mm). After refluxing, the colourless reaction mixture was left in the air. After four days, the oily mass formed thereby was dried thoroughly keeping in a vacuum desiccator over anhydrous CaCl_2 .

Yield: 90 mg (81 %). $\text{C}_{11}\text{H}_{18}\text{N}_4\text{O}$: (222.14). Anal. Cal. for $\text{C}_{11}\text{H}_{18}\text{N}_4\text{O}$: C, 59.42; H, 8.16; N, 25.20 %. Found: C, 59.25; H, 8.35; N, 25.15 %; ^1H NMR (CD_3OD): δ (ppm): 8.28 (1H, s, azomethine proton), 7.19 (1H, d, for imidazole ring proton), 7.06 (1H, d, imidazole ring another proton), 4.00 (3H, s, N-methyl protons), 3.77 (2H, t, $-\text{CH}_2-$ protons close to morpholine ring N), 3.69 (4H, t, $-\text{CH}_2-$ proton of morpholine ring close to N), 2.71 (2H, t, $-\text{CH}_2-$ proton close to imine N), 2.56 (4H, t, $-\text{CH}_2-$ proton of morpholine ring close to O); ^{13}C NMR (CD_3OD): δ (ppm): 154.28(C5), 144.17(C6), 129.22(C8), 126.61(C7), 67.66(C1), 60.27(C3), 59.76(C2), 55.01(C4), 35.75(C9); FT-IR (KBr pellet): (v/cm^{-1}): 1648 (for $\text{C}=\text{N}$), 1440 (morpholine ring N). UV-Vis (CH_3CN): λ_{max} : 277 nm; ESI-MS (positive ion mode in CH_3OH) (m/z): (100%) ($\text{L}+\text{Na}^+$): 245.05 (Theo. 245.14).

2.3. Synthesis of $[\text{Cu}(\text{L})(\mu-1,3-\text{N}_3)]_n(\text{ClO}_4)_n$ (**I**)

The ligand **L** (22 mg; 0.1 mmol) was dissolved in 10 mL of methanol to have a colourless solution. The ligand solution was warmed at 40 °C for five min. $\text{Cu}(\text{ClO}_4)_2 \cdot 6\text{H}_2\text{O}$ (37 mg; 0.1 mmol), dissolved in 10 mL of methanol, was added dropwise to the warm solution of **L** with continuous stirring. After addition of metal solution, a light blue colour was imparted. The resulting reaction mixture was stirred for 30 min. After stirring, 5 mL aqueous solution of NaN_3 (6 mg; 0.1 mmol) was added dropwise to the resulting reaction mixture. On addition of sodium azide solution, the colour turned deep blue. The resulting solution was further stirred for 30 min. Finally, the solution was left in open air for slow evaporation. After 3 days, a dark green crystalline precipitate separated thereby was filtered and was washed thoroughly with chilled

diethyl ether. The compound is soluble in CH₃CN, DMF, DMSO and sparingly soluble in methanol; but it is insoluble in H₂O, THF, CHCl₃, DCM and *n*-hexane.

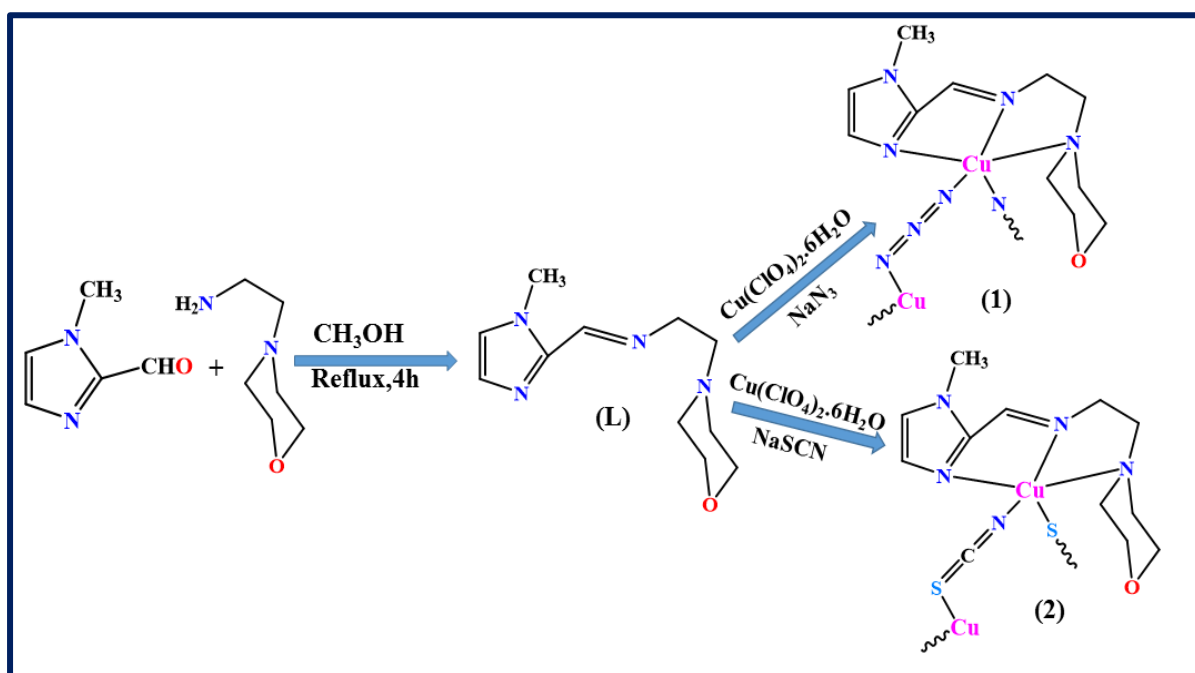
Yield: 36 mg (85 %); C₁₁H₁₈N₇O₅ClCu: (427.184), Anal. Cal. for C₁₁H₁₈N₇O₅ClCu: C, 30.90; H, 4.24; N, 22.94 %; Found: C, 30.98; H, 4.18; N, 22.97 %; FT-IR (KBr pellet): (ν/cm⁻¹): 1639 (for C=N), 2082, 2054 and 2036 (for azide), 1088 and 623 (for perchlorate); UV-Vis (CH₃CN): λ_{max} (nm) : 305, 385 and 669; Λ_M(CH₃CN): 119 ohm⁻¹ cm² mol⁻¹ (1:1 electrolyte).

2.4. Synthesis of [Cu(L)(μ-1,3-SCN)]_n(ClO₄)_n (2)

Compound **2** was synthesized following the same procedure and maintaining the same stoichiometric proportion as for **1**. Here, 5 mL of a methanolic solution of sodium thiocyanate (8 mg, 0.1 mmol) was employed in place of sodium azide. The compound is soluble in CH₃CN, CHCl₃, DMSO, THF and DMF but insoluble in H₂O, MeOH, EtOH, DCM, *n*-hexane and *n*-pentane.

Yield: 34 mg (77 %); C₁₂H₁₈N₅O₅SClCu: (443.37), Anal. Cal. for C₁₂H₁₈N₅O₅SClCu: C, 32.48; H, 4.09; N, 15.79 %; Found: C, 32.58; H, 4.05; N, 15.83 %; FT-IR (KBr pellet): (ν/cm⁻¹): 2089, 2104 (for thiocyanate), 1094 and 625 (for perchlorate), 1641 (for C=N); UV-Vis (CH₃CN): λ_{max} (nm): 308 and 680; Λ_M(CH₃CN): 125 ohm⁻¹ cm² mol⁻¹ (1:1 electrolyte).

Dark green needle shaped single crystals of **1** and **2**, suitable for X-ray diffraction, were harvested from their respective mother liquor. Preparation of the ligand and complexes are depicted in [scheme IV.2](#).



Scheme IV.2. Synthetic scheme of **L** and complexes, **1** and **2**.

Caution: The metal salts of perchlorate and azide with organic ligands are potentially explosive. They should be prepared and handled in small amount with utmost care [42,43].

2.5. Crystallographic data collection and refinement

Dark green needle shaped crystals of **1** and **2** were examined under a microscope. Good diffraction quality single crystals of both complexes were hand-picked from their respective bulk material. High resolution X-ray diffraction data, for **1** at room temperature, and for **2** at low temperature (104 K), were collected on a Bruker-Kappa APEX II CCD diffractometer. The instrument was equipped with a CCD detector. Graphite mono-chromated MoK α (0.71073 Å) radiation was used. The unit cell parameters were determined employing SMART software [44]. Empirical absorption corrections were made using SADABS [45]. The structures were solved using direct methods with the SHELXL-97 program package [46]. Subsequent difference Fourier synthesis and least-square refinement revealed the positions of the remaining non-hydrogen atoms, that were refined anisotropically. Crystal data and structural refinement parameters for **1** and **2** are given in Table IV.1.

Table IV.1. Crystal data and structure refinement for **1** and **2**

CCDC NO.	2112634	2112635
Empirical formula	C ₁₁ H ₁₈ CuN ₇ O ₅ Cl	C ₁₂ H ₁₈ ClCuN ₅ O ₅ S
Formula weight	427.32	443.37
Temperature [K]	273	104
Wavelength [Å]	0.71073	0.71073
Crystal system	Orthorhombic	Monoclinic
Space group	<i>P</i> 2 ₁ 2 ₁ 2 ₁ (#19)	<i>P</i> 2 ₁ / <i>c</i> (#14)
<i>a</i> [Å], <i>b</i> [Å] and <i>c</i> [Å],	6.928(5), 13.564(10) and 18.606(15)	10.84(16), 6.27(9) and 24.82(4)
α [°], β [°] and γ [°]	90, 90 and 90	90, 91.904(5) and 90
Volume [Å ³]	1748.40 (2)	1687.8 (4)
<i>Z</i>	4	4
ρ_{calcd} [mg/cm ³]	1.62	3.59
Absorption coefficient [mm ⁻¹]	1.44	8.03
<i>F</i> (000)	876	1764
θ range for data collection [deg]	2.655 to 27.187	3.049 to 25.076
Limiting indices	-8 < <i>h</i> < 8 -17 < <i>k</i> < 16 -23 < <i>l</i> < 23	-12 < <i>h</i> < 12 -6 < <i>k</i> < 7 -29 < <i>l</i> < 29

Reflections collected/unique	15725/3857 [R _{int} = 0.0363]	11744/2949 [R _{int} = 0.0717]
Completeness of theta	99.4 % (25.242)	98.5% (25.076)
Data / restraints / parameters	3857 / 0 / 272	2949 / 13 / 227
Goodness-of-fit on F ²	1.048	1.188
Final R indices [I>2sigma (I)]	R ₁ = 0.0309 wR ₂ = 0.0686	R ₁ = 0.0960 wR ₂ = 0.2220
R indices (all data)	R ₁ = 0.0380 wR ₂ = 0.0723	R ₁ = 0.1066 wR ₂ = 0.2277
Largest diff. peak and hole	0.212 and -0.225 e.A ⁻³	1.912 and -1.126 e.A ⁻³

Some selected bond lengths and bond angles are listed in [Table IV.2](#).

Table IV.2. Some selected bond lengths (Å) and bond angles (°) for **1** and **2**

Complex 1			
Bond	Distance (Å)	Angle	Angle (°)
Cu1-N2	2.026(3)	N2-Cu1-N4	163.39(11)
Cu1-N3	1.963(3)	N2-Cu1-N7	90.06(13)
Cu1-N5	1.951(3)	N3-Cu1-N2	81.05(12)
Cu1-N4	2.075(3)	N3-Cu1-N4	82.34(12)
Cu1-N7	2.392(4)	N3-Cu1-N7	95.63(14)
		N5-Cu1-N2	100.53(13)
		N5-Cu1-N3	167.45(13)
		N5-Cu1-N4	95.68(12)
Complex 2			
Bond	Distance (Å)	Angle	Angle (°)
Cu1-S1	2.719(3)	N5-Cu1-S1	93.92(2)
Cu1-N5	2.092(8)	N3-Cu1-S1	93.62(2)
Cu1-N3	2.043(8)	N3-Cu1-N5	161.80(3)
Cu1-N4	1.965(8)	N4-Cu1-S1	95.70(3)
Cu1-N6	1.929(8)	N4-Cu1-N5	82.20(3)
		N4-Cu1-N3	80.50(3)
		N6-Cu1-S1	96.90(3)
		N6-Cu1-N4	167.30(4)

Symmetry code: Complex **1**: ½-x, -y, ½+z; Complex **2**: ½-x, ½+y, ½+z

3. Results and discussion

3.1. Syntheses of the complexes

Equimolar reaction of the morpholine based Schiff base ligand (**L**) with copper(II) perchlorate hexahydrate in methanol followed by the addition of stoichiometric amount of sodium azide or sodium thiocyanate afforded, respectively, the polynuclear Cu(II) complexes, **1** and **2**, in satisfactory yield. The ligand was characterised by elemental analysis, ESI-MS (Fig. IV.1), FT-IR and UV-Vis spectroscopy.

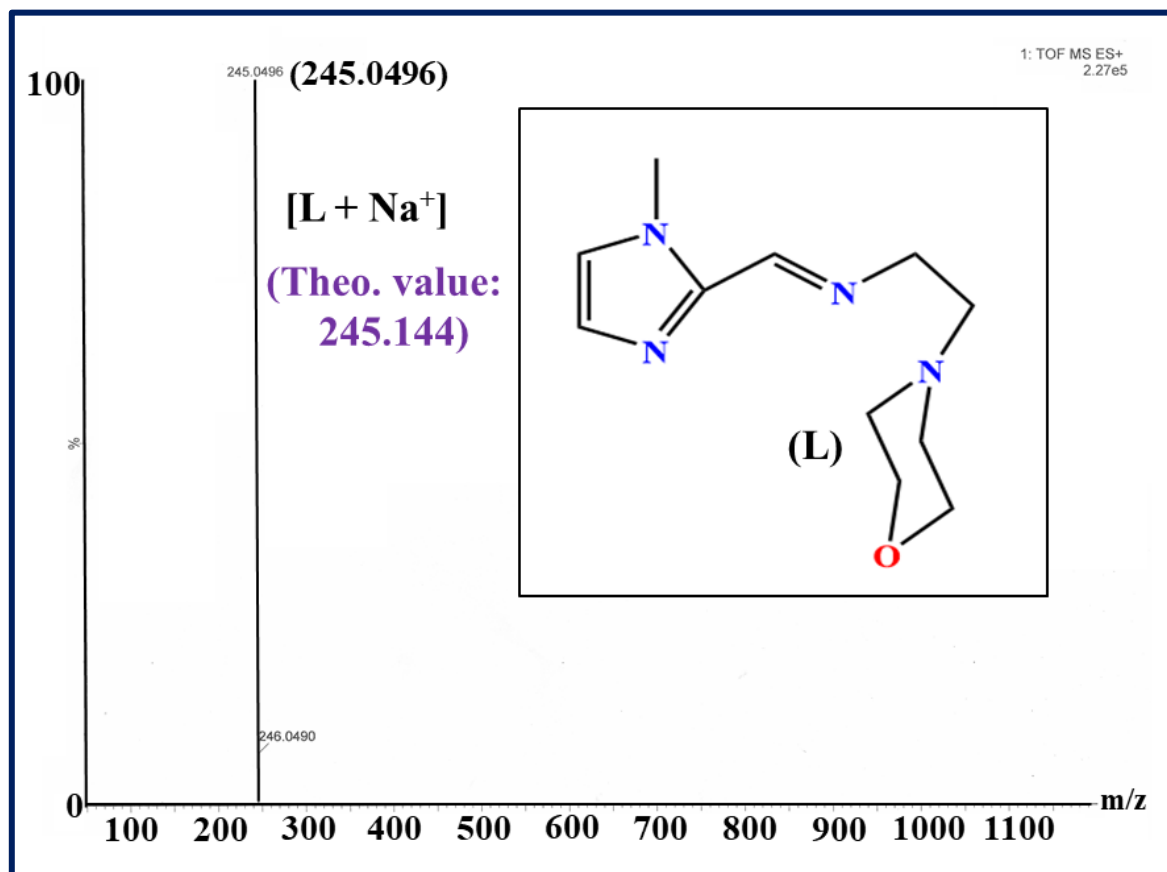
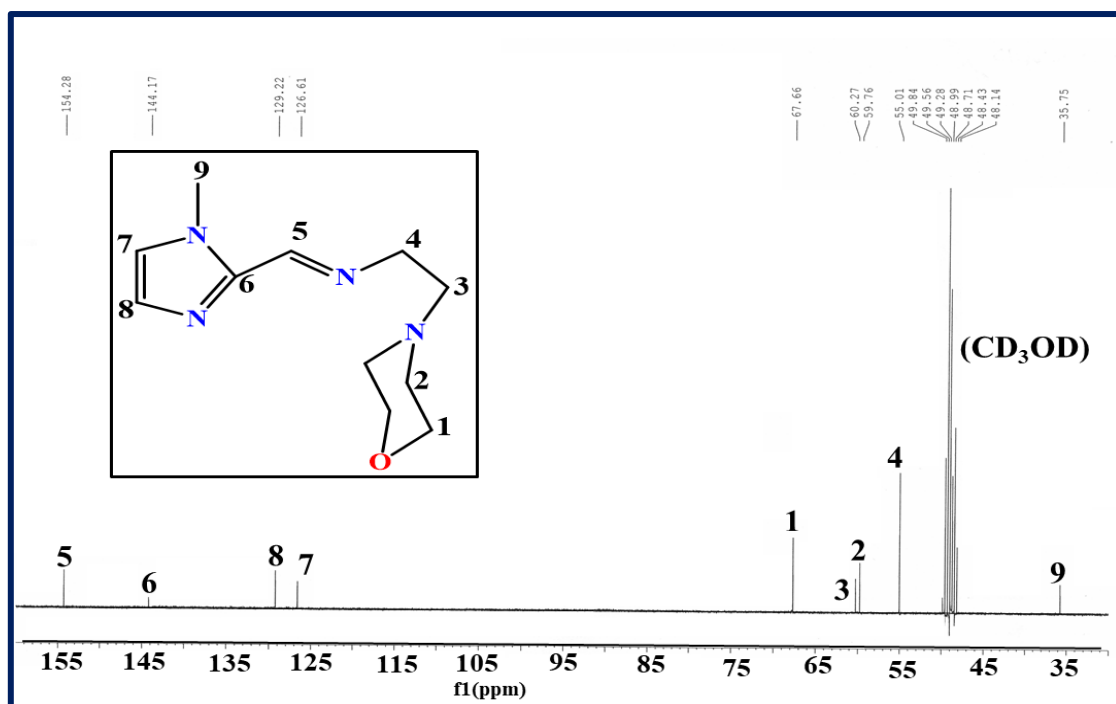
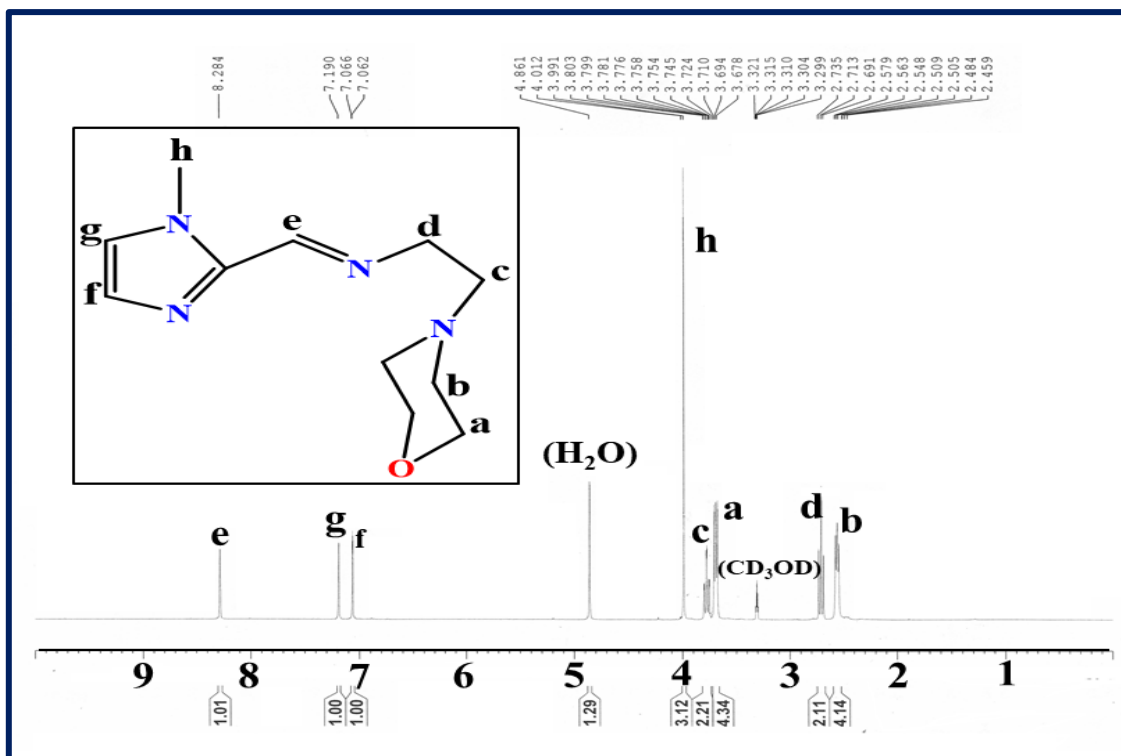


Fig. IV.1. ESI-MS of **L** in methanol.

The complexes were characterised by single crystal X-ray diffraction studies. Additionally, the formation of the ligand was confirmed by ¹H (Fig. IV.2) and ¹³C (Fig. IV.3) NMR spectra.



3.2. Infrared spectra

The FT-IR spectrum of the ligand shows a characteristic band at 1648 cm^{-1} (Fig. IV.4), assigned to the imine ($-\text{C}=\text{N}-$) stretching vibration, that appears at 1639 cm^{-1} in **1** and 1641 cm^{-1} in **2**, suggesting the coordination of the azomethine N atom to the copper(II) centre [47].

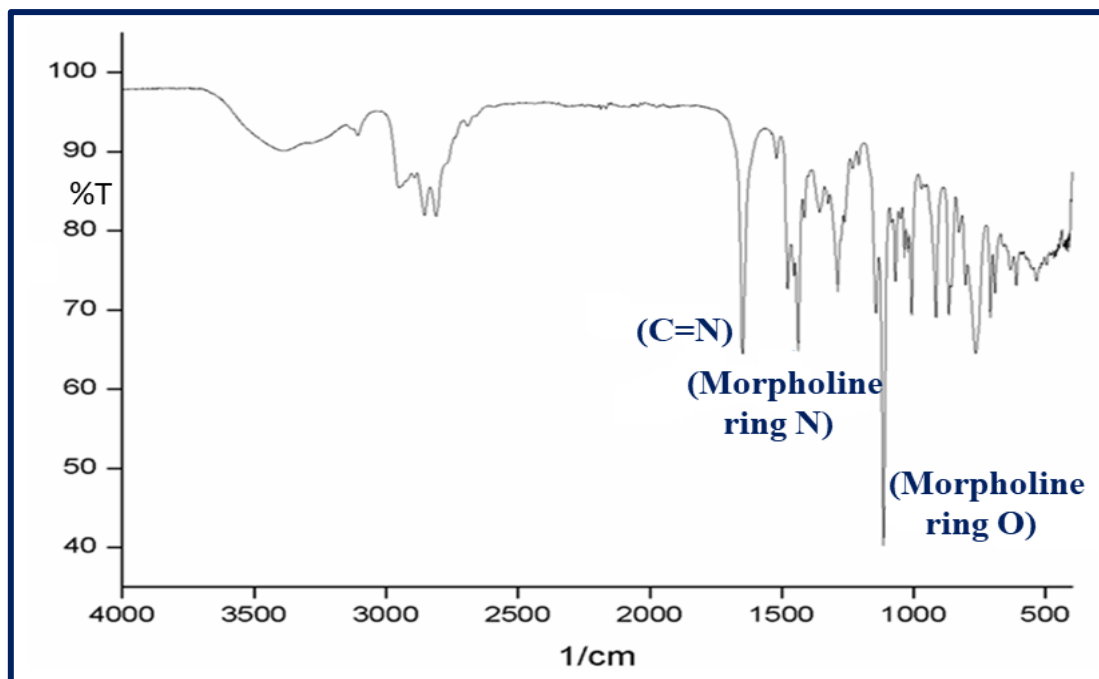


Fig. IV.4. FT-IR spectrum of L.

The three bands at 2083, 2054 and 2037 cm^{-1} in **1** correspond to the μ -1,3 coordinated azido bridge [48]. Complex **2** shows two bands, at 2089 and 2104 cm^{-1} , corresponding to N- and S-bonded thiocyanate bridge, respectively [24, 49-52]. Broad bands at 1088 cm^{-1} in **1** and 1094 cm^{-1} in **2** can be assigned to the asymmetric stretching vibration of non-coordinated perchlorate ion [53,54]. The FT-IR spectra of both **1** and **2** are shown in Figs. IV.5 and IV.6, respectively.

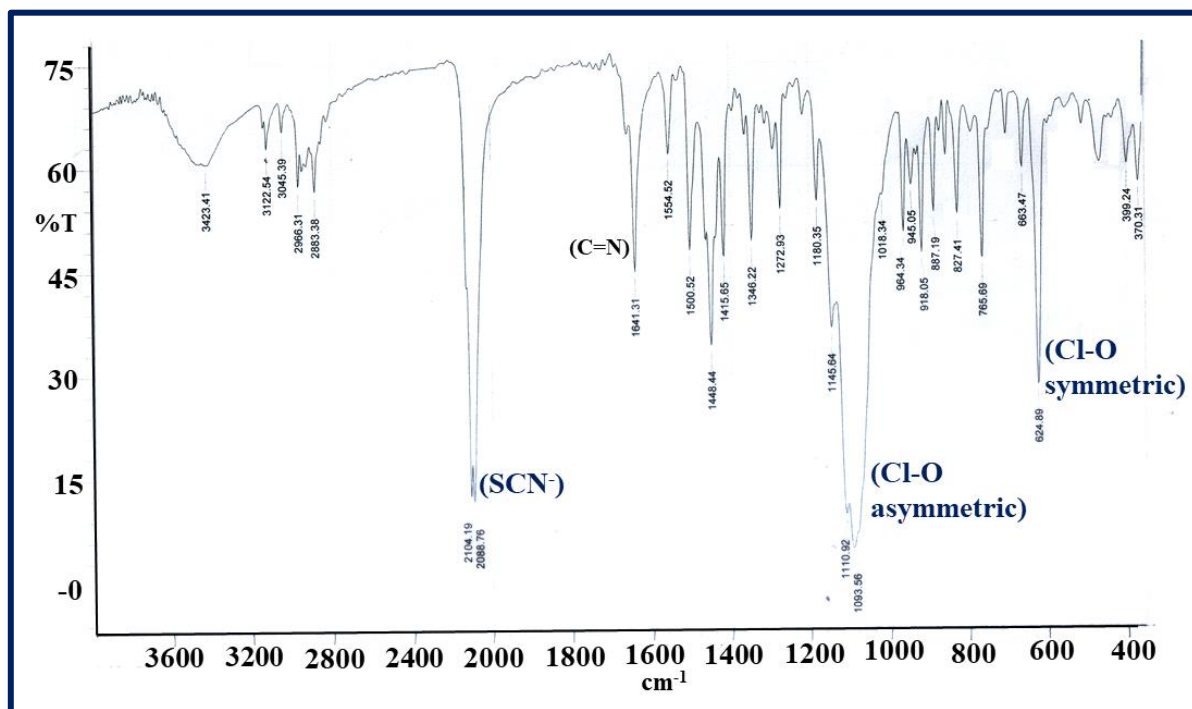


Fig. IV.5. FT-IR spectrum of complex 1.

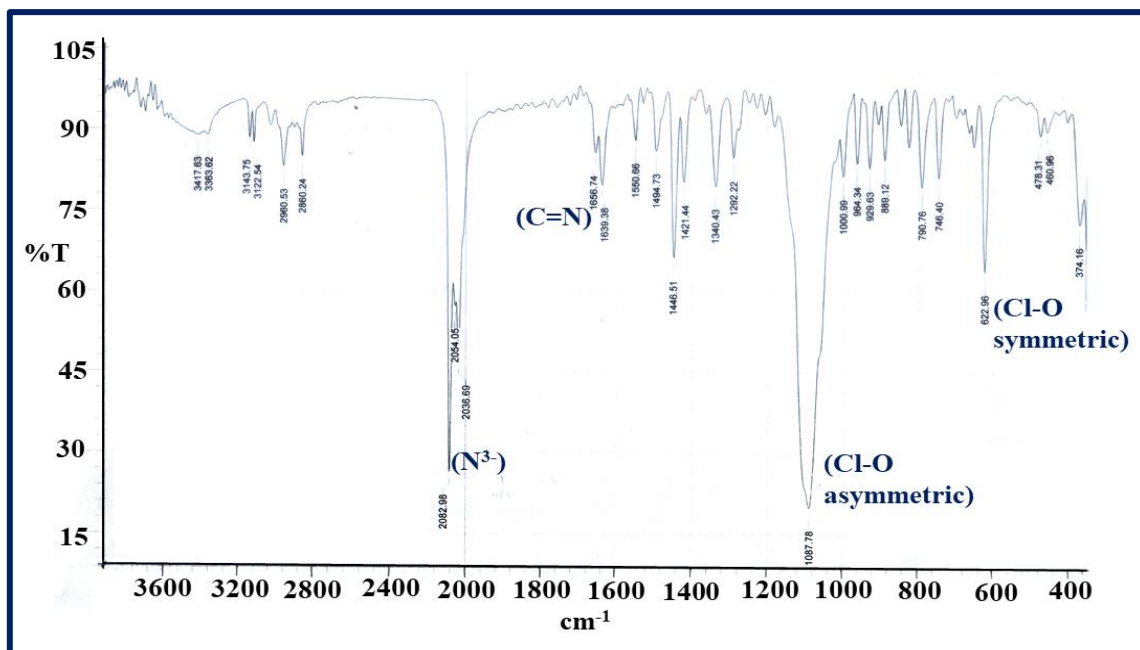


Fig. IV.6. FT-IR spectrum of complex 2.

3.3. Electronic spectra

The electronic spectra of the ligand and its complexes, **1** and **2**, were recorded in acetonitrile solution (Fig. IV.7). The ligand shows a sharp absorption band at 277 nm attributed to a $\pi\text{-}\pi^*$ transition [55]. In compounds **1** and **2**, this transition is shifted respectively to 305 and 308 nm indicating ligand binding. Much weaker but broad transition bands are observed at 669 and 680 nm respectively for **1** and **2**. These are assigned to d-d transition bands. Generally, broad d-d transition band appears at lower energy region below 700 nm. The position and the energetics of this band is characteristic of square-pyramidal copper(II) complexes [56].

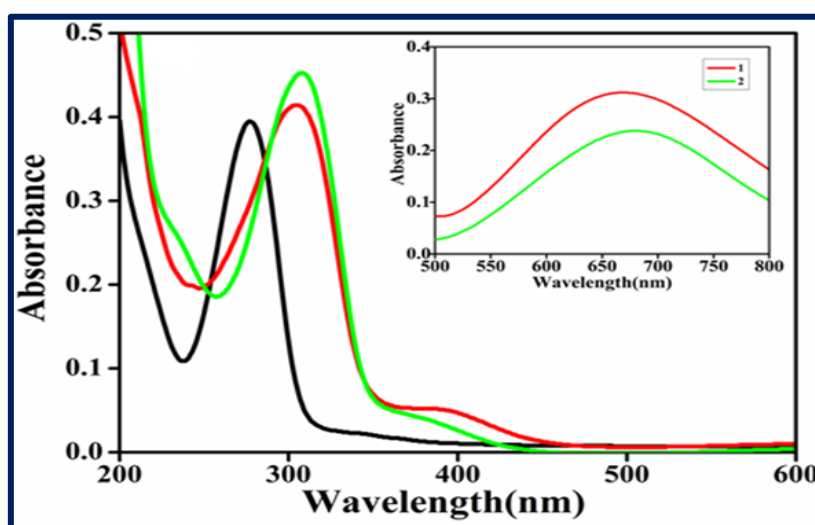


Fig. IV.7. Electronic spectra of **L** (black), **1** (red) and **2** (green) in acetonitrile. Inset: d-d band of **1** and **2**.

3.4. Powder X-ray diffraction

In order to check the phase purity of the bulk materials with that of the simulated patterns (obtained from single crystal structures), we have performed powder X-ray diffraction analyses of both compounds at room temperature. In both compounds, the match between the experimental and simulated powder X-ray diffraction patterns confirms the phase purity of the samples (Figs. IV.8 and IV.9).

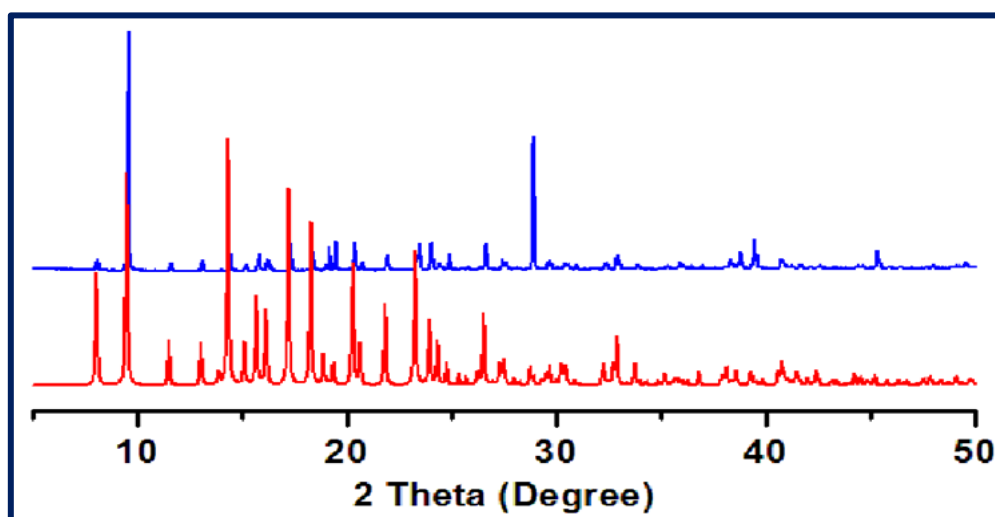


Fig. IV.8. Powder X-ray diffraction pattern of **1**. (red: simulated, blue: as synthesized).

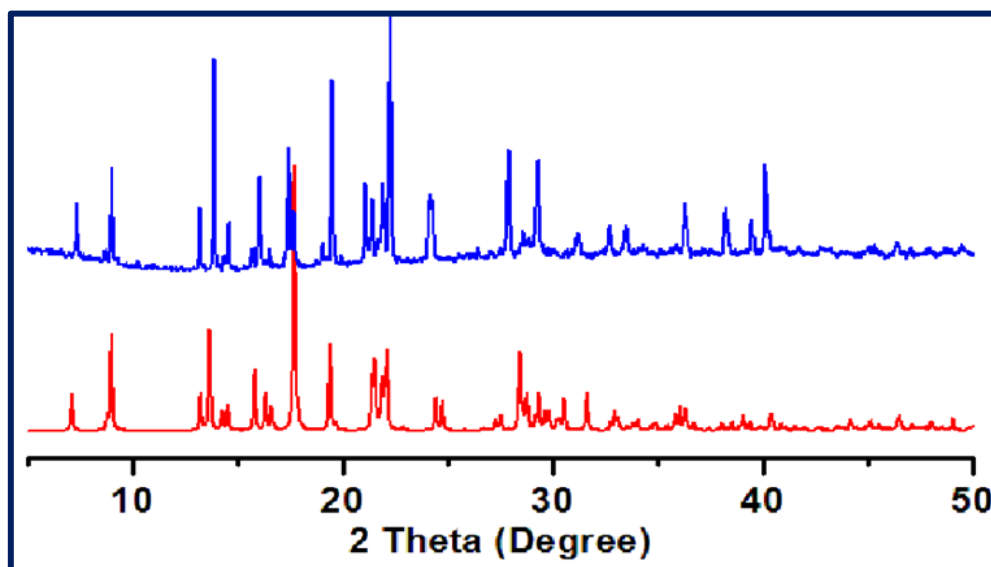


Fig. IV.9. Powder X-ray diffraction pattern of **2**. (red: simulated, blue: as synthesized).

3.5. Crystal structures of compounds **1** and **2**

Single crystal X-ray diffraction data shows that compound **1** crystallizes in the orthorhombic space group $P2_12_12_1$ (#19); whereas compound **2** crystallizes in the monoclinic space group $P2_1/c$ (#14) (Table IV.1). The asymmetric unit of compound **1** contains one **L** ligand, one N_3^-

bridging ligand, one Cu(II) ion and a free ClO_4^- anion, slightly disordered over two very close positions sharing one common oxygen atom (Fig. IV.10a). The asymmetric unit of compound **2** is very similar: it contains one **L** ligand, one SCN^- bridging ligand, one Cu(II) ion and a free (ordered) ClO_4^- anion (Fig. IV.10b).

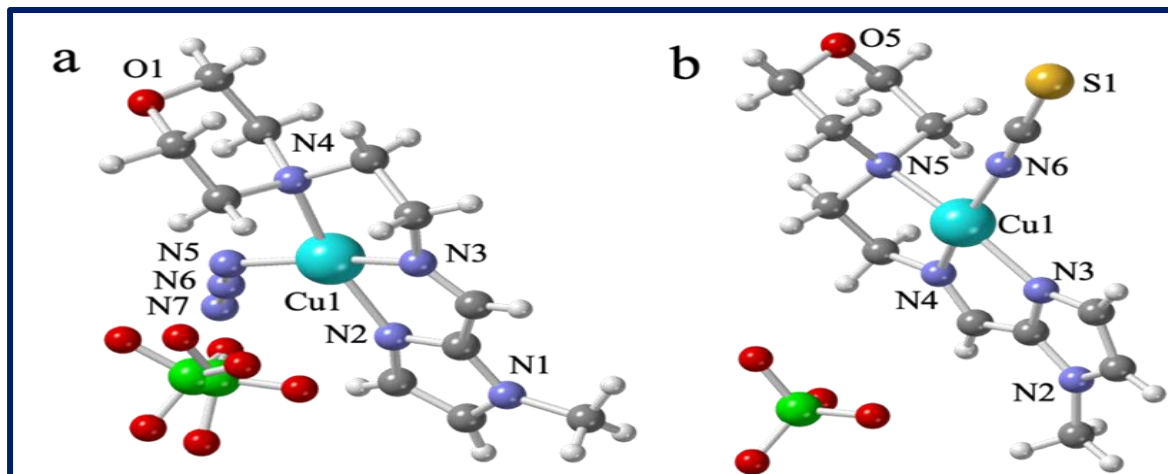


Fig. IV.10. Asymmetric unit of compounds **1** (a) and **2** (b) with the labelling of the main atoms.

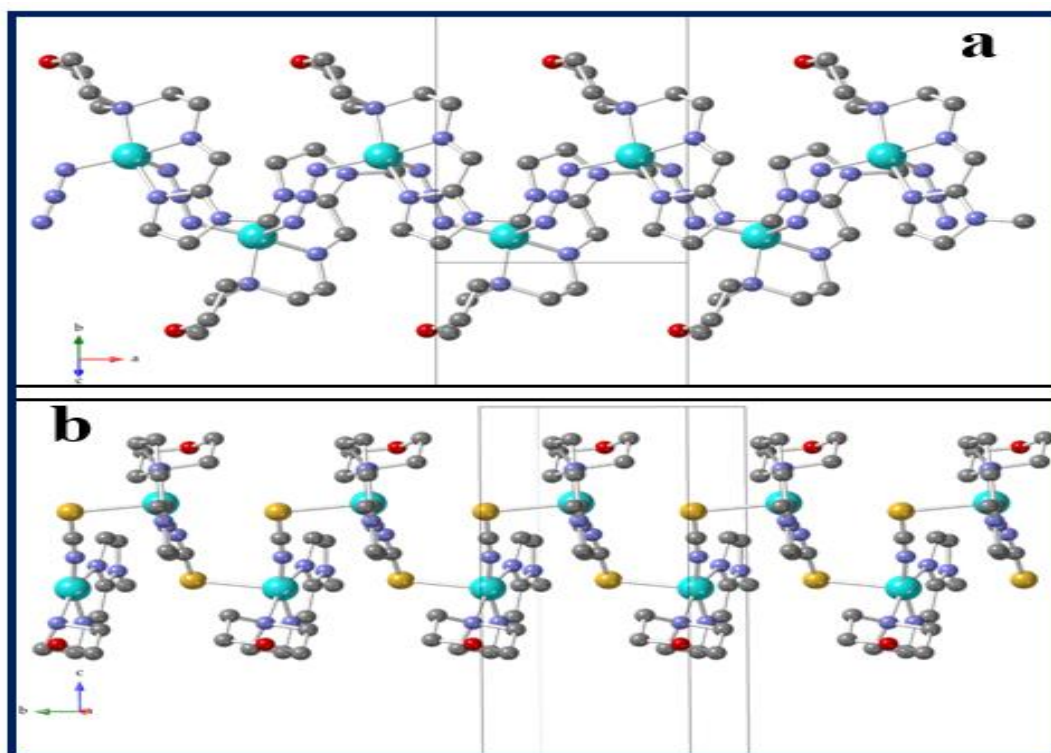


Fig. IV.11. 1D chain-like structures in **1** (a) (single end-to-end azido bridged) and in **2** (b) (single end-to-end thiocyanato bridged). ClO_4^- anions and H atoms are omitted for clarity. Colour code: Cu = light blue, O = red, N = blue, S = yellow and C = grey.

In both compounds the Cu(II) centres are chelated by the Schiff base ligand (**L**), acting as a tridentate chelating N_3 -donor. In compound **1** the Cu(II) ion is also coordinated to two azido

anions that acts as single μ -1,3 bridges, giving rise to regular zigzag chains running along the *a* direction (Fig. IV.11a).

The disordered ClO_4^- anion is semi-coordinated to the Cu(II) ion with a long Cu-O distance of 2.971(4) Å. Compound **2** also presents a zigzag regular chains (running along the *b* direction) where the μ -1,3- N_3^- bridges have been replaced by μ -1,3- SCN^- bridges (Fig. IV.11b).

If we neglect the semi-coordinated ClO_4^- anion in **1**, we can consider that the Cu(II) ions in both compounds are penta-coordinated with CuN_5 and CuN_4S chromophores in **1** and **2**, respectively. In both compounds the coordination geometry is a slightly distorted square pyramid, as indicated by their low Addison parameters (0.06 in **1** and 0.09 in **2**) [57,58]. In both compounds the basal plane is formed by the three N atoms of **L** and by one N atom of a bridging azide (in **1**) or thiocyanate (in **2**). The axial position is occupied by a N atom of the other azide bridge in **1** or by the S atom of the other thiocyanate bridge in **2** (Fig. IV.11). Packing diagram of **1** is shown in Fig. IV.12.

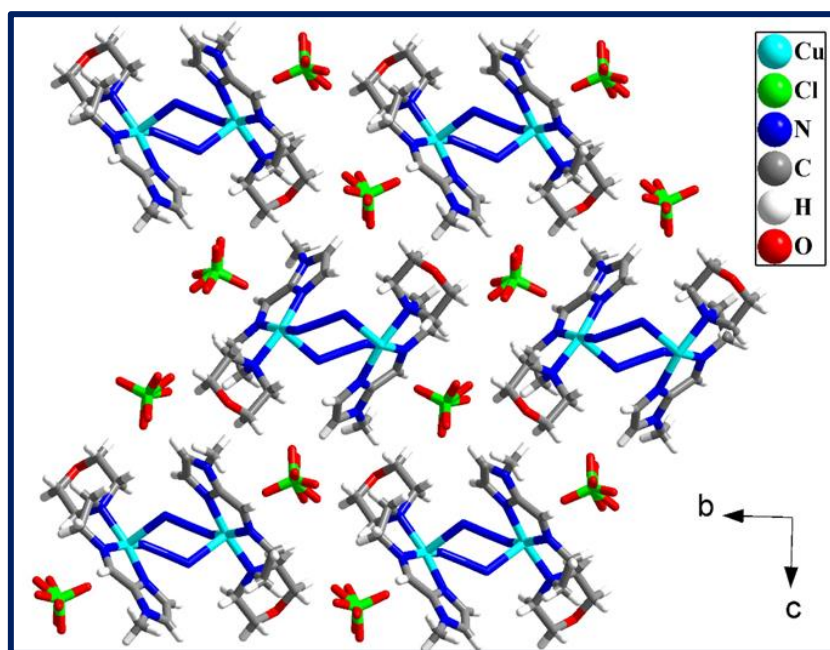


Fig. IV.12. Packing diagram of azido bridged copper(II) polymer (**1**) when it is viewed along the crystallographic *a* axis.

As usually observed, in **1** the axial Cu1-N7 bond is significantly longer (2.392(4) Å) than the basal ones (Cu1-N2 = 2.026(3) Å, Cu1-N3 = 1.963(3) Å, Cu1-N4 = 2.075(3) Å and Cu1-N5 = 1.951(3) Å, Table IV.2) [59-61]. In **2**, the axial Cu1-S1 bond (2.719(3) Å) is also much longer than the basal Cu-N bonds (Cu1-N3 = 2.043(8) Å, Cu1-N4 = 1.965(8) Å, Cu1-N5 = 2.092(8) Å and Cu1-N6 = 1.929(8) Å). These values are consistent with those found in the literature [62]. The intrachain Cu...Cu distance in **1** is 5.7200(6) Å whereas in **2** this

distance is 5.728(9) Å, both within the normal range (5.27-6.62 Å) observed in other similar Cu(II) single-bridged chain compounds [24, 39].

3.6. Magnetic properties

The thermal variation of the $\chi_m T$ product for **1** (χ_m is the molar magnetic susceptibility per Cu(II) ion) shows a room temperature value of *ca.* 0.42 cm³ K mol⁻¹, which is the expected value for an isolate $S = 1/2$ Cu(II) ion. When the sample is cooled, $\chi_m T$ remains nearly constant down to around 50 K and it shows a progressive increase at lower temperatures, reaching a value of 0.95 cm³ K mol⁻¹ at 2 K (Fig. IV.13a). This behaviour indicates the presence of a weak intrachain Cu...Cu ferromagnetic interaction and, accordingly, we have fitted the magnetic data to a simple $S = 1/2$ regular ferromagnetic chain model. This model reproduces very satisfactorily the magnetic data in the whole temperature region with $g = 2.135(2)$ and $J = 2.13(2)$ cm⁻¹ (solid line in Fig. IV.13a, the Hamiltonian is written as $H = -J \sum [S_i S_{i+1}]$).

The ferromagnetic coupling is further confirmed by the isothermal magnetization at 2 K that shows a rapid increase with increasing fields, well above the expected behaviour for two independent $S = 1/2$ centres (solid line in Fig. IV.13b).

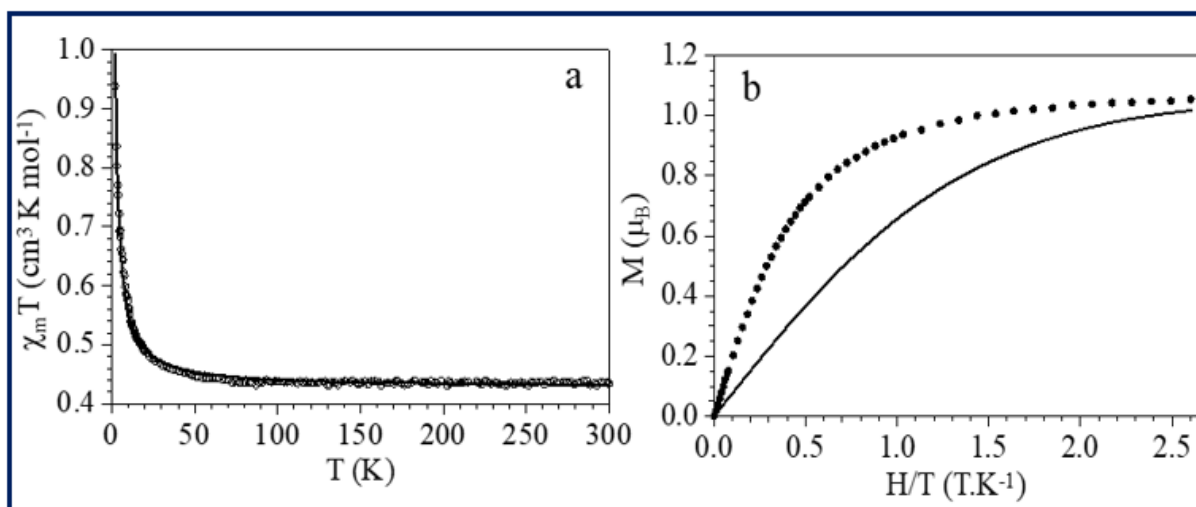


Fig. IV. 13. (a) Thermal variation of the $\chi_m T$ product for compound **1**. Solid line is the fit to the model. (b) Isothermal magnetization at 2 K for compound **1**. Solid line is the best fit to a Brillouin function for a $S = 1/2$ ion.

As observed in compound **1**, the $\chi_m T$ product for compound **2** also shows a room temperature value close to 0.42 cm³ K mol⁻¹, the expected one for an isolated $S = 1/2$ Cu(II) ion (Fig. IV.14a). This value remains constant down to *ca.* 10 K and below this temperature it shows a progressive decrease to reach a value of 0.38 cm³ K mol⁻¹ at 2 K. This behaviour indicates that compound **2** presents a very weak antiferromagnetic intrachain Cu...Cu interaction.

Accordingly, we have fitted the magnetic properties to a simple $S = 1/2$ antiferromagnetic regular chain [63]. This model reproduces very satisfactorily the magnetic data in the whole temperature range with $g = 2.1412(3)$ and $J = -0.277(2) \text{ cm}^{-1}$ (solid line in Fig. IV.14a, the Hamiltonian is written as $H = -J \sum [S_i S_{i+1}]$). This very low J value confirms that the coupling is very weak and antiferromagnetic.

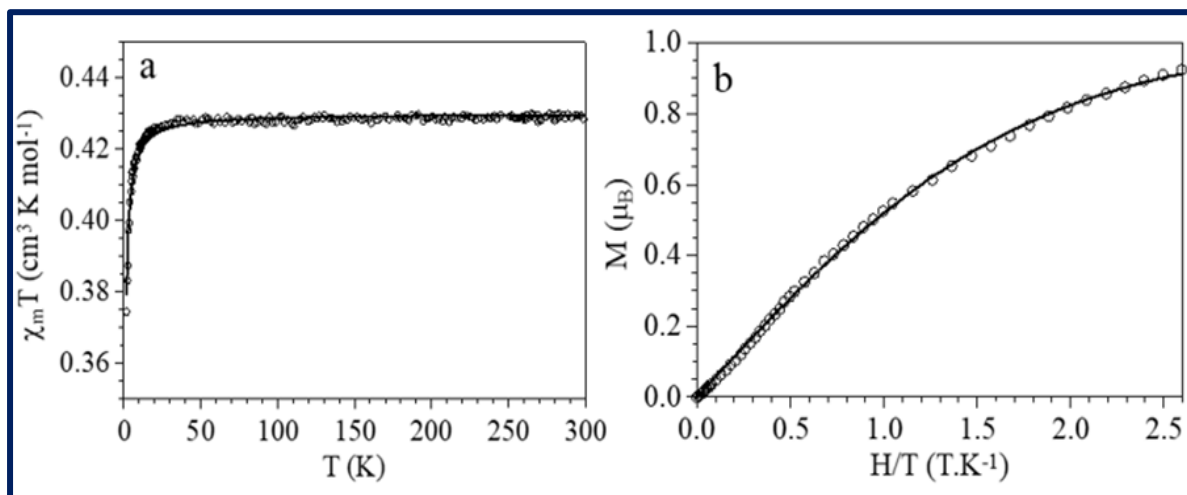


Fig. IV.14. (a) Thermal variation of the $\chi_m T$ product for compound **2**. Solid line is the fit to the model. (b) Isothermal magnetization at 2 K for compound **2**. Solid line is the best fit to a Brillouin function for a $S = 1/2$ ion.

A confirmation of the very weak antiferromagnetic coupling is provided by the isothermal magnetization at 2 K that can be well reproduced with the Brillouin function with $g = 2.03(1)$ and a very weak antiferromagnetic interaction of $-0.29(3) \text{ cm}^{-1}$ (solid line in Fig. IV.14b).

3.7. Coupling mechanism

For d^9 Cu(II) systems, the magnitude of the super-exchange phenomenon is strongly dependent on the bridging mode between the copper centres. Generally, μ -1,3 coordination mode of azido bridges gives rise to antiferromagnetic coupling for different types of metals [1, 64,65]. The e_g atomic orbitals are involved in this super-exchange mechanism. The coupling is strongly antiferromagnetic when the pseudo-halide ligand is bonded to equatorial coordination sites in both copper(II) ions (EE) since the $d_{x^2-y^2}$ orbitals of both Cu(II) ions are involved in this exchange mechanism. In contrast when the azido bridge connects an axial position with an equatorial one (EA), the coupling is much weaker since the overlap between the $d_{x^2-y^2}$ and d_z atomic orbitals is very small.

In compounds **1** and **2** the coordination geometry of the Cu(II) ions is square-pyramidal and the pseudohalide bridging ligand connects an axial with an equatorial coordination site (EA). So, we expect weak coupling between the copper(II) centres. The interaction may be ferro- or

antiferromagnetic depending on their bond parameters in the bridging region. The maximum antiferromagnetic coupling occurs when the M-N-N bond angle is close to 110°. Accidental ferromagnetic coupling interaction may be found for larger bond angles. In **1**, the M-N-N bond angles are 124.2(3)° and 124.0(3)°. These values are similar to those found in other singly μ -1,3-N₃ bridged Cu(II) compounds, where very weak ferromagnetic couplings have been observed, as in **1** (Table IV.3).

Table IV.3. Structural and magnetic parameters for single or double (1,3) bridging azide ligand in Cu(II) complexes

Compounds	Cu···Cu (Å)	Cu-N (Å)	Cu-N (Å)	Cu-N-N (°)	Geom	Mode	J/cm ⁻¹	Ref.
[Cu(N ₃) ₂ (mtn)] _n	6.745	2.708	2.014	87.39	OC	EA	15.6/-2.6	66
[Cu(L1)(μ -1,3-N ₃)] _n (ClO ₄) _n	—	2.266	1.991	136.7	SP	EA	2.69	67
[Cu(L2)(μ -1,3-N ₃)] _n (ClO ₄) _n	—	2.398	1.946	122.5	SP	EA	2.02	67
[Cu ₂ (L2) ₂ (μ -1,3-N ₃) ₂ (ClO ₄) ₂]	5.746	2.950	2.037	123.0	OC	EA	2.4	68
[Cu(L1)(N ₃)] _n (ClO ₄) _n	—	2.355	1.947	126.5	SP	EA	2.15	34
[Cu(L2)(N ₃)] _n (ClO ₄) _n	5.630	2.311	1.965	131.2	SP	EA	3.61	34
1	5.720	2.392	1.951	124.2	SP	EA	2.14	This work

Abbreviations used: mtn = N-methyl-1,3-propane diamine, OC = octahedral geometry, SP = square pyramidal geometry, EA = equatorial-axial bridge. [Cu(L1)(μ -1,3-N₃)]_n(ClO₄)_n, L1 = N,N,2,2,-tetramethyl-3-((pyridine-2-ylmethylene)amino)propan-1-amine; [Cu(L2)(μ -1,3-N₃)]_n(ClO₄)_n, L2 = N,N-dimethyl-2-((pyridine-2-ylmethylene)amino)propan-1-amine; [Cu₂(L2)₂(μ -1,3-N₃)₂(ClO₄)₂], L2 = N,N-dimethyl-3-((pyridine-2-ylmethylene)amino)propan-1-amine; [Cu(L1)(N₃)]_n(ClO₄)_n, L1 = N,N-dimethyl-2-((pyridine-2-ylmethylene)amino)ethan-1-amine; [Cu(L2)(N₃)]_n(ClO₄)_n, L2 = N,N-diethyl-2-((pyridine-2-ylmethylene)amino)ethan-1-amine.

In compound **2**, the M-N-C and M-S-C angles are 175.0(9)° and 94.8(4)°, respectively. These values are similar to those found in other Cu(II) compounds with a single μ -1,3 thiocyanato bridge, that show very weak antiferromagnetic couplings, as observed in compound **2** (Table IV.4).

Table IV.4. Structural and magnetic parameters for the single or double (1,3) bridging thiocyanate ligand in Cu(II) complexes

Compound	Cu...Cu (Å)	Cu-S (Å)	Cu-N (Å)	Cu-S-N (°)	Cu-N-C (°)	Geom	Mode	J/cm ⁻¹	Ref
[AsPh ₄][Cu(SCN) ₃]	5.549 5.559	2.775 2.409	1.966 1.930	98.2 104.1	163.8 165.9	SP	EE EA	-90	69
[{Cu(L)(NCS) ₂ }] _n	5.599	2.770	1.960	97.6	146.5	SP	EA	0	70
[Cu(pyim)(NCS) ₂] _n	6.079	3.174	1.956	104.1	167.1	SP	EA	-0.03	71
[Cu ₂ (bpm)(NCS) ₂] _n	5.328	3.174	1.941	83.1	165.0	OC	EA	-0.6	72
[CuL(μ _{1,3} -NCS)] _n	6.628	2.806	1.954	111.3	173.2	SP	EA	-0.57	73
2	5.728	2.719	1.929	94.8	175	SP	EA	-0.28	This work

Abbreviations used: pyim = 2-(2'-pyridyl)imidazole; bpm = 2,2' bipyrimidine; OC = octahedral geometry, SP = square pyramidal geometry, EA = equatorial-axial bridge; EE = equatorial-equatorial bridge; [{Cu(L)(NCS)₂}]_n, L = 2-methylamino-5-pyridin-2-yl-1,3,4-oxadiazole; [CuL(μ_{1,3}-NCS)]_n, L = 3-((2-(dimethylamino)ethyl)imino)-1-phenylbutan-1-one.

3.8. EPR spectra

EPR spectra of compounds **1** and **2** were recorded from frozen solution in DMF solvent. The magnetic resonance parameters of **1** and **2** are shown in Table IV.5. Both EPR spectra as obtained from frozen solution are characteristic of single μ-1,3 azido and thiocyanato bridged Cu(II) polymers, respectively, due to the d⁹ configuration of Cu(II) complexes with S = 1/2 spin state (Fig. IV.15). Compound **1** shows a rhombic spectrum with g₁ > g₂ ≈ g₃ (Table IV.5), whereas compound **2** shows an axial spectrum with g₁ > g₂ = g₃, (Table IV.5). Both compounds show a hyperfine coupling of the unpaired electron with the I = 3/2 ⁶³Cu and ⁶⁵Cu nuclei, with much higher values for A₁ (Fig. IV.15 and Table IV.5) [74]. The magnetic resonance parameters obtained for **1** and **2** fully agree with the idea that the unpaired electron is located on the d_{x²-y²} orbital [75-77].

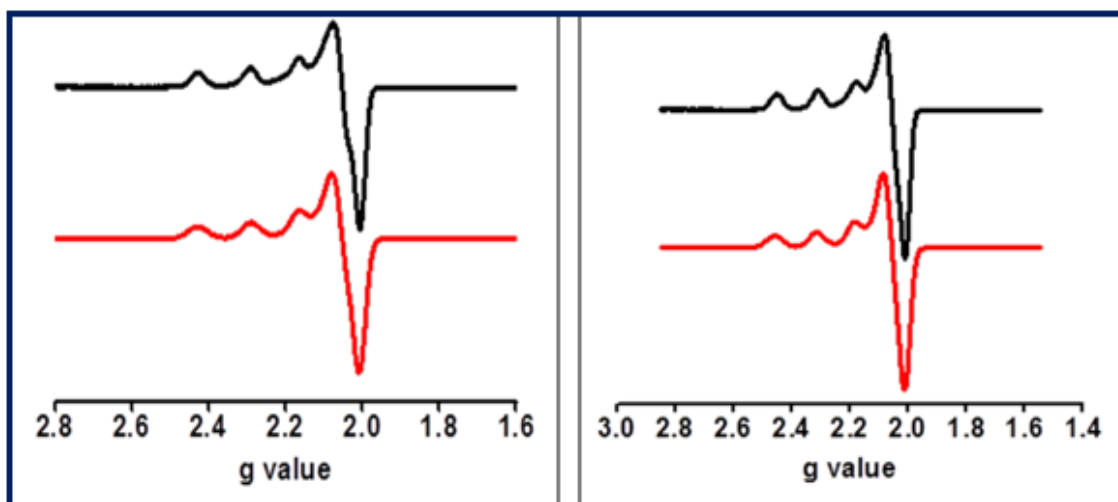


Fig. IV.15. Experimental (black line) and simulated (red line) X-band EPR spectra of **1** (left) and **2** (right) obtained at 143 K in frozen DMF solution.

Table IV.5. Magnetic parameters for **1** and **2**

Complex	g values			A values (G)			Line width (G)
	g_1	g_2	g_3	A_1	A_2	A_3	
1	2.2284	2.0602	2.0519	172.29	17.85	1.77	5.8
2	2.2501	2.0573		177.32	14.85		6.4

4. Conclusions

In summary, the use of azide and thiocyanate as bridging ligands in combination with a morpholine-based tridentate N,N,N-donor Schiff base ligand leads to the formation of two new 1D copper(II) coordination polymers. Compound **1** contains single μ -1,3 azide bridges while **2** contains single μ -1,3 thiocyanate bridges. The magnetic susceptibility measurements reveal the presence of a weak ferromagnetic Cu...Cu intrachain interaction in **1** and a weak antiferromagnetic coupling in **2**, through the single μ -1,3 N_3^- and SCN^- bridges, respectively. Low temperature EPR spectra along with their simulation also corroborate the observed magnetic properties.

5. References

1. O. Kahn, Molecular Magnetism, VCH, Weinheim, 1993.
2. J.S. Miller, M. Drilon, Magnetism: Molecules to Materials, Eds. Wiley-VCH: Weinheim, 2002.
3. T.C. Stamatatos, G.S. Papaefstathiou, L.R. MacGillivray, A. Escuer, R. Vicente, E. Ruiz, S.P. Perlepes, Inorg. Chem. 46 (2007) 8843-8850.
4. S. Sasmal, S. Sarkar, N. Aliaga-Alcalde, S. Mohanta, Inorg. Chem. 50 (2011) 5687-5695.
5. E. Ruiz, P. Alemany, S. Alvarez, J. Cano, J. Am. Chem. Soc. 119 (1997) 1297-1303.
6. A.C. Kathalikkattil, K.K. Bisht, N. Aliaga-Alcalde, E. Suresh, Cryst. Growth Des. 11 (2011) 1631-1641.
7. J. Ribas, A. Escuer, M. Monfort, R. Vicente, R. Cortés, L. Lezama, T. Rojo, Coord. Chem. Rev. 193 (1999) 1027-1068.
8. H.Y. Zang, Y.Q. Lan, G.S. Yang, X.L. Wang, K.Z. Shao, G.J. Xu, Z.M. Su, CrystEngComm 12 (2010) 434-445.
9. M. Das, S. Chatterjee, S. Chattopadhyay, Polyhedron 68 (2014) 205-211.
10. A. Bacchi, M. Carcelli, T. Chiodo, P. Pelagatti, CrystEngComm 12 (2010) 4226-4230.
11. R. Lescouezec, J. Vaissermann, C. Ruiz-Perez, F. Lloret, R. Carrasco, M. Julve, M. Verdaguer, Y. Dromzee, D. Gatteschi, W. Wernsdorfer, Angew. Chem. Int. Ed. 42 (2003) 1483-1486.
12. C. Biswas, S. Chattopadhyay, M.G.B. Drew, A. Ghosh, Polyhedron 26 (2007) 4411-4418.
13. L.M. Toma, R. Lescouezec, F. Lloret, M. Julve, J. Vaissermann, M. Verdaguer, J. Chem. Soc. Chem. Commun. (2003) 1850-1851.
14. Z.N. Chen, H.X. Zhang, K.B. Yu, K.C. Zheng, H. Cai, B.S. Kang, Dalton Trans. (1998) 1133-1136.
15. E.-Q. Gao, S.-Q. Bai, C.-F. Wang, Y.-F. Yue, C. -H. Yan, Inorg. Chem. 42 (2003) 8456-8464.
16. C. Adhikary, S. Koner, Coord. Chem. Rev. 254 (2010) 2933-2958.
17. L. Shen, Y.-Z. Xu, Dalton Trans. (2001) 3413-3414.
18. S. Mondal, P. Chakraborty, N. Aliaga-Alcalde, S. Mohanta, Polyhedron 63 (2013) 96-102.
19. S. Khan, S. Sproules, L.S. Natrajan, K. Harms, S. Chattopadhyay, New. J. Chem. 42 (2018) 1634-1641.
20. C. Adhikary, R. Sen, G. Bocelli, A. Cantoni, S. Chaudhuri, S. Koner, J. Coord. Chem. 62 (2009) 3573-3582.

21. S. Koner, S. Saha, T. Mallah, K.-I. Okamoto, *Inorg. Chem.* 43 (2004) 840-842.
22. P. Cen, W. Yuan, S. Luo, X. Liu, G. Xie, S. Chen, *New J. Chem.* 43 (2019) 601-608.
23. S. Banerjee, M.G.B. Drew, C.-Z. Lu, J. Tercero, C. Diaz, A. Ghosh, *Eur. J. Inorg. Chem.* (2005) 2376-2388.
24. R.A. Bailey, S.L. Kozak, T.W. Michelsen, W.N. Mills, *Coord. Chem. Rev.* 6 (1971) 407-445.
25. F.R. Louka, S.S. Massoud, T.K. Haq, M. Koikawa, M. Mikuriya, M. Omote, R.C. Fischer, F.A. Mautner, *Polyhedron* 138 (2017) 177-184.
26. Z.-X. Miao, M.-X. Li, M. Shao, H.-J. Liu, *Inorg. Chem. Commun.* 10 (2007) 1117-1120.
27. B. Machura, A. Świtlicka, J. Mroziński, B. Kalińska, R. Kruszynski, *Polyhedron* 52 (2013) 1276-1286.
28. C.-M. Liu, S. Gao, D.-Q. Zhang, Y.-H. Huang, R.-G. Xiong, Z.-L. Liu, F.-C. Jiang, D.-B. Zhu, *Angew. Chem. Int. Ed.* 43 (2004) 990-994.
29. M. Mondal, S. Jana, M.G.B. Drew, A. Ghosh, *Polymer* 204 (2020) 122815-122823.
30. I. Banerjee, J. Marek, R. Herchel, M. Ali, *Polyhedron* 29 (2010) 1201-1208.
31. E.-Q. Gao, Y.-F. Yue, S.-Q. Bai, Z. He, C.-H. Yan, *Cryst. Growth Des.* 5 (2005) 1119-1124.
32. A. Escuer, C.J. Harding, Y. Dussart, J. Nelson, V. McKee, R. Vicente, *J. Chem. Soc., Dalton Trans.* (1999) 223-228.
33. Z. Shen, J.-L. Zuo, S. Gao, Y. Song, C.-M. Che, H.-K. Fun, X.-Z. You, *Angew. Chem. Int. Ed.* 112 (2000) 3779-3781.
34. P.S. Mukherjee, T.K. Maji, A. Escuer, R. Vicente, J. Ribas, G. Rosair, F.A. Mautner, N.R. Chaudhuri, *Eur. J. Inorg. Chem.* (2002) 943-949.
35. C.S. Hong, Y. Do, *Angew. Chem. Int. Ed.* 38 (1999) 193-195.
36. C.S. Hong, J. Koo, S.-K. Son, Y.S. Lee, Y.-S. Kim, Y. Do, *Chem. Eur. J.* 7(2001) 4243-4252.
37. J. Ribas, C. Diaz, X. Solans, M. Font-Bardia, *Inorg. Chim. Acta*, 231 (1995) 229-232.
38. J. Cano, G. De Munno, F. Lloret, M. Julve, *Inorg. Chem.* 39 (2000) 1611-1614.
39. N.K. Karan, S. Mitra, T. Matsushita, V. Gramlich, G. Rosair, *Inorg. Chim. Acta* 332 (2002) 87-91.
40. S. Stoll, A. Schweiger, *J. Magn. Reson.* 178 (2006) 42-55.
41. G.A. Bain, J.F. Berry, *J. Chem. Educ.* 85 (2008) 532-536.

42. P.G. Urben (Ed.), Bretherick's Handbook of Reactive Chemical Hazards, Sixth ed., Butterworth-Heinemann, Oxford (1999).
43. W.C. Wolsey, J. Chem. Educ. 50 (1973) A335.
44. Bruker. SMART (Version 5.0) and SAINT (Version 6.02), Bruker AXS Inc., Madison, WI, USA (2000).
45. G.M. Sheldrick, SADABS, Program for empirical correction of area detector data, University of Göttingen, Germany (2000).
46. G.M. Sheldrick, SHELXS-97 and SHELXL-97, Program for crystal structure refinement, University of Göttingen, Germany (1997).
47. N.K. Mandal, B. Guhathakurta, P. Basu, A.B. Pradhan, C.S. Purohit, S. Chowdhury, J.P. Naskar, J. Coord. Chem. 72 (2019) 3625-3644.
48. K. Nakamoto, Infrared and Raman Spectra of Inorganic and Coordination Compounds, John Wiley & Sons, New York, 3rd edn. (1978).
49. J.S. Haynes, A. Kostikas, J.R. Sams, A. Simopoulos and R.C. Thompson, Inorg. Chem. 26 (1987) 2630-2637.
50. B. Żurowska, J. Mroziński, M. Julve, F. Lloret, A. Maslejova, W.S. Dobrowolska, Inorg. Chem. 41 (2002) 1771-1777.
51. H. Grove, M. Julve, F. Lloret, P.E. Kruger, K.W. Törnroos, J. Sletten, Inorg. Chim. Acta, 325 (2001) 115-124.
52. R. de A. Farani, W.M. Teles, C.B. Pinheiro, K.J. Guedes, K. Krambrock, M.I. Yoshida, L.F.C. de Oliveira, F.C. Machado, Inorg. Chim. Acta 361 (2008) 2045-2050.
53. B.J. Hathaway, A.E. Underhill, J. Chem. Soc. (1961) 3091-3096.
54. R.N. Patel, Y.P. Singh, Y. Singh, R.J. Butcher, Polyhedron 104 (2016) 116-126.
55. R. Li, B. Moubaraki, K.S. Murray, S. Brooker, Eur. J. Inorg. Chem. (2009) 2851-2859.
56. A.B.P. Lever, Inorganic Electronic Spectroscopy, Elsevier, Amsterdam, 1984, p. 553.
57. A.W. Addison, T.N. Rao, J. Reedijk, J.V. Rijn, G.C. Verschoor, Dalton Trans. (1984) 1349-1356.
58. B. Guhathakurta, P. Basu, G.S. Kumar, L. Lu, M. Zhu, N. Bandyopadhyay, J.P. Naskar, Polyhedron 110 (2016) 227-234.
59. S. Banerjee, C. Adhikary, C. Rizzoli, R. Pal, Inorg. Chim. Acta 409 (2014) 202-207.
60. S. Sarkar, A. Mondal, J. Ribas, M.G.B. Drew, K. Pramanik, K.K. Rajak, Inorg. Chim. Acta 358 (2005) 641-649.
61. C. Adhikari, S. Koner, Coord. Chem. Rev. 254 (2010) 2933-2958.

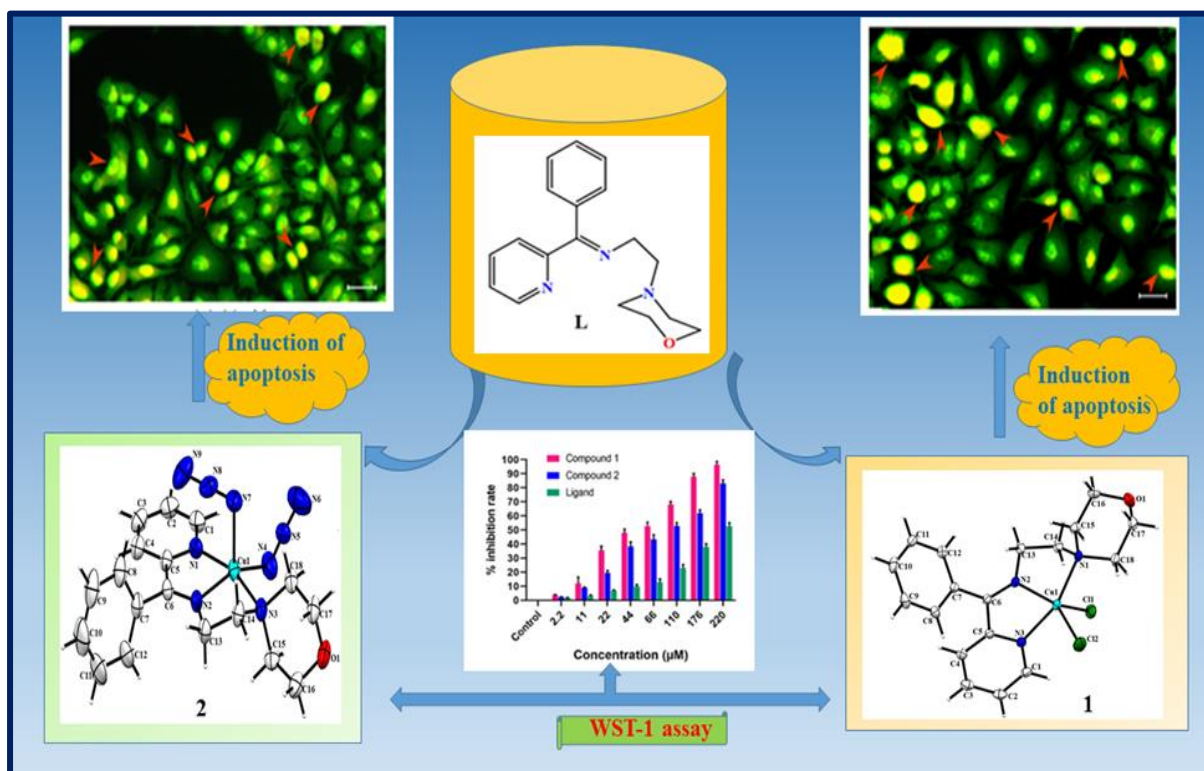
62. J. Lu, H.-T. Liu, D.-Q. Wang, X.-X. Zhang, D.-C. Li, J.-M. Dou, *J. Mol. Struct.* 938 (2009) 299-304.
63. D.B. Brown, J.A. Donner, J.W. Hall, S.R. Wilson, R.B. Wilson, D.J. Hodgson, W.E. Hatfield, *Inorg. Chem.* 18 (1979) 2635-2641.
64. A. Escuer, R. Vicente, J. Ribas, M.S.E. Fallah, X. Solans, M.F. Bardla, *Inorg. Chem.* 32 (1993) 3727-3732.
65. J. Ribas, A. Escuer, M. Monfort, R. Vicente, R. Cortés, L. Lezama, T. Rojo, *Coord. Chem. Rev.* 193 (1999) 1027-1068.
66. P. Bhowmik, S. Biswas, S. Chattopadhyay, C. Diaz, C. J. Gómez-García, A. Ghosh, *Dalton Trans.* 43 (2014) 12414-12421.
67. S. Dalai, P.S. Mukherjee, M.G.B. Drew, T.-H. Lu, N.R. Chaudhuri, *Inorg. Chim. Acta* 335 (2002) 85-90.
68. P.S. Mukherjee, S. Dalai, G. Mostafa, T.-H. Lu, E. Rentachler, N.R. Chaudhuri, *New J. Chem.* 25 (2001) 1203-1207.
69. C.A. White, G.P.A. Yap, N.P. Raju, J.E. Greedan, R.J. Crutchley, *Inorg. Chem.* 38 (1999) 2548-2549.
70. P. Gómez-Saiz, J. García-Tojal, F.J. Arnaiz, M.A. Maestro, L. Lezama, T. Rojo, *Inorg. Chem. Commun.* 6 (2003) 558-560.
71. J. Carranza, J. Sletten, F. Lloret, M. Julve, *Polyhedron* 28 (2009) 2249-2257.
72. M. Julve, M. Verdaguer, G.D. Munno, J.A. Real, G. Bruno, *Inorg. Chem.* 32 (1993) 795-802.
73. P. Talukder, A. Datta, S. Mitra, G. Rosair, M.S. El Fallah, J. Ribas, *Dalton Trans.* (2004) 4161-4167.
74. B.J. Pella, J. Niklas, O.G. Poluektov, A. Mukherjee, *Inorg. Chim. Acta* 483 (2018) 71-78.
75. L. Husarikova, Z. Repicka, J. Moncol, D. Valigura, M. Valko, M. Mazur, *Appl. Magn. Reson.* 44 (2013) 571-582.
76. B. Hathaway, D.E. Billing, *Coord. Chem. Rev.* 5 (1970) 143- 207.
77. K. Das, S. Dolai, P. Vojtíšek, S.C. Manna, *Polyhedron* 149 (2018) 7-16.

CHAPTER-V

Synthesis, characterization, crystal structure, thermal and redox behaviour and antiproliferative studies of morpholine-based two copper(II) compounds

This work has been published in
Applied Organometallic Chemistry
37 (2023) e7120

Graphical Abstract



Highlights

- Two mononuclear Cu(II) complexes were synthesized by using a new morpholine based Schiff base ligand.
- Solid state identity of the Cu(II) complexes have been confirmed by X-ray single crystal structures.
- Spectroscopic properties of the ligand and complexes have been studied.
- Redox and thermal behavior of the complexes were also explored.
- Cytotoxic activities of both the complexes along with the stabilising ligand were screened against non-small human lung cancer cell, A549.

Key words

Schiff base; copper; structure; cancer and anti-proliferation

Abstract

Two novel copper(II) complexes, $[\text{Cu}(\text{L})(\text{Cl})_2](\text{H}_2\text{O})$ (**1**) and $[\text{Cu}(\text{L})(\text{N}_3)_2]$ (**2**), have been synthesized from a morpholine based N,N,N donor tridentate Schiff base ligand, (E)-N-(2-morpholinoethyl)-1-phenyl-1-(pyridin-2-yl)methanimine (**L**). Ligand (**L**) and its stabilized complexes, **1** and **2**, have been comprehensively characterised by different physical and spectroscopic techniques. Solid state single crystal X-ray structures of both **1** and **2** have been determined. Powder X-ray diffraction studies on the bulk samples of **1** and **2** have been executed to demonstrate that the synthesized bulk materials retain their solid phase purity as that exists in the single crystals. Cyclic voltammetric experiments have been done to demonstrate the redox behaviour of **1** and **2**. UV-Vis spectra of the copper(II) complexes with variation in time were accrued to probe that both **1** and **2** retain their stability in solution. Thermo-gravimetric analysis (TGA) has been performed to collate the thermal stability of **1** along with its possible thermal degradation behaviour. Room temperature magnetic moments of **1** and **2** have been determined. Cytotoxic activity of **1** and **2** has been screened against non-small human lung cancer cell, A549.

1. Introduction

Schiff bases, an important privileged class of organic compounds indeed, are deemed universal versatile ligands owing to their ubiquitous diverse anchoring propensities with different metal ions to foster a plethora of complexes with varied configurations [1-5]. These ligands and their complexes display promising catalytic, regulatory, antiradical, antibacterial, antiviral, antifungal, antioxidant and anti-proliferative activities [6-10]. Morpholine based assemblies are of contemporary interest for exhibiting excellent cytotoxic activity [11-13]. In medicinal chemistry, morpholine acts as a good building block as well. The ring oxygen atom in morpholine plays a big role for this manifested bioactivity [14-16]. In our present work, we are concerned with a Schiff base ligand tethered with a morpholine moiety.

Cancer is the most leading cause of death worldwide [17,18]. According to the World Health Organisation (WHO), the year 2020 alone witnessed nearly 10 million fatalities globally out of this dreaded disease [19]. Lung, liver, stomach, breast, colon and rectum cancers are quite common [20-24]. By 2040, an estimated global fatality count will alarmingly reach 29.5 million. Thus, catastrophic disaster-like havoc is on the offing. Dreadful lung cancer (LC) is the most severe amongst all forms of cancer. The five-year survival rate of lung cancer patients is even lower than 20% [25]. This malady is designated as the prime cause of anthropogenic fatality, morbidity and mortality. In the present study, we are concerned with human adenocarcinoma lung cancer cell line, A549. To combat cancer, chemotherapy has still been focused as a prime clinical protocol. Owing to its anticancer efficacies, cis-platin and its suitable derivatives have clinically been used widely. Judged on their promising and remarkable success, platinum based anticancer drugs seem to be indispensable in the management and therapy of cancer. However, platinum-based chemotherapy still suffers from some inherent therapeutic shortcomings. They pose non-negligible dose-limiting harsh side effects in terms of nephro-toxicity, liver toxicity, neuro-toxicity, general toxicity and most importantly drug resistivity [26-30]. Thus, development of new drugs with promising fruitfulness but with tolerable limit of marginalised side effects is the crying need of the day. In this perspective, biocompatible coinage transition metal, copper, is proven to be the front runner. Copper is an essential microelement for most of the aerobic living organisms. Displaying untenable role in redox biology, it functions as a structural and catalytic cofactor in many crucial life-sustaining pathways [31]. Contrary to platinum based agents, copper based systems principally bind DNA double helix in noncovalent mode. Copper complexes display electrostatic, groove and intercalative modes of protein binding propensities [32,33]. It has

truly been demonstrated that copper and copper-anchoring proteins are interlinked with malignancy progression, propagation, angiogenesis and metastasis [34-37]. Consequently, copper based coordination complexes may offer satisfactory anti-proliferative, anticancer and antineoplastic efficacies [38-41]. Again, the underlying viable mechanistic pathways of *in vivo* absorption, assimilation, propagation and excretion of copper have comprehensively been studied [42-45]. All these aspects of copper chemistry rekindled unabated interest over the years to undertake sincere efforts to develop copper based anticancer chemotherapeutic drugs. By this time, a good number of copper coordination complexes as artificial nucleases have successfully been demonstrated to show commendable cytotoxic effects on a variety of cancer cells [46-49]. This can be reckoned readily that the noteworthy copper(II) compound of L. Ruiz-Azuara and co-workers, $[\text{Cu}(\text{II})(4,4'\text{-dimethyl-2,2'}\text{-bipyridine})(\text{acetylacetonate})(\text{NO}_3)(\text{H}_2\text{O})]$, has entered clinical trials (Phase I) [50]. Copper complexes appear to be potential anticancer agents with limiting toxic and dose-limiting effects [51-55]. This wonderful aspect of copper chemistry has aroused our interest as well to work along this line. Herein we wish to report the syntheses, characterisation and structures of two new mononuclear copper(II) complexes stabilised from a novel Schiff base ligand. The ligand bears suitable disposition of pharmacologically crucial morpholine moiety. Redox and thermal behaviour of them has also been expounded. Our present study also encompasses the *in vitro* inhibitory cytotoxic activity of the ligand and its two mononuclear copper(II) complexes against non-small cell lung cancer (NSCL) cell line, A549.

2. Experimental Section

2.1. Materials and methods/ Chemicals

High purity benzoyl pyridine ($\geq 99\%$) and 4-(2-aminoethyl) morpholine (99%) were procured from Sigma Aldrich. Other chemicals like $\text{CuCl}_2 \cdot 2\text{H}_2\text{O}$ and NaN_3 were of reagent grade and were used as such. Commercially available solvents of analytical grade reagent were used as received. For spectroscopic studies and cyclic voltammetric measurements, spectroscopic grade solvents were employed. Dulbecco's Modified Eagles Medium (DMEM), 4',6-diamidino-2-phenylindole (DAPI), Acridine orange (AO), Ethidium bromide (EtBr) and Propidium iodide (PI) were purchased from Himedia, Mumbai, India. Antibiotic- PenStrep and Amphotericin B were procured from MP Biomedicals, United States. Fetal bovine serum (FBS) and water soluble tetrazolium (WST) were purchased from Invitrogen, Carlsbad, CA, United States and Takara Bio Inc, Japan respectively. Copper(II) compounds, **1** and **2**, were dissolved in DMSO and a master concentration of 10 mM was prepared for performing all the cellular

assays. At no point of our experiments did the concentration of DMSO exceed 0.8% (v/v) during treatment. All experiments were performed on cells treated with compounds and ligand for 24 h [54,55].

NMR spectra (^1H , ^{13}C , COSY) of the ligand were recorded on a Bruker 400 MHz (ASCEND) spectrometer at room temperature in suitable deuterated solvents. Chemical shift was followed in ppm with respect to internal standard reference, TMS. Electronic absorption spectra of the ligand and its stabilised copper(II) complexes, **1** and **2**, were recorded on a SHIMADZU UV 1900i spectrophotometer in methanol. Mass spectra (positive ionization mode) were run on a Waters HRMS (XEVO-GTQTOF#YCA351) spectrometer. Magnetic susceptibilities of **1** and **2** were measured at room temperature on a PAR 155 magnetometer. The instrument was standardized with the standard calibrant, $\text{Hg}[\text{Co}(\text{SCN})_4]$. The requisite diamagnetic corrections to the experimentally determined susceptibility values were made with the help of Pascal's constants [56]. FT-IR spectra were recorded by using a SHIMADZU FT-IR-8400S spectrophotometer ($4000\text{--}400\text{ cm}^{-1}$). Powder X-ray diffraction (PXRD) patterns were acquisitioned on a Bruker D8 Advance X-ray diffractometer (1D mode). The patterns were collected with $\text{CuK}\alpha$ ($\lambda = 1.548\text{ \AA}$) radiation generated at 40 kV and 40 mA. Thermogravimetric analysis (TGA) of **1** was performed using a Diamond Pyris 480 (Perkin Elmer) thermal analyser. The data was accrued using $\alpha\text{-Al}_2\text{O}_3$ as a standard under dynamic nitrogen flow rate of 150 ml min^{-1} with a heating rate of $10\text{ }^\circ\text{C min}^{-1}$. Electrical conductivities of the methanolic solutions of **1** and **2** were measured on a Systronics India (Model: 304) direct reading conductivity cell. The conductivity meter was calibrated with aqueous KCl (0.1 M) solution prior use. Electrochemical cyclic voltammetric studies were conducted for **1** and **2** under the blanket of pure and dry N_2 gas in dehydrated and degassed methanol milieu on a CHI 600C (USA) electrochemical workstation at room temperature. The conventional three-electrode configuration was consisted of a BAS Glassy Carbon (GC) working electrode, a platinum wire counter electrode and a Ag/AgCl reference electrode. Tetra-*n*-butyl ammonium perchlorate (TBAP) in 0.1 M concentration served the purpose of indifferent supporting electrolyte.

Caution: Azide salts are potentially explosive and, therefore, hazardous. Although we faced no difficulty, extreme care should be taken to handle this salt and must be used in small quantity [57, 58].

2.2. Synthesis of the ligand (**L**)

0.130 g (1 mmol) of 4-(2-aminoethyl) morpholine was dissolved in 25 mL of methanol to have a colourless solution. 0.183 g (1 mmol) of solid benzoyl pyridine was added all at a time to the morpholine solution at room temperature to obtain a colourless solution. The resulting reaction mixture was heated under reflux for 5 h. After refluxing, the faint yellow solution obtained thereby was kept in the air for slow aerial evaporation. A light-yellow gummy product was imparted after 5 days of standing. This pasty mass so obtained was thoroughly dried in *vacuo* over fused anhydrous calcium chloride. The ligand is soluble in H₂O, MeOH, CH₃CN, DCM and DMSO.

Yield: 0.25 g (85%); Anal. Cal. for. C₁₈H₂₁N₃O (MW 295.168); C, 73.17; H, 7.17; N, 14.22 %; Found: C, 73.13; H, 7.20; N, 14.25%; FT-IR (KBr pellet): (ν/cm^{-1}): 2940, 2855, 2810 (C-H); 1663 (C=N); 1115 (morpholine ring C-N); ESI-MS (positive ion mode in CH₃OH) (m/z): 318.157 [(**L**+Na)]⁺ (100%) (Theo. value 318.168). ¹H-NMR (CD₃OD): δ (ppm): 8.68 (1H, d, pyridine ring proton close to N), 7.98-8.00 (3H, m), 7.64-7.68 (2H, m), 7.51-7.62 (3H, m), 3.65-3.71 (6H, m), 2.75 (2H, t, CH₂ protons of morpholine ring N), 2.48 (4H, t, CH₂ protons of morpholine ring); ¹³C NMR (CD₃OD): δ (ppm): 167.82 (C6), 154.84 (C5), 148.20 (C1), 138.24 (C7), 136.14 (C3), 132.93 (C10), 130.35 (C8), 127.98 (C9), 126.42 (C2), 124.26 (C4), 66.15 (C16), 58.89 (C14), 53.60 (C15), 50.54 (C13); ¹H-NMR (CDCl₃): δ (ppm): 8.73 (1H, d, pyridine ring proton close to N), 8.07-8.03 (3H, m), 7.90 (1H, t), 7.60 (1H, d), 7.51-7.47 (3H, m), 3.70 (4H, t, -CH₂ protons close to morpholine O atom), 3.48 (2H, t, -CH₂ protons close to imine N), 2.49 (4H, t, CH₂ protons of morpholine ring), 1.22 (2H, t); UV-Vis: (CH₃OH): λ_{max} ($\epsilon/\text{M}^{-1}\text{cm}^{-1}$): 261 nm (18 503).

2.3. Synthesis of [CuL(Cl)₂].H₂O (**1**)

0.030 g (0.1 mmol) of **L** was dissolved in 10 mL methanol to have a faint yellow solution. This ligand solution was added dropwise to a 10 mL blue aqueous solution of CuCl₂.2H₂O (0.017 g, 0.1 mmol) with continuous stirring. Within a few minutes of stirring, the colour became green. This reaction mixture was further stirred for 3 h. Finally, the resulting dark green solution was left aside undisturbed at room temperature for slow evaporation. After 3 days, a crystalline compound was harvested by filtration followed by thorough washing with chilled diethyl ether.

Yield: 33 mg (76%); C₁₈H₂₃N₃O₂Cl₂Cu: (447.73); Anal. Cal. for C₁₈H₂₃N₃O₂Cl₂Cu: C, 48.26; H, 5.17; N, 9.38 %; Found: C, 48.22; H, 5.21; N, 9.35; FT-IR (KBr pellet): (ν/cm^{-1}): 3526 (ν O-H, H₂O), 1632 (C=N), 1441(C-C), 1109 (C-N); ESI-MS (positive ion mode in CH₃OH)

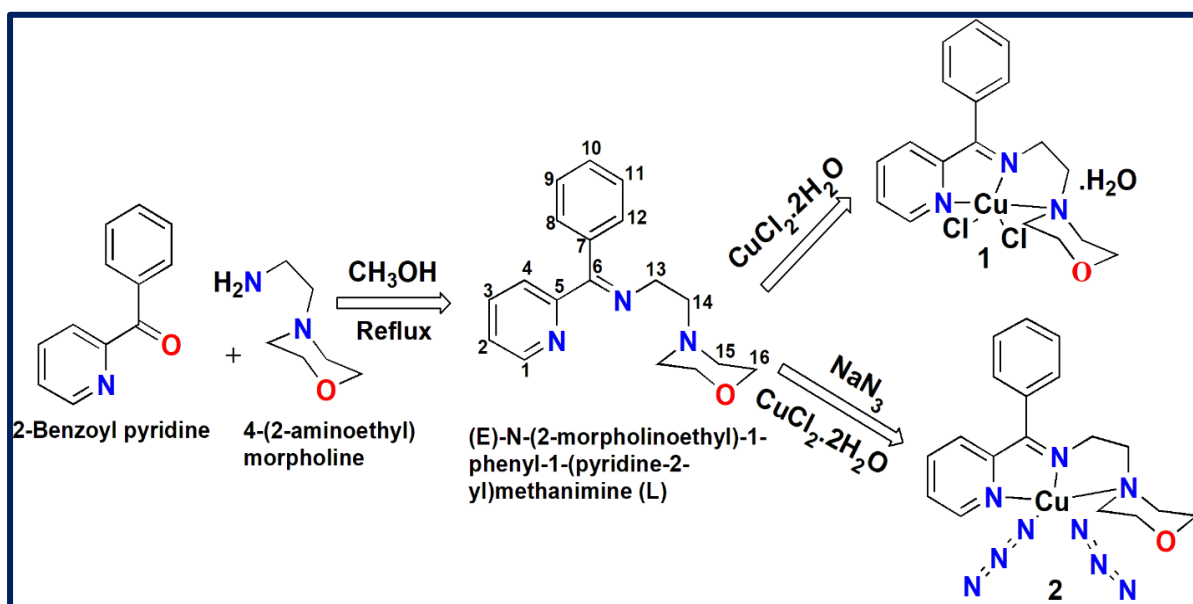
(m/z): 393.216 for (Calcd. 393.668) $[\text{Cu}^{63}\text{L}-(\text{Cl}+\text{H}_2\text{O})]$ (100%) and 395.213 for (Calcd. 395.668) $[\text{Cu}^{65}\text{L}-(\text{Cl}+\text{H}_2\text{O})]$; UV-Vis (CH_3OH): λ_{max} ($\epsilon/\text{M}^{-1}\text{cm}^{-1}$): 274 nm (16 143), 695 nm (1 51); $\Lambda_{\text{M}}(\text{CH}_3\text{OH})$: (Non-electrolyte); $\mu_{\text{eff.}} = 1.82 \mu_{\text{B}}$ at 298 K.

2.4. Synthesis of $[\text{CuL}(\text{N}_3)_2]$ (**2**)

0.030 g (0.1 mmol) of **L** was dissolved in 10 mL of methanol to get a faint yellow solution. A 10 mL methanolic solution of $\text{CuCl}_2 \cdot 2\text{H}_2\text{O}$ (0.017 g, 0.1 mmol) was added dropwise to the ligand solution with continuous stirring. Immediately, the colour of the solution turned green. After 15 min of stirring, a 5 mL aqueous solution of NaN_3 (0.007 g, 0.1 mmol) was added dropwise to the resulting green solution. The reaction mixture was further stirred for 30 min. A deep green solution obtained thereby was kept aside undisturbed in open air for slow evaporation. After 4 days, a dark green crystalline compound was obtained. The crystals were collected through filtration and were washed copiously with chilled diethyl ether.

Yield: 30 mg (66%); $\text{C}_{18}\text{H}_{21}\text{N}_9\text{OCu}$: (442.714); Anal. Cal. for $\text{C}_{18}\text{H}_{21}\text{N}_9\text{OCu}$: C, 48.78; H, 4.78; N, 28.46 %; Found: C, 48.74; H, 4.81; N, 28.49 %; FT-IR (KBr pellet): (ν/cm^{-1}): 2062, 2015 (for azide), 1645 (for $\text{C}=\text{N}$), 1444 ($\text{C}-\text{C}$), 1107 ($\text{C}-\text{N}$); ESI-MS (positive ion mode in CH_3OH) (m/z): 393.054 for (Calcd. 393.109) $[\text{Cu}^{63}\text{L}+\text{Li}]^+-(2\text{N}_2)$ and 395.050 for (Calcd. 395.109) $[\text{Cu}^{65}\text{L}+\text{Li}]^+-(2\text{N}_2)$; UV-Vis (CH_3OH): λ_{max} ($\epsilon/\text{M}^{-1}\text{cm}^{-1}$): 272 nm (21 901), 396 nm (35 21) and 668 nm (268); $\Lambda_{\text{M}}(\text{CH}_3\text{OH})$: (Non-electrolyte); $\mu_{\text{eff.}} = 1.80 \mu_{\text{B}}$ at 298 K.

The synthetic scheme of the ligand and its copper(II) complexes is depicted in [scheme V.1](#).



Scheme V.1. Synthetic route of the ligand (**L**) and its copper(II) complexes, **1** and **2**.

2.5. Cell culture

Human A549 non-small cell lung cancer cells (NSCLC) were purchased from National Center for Cell Science (Pune, India). Cells were maintained in complete Dulbecco's Modified Eagle's Medium (DMEM) supplemented with 1% antibiotic-antimycotic solution (Gibco; Thermo Fisher Scientific, Inc., Grand Island, NY, USA) and 10% FBS (Foetal bovine serum). The culture was maintained for 3-4 days so that cells get enough time to spread as a monolayer. Cells attaining a confluence of 80-90% were then harvested for further analysis. The cells were maintained at 37 °C in a humidified atmosphere containing 5% CO₂ for all the experiments.

2.6. Cell proliferation assay

A standard WST-1 (water-soluble tetrazolium salt) (Roche Applied Science, India) method was utilised to assess cellular viability assays. This method works on the basis of cleavage of tetrazolium into an insoluble purple formazan product by mitochondrial dehydrogenase of intact cells [59]. 4×10^3 cells that were in the exponential growth phase were seeded into 96 well culture plate along with negative untreated control set (only cells). Cells were further treated overnight with various concentrations (2.2-220 μ M) of compounds **1**, **2** and ligand, **L** along with a vehicle control set separately. Simultaneously doxorubicin was taken as positive control and also subjected to concentrations ranging from 0.1-10 μ M. After incubating the cells for 24 h with compounds **1**, **2**, ligand, **L** and doxorubicin, WST-1 reagent was added to the medium and incubated for 2.5 h. The absorbance was measured at 450 nm using a Bio-Rad (model 550) microplate reader. The percentage of cell viability was measured using WST-1 absorption percentage following the protocol of Nandi and co-workers [60].

2.7. Assay of cell viability with Trypan Blue Exclusion assay

The cell viability was also evaluated following the protocol of Trypan Blue Exclusion assay. A549 cells were cultured on 24-well plates until 70% confluence, and then rinsed with PBS (phosphate-buffered saline) and exposed to various concentrations of compounds **1**, **2** and ligand, **L** for 24 h. A negative control and vehicle control was also taken. The adherent cells were trypsinized followed by centrifugation at 2,500 rpm for 6 min to collect the cell pellet for three groups. In fresh medium the cell pellets were re-suspended from which a 10 μ L aliquot was taken and an equal volume of 0.4% trypan blue dye was mixed with it. The absorbance of the samples was measured with a microplate reader at 590 nm wavelength using a MultiSkan GO Microplate Spectrophotometer. The percentage of viable cells was determined by calculating the number of cells able to exclude the dye based on the following formula:

$$\% \text{ Inhibition} = (\text{Total dead cell count} / \text{Total cell count}) \times 100$$

2.8. Colony formation assay

A549 cells were trypsinized and plated into 12-well culture plate at a density of 2×10^3 cells. Cells were treated with compounds **1** and **2** as indicated and cultured for 7-10 days to allow colony formation. Post incubation, colonies were fixed with 4% paraformaldehyde (for 10 min) and stained with 0.1% crystal violet for 15 min. Later extra crystal violet stains were washed out and images of stained colonies were scanned.

2.9. Morphological evaluation

An inverted phase contrast microscope (CKX53; Olympus, Tokyo, Japan) was used to monitor morphological changes in cancerous cells treated with our experimental drug. 4×10^4 A549 cells were grown onto a 2 mm glass plate and were incubated at 37 °C followed by conventional trypsinization. The alterations in morphological appearance of cells were imaged and considered in evaluation after 24 h post-treatment with various concentrations of compounds **1**, **2** and ligand, **L**. The untreated cells were served as negative control.

2.10. Cell cycle assay

During each cell cycle, DNA content varied from one phase to another. Briefly, A549 cell pellets of both **1** and **2** were collected and rinsed thrice with buffer and fixed in ice-cold 70% ethanol overnight at -20 °C prior to staining. The following day, cells were washed again with buffer and were stained with propidium iodide (PI) in the dark for 15 min at room temperature and were then examined for cell cycle distribution by AccuriC6 flow cytometer [61]. Results were expressed as a percentage of cells accumulated in the G0/G1, S and G2/M phases on the basis of differential DNA content.

2.11. Morphological observation of nuclear change

Cells cultured in 6-well plate to a confluence of 70-75% and then treated with two dosage of compounds **1** and **2** for 24 h. Post incubation A549 cells were rinsed and fixation was carried out with 4% paraformaldehyde. Subsequently, 0.1% Triton X was used to permeabilize the cells for better staining. The fixed cells were stained with 0.1 mg/mL DAPI solution, wrapped in aluminium foil and were incubated in dark for 10 min. The surplus stain was rinsed out from plate and viewed under the fluorescence microscope (EVOS FL, Invitrogen).

2.12. Assessment of apoptosis by AO/EtBr staining

To identify the different stages of apoptosis, comprising early, late and necrotic phase, 5×10^4 cells/well were treated with different concentrations of **1** and **2** and harvested after 24 h of treatment. The morphological features of apoptosis induced by both the compounds were evaluated using Acridine Orange-Ethidium Bromide dual (AO/EtBr) staining. The harvested

cells were incubated for 10 min with AO/EtBr in a ratio of 1:1 at room temperature followed by rinsing the extra stain and images were captured under an EVOS FL fluorescence microscope (Invitrogen, USA).

2.13. X-ray crystallography

Green needle shaped single crystals of both **1** and **2**, obtained from respective mother liquor, were selected for data collection under observation through a polarizing microscope. Single-crystal XRD data of both **1** and **2** were accrued employing a Bruker Smart Apex CCD diffractometer at room temperature. The instrument was equipped with graphite monochromated MoK α radiation ($\lambda = 0.71073$ Å). SAINTPlus [62] and SADABS [63] programme packages were used respectively for data reduction and semi-empirical absorption correction. By using direct methods, the structures were solved and were refined through SHELXS-97 programme package software [64]. All the hydrogen atoms were placed geometrically and non-hydrogen atoms were refined anisotropically. The crystal data along with structure refinement of both **1** and **2** are summarized in Table V.1.

Table V.1. Crystal data and structure refinement for **1** and **2**

CCDC NO.	2218689	2218688
Empirical formula	C ₁₈ H ₂₃ CuN ₃ O ₂ Cl ₂	C ₁₈ H ₂₁ CuN ₉ O
Formula weight	447.84	442.99
Temperature [K]	293(2)	273(2)
Wavelength [Å]	0.71073	0.71073
Crystal system and space group	Orthorhombic and <i>Pbca</i>	Monoclinic and <i>P21/c</i>
a [Å], b [Å] and c [Å]	11.04(2), 13.27(3) and 25.87(5)	11.47(10), 16.06(14) and 11.72(11)
α [°], β [°] and γ [°]	90, 90 and 90	90, 112.444(3) and 90
Volume [Å ³]	3794.5(13)	1998.6(3)
Z	8	4
ρ_{calcd} [mg/cm ³]	1.568	1.472
Absorption coefficient [mm ⁻¹]	1.451	1.123
F (000)	1848.0	916
θ range for data collection [deg]	2.423 to 27.163	1.920 to 27.769
Limiting indices	-14 < h < 14, -17 < k < 17, -33 < l < 33	-15 < h < 15, -20 < k < 20, -14 < l < 14

Reflections collected/unique	124959/4210 [R _{int} = 0.0944]	66940/4433 [R _{int} = 0.0573]
Completeness of theta	99.9 % (25.242)	99.9 % (25.242)
Data / restraints / parameters	4210/0/243	4693/0/262
Goodness-of-fit on F ²	1.033	1.050
Final R indices [I>2sigma (I)]	R ₁ = 0.0309 wR ₂ = 0.0686	R ₁ = 0.0960 wR ₂ = 0.2220
R indices (all data)	R ₁ = 0.0594, wR ₂ = 0.1449	R ₁ = 0.0420, wR ₂ = 0.1021
Largest diff. peak and hole	0.446 and -0.585 e.Å ⁻³	0.617 and -0.718 e.Å ⁻³

Some important bond lengths and angles of **1** and **2** are presented in Table V.2. Hydrogen bonding parameters of **1** along with symmetry code are given in Table V.3. Other bonding parameters of **1** and **2** are presented in Tables V.4 and V.5.

Table V.2. Some selected bond lengths (Å) and bond angles (°) of **1** and **2**

Complex 1			
Bond length		Bond angle	
Cu(1)-N(1)	2.067(2)	N(2)-Cu(1)-N(3)	79.39(10)
Cu(1)-N(2)	2.022(3)	N(2)-Cu(1)-N(1)	82.21(10)
Cu(1)-N(3)	1.975(2)	N(3)-Cu(1)-N(1)	160.73(9)
Cu(1)-Cl(1)	2.281(11)	N(2)-Cu(1)-Cl(1)	146.61(8)
Cu(1)-Cl(2)	2.456(12)	N(3)-Cu(1)-Cl(1)	96.31(8)
		N(1)-Cu(1)-Cl(1)	95.88(7)
		N(2)-Cu(1)-Cl(2)	105.76(8)
		N(3)-Cu(1)-Cl(2)	93.65(8)
		N(1)-Cu(1)-Cl(2)	96.82(7)
		Cl(1)-Cu(1)-Cl(2)	107.56(4)
Complex 2			
Bond length		Bond angle	
Cu(1)-N(4)	1.921(3)	N(4)-Cu(1)-N(2)	155.79(13)
Cu(1)-N(2)	1.924(2)	N(4)-Cu(1)-N(1)	96.79(13)
Cu(1)-N(1)	2.046(2)	N(2)-Cu(1)-N(1)	80.48(9)

Cu(1)-N(3)	2.076(3)	N(4)-Cu(1)-N(3)	96.52(13)
Cu(1)-N(7)	2.226(3)	N(2)-Cu(1)-N(3)	82.29(9)
		N(1)-Cu(1)-N(3)	161.81(10)
		N(4)-Cu(1)-N(7)	107.75(14)
		N(2)-Cu(1)-N(7)	96.46(12)
		N(1)-Cu(1)-N(7)	94.37(11)
		N(3)-Cu(1)-N(7)	93.33(11)

Table V.3. Hydrogen bonding parameters of **1**(Å/°)

D-H...A	d(D-H)	d(H...A)	d(D...A)	∠D-H...A	Symmetry
O2-H19...Cl2	0.71(9)	2.62(9)	3.302(4)	160(8)	3/2-x,-1/2+y,z
O(2)-H(20)...Cl(2)	0.91(7)	2.44(7)	3.344(4)	172(5)	1/2+x,1/2-y,1-z
C4-H4...O2	0.93	2.51	3.297(5)	143	x,1+y,z
C15-H15B..Cl1 (Intra)	0.97	2.71	3.384(3)	127	
C17-H17B..Cl1	0.97	2.70	3.579(4)	150	1/2-x,-1/2+y,z

Table V.4. X-H...Cg(π -Ring) interactions for **1**(Å/°)

X-H(I)	Cg(J)	d(H...Cg)	∠X-H...Cg	d(X...Cg)	Symmetry
C3-H3	Cg(5)	2.99	131	3.665(3)	3/2-X,1/2+Y,Z
C9-H9	Cg(4)	2.96	131	3.636(4)	1/2+X,3/2-Y,Z

Cg5, Cg4 are the phenyl rings

Table V.5. Y-X...Cg(π -Ring) interactions for **2**(Å/°)

Y-X(I)	Cg(J)	d(X...Cg)	∠Y-X...Cg	d(Y...Cg)	Symmetry
N8-N9	Cg(1)	3.742(5)	98.1(3)	4.063(3)	X,1/2-Y,1/2+Z

Cg1 is the phenyl ring

3. Result and Discussion

3.1. Synthesis and characterisation

A morpholine based Schiff base ligand (**L**) has been prepared by 1:1 Schiff base condensation of benzoyl pyridine and 4-(2-aminoethyl)morpholine. Mononuclear Cu(II) complexes in optimum yields were prepared by stirring a methanolic solution of CuCl₂·2H₂O with equimolar proportion of **L** for **1**; and a methanolic CuCl₂·2H₂O solution followed by addition of sodium azide with equimolar proportion of the ligand for **2**. After a few days of slow evaporation of the respective mother liquor, green-coloured needle-shaped crystals, suitable for X-ray diffraction studies, were harvested at room temperature. Both **1** and **2** were structurally characterised by single-crystal X-ray crystallography.

ESI mass and ¹H NMR spectra of **L** are given in Figs. V.1 and V.2, respectively.

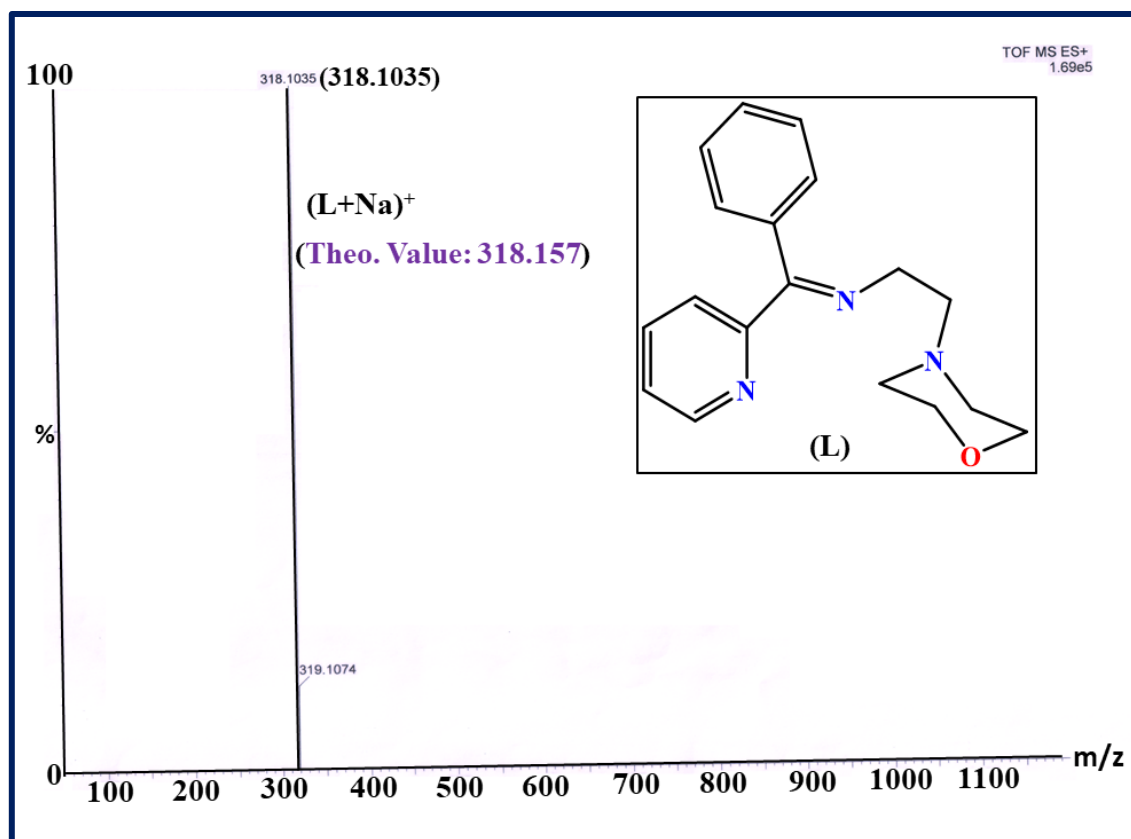


Fig. V.1. ESI mass spectrum of **L** in CH₃OH.

In the 2D COSY NMR experiment, the spin-spin interaction through cross-contour peak has been determined for the adjacent protons. The ¹H-¹H gCOSY NMR spectrum of **L** has been shown in Fig. V.3. The ¹³C NMR spectrum of **L** is depicted in Fig. V.4.

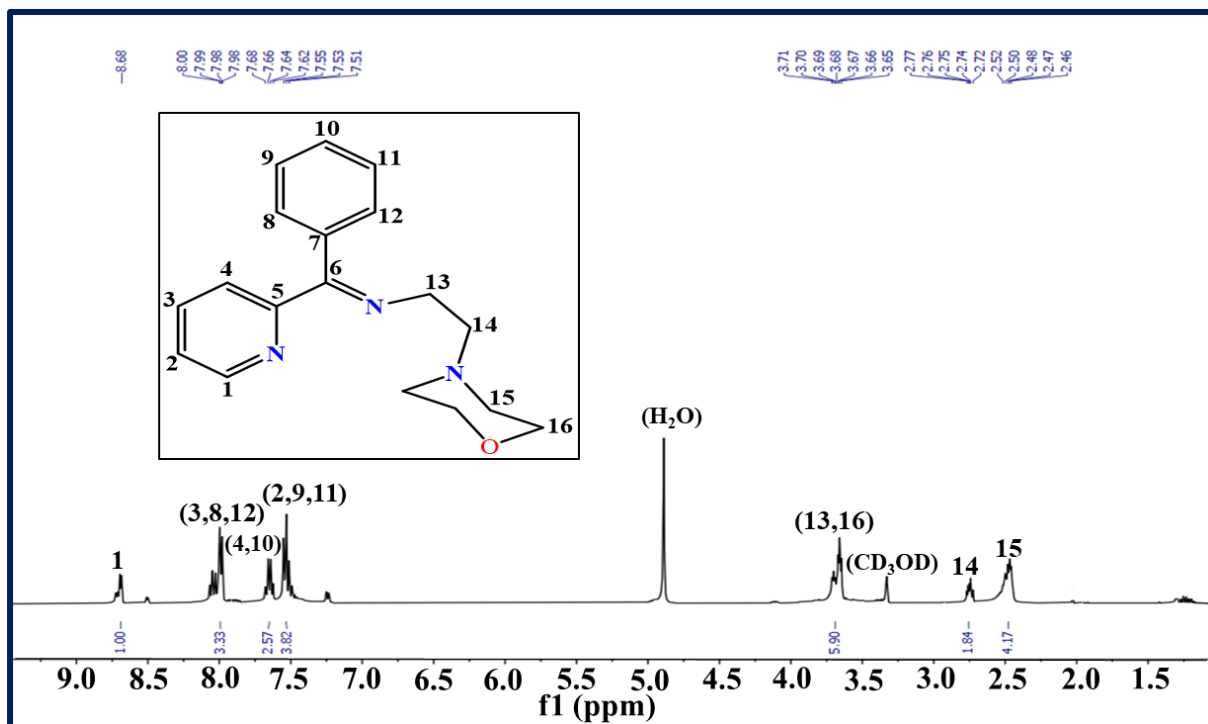


Fig. V.2. ^1H NMR spectrum of **L** in CD_3OD .

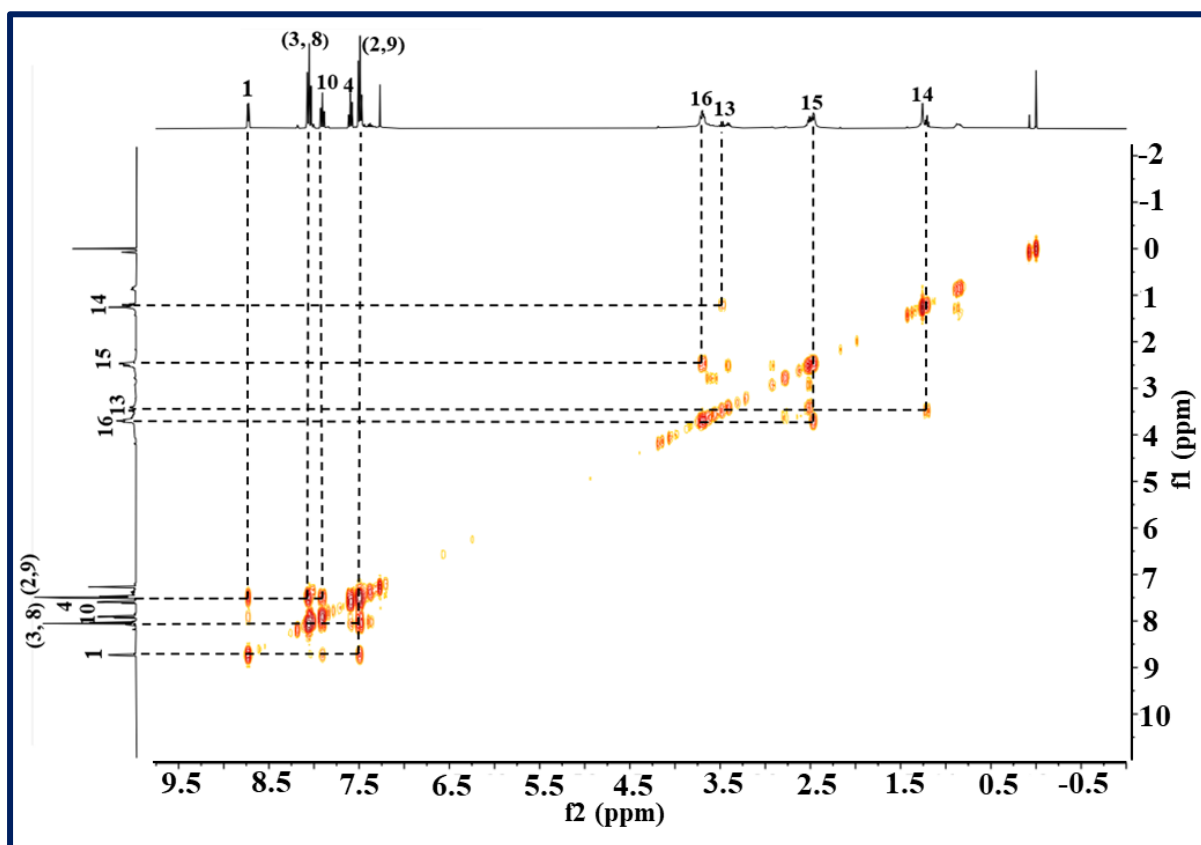


Fig. V.3. ^1H - ^1H gCOSY NMR spectrum of **L** in CDCl_3 .

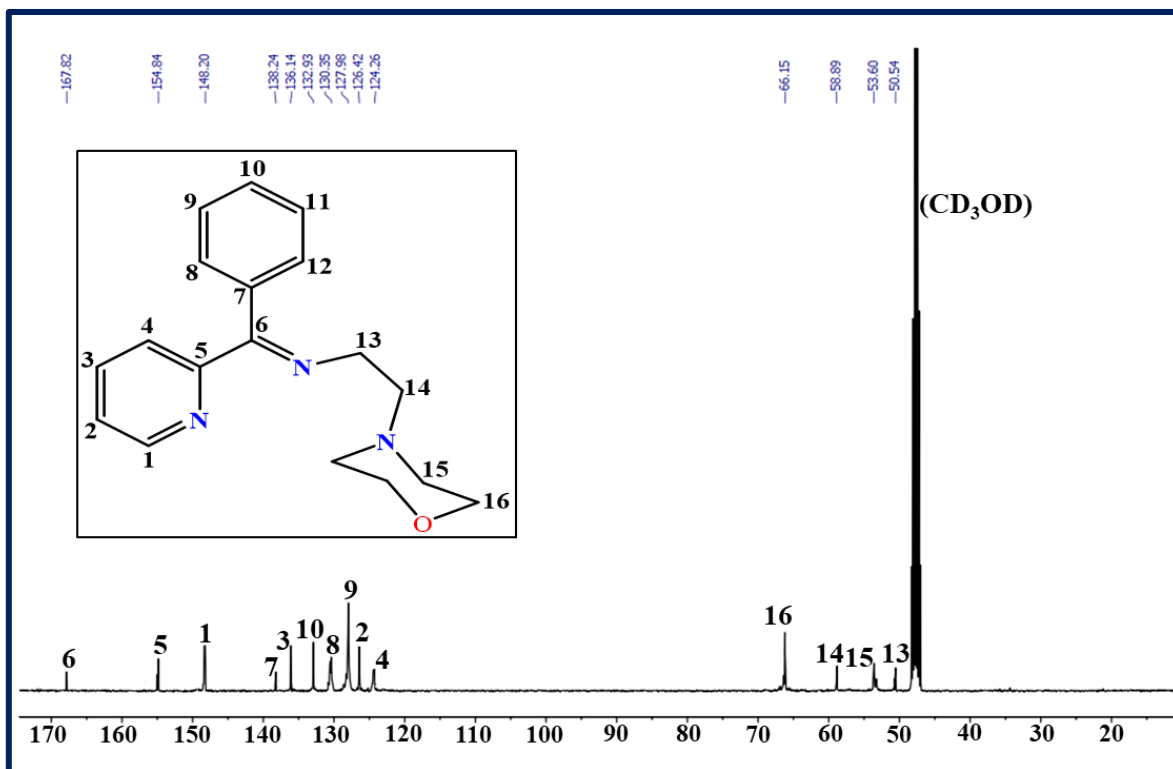


Fig. V.4. ^{13}C NMR spectrum of **L** in CD_3OD .

The FT-IR spectrum of bare **L** shows a characteristic vibrational stretching band at 1663 cm^{-1} . This evidences C=N bond formation (Fig. V.5) [65,66].

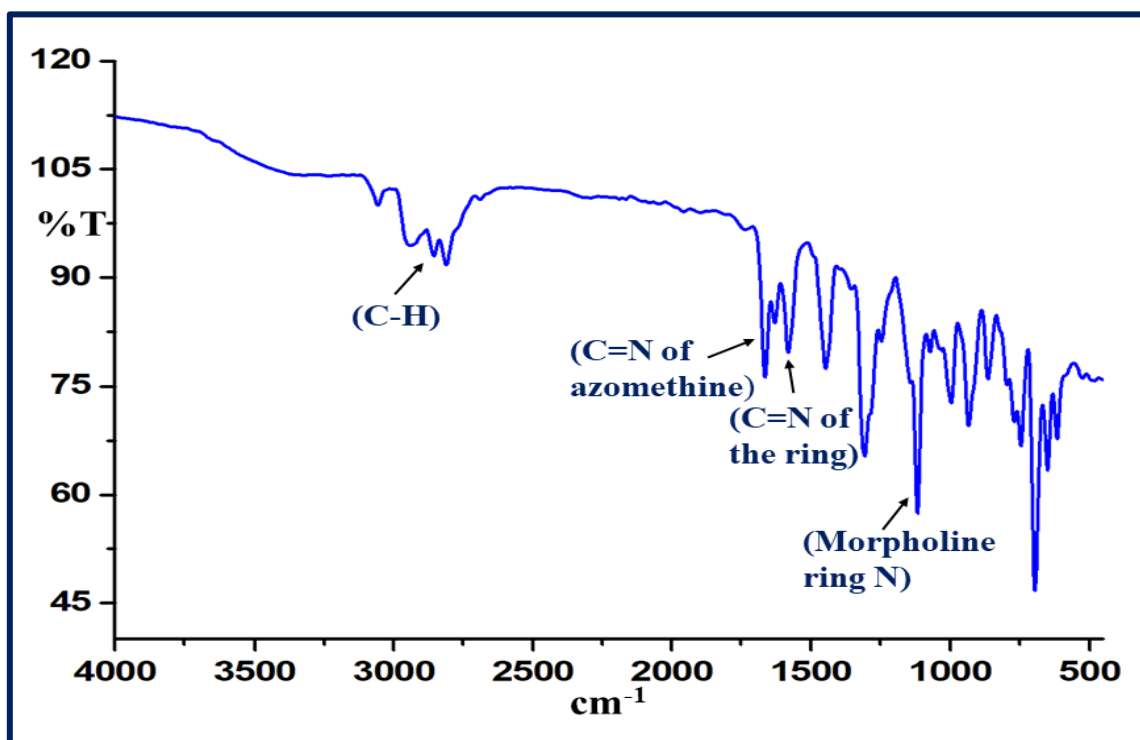


Fig. V.5. FT-IR spectrum of **L**.

Upon complexation, this band shifted bathochromically to lower wavenumber values of 1632 and 1645 cm^{-1} for **1** and **2** respectively. This owes to the coordination of azomethine N of free ligand to copper(II) centers [67,68]. The weakening of the free C=N bond during metallation results in this bathochromic shift [69]. **1** also shows a very broad IR absorption band at 3526 cm^{-1} for non-coordinating water molecule [70] (Figs. V.6 and V.7).

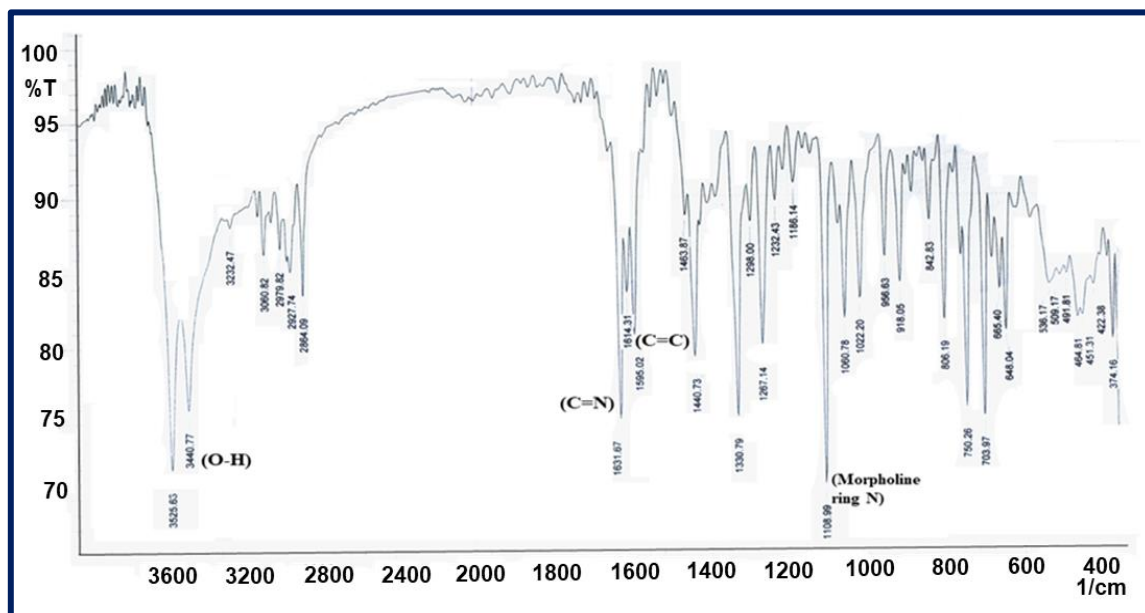


Fig. V.6. FT-IR spectrum of **1**.

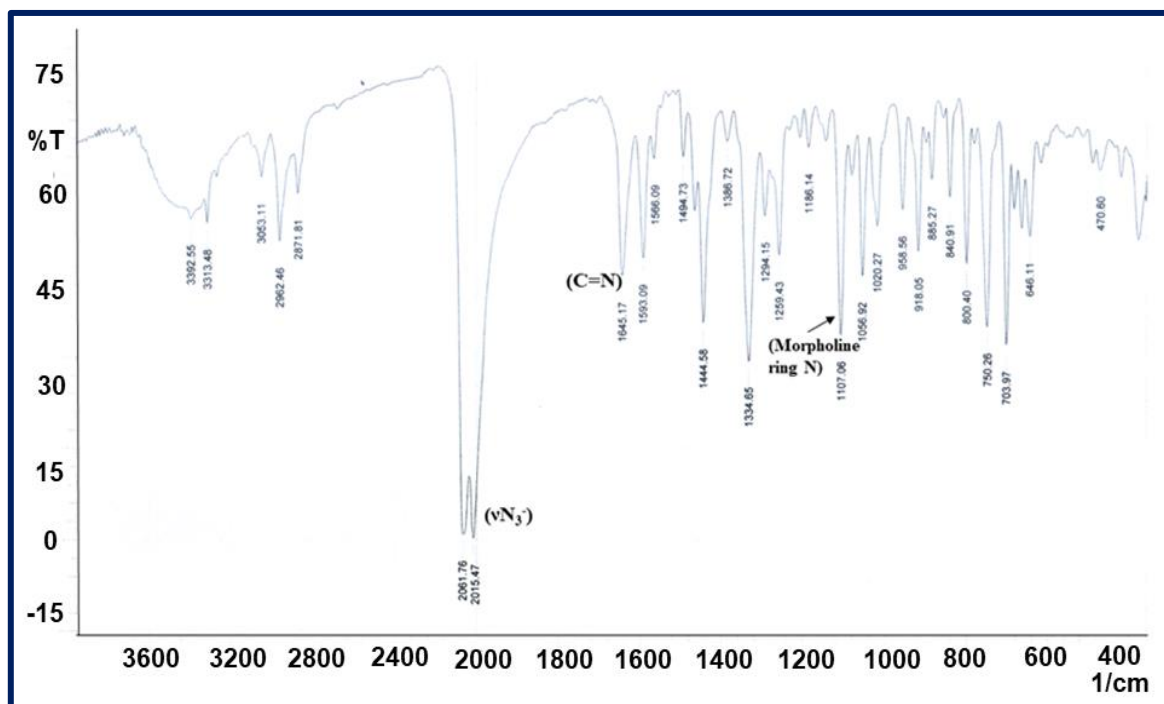


Fig. V.7. FT-IR spectrum of **2**.

The electronic absorption spectra of the ligand (**L**) and its stabilised copper(II) complexes were recorded in methanol as depicted in Fig. V.8. Generally, intense electronic transition bands due to ligand moieties appear in the UV region, while weak and forbidden d-d bands span the visible domain [71,72]. One-electron paramagnetic **1** ($\mu_{\text{eff.}} = 1.82 \mu_{\text{B}}$) and **2** ($\mu_{\text{eff.}} = 1.80 \mu_{\text{B}}$) displayed high-energy intense bands respectively at 274 and 272 nm due to $\pi\text{-}\pi^*$ intra-ligand charge transfer (ILCT) transition [73-75]. The spectrum of **2** also shows an absorption band at 396 nm. This is ascribed to ligand-to-metal charge transfer (LMCT) transition [76]. In the visible domain, a very weak but broad band appeared at 695 and 668 nm for **1** and **2** respectively. These are characteristic d-d bands for Jahn-Teller distorted mononuclear penta-coordinated copper(II) complexes [77].

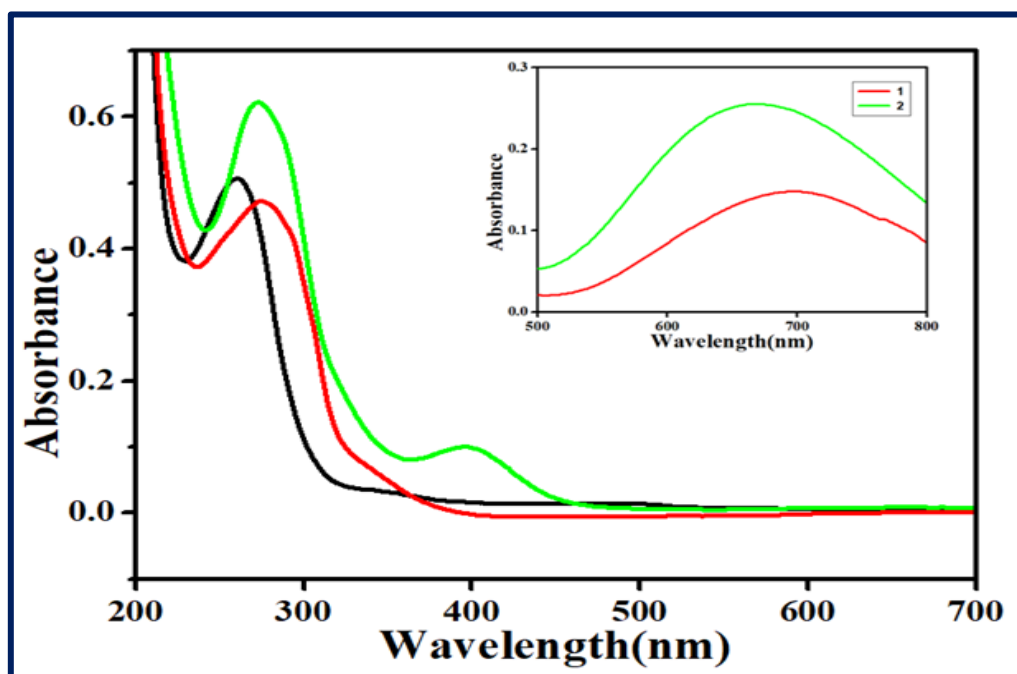


Fig. V.8. UV-Vis spectra of **L** (black), **1** (red) and **2** (green) in methanol. (Inset: d-d bands of **1** and **2**).

3.2. Description of the crystal structures of **1** and **2**

1 and **2** are discrete mononuclear Cu(II) entities. ORTEPs of both **1** and **2** with 30% probability ellipsoids along with atom labelling scheme are shown in Fig. V.9. **1** and **2** crystallise respectively in the orthorhombic *Pbca* space group ($Z = 8$) and monoclinic *P21/c* space group ($Z = 4$). The penta-coordination environment around the metal centres in **1** and **2** is respectively completed by 'N₃Cl₂' and 'N₅' donor sets. The copper(II) center in **1** enjoys three nitrogen donation from the ligand moiety and two chlorides as counter anions; while the homoleptic

donor environment in **2** is fulfilled by three nitrogen donors from **L** and two nitrogen donors from two terminally linked end-on azide ligands.

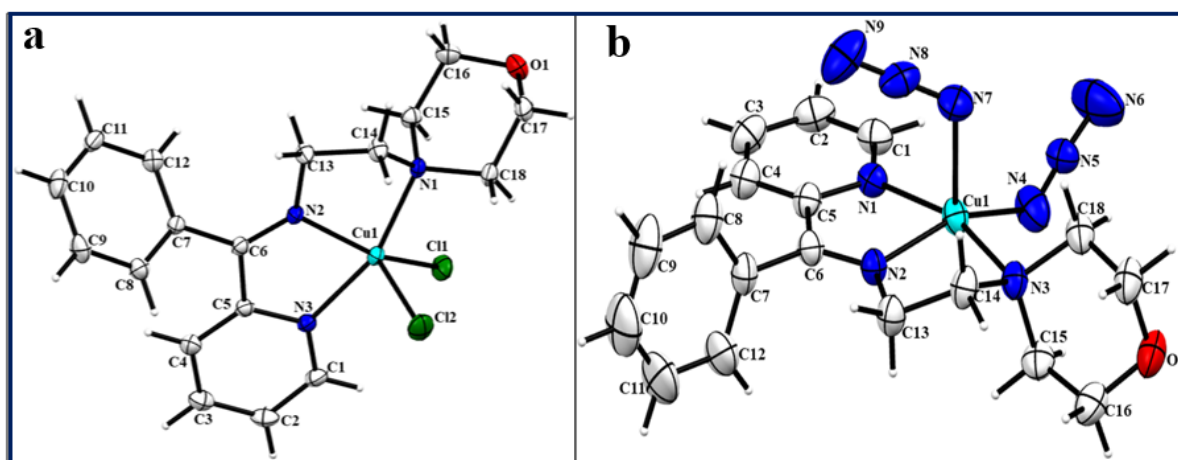


Fig. V.9. (a) ORTEP of **1** with 30% probability ellipsoids. Solvent molecules are omitted for clarity. (b) ORTEP of **2** with 30% probability ellipsoids.

In **1**, the value of Addison's trigonality index parameter, τ_5 comes out to be 0.23 [78-80]. Accordingly, the disposed geometry around the metal center in **1** is distorted square pyramidal. The basal plane around the metal center in **1** is comprised of Cu1-N1; 2.067(2), Cu1-N2; 2.022(3), Cu(1)-N(3); 1.975(2) and Cu1-Cl1; 2.281(11) Å bonds. The apical position is occupied by the Cl(2) atom at a distance of 2.456(12) Å from the metal center. Analogous apical bond distances for chlorine donor atoms are, however, known for mononuclear copper(II) systems in similar geometric disposition [81]. Likewise, the copper(II) center in **2** also exhibits a square pyramidal geometric disposition. The calculated τ_5 value here is of 0.10. As a result, the distortion in **2** is found to be comparatively less. The basal plane around copper(II) in **2** is composed of Cu1-N1; 2.046(2), Cu1-N2; 1.924(2), Cu1-N3; 2.076(3) and Cu1-N4; 1.921(3) Å bonds. The N(7) atom from a terminally disposed azide group occupies the apical position of the square based pyramid. The apical Cu1-N7 bond is of 2.226(3) Å. Two mono-dentate terminal azide groups, N4-N5-N6 and N7-N8-N9, are found to be slightly asymmetric [N4-N5 = 1.068(4), N5-N6 = 1.154(5), N7-N8 = 1.149(4) and N8-N9 = 1.141(5) Å]. The terminal azide group, N4-N5-N6, deviates more from linearity [N4-N5-N6 angle is of 174.30(4)°] in comparison to the other terminally anchored azide group, N7-N8-N9 [N7-N8-N9 angle is of 179.13(4)°]. To the best of our knowledge no mononuclear copper(II) complex in penta-coordination mode with two end-on azido ligands is known. However, only a mononuclear zinc(II) complex is known [82-84]. It is pertinent to note that Schiff base ligands

offer diverse structurally interesting noteworthy coordination complexes [83,84]. The Z values for **1** and **2** are respectively of eight and four. In **1**, two molecular units are linked by Cl···H-C and O···H-C intermolecular hydrogen bonds (Fig. V.10a). Fig. V.10b depicts the H-bonded packing diagram of **2**. The molecular packings of **1** and **2** are shown in Fig. V.11.

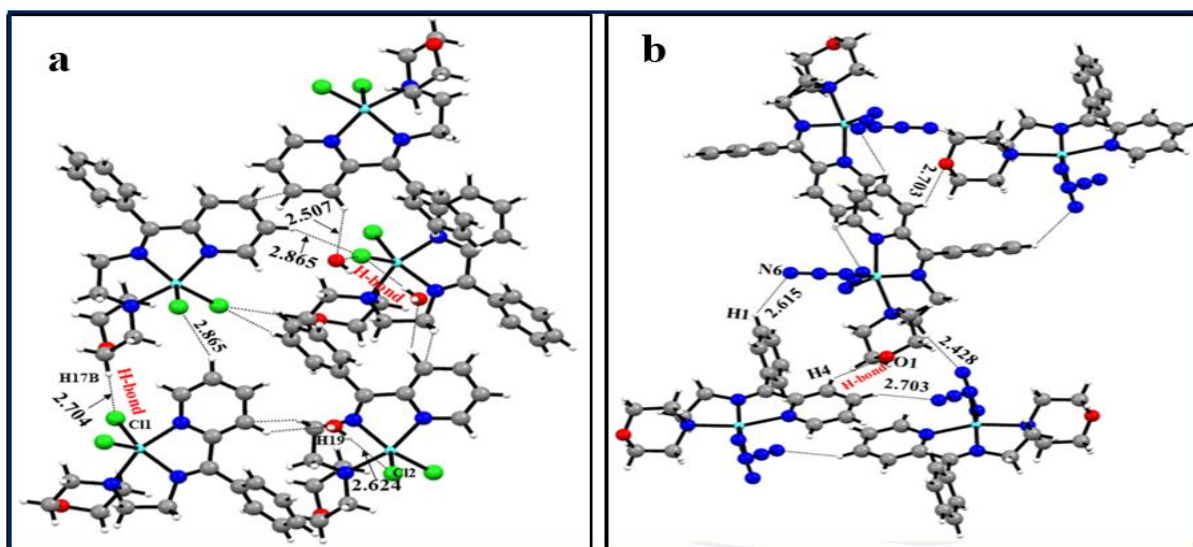


Fig. V.10. (a) Hydrogen bonded, C-H···Cl, O-H···Cl, packing diagram of **1**. (b) Hydrogen bonded, C-H···O and C-H···N, packing diagram of **2**.

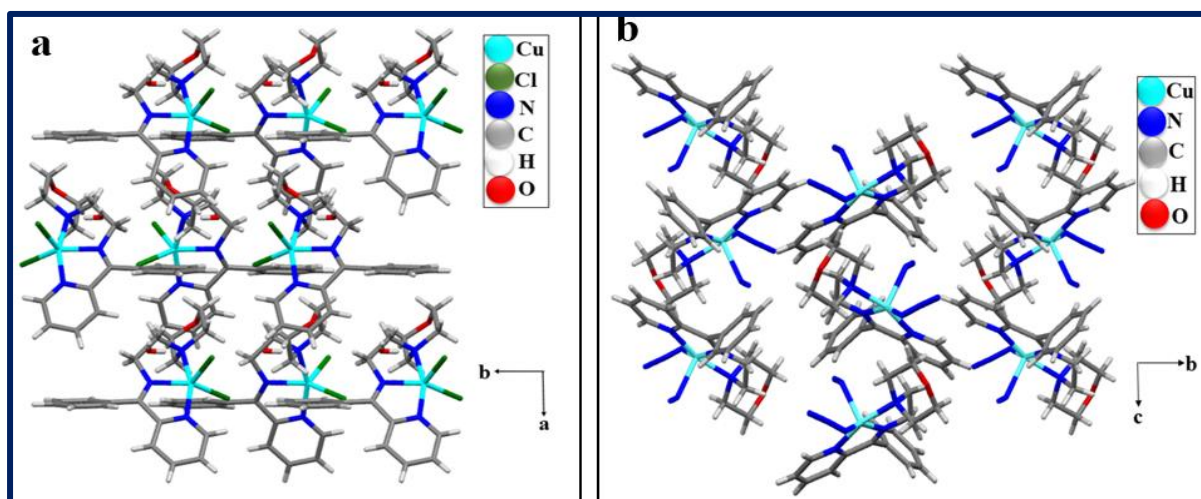


Fig. V.11. (a) The molecular packing of **1** when viewed along crystallographic c axis. (b) The molecular packing of **2** when viewed along crystallographic a axis.

3.3. *In vitro* cell growth inhibition

The cytotoxic effects of the compounds **1**, **2**, and ligand, **L** were evaluated using the WST-1 assay on lung adenocarcinoma cells A549. The WST-1 based assay helped in exploring the metabolic activity of the mitochondria as a measure for the vital status of cells. The

proliferation of cell as well as indirect cell demise can be estimated by this method on a large scale in microtiter plates [85-87]. In presence of active dehydrogenase enzymes, the colorimetric salt WST-1 has permeated into the cytosol of a metabolically active cell and is reduced by cellular mitochondrial dehydrogenases producing an intracellular purple precipitate (formazan), suggesting higher the cell viability more the accumulation of dye. As shown in Fig. V.12a, compound **1** has strongly inhibited the growth and proliferation of cells in a dose dependent manner followed by compound **2** while ligand displaying least cytotoxicity towards the cancerous cell. Additionally, WST-1 assay has helped us to calculate the IC₅₀ value of compounds **1**, **2** and ligand (**L**) for A549 cells which was noted to be 66, 88 and 200 μM respectively (Table V.6).

Table V.6. IC₅₀ values obtained for the selected compounds and ligand

Compound	IC ₅₀ Value (μM)
1	66
2	88
Ligand	200

The IC₅₀ values represent the mean of three independent experiments.

Compound **1** showed better cytotoxicity at a lower dose as compared to compound **2**; whereas ligand exhibited cytotoxicity at almost twice the concentration of compounds **1** and **2** and hence not taken for further experiments. The concentration at which the inhibition was initiated for compounds **1** and **2** was 2.2 and 11 μM respectively.

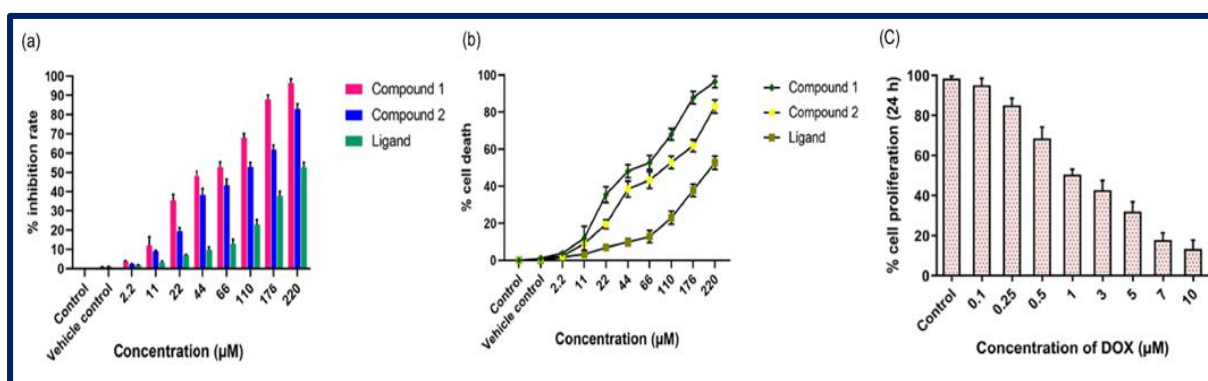


Fig. V.12. *In vitro* growth inhibition of lung adenocarcinoma cells A549 following treatment with compounds for 24 h. The graphs (a) WST-1 assay and (b) Trypan blue assay shows the log dose cytotoxic effects of compounds **1**, **2** and ligand (**L**). (c) Dose-response effects of

positive control, DOX to A549 cell lines. The graphs were prepared as means \pm SD of three separate experiments using GraphPad Prism 6 statistical software.

The cytotoxicity of compounds **1**, **2** and ligand (**L**) was further asserted by trypan blue dye exclusion assay. Fig. V.12b summarizes the cytotoxic effect of both the compounds and ligand as determined by trypan blue dye exclusion assay. The expounded results were in accordance with WST-1 assay. A significant cytotoxic response was noted towards A549 cells by both the compounds, **1** and **2**; while the ligand exhibited the least cytotoxicity. Thus, both the assays reaffirm the sensitivity of the lung adenocarcinoma cells on exposure to compounds, **1** and **2**. Further experiments were carried out for both **1** and **2** with dose values lower than and equal to IC_{50} value. As the ligand did not exhibit any prominent cytotoxicity, so it was not employed in the following assays. Doxorubicin is a widely used chemotherapeutic drug which is routinely used in the treatment of various cancers like breast, liver, lung, ovarian, thyroid, gastric, paediatric cancers, multiple myeloma and sarcoma [86]. During the course of this study, the susceptibility of lung cancer cell line towards doxorubicin was investigated to compare the results of compounds **1**, **2** and ligand (**L**) with an established anticancer drug as positive control. The investigation showed that doxorubicin had an IC_{50} value of $1.1 \mu M$ for A549 cells (Fig. V.12c) which is comparable with the published results [87].

3.4. Compounds, **1** and **2** impede colony formation of A549 cells

To further validate the effect of compounds, **1** and **2** on A549 cell growth and viability, clonogenic cell survival assay was performed. 1×10^3 cancer cells were seeded with and without both the compounds and after 7 days of incubation, the number of colonies formed was counted.

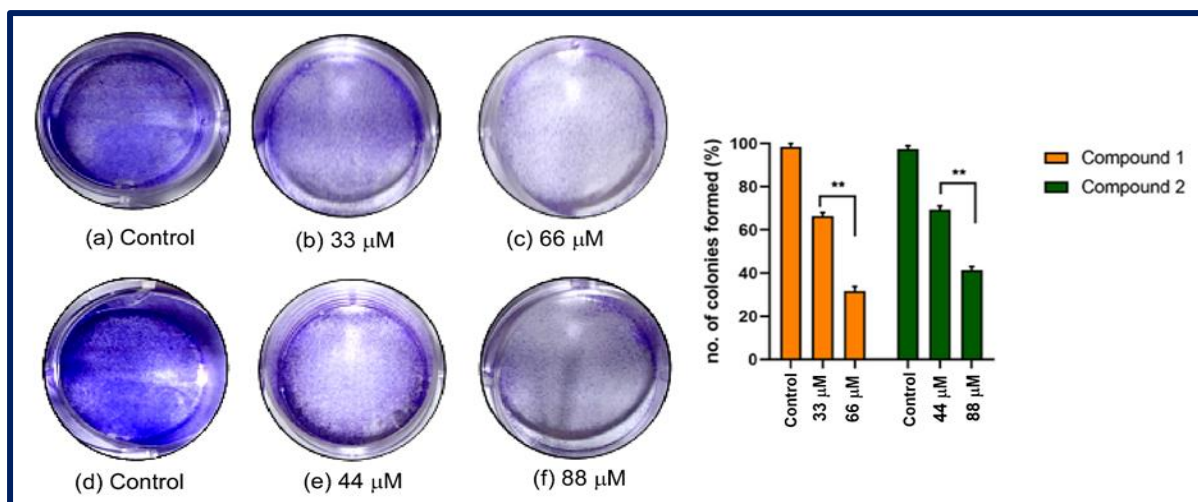


Fig. V.13. Colony forming ability of A549 cells cultured for a week, determined by a colony formation assay. (a-f) Influence of different concentrations of compounds **1** and **2** on colony

forming ability of lung cancer cells. Quantitative analysis of the number of colonies formed in cells treated with various concentrations of compounds (Right panel). Results are representative of at least three independent experiments. The graph represents mean \pm SEM using GraphPad Prism 6 statistical software while the asterisks *, **, *** indicate significant difference at $p < 0.05$, $p < 0.001$ and $p < 0.0001$, respectively, from the untreated control cells.

As illustrated in Fig. V.13a-c, adequate inhibition of colony formation for compound **1** was observed on exposure to 33 and 66 μ M and on the other hand for compound **2** inhibition in colony forming ability was noted for 44 and 88 μ M (Fig. V.13d-f). Nonetheless, at IC₅₀ dose the cell survival, adhesion and colony forming efficiency has further reduced and very few cells were found in well as compared to the full grown cells in untreated set. This effect was not further altered even after cell grown in a drug-free condition for one week.

3.5. Compounds, **1** and **2** induce arrest in cell-cycle progression

Most chemotherapeutic drugs target a physiological comprehending feature of cancerous cells as they inclined to proliferate more actively than normal cells. Most anticancer therapies restrict the growth and proliferation of cancerous cells by arresting the cell cycle progression at a particular phase [88]. *In vitro* assessment has already displayed that the compound has potent antiproliferative activity against A549 cells. Further inhibition of proliferation was examined by measuring cell cycle distribution using propidium iodide stain following treatment with different concentrations of **1** and **2** for 24 h as per the standardized protocol of Nandi and co-workers [89]. The DNA content of A549 cells in different phases of cell cycle was investigated. The histograms from flow cytometer demonstrated an increase in cell population at the sub-G0 phase with concomitant decrease in the proportion of cells in G0/G1, S and G2/M phase of the cell cycle of treated cells in both the compounds when compared with the untreated control cells. In compound **1**, the proportion of cells in S and G2/M phase decreased from 20.7% (control) to 12.2% and 7.2% respectively (Fig. V.14a-c). Compound **2** exhibited a different pattern of reduction in cell number of S and G2/M phase from 15.2% to 10.56% and 6.2% respectively (Fig. V.14d-f). Though the untreated sets demonstrated a presumed pattern with no peak at sub-G0 phase and a broad peak at S and G2/M phase. The increase in the number of cells in the Sub G0 phase was further elevated to 35% and 25% respectively following exposure to 44 and 88 μ M of compounds, **1** and **2**. An increase in the cell population at Sub-G0 phase was a clear indication of apoptotic cells in a dose dependent manner (Fig. V.14; right

panel). Taken together, both compounds **1** and **2** caused growth arrest in the Sub G0 phase of the cell cycle.

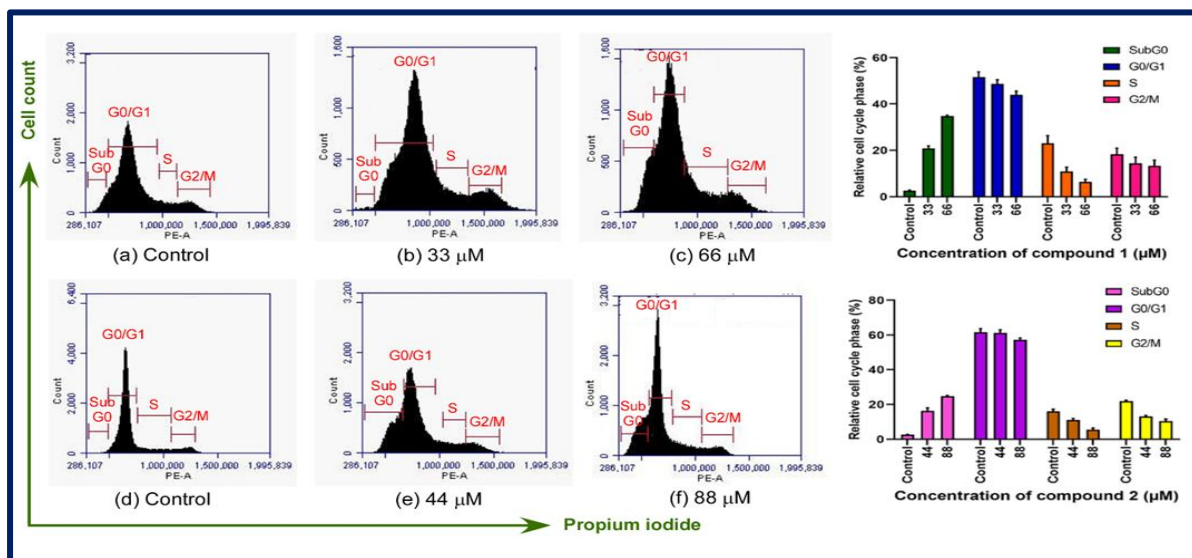


Fig. V.14. Compounds, **1** and **2** induce cell cycle arrest in lung adenocarcinoma cells. Flow cytometry was used to represent cell cycle profiles of A549 cells treated with 33 μM, 66 μM (Compound **1**) and 44 μM, 88 μM (Compound **2**) respectively (a-f). X-axis represents the intensity of propidium iodide, and the Y-axis represents the cell counts. The graph shows the quantitative analysis of cell cycle distribution (Right panel). Values are means ± SD of three independent experiments, each conducted in triplicate.

3.6. Compounds **1** and **2** induce morphological changes in cultured human adenocarcinoma cells A549

Further to validate the cytotoxic effect of the compounds on cancer cells, light microscopy observations were performed to observe the morphology alteration in A549 cells. After treatments with various concentrations for 24 h, Fig. V.15 show bright-field micrographs of A549 cell lines. Dose-dependent morphological changes were visible upon exposure to **1** and **2** like reduced confluence, more bright-circular dead cells and debris were floating, cellular contraction and distorted longer to round shaped acquired due to the loss of adhesion suggesting a cytotoxic and antiproliferative effect (Fig. V.15c, d and g, h). Comparing these results with those of the untreated and vehicle control, no such morphological alterations were observed. Untreated control cells exhibited an extended fusiform shape, well-adherent growth, clear cellular boundaries, higher cell density with lesser cytoplasmic granules (Fig. V.15a, b and e, f).

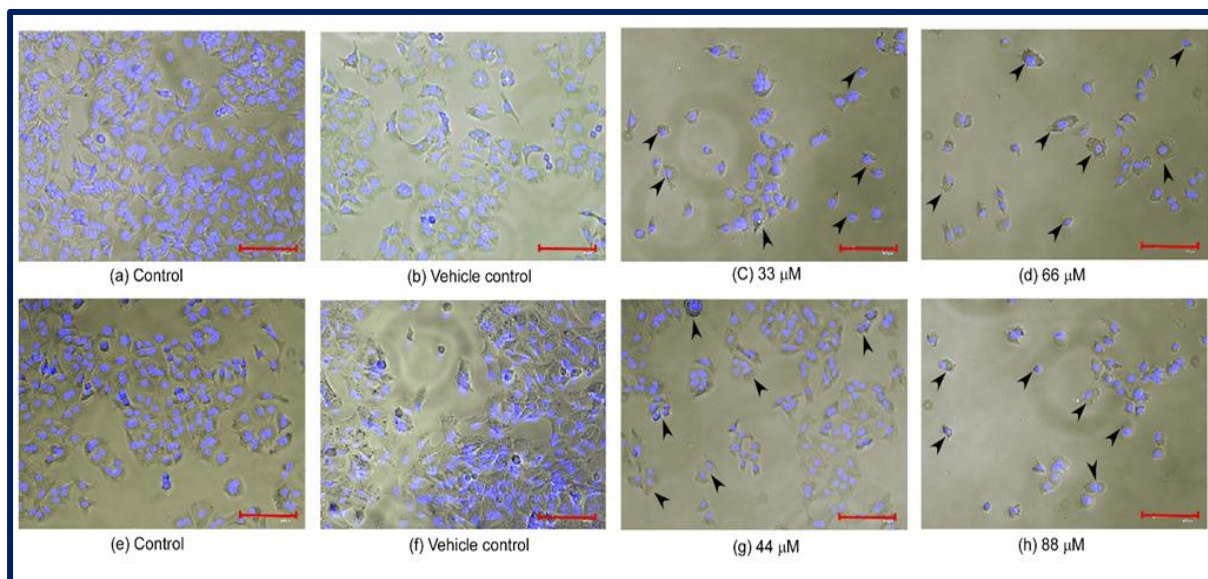


Fig. V.15. Effect of compounds, **1** and **2** on cellular morphological alterations of A549 cancer cells observed under phase contrast light inverted microscope with 10X magnification. Cells were incubated for 24 h with different concentrations of both the compounds (a-f). Scale bar 50 μm . Black arrow signifies the morphological alteration after treatment with compounds, **1** and **2**.

3.7. Compounds **1** and **2** compelled apoptotic induction in A549 cells

Cell death by way of apoptosis is an essential factor for the anticancerous activity of any compound [90]. To evaluate whether the cytotoxicity caused by compounds **1** and **2** towards lung adenocarcinoma cells was induced by apoptosis, various staining techniques have been performed. A fluorescent microscopic study was undertaken to analyse the changes induced by both the compounds in cellular and nuclear morphology of A549 cells and to understand their mode of cell death following staining with DAPI and AO/EtBr dyes. Staining the treated cells with DNA binding dye DAPI, displayed typical morphological features of apoptosis including apoptotic nuclei with bright blue fluorescence, condensed chromatin, deformed and fragmented nuclei with membrane blebbing (indicated by arrow) whereas in untreated and vehicle cells, nuclei were normal with no nuclear disruption indicating healthy cells observed in both the compounds (Fig. V.16a-h). It was also spotted that at higher concentrations i.e. 66 and 88 μM , more cells had exhibited nuclear deformities (Fig. V.16d and h).

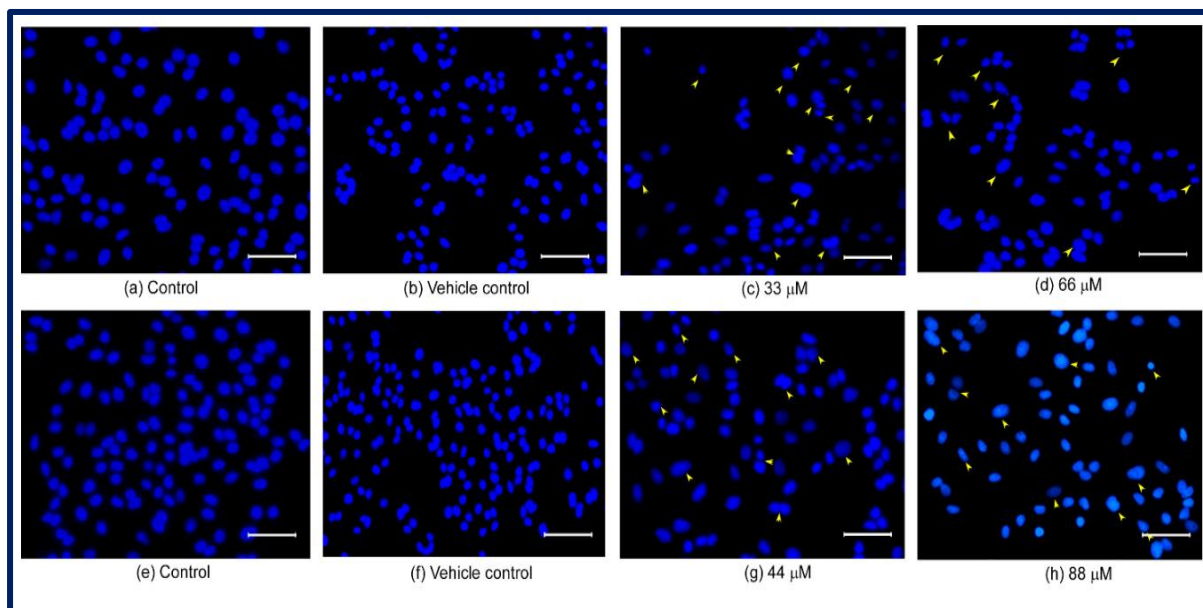


Fig. V.16. Compounds **1** and **2** induce apoptosis of A549 cells. Nuclear changes in apoptotic cells treated with both the compounds are shown by DAPI staining using fluorescence microscopy with 20X magnification. Scale bar 100 μm . Arrow indicates the deformed nuclei after exposure to compounds, **1** and **2**.

After 24 h drug treatment, the morphological abnormalities were observed by double staining with AO/EtBr. Treated A549 cells exhibited nuclear margination and chromatin condensation, which were major consequences of the apoptotic trigger, after treatment of 24 h. In control, cells were intact, healthy with normal cytoplasm and morphology emitting green fluorescence (Fig. V.17a and d). Fluorescence microscopic images of cells treated with lower dose of compounds **1** and **2** distinctly revealed the yellowish green fluorescence representing early apoptotic features (Fig. 17b and e) like cellular shrinkage, membrane blebbing and chromatin condensation other deformities (indicated by arrow) and in higher concentration of treatments, fewer cells fluoresced with yellowish orange along with yellowish green fluorescence indicating the presence of both early as well as late apoptotic cells (Fig. V.17c and f). Late apoptotic cells displayed membrane loss and apoptotic bodies. These characteristic features detected on staining with DAPI and AO/EtBr was typical of apoptotic cells and was quite different from the cells found in untreated control set. Vehicle sets in both cases showed characteristic morphological features as the non-treated ones. This stipulated that exposure of compounds **1** and **2** was potentially competent to trigger apoptosis in most A549 cells.

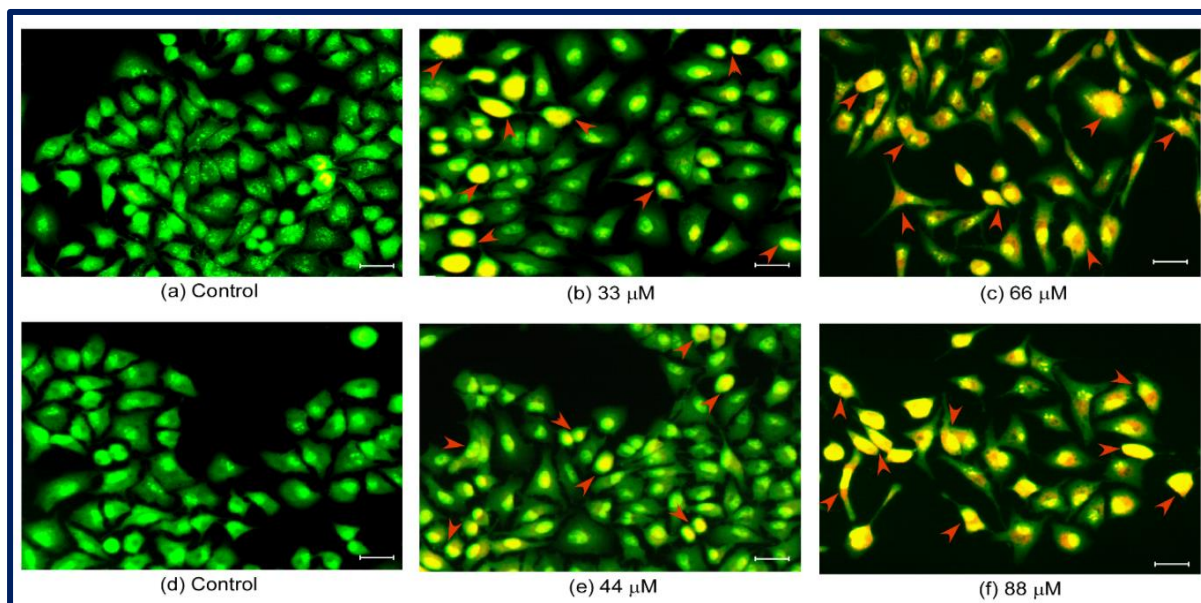


Fig. V.17. Induction of apoptosis with compounds, **1** and **2** in lung adenocarcinoma cells after 24 h incubation. Fluorescence microscopy images of AO/EtBr stained A549 cells (a) and (d) untreated (control) and (b), (c), compound **1** and (e), (f) compound **2** treated at different concentration. AO/EtBr images were recorded using excitation at 460 nm. Viable (light green), early apoptotic (bright green or yellowish green fluorescing) and late apoptosis (yellowish orange fluorescing) cells were observed. Magnification $\times 20$. Scale bar 100 μm . Arrow marks the treated cells showing typical characteristic of apoptosis.

The cytotoxicity assay was evaluated in solution. To check the stability of both **1** and **2** in solution, we have monitored them through UV-Vis spectra with variation in time (Fig. V.18). **1** and **2** are found to be quite stable in solution.

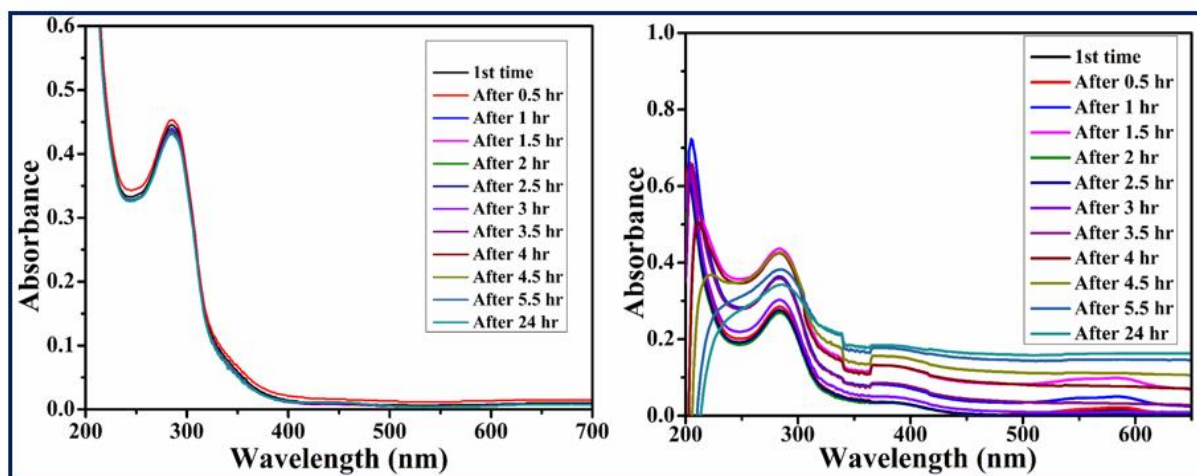


Fig. V.18. UV-Vis spectra of **1** (left) and **2** (right) with variation in time'

3.8. Cytotoxic mechanistic action and structure-activity relationship

To augment the cytotoxic potentiality of both **1** and **2** towards the non-small cell lung cancer cell line, A549 under apoptosis, we employed propidium iodide (PI) staining. The DNA content of A549 cells in different phases of cell cycle was also monitored for cell apoptosis (cell death). Observed activity of **1** and **2** with treated cells is plausibly due to an increase in cell population at the sub-G0 phase with concomitant decrease in the proportion of cells at G0/G1, S and G2/M phase of the cell cycle. Both **1** and **2** showed cell growth arrest in the Sub G0 phase of the cell cycle leading to manifested cytotoxicity [91].

Both **1** and **2** manifest promising activity in comparison to the complexing ligand towards A549. This significant enhancement of activity of **1** and **2** is due to the chelation of the ligand with Cu(II) centers. Extended square pyramidal structural disposition of the copper(II) centers, both in **1** and **2**, accentuated by π - π^* conjugation due to metal ligand chelation is found to be contributing towards enhancement of activity [92]. Inhibitory propensity of **1** against A549 cancer cell lines is observed to be higher than that observed for **2**. Most likely this may be due to the presence of different co-ligand in the coordinating environment. Possibly, this ligand field effect also makes **1** more active towards WST-1 assay.

3.9. Cyclic voltammetry

Electrochemical redox behaviour of **1** and **2** was studied at room temperature in dehydrated degassed methanol. The CV experiments were conducted under dry and pure N₂ atmosphere using GC working electrode. Voltammograms of **1** and **2** are shown in Fig. V.19 and the pertinent data are tabulated in Table V.7. On the positive side of Ag/AgCl reference electrode, **1** and **2**, show oxidative response at 0.591 and 0.585 V respectively. The corresponding reduction peaks for **1** and **2** are discernible respectively at -0.336 and -0.292 V vs Ag/AgCl. The ligand under similar electrochemical environment was found to be electrochemically inert. Accordingly, the manifested redox response can safely be attributed to copper centered. Comparing the observed redox response with that shown by the standard one-electron redox marker, ferrocene; the present response can be assigned to copper(II) to copper(I) reductions. The cathodic to anodic peak potential difference (ΔE_p) for **1** and **2** was found respectively to be 255 and 297 mV at room temperature. The observed i_{pc}/i_{pa} value for **1** is 2.737; while for **2** this value is of 1.729. Accordingly, the observed redox response in both **1** and **2** is designated as irreversible [93]. The observed difference in redox behaviour between **1** and **2** is most likely due to ligand field effects [94].

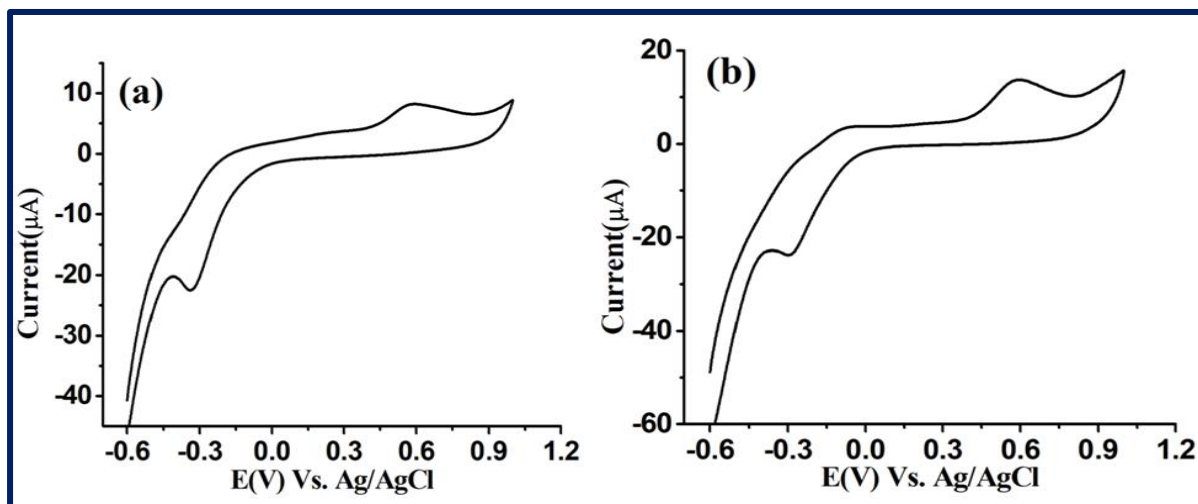


Fig. V.19. CV of the copper(II) complexes, **1**(a) and **2** (b), in methanol at a scan rate of 100 mV s⁻¹.

Table V.7. CV data for **1** and **2**

Complex	E _{pa} (i _{pa})	E _{pc} (i _{pc})	E _{1/2}	i _{pc} /i _{pa}
1	0.591(8.22)	-0.336(-22.5)	0.463	2.737
2	0.589(13.7)	-0.292(-23.7)	0.440	1.729

E_{pc} = cathodic peak potential, V; E_{pa} = anodic peak potential, V; i_{pc} = cathodic peak current and i_{pa} = anodic peak current

3.10. TGA analysis

In order to assess the thermal behaviour of **1**, we have analysed it thermo-gravimetrically. 6.54 mg of **1** was heated in the temperature range of 30-600 °C in an aluminium crucible at the heating rate of 10 °C per min under dynamic nitrogen flow rate of 150 ml per min. The resulting TGA plot of **1** is shown in Fig. V.20.

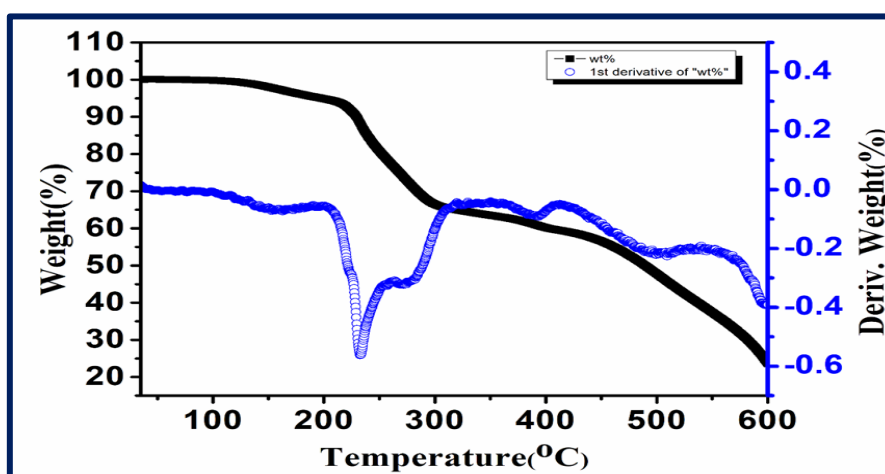


Fig. V.20. TGA curve of **1**.

The thermogram indicates high thermal stability of **1**. It undergoes thermal decomposition in three consecutive steps. In the first step, loss of non-coordinated water molecule (thermal dehydration) occurs in between 100-175 °C [95]. The experimental mass loss of 3.93% for this thermal event is in concordance with the theoretical loss of 4.02%. The second step spans 200-260 °C. The experimental mass loss of 16.86% fairly corresponds to the calculated loss of 16.52%. This is due to the liberation of two coordinated chlorine atoms. Beyond 400 °C, a steady but sharp mass loss took place. This is due to complete combustion of the compound. The black residue is most likely cupric oxide along with little amount of carbon [96]. Compound **2** is explosive due to presence of two azide groups. Owing to safety concerns, thermal analysis has not been realised for **2**. However, our literature survey on analogous copper(II) azide complexes reveal that such systems are thermally stable almost up to 160 °C. Beyond this threshold critical temperature, azide based copper(II) systems explode rendering further thermo-gravimetric characterisation non-realistic [97,98].

3.11. PXRD

Powder X-ray diffraction (PXRD) analysis was performed at room temperature to test the bulk (phase) purity of the powdered crystalline sample of the two compounds, **1** and **2**. The patterns are shown in Fig. V.21. The major PXRD patterns of **1** and **2** (as obtained from respective synthesized bulk powdered samples) are found to be consistent, both in position and intensity, with those of the simulated pattern as obtained from SC-XRD data. This satisfactory concordance is indicative of the phase purity and consistency of the bulk of both **1** and **2**.

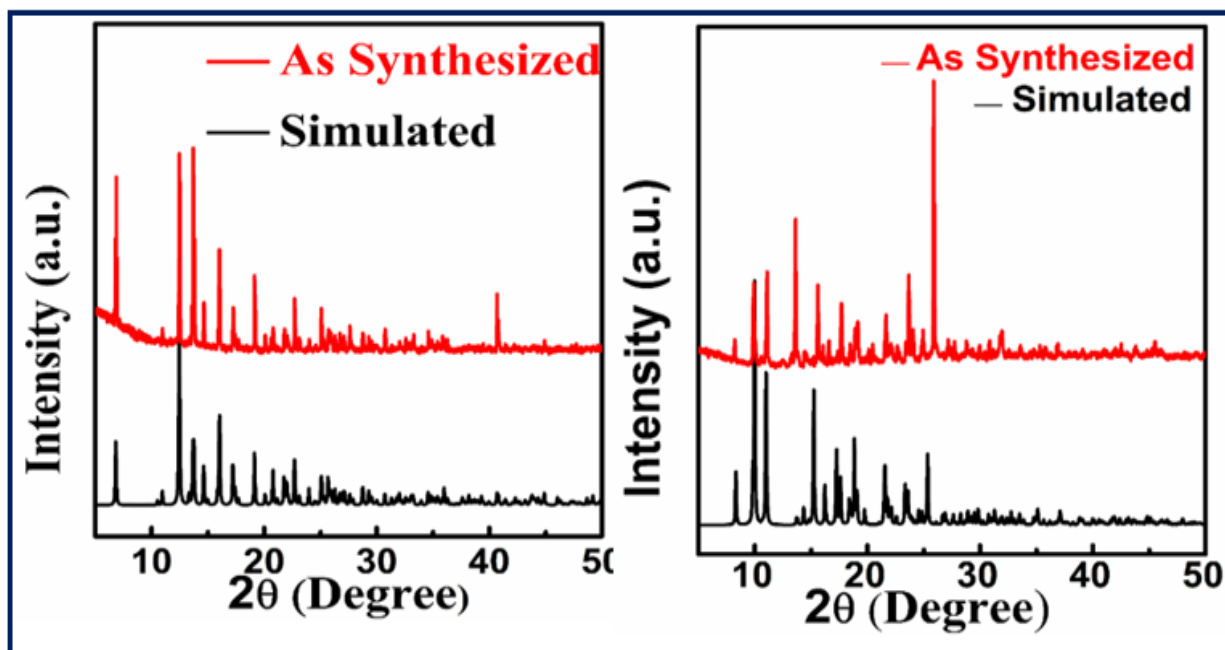


Fig. V.21. Powder X-ray diffraction patterns of **1** (left) and **2** (right).

4. Conclusions

Two mononuclear copper(II) complexes (**1** and **2**), based on a pharmacologically potential molecule, morpholine, dangled Schiff base ligand, were synthesized and thoroughly characterized. The X-ray crystal structures of both the complexes have been determined. Powder X-ray diffraction studies were also undertaken to authenticate the bulk purity of the samples as that retained in the single crystals. Thermal analysis of **1** was also performed to show the thermal stability of the complex. Redox behaviour of the complexes were also monitored to validate the biocompatibility of the complexes. The observed redox response of the two complexes hint that the manifested potential values can even be achieved *in vivo*. The cytotoxic effects of both the complexes were screened against LC cell lines in dose- and time-dependent manner. The ligand manifests no cytotoxic efficacies. On the contrary, low IC₅₀ value of **1** towards non-small cell lung cancer (NSCLC) shows better antiproliferative efficacies of it with low toxicity in comparison to **2**. Both **1** and **2** were induced towards lung adenocarcinoma cells by apoptosis. The expounded results show more cellular nuclear deformities at concentration 66 and 88 μ M respectively for **1** and **2**. The morphological changes in NSCLC cells after treatment with **1** and **2**, monitored with AO/EtBr staining techniques, show annihilation of A549 cancer cell. Our present cytotoxic studies and the corroborated results obtained thereof clearly show that **1** and **2** bear potential prospect and possibility in chemotherapeutic cancer therapy and oncological management.

5. References

1. H. Schiff, Ann. Suppl. 3 (1864) 343.
2. P.G. Cozzi, Chem. Soc. Rev. 33 (2004) 410-421.
3. M.H. Habibi, M. Montazerzohori, A. Lalegani, R.W. Harrington, W. Clegg, J. Fluorine Chem. 127 (2006) 769-773.
4. S. Shahraki, A. Heidari, H.R. Mirzaei, M. Saeidifar, N. Ahmadianasab, H. Mansouri-Torshizi, J. Iran. Chem. Soc. 15 (2018) 697-709.
5. H. Keypour, M. Rezaeivala, L. Valencia, P. Pérez-Lourido, H. R. Khavasi, Polyhedron 28 (2009) 755- 3758.
6. T.L. Yusuf, S.D. Oladipo, S.A. Olagboye, S.J. Zamisa, G.F. Tolufashe, J. Mol. Struct. 1222 (2020) 28857.
7. S.M. Wilkinson, T.M. Sheedy, E.J. New, J. Chem. Educ. 93 (2016) 351-354.
8. S.K. Tadavi, A.A. Yadav, R.S. Bendre, J. Mol. Struct. 1152 (2018) 223-231.
9. R. Chandrasekaran, S.A. Yadav, S. Sivaperumal, J. Cluster Sci. 6 (2019) 1.
10. K.S. Kumar, S. Ganguly, R. Veerasamy, E. De Clercq, Eur. J. Med. Chem. 45 (2010) 5474-5479.
11. K. Ohui, E. Afanasenko, F. Bacher, R. L. X. Ting, A. Zafar, N. Blanco-Cabra, E. Torrents, O. Domotor, N. V. May, D. Darvasiova, E. A. Enyedy, A. Popovic-Bijelic, J. Reynisson, P. Rapta, M. V. Babak, G. Pastorin, V. B. Arion, J. Med. Chem. 62 (2019) 512-530.
12. K. Dhahagani, S.M. Kumar, G. Chakkaravarthi, K. Anitha, J. Rajesh, A. Ramu, G. Rajagopal, Spectrochim. Acta Part A: Mol. Biomol. Spectrosc. 117 (2014) 87-94.
13. P.A. Ajibade, F.P. Andrew, N.L. Botha, N. Solomane, Molecules 25 (2020) 3584.
14. M. Hosseini-Kharat, R. Rahimi, D. Zargarian, Z. M. Lighvan, A. A. Momtazi-Borojeni, T. Sharifi, E. Abdollahi, H. Tavakol, T. Mohammadi, J. Biomol. Struct. Dyn. 37 (2019) 3788-3802.
15. K. Rupak, S. R. Vulichi, K. Suman, Int. J. Chem. Sci. 14 (2016) 1777-1788.
16. J.A. War, S.K. Srivastava, S.D. Srivastava, Spectrochim. Acta Part A: Mol. Biomol. Spectros. 173 (2017) 270-278.
17. L.A. Torre, F. Bray, R.L. Siegel, J. Ferlay, J. Lortet-Tieulent, A. Jemal, CA-Cancer J. Clin. 65 (2015) 87-108.
18. J. Ferlay, I. Soerjomataram, R. Dikshit, S. Eser, C. Mathers, M. Rebelo, D. M. Parkin, D. Forman, F. Bray, Int. J. Cancer 136 (2015) 359-386.

19. J. Ferlay, M. Ervik, F. Lam, M. Colombet, L. Mery, M. Piñeros, Global Cancer Observatory: Cancer Today. Lyon: International Agency for Research on Cancer; 2020.
20. Y. Xia, X. Liu, L. Zhang, J. Zhang, C. Li, N. Zhang, H. Xu, Y. Li, *Cancer Cell Int.* 19 (2019) 81.
21. B. Cvek, V. Milacic, J. Taraba, Q. P. Dou, *J. Med. Chem.* 51 (2008) 6256-6258.
22. P. Baszuk, W. Marciniak, R. Derkacz, A. Jakubowska, C. Cybulski, J. Gronwald, T. Debniak, T. Huzarski, K. Białkowska, S. Pietrzak, M. Muszyńska, J. Kładny, S.A. Narod, J. Lubiński, M.R. Lener, *Biomedicines* 9 (2021) 1628.
23. M. Nurmammat, H. Yan, R. Wang, H. Zhao, Y. Li, X. Wang, K. Nurmaimaiti, T. Kurmanjiang, D. Luo, J. Baodi, G. Xu, J. Li, *ACS Med. Chem. Lett.* 12 (2021) 467-476.
24. L. Quan, X. Luo, L. Xue, J. Li, Y. Ouyang, *J. Inorg. Organomet. Polym. Mater.* 30 (2020) 2744-2755.
25. F. Bray, J. Ferlay, I. Soerjomataram, R. L. Siegel, L.A. Torre, A. Jemal, CA: Cancer J. Clin. 68 (2018) 394-424.
26. S. Dilruba, G.V. Kalayda, *Cancer Chemother. Pharmacol.* 77 (2016) 1103-1124.
27. E. Wong, C. M. Giandomenico, *Chem. Rev.* 99 (1999) 2451-2466.
28. L. Kelland, *Nat. Rev. Cancer* 7 (2007) 573-584.
29. M. Galanski, B. K. Keppler, *Anti-Cancer Agent.* 7 (2007) 55-73.
30. T.C. Johnstone, K. Suntharalingam, S.J. Lippard, *Chem. Rev.* 116 (2016) 3436-3486.
31. V. Culotta, *J. Biol. Inorg. Chem.* 15 (2010) 1-2.
32. M. Alagesan, N.S.P. Bhuvanesh, N. Dharmaraj, *Dalton Trans.* 42 (2013) 7210-7223.
33. X. B. Fu, D. D. Liu, Y. Lin, W. Hu, Z. W. Mao, X. Y. Le, *Dalton Trans.* 43 (2014) 8721-8737.
34. L. M. Balsa, E. J. Baran, I. E. Leon, *Curr. Med. Chem.* 2021, 16.
35. Q. Pan, C.G. Kleer, K.L. van Golen, J. Irani, K.M. Bottema, C. Bias, M. de Carvalho, E.A. Mesri, D.M. Robins, R.D. Dick, G.J. Brewer, S.D. Merajver, *Cancer Res.* 62 (2002) 4854-4859.
36. G. MacDonald, I. Nalvarte, T. Smirnova, M. Vecchi, N. Aceto, A. Dolemeyer, A. Frei, S. Lienhard, J. Wyckoff, D. Hess, J. Seebacher, J.J. Keusch, H. Gut, D. Salaun, G. Mazzarol, D. Disalvatore, M. Bentires-Alj, P.P. Di Fiore, A. Badache, N.E. Hynes, *Sci. Signal.* 7 (2014) 1-12.
37. L.M. Balsa, M.C. Ruitz, L.S.M. de la Parra, E.J. Baran, I.E. Leon, *J. Inorg. Biochem.* 204 (2020) 110975.

38. C. Wittman, F. Bacher, E. A. Enyedy, O. Domotor, G. Spengler, C. Madejski, J. Reynisson, V. B. Arion, *J. Med. Chem.* 65 (2022) 2238-2261.
39. L.M. Balsa, V. Ferraresi-Curotto, M.J. Lavecchia, G.A. Echeverría, O.E. Piro, J. García-Tojal, R. Pis-Diez, A.C. González-Baró, I.E. León. 50 (2021) 9812-9826.
40. L.J. H. Borges, E.S. Bull, C. Fernandes, A.H. Jr., N.F. Azeredo, J.A.L.C. Resende, W.R. Freitas, E.C.Q. Carvalho, L.S. Lemos, H. Jerdy, M.M. Kanashiro, *Eur. J. Med. Chem.* 123 (2016) 128-140.
41. C. Santini, M. Pellei, V. Gandin, M. Porchia, F. Tisato, C. Marzano, *Chem. Rev.* 114 (2014) 815-862.
42. T. Wang, Z. Guo, *J. Curr. Med. Chem.* 13 (2006) 525-537.
43. M. Valko, H. Morris, M.T.D. Cronin, *J. Curr. Med. Chem.* 12 (2005) 1161-1208.
44. A. Gupte, R.J. Mumper, *Cancer Treat. Rev.* 35 (2009) 32-46.
45. B.-E. Kim, T. Nevitt, D.J. Thiele, *Nat. Chem. Biol.* 4 (2008) 176-185.
46. C. Marzano, M. Pellei, F. Tisato, C. Santini, *Anticancer Agents Med. Chem.* 9 (2009) 185-211.
47. A.C. Hangan, G. Borodi, R.L. Stan, E. Pall, M. Cenariu, L.S. Oprean, B. Sevastre, *Inorg. Chim. Acta* 482 (2018) 884-893.
48. D.S. Raja, E. Ramachandran, N.S.P. Bhuvanesh, K. Natarajan, *Eur. J. Med. Chem.* 64 (2013) 148-159.
49. L.A. Alfonso-Herrera, S. Rosete-Luna, D. Hernandez-Romero, J.M. Rivera-Villanueva, J.L. Olivares-Romero, J.A. Cruz-Navarro, A. Soto-Contreras, A. Arenaza-Corona, D. Morales-Morales, R. Colorado-Peralta, *ChemMedChem* 17 (2022) e2022003
50. J. Serment-Guerrero, P. Cano-Sanchez, E. Reyes-Perez, F. Velazquez-Gracia, M.E. Bravo-Gomez, L. Ruitz-Azuara, *Toxicol. Vit.* 25 (2011) 1376-1384.
51. K. H. Thompson, C. Orvig, *Dalton Trans.* (2006) 761-764.
52. D. Griffith, J.P. Parker, C.J. Marmion, *Anti-Cancer Agent Med. Chem.* 10 (2010) 354-370.
53. M.F. Primik, G. Muhlgassner, M.A. Jakupc, O. Zava, P.J. Dyson, V.B. Arion, B.K. Keppler, *Inorg. Chem.* 49 (2010) 302-311.
54. L. de A. Costa, M.H.F. Ottoni, M.G. dos Santos, A.B. Meireles, V.G. de Almeida, W.de F. Pereira, B.A. de Avelar-Freitas, G.E.A. Brito-Melo, *Molecules* 22 (2017) 1789.
55. C. Rodríguez-Burford, D.K. Oelschlager, L.I. Talley, M.N. Barnes, E.E. Partridge, W.E. Grizzle, *Biotech. Histochem.* 78 (2003) 17-21.
56. G.A. Bain, J.F. Berry, *J. Chem. Educ.* 85 (2008) 532-536.

57. P.G. Urben (Ed.), Bretherick's Handbook of Reactive Chemical Hazards, Sixth ed., Butterworth-Heinemann, Oxford, 1999.
58. W.C. Wolsey, J. Chem. Educ., 50 (1973) A335.
59. T.W. Kim, D.W. Hong, C.M. Kang, S.H. Hong, Exp. Mol. Med. 52 (2020) 1730-1743.
60. S. Nandi, S. Chandra, R. Sikder, S. Bhattacharya, M. Ahir, D. Biswal, A. Adhikary, N. R. Pramanik, T. K. Lai, M. G. B. Drew, K. Acharya, J. Agric. Food Chem. 67 (2019) 7660-7673.
61. S. Nandi, S. Adhikary, K. Acharya, J. Food Biochem. 46 (2022) e14021.
62. SMART (V 5.628), SAINT (V 6.45a), XPREP, SHELXTL, Bruker AXS Inc, Madison, USA (2004).
63. G. M. Sheldrick, Siemens Area Correction Absorption Correction Program, University of Göttingen, Göttingen, Germany (1994).
64. G. M. Sheldrick, SHELXL-97 Program for Crystal Structure Solution and Refinement, 1997.
65. N.K. Mandal, N. Bandyopadhyay, P. Arya, S. Chowdhury, N. Raghav, J.P. Naskar, Inorg. Chim. Acta 544 (2023) 121229.
66. T.P. Dionízio, A.C. dos Santos, F.P. da Silva, F. da S. Moura, E. D'Elia, F.M. dos, S. Garrido, M.E. Medeiros, A. Casellato, Electrocatalysis 12 (2021) 137-145.
67. M. Hazra, T. Dolai, A. Pandey, S.K. Dey, A. Patra, Bioinorg. Chem. Appl. 2014 (2014) 104046.
68. Y. Guo, X. Hu, X. Zhang, X. Pu, Y. Wang, RSC Adv. 9 (2019) 41737-41744.
69. C. Şenol, Z. Hayvali, H. Dal, T. Hökelek, J. Mol. Struct. 997 (2011) 53-59.
70. B. Sreenivasulu, M. Vetrichelvan, F. Zhao, S. Gao, J.J. Vittal, Eur. J. Inorg. Chem. (2005) 4635-4645.
71. S.D. Oladipo, B. Omondi, C. Mocktar, Appl. Organomet. Chem. 34 (2020) e5610.
72. D. Lahiri, R. Majumdar, D. Mallick, T.K. Goswami, R.R. Dighe, A.R. Chakravarty, J. Inorg. Biochem. 105 (2011) 1086-1094.
73. S. Zolezzi, A. Decinti, E. Spodine, Polyhedron 18 (1999) 897-904.
74. C.E. Satheesh, P.R. Kumar, N. Shivakumar, K. Lingaraju, P.M. Krishna, H. Rajanaika, A. Hosamani, Inorg. Chim. Acta 495 (2019) 118929.
75. D. Tomczyk, L. Nowak, W. Bukowski, K. Bester, P. Urbaniak, G. Andrijewski, B. Olejniczak, Electrochim. Acta 121 (2014) 64-67.

76. C.E. Satheesh, P.R. Kumar, P. Sharma, K. Lingaraju, B.S. Palakshamurthy, H.R. Raja Naika, *Inorg. Chim. Acta* 442 (2016) 1-9.
77. T.L. Yusuf, S.D. Oladipo, S. Zamisa, H.M. Kumalo, I.A. Lawal, M.M. Lawal, N. Mabuba, *ACS Omega* 6 (2021) 13704-13718.
78. A.W. Addison, T.N. Rao, J. Reedijk, J.V. Rijn, G.C. Verschoor, *J. Chem. Soc., Dalton Trans.* (1984) 1349 -1356.
79. M. Li, A. Ellen, J.H. Espenson, *Inorg. Chem.* 44 (2005) 3690.
80. N.K. Mandal, B. Guhathakurta, P. Basu, A.B. Pradhan, C.S. Purohit, S. Chowdhury, J.P. Naskar, *J. Coord. Chem.* 72 (2019) 3625-3644.
81. A.K. Patel, R.N. Jadeja, H. Roy, R.N. Patel, S.K. Patel, R.J. Butcher, M. Cortijo, S. Herrero, *Polyhedron* 186 (2020) 114624.
82. N. Stevanović, M. Zlatar, I. Novaković, A. Pevec, D. Radanović, I.Z. Matić, M.D. Crnogorac, T. Stanojković, M. Vujčić, M. Gruden, D. Sladić, K. Anđelković, I. Turel, B. Čobeljić, *Dalton Trans.*, 51 (2022) 185-196.
83. D. Sutradhar, H. Chowdhury, S. Banerjee, N.C. Saha, B.K. Ghosh, *Inorg. Chim. Acta* 485 (2019) 86-97.
84. T. Chattopadhyay, M. Mukherjee, K.S. Banu, A. Banerjee, E. Suresh, E. Zangrando, D. Das, *J. Coord. Chem.* 62 (2009) 967-979.
85. A. Guertler, A. Kraemer, U. Roessler, S. Hornhardt, U. Kulka, S. Moertl, A.A. Friedl, T. Illig, E. Wichmann, M. Gomolka, *Radiat. Prot. Dosim.* 143 (2011) 487-490.
86. C.F. Thorn, C. Oshiro, S. Marsh, T. Hernandez-Boussard, H. McLeod, T.E. Klein, R.B. Altman, *Pharmacogenet Genomics* 21 (2011) 440-446.
87. R. Punia, K. Raina, R. Agarwal, R.P. Singh, *PLoS One* 12 (2017) e0182870.
88. D. Alimbetov, S. Askarova, B. Umbayev, T. Davis, D. Kipling, *Int. J. Mol. Sci.* 19 (2018) 1690.
89. S. Nandi, P. Upadhyay, A. Roy, A. Dasgupta, A. Sen, A. Adhikary, K. Acharya, *Environ. Toxicol.* 37 (2022) 52-68.
90. A. Bansal, M.M. Saleh-E-In, P. Kar, A. Roy, N.R. Sharma, *Molecules* 27 (2022) 4597.
91. D.S. Raja, N.S. P. Bhuvanesh, K. Natarajan, *J. Biol. Inorg. Chem.* 17 (2012) 223-237.
92. G. Sharma, N.K. Rana, P. Singh, P. Dubey, D.S. Pandey, B. Koch, *Biomed. Pharmacother.* 88 (2017) 218-231.
93. E. Tas, H. Kara, M. Durgun, A. Kilic, I. Yilmiz, *Synthesis and Reactivity in Inorganic, Metal-Organic, and Nano-Metal Chemistry* 39 (2009) 379-387.

94. P. Mucha, P. Hikisz, K. Gwozdziński, U. Krajewska, A. Leniart, E. Budzisz, RSC Adv. 9 (2019) 31943-31952.
95. N. Kavitha, P.V.A. Lakshmi, J. Saudi Chem. Soc. 21 (2017) 457-466.
96. Y. Guo, X. Hu, X. Zhang, X. Pu, Y. Wang, RSC Adv. 9 (2019) 41737-41744.
97. M. Trivedi, G. Sing, A. Kumar, N.P. Rath, RSC Adv. 4 (2014) 34110-34116.
98. A. Lehle, A. Beghidja, C. Beghidja, O. Mentre, R. Welter, Com. Ren. Chimie. 14 (2011) 462-470.

CHAPTER-VI

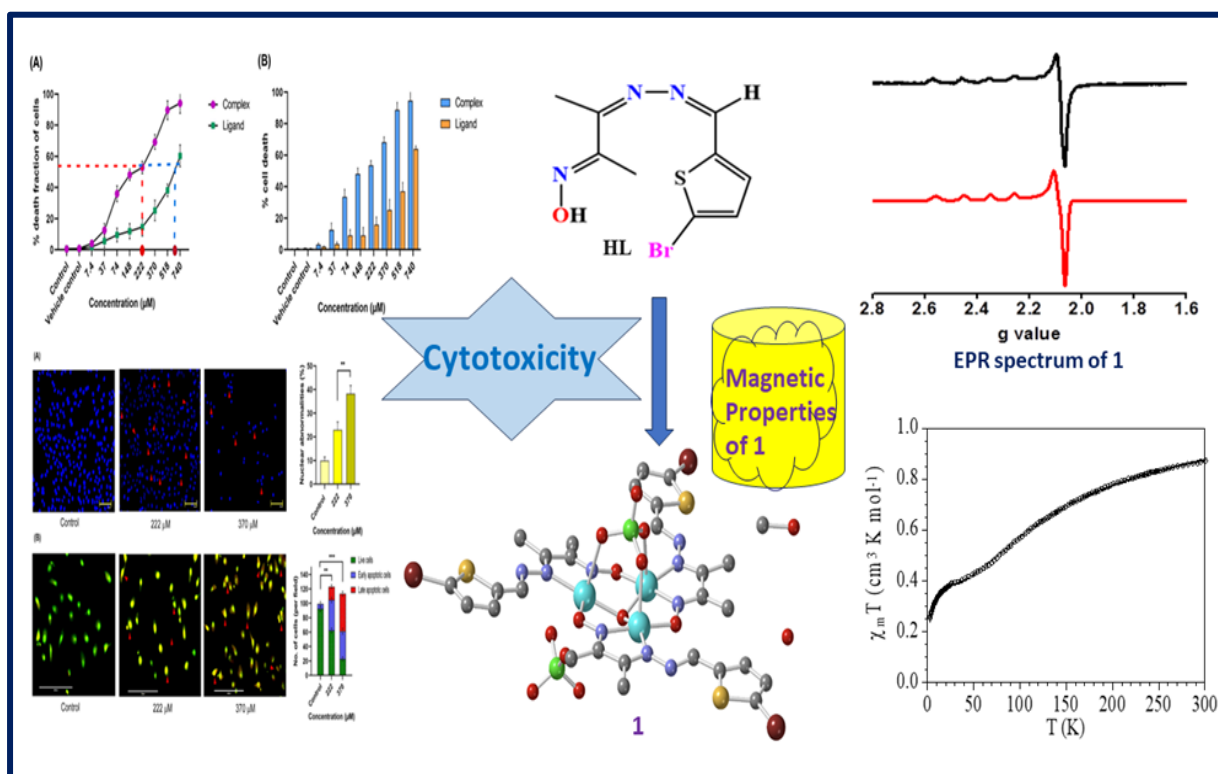
Design, synthesis and structure of a trinuclear copper(II) complex having a Cu_3OH core with regard to aspects of antiproliferative activity and magnetic properties

This work has been published in

New Journal of Chemistry

48 (2024) 5782–5796

Graphical Abstract



Highlights

- A novel triangular trinuclear copper(II) complex (**1**) with a central μ_3 -OH bridge was synthesized by using an oxime based Schiff base ligand (HL).
- **1** has been structurally characterised by single crystal X-ray diffraction.
- The anti-proliferative activity of both **HL** and **1** have been evaluated against human lung cancer cell line, A549.
- The magnetic characterization of **1** with variable-temperature magnetic measurements has been accomplished.
- Low temperature EPR measurements of **1** in frozen DMF solution have been performed.

Key words

Trinuclear copper(II) complex; structure; anti-proliferative activity and magnetic properties

Abstract

We report a novel triangular trinuclear copper(II) complex with a central μ_3 -OH bridge, $[(\text{CuL})_3(\mu_3\text{-OH})(\text{ClO}_4)_2] \cdot \text{CH}_3\text{OH} \cdot \text{H}_2\text{O}$ (**1**), stabilised by the oxime-based Schiff base ligand, 3-(((5-bromothiophen-2-yl)methylene)hydrazineylidene)butan-2-one oxime (**HL**). Comprehensive characterization of **1** has been realised through different analytical and physical methods coupled with spectroscopic techniques. **1** has been structurally characterised by single crystal X-ray diffraction. The anti-proliferative capacity of **HL** and **1** has been evaluated against human lung cancer cell line, A549. Compound **1** shows promising efficacy in contrast to **HL**, which shows a limited cytotoxicity. Contrary to **HL**, **1** has distinctly impeded the proliferation of lung adenocarcinoma A549 cell lines in a dose-dependent way. Compound **1** has been employed as a potential therapeutic agent for promising cellular transformation of malevolent A549 cell lines. The programmed cell death mechanism of **1** reveals characteristic apoptotic changes in cellular morphology like chromatin condensation, fragmented nuclei, nuclear shrinkage along with blebbing, elevated number of nuclear body fragments and distorted nucleus, while round, clear edged, intact nucleus and uniformly stained round nuclei have been observed in the negative control. Variable-temperature magnetic studies show an antiferromagnetic Cu...Cu coupling of $-44.6(2) \text{ cm}^{-1}$. The g value as determined by EPR measurement of **1** in frozen N,N-dimethylformamide solution corroborates the experimental magnetic susceptibility values.

1. Introduction

Cancer, ranked as one of the most aggressive and lethal maladies, lies in the inherent process of cell division. Worldwide, it is the second cause of human mortality. This disease alone kills an alarming number of people all over the world [1-4]. In the year 2021 alone, GLOBOCAN reported 9.6 million cancer death and an approximately 8.1 million new cancer cases. This puts a huge burden on the health and economic well-being of millions of people [5-7]. Cancer persists as a challenge as well as a threat to anthropogenic morbidity, mortality and global health care [8]. Breast, lung, liver, stomach, rectum, skin and colon are some common soft targets of this fatal ailment. Second only to breast cancer, lung cancer threatens humankind with the highest incidence and mortality rate globally [9,10]. New cases of lung cancer and related mortality rate have roughly been increased respectively to 20% and 10% in 2012 and 2020 [5,11]. By 2035, the projected number of fatality out of this malignancy will alarmingly touch 3 million worldwide and by around 2050, the predicted annual cases of infection will hover around 3.5 million [12,13]. Clearly, a catastrophic disaster solely due to lung cancer is in the offing.

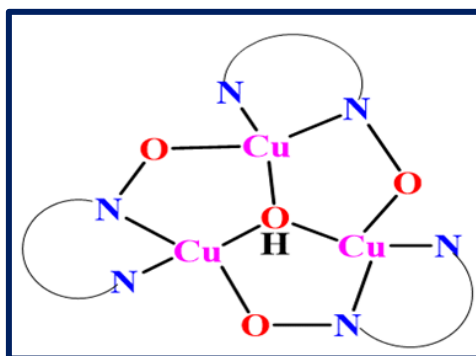
Lung cancer encompasses two major forms – non-small scale lung cancer (NSCLC) and small scale lung cancer (SCLC). Depending on the stage of detection, the therapeutic protocols of lung cancer also vary [14,15]. Besides classical approach like chemotherapy, some of the noted modern clinical protocols for the therapy and management of NSCLC are immunotherapy, targeted therapy, laser therapy, photodynamic therapy. Chemotherapeutic protocols for NSCLC include usage of organic therapeutics like taxol and its derivatives, and inorganic platinum based cisplatin and carboplatin. As a therapeutic drug, the prospect and efficacy of cisplatin are commendable [16-19]. However, cisplatin suffers from a copious number of adverse side effects that limit its applicability and viability. Non-negligible toxic side effects like nephrotoxicity, neurotoxicity, liver toxicity, general toxicity, ototoxicity, haemolysis and most importantly development of resistance to drugs restrict and marginalise the applicability of cisplatin [20-23].

Over the past few decades, major research activities have been focused on developing novel transition metal based compounds to be used as promising anti-malignant agents. Accordingly, a plethora of transition metal based complexes have already been designed and synthesized to be optimally suitable for cytotoxic propensities and wound-recuperating abilities. The ruthenium based approach is noteworthy in this perspective [24-27]. Palladium, gallium, titanium, gold, iron, osmium, rhenium, silver and cobalt compounds also show anti-proliferative activities [28-38].

Being a biocompatible benign bio-element, coinage metal copper seems to be a prospective choice and prognostic marker in this regard. Copper based anticancer agents are so promising that some of them are in the preclinical and clinical trial phase [39-49]. It is worth to emphasizing the key work of L. Ruiz-Azuara and co-workers that had reported a Cu(II) compound: [Cu(II)-(4,4'-dimethyl-2,2'-bipyridine)(acetylacetonate)(NO₃)(H₂O)]. This work is in clinical trials (Phase I) in Mexico [50,51]. Recently, morpholine based mononuclear Cu(II) complexes have been screened by us against lung cancer cell lines A549 [52]. Copper(II) complexes with the Schiff base ligand manifest commendable biological activities due to high DNA binding affinity and biocompatible redox potential [53,54]. The possible mechanism to action of such complexes as anticancer agents are DNA interaction through non-covalent mode, generation of reactive oxygen species (ROS) and mitochondrial toxicity [55-57]. Report on anticancer activity accentuated by trinuclear Cu(II) complexes is indeed very rare. Recently, linear trinuclear Cu(II) complexes with limited cytotoxicity (IC₅₀ > 100 μM) have been reported. The same were screened against human breast (MCF7) and liver cancer (HepG2) cells in a dose-dependent manner [58]. To the best of our knowledge, anti-proliferative activity of μ₃-oxido and/or μ₃-hydroxido bridged triangular trinuclear Cu(II) complex is unprecedented. Addressing this pertinent point, for the first time, herein we are concerned with such a system for its anticancer activity against lung cancer cell lines.

Polynuclear paramagnetic complexes are of contemporary interest owing to their significant applications as molecule-based magnetic materials. Spin coupling between paramagnetic metal centres of such type of exchange coupled systems is propagated through bridging atoms/groups [59-61]. Oxime based ligands have been used in exchange coupled polynuclear systems. Diverse bridging modes of the oxime function can foster homo- and hetero-metallic (M-N-O-M') cores [62-66]. In this context, triangular trinuclear copper(II) complexes having a central oxido/hydroxido bridge with peripheral oximato bridges are noteworthy from the viewpoint of magnetic aspect [67-70]. Accordingly, magnetic studies on trinuclear Cu(II) complexes with a central oxido/hydroxido bridge have become a fascinating area of interest in the last few decades [71-74]. Such systems have drawn keen interest from the magnetic point of view due to their structural diversity and varying coordination environments around each copper centre [75]. Triangular Cu(II) complexes have been studied as model systems since they represent the most basic spin triangle. This has made it possible to thoroughly analyse the magnetic characteristics of geometrically spin-frustrated systems [76,77]. A schematic representation of the μ₃-hydroxido bridged triangular trinuclear

copper(II) core with peripheral oximato bridges, akin to our present work, is shown in scheme VI.1.



Scheme VI.1. A μ_3 -OH bridged triangular trinuclear Cu^{II} core with peripheral oximato bridges.

The three unpaired electrons in this triangular core interact through $\text{Cu}^{\text{II}}\text{-O-Cu}^{\text{II}}$ and Cu-O-N-Cu exchange pathways [78-80]. Such units may show antiferromagnetic (frustrated $S_{\text{total}} = 1/2$) or ferromagnetic ($S_{\text{total}} = 3/2$) coupling. Oxime based oxido-hydroxido bridged hexanuclear copper(II) systems with $\text{Cu}_3\text{O}\cdots\text{H}\cdots\text{OCu}_3$ core have been reported along with their magneto structural correlation [81,82]. Herein we report the synthesis, characterization and crystal structure of a new trinuclear copper(II) complex $[(\text{CuL})_3(\mu_3\text{-OH})(\text{ClO}_4)_2](\text{CH}_3\text{OH})(\text{H}_2\text{O})$ (**1**) having a central μ_3 -OH bridge, stabilised by an oxime based NNO donor Schiff base ligand, 3-(((5-bromothiophen-2-yl)methylene)hydrazineylidene)butan-2-one oxime (**HL**). The anti-proliferative activity of **1** has been screened against lung cancer cell line, A549. We also perform the magnetic characterization of compound **1** with variable-temperature magnetic measurements and EPR spectroscopy.

2. Experimental Section

2.1. Materials

Analytical reagent grade 5-bromothiophene carboxaldehyde (97%) and 2,3-butanedioneminoxime ($\geq 99.0\%$); reagent grade hydrazine hydrate (50-60%) were purchased from Sigma-Aldrich (St. Louis, Missouri, United States). High purity (99.9%) spectroscopic grade methanol, procured from Spectrochem (Mumbai, India), was used for electronic spectroscopic work. Dulbecco's Modified Eagles Medium (DMEM), 4',6-diamidino-2-phenylindole (DAPI), Acridine orange (AO), Ethidium bromide (EtBr) were purchased from Himedia (Mumbai, India). Water-soluble tetrazolium (WST) was purchased from Takara Bio Inc, Japan. Trypan blue dye and crystal violet were purchased from Sigma-Aldrich (St. Louis, Missouri, United States). Antibiotic-PenStrep, Amphotericin B and Foetal bovine serum (FBS)

were procured from MP Biomedicals, United States and Trypsin EDTA from Gibco, Waltham (MA, USA). All other chemicals were of analytical grade and were used as received.

Compound **1** was dissolved in dimethyl sulfoxide (DMSO) (Merck, Kenilworth, NJ, USA) to have a mother stock of 40 mM, which had been further diluted for various experimental assays. Care had been taken so that the concentration of DMSO did not exceed 0.5-0.8% at any point of our experimental procedure.

2.2. Physical measurements

Melting point of the ligand (**HL**) was determined with an electro-thermal digital melting point instrument (SUNSIM, India). It is uncorrected. NMR (^1H and ^{13}C) spectra of **HL** were acquisitioned on a Bruker DPX (300 MHz) spectrometer. Tetramethylsilane (TMS) was used as an internal standard reference. A UV-1900i spectrophotometer (SHIMADZU) (JAPAN) was employed to record the electronic spectra of **HL** and **1** in spectroscopic grade methanol at room temperature. FT-IR spectra ($4000\text{--}400\text{ cm}^{-1}$) of **HL** and **1** were accrued, using KBr pellets, on a SHIMADZU FTIR-8400S spectrophotometer (JAPAN). Electron ionisation mass spectrum of **HL** was recorded on a MStation-JMS-700, JEOL (JAPAN). Ionic conductivity measurement of **1** were performed in methanolic solution at room temperature with a Systronics India direct conductivity meter (Model 304). The conductometer was calibrated using a standard 0.1M KCl solution. EPR measurements on **1** were carried out on a Magnetech GmbH MiniScope MS400 spectrometer. The spectrum was recorded at low temperature (143 K) in frozen N,N-dimethylformamide (DMF) solution. The spectrometer was equipped with a temperature controller, TC H03. The spin resonance spectrometer was equipped with an FC400 frequency detector. EPR spectrum of **1** was simulated using the EasySpin software package [83]. Variable-temperature magnetic susceptibility measurements were carried out in the temperature range 2-300 K with an applied magnetic field of 100 mT on a polycrystalline sample with a mass of 71.872 mg using a Quantum Design MPMS-XL-5 SQUID susceptometer. The susceptibility data were corrected for the sample holder previously measured using the same conditions and for the diamagnetic contribution of the sample as deduced by using Pascal's constant tables [84].

2.3. Solution Preparation for Spectroscopic Studies

2 mM Tris-HCL buffer solution was prepared in millipore water of pH 6.8 to perform all the experiments. A 5 mL (1 mM) stock solution of **1** was prepared in DMSO.

2.4. DNA Binding Studies

The CT-DNA stock solution was prepared by following the standard procedure [85]. DNA solution was de-proteinized followed by ethanol precipitation [86]. It was then sonicated and further dialyzed several times at 5°C under sterile conditions [87]. The purity of the CT-DNA

solution was checked by monitoring the UV absorption spectrum at 260 and 280 nm. The (A₂₆₀/A₂₈₀) ratio was found to be between 1.88 and 1.92 and the (A₂₆₀/A₂₃₀) between 2.12 and 2.22. The concentration of the DNA stock solution was determined by considering the molar extinction coefficient(ϵ) of CT-DNA at 260 nm as 13,200 M⁻¹ cm⁻¹. CT-DNA was added each time to a fixed concentration (12.5 μ M) of complex solution in a cuvette and the spectra were recorded.

2.5. Cell culture

The human lung adenocarcinoma cancer cell line (A549) was obtained from the National Centre for Cell Science (Pune, India) and cultured in Dulbecco's modified Eagle's medium with 10% foetal bovine serum and 100 mg L⁻¹ of antibiotics, namely, penicillin, streptomycin, and amphotericin B, in a humidified chamber containing 5% CO₂. Cells were allowed to reach 80-90% confluence before being trypsinized with trypsin-EDTA for use in experiments. All cell culture experiments were conducted in a biosafety cabinet under sterile condition.

2.5.1. Cell viability assay using WST-1

The viability and proliferation of A549 cells were assessed using the WST-1 reagent (Takara Bio Inc., Japan) according to the manufacturer's protocol. In short, as described by Nandi *et al.* [88] A549 cells were seeded and incubated for 24 h in a 96-well microtiter plate. The cells had been treated with varying concentrations (7.4-740 μ M) of compound **1**. Simultaneously cisplatin used as a positive control drug and DMSO was used as vehicle control set separately in triplicate and incubated at 37 °C for 24 h. The following day, 5 μ L of WST-1 reagent was added to each well and incubated in the dark for 3 h at 37 °C. Analysis was done at 450 nm through Bio-Rad (model 550) microplate reader. The IC₅₀ value was determined with GraphPad Prism software (version 9.03).

2.5.2. Evaluation of A549 cell count and viability by trypan blue assay

Trypan blue dye exclusion assay was used to determine the effect of a drug on the viability of cancer cells. Briefly, the cells were seeded at a density of 1 \times 10⁵ cells per well in a 12-well culture plate and treated with different concentrations of **1** along with a negative control and vehicle control set separately in triplicate. The next day, cells were trypsinized and cell pellets were collected by centrifugation. Then the cell pellets were diluted in serum-free media and 10 μ L aliquot from the original stock was mixed with an equal volume of 0.4% trypan blue dye. Detectable fluorescence of trypan blue was measured at 585 nm through a Bio-Rad (model 550) microplate reader. The readings were recorded and the percentage inhibition of cell viability was calculated based on the following formula:

$$\% \text{ Inhibition} = (\text{Total dead cell count} / \text{Total cell count}) \times 100$$

2.5.3. Colony formation assay

A549 cells were introduced into a 12-well plate at a density of 4×10^3 cells per well and they were treated with the vehicle as well as with compound **1** at 222 and 370 μM the following day. After washing the cells with PBS, new medium was added. The cells were then grown for seven days at 37 °C in an incubator. On the eighth day, the cells were rinsed with PBS, fixed with 4% PFA, and stained for 0.5 h with 0.1% crystal violet. After that, colonies were rinsed with distilled water and photographs were taken.

2.5.4. Cytomorphological observation of A549 cells by bright field microscopy/fluorescence microscopy

A549 cells were cultured overnight in 60-mm tissue culture dish for cell adhesion and treated with 222 and 370 μM compound **1** for 24 h. The morphological changes of cells were observed using a phase contrast microscope. Further fluorescent staining with 1 $\mu\text{g mL}^{-1}$ DAPI for 15 min in the dark was carried out for better visualisation of cell with nucleus under a fluorescence microscope (FLoid Imaging Station, Life Technologies, Waltham, MA, USA).

2.5.5. In vitro cell wound repair assay

The *in vitro* scratch wound repair assay was a modification of a previously described methodology of Nandi *et al.*, [89]. Briefly, 5×10^4 A549 cells per mL were cultured in 6-well plates to confluence as monolayers under standard condition. Upon reaching a confluence of more than 75% for cultured cells, linear wounds were made with a 100 μL pipette tip on cell monolayers followed by incubation with serum-free conditioned media for 24 h. Circumferential wound gaps were measured by ImageJ software and the percentage of wound repair was calculated.

2.5.6. Nuclear morphology by DAPI staining under inverted fluorescent microscope

The DAPI staining technique was utilized to recognize the obvious signs of apoptosis in cancerous cells. A549 cells (5×10^4 cells per mL) were cultured in a 6-well culture plate overnight. Subsequently, cells were subjected to drug treatment at a concentration of 222 and 370 μM . To examine alterations in nuclear morphology, treated cells were rinsed with phosphate-buffered saline (PBS) and fixed with 4% paraformaldehyde for 10 min. More cells were washed with PBS and permeabilized with 0.1% TritonX-100. Finally, cells were exposed to DAPI (1 $\mu\text{g mL}^{-1}$ in PBS) for 15 min and were visualized under a fluorescence microscope (FLoid Imaging Station, Life Technologies, Waltham, MA, USA).

2.5.7. Direct fluorescence microscopic analysis for apoptosis induction

Dual staining with acridine orange/Ethidium bromide (AO/EB) was performed to distinguish viable, apoptotic and necrotic cells with distinct morphological alterations in a cultured plate. 2×10^3 cells were grown in a 6-well plate and then the cells were treated with 222 and 370 μM

compound **1** and kept overnight. The following day, the cells were stained with the acridine orange (AO, 5 mg mL⁻¹) and ethidium bromide (EB, 3 mg mL⁻¹) mixture. The extra unbound dye residues were rinsed with phosphate buffer saline prior to fluorescence microscopic visualisation.

2.5.8. Data analysis and statistics

Data are presented as the mean \pm standard deviation and SEM. All experiments were repeated at least three times. For paired comparisons, Student's t-test was used to determine the P-values. For multiple paired comparisons, analysis of variance and Post hoc tests were used to determine the P-values. Prism9 software was used for all statistical analyses. Statistically, significance was defined as $P < 0.05$.

2.6. Synthesis of the ligand (**HL**)

Biacetyl monoxime monohydrazone (BMMH) (115 mg, 1 mmol) was dissolved in 30 mL of methanol to have a colourless solution. 5-bromothiophene carboxaldehyde (90 μ L, 1 mmol) was added to the above solution. The resulting solution turned light yellow. The reaction mixture was refluxed for 4 h in the presence of pre-activated molecular sieves (4 Å x 1.5 mm). The dark yellow solution obtained was left undisturbed in air for slow evaporation. After four days, a yellow crystalline solid was obtained. It was filtered and thoroughly washed with cold diethyl ether. The compound was dried *in vacuo* over CaCl₂. The synthesized ligand is soluble in methanol, DCM, DMF, DMSO and THF. It is insoluble in *n*-hexane, *n*-pentane and H₂O.

Yield: 210 mg (72%); m.p.: 170 °C; Anal. Calc. for C₉H₁₀N₃OSBr: C, 37.48; H, 3.49; N, 14.57%; Found: C, 37.44; H, 3.54; N, 14.53%; ¹H NMR (DMSO-d₆): δ (ppm): 11.69 (1H, s, -OH proton), 8.77 (1H, s, for azomethine proton), 7.45 (1H, d, ring proton of thiophene), 7.33 (1H, d, another ring proton of thiophene), 2.02 (s, 3H, -CH₃ proton), 1.92 (s, 3H, -CH₃ proton); ¹³C NMR (DMSO-d₆): δ (ppm): 156.04(C3), 155.35(C1), 154.91(C6), 140.51(C5), 135.10(C8), 132.30(C7), 117.87(C9), 13.10(C4), 9.73(C2); FT-IR (KBr): (ν /cm⁻¹): 3229 (for -OH stretching), 1610 (for C=N), 1423 (C=N of oxime), 1360 (for -CH₃ asymmetric); UV-Vis (CH₃OH): λ_{max} (ϵ /M⁻¹ cm⁻¹): 248 nm (26 288) and 351 nm (22 989); EI-MS (CH₃OH) (m/z): (100%) (**HL**): 287.981 (Theo. Value: 288.080).

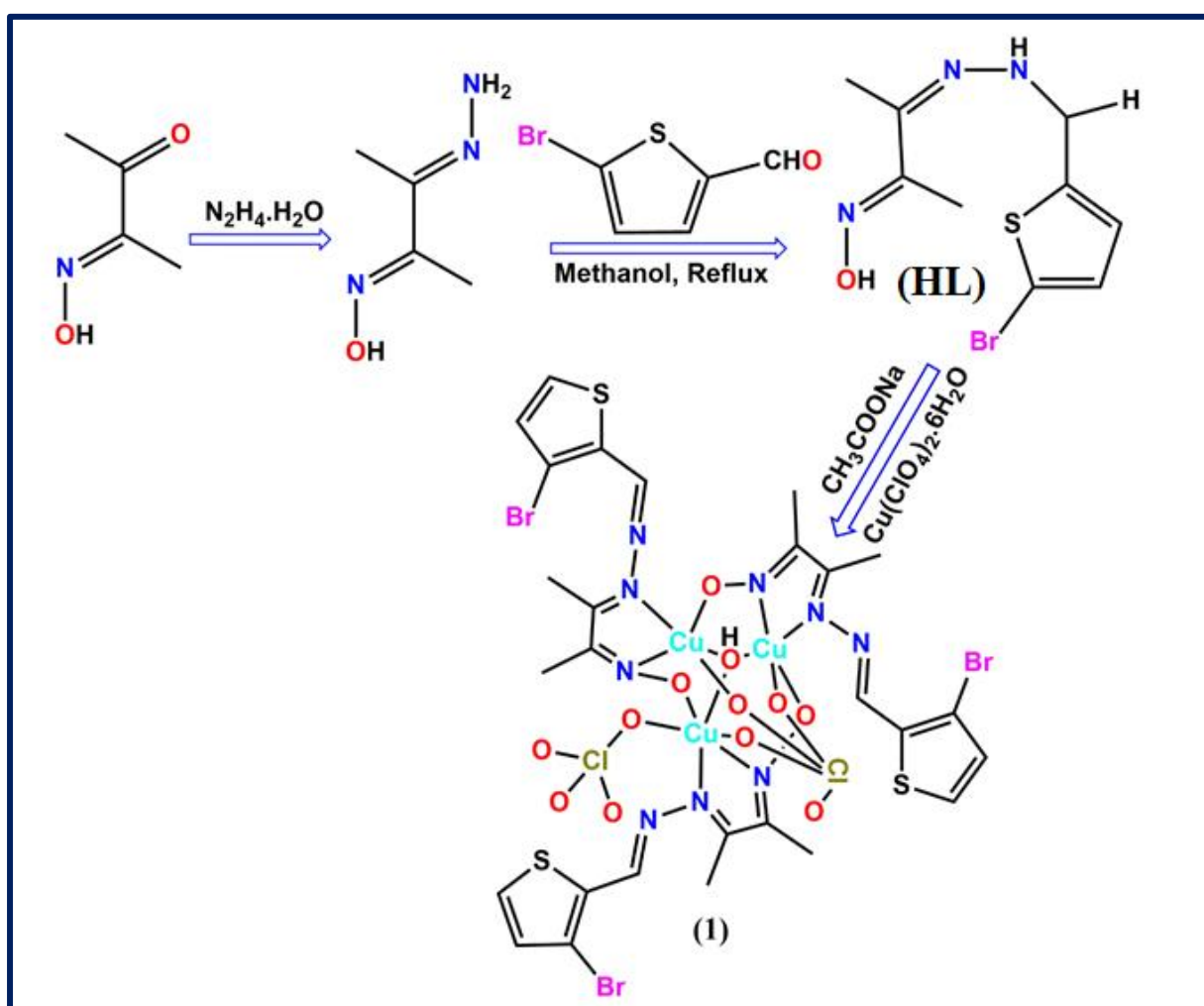
2.7. Synthesis of complex [(CuL)₃(μ_3 -OH)(ClO₄)₂] \cdot CH₃OH \cdot H₂O (**1**)

The ligand **HL** (57 mg, 0.2 mmol) was dissolved in 15 mL of methanol to obtain a light yellow solution. Anhydrous sodium acetate (17 mg, 0.2 mmol) was added to this solution, followed by Cu(ClO₄)₂·6H₂O (74 mg, 0.2 mmol) under stirring. Immediately, the colour of the solution turned dark green. The solution was stirred for 2 h and was filtered and kept undisturbed for slow evaporation at room temperature. A green crystalline compound was obtained after 2 days. It was filtered, washed thoroughly with cold diethyl ether and dried *in vacuo* at room

temperature over calcium chloride. The green compound is soluble in methanol, acetonitrile, dichloromethane, DMF and DMSO.

Yield: 30 mg (23%); Anal. Calc. for, $C_{28}H_{34}N_9O_{14}S_3Br_3Cl_2Cu_3$: C, 25.49; H, 2.60; N, 9.56 %; Found: C, 25.45; H, 2.63; N, 9.53 %; FT-IR (KBr): (ν/cm^{-1}): 3425 (for -OH stretching), 1608, 1576 (for C=N), 1423 (C=N of oxime), 1144, 1113, 1088 and 627 (for ClO_4 stretching); UV-Vis (CH_3OH): λ_{max} ($\epsilon/M^{-1} cm^{-1}$): 277 nm (37 797), 356 nm (07 577) and 634 nm (2 61); $\Lambda_M(CH_3OH)$: $165 \Omega^{-1}cm^2mol^{-1}$ (1:2 electrolyte).

Shining needle shaped dark green crystals were grown by direct diffusion of *n*-hexane into a moderately concentrated DCM solution of compound **1**. The synthetic route to **HL** and **1** is shown in scheme VI.2.



Scheme VI.2. Synthetic route to **HL** and **1**.

Caution: Perchlorate salts and their metal complexes with organic ligands are potentially explosive particularly during heating and shocking [90,91]. Although we did not face any difficulty during our work, utmost care must be taken during their handling.

2.8. Crystallographic data collection and refinement

Single dark green needle-shaped crystals of **1** were used. A suitable crystal of **1** with dimensions $0.12 \times 0.21 \times 0.24 \text{ mm}^3$ was selected and mounted. The crystal data was collected on a Bruker D8 Venture Microfocus APEX-II diffractometer with a Mo-K α (graphite-monochromated) radiation source ($\lambda = 0.71073 \text{ \AA}$) (equipped with a CCD area detector) at low temperature ($T = 145(2) \text{ K}$). The diffraction data was collected with a ω scan width of 1.00° and exposure time 10s. The data collection for **1** was managed by the APEX3(v2017.3-0) software and processed through SAINT. Data were measured using ω/ϕ scans with Mo K α radiation. The diffraction pattern was indexed and the total number of runs and images was based on the strategy calculation from the program Bruker APEX2 [92]. The maximum resolution that was achieved was $\Theta = 21.00^\circ$ (0.99 \AA). The structure was solved and the space group $P-1$ (# 2) was determined by the ShelXT 2014/5 solution program package using iterative methods [93,94]. Olex2 1.5-dev was used as the graphical interface [95]. Data reduction, scaling and absorption corrections were performed using Bruker SAINT. Data reduction, scaling and absorption corrections were performed using Bruker SAINT. The final completeness is 99.85% out to 21.00° in Θ . SADABS 2016/2 was used for absorption corrections [96]. The absorption coefficient of **1** is 4.435 mm^{-1} at wavelength(λ) 0.71073 \AA . The minimum and maximum transmissions are respectively of 0.495 and 0.746. The model was refined with olex2.refine1.5-dev using full matrix least squares minimisation on F^2 [97]. All non-hydrogen atoms were refined anisotropically. Hydrogen atom positions were calculated geometrically and refined using the riding model. Hydrogen atom positions were calculated geometrically and refined using the riding model. The crystallographic refinement data of **1** are tabulated in Table VI.1. Some selected bond lengths in \AA and bond angles in $^\circ$ are tabulated in Table VI.2.

Table VI.1. Crystal data and structure refinement for **1**

CCDC NO.	2270365
Empirical formula	$\text{C}_{28}\text{H}_{33}\text{Br}_3\text{Cl}_2\text{Cu}_3\text{N}_9\text{O}_{14}\text{S}_3$
Formula weight	1317.077
Temperature [K]	145(2)
Wavelength [\AA]	0.71073
Crystal system and Space group	Triclinic and $P-1$
a [\AA], b [\AA] and c [\AA]	8.140(5), 14.632(10) and 19.569(11)

α [°], β [°] and γ [°]	85.11(4), 85.25(2) and 74.26(2)
Volume [Å ³]	2231(2)
Z and ρ_{calcd} [mg/cm ³]	2 and 1.961
Absorption coefficient [mm ⁻¹] and F(000)	4.435 and 586
Crystal size [mm]	0.12 × 0.21 × 0.24
Limiting indices	-8 ≤ h ≤ 8, -14 ≤ k ≤ 14, -19 ≤ l ≤ 19
Reflections collected/unique	24437/3404 [Rint = 0.1042]
Completeness of theta	99.9% (25.242)
Data / restraints / parameters	3404/0/547
Goodness-of-fit on F ²	1.0791
Final R indices [I > 2σ(I)]	R ₁ = 0.0494, wR ₂ = 0.1176
R indices (all data)	R ₁ = 0.0771, wR ₂ = 0.1372
Largest diff. peak and hole	1.5671 and -0.7822 e.Å ⁻³

Table VI.2. Selected bond lengths in Å and angles in ° for **1**

Bonds	Length/Å	Angles	Angle/°	Angles	Angle/°
Cu1-O2	1.941(6)	O1-Cu1-O2	91.4(3)	N8-Cu3-O4	101.5(3)
Cu1-O1	1.964(7)	O5-Cu1-O2	90.5(2)	N8-Cu3-O1	166.9(3)
Cu1-O5	1.968(6)	O5-Cu1-O1	97.4(2)	N8-Cu3-N7	80.8(3)
Cu1-N2	2.042(7)	N2-Cu1-O2	100.2(3)	O3-Cu2-O1	91.4(2)
Cu1-N1	2.344(7)	N2-Cu1-O1	159.2(3)	O6-Cu2-O1	92.3(2)
Cu3-O4	1.936(6)	N2-Cu1-O5	99.7(3)	O6-Cu2-O3	96.7(3)
Cu3-O1	1.951(7)	N1-Cu1-O2	176.8(3)	N4-Cu2-O1	88.2(3)
Cu3-N7	176.9(3)	N1-Cu1-O1	87.0(3)	N4-Cu2-O3	175.4(3)
Cu3-N8	91.3(3)	N1-Cu1-O5	92.4(3)	N4-Cu2-O6	88.0(3)
Cu2-O1	87.0(3)	N1-Cu1-N2	80.6(3)	N5-Cu2-O1	166.1(3)
Cu2-O3	100.3(3)	O1-Cu3-O4	90.6(2)	N5-Cu2-O3	100.3(3)
Cu2-O6	80.6(3)	N7-Cu3-O4	176.6(3)	N5-Cu2-O6	93.7(3)
Cu2-N4	159.2(3)	N7-Cu3-O1	87.3(3)	N5-Cu2-N4	79.5(3)

3. Results and discussion

3.1. Synthesis and IR spectroscopy

The ligand **HL** was synthesized by equimolar Schiff base condensation of 5-bromo-2-thiophene carboxaldehyde and biacetyl monoxime monohydrazone (BMMH) with satisfactory yield. The trinuclear copper(II) complex was obtained by equimolar reaction of the synthesized ligand (**HL**) and copper(II) perchlorate hexa-hydrate in methanol at room temperature. **HL** has been characterised by EI-MS, ^1H and ^{13}C NMR spectra. The EI-MS of **HL** is shown in Fig. VI.1.

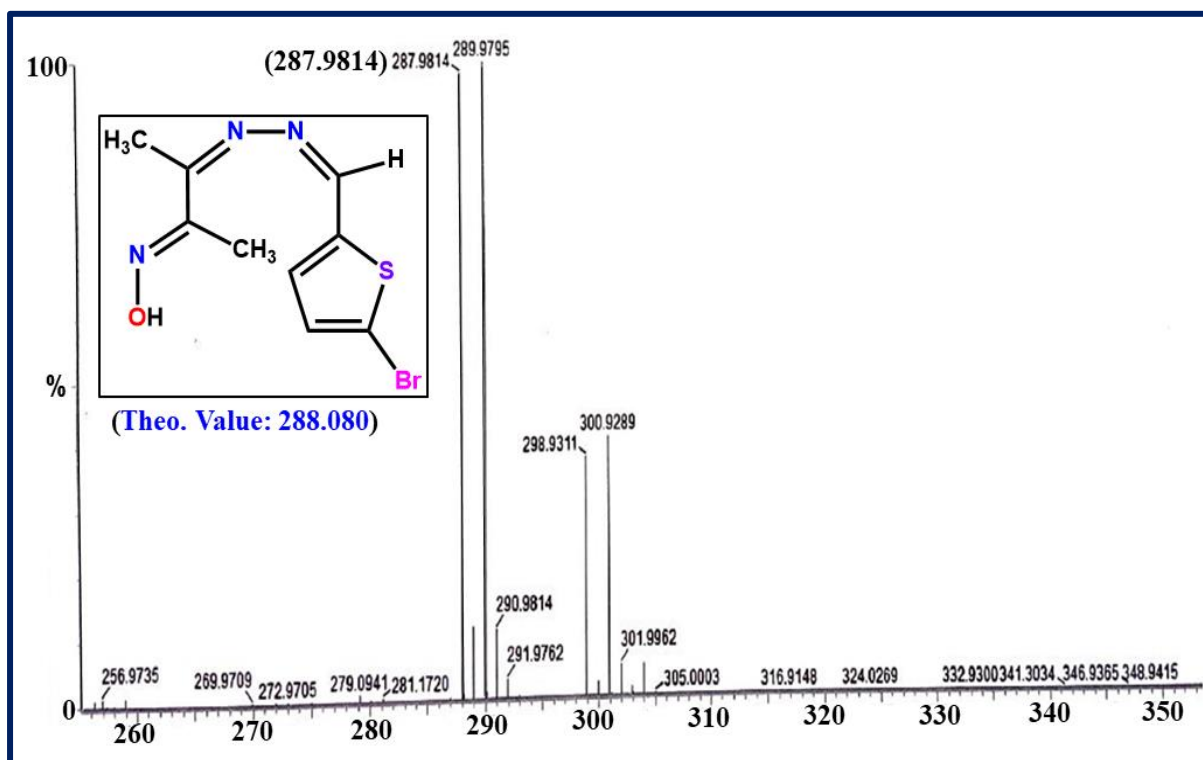


Fig. VI.1. EI-MS spectrum of ligand (**HL**) in methanol.

The ^1H and ^{13}C NMR spectra of **HL** are shown in Fig. VI.2 and Fig. VI.3, respectively.

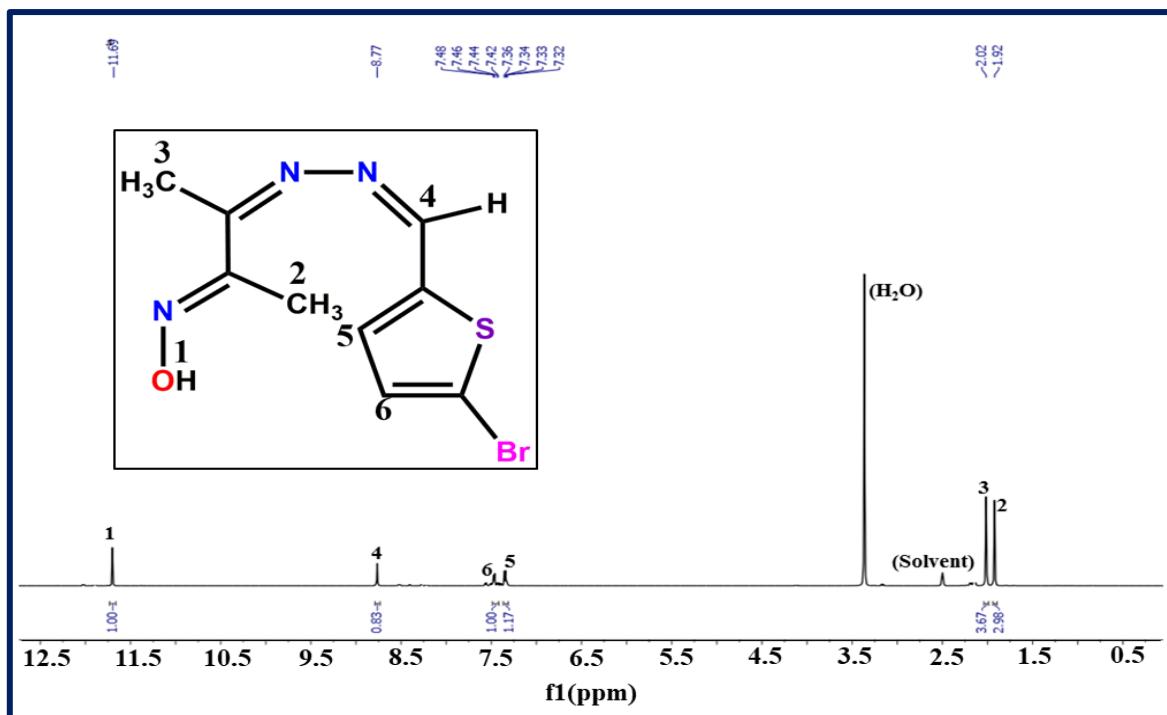


Fig. VI.2. ¹H NMR spectrum of **HL** in DMSO-d₆.

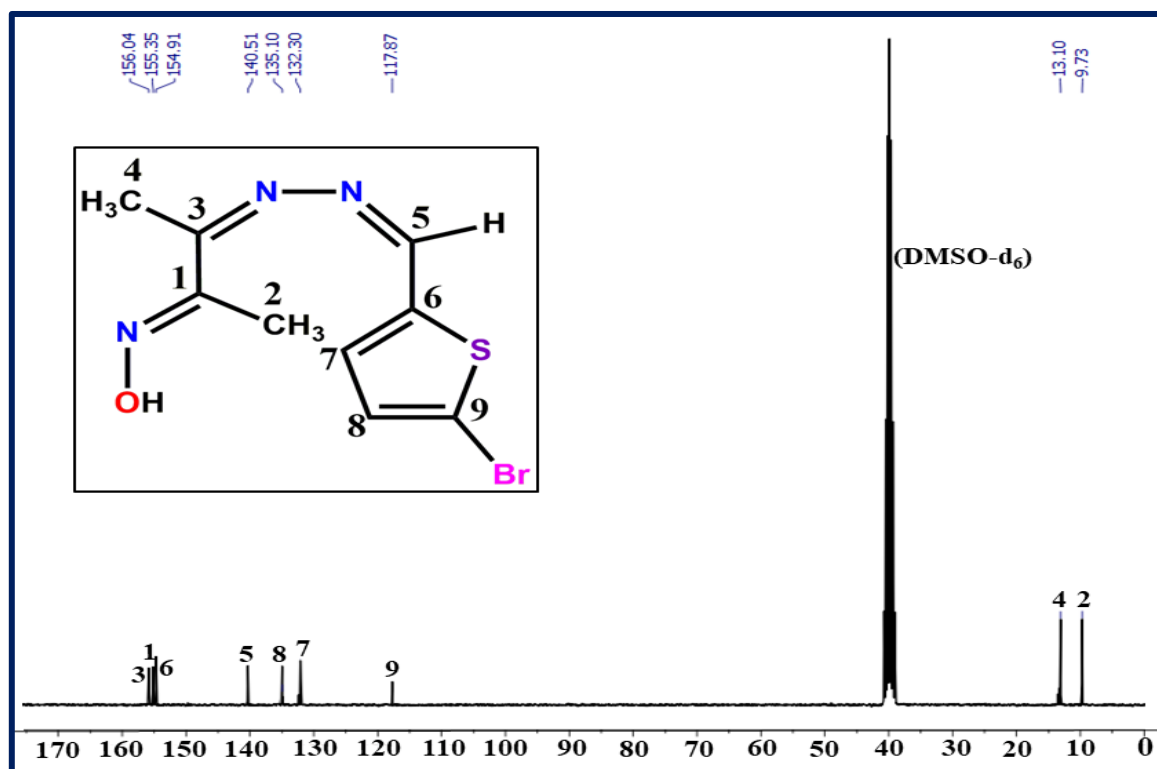


Fig. VI.3. ¹³C NMR spectrum of **HL** in DMSO-d₆.

In the FT-IR spectrum of **HL**, we have a characteristic sharp band at 1610 cm⁻¹ which can be assigned to the imine stretching vibration (Fig. VI.4). This band at 1610 cm⁻¹ is slightly shifted to a lower wavenumber of 1604 cm⁻¹ during complexation, indicative of the coordination of the nitrogen atom of the imine group to the metal center [98]. The free -OH group of the oxime

fragment of **HL** shows a broad band around 3229 cm^{-1} . A sharp band also appears at 1423 cm^{-1} for the C=N stretching vibration of oxime.

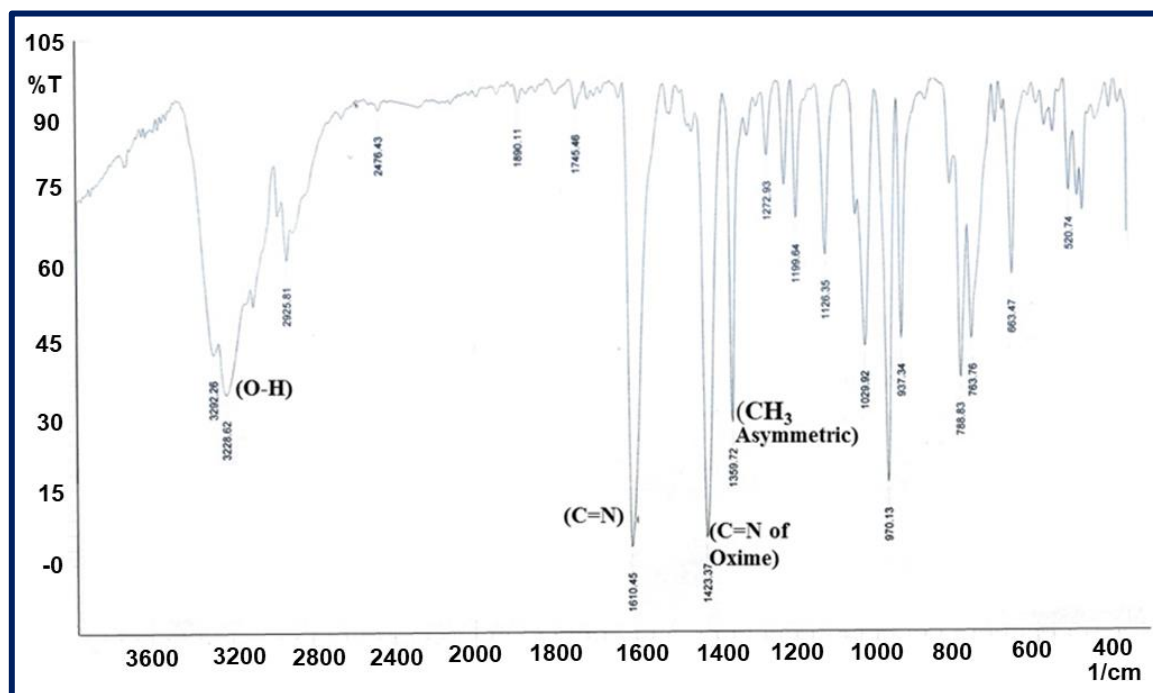


Fig. VI.4. FT-IR spectrum of **HL**.

Compound **1** displays split bands at 1144, 1113 and 1088 cm^{-1} due to the asymmetric Cl-O stretching vibration and a single sharp band at 627 cm^{-1} attributed to the symmetric Cl-O stretching. These split bands are indicative of perchlorate ion coordination to the metal centre through oxygen, as confirmed by the X-ray structure [99,100] (Fig. VI.5).

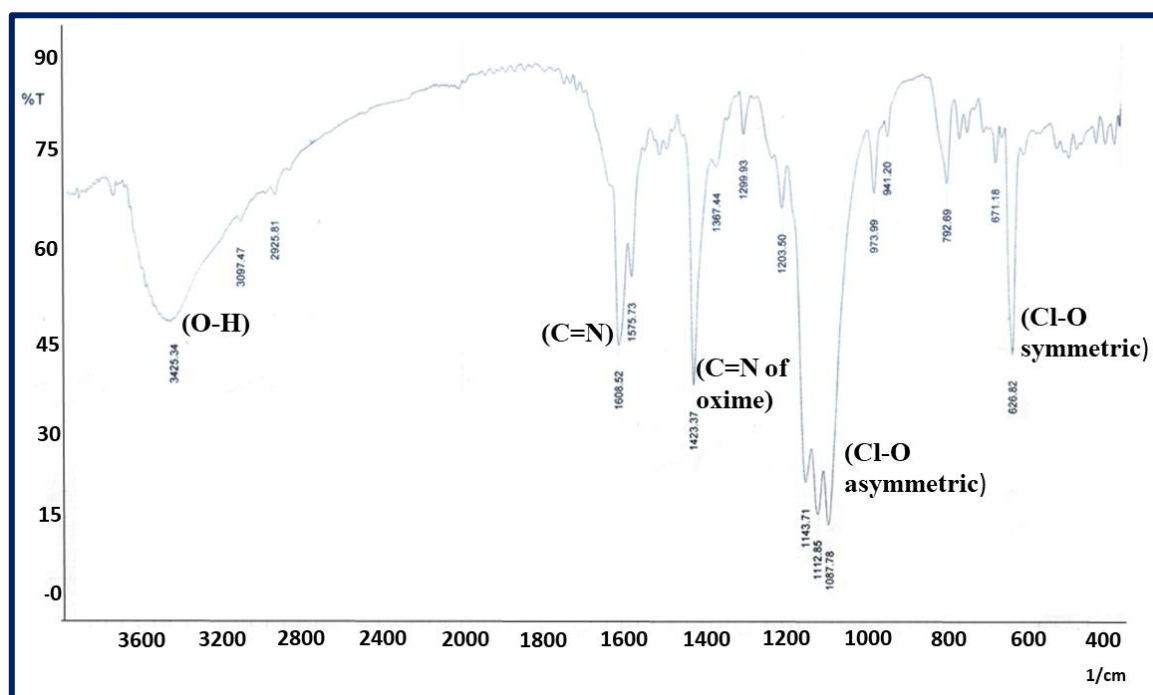


Fig. VI.5. FT-IR spectrum of complex **1**.

3.2. Electronic spectra

The electronic absorption spectra of both **HL** and **1** were recorded in methanol (Fig. VI.6). The spectrum of free **HL** shows two intratransitions at 248 and 351 nm, whereas compound **1** shows bands at 277 and 356 nm. The bands at 351 nm in **HL** and 356 nm in **1** may be assigned to the $n-\pi^*$ charge transfer transitions [101]. The higher energy bands, in the range of 200-300 nm, are associated with the intra-ligand $\pi-\pi^*$ charge-transfer transitions [102,103]. A broad band has also been observed at 634 nm with a low molar extinction coefficient value for **1** ($261 \text{ M}^{-1} \text{ cm}^{-1}$, inset in Fig. VI.6) that can be assigned to the d-d transition band in copper(II) [104,105]. Following our literature survey, two dinuclear oxime based Cu(II) complexes having different non-coordinated counter anions exhibited broad absorption bands in the visible domain at 636 and 635 nm. Additionally, sharp characteristic bands were also found at 427 and 426 nm owing to ligand to metal charge transfer transitions [81]. Moreover, an oxime based mononuclear Cu(II) complex shows characteristics bands at 402 and 624 nm, respectively, for the $\pi-\pi^*$ and d-d transitions [106]. All these reported d-d bands are similar to that obtained in the case of **1**. However, **1** manifests a low ligand to metal charge transfer band in contrast with the previously reported mono and dinuclear Cu(II) complexes under comparison. This may arise most likely due to different ligand environments.

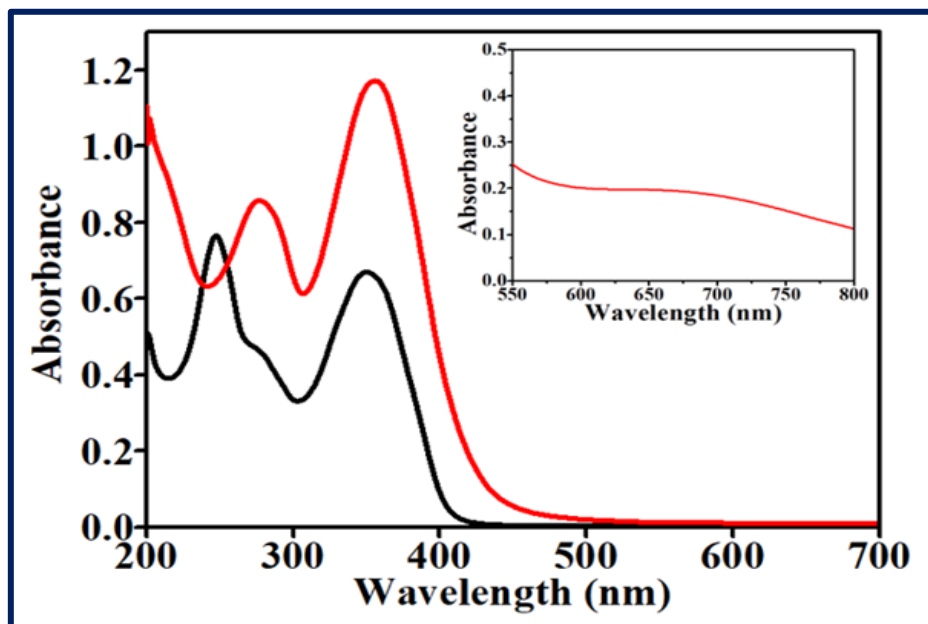


Fig. VI.6. UV-Vis spectra of **HL** (black) and **1** (red) in methanol (Inset: d-d band).

3.3. Description of the crystal structure of $[(\text{CuL})_3(\mu_3\text{-OH})(\text{ClO}_4)_2] \cdot \text{CH}_3\text{OH} \cdot \text{H}_2\text{O}$ (**1**)

Compound **1** crystallizes in the triclinic $P-1$ space group. An ORTEP view with 50% probability ellipsoids of **1** is shown in Fig. VI.7 (left). The asymmetric unit of **1** contains three **L**⁻ ligands,

three Cu^{II} ions, a $\mu_3\text{-OH}$ group, and two coordinated ClO_4^- anions, with methanol and water molecules as solvent of crystallization. The molecular structure of **1** contains a discrete trinuclear copper(II) core, with a central μ_3 -hydroxido bridge, surrounded by three L^- ligands and further stabilized by two coordinated perchlorate counter anions [Fig. VI.7 (left)].

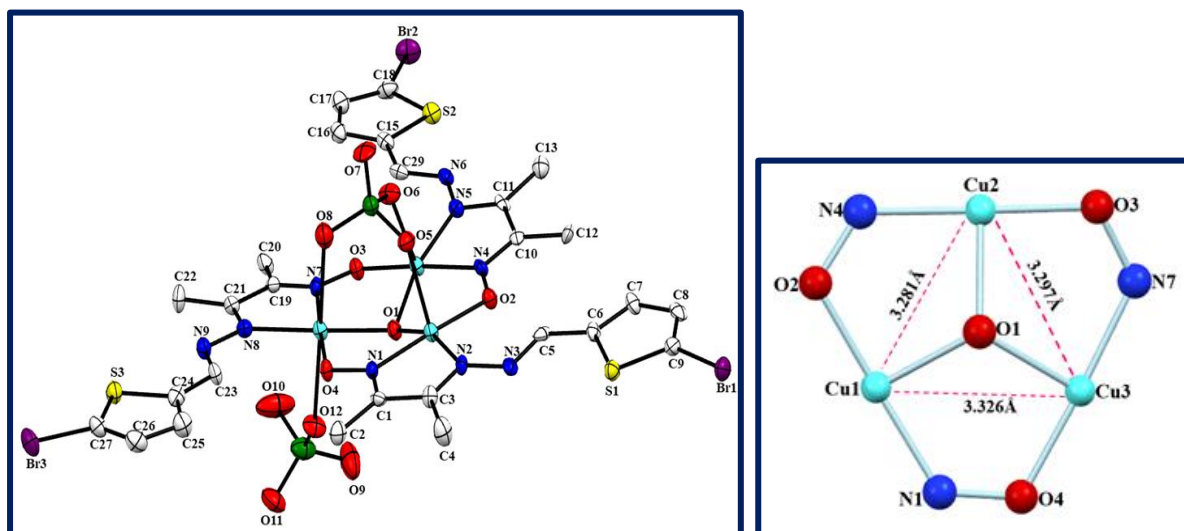


Fig. VI.7. Molecular structure of **1** with atomic displacement parameters (50% probability ellipsoids) (left). The *inverse*-metallacrown core as present in **1** (right).

The Cu1-Cu2, Cu2-Cu3 and Cu3-Cu1 distances are very similar: 3.281, 3.297 and 3.326 Å, respectively, with an average value of 3.301 Å. As a result of the μ_3 -hydroxido bridge, the three copper(II) centres adopt a near-equilateral triangular shape [107,108]. The Cu_3 triangle is capped on one side by the O1 atom of the central $\mu_3\text{-OH}^-$ ion and by a ClO_4^- anion (coordinated to the three Cu^{II} ions) on the other side. Cu1 and Cu2 centres show similar square pyramidal N_2O_3 coordination environments, whereas Cu3 shows an octahedral N_2O_4 environment. Both Cu1 and Cu2 shows a distorted square pyramidal environment with Addison's parameters, τ , of 0.29 for Cu1 and 0.15 for Cu2 [109,110]. The basal positions are occupied by two N donor atoms from the L^- ligand, one O atom from an adjacent L^- ligand and the O atom of the central hydroxido bridge. The axial position is occupied by an O atom from a perchlorate ion. As usual, the axial bond distances (Cu1-O5 = 2.344 Å and Cu2-O6 = 2.424 Å) are longer than the basal ones (in the range 1.906-2.042 Å, Table VI.2). Cu3 shows a distorted N_2O_4 octahedral environment. The equatorial positions are occupied by two N atoms from the L^- ligand, one O atom from an adjacent L^- ligand and the O atom of the central hydroxido bridge (similar to the basal plane of Cu1 and Cu2). The axial positions are occupied by two O atoms from two ClO_4^- coordinated anions, again with much longer Cu-O bond distances (2.449 and 2.639 Å) than the equatorial ones (in the range 1.936-3.046 Å, Table VI.2). The Cu-N(oxime) and Cu-N(imine)

bond lengths are in the range of 1.951-1.964 Å and 2.041-2.046 Å, respectively. These values are within the normal range observed in other similar trinuclear copper(II) complexes [111-114]. One of the two coordinated ClO_4^- anions is connected through three O atoms (O5, O6 and O8) to the three Cu centres with Cu-O bond distances of Cu1-O5 = 2.344 Å, Cu2-O6 = 2.424 Å and Cu3-O8 = 2.639 Å. Consequently, this perchlorate acts as a μ_3 -perchlorato-O,O',O'' capping ligand [115]. The average Cu-O(perchlorate) bond distance is 2.464 Å. This rather long Cu-O(perchlorate) bond indicates that the perchlorate anions are weakly bound to the copper centres, as already observed in other similar trinuclear Cu_3 complexes [116]. This weak ligation has further been confirmed by the electrical conductivity measurements in solution. Compound **1** in methanol behaves as a 1:2 electrolyte. This is indicative of the total dissociation of the two ClO_4^- anions in solution. As expected for a quasi-equilateral triangle, the intra-trimer Cu1-O1-Cu2, Cu2-O1-Cu3 and Cu3-O1-Cu1 bond angles are very similar: 112.4, 111.5 and 113.5°, respectively. The sum of these angles is less than 360° by 22.6°. This is due to the lack of planarity of the Cu_3O core (the O atom is located 0.538 Å away from the Cu_3 plane). Therefore, O1 shows a hybridization in between sp^2 and sp^3 [117]. In the domain of metalla-crown (MC) topology, the trinuclear copper core in **1** can be described as *inverse-9-metallacrown-3* (Fig. VI.7(right)) [118].

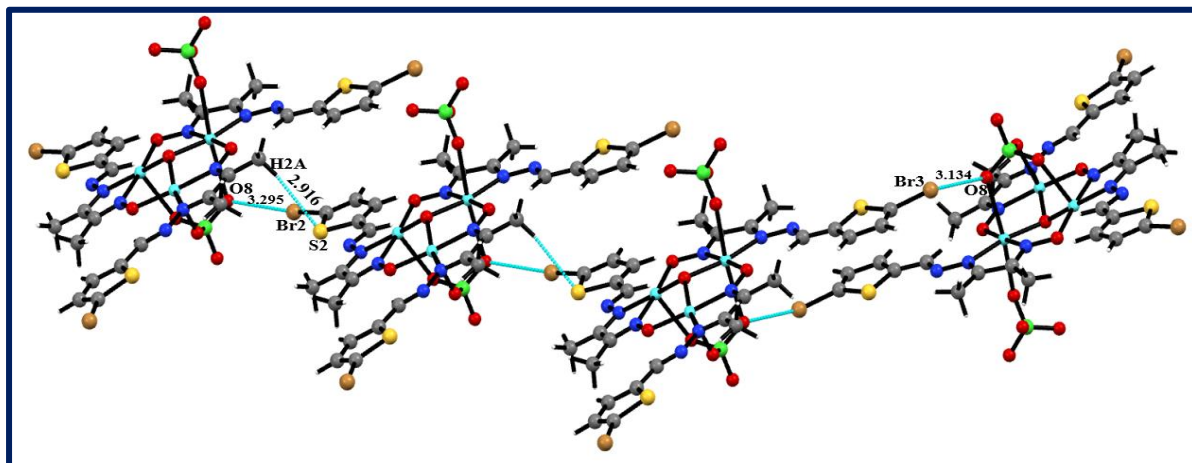


Fig. VI.8. H-bonded chain view of **1** through intermolecular interaction of $\text{C-Br}\cdots\text{O}$ and $\text{C-H}\cdots\text{S}$. Solvent molecules are omitted for clarity. The H-bonds are indicated by dashed line. As can be seen in Fig. VI.8, there is a weak $\text{C2-H2A}\cdots\text{S2}$ and two $\text{O}\cdots\text{Br}$ interactions that connect the trimers to form a chain of trimers. Additionally, there are several intra-trimer $\text{C-H}\cdots\text{O}$ interactions that connect different L^- ligands as well as H-bonds connecting the water molecule (O13) of crystallization with the two perchlorate anions (O6, O9 and O12) and with the central μ_3 -OH group (Table VI.3).

Table VI.3. Shorter intra- and inter-trimer interactions in compound **1**

Atoms	D-H (Å)	H···A (Å)	D-H···A (°)	D···A (Å)
*C5-H5···O2	0.950	2.121	149.4	2.978
*C14-H14···O3	0.950	2.200	138.9	2.982
*C23-H23···O4	0.950	2.088	157.2	2.987
C2-H2A···S2	0.980	2.916	171.4	3.887
O8···Br3				3.134
O8···Br2				3.295
O1···O13				2.695
O12···O13				3.015
O9···O13				2.739
O6···O13				2.891

* Intra-trimer H-bonds.

3.4. DNA binding

To explore the interaction of a complex with DNA, UV-Visible spectroscopic analysis is one of the useful methods [119]. Electronic absorption titrations for **1** was carried out in the absence and presence of CT-DNA employing Tris buffer (pH = 6.8) at 20 °C (Fig. VI.9). In the absorption spectra, **1** displayed absorption maxima at 364 nm corresponding to metal-to-ligand charge-transfer bands (MLCT) bands. 12.5 µM of complex **1** was titrated against increasing the concentration of CT-DNA (0-135 µM). The absorption spectra with the concomitant changes in intensity and wavelength were followed. Our expounded results clearly indicated that **1** shows 41.98% hypochromism with slight bathochromic shifts as a result of the intercalation binding mode of the complex and DNA base pairs. The binding constants (K_b) for **1** was calculated from the Wolfe–Shimmer equation [eqn (1)] [120] in order to compare the interaction intensity with CT-DNA.

$$\frac{[DNA]}{\epsilon_a - \epsilon_f} = \frac{[DNA]}{\epsilon_b - \epsilon_f} + \frac{1}{k_b(\epsilon_b - \epsilon_f)} \quad \text{.....(1)}$$

where ϵ_a is the extinction coefficient at the given DNA concentration as determined from Abs/[complex]. ϵ_f and ϵ_b correspond respectively to the extinction coefficient of the free complex and of the complex fully bound to DNA. The Wolfe–Shimmer binding constant (K_b)

can be obtained from the ratio of the slope of the linear plots of $[\text{DNA}]/(\epsilon_a - \epsilon_f)$ vs. $[\text{DNA}]$ and the intercept. The binding constant value for **1** was found to be $8.48 \times 10^4 \text{ M}^{-1}$.

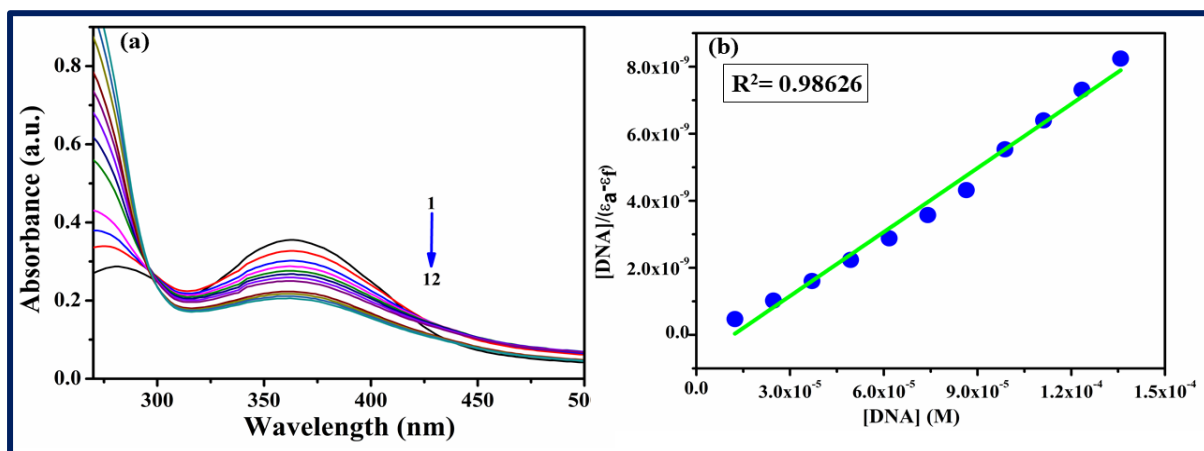


Fig. VI.9. (a) Absorption spectra of **1** ($12.5 \mu\text{M}$) in Tris-HCl buffer ($\text{pH} = 6.8$) with increasing amount of DNA ($135 \mu\text{M}$) at room temperature. (b) linear plots of $[\text{DNA}]/(\epsilon_a - \epsilon_f)$ vs. $[\text{DNA}]$.

3.5. CD spectra

The circular dichroism (CD) spectra of CT-DNA and its interaction with **1** are shown in Fig. VI.10. The CD signal peak, as the blank control, changed to a certain extent after the addition of **1**.

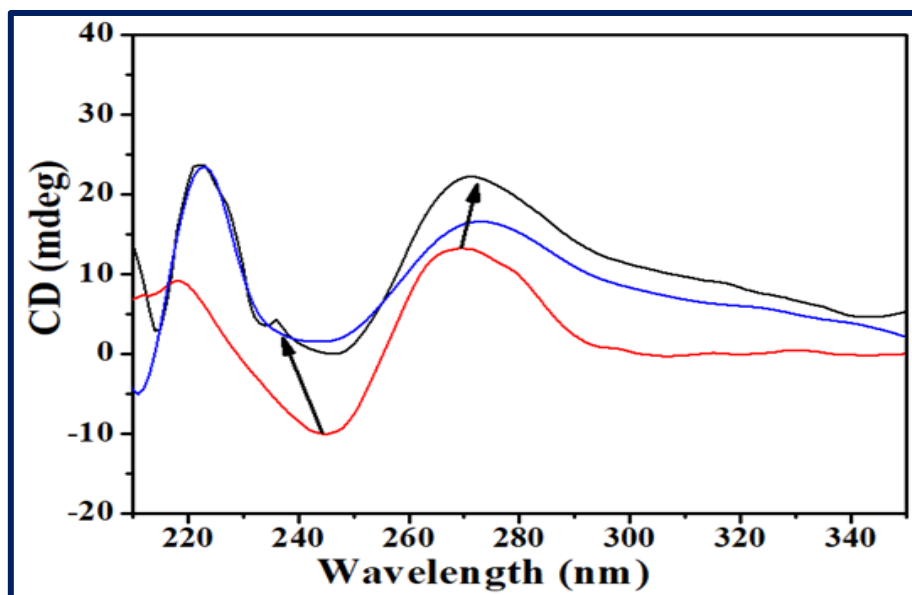


Fig. VI.10. CD spectra of interaction between **1** and CT-DNA. $C_{\text{DNA}} = 135 \mu\text{M}$.

As can be seen, the negative peak intensity decreased while the positive peak increased with certain degrees of red shift. Among them, the positive peak signal was enhanced in the CD spectrum due to the base stacking effect of DNA after the interaction of **1** with DNA base pair.

As a result, the double helix was more compact. The decrease and red shift of the negative peaks indicate that **1** destroyed the right-hand helicity of DNA molecules [121]. The results shows that **1** interacts with CT-DNA in an intercalated manner. The change of the spectral pattern of the positive and negative peaks confirms the interaction of DNA with **1**.

3.6. Biological study

In order to investigate the potential cytotoxicity of compound **1** against cancer cells, we have used the human lung adenocarcinoma cell (A549) as a model cell line to determine the effects of **1** on carcinoma cell proliferation.

3.6.1. Complex induced potent cytotoxic effects and inhibition of cell colony forming tendency

Water soluble tetrazolium 1 (WST-1) was utilised to investigate the cytotoxic activity of human lung adenocarcinoma cell line, A549. The WST-1 assay is based on the amount of formazan dye formed directly through the metabolic activity of cells. To the best of our knowledge, this is the first report on the biological cytotoxic activity of any trinuclear copper(II) compound. The *in vitro* cytotoxicity of **HL** and **1**, along with standard drug cisplatin as a positive control and DMSO as a vehicle control, was studied using the WST-1 assay. The *in vitro* biological effects of **HL** and **1** on A549 cell proliferation are depicted in Fig. VI.11A. There was a dose-dependent activity; with an increase in the concentrations of Compound **1**, the percentage of cell viability decreased with moderate cytotoxicity when compared with **HL**. On the other hand, **HL** displayed almost negligible cytotoxicity even at the highest dose of 518 μM . The 50% inhibition of cell growth (IC_{50} value) for **1** and **HL** was calculated by applying a non-linear regression curve fit analysis and was recorded as 222 and 592 μM respectively (Table VI.4).

Table VI.4. IC_{50} values for **1** and **HL**. IC_{50} values represent the mean of three independent

Compounds	IC_{50} value (μM)
1	222 \pm 0.87
HL	592 \pm 1.26

Cisplatin was used as a positive control in A549 cell lines because it is considered as the most common and effective anticancer drug in lung cancer treatment regimens as mentioned in our introductory part. The lung cancer A549 cells were then subjected to cytotoxic studies with cisplatin as a standard drug for comparison, and its IC_{50} value of cisplatin was recorded to be 1.75 μM (Fig. VI.11B).

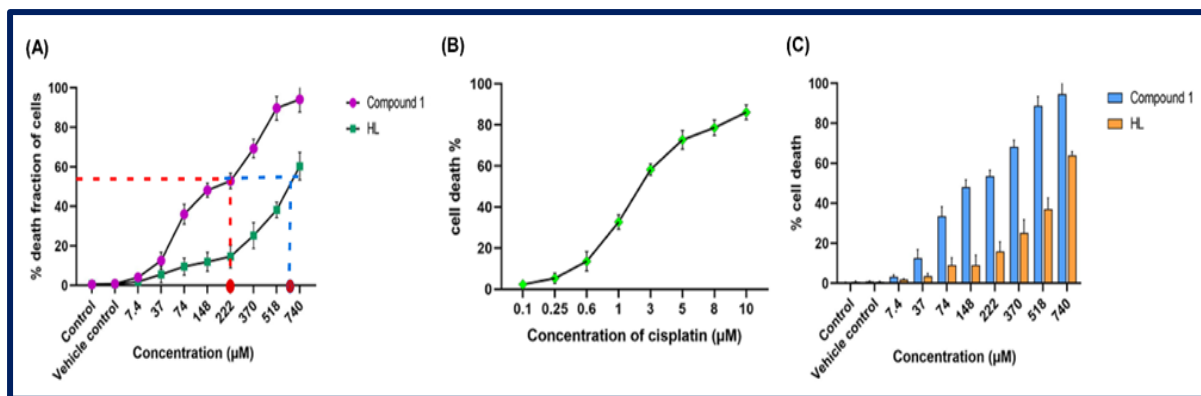


Fig. VI.11. Measurement of cytotoxic activity in A549 cells by (A) WST-1 assay with compound **1** and **HL** (B) WST-1 assay performed with positive control cisplatin (C) Trypan blue viability assay. Results indicate the percentage of live or viable cells as compared to the total number of cells for each sample. Data were collected from two independent experiments with three replicates per sample and were analysed with Two-Way ANOVA. Error bars are standard deviations. Data are shown as the mean \pm SD of three independent experiments.

The cytotoxic effect of **1** was further confirmed by trypan blue dye exclusion assay. Corresponding to WST-1 results, close cytotoxic response was noted from A549 cells on treatment with **1**, demonstrating prominent changes in their ability to exclude trypan blue until 24 h (Fig. VI.11C). The expounded results have positively hinted that **1** exerts potent cytotoxic effect than its stabilising ligand, **HL**, against human lung cancer cells. So, further studies were carried out on **1** taking two concentrations i.e. 222 and 370 μM respectively which are IC₅₀ and above IC₅₀ values, respectively.

The apoptotic nature of the complex and ligand was also screened against breast cancer cell line MCF-7 by WST-1 assay (Fig. VI.12). Complex **1** revealed an IC₅₀ value of 224 ± 0.25 μM against breast cancer cell line (MCF-7).

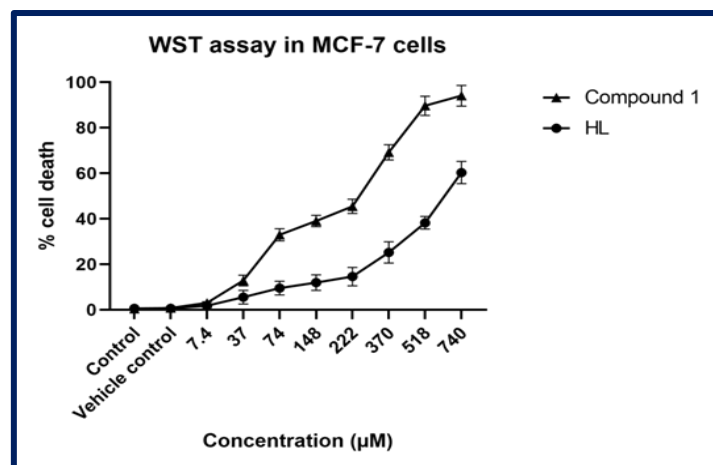


Fig. VI.12. Measurement of cytotoxic activity in MCF-7 cells by WST assay with **1** and **HL**.

It is pertinent to note that similar high IC₅₀ value $\geq 100 \mu\text{M}$ was also observed in human MCF-7 breast and HepG2 liver cancer cells by treatment with linear trinuclear Cu(II) complexes [58]. Some mononuclear/ dinuclear Cu(II) complexes show prominent cytotoxicity with lower IC₅₀ values [122-124]. Triangular trinuclear Cu(II) complexes usually show lower cytotoxicity in comparison to mono/di nuclear Cu(II) complexes.

The inhibitory effect of **1** on the proliferation of A549 cells was determined with colony formation assay. Cultured A549 cells were treated with the complex at the two mentioned concentrations (222 and 370 μM) for a week, and then stained with crystal violet. As depicted in Fig. VI.13, compound **1** suppress the colony formation tendency of A549 cells while the control and vehicle wells had almost fully grown cells. Cumulatively these results show that **1** has a dual effect: (i) decrease cell viability and (ii) inhibit the colony formation in a persistent way.

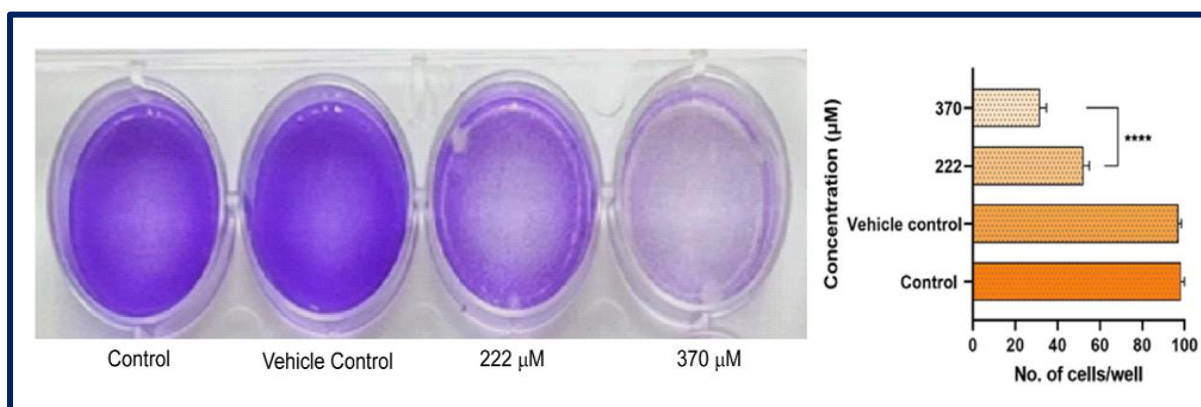


Fig. VI.13. Complex suppressed colony formation ability of lung adenocarcinoma cells at the indicated doses for appropriate time. The colony formation rate of cells was calculated and represented (Right panel). The data are presented as the mean \pm SD of three separate experiments. (* $P < 0.05$, ** $P < 0.01$, *** $P < 0.001$ significant differences between treatment group and control group).

3.6.2. Morphological changes induced by complex **1**

Image analysis with phase contrast microscopy is a non-destructive cell imaging method, which allows one to visualise and analyse apoptosis without influencing the cell behaviour [125]. The results of microscopic image analyses established that **1** has a moderate toxic effect against A549 cells which led to alteration in the cell structure. In the negative control set, the cell appeared to be normal bearing usual morphology with strong adhesion, whereas in treated set, changes in morphology such as cellular shrinkage accompanied by round cells, elongated and distorted cells, poor cellular adhesion and reduced cell number with visible cellular debris were clearly observed (Fig. VI.14).

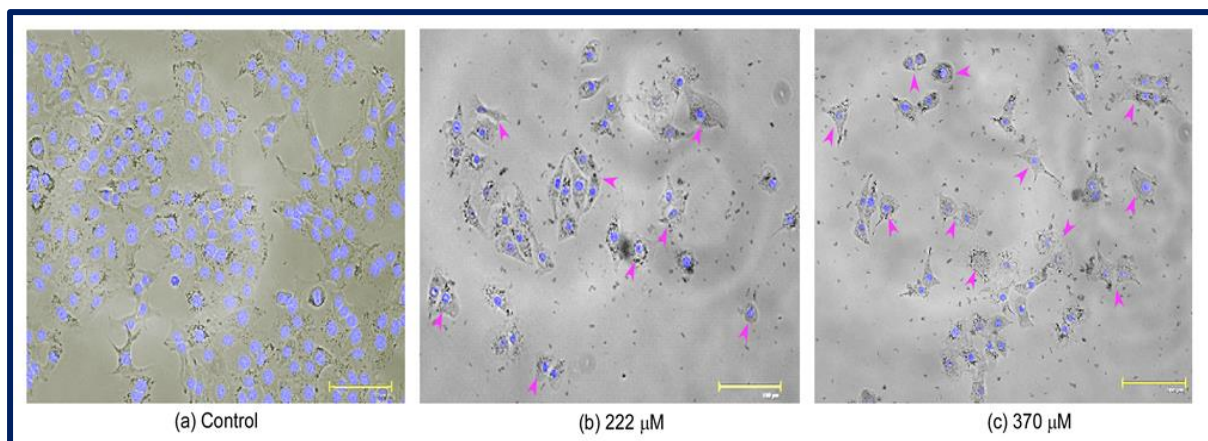


Fig. VI.14. Morphological alterations of lung adenocarcinoma A549 cells under inverted phase contrast microscopy. (a) control and, (b) and (c) cells exposed with complex. Magnification 40x.

3.6.3. Apoptotic cell death in A549 cells induced by complex 1

Studying apoptosis is a key point in cancer research since a dearth or a surplus of apoptosis is the sole cause for cancer. At present, several *in vitro* procedures are at hand to study apoptosis including various morphological staining methods like acridine orange and ethidium bromide (AO/EB), DAPI (4',6-diamidino-2-phenylidole), Hoechst staining, etc. [126]. Hence, in order to decipher the cytotoxic mode of action of **1** against A549 cancer cells, staining experiments were conducted using DAPI and AO/EB. To determine the involvement of apoptosis in complex **1**-induced cytotoxicity in A549 cells, initial evaluation was carried out with fluorescent DNA binding dye, DAPI. Fig. VI.15A shows how treatment with **1** causes characteristic apoptotic changes in cellular morphology as chromatin condensation with irregular edges around the nucleus, fragmented nuclei, nuclear shrinkage as well as blebbing, elevated number of nuclear body fragments and distorted nucleus, whereas round, clear edged, intact nucleus and uniformly stained round nuclei were observed in the negative control.

Further fluorescence microscopic observations of the A549 cells stained with AO/EB validate the presence of early and late apoptotic stages of cells along with the prominent apoptotic features. Acridine orange (AO) being an important dye stains the nuclei green in both living and dead cells, while ethidium bromide (EB) stains only those cells that have lost their membrane integrity [127]. When complex **1**-treated A549 cells were stained with AO/EB dye mixture, a major proportion of cells showed cellular shrinkage, condensed or fragmented chromatin, membrane blebbing with distorted cellular morphology (Fig. VI.15B). Cells emitting yellowish green fluorescence were marked as early apoptotic as notably visible in 222 μM concentration along with a few cells emitting yellowish orange indicating the presence of both early and late apoptotic cells.

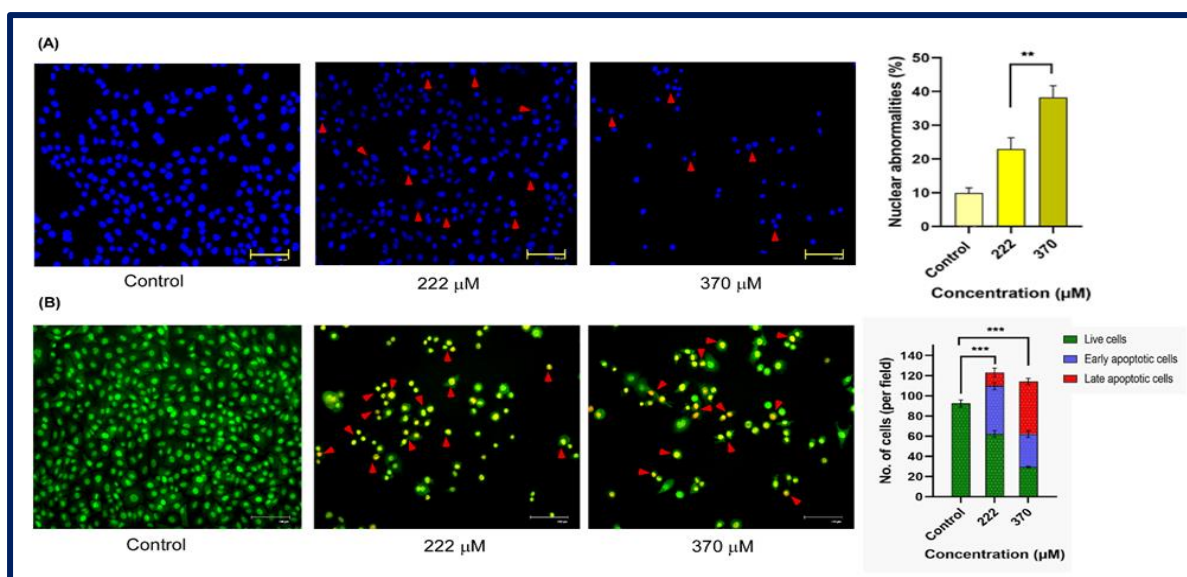


Fig. VI.15. Apoptosis induction studies of complex (**1**) in A549 cells. (A) DAPI staining. Arrows represent the nuclear anomalies which increased with increasing dose of complex. The percentage of nuclear abnormalities in respective set of experiment represented in bar graph (right panel). (B) Acridine orange and Ethidium bromide (AO/EB) staining by fluorescence microscope. Arrow indicates early apoptotic (EA) and late apoptotic (LA) cells. The bar graph depicts the population of cells in different phases (right panel). Scale bar denotes 200 μM. Magnification 45×. All the experiments were performed after 24 h incubation. Values represent the means ± standard deviation (SD), and all samples were measured independently in triplicate. Differences among the groups were compared by one-way ANOVA, and the asterisks indicate significant differences between treatment group and control group (* $P < 0.05$, ** $P < 0.01$, *** $P < 0.001$).

At high concentration of 370 μM, most of the cells fluoresced yellowish orange to bright orange indicating the late apoptotic stage. In contrast, non-apoptotic or live cells appeared wholly green in colour with no alternation in their morphology in the control. The results significantly reveal that cell death induced by **1** in A549 cells is due to apoptosis. By counting the number of yellowish orange, yellowish green and green cells, the apoptotic rate was calculated (Fig. VI.15B, right panel). Based on these results, complex **1** might be a possible choice for further test of the anticancer activity against human lung adenocarcinoma cells for both *in vitro* and *in vivo* procedures.

3.6.4. Effect of complex (**1**) on the migration of A549 cells

Customarily, cells tend to migrate, which is essential for growth and to ensure proper tissue functions. In cancer cells, the migratory property leads to invasion and metastasis. This is the prime reason for the mortality of lung cancer patients [128]. To study the effect of **1** on the

migration of A549 cells, experiments were conducted for 24 h till the induced wound was completely closed in wound-healing assays. As can be seen in Fig. VI.16, the migration ability of A549 cells decreases as the amount of complex **1** covering the wound increases, whereas the negative control cells show almost 90 % of wound closure after 24 h.

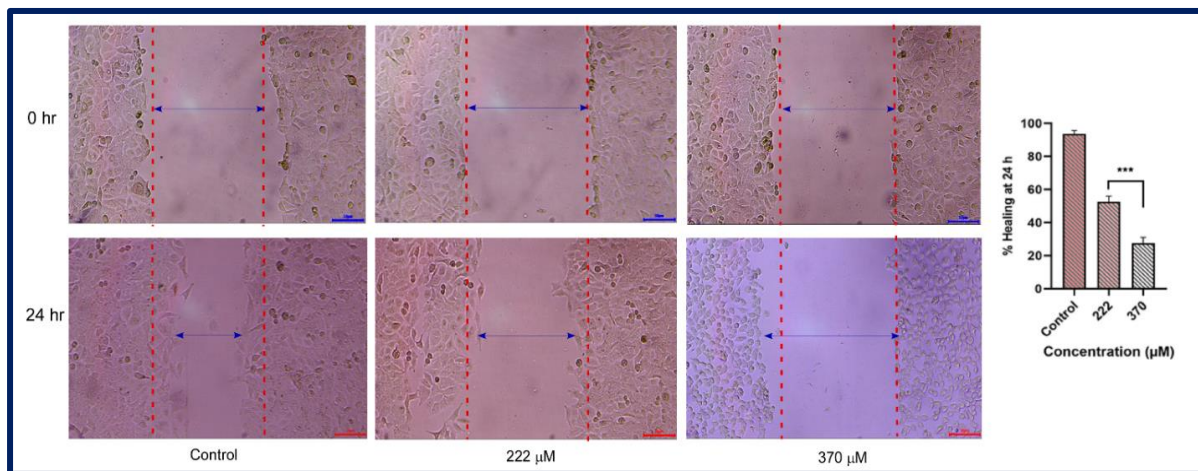


Fig. VI.16. Wound-healing assay of A549 cells after exposure to complex (**1**). Representative wound-healing images taken at 0 h and 24 h with respective wound-closure ratios (Left panel). Wound-closure analysis after complex normalized to 0% at 0 h. Experiments were repeated three times. Bars represent standard deviation from one representative experiment (Right panel). Magnification 100x.

3.6.5. Cell death mechanism

There are several comprehensive studies that focus on the diverse roles of inorganic compounds in cancer therapy [129]. Copper based complexes are favourable next-generation non-platinum anticancer agents and chemotherapeutics [130]. Our compound exhibits a regular cell death against A549 lung cancer cells and in reference to other studies conducted previously, we infer that trinuclear copper(II) complexes induces cell death through diverse mechanisms, encompassing reactive oxygen species (ROS) responses, mitochondrial dysfunction and apoptosis through an intrinsic pathway. Similarly, Gul *et al.*, in 2020 reported two copper(II) complexes, Cu1 and Cu2 with isoquinoline derivatives as ligands that interacted via the mitochondrial-mediated pathway against A549 cells [131]. Yip *et al.*, 2011 found that disulfiram (DSF) can manifest strong copper-dependent toxicity *in vitro* against cultured breast cancer cells [132]. The combined application of disulfiram and Cu^{2+} inhibited breast cancer cell colony formation, induced ROS production and subsequently activated downstream apoptosis-related pathways, thereby induced breast cancer cell apoptosis. Again, *in vitro* antitumor effects of a Cu(II) complex, $[\text{Cu}(4\text{-fh})(\text{phen})(\text{ClO}_4)_2]$, had been reported to act against melanoma B16F10 cells through DNA-damage, G0/G1 cell cycle arrest and triggered

apoptosis [133]. Reports on promising *in vitro* anti-proliferative efficacy of copper(II) complexes against lung carcinoma cell NCI-H460 are also there. For ready reckoning, $[\text{Cu}(\text{L1})\text{Cl}]\text{Cl}\cdot 2\text{H}_2\text{O}$ induced cell death by apoptosis via cell cycle arrest at sub-G1 populations, plasma membrane blebbing, fragmentation and condensation of chromatin, alterations in mitochondria along with distinct changes on the cell surface [134]. Novel water-soluble ternary copper(II) mixed ligand complexes, $[\text{Cu}(4\text{-mphen})(\text{tyr})(\text{H}_2\text{O})]\text{NO}_3\cdot 2\text{H}_2\text{O}$ and $[\text{Cu}(5\text{mphen})(\text{tyr})(\text{H}_2\text{O})]\text{NO}_3\cdot 2\text{H}_2\text{O}$, had been demonstrated to display apoptotic activity against adenocarcinomic human alveolar basal epithelial cell, A549. These two complexes were also demonstrated to cause DNA damage possibly through significant induction of ROS-mediated oxidative damage in the cancer cell and varying degrees of cytotoxic and genotoxic damage in the cancer cell line [135].

To ascertain the stability of **1** during our anti-proliferative assay, its UV-Vis spectra in 0.5% DMSO solution in time-variation mode were monitored (Fig. VI.17). **1** retained its unaltered identity in terms of structural rigidity in 0.5% DMSO solution. This prompted us to deploy 0.5% DMSO solution of **1** in our undertaken bio-assays.

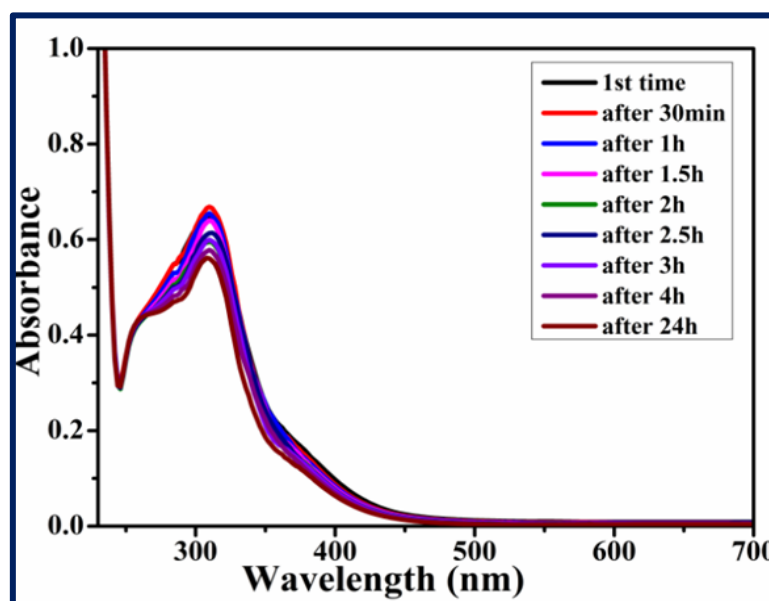


Fig. VI.17. UV-Vis spectra of **1** in 0.5% DMSO with variation in time mode.

3.7. Magnetic properties

The thermal variation of the product of the molar magnetic susceptibility per Cu_3 trimer times the temperature ($\chi_m T$) shows a value close to $0.9 \text{ cm}^3 \text{ K mol}^{-1}$ at room temperature (Fig. VI.18). When the sample is cooled, the $\chi_m T$ value shows a continuous decrease to reach a plateau of around $0.4 \text{ cm}^3 \text{ K mol}^{-1}$ below 50 K. At lower temperatures, $\chi_m T$ shows a further decrease to reach a value of $0.25 \text{ cm}^3 \text{ K mol}^{-1}$ at 2 K. This behaviour clearly indicates the presence of

predominant antiferromagnetic Cu···Cu interactions inside the Cu₃ triangle, giving rise to spin frustration since in a triangular array of spins, it is not possible to simultaneously satisfy the three possible spin pairings in an antiferromagnetic way [59-61]. Since complex **1** shows a quasi-equilateral triangle, we have fitted the magnetic properties of **1** with a simple model of an equilateral $S = \frac{1}{2}$ triangle with the following Hamiltonian: $H = -2J[S_1S_2 + S_2S_3 + S_1S_3]$ including a weak inter-trimer coupling (zj , to account for the decrease at very low temperatures) and a paramagnetic monomeric impurity, using the program PHI [136]. This model reproduces very satisfactorily the magnetic data in the whole temperature range with $g = 2.144(4)$, $J = -44.6(2) \text{ cm}^{-1}$, $zj = -2.0(1) \text{ cm}^{-1}$ and a $S = \frac{1}{2}$ paramagnetic impurity of 2.2(1)% (solid line in Fig. VI.18).

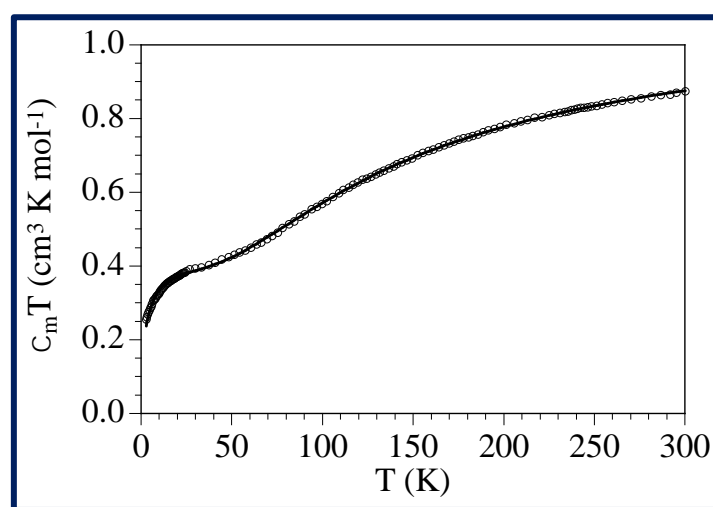


Fig. VI.18. Thermal variation of $\chi_m T$ per Cu₃ trimer in **1**. Solid line shows the best fit to the equilateral $S = \frac{1}{2}$ trimer model.

3.8. Magneto-structural correlation

It is well established that in triangular Cu₃ complexes with a central O atom, the strength of the antiferromagnetic coupling mainly depends on the Cu-O-Cu bond angles since these angles are closely related to the planarity of the Cu₃O entity. The larger the angle, the larger the planarity and, accordingly, the stronger the antiferromagnetic coupling [137]. Additionally, there are other factors that may affect the effective overlap of the magnetic orbitals and, therefore, the magnetic coupling as: (i) the deviation of the μ_3 -O centre from the centroid of the Cu₃ triangle (the higher the deviation, the weaker the coupling), (ii) the Cu···Cu distance in the triangle and (iii) the co-planarity of the equatorial coordination plane around each copper centre (the greater the co-planarity, the stronger the magnetic coupling).

Since complex **1** contains: (i) a central μ_3 -OH bridge, (ii) a μ_3 -perchlorato-O,O',O'' capping ligand connecting the three Cu^{II} ions and (iii) a Cu₃ core surrounded by peripheral oximates, we have performed a search in the CCDC database (consulted in October 2023) [116,138-142],

to look for complexes similar to complex **1**. This search shows that there are only six trinuclear copper(II) complexes reported with these characteristics. Unfortunately, only three of them have been magnetically characterized (Table VI.5) [138-140]. In these three examples, the magnetic coupling is strong and antiferromagnetic, although the lack of more examples precludes a clear magneto-structural correlation. Furthermore, two of them have been fitted with an antisymmetric exchange and, therefore, the J values cannot be compared with the other case where a symmetric exchange model has been used. Nevertheless, we can compare compound **1** ($J = -89.2 \text{ cm}^{-1}$) with compound KUPRAP ($J = -148 \text{ cm}^{-1}$) [139]. In compound KUPRAP the average Cu-O-Cu bond angle is larger compared to that in compound **1** (115.42° vs. 112.44°), the average dihedral Cu-N-O-Cu angle is lower (6.05° vs. 10.16°) and the average Cu...Cu distance is shorter (3.212 \AA vs. 3.301 \AA). All these structural parameters indicate that the magnetic coupling in KUPRAP must be stronger than that in **1**, in agreement with the experimental results (-148 cm^{-1} vs. -89.2 cm^{-1}) (Table VI.5).

Table VI.5. Comparison of structural and magnetic parameters of some oxime based μ_3 -OH bridged trinuclear copper(II) complexes

Complex (CCDC)	Cu...Cu (Å)	α ($^\circ$) ^a	θ ($^\circ$) ^b	J (cm^{-1}) ^c	z_j (cm^{-1})	Ref.
1	3.281 3.297 3.326	112.40 111.46 113.45	9.37 20.34 0.77	-89.2	-2.0	This work
ACAFIW	3.203 3.225 3.217	111.06 112.47 111.89	8.70 8.17 11.44	-441(2) ^d		138
KUPRAP	3.198 3.221 3.216 3.214 3.215 3.205	114.92 116.89 115.91 114.91 115.48 114.42	6.37 0.17 12.37 3.99 2.23 11.18	-148	-7.65 ^e	139
YIZNOM	3.215 3.215 3.227	117.17 116.12 114.99	12.82 4.85 3.74	-636 ^d	-0.13 ^e	140

ACAFIW = $[\text{Cu}_3(\text{OH})(\text{ClO}_4)_2(\text{mpko})_3] \cdot \text{CH}_3\text{OH}$, (mpko = methyl(2-pyridyl)ketone oxime); KUPRAP = $\{[\text{Cu}_3(\text{NHDEPO})_3(\mu_3\text{-O})(\text{ClO}_4)_2(\mu\text{-H})](\text{ClO}_4)_7\} \cdot 4\text{H}_2\text{O}$ (NHDEPO = 3-[3-(diethylamino)propylimino]butan-2-one oxime); YIZNOM = $\{[\text{Cu}_3(\text{HL})_3(\text{ClO}_4)(\mu_3\text{-O})_2(\mu\text{-H})](\text{ClO}_4)_7\}$, (HL = 3-[3-(dimethylamino)propylimino]-butan-2-one oxime). (a) α = Cu-O-Cu angle; (b) θ = Cu-N-O-Cu torsion angle; (c) the Hamiltonian is $H = -J[S_1S_2 + S_2S_3 + S_3S_1]$; (d) antisymmetric exchange; (e) θ value (Weiss correction of the temperature).

3.9. EPR spectroscopy

The EPR spectrum of **1**, recorded in a frozen N,N-dimethylformamide (DMF) solution at 143 K (Fig. VI.19), displays four hyperfine lines in the parallel (g_{\parallel}) region, corresponding to the hyperfine coupling with the $I = 3/2$ nuclear spin of ^{63}Cu and ^{65}Cu nuclei (with natural abundances of 69.7% and 30.3%, respectively). Compound **1** shows a rhombic EPR spectrum with $g_{\perp} > 2.2 > g_{\parallel}$ and $A_{\perp} > A_{\parallel}$. This spectrum can be very well simulated with a linewidth of 3 G, $g_{\perp} = 2.4000$, $g_{\parallel} = 2.0849$, $A_{\perp} = 128.7$ G and $A_{\parallel} = 12.21$ G (red line in Fig. VI.19). These values and the observed EPR spectrum agree with a Cu^{II} ion with an electronic ground state in which the unpaired electron mainly occupies the $d_{x^2-y^2}$ orbital [143]. The magnetic parameter values of **1** are shown in Table VI.6.

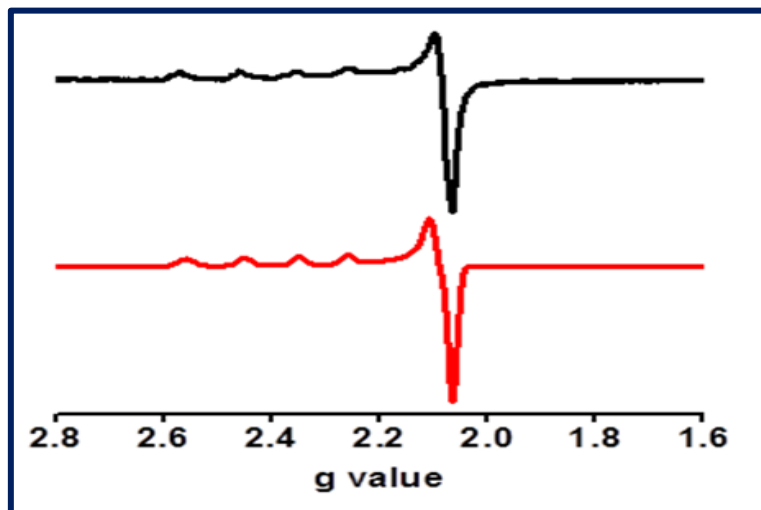


Fig. VI.19. X-band EPR spectra of **1** in frozen DMF solution. Red (simulation) and black (experimental).

Table VI.6. Magnetic parameters of **1**

Complex	g value		A value (G)		Line width(G)
	g_1	g_2	A_1	A_2	
1	2.4000	2.0849	128.7	12.21	3

4. Conclusions

In this work, we have successfully synthesized and characterised a novel Schiff base ligand, 3-(((5-bromothiophen-2-yl)methylene)hydrazineylidene)butan-2-one oxime (**HL**), and a rare triangular trinuclear copper(II) complex (**1**) with a central μ_3 -OH bridge and a capping ClO_4^- anion connecting the three Cu^{II} ions. Both **HL** and **1** have been screened against lung adenocarcinoma cell lines A549. In contrast to the ligand **HL**, significant cell death has been induced by **1** in A549 cells. The IC_{50} value for **1** is found to be much lower than that of **HL**. Cellular cell death induced by **1** is due to apoptosis. **1** displays elevated outstanding potency against A549 cells. Based on these results, compound **1** might be a possible choice of anticancer medication against human lung adenocarcinoma cells (A549) for both *in vitro* and *in vivo* experimental procedures. In addition, the magnetic properties of **1** show the presence of a moderate antiferromagnetic coupling that can be rationalized from the structural parameters.

5. References

1. L.A. Torre, F. Bray, R.L. Siegel, J. Ferlay, J. Lortet-Tieulent, A. Jemal, CA-Cancer J. Clin. 65 (2015) 87-108.
2. H.K. Matthews, C. Bertoli and R.A.M. de Bruin, Nat. Rev. Mol. Cell Biol. 23 (2022) 74-88.
3. D. Hanahan, Cancer Discov. 12 (2022) 31-46.
4. C.P. Wild, E. Weiderpass and B.W. Stewart, Word cancer report: cancer report for cancer prevention, IARC, Newyork, 2020.
5. H. Sung, J. Ferlay, R.L. Siegel, M. Laversanne, I. Soerjomataram, A. Jemal and F. Bray, CA-Cancer J. Clin. 71 (2021) 209-249.
6. B.S. Chhikara and K. Parang, Chem. Bio. Lett. 10 (2023) 451.
7. J. Ferlay, M. Colombet, I. Soerjomataram, Int. J. Cancer 149 (2021) 778-789.
8. The global challenge of cancer. Nat. Cancer 1 (2020) 1-2.
9. World Health Organization, Cancer facts sheets, lung cancer, <https://www.who.int/news-room/fact-sheets/detail/cancer>.
10. R.L. Siegel, K.D. Miller, H.E. Fuchs, A. Jemal, CA- Cancer J. Clin. 72 (2022) 7-33.
11. F. Bray, J. Ferlay, I. Soerjomataram, R.L. Siegel, L.A. Torre, A. Jemal, CA-Cancer J. Clin. 68 (2018) 394-424.
12. J. Didkowska, U. Wojciechowska, M. Mańczuk and J. Lobaszewski, Ann. Transl. Med. 4 (2016) 1-11.
13. R. Sharma, Int. J. Clin. Oncol. 27 (2022) 665-675.
14. B.C. Bade and C.S.D. Cruz, Clin. Chest Med. 41 (2020) 1-24.
15. K. Moghissi, J. Kastelik, P. Barber and P.S. Nia, *Perspectives in Lung Cancer*, Bentham Books, Singapore, 2020.
16. S.P. Fricker, Dalton Trans. (2007) 4903-4917.
17. N.K. Singh, P.N. Yadav, A.A. Kumbhar, Y.R. Pokhrel, P.N. Yadav, J. Inorg. Biochem. 210 (2020) 111134.
18. American Cancer Society, Treating Non-Small Cell Lung Cancer, <https://www.cancer.org/cancer/lung-cancer/treating-non-small-cell.html>.
19. Y. Gao, P. Dorn, S. Liu, H. Deng, S.R. R. Hall, R.W. Peng, R.A. Schmid, T.M. Marti, Cancer Cell Int. 19 (2019) 1-14.
20. S. Dilruba, G.V. Kalayda, Cancer Chemother. Pharmacol. 77 (2016) 1103-1124.
21. T.C. Johnstone, K. Suntharalingam, S.J. Lippard, Chem. Rev., 116 (2016) 3436-3486.

22. M.S. Galanski, B.K. Keppler, *Anti-Cancer Agent*. 7 (2007) 55-73.
23. Y. Jung, S. J. Lippard, *Chem. Rev.* 107 (2007) 1387-1407.
24. Y.G. Gonçalves, A.B. Becceneri, A.E. Graminha, V.M. Miranda, R.R. Rios, F. Rinaldi-Neto, M.S. Costa, A.C. R. Gonçalves, V.M. Deflon, K.A. G. Yoneyama, P.I. S. Maia, E.F. Franca, M.R. Cominetti, R.S. Silva, G.V. Poelhsitz, *Dalton Trans.* 52 (2023) 9590-9606
25. A.E. Graminha, J. Honorato, R.S. Correa, M.R. Cominetti, A.C.S. Menezes, A.A. Batista, *Dalton Trans.* 50 (2021) 323-335.
26. G.F. Grawe, K.M. Oliveira, C.M. Leite, T.D. de Oliveira, J. Honorato, A.G. Ferreira, E.E. Castellano, M.R. Cominetti, R.S. Correa, A.A. Batista, *Dalton Trans.* 51 (2022) 1489-1501.
27. J. Jiang, Q. Chen, T. Huan, Y. Nie, Z. Dai, D. Li, X. Xu, J. Lu, Z. Hua, H. Xu, *Dalton Trans.* 52 (2023) 14338-14349.
28. T.J. Carneiro, A.S. Martins, M.P. M. Marques, A.M. Gil, *Front. Oncol.* 10 (2020) 590970.
29. M.N. Alam, F. Huq, *Coord. Chem. Rev.* 316 (2016) 36-67.
30. T. Lazarević, A. Rilak, Ž.D. Bugarčić, *Eur. J. Med. Chem.* 142 (2017) 8-31.
31. W.A. Wani, U. Baig, S. Shreaz, R.A. Shiekh, P.F. Iqbal, E. Jameel, A. Ahmad, S.H. Mohd-Setapar, M. Mushtaque, L.T. Hun, *New J. Chem.* 40 (2016) 1063-1090.
32. T. Nabiyeva, C. Marschner, B. Blom, *Eur. J. Med. Chem.* 201 (2020) 112483.
33. C. R. Munteanu, K. Suntharalingam, *Dalton Trans.* 44 (2015) 13796-13808.
34. Y. Liu, Y. Wang, S. Song, H. Zhang, *Chem. Sci.* 12 (2021) 12234.
35. X. Li, Z. Shi, J. Wu, J. Wu, C. He, X. Hao, C. Duan, *Chem. Commun.* 56 (2020) 7537-7548.
36. M. Gallardo-Villagrán, L. Paulus, J. L. Charissoux, D.Y. Leger, P. Vergne-Salle, B. Therrien, B. Liagre, *Dalton Trans.* 51 (2022) 9673-9680.
37. R. Paprocka, M. Wiese-Szadkowska, S. Janciauskiene, T. Kosmalski, M. Kulik, A. Helmin-Basa, *Coord. Chem. Rev.* 452 (2022) 214307.
38. M. Kedia, S. Khatun, U. Phukon, B. Shankar, A.K. Rengan, M. Sathiyendiran, *Dalton Trans.* 52 (2023) 14314-14318.
39. S.U. Parsekar, K. Paliwal, P. Haldar, P.K.S. Antharjanam, M. Kumar, *ACS Omega* 7 (2022) 2881-2896.
40. C. Santini, M. Pellei, V. Gandin, M. Porchia, F. Tisato, C. Marzano, *Chem. Rev.* 114 (2014) 815-862.

41. M. Das, S. Mukherjee, M.M. Islam, I. Choudhuri, N. Bhattacharyya, B.C. Samanta, B. Dutta, T. Maity, *ACS Omega* 7 (2022) 23276-23288.
42. N. Biswas, S. Khanra, A. Sarkar, S. Bhattacharjee, D.P. Mandal, A. Chaudhuri, S. Chakraborty, C.R. Choudhury, *New J. Chem.* 41 (2017) 12996-13011.
43. M.S. Galanski, V.B. Arion, M.A. Jakupcic, B.K. Keppler, *Curr. Pharm. Des.* 9 (2003) 2078-2089.
44. R.W.-Y. Sun, D.-L. Ma, E.L. -M. Wong, C.-M. Che, *Dalton Trans.* (2007) 4884-4892.
45. Y. Li, K.-N. Wang, L. He, L.-N. Ji, Z.-W. Mao, *J. Inorg. Biochem.* 205 (2020) 110976.
46. M.N. Ahamad, K. Iman, M.K. Raza, M. Kumar, A. Ansari, M. Ahmad, M. Shahid, *Bioorg. Chem.* 95 (2020) 103561.
47. M.K. Gond, N. Rai, B. Chandra, V. Gautam, S. Garai, R.J. Butcher, M.K. Bharty, *Dalton Trans.* 52 (2023) 10213-10221.
48. Y. Chen, Z. Ke, L. Yuan, M. Liang, S. Zhang, *Dalton Trans.* 52 (2023) 12318-12331.
49. W. Lu, J. Tang, Z. Gu, L. Sun, H. Wei, Y. Wang, S. Yang, X. Chi, L. Xu, *J. Inorg. Biochem.* 238 (2023) 112030.
50. J. Serment-Guerrero, P. Cano-Sanchez, E. Reyes-Perez, F. Velazquez-Gracia, M.E. Bravo-Gomez, L. Ruitz-Azuara, *Toxicol. Vit.* 25 (2011) 1376-1384.
51. C.S. Novoa-Ramírez, A. Silva-Becerril, M.M. González-Ballesteros, V. Gomez-Vidal, M. Flores-Álamo, L. Ortiz-Frade, J. Garcia-Mora, L. Ruiz-Azuara, *J. Inorg. Biochem.* 242 (2023) 112097.
52. N.K. Mandal, S. Nandi, K. Acharya, J.P. Naskar, *Appl. Organomet. Chem.* 37 (2023) e7120.
53. M. Anjomshoa, H. Hadadzadeh, M. Torkzadeh-Mahani, S. J. Fatemi, M. Adeli-Sardou, H.A. Rudbari, V.M. Nardo. *Eur. J. Med. Chem.* 96 (2015) 66-82.
54. P. Adak, B. Ghosh, A. Bauza, A. Frontera, A.J. Blake, M. Corbella, C.D. Mukhopadhyay, S.K. Chattopadhyay, *RSC Adv.* 6 (2016) 86851-86861.
55. G.-Y. Li, K.-J. Du, J.-Q. Wang, J.-W. Liang, J.-F. Kou, X.-J. Hou, L.-N. Ji, H. Chao, *J. Inorg. Biochem.* 119 (2013) 43-53.
56. K.E. Prosser, S.W. Chang, F. Saraci, P.H. Le, C.J. Walsby, *J. Inorg. Biochem.* 167 (2017) 89-99.
57. G. Ramesh, S. Daravath, M. Swathi, V. Sumalatha, D.S. Shankar, S. Shivaraj, *Chem. Data Collect.* 28 (2020) 100434.

58. H.H. Nguyen, T.T. Pham, N.O. Pham-Thi, V.H. Tran, C.D. Le, B.V. Hoi, T.N. Trieu, C.T. Pham, *J. Mol. Struct.* 1249 (2022) 131680.
59. O. Kahn, *Molecular Magnetism*, VCH, Weinheim, Germany, 1993.
60. J.K. McCusker, E.A. Schmitt, D.N. Hendrickson, in *Magnetic Molecular Materials*, ed. D. Gatteschi, O. Kahn, J.S. Miller and F. Palacio, Kluwer, Dordrecht, 1991.
61. *Magnetism: Molecules to Materials*, ed. J.S. Miller, M. Brillon, Wiley-VCH, Weinheim, Germany, 2002.
62. P. Chaudhuri, *Coord. Chem. Rev.* 243 (2003) 143-190.
63. M.E. Keeney, K. Osseo-Asare and K.A. Woode, *Coord. Chem. Rev.* 59 (1984) 141-201.
64. S. Khanra, B. Biswas, C. Golze, B. Buchner, V. Kataev, T. Weyhermüller, P. Chaudhuri, *Dalton Trans.* (2007) 481-487.
65. P. Chaudhuri, T. Weyhermüller, R. Wagner, S. Khanra, B. Biswas, E. Bothe, E. Bill, *Inorg. Chem.* 46 (2007) 9003-9016.
66. C.J. Milios, C.P. Raptopoulou, A. Terzis, F. Lloret, R. Vicente, S.P. Perlepes, A. Escuer, *Angew. Chem. Int. Ed.* 43 (2004) 210-212.
67. T.S. M. Abedin, L.K. Thompson, D.O. Miller, E. Krupicka, *Chem. Commun.* (2003) 708-709.
68. N.F. Curtis, O.P. Gladkikh, S.L. Heath, K.R. Morgan, *Aust. J. Chem.* 53 (2000) 577-582.
69. Y. Agnus, R. Louis, B. Metz, C. Boudon, J.P. Gisselbrecht, M. Gross, *Inorg. Chem.* 30 (1991) 3155-3161.
70. T. Afrati, C.M. Zaleski, C. Dendrinou-Samara, G. Mezei, J.W. Kampf, V.L. Pecoraro, D.P. Kessissoglou, *Dalton Trans.* (2007) 2658-2668.
71. R.J. Butcher, C.J. O'Connor, E. Sinn, *Inorg. Chem.* 20 (1981) 537-545.
72. P.A. Angaridis, P. Baran, R.R. Boca, F. Cervantes-Lee, W. Haase, G. Mezei, R.G. Raptis, R. Werner, *Inorg. Chem.* 41 (2002) 2219-2228.
73. T.C. Stamatatos, J.C. Vlahopoulou, Y. Sanakis, C.P. Raptopoulou, V. Psycharis, A.K. Boudalis, S.P. Perlepes, *Inorg. Chem. Commun.* 9 (2006) 814-818.
74. M. Angaroni, G.A. Ardizzoia, T. Beringhelli, G. La Monica, D. Gatteschi, N. Masciocchi, M. Moret, *Dalton Trans.* (1990) 3305-3309.
75. W. Cañon-Mancisidor, E. Spodine, V. Paredes-Garcia, D. Venegas-Yazigi, *J. Mol. Model* 19 (2013) 2835-2844.
76. S. Ferrer, J.G. Haasnoot, J. Reedijk, E. Müller, M.B. Cingi, M. Lanfranchi, A.M. Lanfredi, J. Ribas, *Inorg. Chem.* 39 (2000) 1859-1867.

77. J.E. Greedan, J. Mater. Chem. 11 (2001) 37-53.
78. R. Beckett, R. Colton, B.F. Hoskins, R.L. Martin, D.G. Vince, Aust. J. Chem. 22 (1969) 2527-2533.
79. R. Beckett, B.F. Hoskins, Dalton Trans. (1972) 291-295.
80. Y.-B. Jiang, H.-Z. Kou, R.-J. Wang, A.-L. Cui, J. Ribas, Inorg. Chem. 44 (2005) 709-715.
81. L.K. Das, M.G.B. Drew, C. Diaz, A. Ghosh, Dalton Trans. 43 (2014) 7589-7598.
82. S. Karmakar, O. Das, S. Ghosh, E. Zangrando, M. Johann, E. Rentschler, T. Weyhermüller, S. Khanra, T.K. Paine, Dalton Trans. 39 (2010) 10920-10927.
83. S. Stoll and A. Schweiger, J. Magn. Reson. 178 (2006) 42-55.
84. G.A. Bain, J.F. Berry, J. Chem. Educ. 85 (2008) 532-536.
85. R. Bhowmick, A.S.M. Islam, U. saha, G.S. Kumar, M. Ali, New J. Chem. 42 (2018) 3435-3443.
86. G.H. Jeffery, J. Bassett, J. Mendham, R.C. D. Addison, Vogel's Text Book of Quantative Chemical Analysis; Wesley Longman Limited: United Kingdom, 5th ed.; 1989.
87. G.M. Sheldrick, Acta Crystallogr. Sec A: Found. Adv. 78 (2015) 3-8.
88. S. Nandi, S. Chandra, R. Sikder, S. Bhattacharya, M. Ahir, D. Biswal, A. Adhikary, N.R. Pramanik, T.K. Lai, M.G.B. Drew, K. Acharya, J. Agric. Food Chem., 67 (2019) 7660-7673.
89. S. Nandi, P. Upadhyay, A. Roy, A. Dasgupta, A. Sen, A. Adhikary, K. Acharya, Environ. Toxicol. 37 (2022) 52-68.
90. P.G. Urban (Ed.), Bretherick's Handbook of Reactive Chemical Hazards, Sixth ed., Butterworth-Heinemann, Oxford, 1999.
91. W.C. Wolsey, J. Chem. Educ. 50 (1973) A335.
92. APEX2 suite for crystallographic software, Bruker axs, Madison, WI (1995).
93. SAINT - Software for the Integration of CCD Detector System Bruker Analytical X-ray Systems; Bruker Axs: Madison, WI (1995).
94. G.M. Sheldrick, ShelXT-Integrated space-group and crystal-structure determination, Acta Cryst. A71 (2015) 3-8.
95. O.V. Dolomanov, L.J. Bourhis, R.J. Gildea, J.A.K. Howard, H. Puschmann, Olex2: A complete structure solution, refinement and analysis program, J. Appl. Cryst. 42 (2009) 339-341.
96. L. Krause, R. Herbst-Irmer, G.M. Sheldrick, D.J. Stalke, Appl. Cryst. 48 (2015) 3-10

97. L.J. Bourhis, O.V. Dolomanov, R.J. Gildea, J.A.K. Howard, H. Puschmann, *Acta Cryst. A* 71 (2015) 59-71.
98. N.K. Mandal, C.J. Gómez-García, P. Saha, J.P. Naskar, *J. Coord. Chem* 76 (2023) 705-719.
99. Y. Fukuda, A. Shimura, M. Mukaida, E. Fujita, K. Sone, *J. Inorg. Nucl. Chem.* 36 (1974) 1265-1270.
100. N.K. Mandal, N. Bandyopadhyay, P. Arya, S. Chowdhury, N. Raghav, J.P. Naskar, *Inorg. Chim. Acta* 544 (2023) 121229.
101. A. Golcu, M. Tumer, H. Demirelli, R.A. Wheatley, *Inorg. Chim. Acta* 358 (2005) 1785-1797.
102. T.L. Yusuf, S.D. Oladipo, S. Zamisa, H.M. Kumalo, I.A. Lawal, M.M. Lawal, N. Mabuba, *ACS Omega* 6 (2021) 13704-13718.
103. C.E. Satheesh, P.R. Kumar, N. Shivakumar, K. Lingaraju, P.M. Krishna, H. Rajanaika, A. Hosamani, *Inorg. Chim. Acta* 495 (2019) 118929.
104. M. Dieng, I. Thiam, M. Gaye, A.S. Sall, A.H. Barry, *Acta Chim. Slov.*, 53 (2006) 417-423.
105. N.K. Mandal, B. Guhathakurta, P. Basu, A.B. Pradhan, C.S. Purohit, S. Chowdhury, J.P. Naskar, *J. Coord. Chem.* 72 (2019) 3625-3644.
106. A. Zengin, K. Karaoğlu, M. Emirik, E. Menteşe, K. Serbest, *J. Mol. Struc.* 1193 (2019) 444-449.
107. J.P. Naskar, B. Guhathakurta, P. Basu, N. Bandyopadhyay, G.S. Kumar, M. Zhu, L. Lu, *Inorg. Chim. Acta* 462 (2017) 158-166.
108. S. Sengupta, S. Khan, S.K. Chattopadhyay, I. Banerjee, T.K. Panda, S. Naskar, *Polyhedron* 182 (2020) 114512.
109. A.W. Addison, T.N. Rao, J. Reedijk, J.V. Rijn, G.C. Verschoor, *Dalton Trans.* (1984) 1349-1356.
110. B. Guhathakurta, P. Basu, G.S. Kumar, L. Lu, M. Zhu, N. Bandyopadhyay, J.P. Naskar, *Polyhedron* 110 (2016) 227-234.
111. F.Z.C. Fellah, J.-P. Costes, L. Vendier, C. Duhayon, S. Ladeira, J.-P. Tuchagues, *Eur. J. Inorg. Chem.* (2012) 5729-5740.
112. M. Kwiatkowski, E. Kwiatkoski, A. Olechnowicz, D. M. Ho, E. Deutsch, *Inorg. Chim. Acta*, 150 (1988) 65-73.

113. S. Naiya, B. Sarkar, Y. Song, S. Ianelli, M.G.B. Drew, A. Ghosh, *Inorg. Chim. Acta*, 363 (2010) 2488-2495.
114. J.-P. Costes, F. Dahan, J.P. Laurent, *Inorg. Chem.* 25 (1986) 413-416.
115. D. Maity, P. Mukherjee, A. Ghosh, M.G. B. Drew, C. Diaz, G. Mukhopadhyay, *Eur. J. Inorg. Chem.* (2010) 807-813.
116. P. Chakrabarti, V.G. Puranik, J.P. Naskar, S. Hati, D. Datta, *Ind. J. Chem.* 39A (2000) 571-578.
117. H.-D. Bian, J.-Y. Xu, W. Gu, S.-P. Yan, P. Cheng, D.-Z. Liao, Z.-H. Jiang, *Polyhedron* 22 (2003) 2927-2932.
118. T. Afrati, C. Dendrinou-Samara, C. Raptopoulou, A. Terzis, V. Tangoulis, A. Tsipis, D. P. Kessissoglou, *Inorg. Chem.* 47 (2008) 7545-7555.
119. L. Shivakumar, K. Shivaprasad, H.D. Revanasiddappa, *Spectrochim. Acta, A* 107 (2013) 203-212.
120. A. Wolfe, G.H. Shimer, T. Meehan, *Biochemistry* 26 (1987) 6392-6396.
121. X.-T. Song, Y. Zhou, G.-B Liu, H.-C. Guan, S.-M. Yue, *J. Coord. Chem.* 76 (2023) 345-370.
122. Y.-Q. Gu, Y.-J. Zhong, M.-Q. Hu, H.-Q. Li, K. Yang, Q. Dong, H. Liang, Z.-F. Chen, *Dalton Trans.* 51 (2022) 1968-1978.
123. Q. Peña, G. Sciortino, J.-D. Maréchal, S. Bertaina, A.J. Simaan, J. Lorenzo, M. Capdevila, P. Bayón, O. Iranzob, Ò. Palacios, *Inorg. Chem.* 60 (2021) 2939–2952.
124. H.-Q. Zhang, X. Lu, J.-L. Wu, M.-Q. Ou, N.-F. Chen, H. Liang, Z.-F. Chen, *Dalton Trans.* 53 (2024) 3244-3253.
125. R. Sakthivel, D.S. Malar, K.P. Devi, *Biomed. Pharmacother.* 105 (2018) 742-752.
126. D. Ribble, N.B. Goldstein, D.A. Norris, Y.G. Shellman, *BMC Biotechnol.* 5 (2005) 12.
127. A. Byczkowska, A. Kunikowska, A. Kaźmierczak, *Protoplasma* 250 (2013) 121-128.
128. R. Gomez-Casal, C. Bhattacharya, N. Ganesh, L. Bailey, P. Basse, M. Gibson, M. Epperly, V. Levina, *Mol. Cancer* 12 (2013) 94.
129. W. Zhang, W.C. Cho, S. H. Bloukh, Z. Edis, W. Du, Y. He, H.Y. Hu, T.L. M. T. Hagen, M. Falahati, *Int. J. Biol. Macromol.* 212 (2022) 358-369.
130. R.A.C. Souza, W.R.P. Costa, E.F. Faria, M.A. de S. Bessa, R. de P. Menezes, C.H.G. Martins, P.I.S. Maia, V.M. Deflon, C.G. Oliveira, *J. Inorg. Biochem.* 223 (2021) 111543.
131. N.S. Gul, T.M. Khan, M. Chen, K.B. Huang, C. Hou, M.I. Choudhary, H. Liang, Z. F. Chen, *J. Inorg. Biochem.* 213 (2020) 111260.

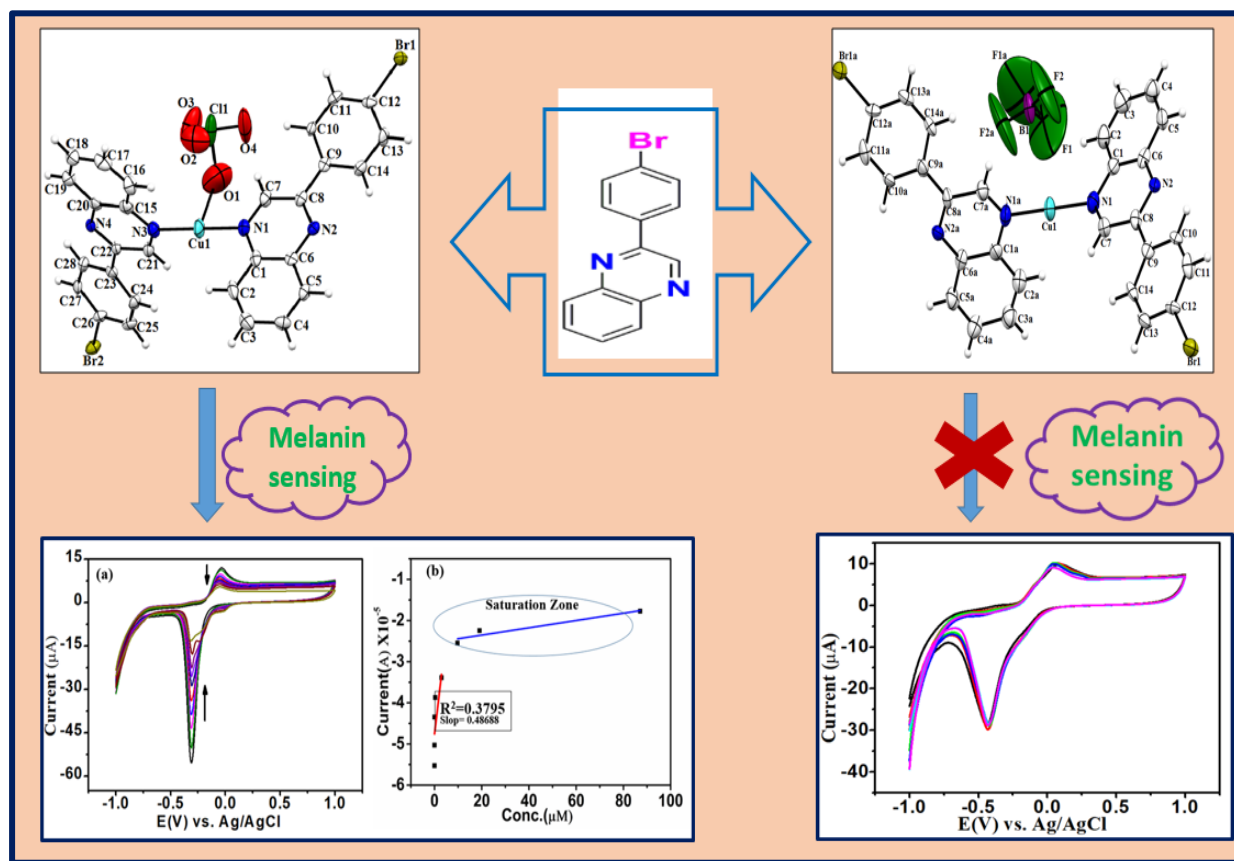
132. N.C. Yip, I.S. Fombon, P. Liu, S. Brown, V. Kannappan, A. L. Armesilla, B. Xu, J. Cassidy, J. L. Darling, W. Wang, *Br. J. Cancer* 104 (2011) 1564-1574.
133. P.H.A. Machado, D.A. Paixão, R.C. Lino, T.R. de Souza, N.J.de S. Bontempo, L.M. Sousa, F.V.P.de V. Azevedo, P.C. Orsolin, P.M.A.P. Lima, I.C. Martins, J.F.da C. Guerra, S.C. Teixeira, T.G. Araújo, L.R. Goulart, S. Morelli, W. Guerra, R.J.de O. Júnior, *Sci. Rep.* 11 (2021) 24450.
134. L.L.F. Maciel, W.R. de Freitas, E.S. Bull, C. Fernandes, A. Horn Jr, J.C. de A. Almeida, M.M. Kanashiro. *J. Inorg. Biochem.* 210 (2020) 111166.
135. M.F. Abdullah, N. Cinkilic, O. Vatan, D. Inci, R. Aydin, *bioRxiv*, doi: <https://doi.org/10.1101/2022.08.12.503805>.
136. N.F. Chilton, R.P. Anderson, L.D. Turner, A. Soncini, K.S. Murray, *J. Comput. Chem.* 34 (2013) 1164-1175.
137. S. Ferrer, F. Lloret, E. Pardo, J.M. Clemente-Juan, M. Liu-González, S. García-Granda, *Inorg. Chem.* 51 (2012) 985-1001.
138. L. Martínez, C. Bazzicalupi, A. Bianchi, F. Lloret, R. González, C. Kremer, R. Chiozzzone *Polyhedron* 138 (2017) 125-132.
139. D. Maity, P. Mukherjee, A. Ghosh, M.G.B. Drew, C. Diaz, G. Mukhopadhyay, *Eur. J. Inorg. Chem.* (2010) 807-813.
140. L.K. Das, M.G.B. Drew, C. Diaz, A. Ghosh, *Dalton Trans.* 43 (2014) 7589-7598.
141. B.D. Roach, R.S. Forgan, E. Kamenetzky, S. Parsons, P.G. Plieger, F.J. White, S. Woodhouse, P.A. Tasker, *Molecules* 27 (2022) 6421.
142. Y. Agnus, R. Louis, B. Metz, C. Boudon, J.P. Gisselbrecht, M. Gross, *Inorg. Chem.* 30 (1991) 3155-3161.
143. L. Husáriková, Z. Repická, J. Moncol, D. Valigura, M. Valko, M. Mazur, *Appl. Magn. Reson.* 44 (2013) 571-582.

CHAPTER-VII

**Syntheses, crystal structures and spectroscopic properties of copper(I)
complexes stabilized from a quinoxaline based ligand: Enzyme-less
electrochemical sensing of melanin**

MS is under preparation

Graphical Abstract



Highlights

- Two novel mononuclear copper(I) complexes, **1** and **2**, were synthesized by using an quinoxaline based probe (**bpq**).
- **1** and **2** have been structurally characterised by single crystal X-ray diffraction.
- Enzyme-less electrochemical sensor was developed in phosphate buffered saline (PBS, pH = 7.4) for determination of melanin.
- The proposed sensor, modified with **1**, detects melanin at very low concentration.
- The modified sensor offers good reproducibility and demonstrates its application in real sample specimen like hair.

Key words

Copper(I) complexes; crystal structures; modified electrodes and melanin sensing

Abstract

In this work, two novel copper(I) complexes, $[\text{Cu}(\text{bpq})_2(\text{ClO}_4)]$ (**1**) and $[\text{Cu}(\text{bpq})_2]\text{BF}_4$ (**2**) have been synthesized from a quinoxaline based probe, 2-(4-bromophenyl)quinoxaline (**bpq**). **1** and **2** have comprehensively been characterized by C, H and N microanalyses, FT-IR, UV-Vis (solution and solid phase) and electrical conductivity measurements in solution phase. Solid state single crystal structures of both the Cu(I) complexes have been determined. Deploying a modified electrode of **1**, for the first time, herein, we report the enzyme-less selective and sensitive electrochemical sensing leading to the detection of melanin, a ubiquitous yet unique natural pigment. Contrary to **1**, the analogous modified electrode of **2** offers no significant electrochemical sensing. Modification of electrode has been achieved by drop casting method at the surface of a glassy carbon (GC) electrode. The electrochemical sensing has been accomplished at the physiological pH of 7.4 employing phosphate buffer saline (PBS). Our modified electrode manifests dislocation and transportation of electrons from the surface of the electrode to melanin. The presently devised sensor can detect melanin at a very low concentration range of 0.003 to 200 μM . The LOD and LOQ values are found respectively to be of 2.51 and 7.61 μM . Subsequently, this sensor has successfully been applied for the sensing of melanin in real sample specimen like hair.

1. Introduction

Melanin, a term coined by Berzelius and derived from the Greek word ‘melanos’ meaning ‘black’, is a Nature’s ubiquitous yet unique class of pigments present throughout the biosphere. Consisting of small group of distinct bio-macromolecules, these ‘natural’ pigments offer a plethora of structures, diverse functions and varied manifestations. From camouflaging and self-protection to energy harvesting — melanin is indispensable. The regal stripes of tigers, colourful wings of butterflies and the very survival of polar bears in sub-zero temperatures are due to these pigments. In humans, they are responsible for pigmentation in skin, light absorption and free radical scavenging in iris and retina [1-4]. Melanin’s usage spans diverse fields like opto-bioelectronics, biomimetics, biomedicines, mussel-inspired interface modifications and designing of semiconductors based on amorphous materials. Being a redox active material with high dielectric value, it can be employed in the making of flexible super-capacitor electrodes and in redox tagging. All these aspects are due to melanin’s mechanical flexibility in terms of ‘versatility’ or ‘mechanical suppleness’ coupled with biocompatibility, multi-foldedness, tunability and specificity [5-9]. From constitutional viewpoint, melanin is a heterogeneous mixture of macromolecules. Eumelanin pigment, commonly known as melanin, is a brown-black pigment. Such pigments, a class of poly-indolequinone biopolymers, are derived from the oxidation of tyrosine in animals by tyrosinase [10,11]. They show distinct physical properties that are conducive to diverse biological functions [12,13]. Its epidermal concentration is a biomarker of low skin cancer [14]. Eumelanin consists of a mixture of 5,6-dihydroxyindole (DHI), 5,6-dihydroxyindole-2-carboxylic acid (DHICA) and pyrrole units [15,16].

Melanin pigments are of great contemporary interest from biotechnological point of view as well. They offer promising application in pharmaceutical, electronic, cosmetic and in food processing industries [17-19]. Biologically fabricated anode, made from synthetic melanin material, has also being used for energy storage devices [20]. Again, melanin is present as one of the major chromophores in the superficial skin layer. Accordingly, quantitative evaluation of melanin is crucial for the diagnosis, therapy and prevention of diverse dermatological diseases and pigmentation disorders (both hyper- and hypomelanotic) including cancers. Keeping all these points under consideration, melanin determination is of contemporary sufficient significance. Diffuse reflectance spectroscopy (DRS) is one of the most widely used methods for the evaluation of this human skin chromophore [21-23]. However, till date there is no accurate method for the determination of the proportion of different monomeric units as present in melanin [24]. Intensive research work is underway to develop easy but accurate,

reliable and viable method for the detection of melanin in real samples. Spectroscopic methods based on electron paramagnetic resonance (EPR) spectroscopy [25], photoacoustic spectroscopy [26] are in vogue. Chromatographic methods at the level of HPLC [24] also need to be mentioned. HPLC method has successfully been applied to analyse melanin in nevi, feathers and melanomas. Electrochemical methods [27,28] are also successful for human epidermis and melanocytes [29,30]. All these methods for the quantification of melanin in pigmented tissues require isolation of melanin. Several studies showed that [31-34] sensors have made growing area of research progress for the biological important compound including antioxidant and various drugs active substance.

Of late electrochemical sensors, specifically modified electrodes, are proven to be promising in terms of enhanced accuracy, easiness, rapidity and reproducibility with desired degree of cost-effectiveness. These aspects of electrochemical sensing of melanin rekindle unabated interest for the development of reliable methods for electrochemical detection and determination of melanin. Such type of sensors consists of two electrodes — a working electrode and an auxiliary electrode coupled with a closed circuit and a transducer for requisite charge transport [35-36]. This charge transportation may either be electronic or ionic. A combination of both the two may exist as well. Chemical reaction between the modified working electrode surface and the intended analyte may also give rise to charge transfer. It is a point to reckon that a Pt electrode, modified with 2,5-dimethylfuran (2,5-DMF), had been developed for the determination of melanin through electrochemical sensing by Duran *et al.* [37]. However, to the best of our knowledge, electrode modified by coordination complexes of transition metal ions for the detection of melanin is hitherto not known. In the present work, we are concerned with the same.

Phosphorescent copper(I) complexes have surged unabated interest of many researchers in this respect. Such copper(I) systems manifest truly interesting properties and significant application in diverse fields such as organic light emitting diodes [38,39], optoelectronics and photovoltaics [40] and biological systems [41]. Closed-shell d^{10} copper(I) being ‘soft’, in terms of Pearson’s ‘Hard-Soft’ classification, yields stable complexes with ‘soft’ ligands like π -acids, imino N, -P and thiaethers etc. The most commonly accessible coordination geometries of copper(I) are tetrahedral to distorted tetrahedral geometries with coordination number 4. A multitude of two-coordinate linear, three-coordinate triangular to T-shaped; square-pyramidal and trigonal bipyramidal geometries with coordination number 5 are known [42-46]. The flexible coordination geometry around the center of Cu(I) complexes make them excellent

candidates for luminescent-sensing materials [47-49]. For ready reckoning, McMillin's work on Cu(I)-bis(1,10-phenanthrolines) systems adorned with room temperature luminescent properties can be cited [50,51]. But, such entities have lesser been known in the context of sensing of analytes. However, gas sensing aspects of copper(I) complexes are truly known [52,53]. Again, enzyme-less electrochemical sensors based on transition metal oxides are known to exist for the detection of neurotransmitter biomarkers [54]. Curiously, development of modified electrodes based on copper(I) compounds for reliable melanin sensing is unprecedented. Herein, we wish to report the syntheses and comprehensive characterization of two new Cu(I) complexes having various coordination modes stabilised with an imino nitrogen donor ligand, 2-(4-bromophenyl)quinoxaline (**bpq**). An electrochemical melanin sensor was developed through modification of the glassy carbon working electrode with one of these Cu(I) complexes. Selective and reliable melanin sensing have accordingly been accomplished at the physiological pH of 7.4 with this modified electrode. This sensing of melanin has even been accomplished with real sample specimen like hair.

2. Experimental section

2.1. Materials and method

Reagent-grade 2-(4-bromophenyl)quinoxaline (96%) and hydrazine hydrate (50-60%) were procured from Sigma-Aldrich, USA (St. Louis, Missouri, United States). Melanin (synthetic) and solid $\text{Cu}(\text{BF}_4)_2 \cdot n\text{H}_2\text{O}$ (A.R. grade) were also purchased from Sigma-Aldrich (St. Louis, Missouri, United States). Other reagent-grade chemicals like $\text{Cu}(\text{ClO}_4)_2 \cdot 6\text{H}_2\text{O}$ were purchased from LOBA Chemie (Mumbai, India) and were used as received. All solvents were of analytical grade. Having obtained commercially they were used as received without any prior purification and drying.

2.2. Physical measurements

The FT-IR spectra (KBr disc) of the copper(I) complexes were recorded employing a Shimadzu FT-IR 8400S spectrophotometer in the range $4000\text{-}400\text{ cm}^{-1}$ (Japan). Solution phase electronic spectra for the copper(I) complexes were accrued on a SHIMADZU UV-1900i spectrophotometer (Japan). Solid state electronic spectra of the copper(I) compounds were recorded on a Perkin Elmer UV-Vis spectrophotometer, Lambda 35. Electrochemical cyclic voltammetric (CV) experiments were performed in degassed dichloromethane on an electrochemical workstation CHI600C, USA using 0.1 M TBAP as the supporting electrolyte. Employing a Systronics (India) direct reading conductivity meter (model 304), electrical conductivities of **1** and **2** in DMF at room temperature were measured. Single crystal X-ray diffraction data of the Cu(I) complexes, **1** and **2**, were collected on a Bruker APEX II (Smart)

diffractometer at low temperature. Powder X-ray diffraction data of **1** and **2** were collected on a Bruker D8 (advance) diffractometer with a Cu K α radiation ($\lambda = 1.5418 \text{ \AA}$) source. During data collection the source was operated at 40 kV and 40 mA. The PXRD data was collected in the range of 2θ (5° to 50°) with a scan rate of 0.2 s per step under ambient condition.

2.3. Fabrication of GCE/**1** Electrode

For electrochemical measurement, the GCE was polished with Al_2O_3 powder for 5 min and rinsed thoroughly with distilled water and acetone followed by drying in an open air. 1 mg of **1** was dispersed in 1 mL degassed DCM through sonication under ultrasonic oscillation to have a yellow suspension. The GCE, so modified, was fabricated by the drop casting of the yellow suspension onto the surface of pre-treated GCE. Finally, it was dried under a heating bulb to evaporate DCM. In this way, GCE/**1** was prepared for subsequent CV measurements.

2.4. Sample preparation

A stock solution of melanin was prepared for electrochemical measurements by dissolving in water under sonication for 1 h. CV experiments were done for melanin sensing in PBS (pH = 7.4). For real sample monitoring, the hair sample was dissolved in a 0.1 M NaOH solution and was boiled until dissolved. For electrochemical analysis, the pH of the hair solution was fixed at 7.4.

2.5. Synthetic procedure of $[\text{Cu}(\text{bpq})_2(\text{ClO}_4)]$ (**1**)

$[\text{Cu}(\text{bpq})_2(\text{ClO}_4)]$ was prepared by 2:1 stoichiometric reaction of 2-(4-bromophenyl) quinoxaline (bpq) and $\text{Cu}(\text{ClO}_4)_2 \cdot 6\text{H}_2\text{O}$. 0.143 g (0.5 mmol) of bpq was dissolved in 10 mL of methanol to have a colourless solution. A 5 mL blue methanolic solution of $\text{Cu}(\text{ClO}_4)_2 \cdot 6\text{H}_2\text{O}$ (0.093 g, 0.25 mmol) was added dropwise to the ligand solution under stirring. The resulting light green solution was heated to boiling on a water bath. To this hot solution, 0.03 mL of hydrazine hydrate (1 mmol) diluted in 3 mL of methanol, was added dropwise with continuous stirring. Within a few min, yellowish-orange compound started precipitating. After 5 min, it was filtered out hurriedly and dried in a vacuum desiccator over fused CaCl_2 . It is highly soluble in THF, DMSO and DMF but partly soluble in protic solvents.

Yield: 95 mg (52 %); $\text{C}_{28}\text{H}_{18}\text{CuBr}_2\text{N}_4\text{O}_4\text{Cl}$: (733.184), Anal. Cal. for $\text{C}_{28}\text{H}_{18}\text{CuBr}_2\text{N}_4\text{O}_4\text{Cl}$: C, 45.85; H, 2.48; N, 7.64; found: C, 45.89; H, 2.45; N, 7.67 %. FT-IR (KBr) (v/cm^{-1}): 3064 (C-H aromatic), 1587 (C=N aromatic), 1487 (C=C aromatic), 1144_m, 1119_s, 1087_m, 1074_s and 623 (ClO_4). UV-Vis (DCM): λ_{max} ($\epsilon/\text{M}^{-1}\text{cm}^{-1}$): 339 nm (25 965); UV-Vis: λ_{max} (nujol): 323, 377 and 395 nm; Λ_{M} (DMF): 08 $\text{ohm}^{-1} \text{cm}^2 \text{mol}^{-1}$ (non-electrolyte).

2.6. Synthetic procedure of $[(Cu(bpq)_2)]BF_4$ (**2**)

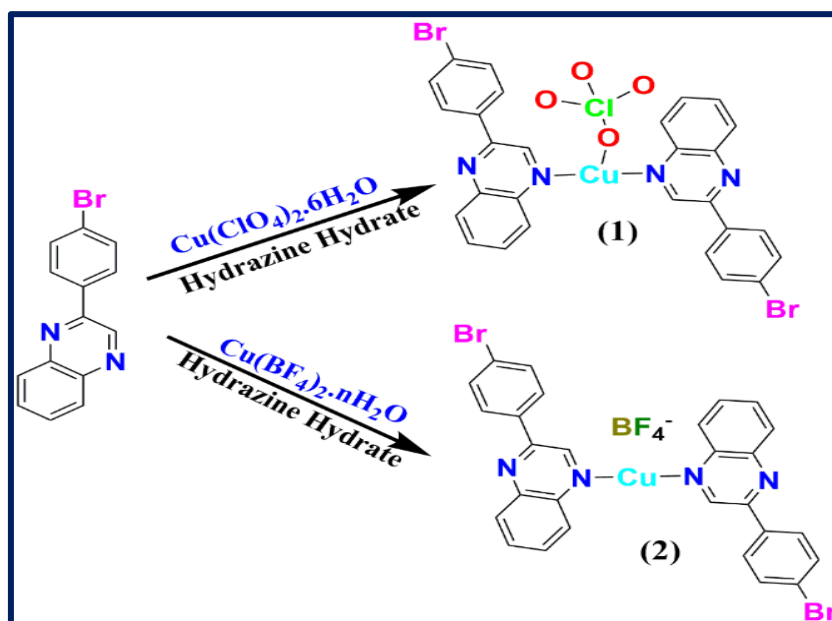
Complex **2** was prepared following the same procedure as that had been adopted for **1**. Here, a 5 mL blue methanolic solution of hydrated copper(II) tetrafluoroborate, $Cu(BF_4)_2 \cdot nH_2O$ (0.059 g, 0.25 mmol) was added to a 15 mL colourless methanolic solution of bpq (0.143 g, 0.5 mmol). The resulting light green solution was heated to boiling on a water bath. A 3 mL methanolic solution of hydrazine hydrate (0.03 mL, 1 mmol) was added dropwise to the previous reaction mixture under stirring condition. After 5 min, reddish-orange precipitate started separating from the reaction mixture. The compound so separated was filtered out immediately, washed with 5 mL of methanol and was dried *in vacuo* over anhydrous $CaCl_2$. The compound is soluble in DCM, THF and DMF.

Yield: 79 mg (44%); $C_{28}H_{18}CuBr_2N_4BF_4$: (720.00), Anal. Cal. for $C_{28}H_{18}CuBr_2N_4BF_4$: C, 46.65; H, 2.52; N, 7.78. Expt. found: C, 46.62; H, 2.55; N, 7.72 %; FT-IR (KBr) (ν/cm^{-1}): 1586 (C=N of aromatic), 1489 (C=C of aromatic ring), 1073_m, 1048_b, 1008_s, 973, 961 (BF_4); UV-Vis (DCM) λ_{max} ($\epsilon/M^{-1}cm^{-1}$): 350 nm (22 466), UV-Vis: λ_{max} (nujol): 322, 378 and 397 nm; Λ_M (DMF): 61 ohm⁻¹ cm² mol⁻¹ (1:1 electrolyte).

Both **1** and **2** are indefinitely stable in the solid state on preservation in a vacuum desiccator.

Caution: Although we met with no unpleasant incident, utmost care should be taken while handling perchlorate salt since it detonates when comes in contact with heat or experiences shock particularly in solid state. Manipulations only with a meagre amount of this salt is recommended [55].

The synthetic route of both **1** and **2** is shown in scheme VII.1.



Scheme VII.1. Synthetic route for the preparation of **1** and **2**.

2.7. X-ray Crystallography

Shining needle-shaped lemon yellow crystals of **1** and orange-yellow crystals of **2** were obtained by direct diffusion of chilled diethyl ether into the filtrate of their respective methanolic mother liquor. Suitable crystals with appropriate sizes were examined under a microscope and were mounted for X-ray data collection. X-ray data of **1** and **2** were collected at low temperature on a Bruker D8 Venture Microfocus APEX-II diffractometer. The diffractometer was equipped with a Mo-K α (graphite monochromated) radiation source ($\lambda = 0.71073 \text{ \AA}$). The diffraction data of **1** and **2** were collected with a ω scan width of 1.00° and an exposure time of 10 s. The data collection for **1** and **2** were managed by the software package, APEX3(v2017.3-0). The diffraction pattern was indexed and BRUKAR APEX 2 program was used to determine the total number of runs and images [56]. The space groups of **1** ($P21/n$) and **2** ($Pbcn$) were determined by the ShelXT 2014/5 program package using iterative methods [57,58]. Data reduction was carried out using Bruker SAINT and empirical absorption corrections were made using SADABS [59]. The model was refined with SHELXL-2016/6 using full matrix least squares minimisation on F^2 [60]. All non-hydrogen atoms were refined anisotropically. Hydrogen atom positions were calculated geometrically and were refined using the riding model. The crystal data and structural refinement data of **1** and **2** are summarised in Table VII.1. Some selected bond lengths and bond angles of **1** and **2** are included in Table VII.2.

Table VII.1. Crystal data and structure refinement for **1** and **2**

	1	2
CCDC No	2121272	2359336
Empirical formula	$\text{C}_{28}\text{H}_{18}\text{CuBr}_2\text{N}_4\text{O}_4\text{Cl}$	$\text{C}_{28}\text{H}_{18}\text{BBr}_2\text{CuF}_4\text{N}_4$
Formula weight	733.26	720.62
Temperature [K]	148(2)	219(2)
Wavelength [\AA]	0.71073	0.71073
Crystal system	Monoclinic	Orthorhombic
Space group	$P21/n$	$Pbcn$
Unit cell dimensions		
a [\AA], b [\AA] and c [\AA]	5.8307(5), 31.367(3) and 4.4212(12)	5.907(2), 14.428(6) and 31.187(13)
α [$^\circ$], β [$^\circ$] and γ [$^\circ$]	90, 90 and 90	90, 90 and 90
Volume [\AA^3]	2637.5 (4)	2657.9(19)
Z	4	4
ρ_{calcd} [mg/cm^3]	1.847	1.801
Absorption coefficient	4.004	3.883

[mm ⁻¹]		
F (000)	2575	1416
Θ range for data collection [deg]	2.406 to 27.269	2.612 to 25.000
Limiting indices	-6<h<7, -38<k<40, -18<l<18	-6<h<7, -17<k<17, -37<l<37
Data/restraints/parameters	5905/0/361	2341/0/182
Goodness-of-fit on F ²	1.039	1.047
Final R indices [I>2σ(I)]	R ₁ = 0.0859, wR ₂ = 0.2294	R ₁ = 0.1117, wR ₂ = 0.2659
R indices (all data)	R ₁ = 0.1229, wR ₂ = 0.2538	R ₁ = 0.1589, wR ₂ = 0.293
Largest diff. peak and hole	3.572 and -1.693 e.Å ⁻³	1.528 and -2.149 e.Å ⁻³

Table VII.2. Selected bond lengths (Å) and bond angles (°) for **1** and **2**

Complex 1			
Bond length		Bond angle	
Cu(1)-O(1)	2.768(18)	N(1)-Cu(1)-O(1)	96.0(4)
Br(1)-C(26)	1.887(7)	N(3)-Cu(1)-O(1)	85.7(4)
Cu(1)-N(1)	1.905(7)	N(1)-Cu(1)-N(3)	178.0(3)
Cu(1)-N(3)	1.906(7)	O(1)-Cu(1)-Cl(1)	88.6(4)
Cl(1)-O(1)	1.679(15)	O(4)-Cl(1)-O(1)	87.9(8)
Complex 2			
Bond length		Bond angle	
Cu(1)-N(1)	1.873(8)	N(1)-Cu(1)-N(1a)	177.0(7)
Cu(1)-N(1a)	1.874(8)	C(7)-N(1)-Cu(1)	121.2(9)
Br(1)-C(12)	1.901(11)	C(1)-N(1)-Cu(1)	120.7(8)
N(1)-C(1)	1.418(17)	F(1)-B(1)-F(2)	104(2)
F(1)-B(1)	1.14(2)	C(13)-C(12)-Br(1)	119.6(8)

3. Results and discussion

3.1. Synthesis and IR Spectroscopy of complexes **1** and **2**

Both the copper(I) complexes were synthesised by using **bpq**, (2-(4-bromophenyl) quinoxaline), and copper(II) salts of perchlorate and tetrafluoroborate for complexes, **1** and **2** respectively. The reactions were carried out on a water bath by *in situ* reduction of copper(II) ions with hydrazine hydrate. The FT-IR spectrum of free **bpq** shows characteristic band at 1608 cm⁻¹ for C=N stretching vibration of the aromatic ring [61]. This band shifted to lower

wavenumber values: from 1608 to 1587 cm^{-1} in **1** and to 1586 cm^{-1} in **2**. This is indicative of the coordination of imine nitrogen atom of bpq to the copper(I) center in **1** and **2** [62,63]. The FT-IR spectrum of **1** also shows characteristic split bands at 1143, 1118, 1087, 1074 and 1053 cm^{-1} . This is indicative of the coordinated perchlorate ion in **1** [64]. The B-F stretching bands for tetrafluoroborate counter ion were observed at 1073, 1048, 1008, 973 and 961 cm^{-1} for **2**. The FT-IR spectra of both **1** and **2** are given in Fig. VII.1. and Fig. VII.2, respectively.

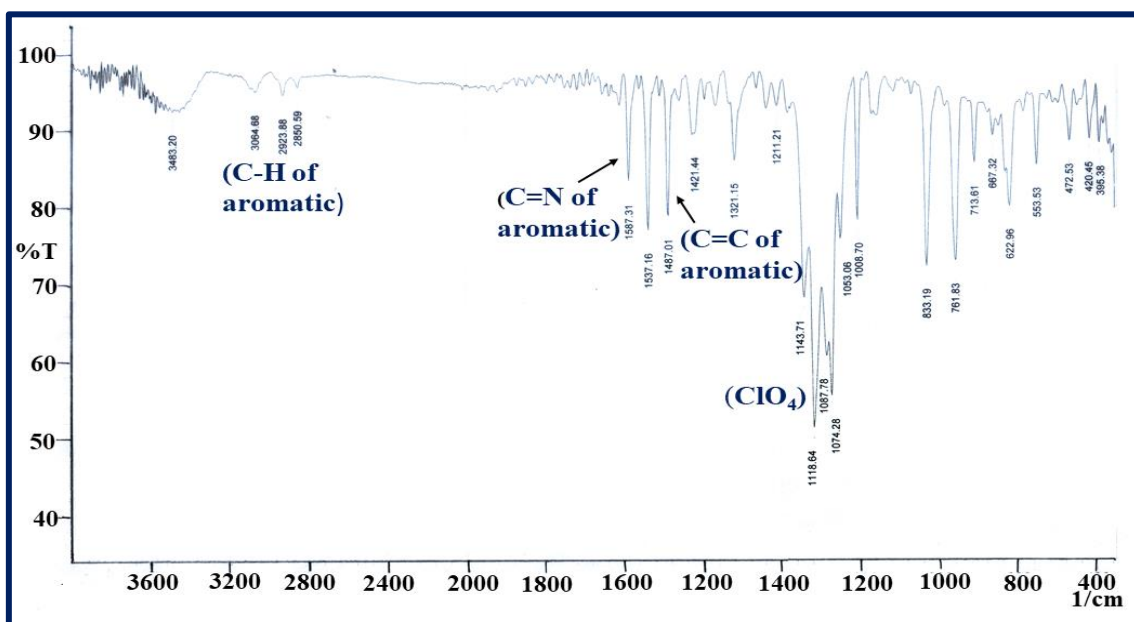


Fig. VII.1. FT-IR spectrum of **1**.

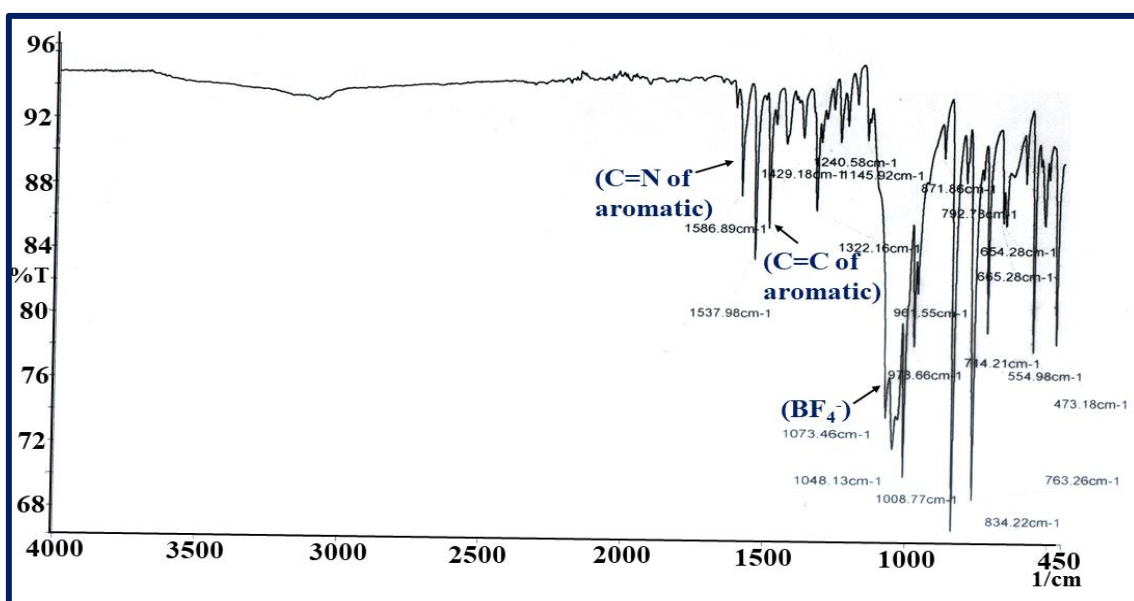


Fig. VII.2. FT-IR spectrum of **2**.

3.2. Electronic spectra

Solution phase electronic spectra of both **1** and **2** were recorded in degassed DCM [Fig. VII.3 (left)]. **1** and **2** show only one characteristic band at 339 and 350 nm respectively. This charge transfer band may arise from metal to quinoxaline charge transfer. In solid state electronic spectrum, **1** displays bands at 323, 377 and 395 nm. These additional bands may encompass some kind of charge transfer involving Cu(I)-oxygen bond. Similar electronic behaviour had also been reported by Munakata *et al.* [65]. Akin to **1**, **2** shows bands at 322, 378 and 397 nm. The solid state electronic spectra of **bpq** and the Cu(I) complexes, **1** and **2**, are shown in Fig. VII.3 (right).

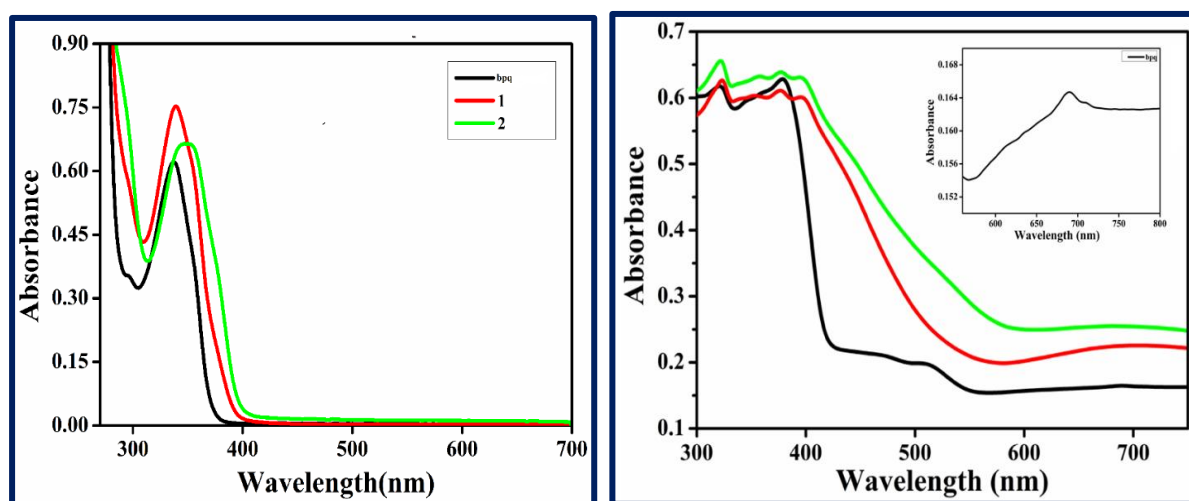


Fig. VII.3. Absorption spectra of **bpq** and complexes, **1** and **2** in degassed DCM at room temperature (left). Solid state electronic spectra of **bpq** (black) and complexes, **1** (red) and **2** (green) (right).

3.3. Structural description of **1** and **2**

Single crystal X-ray diffraction studies reveal that complex **1** is a tri-coordinate Cu(I) system. The 'N₂O' tri-coordination is satisfied by two nitrogen donor atoms - one from each quinoxaline moiety and one lone oxygen atom from the coordinated perchlorate counter ion. **1** crystallizes in the monoclinic *P2₁/n* space group. Two Cu-N bond lengths are almost alike and they are of 1.905(7) and 1.906(7) Å. Perchlorate ion is weakly bound to the copper center. Cu1-O1 bond length is 2.768(18) Å. This bond length is somewhat elongated and consequently weak. This type of weak perchlorate coordination had previously been observed in an analogous slightly bent T-shaped copper(I) system in its N₂O coordination environment [66]. Our Cu-N bond lengths are also comparable with the Cu-N bond lengths of this discrete mononuclear copper(I) complex. **1** is also a slightly bent T-shaped planar molecule with the N(1)-Cu(1)-N(3) bond angle of 178°. Like **1**, three-coordinate mononuclear copper(I)

complexes are, however, well known [67,68]. The ORTEP (50% probability ellipsoid) with atom labelling scheme of both **1** and **2** is depicted in Fig. VII.4.

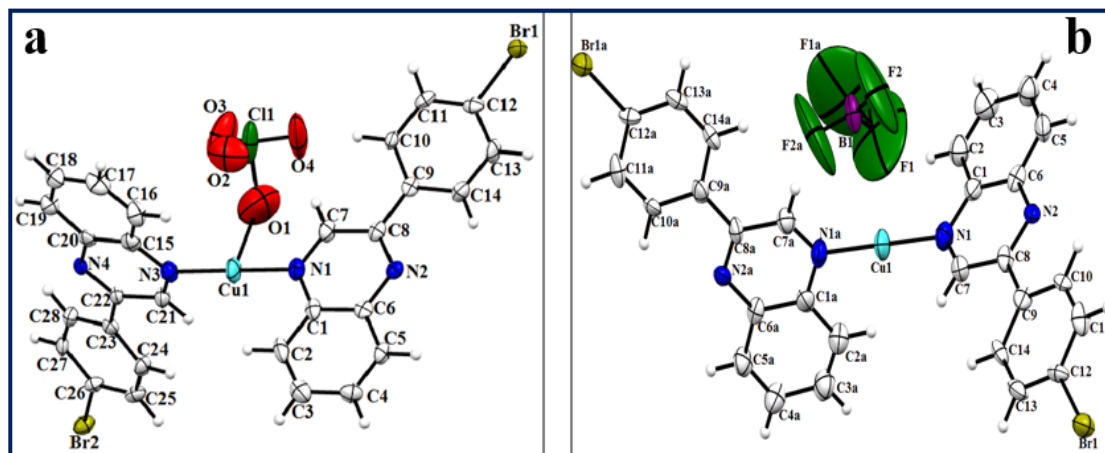


Fig. VII.4. ORTEP view of **1** (a) and **2** (b) with 50% probability ellipsoid.

On the contrary, **2** is a two-coordinate discrete mononuclear copper(I) system. The copper(I) center in **2** is tethered by two nitrogen donor atoms, each from one quinoxaline moiety. **2** bears the counter anion BF_4^- outside the coordination sphere. It crystallises in the triclinic system with *Pbcn* space group. The copper(I) center in **2** enjoys a slightly distorted linear geometry with two almost identical Cu-N bond lengths of 1.873(8) and 1.874(8) Å. The N(1)-Cu(1)-N(1) bond angle is of 177.0(7)°. Similar Cu-N bond lengths had been reported for linear copper(I) complexes with similar ‘NN’ coordination environment [69]. Many linear two-coordinate copper(I) complexes have been documented [70,71]. However, very few two-coordinate linear Cu(I) complexes with nitrogen donors are known [72]. Both the unit cells, as present in the asymmetric units of **1** and **2**, contain four molecules ($Z = 4$) (Fig. VII.5). Our bond valence sum (BVS) calculation (0.848 for **1** and 0.914 for **2**) shows that the copper center in both **1** and **2** is in ‘+I’ oxidation state [73].

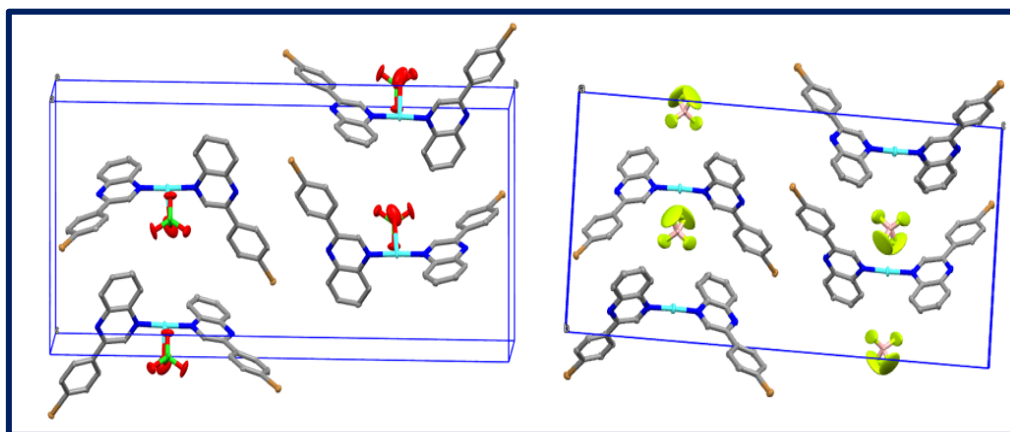


Fig. VII.5. Inner view of the unit cell of both **1** (left) and **2** (right).

3.4. Cyclic voltammetry

In order to delve into the redox behaviour of **1** and **2**, we have taken recourse to execute cyclic voltammetric experiments (Fig. VII.6) of them. The experiments were performed under dry N₂ atmosphere at a scan rate of 100 mV s⁻¹ in degassed DCM using tetrabutylammonium perchlorate (TBAP) as the supporting electrolyte. Complex **1** shows an oxidative quasi-reversible voltammogram with a half-wave potential of 0.699 V vs. Ag/AgCl. Compared with the standard ferrocene/ferrocenium couple, under the same experimental conditions, it is revealed that **1** involves only one electron for the oxidative response. In DCM-water saturated solution, **1** shows irreversible redox response under the same experimental conditions. The redox process is metal-based since the quinoxaline-based ligand (**bpq**) is not electro-active in the potential window of present investigation. Accordingly, the observed redox response can



On addition of water (0.5 µL) to the degassed DCM solution of **1**, as used for cyclic voltammetry, the potential of the couple (1) is lowered. This hints that in presence of water oxidation of **1** becomes favourable.

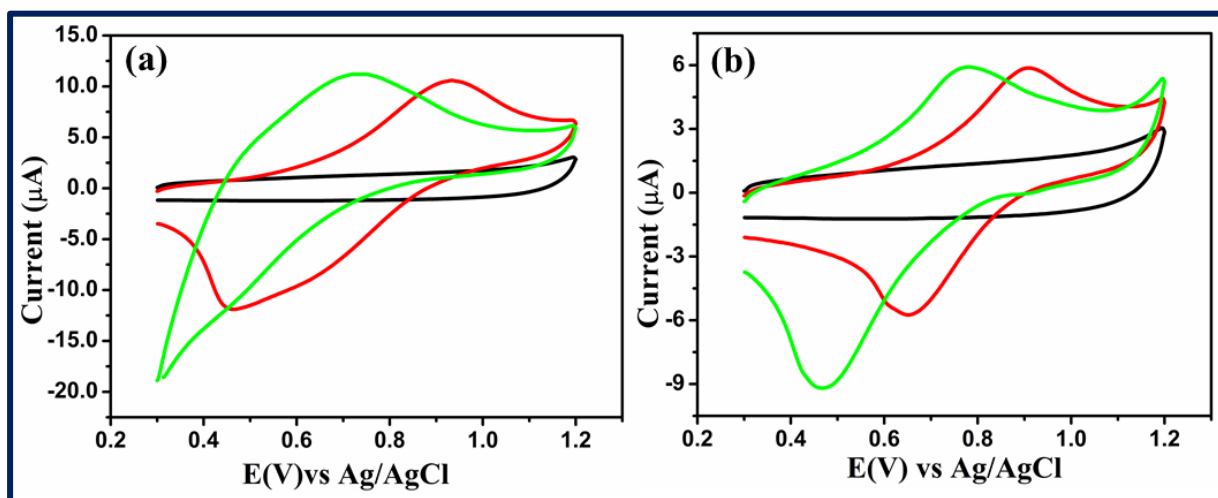


Fig. VII.6. (a) Cyclic voltammograms of ligand (black line), complex **1** (red line) in degassed DCM solvent and in DCM saturated in water (green line) under dry N₂ atmosphere. (b) Cyclic voltammograms of ligand (black line), complex **2** (red line) in degassed DCM solvent and in DCM saturated in water (green line) under dry N₂ atmosphere.

Complex **2** manifests almost reversible voltammogram with a half-wave potential value of 0.78 V vs Ag/AgCl with a cathodic peak current (*i*_{pc}) value of -5.7491 µA with its corresponding anodic peak current (*i*_{pa}) value of 5.8695 µA. Clearly, the ratio of *i*_{pc} to *i*_{pa} (0.979) closely approaches to unity. This oxidative response involves only one electron as deciphered on

comparing with the standard redox couple, Fc/Fc^+ under the same electrochemical conditions. In DCM-water saturated solution, **2** shows almost reversible redox response as noted



3.5. Melanin sensing

In order to investigate the electrochemical sensing of melanin, cyclic voltammetric (CV) technique was employed using GCE/**1** modified electrode. For this proposed sensor, the potential window was chosen as -1 to +1 V. In this technique, the reduction peak current successively decreases with successive addition of melanin concentration (0.003 to 200 μM) (Fig. VII.7). The GCE/**1** modified electrode showed a linear range (0.003 μM to 5 μM) with a LOD value of 2.52 μM . Under identical condition, the limit of quantification (LOQ) value was found to be 7.61 μM [74,75].

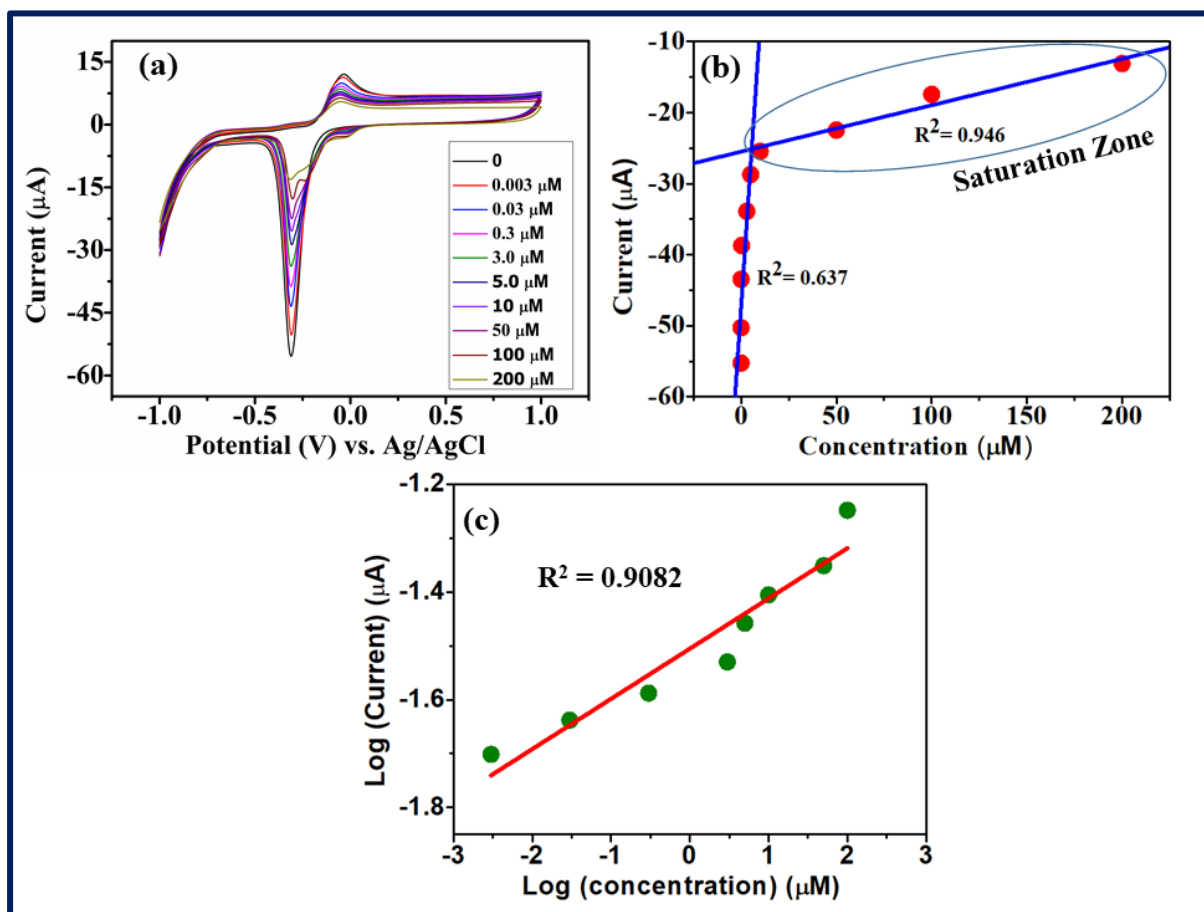


Fig. VII.7. CVs of the GCE/**1** in PBS (pH=7.4) with melanin concentration (0.003 μM to 200 μM). (b) plot of peak current vs concentration. (c) Log current vs Log concentration plot.

However, no electrochemical response was observed with the addition of melanin with different concentration (0.001 μM -2 μM) for modified electrode of **2** (Fig. VII.8).

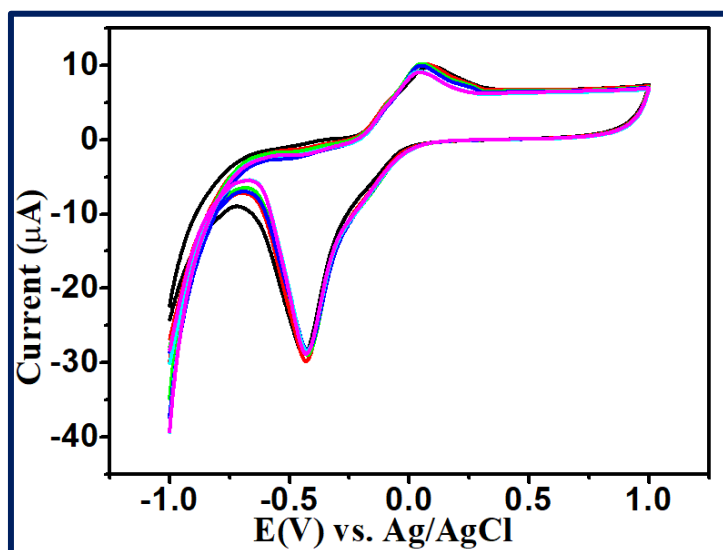


Fig. VII.8. CVs of the GCE/2 in PBS (pH=7.4) with melanin concentration (0.001 μ M-2 μ M).

The CV of bare GC was run in PBS (pH=7.4) buffer solution under the potential range of -1 to +1 V. Varying concentration of melanin solution was added and CV was run under the same experimental condition (Fig. VII.9). No noticeable change was, however, observed in the reduction or oxidation direction in comparison with the bare GC peak. Accordingly, we safely conclude that melanin is electrochemically silent or dormant.

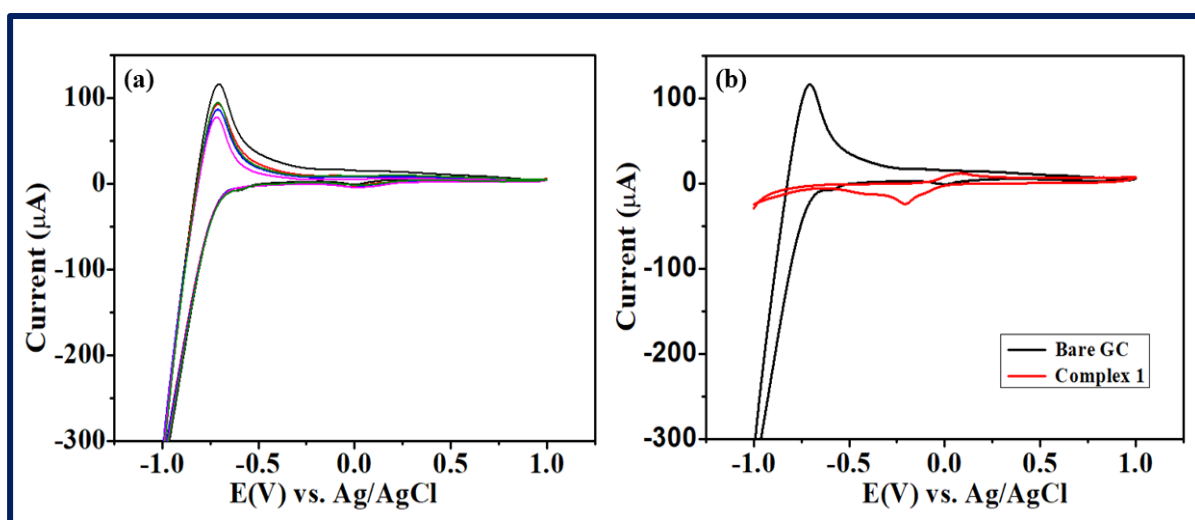


Fig. VII.9. (a) Curves of bare GCE with melanin and (b) CV of bare GCE (black) and complex 1 (red) in 0.1 M PBS (pH=7.4).

To know the effect of scan rate, we have run CV at a fixed concentration with different scan rates (10 -150 mVs^{-1}) at PBS buffer (pH=7.4). From the Fig. VII.10a, it is clearly observed that the reduction peak currents as well as the oxidation peak currents increase with concomitant

increase in sweep rate. But the extent of magnitude for the reduction is higher than oxidation. A linear dynamic plot of current vs square root of scan rate is depicted in Fig. VII.10b.

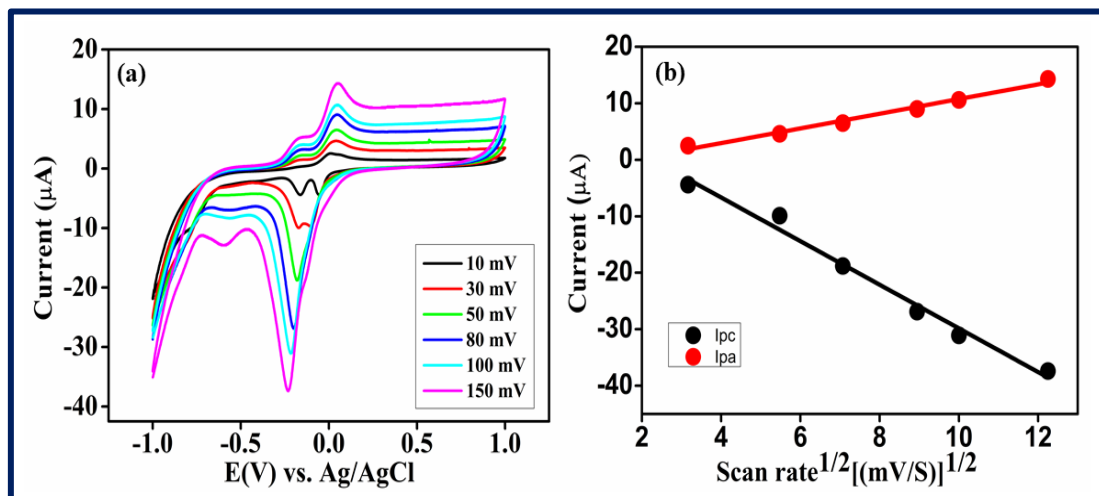


Fig. VII.10. (a) CV of GCE/1 of melanin (0.5 μM) in PBS medium at different scan rates and (b) linear dynamic plot of current vs square root of scan rate.

3.5.1. Interference and selectivity studies

Interferences studies were done of some organic and inorganic salt for the proposed melanin sensor through CV experiment at a particular concentration of melanin (0.5 μM) in PBS (pH = 7.4) (Fig. VII.11). Variation in percentage of the interferents were calculated through CV measurement by the given formula: $j_{pc}(\text{melanin}) = [j_{pc}(\text{melanin}) - j_{pc}(\text{Interferents})] / j_{pc}(\text{melanin})$; (j_{pc} = cathodic peak current). The results of variation in percentage are depicted in Table VII.3.

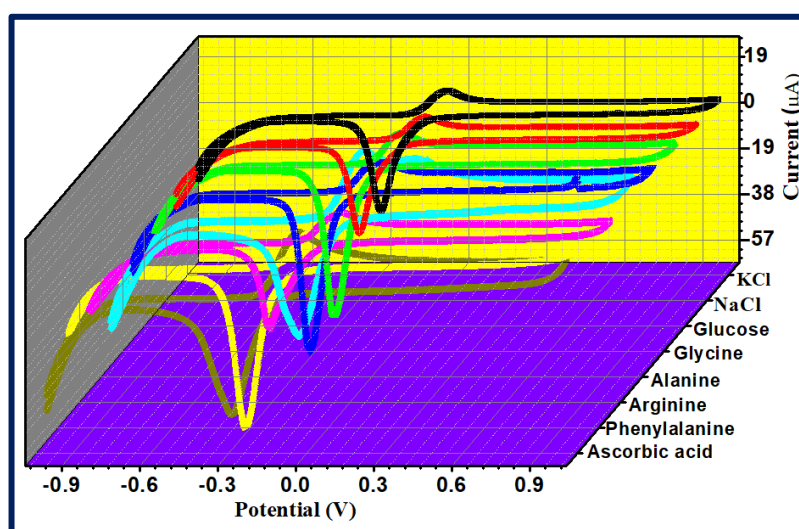


Fig. VII.11. CV curves at 50 mVs⁻¹ of the GCE/1 for melanin (0.5 μM) in PBS buffer (pH=7.4) in comparison to organic and inorganic interferences.

Table VII.3. Percentage of variation of interferents (j_{pc} %) at a particular concentration of melanin (0.5 μ M).

Interference	Concentration (mM)	Percentage variation, j_{pc} %
KCl	1	0.08
NaCl	1	0.10
Glucose	1	0.06
Glycine	1	0.02
Alanine	1	0.10
Arginine	1	0.14
Phenylalanine	1	0.10
Ascorbic acid	1	0.04

3.5.2. Reproducibility and stability

To check the reproducibility and stability of the modified electrode, the cyclic voltammetry (CV) analysis was performed at 50 mVs^{-1} . Four fabricating modified electrodes were preapred for reproducibility test and measurements were taken at the same experimental condition at a particular cocentration of melanin (0.5 μ M) (Fig. VII.12). The reduction peak current remains intact over different electrodes.

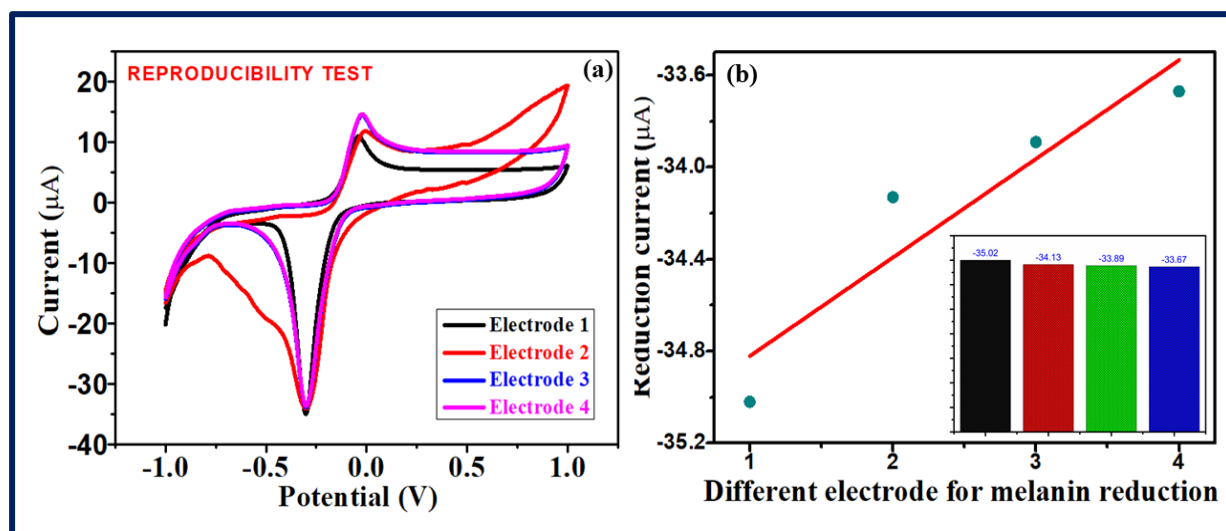


Fig. VII.12. (a) Reproducibility test and (b) electrochemical reduction current

The stability also check at the same experimental condition over a day. The coated electrode was stored in a vacuum desiccator for electrochemical mesuremnets. It clearly preceived that

the electrode decreases the reduction current for each electrochemical measurement (Fig. VII. 13).

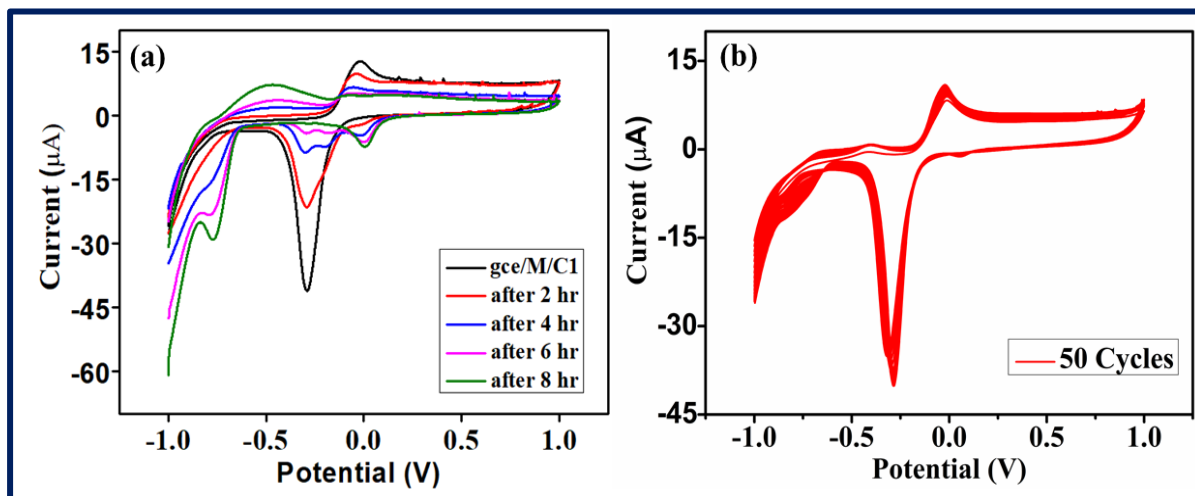


Fig. VII.13. Stability test with variation in time (left) and CV curves with 50 cycles (right) of melanin (0.5 μM).

3.5.3. pH effect

The effect of pH on melanin sensing was followed by monitoring CV at a scan rate of 50 mVs⁻¹ with different pH (3.5-10). The reduction peak current decreases as pH decreases, as does the peak current greater than 8.2. It clearly indicates that the melanin reduction does not occur in a highly acidic medium. Fig. VII.14 displays the highest reduction peak current for the proposed melanin sensing in the pH range 7 to 8.2. The solubility of melanin also increases in alkaline medium [76]. Consequently, the pH value of 7.4 was maintained for the subsequent measurements as have been undertaken for melanin sensing.

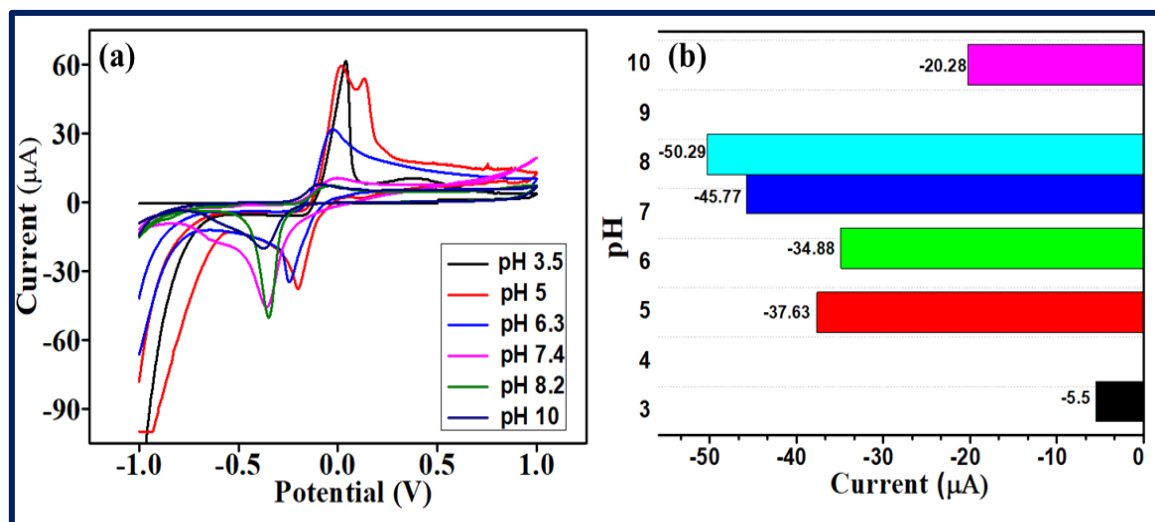


Fig. VII.14. (a) CV of melanin at different pH and (b) A bar plot of pH against current.

3.5.4. Real sample analysis

In order to demonstrate its application in real sample, we have taken recourse to prepare hair sample by dissolving hair in dilute sodium hydroxide under boiling condition. Different amount of melanin in the micro-molar concentration range was added to the hair sample as shown in Fig. VII.15. The percentage of recovery were found to be 107 and 103%, respectively. Furthermore, the limit of detection (LOD) value for real sample analysis is determined. The LOD value suggests that proposed method for detection of melanin is promising for real sample analysis. The values found from the experiment are presented in Table VII.4.

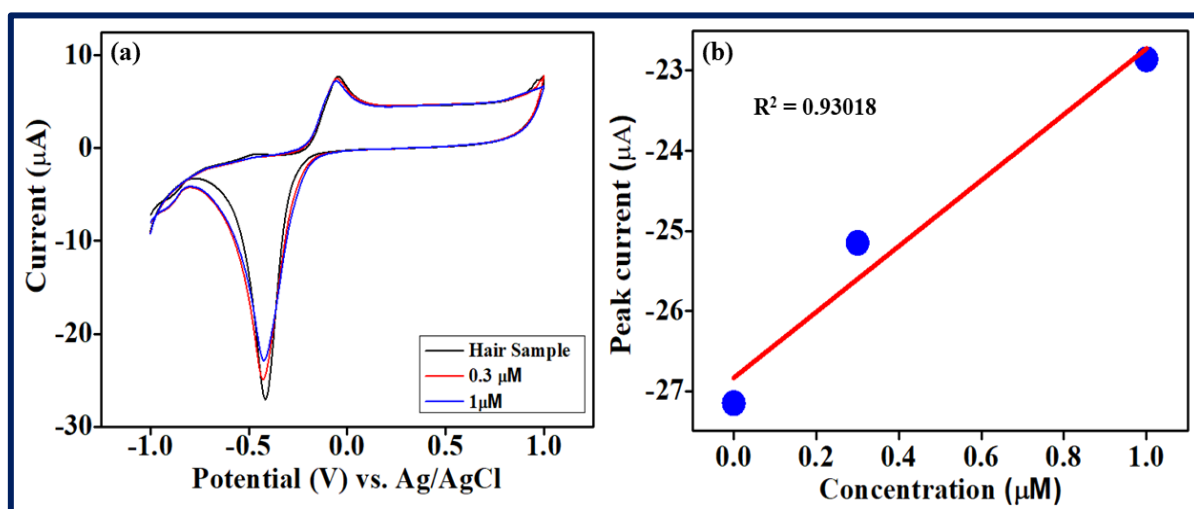


Fig. VII.15. Analysis of melanin in real sample with the addition of different amount of melanin concentration. (b) peak current vs concentration plot.

Table VII.4. Determination of melanin in real sample by addition method at the electrolytic cell presence of GCE/1

Sample	Melanin Added (μM)	Average found (μM)	Recovery (%)	LOD (μM)
Hair sample	0	0.3	0	0.378
	0.6	0.646	107	
	1.3	1.346	103	

3.6. PXRD

Powder X-ray diffraction analysis of both the Cu(I) complexes, **1** and **2**, was performed to check the homogeneity and phase purity of the bulk compound. Most of the major peaks of simulated pattern as obtained from single crystal diffraction matched well with the powder pattern of both **1** and **2**. The phase purity of the bulk materials of **1** and **2** were confirmed on

the basis of major peak position identity. The PXRD pattern of both **1** and **2** have been shown in Fig. VII.16.

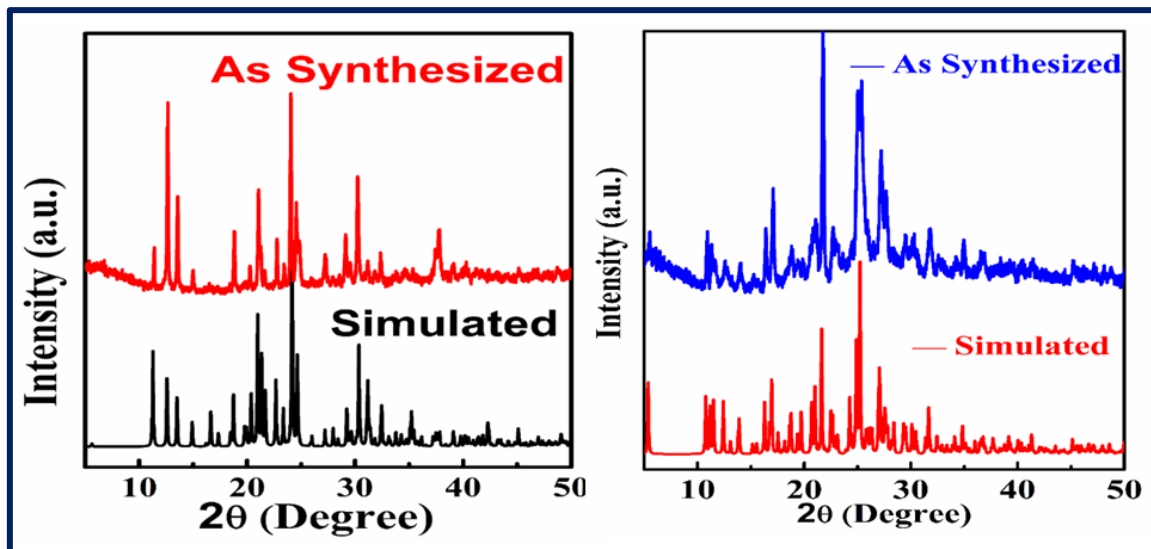


Fig. VII.16. X-ray powder diffraction patterns of **1** (left) and **2** (right).

4. Conclusions

In this work, we have successfully synthesized two novel copper(I) complexes stabilised from a quinoxaline derivative, 2-(4-bromophenyl)quinoxaline (**bpq**). Both the complexes have been comprehensively characterised by different analytical methods and spectroscopic techniques. The crystal structures of both of them have been determined. One is a tri-coordinated bent T-shaped planar molecule; while the other is an almost linear bi-coordinated copper(I) system. Herein, for the first time, an electrochemical melanin sensor has been developed employing a modified glassy carbon electrode with one of the copper(I) complexes. The sensing has been monitored by cyclic voltammetric experiments. The LOD and LOQ values were found to be promising. The efficacy of the sensing propensity of our novel sensor has been corroborated with specimen hair sample.

5. References

1. J. Borovanský, P.A. Riley, Eds. pp. 1-19, Wiley-VCH Verlag GmbH & Co. KGaA, 1st edition, 2011.
2. H.Z. Hill, W. Li, P. Xin, D.L. Mitchell, *Pigment Cell Res.* 10 (1997) 158-161.
3. L. Guo, W. Li, Z. Gu, L. Wang, L. Guo, S. Ma, C. Li, J. Sun, B. Han, J. Chang, *Int. J. Mol. Sci.* 24 (2023) 4360.
4. M. d'Ischia, A. Napolitano, A. Pezzella, P. Meredith, M. Buehler, *Angew. Chem. Int. Ed.* 59 (2020) 11196 -11205.
5. A.B. Mostert, *Polymers* 13 (2021) 1670.
6. G. Prota, *Melanins and Melanogenesis*. New York: Academic Press; 1992, pp. 1-290.
7. S. Ito, *Advances in chemical analysis of melanins*. In: J.J. Nordlund, R.E. Boissy, V.J. Hearing, R.A. King, J.P. Ortonne. *The Pigmentary System: Physiology and Pathophysiology*. New York: Oxford University Press, 1998. pp. 439-450.
8. P. Kumar, E.D. Mauro, S. Zhang, A. Pezzella, F. Soavi, C. Santato, F. Cicoira, J. Mater. Chem. C 4 (2016) 9516-9525.
9. X. Liu, H. Liu, H. Zheng, Y. Fang, *Prog. Org. Coat.* 152 (2021) 106138.
10. A.A. R. Watt, J.P. Bothma, P. Meredith, *Soft Matter* 5 (2009) 3754-3760.
11. M. d'Ischia, K. Wakamatsu, A. Napolitano, S. Briganti, J.C. Garcia-Borron, D. Kovacs, P. Meredith, A. Pezzella, M. Picardo, T. Sarna, J.D. Simon, S. Ito, *Pigment Cell Melanoma Res.* 26 (2013) 616-633.
12. P Meredith, T. Sarna, *Pigment Cell Res.* 19 (2006) 572-594.
13. J.D Simon, D. Peles, K. Wakamatsu, S. Ito, *Pigment Cell Melanoma Res.* 22 (2009) 563-579.
14. N. Mujahid, Y. Liang, R. Murakami, H. G. Choi, A.S. Dobry, J. Wang, Y. Suita, Q.Y. Weng, J. Allouche, L.V. Kemeny, A.L. Hermann, E.M. Roider, N.S. Gray, D.E. Fisher, *Cell Rep.* 19 (2017) 2177-2184.
15. R.A. Nicolaus, G. Prota, C. Santacrose, G. Scherillo, D. Sica, *Gazzetta Chim. Ital.* 99 (1967) 323-350.
16. G.A. Swan, A. Waggott, *J. Chem. Soc. Perkin. I* 10 (1970) 1409-1418.
17. P.M. Plonka, M. Garbacka, *Acta. Biochim. Pol.* 53 (2006) 429-443.
18. N.N. Gessler, A.S. Egorova, T.A. Belozerskaya, *Appl. Biochem. Microbiol.* 50 (2014) 105-113.

19. M. d'Ischia, K. Wakamatsu, F. Cicoira, E.D. Mauro, J.C. Gracia-Borrón, S. Commo, I. Galvan, G. Ghanem, K. Kenzo, P. Meredith, A. Pezzella, C. Santato, T. Sarna, J.D. Simon, L. Zecca, F.A. Zucca, A. Napolitano, S. Ito, *Pigment Cell Melanoma Res.* 28 (2015) 520-544.
20. Y.J. Kim, W. Wu, S.-E. Chun, J.F. Whitacre, C.J. Bettinger, *PNAS* 110, 20912-20917.
21. J.B. Dawson, D.J. Barker, D.J. Ellis, E. Grassam, J.A. Cotterill, G.W. Fisher, J.W. Feather, *Phys. Med. Biol.* 25 (1980) 695-709.
22. J.W. Feather, M. Hajizadeh-Saffar, G. Leslie, J.B. Dawson, *Phys. Med. Biol.* 34 (1989) 807-820.
23. I. Nishidate, Y. Aizu, H. Mishina, *J. Biomed. Opt.* 9 (2004) 700-710.
24. K. Wakamatsu, S. Ito, *Pigment Cell Res.* 15 (2002) 174-183.
25. K. J. Reszka, Z. Matuszak, C. F. Chignell, *Free Radical Biology & Medicine* 25 (1998) 208-216.
26. T. Watanabe, A. Tamura, Y. Yoshimura, H. Nakazawa, *Anal. Biochem.* 254 (1997) 267-271.
27. C.-L. Serpentine, C. Gauchet, D. Montauzon, M. Comtat, J. Ginestar, N. Paillous, *Electrochim. Acta* 45 (2000) 1663-1668.
28. R. Xu, C.T. Prontera, E.D. Mauro, A. Pezzella, F. Soavi, C. Santato, *APL Materials* 5 (2017) 126108.
29. S. Ito, *J. Invest. Dermatol.* 1993 (100) 166S-171S.
30. S. Ito, K. Wakamatsu, H. Ozeki, *Pigment Cell Res.* 13 (2000) 103-109.
31. B. Aksoy, Ö. Güngör, S. Köytepe, T. Seçkin, *Polymer-Plastics Techno. Engineering* 2016 (55) 119-128.
32. S.T. Duran, C.B.A. Hassine, M. Burç, Ö. Güngör, *Anal. Bioanal. Electrochem.* 12 (2020) 857-869.
33. S.T. Duran, N. Ayhan, B. Aksoy, S. Köytepe, A. Paşahan, *Polym. Bull.* 77 (2020) 5065-5082.
34. S.T. Duran, *J. Sci.* 32 (2019) 426-438.
35. G. Maduraiveeran, M. Sasidharan, V. Ganesan, *Biosens. Bioelectron.* 103 (2018) 113-129.
36. M. Burç, S. Köytepe, S.T. Duran, N. Ayhan, B. Aksoy, Turgay Seçkin, *Measurement* 151 (2020) 107103.
37. M. Burç, D. Asma, S.T. Duran, Macdo. *J. Chem. Chem. Eng.* 40 (2021) 289-297.

38. N. Kandasamy, N. Keerthi. J. Jeyasekaran, ACS Appl. Electron. Mater. 5 (2023) 4805-4815.
39. M. Osawa, M. Hoshino, M. Hashimoto, I. Kawata, S. Igawaa, M. Yashima, Dalton Trans. 44 (2015) 8369-8378.
40. E. Cariati, E. Lucenti, C. Botta, Coord. Chem. Rev. 306 (2016) 566-614.
41. X. Zhang, Z. Chi, Y. Zhang, S. Liu and J. Xu, J. Mater. Chem. C 1 (2013) 3376-3390
42. H.V.R. Dias, Pure Appl. Chem. 82 (2010) 649-656.
43. M. Wallesch, D. Volz, D.M. Zink, U. Schepers, M. Nieger, T. Baumann, S. Bräse, Chem. Eur. J. 20 (2014) 6578-6590.
44. A. Barbieri, G. Accorsi, N. Armaroli, Chem. Commun. (2008) 2185-2193.
45. K. Tsuge, Y. Chishina, H. Hashiguchi, Y. Sasaki, M. Kato, S. Ishizaka, N. Kitamura, Coord. Chem. Rev. 306 (2016) 636-651.
46. A. Schlachter, K. Tanner, P.D. Harvey, Coord. Chem. Rev. 448 (2021) 214176.
47. A. Kobayashi, M. Kato, Chem. Lett. 46 (2017) 154-162.
48. E. Cariati, E. Lucenti, C. Botta, U. Giovanella, D. Marinotto, S. Righetto, Coord. Chem. Rev. 306 (2016) 566-614.
49. S. Perruchas, Dalton Trans. 50 (2021) 12031-12044.
50. D.R. McMillin, K.M. McNett, Chem. Rev. 98 (1998) 1201-1219.
51. S. Mahadevan, M. Palaniandavar, Inorg. Chem. 37 (1998) 693-700.
52. V. Singh, J. Sinha, A. Nanda, S.A. Shivashankar, N. Bhat, S. Avasthi, Inorg. Chem. 60 (2021) 17141-17150.
53. B. Wolpert, O.S. Wolfbeis, V.M. Mirsky, Sens. Accutators B: Chem. 142 (2009) 446-450.
54. R.R. Poolakkandy, M.M. Menampambath, Electrochem. Sci. Adv. 1 (2021) e2000024.
55. P. G. Urben (Ed.), Bretherick's Handbook of Reactive Chemical Hazards, Sixth Ed. Butterworth-Heinemann, Oxford, 1999.
56. APEX2 suite for crystallographic software, Bruker AXS, Madison, WI (1995).
57. SAINT - Software for the Integration of CCD Detector System Bruker Analytical X-ray Systems; Bruker AXS: Madison, WI (1995).
58. G.M. Sheldrick, ShelXT-Integrated space-group and crystal-structure determination, Acta Cryst. A71 (2015) 3-8.
59. Bruker. SAINT and SADABS; Bruker AXS Inc.: Madison, Wisconsin, USA (2004).
60. G.M. Sheldrick. Crystal structure refinement with SHELXL. Acta Crystallogr. C71 (2015) 3-8.

61. M. Ghaemy, F.H. Nasr, J. Appl. Polym. Sci. 124 (2012) 1707-1715.
62. S.S. Sreejith, N. Mohan, N. Aiswarya, M.R.P. Kurup, Polyhedron 115 (2016) 180-192.
63. N.A. Mangalam, M.R.P. Kurup, Spectrochim. Acta A: Mol. Biomol. Spectrosc. 71 (2009) 2040-2044.
64. K. Nakamoto, Infrared and Raman Spectra of Inorganic and Coordination Compounds, (1978) New York: John Wiley and Sons.
65. M. Munakata, S. Kitagawa, N. Ujimar, M. Nakamura, N. Maekawa, H. Mastuda, Inorg. Chem. 1993 (32) 826-832.
66. J.P. Naskar, S. Chowdhury, M.G.B. Drew, D. Datta, New J. Chem. 26 (2002) 170-175.
67. S. Liu, J. Zhang, C. Liu, G. Yin, M. Wu, C. Du, B. Zhang, Polyhedron 218 (2022) 115761.
68. T.N. Sorrell, M.R. Malachowski, Inorg. Chem. 22 (1983) 1883-1887.
69. H.-C. Liang, E. Kim, C.D. Incarvito, A.L. Rheingold, K.D. Karlin, Inorg. Chem. 41 (2002) 2209-2212.
70. K.K. Manar, S. Chakraborty, V.K. Porwal, D. Prakash, S.K. Thakur, A.R. Choudhury, S. Singh, ChemistrySelect 5 (2020) 9900-9907.
71. J. Li, L. Wang, Z. Zhao, X. Li, X. Yu, P. Huo, Q. Jin, Z. Liu, Z. Bian, C. Huang, Angew. Chem. Int. Ed. 59 (2020) 8210-8217.
72. J.W. Tye, Z. Weng, A.M. Johns, C.D. Incarvito, J.F. Hartwig, J. Am. Chem. Soc. 130 (2008) 9971-9983.
73. I.D. Brown, D. Altermatt, Acta Cryst. Sec. B 41 (1985) 244.
74. H. Alwael, A.S. Alharthi, M.M. Dabi, M. Oubaha, M.S. El-Shahawi, Electrochem. Commun. 162 (2024) 107686.
75. W.D. Adane, B.S. Chandravanshi, M. Tessema, Sens. Actuators B: Chem. 390 (2023) 134023.
76. X. Guo, S. Chen, Y. Hu, G. Li, N. Liao, X. Ye, D. Liu, C. Xue, J. Food Sci. Technol. 51 (2014) 3680-3690.

List of Publications

Thesis Work

1. **N.K. Mandal**, B. Guhathakurta, P. Basu, A.B. Pradhan, C.S. Purohit, S. Chowdhury, J.P. Naskar
DNA and RNA binding studies on a novel bromo-bridged dimeric copper(II) complex stabilized from a Schiff base ligand
Journal of Coordination Chemistry 72 (2019) 3625-3644
2. **N.K. Mandal**, N. Bandyopadhyay, P. Arya, S. Chowdhury, N. Raghav, J.P. Naskar
Synthesis, characterization, structure, *in vitro* enzymatic activity and sensing aspects of a copper(II) complex stabilized from a naphthaldehyde based Schiff base ligand
Inorganica Chimica Acta 544 (2023) 121229
3. **N.K. Mandal**, C.J Gómez-García, P. Saha, J.P. Naskar
Syntheses of two copper(II) coordination polymers from a morpholine-based tridentate Schiff base ligand: crystal structures and magnetic properties
Journal of Coordination Chemistry 76 (2023) 705-719
4. **N.K. Mandal**, S. Nandi, K. Acharya, J.P. Naskar
Synthesis, characterization, crystal structure, thermal and redox behaviour and antiproliferative studies of morpholine-based two copper(II) compounds
Applied Organometallic Chemistry 37 (2023) e7120
5. **N.K. Mandal**, S. Nandi, S. Benmansour, C.J. Gómez-García, K. Acharya, J.P. Naskar
Design, synthesis and structure of a trinuclear copper(II) complex having a Cu₃OH core with regard to aspects of antiproliferative activity and magnetic properties
New Journal of Chemistry 48 (2024) 5782-5796
6. **N.K. Mandal**, B.B. Show, J.P. Naskar
Syntheses, crystal structures and spectroscopic properties of copper(I) complexes stabilized from a quinoxaline based ligand: Enzyme-less electrochemical sensing of melanin
MS under preparation

Other Work

7. **N.K. Mandal**, P. Arya, N. Raghav, S. Chowdhury, J.P. Naskar
Design, synthesis, crystal structure, photophysical behavior and aggregation-induced emission of a novel pyrene scaffold multifunctional Schiff base ligand: inhibition of digestive enzymes and docking studies
New Journal of Chemistry 47 (2023) 14551-14568
8. D. Mukherjee, K. Sarkar, S. Reja, M. Bakibillah, S. Guha, **N.K. Mandal**, J.P. Naskar, R.K. Das
Mononuclear Zn(II) Complex Based on N2O Ligand Compartment: First Case to Detect Nitro Explosives
Journal of Fluorescence 2023 (<https://doi.org/10.1007/s10895-023-03431-9>)
9. N. Bandyopadhyay, **N.K. Mandal**, L. Haque, S. Das, S. Chowdhury, J.P. Naskar
Synthesis, crystal structure, Hirshfeld surface analysis and theoretical studies of an oxime-based ligand: DNA binding and docking studies of its novel Pd (II) complex
Journal of Molecular Structure 1310 (2024) 138358
10. B. Guhathakurta, **N.K. Mandal**, S. Benmansour, C.J. Gómez-García, J.P. Naskar
A rare example of a dimeric copper(II) complex with a double nitrate $\kappa^1-O,O';\kappa^2-O$ bridge: synthesis, crystal structure, magnetic properties and Hirshfeld surface analysis
MS under preparation



DNA and RNA binding studies on a novel bromo-bridged dimeric copper(II) complex stabilized from a Schiff base ligand

Naba Kr Mandal^a, Bhargab Guhathakurta^a, Pritha Basu^b,
Ankur Bikash Pradhan^a, Chandra Shekhar Purohit^c, Shubhamoy Chowdhury^d
and Jnan Prakash Naskar^a

^aDepartment of Chemistry, Jadavpur University, Kolkata, India; ^bDepartment of Chemistry, Sunderwati Mahila College, Bhagalpur, Bihar, India; ^cSchool of Chemical Sciences, National Institute of Science Education and Research, Bhubaneswar, India; ^dDepartment of Chemistry, University of Gour Banga, Malda, India

ABSTRACT

A novel red copper(II) compound, bis(μ -bromo)bis(2-(benzothiazol-2-yl-hydrazono)-1,2-diphenyl-ethanone)-dicopper(II) (**1**), has been fostered by equimolar reaction of a Schiff-base ligand, 2-(benzothiazol-2-yl-hydrazono)-1,2-diphenyl-ethanone (LH), with copper(II) bromide in satisfactory yield. **1** has thoroughly been characterized by C, H and N elemental analyses, FT-IR and UV-vis (both in solid state and in solution) spectroscopies, and room-temperature magnetic susceptibility and conductivity measurements. Dimeric **1** bears symmetric rare bromo-bridges in its crystal structure. **1** retains its solid-state identity even in a protic solvent like methanol. **1** in methanol displays two-step one-electron redox response. Theoretical calculations based on DFT were executed to probe the electronic structure of **1** and to augment its color. DNA- and RNA-binding aspects of both LH and **1** have been explored. Thermodynamic binding parameters have been determined. LH is a major-groove binder to DNA, while **1** manifests itself as a minor-groove binder. This binding has been corroborated through molecular docking. Nucleic acid binding aspect of such type of rare bromo-bridged red copper(II) dimer is unprecedented.

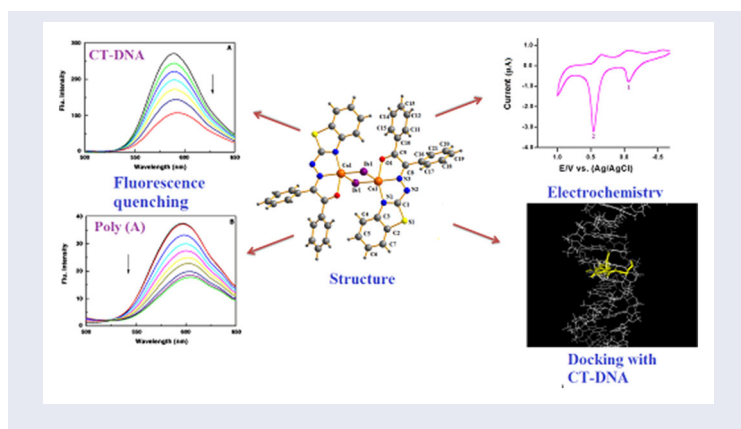
ARTICLE HISTORY

Received 24 October 2019

Accepted 24 November 2019

KEYWORDS

Schiff-base; copper;
structure; DNA; docking

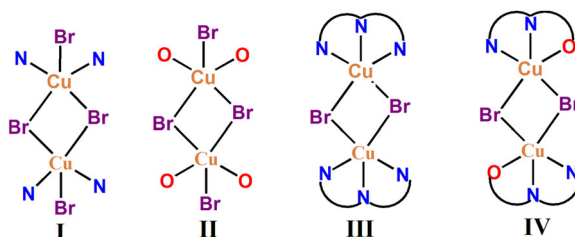


1. Introduction

Binuclear copper(II) complexes are of contemporary interest. The reasons are myriad. Such assemblies encompass a special echelon in copper coordination chemistry. Binuclear copper(II) compounds are the probing systems for different theories and models in magnetochemistry [1, 2]. From a biological viewpoint, they serve as DNA molecular probes [3]. For the development of novel anticancer drugs with lower toxicity but with pronounced potentiality, copper(II) dimers are the ideal choice for their commendable antiproliferative efficacies [4]. These assemblies even perform excellent DNA-strand scission [5, 6]. Accordingly, they are optimum candidates from the viewpoint of genetic engineering. Again, such systems are important in enzymatic catalytic reaction [7, 8]. A plethora of copper(II) dimers with varying bridging entities are known to exist. For ready reckoning, end-on azido [9], end-to-end azido [10], end-to-end thiocyanate [11], bis(μ -sulphato)- [12], alkoxo- [13, 14], hydroxo- [15, 16], and imidazolate-bridged [17] dinuclear copper(II) compounds have been reported. In the halo-bridged family, chloro-bridged copper(II) dimers are comfortably common, while bromo-bridged systems are really less known. Copper(II) dimers having bis(μ -iodo) [18, 19] and bis(μ -fluoro) entities are also known [20]. Our literature search reveals that N,O-donor Schiff-base ligand has been employed to foster dimeric chloro-bridged copper(II) compound [21]. This prompted us to generate bromo-bridged system using this type of ligand. It is a point to note that symmetric bromo-bridged dimeric copper(II) compound, generated from N,O-donor Schiff-base ligand, is unprecedented. Here, we are concerned with such type of bromo-bridged copper(II) dimer.

For bis(μ -bromo)-bridged copper(II) complexes, various bridging modes have been known to exist. Among the bridging modes, as shown in Scheme 1, I is the most common. This mode is rampant in a multitude of copper(II) complexes [22–25]. Compounds bearing other modes, II [26] and III [27–29], have also been known along with their magnetic studies.

Ours is the rare IV mode. Prior to this work, only one example of such mode is known in a copper(II) dimer. This has been stabilized from a L-leucine based ligand [30]. Halo-bridged dinuclear copper(II) complexes with N_2Cl_3 coordination environment having pyridine-based ligand show chromotropic behavior. These properties have



Scheme 1. Different modes of bromo-bridges as observed in copper(II) dimers.

been attributed to structural changes accentuated in different solvents [31]. Of late, monomeric copper(II) complexes, stabilized from a Schiff base ligand, have been studied to show DNA- and RNA-binding efficacies [32]. Again, chromone-based monomeric copper(II) complexes with N,N-donor ligand have been shown to manifest DNA/RNA-binding interaction with remarkable cytotoxic propensities [33]. It is pertinent to note that DNA- and RNA-binding studies on bromo-bridged copper(II) dimer evaded earlier attention. Herein, for the first time we have taken initiative to study the DNA/RNA-binding interaction of a symmetric rare bromo-bridged binuclear copper(II) complex. In this work, synthesis, characterization, structure, spectroscopic and redox aspects of a novel red dimeric bis(μ -bromo)-bridged Cu(II) complex (**1**) having a rare CuN_2OBr_2 chromophore have been reported along with its DNA/RNA-binding studies.

2. Experimental

2.1. Materials

2-Hydrazino-benzothiazole and benzil were procured from Aldrich, USA and Loba Chemie, India, respectively. Copper(II) bromide was purchased from Sigma-Aldrich. All other chemicals and solvents were of analytical reagent grade and used as received.

2.2. Nucleic acids and buffer

Polyriboadenylic acid [Poly(A)] as potassium salt and calf-thymus (CT) DNA (Type I, 42 mol% GC) were both purchased from Sigma-Aldrich Corporation (St. Louis, MO, USA). 10 mM citrate-phosphate (CP) buffer in the presence of 2% DMSO at pH 7.0 was employed for all biophysical studies. Nucleic acid solutions were also prepared in the same buffer. The buffer solution was filtered through Millipore membrane filters (0.22 μm pore size). The Millipore membrane filters had been procured from Millipore, India Pvt. Ltd., Bangalore, India. The concentrations of the CT DNA and Poly(A) were determined spectrophotometrically by considering the molar absorption coefficient value of 13,200 $\text{M}^{-1}\text{cm}^{-1}$ (base pairs) [34] and 10,000 $\text{M}^{-1}\text{cm}^{-1}$ [35], respectively.

2.3. Physical measurements

To determine the melting point of **1**, an electro-thermal digital melting point apparatus was used. The value is not corrected. FT-IR spectrum (KBr disc) [s = sharp] of **1** was

recorded from 400 to 4000 cm^{-1} on a Shimadzu FTIR 8400S spectrophotometer. To have the C, H and N micro-analytical data, a Perkin Elmer 2400 II elemental analyzer was employed. On a Shimadzu UV-160A spectrophotometer, UV-vis spectrum of the compound was recorded in methanol. UV-vis spectrum of **1** in solid state was run on a Perkin Elmer LAMBDA 35 UV-vis spectrophotometer. The magnetic susceptibility of **1** was measured with a PAR 155 vibrating sample magnetometer at 298 K. For the calibration of the magnetometer, $\text{Hg}[\text{Co}(\text{SCN})_4]$ was used as the calibrant. Following Pascal's constants, the magnetic susceptibility data were corrected for requisite diamagnetism. The electrochemical redox behavior of our title compound was investigated employing a conventional three-electrode configuration on a BAS Epsilon Electrochemical workstation (Model CV-50) in methanol at 298 K. A glassy carbon working electrode, a platinum-wire auxiliary electrode and a Ag/AgCl reference electrode completed the conventional three-electrode assembly. 0.1 M tetra-*n*-butylammonium perchlorate (TBAP) was used as the indifferent electrolyte. Dry and degassed nitrogen gas was purged for 10 min to maintain an inert atmosphere during our CV data acquisition. The cell was blanketed with pure nitrogen during scanning. The electrical conductivity was measured in methanol on a Systronics (India) direct reading conductivity meter (Model 304) at room temperature. To calibrate the meter, 0.1 M KCl solution in water was employed.

2.4. Computational details

The GAUSSIAN-09 Revision C.01 program package was employed for all theoretical calculations [36]. The gas phase geometries of the molecules, LH and its bromo-bridged copper(II) dimer (**1**), were fully optimized without any restrictions of symmetry in singlet ground states with the gradient-corrected DFT level coupled with the level of three parameter-fit of the exchange and correlation functional of Becke B3LYP [37] which includes the correlation functional of Lee *et al.* (LYP) [38]. The basis set LANL2DZ with effective core potential (ECP) was employed for Cu and bromine following the associated valence double zeta basis set of Hay and Wadt [39–41]. This is in combination with the 6-31 + G(d) basis set selected for hydrogen, carbon, nitrogen and oxygen [42, 43].

2.5. Methods for DNA and RNA binding

2.5.1. Spectrophotometric study

All spectrophotometric studies were executed on a Jasco V660 double-beam monochromatic spectrophotometer (Jasco International Co. Ltd., Hachioji, Japan) at room temperature. The spectrophotometer was connected with a thermoelectrically controlled cell-holder with a temperature controller to keep the temperature steady during the experiment. The spectrophotometric measurements were carried out in a matched quartz cuvette of 1 cm path length (Hellma, Germany). Following our earlier protocol, we performed the experiment as described herein [27]. In each set of scanning, the self-absorption values of DNA and Poly(A) were eliminated.

The binding constants (*K*) for the anchoring of LH and **1** with DNA and Poly(A) were determined in the spirit of Benesi-Hildebrand (BH) equation [44],

$$A_0/\Delta A = A_0/\Delta A_{\max} + (A_0/\Delta A_{\max}) \times 1/K \times 1/L_t \quad (1)$$

where $\Delta A = A_0 - A$, ΔA_{\max} = maximum reduced absorbance, A_0 = maximum absorbance at λ_{\max} , A = reduced absorbance and L_t = nucleotide concentration.

2.5.2. Fluorescence spectroscopic and ethidium bromide displacement studies

Spectrofluorimetric studies were performed on a PTI QM-400 spectrofluorimeter. Here, we have explored the binding propensities of LH and **1** with the nucleotides by fluorescence titrimetric methods. Three different temperatures were considered employing a temperature controller unit in fluorescence free quartz cuvettes of 1 cm path length following earlier methods [45]. The binding constants of **1** and LH with DNA and Poly(A) were evaluated by the Benesi-Hildebrand (BH) equation. Ethidium bromide (EB)-displacement assay was performed for **1** and LH with DNA and Poly(A) in 50 mM Tris-HCl buffer (pH = 7.0) in the presence of 2% DMSO in fluorescence free quartz cuvettes of 1 cm path length at 25 °C. Initially, the fluorescence intensity of a pre-equilibrated mixture of CT DNA and Poly(A) (50 μ M) and EB (7 μ M) was recorded at 590 nm. Then, **1** and LH were added to the earlier complex and the change in fluorescence intensity was monitored carefully [46]. IC_{50} values for the complexes have subsequently been determined following the protocol described earlier [47]. The same experiment was repeated for LH following similar methodology.

2.5.3. Thermodynamic studies: temperature dependent spectrofluorometry

Temperature dependent fluorescence titration experiments, both for **1** and LH, were carried out on a PTI QM-400 spectrofluorimeter at three different temperatures (15, 25 and 35 °C). The instrument was accentuated with a thermometric cell temperature programmer and temperature controller. The binding constant for each case was evaluated by the BH plot as alluded in Section 2.5.1.

From van't Hoff plot ($\ln K'$ vs. $1/T$), different thermodynamic parameters were determined. The binding enthalpy change (ΔH°) has been ascertained from the slope of the plot.

$$\partial \ln(K')/\partial(1/T) = -\frac{\Delta H^\circ}{R} \quad (2)$$

Employing the following equation, Gibbs free energy change (ΔG°) was determined at a definite temperature.

$$\Delta G^\circ = -RT \ln(K') \quad (3)$$

Finally, entropy change (ΔS°) during binding was ascertained following the thermodynamic Eq. 4.

$$\Delta S^\circ = (\Delta H^\circ - \Delta G^\circ/T) \quad (4)$$

2.5.4. Circular dichroism studies

The conformational changes of DNA and RNA due to the binding of **1** and LH were monitored by a JASCO J815 unit equipped with a temperature programmer (model PFD 425L/15) at 298 K.

The CD spectra of fixed concentration of DNA/RNA were first monitored and then with increasing concentration of the ligand and complex in a rectangular strain free quartz cuvette of 1 cm path length. The CD spectra were recorded from 400 to 230 nm at a scan speed of 100 nm min⁻¹ keeping a band width of 1.0 nm at a sensitivity of 100 millidegrees. During each measurement of the CD spectrum, we performed the requisite base line correction, smoothing and normalization to nucleotide concentration. The calibration of the CD unit was routinely checked employing an aqueous solution of d-10 ammonium camphor sulphonate.

2.5.5. Molecular docking study

Molecular docking study was employed to have an idea about the possible binding location of the ligand and complex with protein. The native structure of CT DNA was taken from RSC Protein Data Bank having PDB ID: BDL001. Docking studies were performed with the AutoDock 4.2 software, which utilizes the Lamarckian Genetic Algorithm (LGA). For the docking of LH and **1** with CT DNA, the required file for LH and **1** were generated through the combined use of the Gaussian 09W and AutoDock 4.2 software packages. The optimized geometries of LH and **1** were obtained from DFT//B3LYP/6-31G level of theory using Gaussian 09W suite of programs and the resulting geometries were read in the Gauss view 5 software in a compatible file format. From this, the requisite file was generated in AutoDock 4.2. The grid box was set to 110, 110 and 110 Å, respectively, along X, Y and Z axes with a grid spacing of 0.37 Å in order to recognize the binding site of both LH and **1** in CT DNA. The employed AutoDocking parameters were as follows: GA population size = 150; maximum number of energy evaluations = 250 000; GA crossover mode = two points. The lowest binding energy conformer was selected from 10 different conformations for each docking simulation and the resulting minimum energy conformation was chosen for further analyses. The PyMOL software package was used for better visualization of the docked conformations.

2.6. Syntheses

2.6.1. Preparation of ligand (LH)

LH was generated following our previously reported method [21].

2.6.2. Preparation of [Cu₂(μ-Br)₂(L)₂] (**1**)

0.017 g (0.05 mmol) of LH was dissolved in 20 mL of methanol to have a straw-yellow solution. 0.015 g (0.05 mmol) of solid CuBr₂ was added all at a time to the ligand solution with constant stirring. Immediately the color of the solution turned pinkish red. The stirring was continued for 2 h. After stirring, the resulting reaction mixture was left for aerial evaporation. After 3 days, wine-red crystalline compound was harvested. The separated compound was filtered and washed thoroughly with chilled diethyl ether. Subsequently it was dried in a vacuum desiccator over anhydrous fused CaCl₂. Yield: 0.018 g (75%). m.p. > 200 °C. Elemental analyses for C₄₂H₂₈Br₂Cu₂N₆O₂S₂ (MW = 999.476): Found (%): C, 50.40; H, 2.85; N, 8.37; calcd. (%): C, 50.42; H, 2.82; N, 8.40. FT-IR (KBr): ν[cm⁻¹]: 1559 s [ν(C=N)], 1537 s, 1462 s [ν(C=C) of phenyl ring skeletal].

UV-vis (MeOH): $\lambda_{\text{max}}/\text{nm}$ ($\epsilon/\text{M}^{-1}\text{cm}^{-1}$) 203 (26,310), 252 (12,960), 290 (7,749), 535 (5,794). UV-vis (Solid state): $\lambda_{\text{max}}/\text{nm}$ 250, 295, 531. Λ_{M} (MeOH): $22\text{ ohm}^{-1}\text{cm}^2\text{mol}^{-1}$ (non-electrolyte). $\mu_{\text{eff}}(\text{BM})$: 1.94 (at 298 K) per Cu atom. Needle-shaped glittering single crystals, fit for X-ray structure determination, were developed by standing a dilute methanolic solution of the compound in a refrigerator for a fortnight. The compound is soluble in CH_3OH , $\text{C}_2\text{H}_5\text{OH}$, THF, DMSO, DMF and partly soluble in DCM. The compound is insoluble in CH_3CN , C_6H_6 , n-hexane and n-pentane.

2.7. Crystal structure determination

An appropriate shining red, needle-shaped single-crystal of **1** was selected for X-ray crystallography under visualization through a microscope. Intensity data of **1** were collected on a Bruker-Kappa APEX II CCD diffractometer. The diffractometer was equipped with a 1 K charge-coupled device (CCD) area detector employing graphite monochromated Mo- K_{α} radiation ($\lambda = 0.71073\text{ \AA}$) at 296(2) K. The cell parameters were determined using SMART software [48]. For the reduction and correction of the collected data, SAINTPlus was used [48]. Employing SADABS absorption corrections were done [49]. Finally by the direct method with SHELXL-97 program package, the structure was solved [50]. The refinement by full-matrix least-squares method was executed on all F^2 data with SHELXL-97. For all non-hydrogen atoms, anisotropic refinement was performed. Subsequently the additional hydrogen atoms were positioned by riding model. The cycle of full-matrix least-squares methods for refinement was performed on the basis of observed reflections and the variable parameters. The structural refinement data for **1** are shown in Table 1. Selected bond lengths and angles of **1** are tabulated in Table 2.

3. Results and discussion

3.1. Synthesis and formulation

LH has been synthesized by the 1:1 Schiff-base condensation of 2-hydrazino-benzothiazole and benzil in methanol. The synthetic scheme has been outlined in Scheme 2.

LH can exist in two forms, keto and enol. Thus, the ligand can undergo keto-enol tautomerism. The keto form is more stable than the enol form. However, during complex formation, the enol form binds the metal ion [21].

Our subsequent reaction of LH with CuBr_2 in methanol afforded a red dimeric bis(μ -bromo)-bridged Cu(II) complex in satisfactory yield. In the FT-IR spectrum of LH, three strong absorption bands have been observed (Figure S1). These have been reported earlier by us along with assignments [21]. The $\nu(\text{C}=\text{N})$ stretching frequency was observed at 1595 cm^{-1} for **1**. The aromatic $\text{C}=\text{C}$ ring vibrations were observed from 1537 to 1462 cm^{-1} (Figure S2). The Cu-Br stretching frequency is generally observed from 200 to 400 cm^{-1} . Here we could not observe it due to the limitation of the window ($400\text{--}4000\text{ cm}^{-1}$) of the spectrophotometer used. Red copper(II) compounds are scarce indeed. Nitrocyenin (NC), a brilliant red mononuclear copper(II) protein, is known to present in a chemoautotrophic bacterium, *Nitrosomonas europaea* [51]. This microorganism derives energy currency from the oxidation of ammonia to

Table 1. Crystal data and structure refinement for **1**.

CCDC no.	1831458
Empirical formula	C ₄₂ H ₂₈ Br ₂ Cu ₂ N ₆ O ₂ S ₂
Formula weight	999.743
Temperature [K]	296(2)
Wavelength [Å]	0.71073
Crystal system	Monoclinic
Space group	P2 ₁ /n
Unit cell dimensions	
a [Å]	10.1790(5)
b [Å]	14.3499(7)
c [Å]	13.0811(7)
α [°]	90
β [°]	95.615(3)
γ [°]	90
Volume [Å ³]	1901.56(17)
Z	2
ρ _{calcd} [mg/cm ³]	1.753
Absorption coefficient [mm ^{−1}]	3.377
F (000)	1004
Crystal size [mm]	0.7 × 0.51 × 0.24
Θ range for data collection [deg]	2.112 to 26.321
Limiting indices	−12 < h < 12, −16 < k < 17, −16 < l < 14
Absorption correction	Semi-empirical from equivalents
Max. and min. transmission	0.7454 and 0.5831
Reflections collected/unique	9574/3841 [R _{int} = 0.0327]
Completeness of theta = 25.242	99.9%
Refinement method	Full-matrix least-squares on F ²
Data/restraints/parameters	3841/0 /253
Goodness-of-fit on F ²	1.036
Final R indices [I > 2σ(I)]	R ₁ = 0.0340, wR ₂ = 0.0801
R indices (all data)	R ₁ = 0.0503, wR ₂ = 0.0870
Largest diff. peak and hole	0.586 and −0.479 e.Å ^{−3}

nitrite. In the perspective of global nitrogen cycle, this prokaryote offers ubiquitous role. One true example of the synthetic analogue of this red mononuclear copper(II) system has been published recently [52]. To the best of our knowledge, such example is hitherto unknown for binuclear copper(II) system. **1** is red and shows an absorption band at 535 nm with ϵ value of $5794 \text{ M}^{-1} \text{ cm}^{-1}$. Accordingly, we have taken recourse to perform DFT calculations on **1** to delve into the electronic structure of it in comparison to its stabilizing ligand, LH. **1** is soluble in most of the protic solvents like methanol, ethanol, tetrahydrofuran, but sparingly soluble in chloro-solvents like dichloromethane and dichloroethane. It is insoluble in acetonitrile, n-hexane and n-pentane. The UV-vis spectrum of **1** retains its identical identity, in terms of peak position, both in the solid state as well as in methanolic solution (Figure S3). This testifies that the compound retains its solid-state dimeric identity even in a methanolic solution as well. Again, the compound is a non-electrolyte in methanol. **1** displays two well separated CV responses in solution. These data also corroborate that the dimeric core in **1** as observed in its solid state retains as such in solution phase.

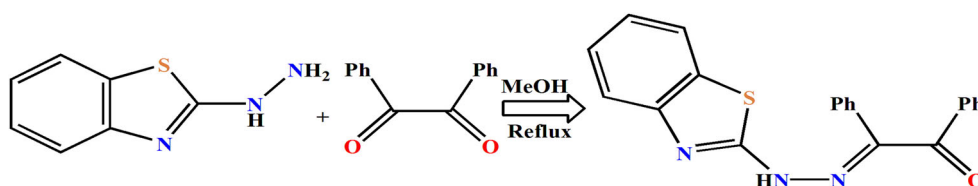
3.2. Electronic spectra of LH and **1**

LH shows an intraligand charge-transfer band in methanol at 355 nm with an ϵ value of $19,070 \text{ M}^{-1} \text{ cm}^{-1}$ (Figure S5) [21]. The CT band appears in **1** around 535 nm in methanol with attenuated intensities (Figure S5). In general, the extent of red-shift

Table 2. Selected experimental and optimized bond distances (Å) and angles (°) for **1**.

Bond	Experimental	Optimized	Bond	Experimental	Optimized
C(1)–N(1)	1.318(4)	1.32731	C(1)–N(2)	1.369(4)	1.34573
C(1)–S(1)	1.719(3)	1.77209	C(8)–N(3)	1.320(4)	1.31958
C(9)–O(1)	1.255(4)	1.23853	N(1)–Cu(1)	2.006(2)	2.09773
N(2)–N(3)	1.312(3)	1.32196	N(3)–Cu(1)	1.970(3)	2.02945
O(1)–Cu(1)	2.036(2)	2.13576	Br(1)–Cu(1)	2.3811(5)	2.45261
			Cu(1)–Br(1)#1	2.7729(5)	2.68475
Angle	Experimental	Optimized	Angle	Experimental	Optimized
N(3)–N(2)–C(1)	108.4(3)	111.14837	N(2)–N(3)–Cu(1)	119.2(2)	117.26360
C(8)–N(3)–Cu(1)	117.2(2)	120.19769	C(9)–O(1)–Cu(1)	112.72(19)	110.77917
C(1)–S(1)–C(2)	89.19(15)	88.63818	Cu(1)–Br(1)–Cu(1)#1	84.756(17)	79.83530
N(3)–Cu(1)–N(1)	78.99(10)	76.99089	N(3)–Cu(1)–O(1)	79.00(9)	74.65197
N(1)–Cu(1)–O(1)	156.22(10)	152.53914	N(3)–Cu(1)–Br(1)	165.22(8)	161.03877
N(1)–Cu(1)–Br(1)	105.27(7)	106.12978	O(1)–Cu(1)–Br(1)	93.98(6)	96.84599
N(3)–Cu(1)–Br(1)#1	97.70(8)	99.00547	N(1)–Cu(1)–Br(1)#1	101.94(7)	104.12978
O(1)–Cu(1)–Br(1)#1	89.82(7)	92.84599	Br(1)–Cu(1)–Br(1)#1	95.243(17)	98.16464

Symmetry transformations used to generate equivalent atoms: #1 – x + 1, –y + 1, –z + 1.

**Scheme 2.** Synthetic scheme of LH.

depends on the charge on the central metal ion. The higher the charge on the metal ion, the lower is its red-shift. For the sake of comparison, here we have performed calculations on an analogous Zn(II) complex of LH. Being a d^{10} spherically symmetrical system, Zn(II) enjoys no CFSE. Our Mulliken population analyses show that the residual charge on Zn center in the same geometry with analogous ligand environment is 1.08 and that on Cu is 0.23 in **1**. The HOMO–LUMO gap in LH is 2.893 eV. This gap is of 0.558 eV in **1** (Figure 1). Accordingly, the absorption band at 535 nm with an ϵ value of $5,794 \text{ M}^{-1}\text{cm}^{-1}$ (Figure S5) brings about red color in **1** in its methanolic solution. That way, **1** is akin to nitrocyanin. The geometry optimized structures of **1** and zinc(II) compound at the same coordination environment are shown in Figure S4.

3.3. Molecular structure of $[\text{Cu}_2(\mu\text{-Br})_2(\text{L})_2]$ (**1**)

The X-ray crystal structure (Figure 2) of **1** has been determined. **1** is a bis(μ -bromo)-bridged dimeric copper(II) complex. It is a centrosymmetric copper(II) dimer with two CuLBr sub-units. Each penta-coordinated copper center in **1** is in “ N_2OBr_2 ” coordination environment. Each copper center in **1** enjoys three donations from the approaching ligand moiety. One is oxygen (O1) from enol moiety and the two others are one nitrogen (N1) from the benzothiazole ring and one imine nitrogen (N3) of Schiff base. This penta-coordination around each copper center has been fulfilled by the additional donation of two symmetrically disposed doubly bridged bromide centers, (Br1) and (Br1#1) (Figure S6).

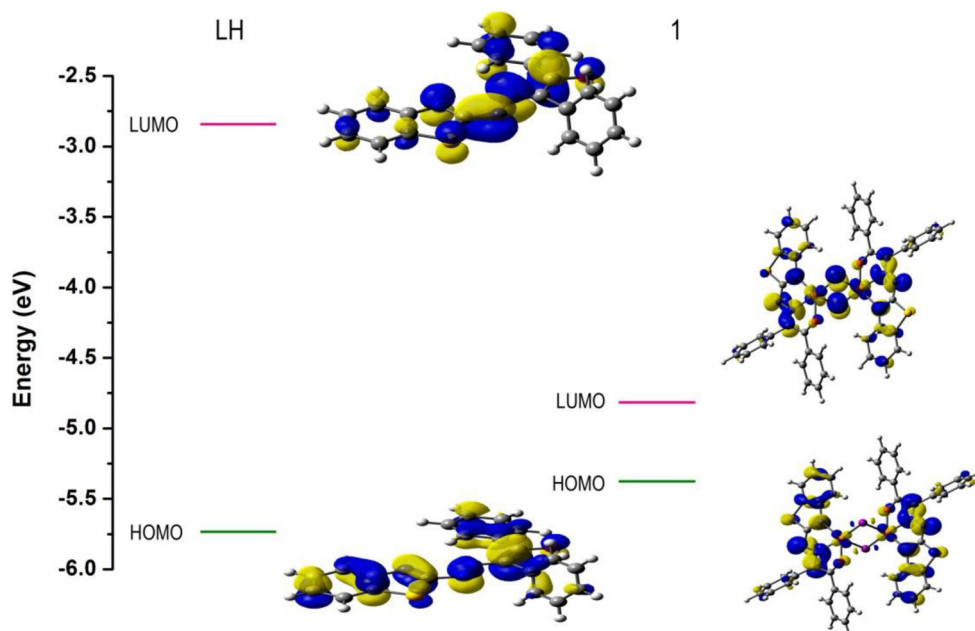


Figure 1. HOMO, LUMO energy and their contour diagram of orbitals of LH and **1**.

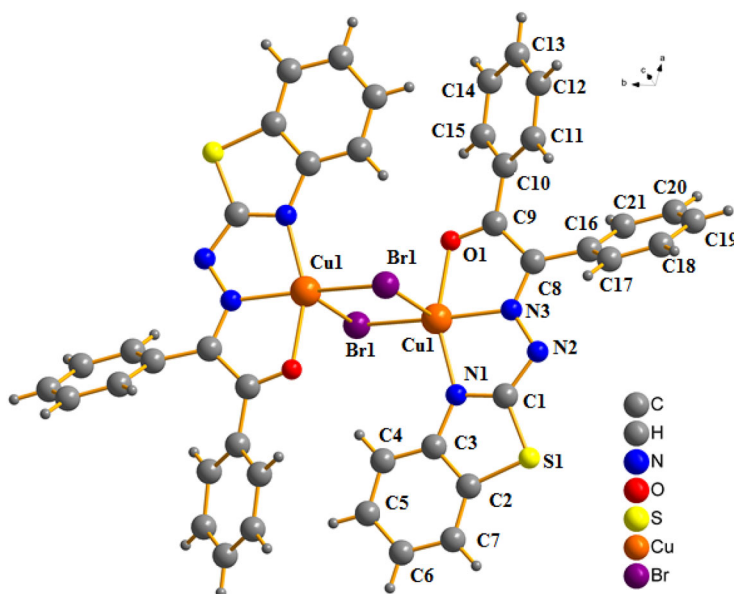


Figure 2. Molecular structure of **1** in ball and stick diagram.

Here, each metal center prefers to adopt the square pyramidal geometry rather than trigonal bipyramidal geometry. To augment the geometry around each copper center in **1**, we have determined the geometry index or structural parameter (τ). For the penta-coordinated complex this geometry index or structural parameter (τ_5) may either be zero or unity. The trigonality index (τ_3) value is zero for a regular square

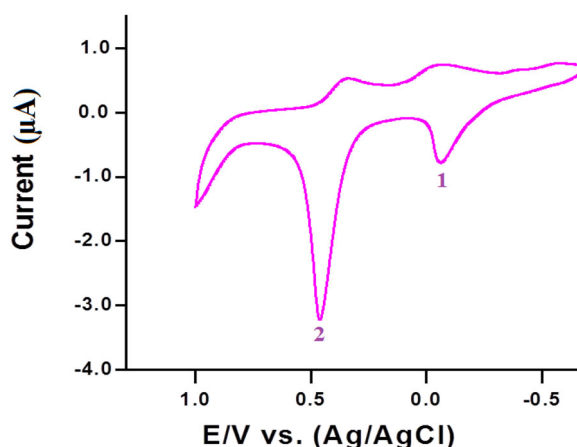


Figure 3. CV of **1** in methanol at a scan rate of 100 mV s^{-1} . Analyte conc. was $3.22 \times 10^{-4} \text{ M}$.

pyramidal geometry and is of unity for a perfectly trigonal bipyramidal geometric disposition [53–55]. Now, considering $\text{N}(3)\text{--Cu}(1)\text{--Br}(1) = 165.22^\circ$ and $\text{N}(1)\text{--Cu}(1)\text{--O}(1) = 156.22^\circ$ as the two largest angles around each copper center in **1**, the τ_5 value comes out 0.15. Thus, the geometry around each copper center in **1** is square pyramidal with some degree of distortion. The structural core in **1** has also been characterized by the Cu–Cu distance of 3.486 \AA and an acute angle of $\text{Cu}1\text{--Br}1\text{--Cu}1\#1$, 84.76° . From the X-ray crystallographic data it is revealed that the four basal bonds $\text{Cu}1\text{--N}3$, $\text{Cu}1\text{--N}1$, $\text{Cu}1\text{--O}1$ and $\text{Cu}1\text{--Br}1$ are 1.970 , 2.006 , 2.036 and 2.381 \AA , respectively. Collectively they form the square-based basal plane around Cu1. The $\text{Cu}1\text{--Br}1\#1$ bond is longer and Br1#1 occupies the apical site of the square-based pyramid around Cu1. The $\text{Cu}1\text{--Br}1\#1$ bond distance (2.773 \AA) is longer in comparison to earlier reports for analogous chloro-bridged Cu(II) dimers [21, 56]. For ready reckoning, Cu...Cu distance as found earlier for mode I (Scheme 1) is 3.626 \AA and $\text{Cu}1\text{--Br}1\text{--Cu}2$ angle is 87.00° [24]. For bridging modes II and III, the Cu...Cu distances are found, respectively, to be 3.714 and 3.803 \AA , while Cu–Br–Cu angles, respectively, are 85.51 and 92.14° . In **1**, copper-to-copper separation is 3.486 \AA and the respective angle is 84.76° . Thus, Cu...Cu bond distance in **1** is found to be shorter. However, the $\text{Cu}1\text{--Br}1\#1$ bond distance (2.773 \AA) is comparable with the respective bond distance value (2.706 \AA) as observed previously for a bis(μ -bromo)-bridged copper(II) dimer having “ N_2Br_3 ” donor sites [22]. In **1**, copper-to-copper bond distance (3.486 \AA) is found to be longer when compared to analogous chloro-bridged dimer with the same ligand [21].

3.4. Electrochemistry

The redox property of **1** was studied by CV in methanol (Figure 3) with a GC electrode at a scan rate of 100 mV s^{-1} under N_2 atmosphere. Two oxidative peaks were observed for **1** on the positive side of Ag/AgCl reference electrode. The corresponding reductive peaks were also found. The CV data for **1** is shown in Table 3. LH was found to be potentially inert within our potential domain of interest. Thus, the observed redox response is truly metal centered. Comparing with the standard redox couple,

Table 3. Cyclic voltammetric data for **1**.

$E_{pa1}(i_{pa1})$	$E_{pc1}(i_{pc1})$	$E_{1/2}(1)$	$I_{pc}/I_{pa}(1)$	$E_{pa2}(i_{pa2})$	$E_{pc2}(i_{pc2})$	$E_{1/2}(2)$	$I_{pc}/I_{pa}(2)$
0.076 (7.49)	0.072 (7.55)	0.074	1.05	0.35 (5.072)	0.465 (33.88)	0.408	6.679

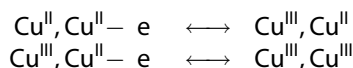
E_{pc1} , E_{pc2} = cathodic peak potential, V; E_{pa1} , E_{pa2} = anodic peak potential, V; i_{pc1} , i_{pc2} = cathodic peak current, μA ; i_{pa1} , i_{pa2} = anodic peak current, μA ; $E_{1/2} = 0.5(E_{pc} + E_{pa})$, V.

Fc/Fc^+ , it can be inferred that each redox couple as observed here involves only one electron. Accordingly, the observed response can be assigned as one electron two-step process involving one electron in each step.

Couple 2 is irreversible, whereas couple 1 is almost quasi-reversible in nature. The i_{pc}/i_{pa} value for couple 2 is 6.679 in **1**. During CV experiment a mixed-valence species, $Cu(III)/Cu(II)$, is formed in the intermediate redox step. For such type of mixed-valence species, the extent of stability can be realized electrochemically by evaluating conproportionation constant (K_{con}). The conproportionation constant may be represented as:

$$K_{con} = \frac{[Cu(III)Cu(II)]^2}{[Cu(III)Cu(III)][Cu(II)Cu(II)]} = \exp \left[\frac{nF(\Delta E)}{RT} \right]$$

where $\Delta E = [E_{1/2}(Ox2) - E_{1/2}(Ox1)]$. The greater is the stability of the mixed valence species, the higher is the value of K_{con} [57, 58]. The magnitude of K_{con} was found to be 3.72×10^3 by taking ΔE for **1** as 0.378 V *versus* SCE (after reference conversion to SCE). The stability of the mixed-valence species also depends on ligand unsaturation [59]. The redox response in **1** can be written as:



For dinuclear copper(II) system, similar redox response is, however, known [21, 60].

3.5. DNA and RNA binding aspect

3.5.1. Spectrophotometric study

Absorption spectroscopy is one of the powerful techniques commonly employed to characterize ligand and complex and their binding with nucleic acids. We have a characteristic spectrum of both **1** and LH in the wavelength of 300–600 nm range. **1** has a characteristic band at 535 nm, while LH has a band at 355 nm. The absorption intensity of **1** and LH decreases gradually with increasing concentration of both CT DNA and Poly(A) but the magnitude of decrement is higher for ligand in comparison to the complex. Poly(A) shows much higher hypochromic effect with ligand than CT DNA (Figures 4 and S7). This hypochromic effect is indicative of strong intermolecular interaction involving effective overlap of the π -electron cloud of **1** and LH with those base pairs of nucleic acids. The affinity constant values were calculated for each system with the B-H plots (Figure S8) and equation as described in Section 2.5.1. The binding affinity (K) values follow the trend ligand-Poly(A) > ligand-CT DNA > complex-Poly(A) > complex-CT DNA. The observed values are shown in Table 4.

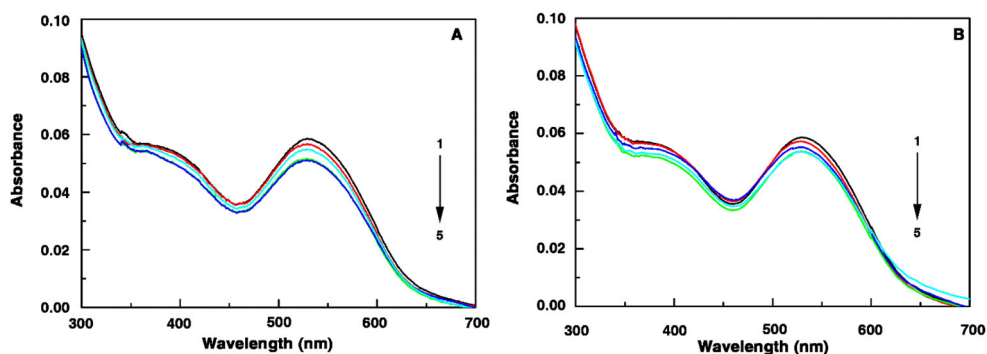


Figure 4. Change of absorption spectra of complex (curve 1) on increasing concentration of (A) CT DNA and (B) Poly(A) (curves 2–5).

Table 4. Binding parameters as obtained from absorption spectroscopy.

System	$K \times 10^{-4} \text{ (M}^{-1}\text{)}$
Ligand + DNA	1.013 ± 0.05
Ligand + Poly(A)	1.238 ± 0.02
Complex + DNA	0.779 ± 0.03
Complex + Poly(A)	0.912 ± 0.06

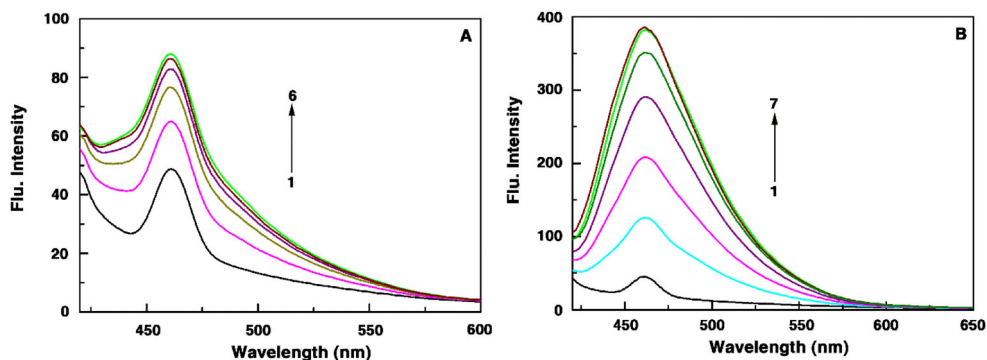


Figure 5. Fluorescence titration of complex (curve 1) with increasing concentration of (A) CT DNA (curves 2–6) and (B) Poly(A) (curves 2–7).

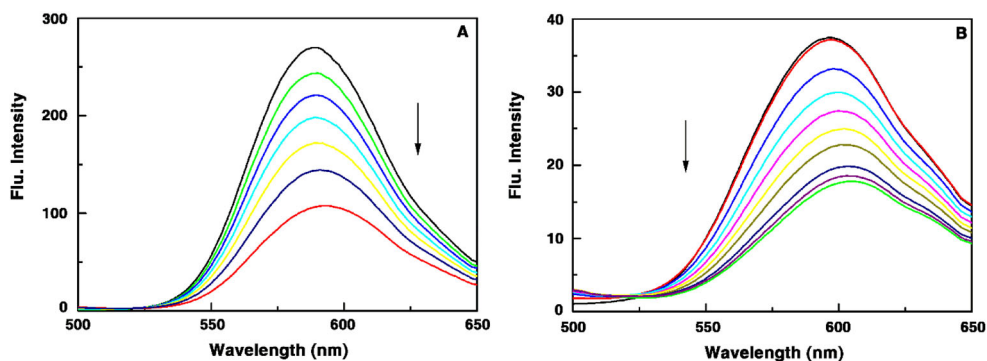
3.5.2. Spectrofluorimetric study

The interaction of **1** and LH with CT DNA and Poly(A) was further characterized by spectrofluorimetric study. We have a characteristic fluorescence spectrum for **1** and LH in the 400–650 nm wavelength range. Complex has a maximum value at 460 nm. The intensity was enhanced with gradual addition of both DNA and Poly(A) which indicates the strong association of nucleic acid with complex (Figure 5).

Bare LH displays a low-intensity band at 403 nm, but on complexation with CT DNA, a new band at 430 nm emerges (Figure S9). With Poly(A) this new band comes out at 450 nm. This authenticates that LH undergoes strong binding in both DNA and Poly(A) with concomitant emergence of new bands of pronounced intensity. The observed magnitude of band-intensity enhancement was maximum for ligand-Poly(A) binding followed by ligand-DNA, complex-Poly(A) and the complex-DNA.

Table 5. Binding parameters as observed from fluorescence spectroscopy.

System	$K \times 10^{-4} \text{ (M}^{-1}\text{)}$
Ligand + DNA	1.010 ± 0.05
Ligand + Poly(A)	1.275 ± 0.03
Complex + DNA	0.987 ± 0.01
Complex + Poly(A)	1.064 ± 0.02

**Figure 6.** Quenching of fluorescence intensity of (A) EB-CT DNA and (B) EB-Poly(A) complex with addition of increasing concentration of **1**.

The binding values as determined by us from UV-vis titration also follow the same trend. The sequence runs as ligand-Poly(A) > ligand-CT DNA > complex-Poly(A) > complex-CT DNA. All the binding constants were calculated from the B-H plot and are listed in Table 5 (Figure S10).

3.5.3. Ethidium bromide displacement assay

Ethidium bromide (EB) displacement assay was employed for the determination of mode of binding of complex and ligand with nucleic acids. EB is a well-known classical DNA-intercalator commonly used as a fluorescent tag. On displacement of EB from its EB-DNA complex by a molecule, the fluorescence intensity lessens. This is suggestive of the intercalation of the molecule inside the helix. On addition of **1** to the EB-DNA and EB-Poly(A) complex, we observed a quenching in fluorescence intensity and it reaches half of the initial value after addition of $21 \mu\text{M}$ and $39 \mu\text{M}$ concentration of **1** for EB-DNA and EB-Poly(A), respectively (Figures 6 and S11). It indicates the intercalative nature of the binding of complex with DNA and partial intercalative binding or groove binding nature of complex with Poly(A) as the IC_{50} value was high for Poly(A).

On gradual addition of LH to EB-DNA and EB-Poly(A) complex, no significant change was observed in fluorescence intensity although LH binds both CT DNA and Poly(A) more strongly than complex. Thus, we can conclude that LH is unable to displace EB from its complex with DNA and Poly(A). This observation indicates possible groove-binding or partial intercalative binding nature of ligand towards the nucleic acid.

Table 6. Thermodynamic parameters as obtained from temperature dependent fluorescence study.

System	ΔG^0 (kcal/mol)	ΔH^0 (kcal/mol)	$T\Delta S^0$ (kcal/mol)
Ligand + DNA	−5.462	−8.187	−2.724
Ligand + Poly(A)	−5.600	−7.718	−2.118
Complex + DNA	−5.448	−7.829	−2.381
Complex + Poly(A)	−5.496	−7.787	−2.292

3.5.4. Thermodynamics of the interaction

Temperature-dependent fluorescence titration studies were carried out at three different temperatures and binding constant values were calculated as described in the material method section by B-H plots. This is also used to determine the thermodynamic parameters of the binding phenomenon of complex and ligand with DNA and Poly(A). The thermodynamic parameters were calculated by using van't Hoff plots. The values of the thermodynamic parameters for both the complex and ligand with CT DNA and Poly(A) are given in Table 6.

The van't Hoff plot for binding is presented in Figure S12. Thermodynamic parameters, presented in Table 6, show that the binding was driven by negative enthalpy and entropy change in every case.

Common forms of interaction between small molecules and macromolecules are hydrogen bonding, van der Waals forces, hydrophobic and electrostatic interaction. From the underlying thermodynamic parameters, we can predict those binding modes. The values of positive enthalpy ($\Delta H > 0$) and entropy ($\Delta S > 0$) changes suggest a hydrophobic interaction, while van der Waals force or hydrogen bond formation may occur when the enthalpy ($\Delta H < 0$) and entropy ($\Delta S < 0$) changes become negative [61]. In our case, the negative enthalpy and entropy changes for the binding process indicates that the binding may occur *via* van der Waals interaction or hydrogen bond formation.

3.5.5. Circular dichroism studies

Conformational changes of CT DNA and Poly(A) due to the interaction with the Cu complex and ligand were followed by circular dichroism studies. The CD spectra of DNA and Poly(A) are shown in Figure 7. DNA has a characteristic positive band at 275 nm and a negative band at 245 nm in its CD spectrum due to base stacking and polynucleotide helicity, respectively. Here we observed a distinct change in CD spectrum of CT DNA due to association with **1** and LH as represented in Figure 7(A,C). Poly(A) shows characteristic positive and negative bands at 265 and 247 nm, respectively. The spectral pattern of Poly(A) was also changed in the presence of both the complex and ligand as shown in Figure 7(B, D). Although the magnitude of the spectral changes of both DNA and Poly(A) were not very large but the nature of the spectral changes indicates that both the complex and ligand bind with DNA and Poly(A).

1 shows groove-binding with CT-DNA as has been deciphered from our molecular docking studies. Secondary structure of DNA is perturbed markedly by the intercalative binding of DNA with small molecules [62, 63]. However, groove-binding imparts substantially low impact on the native CD spectra of nucleic acids. This situation has been demonstrated recently for copper(II) systems stabilized from Schiff base ligands [64]. **1**,

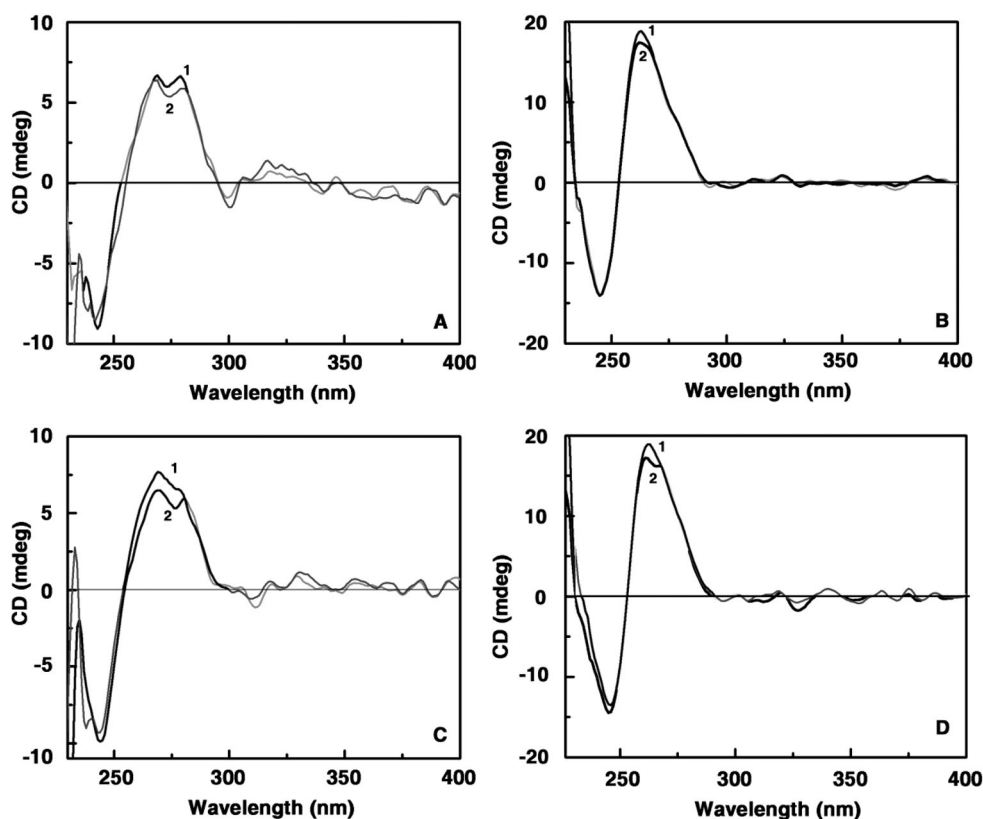


Figure 7. CD spectra of (A) free CT DNA (1) and CT DNA in presence of Cu complex (2), (B) free poly(A) (1) and poly(A) in the presence of Cu complex (2), (C) free CT DNA (1) and CT DNA in the presence of ligand (2) and (D) free poly(A) (1) and poly(A) in the presence of ligand (2).

a copper(II) dimer, generated out of a Schiff base ligand, also shows groove-binding as evidenced from our CD spectra.

3.6. Molecular docking

To have an idea about the possible location of LH and **1** in the DNA environment, we have taken recourse to molecular modelling study. The details of the adopted method are given in [Section 2.5.5](#). [Figure 8](#) represents the docked conformation of LH and **1** with DNA.

It is observed that major groove of DNA is the most suitable position for the binding in the case of LH. However, for **1** minor groove is the most suitable position. The free energies of binding for LH and **1** with DNA were found to be -5.82 and $-5.26 \text{ kcal mol}^{-1}$, respectively, as revealed from molecular docking analyses. Respective binding constants as found from molecular docking were 1.54×10^4 and $1.01 \times 10^4 \text{ M}^{-1}$ for LH and **1**, respectively. The data as obtained from the molecular docking analyses are in good concordance with that obtained from UV-vis and fluorescence titrimetric analyses. In both cases, the possible contribution of negative free energy change for the binding process may be attributed due to the van der Waals

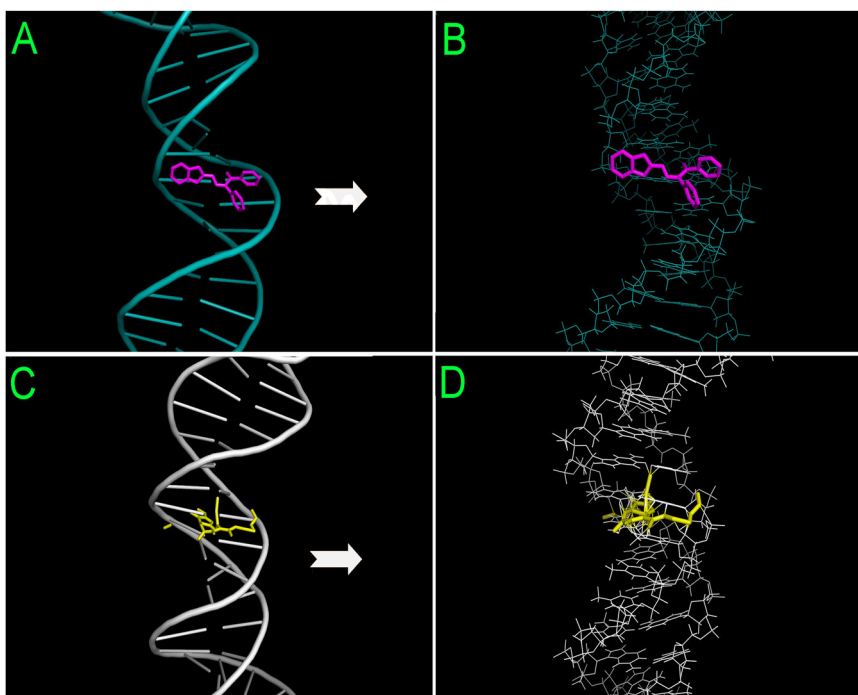


Figure 8. Stereo-view of the docked conformation of LH (A and B) and **1** (C and D) with CT DNA.

stacking interactions, hydrophobic as well as weak electrostatic interactions. Hydrophobic interaction and van der Waals contacts along with H-bonding by N or O atom may contribute to the stronger binding of ligand to CT DNA compared to **1**.

The magnitude of binding constant is a useful parameter to assess the binding abilities of small molecules with nucleic acids. Here for **1**, the binding constant values with DNA and RNA are found, respectively, to be 0.779×10^4 and $0.912 \times 10^4 \text{ M}^{-1}$. These values are close to the respective values, 7.6×10^3 and $6.5 \times 10^3 \text{ M}^{-1}$, as have been reported for a mononuclear copper(II) complex [65]. **1** shows higher RNA binding abilities than DNA. This is indicative of the inherent hypochromic effect of RNA. Again, the binding constant value as obtained for azo-bridged binuclear copper(II) complex with DNA was found to be $17.75 \times 10^4 \text{ M}^{-1}$ [66]. Most likely this higher value owes to the bridging azo moieties. The DNA binding constant values as obtained for a group of mononuclear copper(II) complexes, derived from a Schiff base ligand, were found to be 7.35×10^4 , 2.51×10^4 , 3.46×10^4 and $0.94 \times 10^4 \text{ M}^{-1}$ [67]. These values are akin to us.

4. Conclusion

We have synthesized and characterized a novel centrosymmetric bis(μ -bromo)-bridged red copper(II) dimer (**1**) from our previously reported Schiff base ligand, 2-(benzothiazol-2-yl-hydrazono)-1,2-diphenyl-ethanone (LH). The X-ray crystal structure of **1** has been determined. In CV, **1** generates a mixed-valence species. The DNA and Poly(A)

binding aspects of both LH and **1** have been demonstrated by several spectrophotometric and spectrofluorimetric methods. Docked conformer of LH reveals its major DNA-groove binding, while **1** is a minor DNA-groove binder. Comparing with our earlier report, it is evident that chloro-bridged copper(II) dimer of LH is superior to its bromo counterpart (**1**) in terms of DNA-binding. Most likely this is due to the presence of bulky bromide bridges. However, studies on DNA- and RNA-binding aspects of symmetric bromo-bridged copper(II) dimer is hitherto unprecedented. In this perspective, the significance and prospect of the present work is apparent.

Acknowledgements

We solicit to thank our esteemed reviewers for valuable suggestions to put the entire work into context.

Disclosure statement

No potential conflict of interest was reported by the authors.

Funding

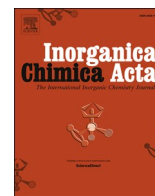
NKM gratefully acknowledges the University Grants Commission, New Delhi, India for his fellowship. Financial support received from Jadavpur University, Kolkata 700 032, India under RUSA 2.0 is sincerely acknowledged.

References

- [1] O. Kahn. *Acc. Chem. Res.*, **33**, 647 (2000).
- [2] E. Pardo, J. Faus, M. Julve, F. Lloret, M.C. Muñoz, J. Cano, X. Ottenwaelde, Y. Journaux, R. Carrasco, G. Blay, I. Fernández, R. Ruiz-García. *J. Am. Chem. Soc.*, **125**, 10770 (2003).
- [3] X. Zhang, Y. Wang, Q. Zhang, Z. Yang. *Spectrochim. Acta A*, **77**, (2010).
- [4] L.M. López-Martínez, H. Santacruz-Ortega, R.E. Navarro, M. Inoue, R. Sugich-Miranda, J. Hernández-Paredes, I. Castillo, R.R. Sotelo-Mundo. *Polyhedron*, **127**, 438 (2017).
- [5] S. Das, C. Madhavaiah, S. Verma, P.K. Bharadwaj. *Inorg. Chim. Acta*, **358**, 3236 (2005).
- [6] S. Thyagarajan, N.N. Murthy, A.A.N. Sarjeant, K.D. Karlin, S.E. Rokita. *J. Am. Chem. Soc.*, **128**, 7003 (2006).
- [7] R.H. Holm, P. Kennepohl, E.I. Solomon. *Chem. Rev.*, **96**, 2239 (1996).
- [8] R.L. Lieberman, A.C. Rosenzweig. *Nature*, **434**, 177 (2005).
- [9] S. Koner, S. Saha, T. Mallah, K.I. Okamoto. *Inorg. Chem.*, **43**, 840 (2004).
- [10] S. Shit, P. Talukder, J. Chakraborty, G. Pilet, M. Salah El Fallah, J. Ribas, S. Mitra. *Polyhedron*, **26**, 1357 (2007).
- [11] J.A.R. Navarro, M.A. Romero, J.M. Salas, M. Quirós, E.R.T. Tiekink. *Inorg. Chem.*, **36**, 4988 (1997).
- [12] H. Endres, D. Noethe, E. Rossato, W.E. Hatfield. *Inorg. Chem.*, **23**, 3467 (1984).
- [13] M.G. Alvarez, G. Alzueta, J. Borrás, M. Pitié, B. Meunier. *J. Biol. Inorg. Chem.*, **8**, 644 (2003).
- [14] S.-C. Cheng, H.-H. Wei. *Inorg. Chim. Acta*, **340**, 105 (2002).
- [15] L.-P. Lu, M.-L. Zhu, P. Yang. *J. Inorg. Biochem.*, **95**, 31 (2003).
- [16] E. Ruiz, P. Alemany, S. Alvarez, J. Cano. *J. Am. Chem. Soc.*, **119**, 1297 (1997).
- [17] D. Li, S. Li, D. Yang, J. Yu, J. Huang, Y. Li, W. Tang. *Inorg. Chem.*, **42**, 6071 (2003).
- [18] T.S. Lobana, R.J. Butcher. *Transi. Met. Chem*, **29**, 291 (2004).

- [19] T.S. Lobana, S. Khanna, R.J. Butcher, A.D. Hunter, M. Zeller. *Inorg. Chem.*, **46**, 5826 (2007).
- [20] F.J. Rietmeijer, R.A.G. De Graaff, J. Reedijk. *Inorg. Chem.*, **23**, 151 (1984).
- [21] B. Guhathakurta, P. Basu, C.S. Purohit, N. Bandyopadhyay, G.S. Kumar, S. Chowdhury, J.P. Naskar. *Polyhedron*, **126**, 195 (2017).
- [22] M.A. Romero, J.M. Salas, M. Quirós, M.P. Sánchez, J. Romero, D. Martín. *Inorg. Chem.*, **33**, 5477 (1994).
- [23] P. Singh, D.Y. Jeter, W.E. Hatfield, D.J. Hodgson. *Inorg. Chem.*, **11**, 1657 (1972).
- [24] W.E. Marsh, T.L. Bowman, W.E. Hatfield, D.J. Hodgson. *Inorg. Chim. Acta*, **59**, 19 (1982).
- [25] H. Endres. *Acta Crystallogr. B Struct. Sci.*, **34**, 3736 (1978).
- [26] C.P. Landee, R.E. Greeney. *Inorg. Chem.*, **25**, 3771 (1986).
- [27] S. Chakrabarty, P. Sarkhel, R.K. Poddar. *Inorg. Chem.*, **61**, 3260 (2008).
- [28] R. Li, B. Moubaraki, K.S. Murray, S. Brooker. *Dalton Trans.*, **37**, 6014 (2008).
- [29] D.K. Towle, S.K. Hoffmann, W.E. Hatfield, P. Singh, P. Chaudhuri, K. Wiegardt. *Inorg. Chem.*, **24**, 4393 (1985).
- [30] D. Žilić, B. Rakvin, D. Milić, D. Pajić, I. Dilović, M. Cametti, Z. Džolić. *Dalton Trans.*, **43**, 11877 (2014).
- [31] A. Shirvan, H. Golchoubian, E. Bouwman. *J. Mol. Struct.*, **1195**, 769 (2019).
- [32] S. Zehra, T. Roisnel, F. Arjmand. *ACS Omega*, **4**, 7691 (2019).
- [33] F. Arjmand, Z. Afsan, T. Roisnel. *RSC Adv.*, **8**, 37375 (2018).
- [34] P. Basu, D. Bhowmik, G.S. Kumar. *J. Photochem. Photobiol. B: Biol.*, **129**, 57 (2013).
- [35] C. Ciatto, M.L. D'Amico, G. Natile, F. Secco, M. Venturini. *Biophys. J.*, **77**, 2717 (1999).
- [36] M.J. Frisch, G.W. Trucks, H.B. Schlegel, G.E. Scuseria, M.A. Robb, J.R. Cheeseman, G. Scalmani, V. Barone, B. Mennucci, G.A. Petersson, H. Nakatsuji, M. Caricato, X. Li, H.P. Hratchian, A.F. Izmaylov, J. Bloino, G. Zheng, J.L. Sonnenberg, M. Hada, M. Ehara, K. Toyota, R. Fukuda, J. Hasegawa, M. Ishida, T. Nakajima, Y. Honda, O. Kitao, H. Nakai, T. Vreven, J.A. Montgomery, Jr., J.E. Peralta, F. Ogliaro, F. Bearpark, J.J. Heyd, E. Brothers, K.N. Kudin, V.N. Staroverov, R. Kobayashi, J. Normand, K. Raghavachari, A. Rendell, J.C. Burant, S.S. Iyengar, J. Tomasi, M. Cossi, N. Rega, J.M. Millam, M. Klene, J.E. Knox, J.B. Cross, V. Bakken, C. Adamo, J. Jaramillo, R. Gomperts, R.E. Stratmann, O. Yazyev, A.J. Austin, R. Cammi, C. Pomelli, J.W. Ochterski, R.L. Martin, K. Morokuma, V.G. Zakrzewski, G.A. Voth, P. Salvador, J.J. Dannenberg, S. Dapprich, A.D. Daniels, O. Farkas, J.B. Foresman, J.V. Ortiz, J. Cioslowski, D.J. Fox. *Gaussian 09, Revision C.01*, Gaussian Inc., Wallingford, CT (2009).
- [37] A.D. Becke. *J. Chem. Phys.*, **98**, 5648 (1993).
- [38] C. Lee, W. Yang, R.G. Parr. *Phys. Rev. B*, **37**, 785 (1988).
- [39] P.J. Hay, W.R. Wadt. *J. Chem. Phys.*, **82**, 299 (1985).
- [40] W.J. Hehre, R. Ditchfield, J.A. Pople. *J. Chem. Phys.*, **56**, 2257 (1972).
- [41] J.D. Dill, J.A. Pople. *J. Chem. Phys.*, **62**, 2921 (1975).
- [42] P.C. Hariharan, J.A. Pople. *Theoret. Chim. Acta*, **28**, 213 (1973).
- [43] T. Clark, J. Chandrasekhar, G.W. Spitznagel, P. von Rague Schleyer. *J. Comput. Chem.*, **4**, 294 (1983).
- [44] H.A. Benesi, J.H. Hildebrand. *J. Am. Chem. Soc.*, **71**, 2703 (1949).
- [45] K. Bhadra, M. Maiti, G.S. Kumar. *Biochim. Biophys. Acta*, **1770**, 1071 (2007).
- [46] P. Basu, G.S. Kumar. *RSC Adv.*, **5**, 29953 (2015).
- [47] J.-H. Tan, Y.-J. Lu, Z.-S. Huang, L.-Q. Gu, J.-Y. Wu. *Eur. J. Med. Chem.*, **42**, 1169 (2007).
- [48] Bruker. *SMART (Version 5.0) and SAINT (Version 6.02)*, Bruker AXS Inc., Madison, WI, USA (2000).
- [49] G.M. Sheldrick. SADABS, program for empirical correction of area detector data, University of Göttingen, Germany (2000).
- [50] G.M. Sheldrick. SHELXS97 and SHELXL97, program for crystal structure refinement, University of Göttingen, Germany (1997).
- [51] R.L. Lieberman, D.M. Arciero, A.B. Hooper, A.C. Rosenzweig. *Biochemistry*, **40**, 5674 (2001).
- [52] N.K. Shee, S.G. Patra, M.G.B. Drew, D. Datta. *J. Coord. Chem.*, **69**, 3691 (2016).
- [53] A.W. Addison, T.N. Rao, J. Reedijk, J.V. Rijn, G.C. Verschoor. *Dalton Trans.*, 1349 (1984).

- [54] K.P. Maresca, G.H. Bonavia, J.W. Babich, J. Zubieta. *Inorg. Chim. Acta*, **284**, 252 (1999).
- [55] M. Li, A. Ellern, J.H. Espenson. *Inorg. Chem.*, **44**, 3690 (2005).
- [56] G.R. Desiraju, H.R. Luss, D.L. Smith. *J. Am. Chem. Soc.*, **100**, 6375 (1978).
- [57] S.K. Mondal, L.K. Thompson, K. Nag, J.P. Charland, E.J. Gabe. *Inorg. Chem.*, **26**, 1391 (1987).
- [58] W. Zhang, S. Liu, C. Ma, D. Jiang. *Polyhedron*, **17**, 3835 (1998).
- [59] J.P. Naskar, C. Biswas, B. Guhathakurta, N. Aliaga-Alcalde, L. Lu, M. Zhu. *Polyhedron*, **30**, 2310 (2011).
- [60] J.P. Naskar, B. Guhathakurta, L. Lu, M. Zhu. *Polyhedron*, **43**, 89 (2012).
- [61] X.-B. Fu, G.-T. Weng, D.-D. Liu, X.-Y. Le. *J. Photochem. Photobiol. A: Chem.*, **276**, 83 (2014).
- [62] S.S. Jain, M. Polak, N.V. Hud. *Nucleic Acids Res.*, **31**, 4608 (2003).
- [63] J.L. Mergny, G. Duval-Valentin, C.H. Nguyen, L. Perrouault, B. Faucon, M. Rougee, T. Montenay-Garestier, E. Bisagni, C. Helene. *Science*, **256**, 1681 (1992).
- [64] S. Banerjee, P. Ghorai, P. Brandao, D. Ghosh, S. Bhuiya, D. Chattopadhyay, S. Das, A. Saha. *New J. Chem.*, **42**, 246 (2018).
- [65] M. Tripathi, G.C. Giri, D. Das, R. Pande, S. Sarkar, S. Giri, G. Roymahapatra, A. Sarkar. *Nucleotides Nucl. Acids*, **37**, 563 (2018).
- [66] A. Pradhan, S. Halder, K.B. Mallik, M. Ghosh, M. Bera, N. Sepay, D. Schollmeyer, S.K. Ghatak, S. Roy, S. Saha. *Inorg. Chim. Acta*, **484**, 197 (2019).
- [67] S. Kathiresan, S. Mugesh, J. Annaraj, M. Murugan. *New J. Chem.*, **41**, 1267 (2017).



Synthesis, characterization, structure, *in vitro* enzymatic activity and sensing aspects of a copper(II) complex stabilized from a naphthaldehyde based Schiff base ligand

Naba Kr Mandal^a, Nirmalya Bandyopadhyay^a, Priyanka Arya^b, Shubhamoy Chowdhury^c, Neera Raghav^b, Jnan Prakash Naskar^{a,*}

^a Department of Chemistry, Jadavpur University, Kolkata 700 032, India

^b Department of Chemistry, Kurukshetra University, Kurukshetra 136 119, Haryana, India

^c Department of Chemistry, Gour Banga University, Malda, West Bengal 732 103, India

ARTICLE INFO

Keywords:

Schiff base
Copper
Structure
Enzymatic activity
Molecular docking
Fluorescence quenching

ABSTRACT

A mononuclear copper(II) complex, $[\text{CuL}(\text{ClO}_4)(\text{H}_2\text{O})]\cdot\text{THF}$ (**1**), from a naphthaldehyde based Schiff base probing ligand, 1-(benzothiazol-2-yl-hydrazonomethyl)-naphthalen-2-ol (**LH**), has been prepared and characterized by FT-IR, UV-vis, EPR, CHN analysis, electrical conductivity and magnetic susceptibility measurements. The X-ray crystal structure of **1** has also been determined. *In vitro* enzymatic activity of **LH** and **1** on digestive enzymes like amylase, trypsin and lipase has been investigated. Molecular docking studies have also been performed to corroborate this bioactivity. **LH** displays quenching of fluorescence intensity only upon addition of a Cu^{2+} ion at 459 nm. Other metal ions under present study, however, offer no influence. The low limit of detection value, 0.35 μM , indicates that **LH** offers high selectivity towards Cu^{2+} . Calculations at the level of DFT were also undertaken to have an insight into the electronic environment of both **LH** and **1**.

1. Introduction

Digestive enzymes help in the digestion of food stuffs into proper simple subunits to be fit for subsequent absorption. Studies on digestive enzymes primarily help to monitor nutrient digestibility. Moreover, digestive enzymes are important from the point of view of medicinal research as well as industrial applications [1]. Digestive enzymes span from microscopic to macroscopic living organisms. For ready reckoning, the role of energy currency as required to assemble the different bacterial cell constituents can be mentioned. This requisite energy is derived from the breaking down of various organic substrates like starch, lipids and proteins aided by digestive enzymes [2]. Amylase enzymes help to hydrolyze polysaccharide starch molecules [3]. Lipase enzymes hydrolyze long chain triglycerides. They aid in biotechnological applications [4]. Schiff base metal complexes offer a plethora of pharmacological attributes leading to their prospective biomedical applications [5]. Schiff base metal complexes display anti-microbial, antiviral, anti-fungal, anti-inflammatory and anti-cancer properties [6]. However, to the best of our knowledge, studies of Schiff base copper(II) complexes on digestive enzymes is rare indeed. Of late extracellular

amylase production, accentuated by a tetra-dentate Schiff base copper (II) complex, has been reported [7]. Copper(II) complex from a Schiff base ligand towards trypsin inhibition is also known [8]. Strikingly, the lipase activity of any Schiff base copper(II) complex evaded earlier attention.

Chemosensors are compounds that selectively bind specific counterparts with noticeable changes in their optical signal, magnetic property, electrical property and many other attributes. Fluorescent chemosensors have drawn unabated contemporary interest because of their potential implications in environmental and medicinal research. Fluorescent sensors manifest ubiquitous advantages due to their convenient handling, high specificity coupled with pronounced sensitivity [9]. Copper, the third most abundant element in the human body after iron and zinc, plays a crucial role in diverse biological processes like oxygen transport activation, signal transduction and cellular energy generation [10]. However, owing to its inherent toxicity, copper is a significant pollutant to natural environment and habitat as well [11]. In this perspective, selective but sensitive sensing of copper is of utmost importance. Over the past several years, a good number of fluorescence based chemosensors have been reported emphasizing the detection of

* Corresponding author.

E-mail address: jpnaskar@rediffmail.com (J. Prakash Naskar).

<https://doi.org/10.1016/j.ica.2022.121229>

Received 1 August 2022; Received in revised form 26 September 2022; Accepted 27 September 2022

Available online 30 September 2022

0020-1693/© 2022 Elsevier B.V. All rights reserved.

copper(II) ions [12]. The World Health Organization (WHO) recommends 10–12 mg/day of copper(II) intake for an adult human being. Again, the average concentration of blood copper under normal physiological conditions should not exceed the limit of 100–150 µg/dL (15.7–23.6 µM) [13]. Imbalance of Cu²⁺ poses serious health hazards like gastrointestinal catarrh, hypoglycemia, dyslexia Menke's and Wilson's [14] and Alzheimer's diseases [15]. Fluorescent molecular probes can even quantitatively sense metal ions in biological samples [16].

Here we wish to report the interaction of a naphthaldehyde based Schiff base probing ligand, 1-(benzothiazol-2-yl-hydrazonomethyl)-naphthalen-2-ol (**LH**) and its mononuclear copper(II) complex, [CuL(ClO₄)(H₂O)].THF (**1**), with amylase, trypsin and lipase. We also wish to report a simple yet convenient method for the selective detection of copper(II) ions employing **LH** with a commendable low LOD value. The binding mode of **LH** with Cu²⁺ has been confirmed by the single crystal X-ray structure of its copper(II) complex. For copper(II) systems, the crystal structures are, however, known with its sensing probes [17].

2. Experimental

2.1. Materials and measurements

All analytical reagent grade chemicals were procured from commercial suppliers and were used as received without further purification. 2-hydroxy-1-naphthaldehyde and 2-hydrazino benzothiazole were purchased from Aldrich, USA. (St. Louis, MO, USA). Melting point of the probe was determined with the aid of an electro-thermal digital melting point apparatus (SUMSIM India). C, H and N microanalytical data were acquired on a Perkin-Elmer 2400II elemental analyzer. FT-IR spectra (KBr pellets) of both **LH** and **1** were recorded on a Perkin Elmer spectrophotometer. UV–vis absorption spectra were recorded on a Shimadzu UV-160A spectrophotometer. A Bruker DPX300 MHz spectrometer was used to run both ¹H NMR (300 MHz) and ¹³C NMR (76 MHz) spectra (in DMSO-d₆, reference: TMS) of **LH**. An ESI mass spectrum of **LH** was recorded on a Waters Q-TOF Micro YA263 spectrometer in acetonitrile in the positive ionization mode. Fluorescence emission spectra were run on a Perkin Elmer spectrophotometer (Model LS-55). Conductivity measurement of **1** was performed on a Systronics (India) direct reading conductivity meter (model 304) at room temperature. A PAR 155 vibrating sample magnetometer fitted with a walker scientific L75FBAL magnet, calibrated with Hg[Co(SCN)₄], was used to determine the magnetic susceptibility of **1** at room temperature. The magnetic susceptibility data were corrected for diamagnetism using Pascal's constants [18]. The program package GAUSSIAN-09 Revision C.01 was used for all calculations [19]. The gas phase geometries of the compounds were fully optimized with symmetry restrictions in the singlet ground state with the gradient-corrected DFT level coupled with B3LYP [20]. The LanL2DZ basis set was used for **LH** and **1** [21]. The HOMOs and LUMOs of **LH** and **1** were calculated with the TD-DFT method, and the solvent effect (in methanol) was simulated using the polarizing continuum model with the integral equation formalism (C-PCM) [22].

Powder X-ray diffraction analysis of **1** was done on a Bruker D8 advance X-ray diffractometer with Cu Kα radiation (λ = 1.548 Å) generated at 40 kV and 40 mA.

Caution: Perchlorate salts of metal complexes are potentially explosive [23]. It should be handled in small quantities with the utmost caution.

2.2. Synthesis

2.2.1. Synthesis of 1-(benzothiazol-2-yl-hydrazonomethyl)-naphthalen-2-ol (**LH**)

The Schiff base ligand (**LH**) was synthesized following the method reported earlier [24].

Yield: 0.028 g (89 %); m.p. 243–245 °C (lit. 242–243 °C); Anal. Calcd. for C₁₈H₁₃N₃OS: C, 67.69; H, 4.11; N, 13.16. Found: C, 67.66; H,

Table 1

Crystal data and structure refinement for **1**.

Complex	
CCDC No.	1,900,538
Empirical formula	C ₂₂ H ₂₂ N ₃ CuO ₇ SCl
Formula weight	571.47
Temperature [K]	293(2)
Wavelength [Å]	0.71073
Crystal system	Triclinic
Space group	P-1
Unit cell dimensions	
<i>a</i> [Å]	9.9550(2)
<i>b</i> [Å]	9.9777(2)
<i>c</i> [Å]	13.7706(3)
α [°]	105.8940(10)
β [°]	90.228(2)
γ [°]	117.2250(10)
Volume [Å ³]	1156.34(4)
Absorption coefficient [mm ⁻¹]	1.201
θ range for data collection	2.327° < θ < 30.565°
Absorption correction	Semi-empirical from equivalents
Refinement method	Full-matrix least-squares on <i>F</i> ²
<i>Z</i>	2
ρ _{calcd} [gm/cm ³]	1.641
<i>F</i> (000)	586
Crystal size [mm]	0.386 × 0.346 × 0.148
Limiting indices	−14 ≤ <i>h</i> ≤ 14 −14 ≤ <i>k</i> ≤ 14 −19 ≤ <i>l</i> ≤ 19
Reflections collected/unique	24728/7050 [Rint = 0.0396]
Data/restraints/parameters	7050/0/324
<i>R</i> ₁ , all data, <i>R</i> ₁ [<i>I</i> > 2σ(<i>I</i>)]	0.0613, 0.0403
<i>wR</i> ₂ , all data, <i>wR</i> ₂ [<i>I</i> > 2σ(<i>I</i>)]	0.1095, 0.0998
<i>S</i> on <i>F</i> ²	1.040
Largest diff. peak and hole [eÅ ⁻³]	0.451 and −0.339

4.13; N, 13.14; FT-IR (KBr, cm⁻¹): 3435(vb) [ν(O—H)], 2926(s) [ν(N—H)], 1624(s) [ν(C=N) of azomethine], 1587(w) [ν(C=N) of benzothiazole]; UV–vis (THF): λ (ε, M⁻¹cm⁻¹) = 407 (12 000), 381 (16 000), 335 (99 000), 248 (16 000), 244 (28 599) nm; ¹H NMR (300 MHz, DMSO-d₆) δ (ppm): 9.17 (s, 1H), 8.61 (s, 1H), 7.09–7.89 (ring proton, 10H), 4.01 (s, 1H); ¹³C NMR (76 MHz, DMSO-d₆, TMS) δ [ppm]: 166.362, 157.788, 110.175 and 118.897–132.723 (all aromatic carbons). ESI-MS (positive ion mode in CH₃CN) (*m/z*): 320.001 (calcd. 320.112) for [**LH** + H]⁺.

2.2.2. Synthesis of **1**

LH (0.012 g, 0.03 mmol) was dissolved in 10 mL THF to obtain a light yellow solution. 0.011 g (0.03 mmol) of Cu(ClO₄)₂·6H₂O, dissolved in 3 mL of THF, was added dropwise to the ligand solution with constant stirring. The resulting green solution was stirred for 15 min at room temperature. After stirring, the resulting reaction mixture was left for slow aerial evaporation. On slow evaporation, a green mass was obtained and it was thoroughly washed with diethyl ether and was vacuum dried over fused CaCl₂. The compound is soluble in DMF, THF, CH₃COCH₃, CH₃OH and CH₃CN. It is insoluble in *n*-hexane and *n*-pentane.

Yield: 0.014 g (62 %); Anal. Calcd. for C₂₂H₂₂ClCuN₃O₇S: C, 46.23; H, 3.88; N, 7.35. Found: C, 46.19; H, 3.90; N, 7.33; FT-IR (KBr, cm⁻¹): 3470(vb) [ν(O—H)], 2924(m) [ν(N—H)], 1537(s) [ν(C=N) of azomethine], 1500(m) [ν(C=N) of benzothiazole]; 1121, 1095, 1045(s) [ν(ClO₄)]; 625(s) [δ(ClO₄)]; UV–vis (MeOH): λ (ε, M⁻¹cm⁻¹) = 660 (153), 435 (15 000), 326 (16 168), 280 (22 204), 244 (28 599) nm; ESI-MS (positive ion mode in acetonitrile) (*m/z*): Found: 380.988 (Calc.: 381.006) for [⁶³Cu(L) + H⁺· (THF + H₂O + ClO₄)] with 100 % intensity and 382.990 (cal.: 383.006) for [⁶⁵Cu(L) + H⁺· (THF + H₂O + ClO₄)] with 33 % intensity (Fig.S5); Λ_M (in MeOH): Non-electrolyte. μ_{eff} = 1.91B.M.

Table 2
Hydrogen bonds (Å and °) for **1**.

D–H...A	d(D–H)	d(H...A)	d(D...A)	∠(D–H–A)	Symmetry code
C(3)–H(3)... O(5)	0.93	2.46	3.194(3)	135.6	
N(2)–H(2)... O(7)	0.86	1.92	2.692(2)	148.4	x,y-1,z
O(5)–H(51)... O(3)	0.75(3)	2.06(4)	2.787(3)	166(4)	-x + 2, -y + 1, -z + 1
O(5)–H(51)... Cl(1)	0.75(3)	2.99(3)	3.6579 (19)	151(3)	-x + 2, -y + 1, -z + 1
O(5)–H(52)... O(6)	0.81(4)	1.93(4)	2.705(2)	160(3)	-x + 2, -y + 1, -z +

2.3. X-ray data collection and structure determination

Shining needle shaped green single crystals of **1**, suitable for X-ray crystallography, were grown by direct diffusion of diethyl ether into a moderately concentrated mother liquor at room temperature. The crystals were chosen under visualization through an optical microscope. The data for **1** was collected with a Bruker-Kappa APEX II CCD diffractometer at 293(2) K. The diffractometer was equipped with a 1 K charge-coupled device area detector. Data collection had been performed using MoK α radiation (0.71073 Å). SMART software was used to determine the cell parameters [29]. The reduction and correction of the collected data was done by using the SAINTplus software [29]. Using SADABS software, absorption corrections had been done [30]. Using the direct method with SHELXL-97 program suites, we solved the structure [31]. The refinement by full-matrix least-squares methods on all F² data was done by the SHELXL-97 program. The cycle of full-matrix least square refinement had been performed on the basis of observed reflections and variable parameters. Crystal data and structure refinement parameters of the crystal have been summarized in Table 1. Some selected bond lengths and bond angles are tabulated in Table S1. The hydrogen bonding data are given in Table 2.

2.4. Trypsin assay

Trypsin inhibition studies were carried out following the previously described assay [25] with slight modification. The experiment was

performed for **LH** and **1** at varying concentrations. Trypsin stock solution (1 mg/mL) was prepared in 0.1 M phosphate buffer (pH 7.4). 150 enzyme units were incubated with 200 μ L samples for half an hour and the 20 μ L substrate (Bz-D, L-Arg- β NA) was added. The reaction was stopped by adding butanol and was read spectrophotometrically at 520 nm. The experiments were performed in triplicate and the % activity was determined from the average value. Curcumin was taken as a control at its respective concentration.

2.5. Amylase assay

Amylase studies were performed as had been described earlier [25] using the DNS method. 10 mg/mL amylase stock solution was prepared in 0.1 M phosphate buffer at pH 7. 200 μ L of samples at varying concentrations were incubated with 13 enzyme units for half an hour. 1 mL of 0.2 % starch solution was added as substrate and the enzyme inhibition was estimated by adding 3,5-dinitrosalicylic acid (DNS). The reaction mixture was heated for 10 min after adding DNS and the absorbance was noted after dilution at 540 nm taking curcumin as a control for the synthesized compounds.

2.6. Lipase assay

Lipase studies were performed colorimetrically using olive oil as substrate. 200 μ L of samples were incubated with 1.65 mL of lipase solution (prepared 2 mg/mL in 0.2 M tris buffer of pH 7.7). After 1 h, 1 mL olive oil substrate was added to the reaction mixture and was kept for 24 h. The reaction was stopped after 24 h by adding 6 mL ethanol and was then titrated with 50 mM NaOH solution using phenolphthalein indicator. Orlistat, a known lipase inhibitor, was taken as a control.

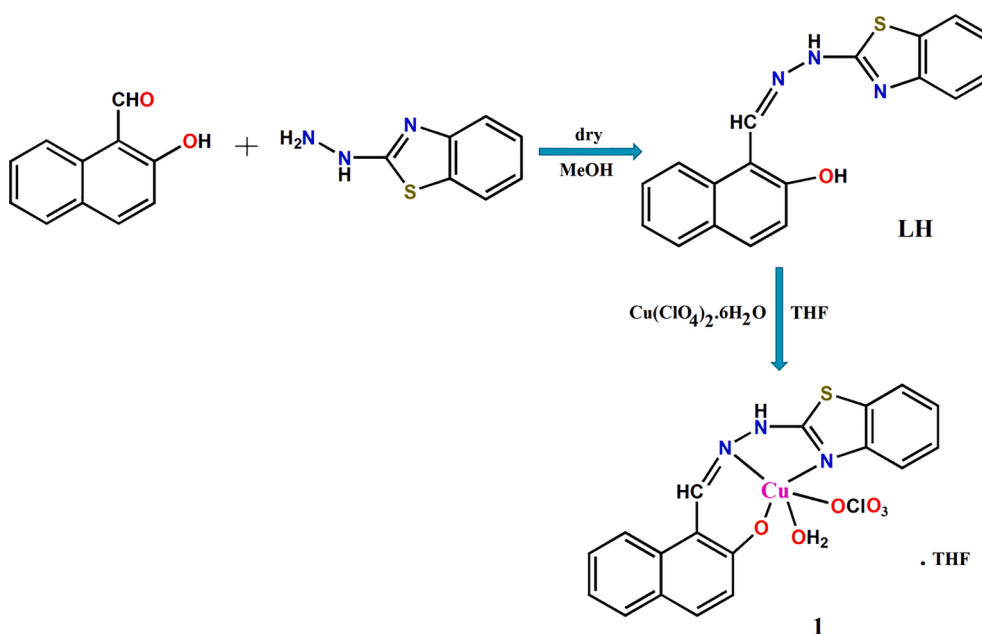
% Inhibition was calculated using the following formula:

$$\% \text{ Inhibition} = [(A_C - A_S)/A_C] \times 100$$

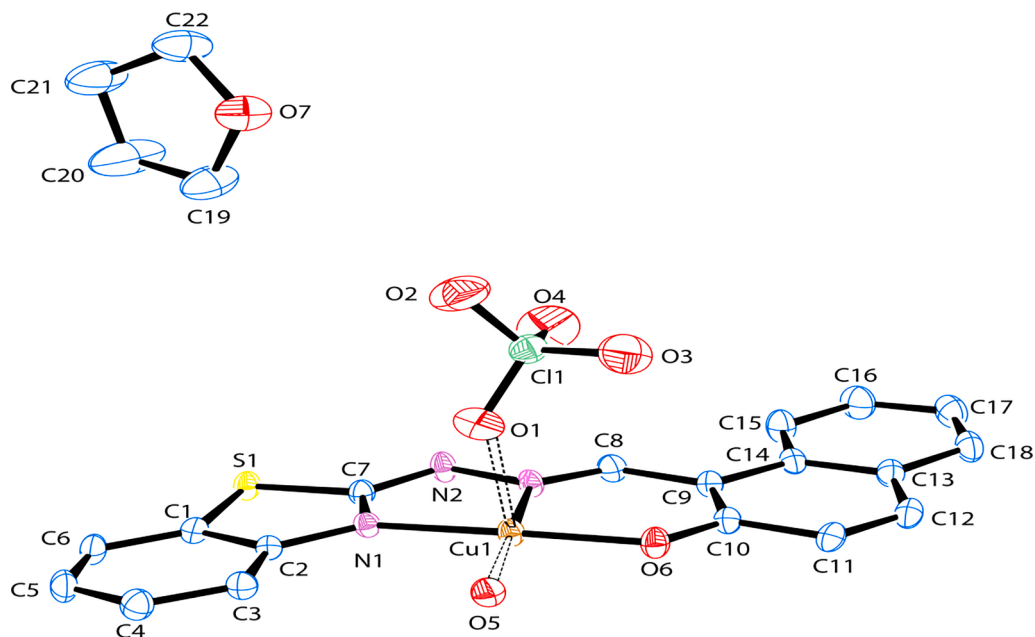
where, A_C and A_S represent absorbance of control and sample respectively.

2.7. Molecular docking studies

All the docking experiments were performed using iGEMDOCK that requires ligand and enzyme active sites. The structures of trypsin,



Scheme 1. Synthetic route of **LH** and **1**.

Fig. 1. ORTEP of **1** with 30% probability ellipsoid.

amylase and lipase were retrieved from the Protein Data Bank (<https://www.rcsb.org/>) as Trypsin (1avw) [26], Amylase (1dhk) [27] and Lipase (1lbs) [28]. The structures of **LH** and **1** were drawn in Chem 3D and were saved after minimizing the energy as pdb file. After loading the prepared ligand and the binding site, slow docking parameters were set as: screening population size = 300, generations = 80, number of solutions = 10, radius = 8 Å. Finally, the output files obtained thereby as best pose were visualized by using DS visualizer and further the interactions with the enzymes were computed.

2.8. Sensing experiments

In DMSO solvent, the sensing study on **LH** was carried out with different metal ions (Al^{3+} , Na^+ , K^+ , Mg^{2+} , Ca^{2+} , Pb^{2+} , Hg^{2+} , Zn^{2+} , Cd^{2+} , Cr^{3+} , Mn^{2+} , Fe^{2+} , Fe^{3+} , Co^{2+} , Ni^{2+} and Cu^{2+}). For studies of absorption and emission titration experiments, **LH** and metal ions had been added in such a manner that the final concentration was consistently at 55 μM .

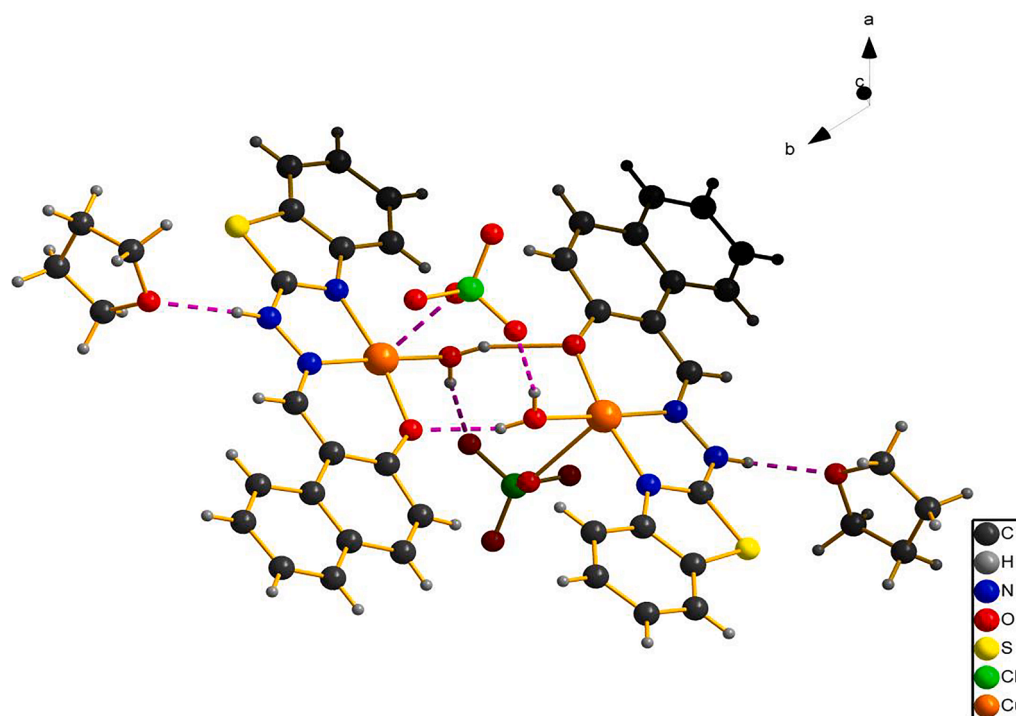
Fig. 2. Hydrogen bonded diagram of **1**.

Table 3*In vitro* analysis of LH and 1 towards extracellular digestive enzymes.

Conc.	% Trypsin Inhibition			% Amylase Inhibition			% Lipase Inhibition		
	Curcumin	Ligand	Complex	Curcumin	Ligand	Complex	Orlistat	Ligand	Complex
10 ⁻³ M	85.36 ± 1.29	51.29 ± 1.32	72.33 ± 0.98	55.70 ± 2.12	17.07 ± 1.23	21.39 ± 0.88	86.29 ± 1.26	63.52 ± 2.19	79.28 ± 1.28
10 ⁻⁴ M	69.88 ± 2.26	46.87 ± 1.68	65.94 ± 2.03	38.47 ± 1.25	12.23 ± 2.02	17.87 ± 1.38	80.38 ± 2.66	58.48 ± 1.98	75.31 ± 2.10
10 ⁻⁵ M	56.28 ± 2.45	30.16 ± 1.23	54.68 ± 1.56	25.05 ± 1.38	9.23 ± 1.13	12.42 ± 1.21	71.98 ± 2.93	50.87 ± 2.43	69.26 ± 1.85
10 ⁻⁶ M	48.76 ± 1.88	26.27 ± 1.73	19.94 ± 1.09	18.75 ± 2.17	4.06 ± 1.27	8.36 ± 1.25	67.52 ± 1.28	31.48 ± 1.87	64.19 ± 2.06
10 ⁻⁷ M	39.64 ± 2.04	19.94 ± 1.09	36.19 ± 1.63	14.02 ± 1.35	1.24 ± 1.42	5.96 ± 1.82	59.86 ± 2.27	26.32 ± 2.09	50.75 ± 1.98

3. Results and discussion

3.1. Synthesis and general characterization

LH, 1-(benzothiazol-2-yl-hydrazonomethyl)-naphthalen-2-ol, was synthesized by an equimolar Schiff base condensation of 2-hydroxy-1-naphthaldehyde with 2-hydrazino benzothiazole in methanol. **LH** was characterized by ¹H and ¹³C NMR, FT-IR and ESI mass spectroscopy [Figs. S1-S4]. Our subsequent 1:1 stoichiometric reaction of **LH** and Cu (ClO₄)₂·6H₂O in THF enabled us to afford **1**. The synthetic route of **LH** and **1** has been illustrated in scheme 1.

Free ligand exhibits FT-IR stretching vibrations at 3435(vb) [ν(O—H)], 2926(s) [ν(N—H)], 1624(s) [ν(C=N) of azomethine] and 1587(w) cm⁻¹ [ν(C=N) of benzothiazole]. In the FT-IR spectrum of **1**, corresponding bands have been assigned at 3429 [ν(O—H)], 2923 [ν(N—H)], 1618–1600 [ν(C=N) of azomethine] and 1577 cm⁻¹ [ν(C=N) of benzothiazole] (Fig. S6). A characteristic broad but split band at 1116–1045 cm⁻¹ indicates that the perchlorate ion is directly coordinated to the central metal ion of **1** [32]. The electronic absorption spectrum of **LH** in THF shows absorption bands at 407, 381, 335, 248 and 244 nm (Fig. S7). These are due to n→π* and π→π* transitions, characteristic of a carbonyl group [33]. UV–vis spectrum of **1** in methanol shows characteristic bands at 435, 326, 280 and 244 nm (Fig. S7). The d-d transition band is observed at 660 nm which is indicative of a five coordinated square-pyramidal geometry [34]. The X-band EPR spectrum of solid **1** was recorded on a JEOLJES- FA200 EPR spectrometer at room temperature (Fig. S8). The observed g value was 2.06. This g value is compatible with the Jahn-Teller distorted copper(II) compound in distorted square-pyramidal geometry [35].

3.2. Molecular structure of [CuL(ClO₄)(H₂O)].THF

1 is a monomeric Cu(II) complex, [CuL(ClO₄)(H₂O)].THF, with N,N, O donor Schiff base ligand as illustrated in Fig. 1. The central copper atom is nested in a penta-coordinated environment involving two Cu–N bonds and three Cu–O bonds. **1** crystallizes in triclinic *P*-1 space group with two asymmetric units per unit cell. The geometry index (τ₅) has been determined to augment the geometry around the copper center in **1**. By definition, τ₅ = (α-β)/60°, where α and β are the largest and second largest bond angles in a complex. For a penta-coordinated complex, τ₅ may either be zero or unity. For a perfectly square pyramidal geometry, τ₅ would be zero. This value is unity in a regular trigonal bipyramidal core [36–38]. Considering [N(3)-Cu(1)-O(5) = 176.07(8)° and O(6)-Cu(1)-N(1) = 170.88(7)°] respectively as α and β, τ₅ value here comes out to

be 0.0865. This magnitude is indicative of a distorted square-pyramidal geometry around the copper center.

The four basal bonds, [Cu(1)-N(1), Cu(1)-N(3), Cu(1)-O(6) and Cu(1)-O(5)] are respectively of 1.9781(16), 1.9447(17), 1.8926(14) and 1.9793(14) Å. Collectively they form a square based basal plane around the copper centre in **1**. O(1) occupies the apical site of the square based pyramid. One perchlorato oxygen, O(1), is weakly bonded to the copper center. The crystal structure has been stabilized through THF solvent mediation. **1** undergoes dimerization through hydrogen bonding (Fig. 2).

3.3. Enzymes assay

Digestive enzymes are the enzymes secreted by various parts of the body, that primarily aim at breaking down food components. Out of the various enzymes, trypsin, amylase and lipase are the enzymes that significantly help in food digestion by breaking down proteins, carbohydrates and fats respectively. Amylase and trypsin inhibitors can be successfully used as anti-pancreatitis agents.

Trypsin is a serine protease found in the small intestine that helps in hydrolyzing proteins. This proteolytic enzyme is widely used as an anti-inflammatory agent and as a promoter in tissue repair. Although having much importance, if trypsin activation exceeds a certain limit, then it can damage cells and can lead to pancreatitis. Hence, trypsin activity needs to be regulated. **1** manifests appreciable inhibition towards trypsin at moderate concentrations.

Amylase is responsible for digestion of carbohydrates by breaking down of starch into sugars. High amylase levels can also lead to acute pancreatitis. Curcumin, taken as a control, is known to inhibit α-amylase appreciably. However, **1** exhibits little inhibition towards α-amylase.

Lipases are responsible for the breaking down of fats into fatty acids and glycerol. Lipase inhibitors are primarily used as anti-obesity agents as they tend to decrease the gastrointestinal absorption of fats by preventing the hydrolysis of dietary triglycerides. **LH** and **1** inhibited lipase by almost 50 % at a lower concentration i.e. 10⁻⁷ M. This demonstrates the potential of them to act as anti-obesity agents. The results of *in vitro* studies are shown in Table 3.

3.4. Docking analysis

Molecular docking studies reveal that none of the compounds is directly attached to the amino acids of the catalytic triads of the enzymes — trypsin, amylase and lipase. However, the interaction with other active amino acids leads to conformational changes in enzymes, which

Table 4*In silico* analysis of the synthesized ligand (**LH**) and its complex (**1**) towards extracellular digestive enzymes.

Docking parameters		Trypsin			Amylase			Lipase		
		Curcumin	Ligand	Complex	Curcumin	Ligand	Complex	Orlistat	Ligand	Complex
Energy (kCal/mol)	Total	-106.636	-98.9765	-104.24	-95.3669	-82.5903	-104.443	-85.796	-84.7505	-85.1988
	VDW	-86.6059	-89.1898	-73.4211	-71.4793	-71.3879	-76.4021	-63.4156	-73.7099	-38.8634
	HB	-20.03	-9.78667	-30.8194	-23.8876	-11.2024	-28.0407	-22.3804	-11.0406	-46.3354
Total no. of interactions(Ligand-Enz)		6	8	11	8	13	18	4	11	5
No. of H-bonds		5	2	10	6	3	8	1	2	1
No. of Hydrophobic bonds		1	6	1	2	10	10	3	9	4

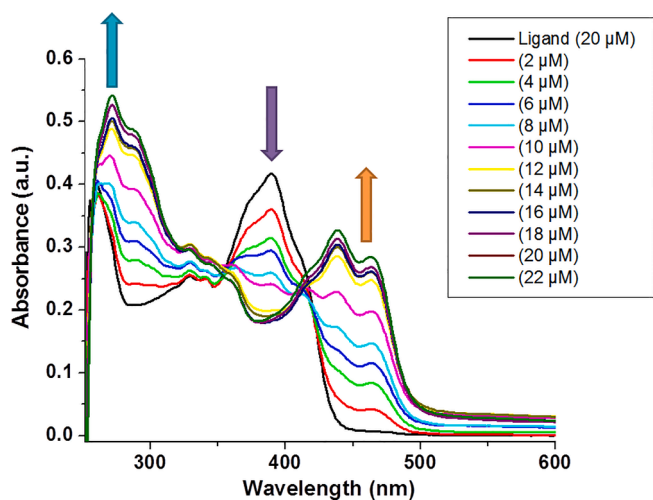


Fig. 3. Absorption spectra of LH (concentration 20 μM) in presence of 0, 2, 4, 6, 8, 10, 12, 14, 16, 18, 20 and 22 μM of Cu^{2+} ion in DMSO at room temperature.

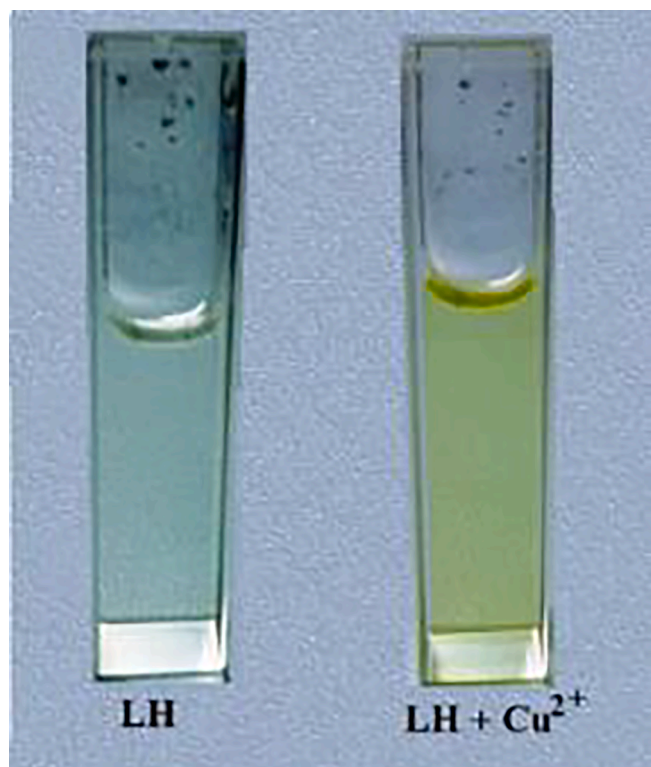


Fig. 4. Color change of LH (20 μM) on addition of copper(II).

directly affect their interaction with the substrate and hence result in decreased or increased activity of the enzyme. The total energy of a predicted pose of an inhibitor with an enzyme active site as a sum total of van der Waals (VDW), H-bonding (HB) and electrostatic energy is presented in Table 4. 2-D and 3-D figures of the respective enzymes are compiled in Tables S2 and S3, respectively. The colour code for different interactions is compiled in the figures itself.

3.5. Absorption studies

By UV–visible absorption spectroscopy, the complex ion of Cu^{2+} with LH was investigated in DMSO solution. The absorption spectra of LH (20 μM) were recorded with different concentrations of Cu^{2+} (0–22 μM)

at room temperature (Fig. 3).

In the absence of copper ion, LH exhibited absorption bands at 271, 390 and 440 nm. On addition of different concentrations of copper ion, a significant change was observed in all absorption bands. With addition of Cu^{2+} , the band at 390 nm weakened and those at 270 and 440 nm intensified. This result clearly indicates that the probe (LH) anchors Cu^{2+} with remarkable selectivity towards Cu^{2+} . Fig. 4 shows color change of LH on addition of Cu^{2+} ion.

3.6. Cu^{2+} ion sensing by fluorescence studies

To explore the photophysical properties of our probe LH, fluorescence emission studies were executed by various methods. On excitation at 390 nm, LH (20 μM) shows an emission band at 459 nm in DMSO solvent at room temperature.

The fluorescence emission intensity of LH noticeably diminishes on the addition of Cu^{2+} . The probe LH is thus a selective binder of Cu^{2+} . The fluorescence quenching occurred in emission band at 459 nm. A titration experiment was also performed with the gradual addition of Cu^{2+} to the solution of LH. When Cu^{2+} ions with varying concentrations (0–22 μM) were added to LH, a systematic fluorescence quenching was observed (Fig. 5). With the addition of a small amount of Cu^{2+} , the quenching occurred with enhanced rapidity. However, this quenching of fluorescence intensity gradually weakened with the continuous addition of Cu^{2+} .

With 20 μM LH probe, the fluorescence efficacies were monitored towards different metal ions as shown in Fig S8. For selectivity determination, one equivalent amount of LH was exposed to one equivalent of various metal ion solution under current investigation (Al^{3+} , Na^+ , K^+ , Mg^{2+} , Ca^{2+} , Pb^{2+} , Hg^{2+} , Zn^{2+} , Cd^{2+} , Cr^{3+} , Mn^{2+} , Fe^{3+} , Fe^{2+} , Co^{2+} , Ni^{2+} and Cu^{2+}). However, only on addition of Cu^{2+} , a significant change was noticed. Only Cu^{2+} ion showed fluorescence quenching with characteristic emission.

The selectivity of LH for Cu^{2+} had been checked in the presence of other metal ions (Fig. 6). A DMSO solution of the fluorescence probe LH was exposed to 1.0 equivalent of Cu^{2+} in the presence of other metal ions in the equivalent concentration. Only Fe^{3+} ions were able to reduce the negligible amount of emission intensity. No other alkali or alkaline metal ion was able to quench the fluorescence intensity of LH. The relative changes in fluorescence intensity of LH with Cu^{2+} along with other relevant metal ions are shown in Fig. 7.

Job's plot of the probe LH was done with Cu^{2+} varying different equivalent concentration of both by measuring fluorescence intensity (Fig. S9). At the same equivalent mixture condition, plot shows a significant break. This clearly indicates that the probe LH forms a complex with Cu^{2+} in a 1:1 M proportion. It is pertinent to note that our crystal structure of the copper complex of LH also confirms this stoichiometric proportion (Fig. 1). From the Benesi-Hildebrand plot, the binding constant value (K_a) was found to be $3.05 \times 10^4 \text{ M}^{-1}$ (Fig. S10).

3.7. Limit of detection (LOD) determination

Following 3σ method, the limit of detection (LOD) value of the present probe for copper(II) ion had been evaluated [39]. The determined LOD value was 0.35 μM . The World Health Organization has set the LOD value of 31.5 μM (maximum adoptable) [40]. In comparison, our LOD value is significantly lower (Fig. 8). This low LOD value clearly indicates that the probe, LH, offers high sensitivity towards Cu^{2+} . We take recourse to comparing our present result with some recently published Cu^{2+} probes [41–47] (Table S4). From this comparison, it is obvious that our present probe is superior to most of the currently reported probes. However, a recently published naphthaldehyde based sensor, akin to our probe, has been found to manifest the best efficacy [44]. Additionally, a good linear dynamic relationship at 459 nm was obtained between fluorescence intensity and Cu^{2+} ion concentration with an R value of 0.98732. This obtained value suggests more accurate

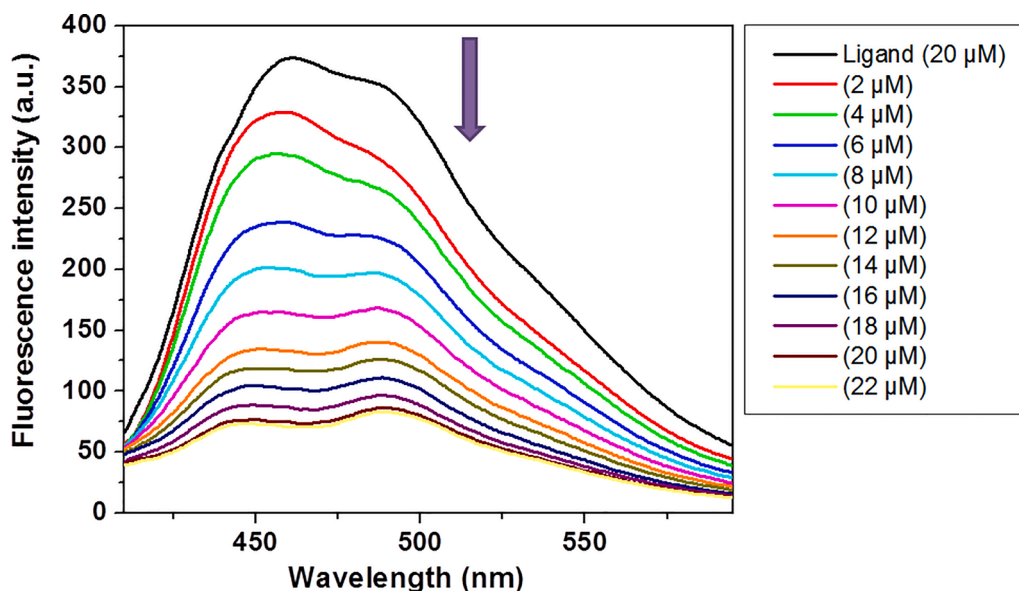


Fig. 5. Emission spectra of LH (20 μM) in presence of 0, 2, 4, 6, 8, 10, 12, 14, 16, 18, 20 and 22 μM of Cu^{2+} ions in DMSO at room temperature. $\lambda_{\text{ex}} = 390 \text{ nm}$.

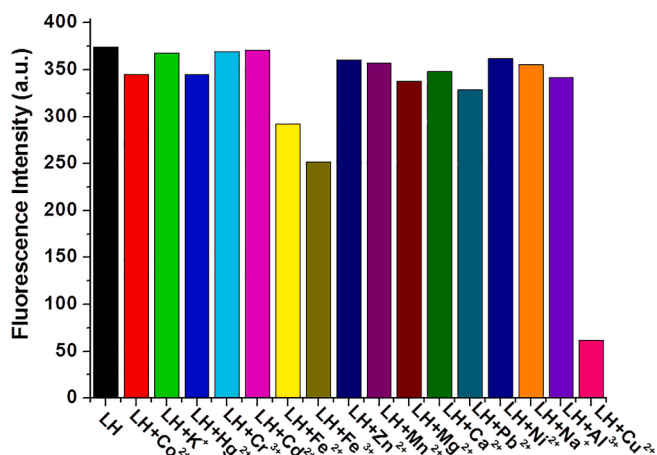


Fig. 6. Relative fluorescence intensity changes of LH in presence of different metal ions in DMSO.

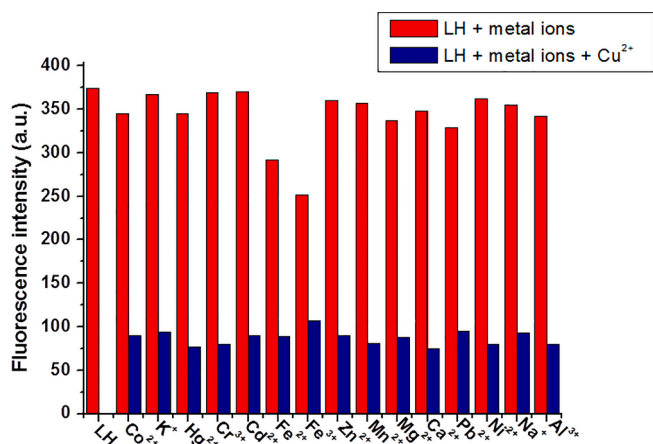


Fig. 7. Relative fluorescence intensity changes of LH in presence of Cu^{2+} along with relevant other metal ions in DMSO.

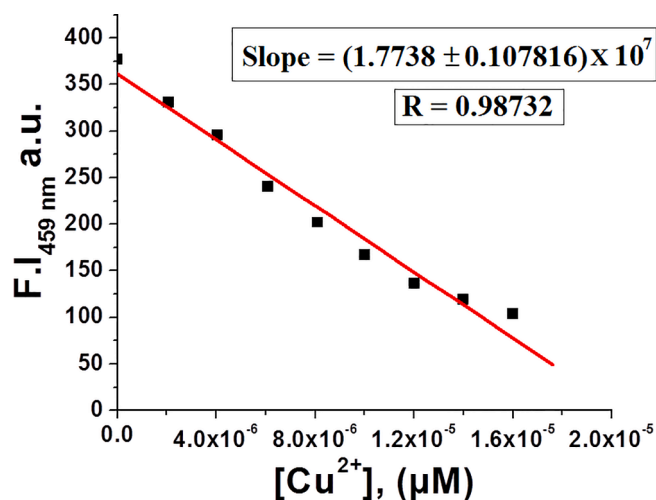


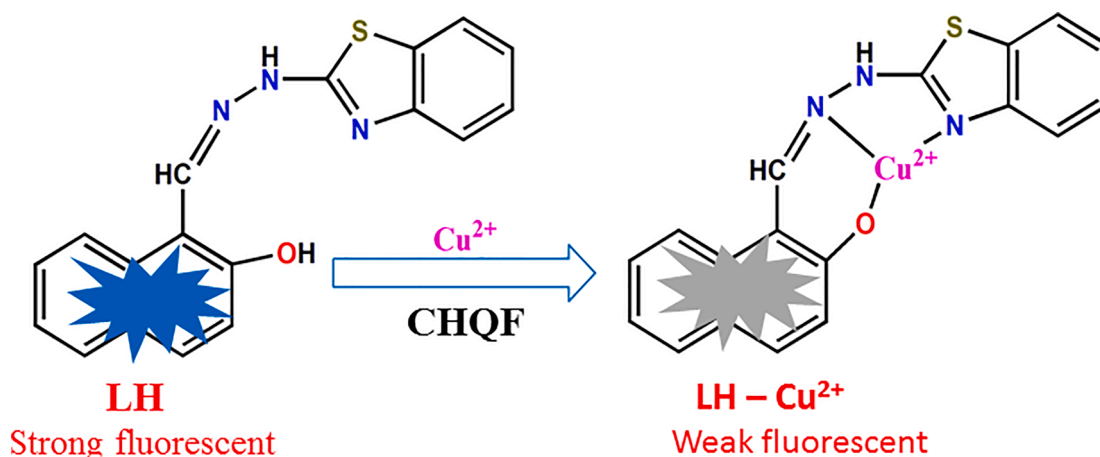
Fig. 8. Linear dynamic plot of F.I. (at 459 nm) vs $[\text{Cu}^{2+}]$ for the determination of S (slope). $[\text{LH}] = 20 \mu\text{M}$ with standard deviation 2.1831; LOD (Cu^{2+}) = $(3 \times 2.1831) / 1.7738 \times 10^7 = 0.35 \mu\text{M}$.

detection of Cu^{2+} ion (Fig. 8). Our present low LOD value has been compared with some other previously reported sensors and has been tabulated in Table S4

We also checked the copper(II) sensing aspect of LH (20 μM) in methanol, acetone and acetonitrile along with DMSO. We observed promising changes in fluorescence intensity in DMSO. For the rest of the solvents, the response was poor (Fig. S12).

3.8. Sensing mechanism

To augment the proposed sensing mechanism of the present fluorescent probe LH, we had taken recourse to monitoring the fluorescence phenomenon of LH (20 μM) in DMSO solution towards different metal ions. On excitation at 390 nm, a strong emission band was observed at 499 nm for the fluorescent sensor LH in DMSO solvent at room temperature. However, a distinct fluorescence quenching was observed only for the Cu^{2+} ion during our experiment over other tested metal ions as shown in Fig. S8. Most likely this can be attributed to the paramagnetic



Scheme 2. Proposed sensing mechanism of LH.

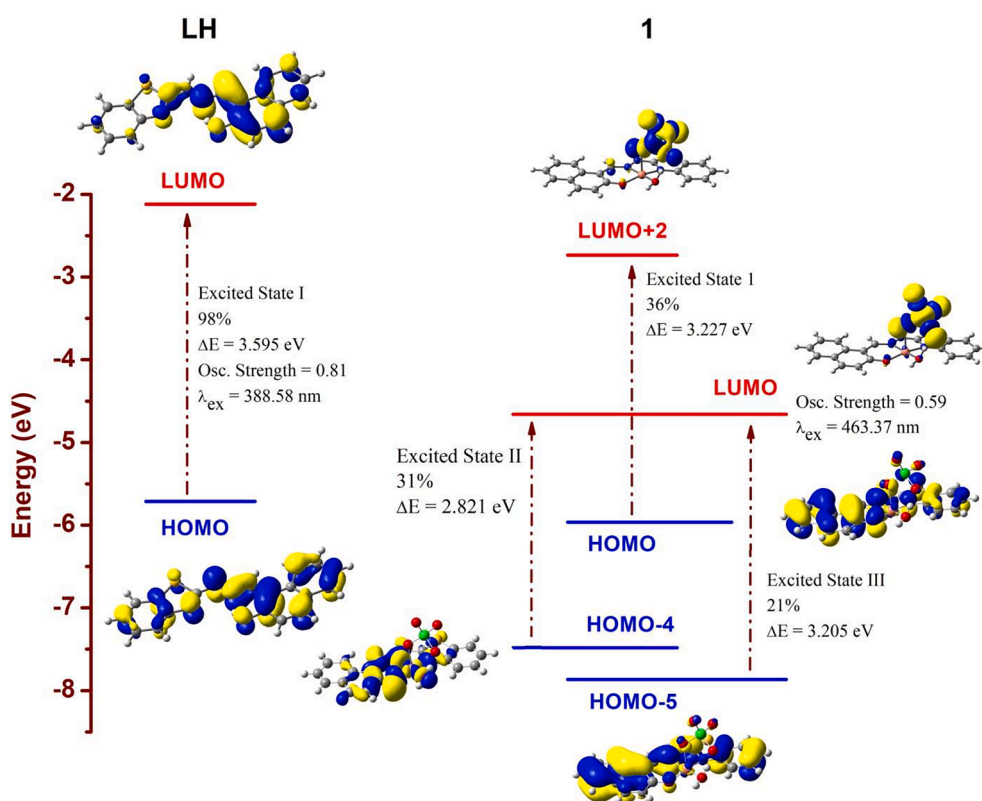


Fig. 9. Molecular orbital diagram and excitation energies for LH and 1.

behaviour of Cu^{2+} ion. Due to the formation of the LH-Cu^{2+} complex, a photoinduced energy/charge transfer occurs from metal to fluorophore. This pathway, the chelation-quenched fluorescence (CHQF) sensing mechanism, caused by the complexation of LH with Cu^{2+} is most likely operative here [48]. Earlier, LH had been reported for time dependent selectivity for copper(II) ion through the turn-on mode. The authors proposed that the binding mode of LH with Cu^{2+} is either through N or S of the benzothiazole ring in an acetonitrile milieu. For the chelation of Cu^{2+} with a S donor atom, strong fluorescence was observed; while a non-fluorescence situation resulted for anchoring through a N atom [49]. Here, we have confirmed the unambiguous binding mode of LH with Cu^{2+} solely through the N donor atom by single crystal X-ray structure as depicted in Fig. 1. The fluorescence intensity was quenched upon the continuous addition of Cu^{2+} . Other tested metal ions under the

present study, however, failed to quench fluorescence intensity. Possibly this may be attributed to the not so stable coordination geometry arising out of unfavourable anchoring of other metal ions other than copper with LH in DMSO. The proposed sensing mechanism is shown in scheme 2.

3.9. DFT calculations

Calculated bond parameters as obtained by DFT are consistent with the crystallographic data of 1 and are tabulated in Table S5. The calculated bond distances of Cu1–N1, Cu1–N3, Cu1–O3, Cu1–O5 and Cu1–O6 are a little bit longer than their respective crystallographic values. For 1, the computed angles lie within $\pm 5^\circ$ deviation from their respective experimental values. The optimized bond parameters of free ligand (LH) and both optimized as well as experimental bond

parameters of coordinated ligand are almost the same. Thus, our calculated bond lengths and bond angles are in fair agreement with the experimental data. The manifested overall variations are reasonable since being carried out *in vacuo* at 0 K, theoretical optimization cannot match exactly with the experimental data set. Again, the deviation of the calculated bond parameters from the experimental data may arise due to conformational changes induced by the crystal field perturbation and temperature effect. This may be due to the basis sets chosen for calculations [50]. To get insight into the electronic absorption aspects of **LH** and **1**, TD-DFT calculations were carried out with the optimized structures. The evaluated transition energies of **LH** and **1**, using the LanL2DZ basis set and TD-SCF calculation, are shown in Fig. 9. The molecular orbitals (MOs) of **LH** at the first lower excited state were ascribed to the HOMO → LUMO transition found at 388.58 nm against the experimental absorption at 390 nm. For free **LH**, the HOMO-LUMO energy gap was found to be 3.595 eV; while the HOMO-4 → LUMO value for **1** was 2.821 eV. In **1**, comparatively less amount of energy is required to excite the electron due to decrease in energy gap as compared to free **LH**. This results in a bathochromic shift in the absorption spectrum. However, the main MO contributions of **1** at the third lower excited states were analyzed to be the HOMO-5 → LUMO, HOMO-4 → LUMO and HOMO → LUMO + 2 transitions found at 463.37 nm against the experimental λ^{max} value of 465 nm.

3.10. Powder X-ray diffraction

Powder X-ray diffraction of **1** was done to check the phase purity of the bulk materials. Simulated patterns as obtained from SC-XRD are in good agreement with the powder pattern. This confirms the phase purity of the bulk materials of **1** (Fig. S13).

4. Conclusions

In summary, we have synthesized a novel mononuclear Cu(II) complex (**1**) from a naphthaldehyde based Schiff base ligand (**LH**) and was thoroughly characterized. The crystal structure of the copper(II) complex of **LH** has also been determined. *In vitro* enzymatic studies employing amylase, trypsin and lipase were carried out for both **LH** and **1**. *In silico* analysis of **LH** and **1** have also been carried out towards extracellular digestive enzymes. **1** shows inhibition towards the tested enzymes. This study reveals that both **LH** and **1** can be used as anti-obesity agents due to their strong inhibition towards lipase at lower concentrations. Accordingly, the present work may bear some significant biological perspective. In addition, the fluorescent probe (**LH**) shows selectivity towards the Cu^{2+} ion in organic milieu. In the absence of Cu^{2+} ions, the probe shows an emission band at 459 nm while on addition of the Cu^{2+} , it shows significant fluorescence quenching. Our Job's plot analysis confirms a 1:1 binding stoichiometry of the probe with the Cu^{2+} ion. The present work demonstrates a rare situation where the solid state crystal structure of the probe-metal system has been deciphered. This probe offers high selectivity coupled with significant sensitivity towards Cu(II) ion with satisfactory low LOD value of 0.35 μM . Based on this outcome, the present contribution may draw attention at least to the monitoring of copper(II) ions in industrial and environmental samples.

Declaration of Competing Interest

The authors declare that they have no known competing financial interests or personal relationships that could have appeared to influence the work reported in this paper.

Data availability

Data will be made available on request.

Acknowledgement

NKM is thankful to the UGC, New Delhi, India for a senior research fellowship. Various help from Prof. Chandra Sekhar Purohit, School of Chemical Science, NISER, Bhubaneswar, Odisha 751 005, India is gratefully acknowledged.

Appendix A. Supplementary data

Supplementary data to this article can be found online at <https://doi.org/10.1016/j.ica.2022.121229>.

References

- [1] (a) M. Furne, M.C. Hidalgo, A. Lopez, M. Gracia-Gallego, A.E. Morales, A. Domezain, J. Domezain, A. Sanz, *Aquaculture* 250 (2005) 391-398; (b) R.D. Schmid, R. Verger, *Angew. Chem. Int. Ed.* 37 (1998) 1608-1633; (c) M. Hirota, M. Ohmura, H. Baba, J. Gastro. 41 (2006) 832-836.
- [2] (a) N.Y. Ensari, B. Otludil, M.C. Aytekin, *Starch/Stärke* 47 (1995) 315-321; (b) M. E. Fárez-Vidal, A. Fernandez-Vivas, J.M. Arias, *J. Appl. Bacterio.* 73 (1992) 148-156.
- [3] (a) N.S. Reddy, A. Nimmagadda, K.R.S.S. Rao, *African J. Biotech.* 2 (2003) 645-648; (b) K. Yamane, B. Maruo, *J. Bact.* 120 (1974) 792-798.
- [4] F. Hasan, A.A. Shah, A. Hameed, *Enzyme Microb. Technol.* 39 (2006) 235-251.
- [5] (a) W.A. Zoubi, A.A.S. Al-Hamdani, S.D. Ahmed, Y.G. Ko, *J. Phys. Org. Chem.* 31 (2018) e3752; (b) M.S. More, P.G. Joshi, Y.K. Mishra, P.K. Khanna, *Mater. Today Chem.* 14 (2019) 100195; (c) A. Kajal, S. Bala, S. Kamboj, N. Sharma, V. Saini, *J. Catalysts* (2013) 893512.
- [6] (a) C. Biswas, A. Chatterjee, V. Vijayan, C.S. Purohit, M.S. Kiran, R. Ghosh, *Inorg. Chem. Commun.* 136 (2022) 109178-109183. (b) M.N. Uddin, S.S. Ahmed, S.M.R. Alam, *J. Coord. Chem.* 73 (2020) 3109-3149; (b) S. Patil, S.D. Jadhav, U.P. Patil, *Arch. Appl. Sci. Res.* 4 (2012) 1074-1078.
- [7] B. Otludil, B.A. Otludil, R. Demir, V. Tolan, H. Temel, *Biotechnol. Biotechnol. Equip.* 29 (2005) 105-110.
- [8] (a) D. Iyaguchi, S. Kawano, K. Takada, E. Toyota, *Bioorganic & Medicinal Chemistry* 18 (2010) 2076-2080; (b) E. Toyota, K.K.S. Ng, H. Sekizaki, K. Itoh, K. Tanizawa, M.N. G. James, *J. Mol. Biol.* 305 (2001) 471-479.
- [9] (a) Z. Liu, W. He, M. Pei, G. Zhang, *Chem. Commun.* 51 (2015) 14227-14230; (b) C.-Y. Lai, B.G. Trewyn, D.M. Jeftinija, K. Jeftinija, S. Xu, S. Jeftinija, V.S.-Y. Lin, *J. Am. Chem. Soc.* 125 (2003) 4451-4459.
- [10] (a) B. Muthuraj, R. Deshmukh, V. Trivedi, P.K. Iyer, *ACS Appl. Mater. Interfaces* 6 (2014) 6562-6569; (b) A.M. Abu-Dief, L.A.E. Nassr, *J. Iran. Chem. Soc.* 12 (2015) 943-955; (c) Y. Wang, S. Liu, H. Chen, Y. Liu, H. Li, *Dyes Pigments* 142 (2017) 293-299.
- [11] (a) E. Merian, *Analysis and Biological Relevance*, VCH, Weinheim, 1991, p. 893; (b) E. Merian, *Metals and Their Compounds in the Environment*, VCH, Weinheim, Germany, 1991; (c) D.W. Domaille, E.L. Que, C.J. Chang, *Nat. Chem. Biol.* 4 (2008) 168-175.
- [12] (a) S.-P. Wu, T.-H. Wang, S.-R. Liu, *Tetrahedron* 66 (2010) 9655-9658; (b) T. Li, Z. Yang, Y. Li, Z. Liu, G. Qi, B. Wang, *Dyes Pigments* 88 (2011) 103-108; (c) H.S. Jung, P. S. Kwon, J.W. Lee, J.I. Kim, C.S. Hong, J.W. Kim, S. Yan, J.Y. Lee, J.H. Lee, T. Joo, J.S. Kim, *J. Am. Chem. Soc.* 131 (2009) 2008-2012; (d) A. Saravanan, G. Subashini, S. Shyamsivappan, T. Suresh, K. Kadirvelu, N. Bhuvanesh, R. Nandhakumar, P.S. Mohan, *J. Photochem. Photobiology A: Chem.* 364 (2018) 424-432; (e) M. Sadiq, R. Naz, J. Khan, R. Khan, *J. Fluores.* 18 (2018) 1281-1294.
- [13] (a) J.R. Barrull, M. d'Halluin, E.L. Grogne, F.-X. Felpin, *Chem. Commun.* 52 (2016) 6569-6572; (b) X. Ma, Z. Tan, G. Wei, D. Wei, Y. Du, *Analyst* 137 (2012) 1436-1439.
- [14] (a) D.J. Waggoner, T.B. Bartnikas, J.D. Gitlin, *Neurobiol. Dis.* 6 (1999) 221-230; (b) C. Vulpe, B. Levinson, S. Whitney, S. Packman, J. Gitschier, *Nat. Genet.* 3 (1993) 7-13; (c) P.C. Bull, G.R. Thomas, J.M. Rommens, J.R. Forbes, D.W. Cox, *Nat. Genet.* 5 (1993) 327-337.
- [15] Y.H. Hung, A.I. Bush, R.A. Cherny, *J. Biol. Inorg. Chem.* 15 (2010) 61-76.
- [16] (a) P. Jiang, Z. Guo, *Coord. Chem. Rev.* 248 (2004) 205-229; (b) F. Pina, M.A. Bernardo, E. Garcia-Espana, *Eur. J. Inorg. Chem.* (2000) 2143-2157.
- [17] (a) G.K. Patra, R. Chandra, A. Ghorai, K.K. Shrivastava, *Inorg. Chim. Acta* 462 (2017) 315-322; (b) M. Boiocchi, L. Fabbri, M. Licchelli, D. Sacchi, M. Vázquez, C. Zampa, *Chem. Commun.* (2003) 1812-1813.
- [18] G.A. Bain, J.F. Berry, *J. Chem. Educ.* 85 (2008) 532-536.
- [19] M.J. Frisch, G.W. Trucks, H.B. Schlegel, G.E. Scuseria, M.A. Robb, J.R. Cheeseman, G. Scalmani, V. Barone, B. Mennucci, G.A. Petersson, H. Nakatsuji, M. Caricato, X. Li, H.P. Hratchian, A.F. Izmaylov, J. Bloino, G. Zheng, J.L. Sonnenberg, M. Hada, M. Ehara, K. Toyota, R. Fukuda, J. Hasegawa, M. Ishida, T. Nakajima, Y. Honda, O. Kitao, H. Nakai, T. Vreven, J.A. Montgomery Jr., J.E. Peralta, F. Ogliaro, M. Bearpark, J.J. Heyd, E. Brothers, K. N. Kudin, V.N. Staroverov, R. Kobayashi, J. Normand, K. Raghavachari, A. Rendell, J.C. Burant, S.S. Iyengar, J. Tomasi, M. Cossi, N. Rega, J.M. Millam, M. Klene, J.E. Knox, J.B. Cross, V. Bakken, C. Adamo, J. Jaramillo, R. Gomperts, R.E. Stratmann, O. Yazyev, A.J. Austin, R. Cammi, C. Pomelli, J.W. Ochterski, R.L. Martin, K. Morokuma, V.G. Zakrzewski, G.A. Voth, P. Salvador, J.J. Dannenberg, S. Dapprich, A.D. Daniels, Ö. Farkas, J.B. Foresman, J. V. Ortiz, J. Cioslowski, D.J. Fox, *Gaussian 09, Revision C.01*, Gaussian Inc., Wallingford, CT, 2009.

- [20] (a) A.D. Becke, *J. Chem. Phys.* 98 (1993) 5648; (b) C. Lee, W. Yang, R.G. Parr, *Phys. Rev. Sect. B* 37 (1988) 785-789.
- [21] P.J. Hay, W.R. Wadt, *J. Chem. Phys.* 82 (1985) 299-310.
- [22] (a) V. Barone, M. Cossi, *J. Phys. Chem. A* 102 (1998) 1995-2001; (b) J. Tomasi, B. Mennucci, R. Cammi, *Chem. Rev.* 105 (2005) 2999-3094.
- [23] W.C. Wolsey, *J. Chem. Educ.* 50 (1973) A335-A337.
- [24] S.R. Girish, V.K. Revankar, V.B. Mahale, *Transition Met. Chem.* 21 (1996) 401-405.
- [25] P. Arya, N. Raghav, *J. Mol. Struct.* 1228 (2021), 129774.
- [26] L. Migliolo, A.S. de Oliveira, E.A. Santos, O.L. Franco, M.P. de Sales, *J. Mol. Graphics and Modelling* 29 (2010) 148-156.
- [27] F. Xie, W. Zhang, S. Gong, X. Gu, X. Lan, J. Wu, Z. Wang, *Food Chem.* 271 (2019) 62-69.
- [28] D.I. Habeych, P.B. Juhl, J. Pleiss, D. Vanegas, G. Eggink, C.G. Boeriu, *J. Mol. Catalysis B: Enzymatic* 71 (2011) 1-9.
- [29] Bruker, SMART (Version 5.0) and SAINT (Version 6.02). Bruker AXS Inc., Madison, Wisconsin, USA, 2000.
- [30] G. M. Sheldrick, SADABS, Program for Empirical Correction of Area Detector Data, University of Göttingen, Germany, 2000.
- [31] G.M. Sheldrick, SHELXS97 and SHELXL97, University of Göttingen, Germany, Program for Crystal Structure Refinement, 1997.
- [32] Y. Fukuda, A. Shimura, M. Mukaida, E. Fujita, K. Sone, *J. Inorg. Nucl. Chem.* 36 (1974) 1265-1270.
- [33] M.H. Habibi, M. Mikhak, *Spectrochim. Acta part A: Molecular and Biomolecular Spectroscopy* 96 (2012) 501-505.
- [34] B.J. Hathaway, R.J. Dudley, P. Nicholls, *J. Chem. Soc. A* (1969) 1845-1848.
- [35] M. Kumar, S.U. Parsekar, N. Duraipandy, M.S. Kiran, A.P. Koley, *Inorg. Chim. Acta* 484 (2019) 219-226.
- [36] A.W. Addison, T.N. Rao, J. Reedijk, J.V. Rijn, G.C. Verschoor, *Dalton Trans.* (1984) 1349-1356.
- [37] M. Li, A. Ellern, J.H. Espenson, *Inorg. Chem.* 44 (2005) 3690-3699.
- [38] K.P. Maresca, G.H. Bonavia, J.W. Babich, J. Zubieta, *Inorg. Chim. Acta* 284 (1999) 252-257.
- [39] V. Thomsen, D. Schatzlein, D. Mercuro, *Spectros.* 18 (2003) 112-114.
- [40] J.H. Kang, S.Y. Lee, H.M. Ahn, C. Kim, *Inorg. Chem. Commun.* 74 (2016) 62-65.
- [41] P. Torawane, S.K. Sahoo, A. Borse, A. Kuwar, *Lumines.* 32 (2017) 1426-1430.
- [42] K. Rout, A.K. Manna, M. Sahu, J. Mondal, S.K. Singh, G.K. Patra, *RSC Adv.* 9 (2019) 25919-25931.
- [43] Y.R. Bhorge, H.-T. Tsai, K.-F. Huang, A.J. Pape, S.N. Janaki, Y.-P. Yen, *Spectrochim. Acta Part A: Molecular and Biomolecular Spectroscopy* 130 (2014) 7-12.
- [44] N. Xiao, C. Zhang, *Inorg. Chem. Commun.* 107 (2019), 107467.
- [45] G.J. Park, G.R. You, Y.W. Choi, C. Kim, *Sens. Actuators, B* 229 (2016) 257-271.
- [46] S. Ghosh, A. Ganguly, M.R. Uddin, S. Mandal, M.A. Alam, N. Guchhait, *Dalton Trans.* 45 (2016) 11042-11051.
- [47] C.-Y. Chou, S.-R. Liu, S.-P. Wu, *Analyst* 138 (2013) 3264-3270.
- [48] Z. Guo, Q. Niu, T. Li, T. Sun, H. Chi, *Spectrochim. Acta Part A: Molecular and Biomolecular Spectroscopy* 213 (2019) 97-103.
- [49] Z. Zhang, S. Yuan, E. Wang, *J. Fluoresc.* 28 (2018) 1115-1119.
- [50] A. Bhattacharya, J.P. Naskar, S. Majumder, R. Ganguly, P. Mitra, S. Chowdhury, *Inorg. Chim. Acta.* 425 (2015) 124-133.



Syntheses of two copper(II) coordination polymers from a morpholine-based tridentate Schiff base ligand: crystal structures and magnetic properties

Naba Kr Mandal^a, Carlos J. Gómez-García^b, Pinaki Saha^c and Jnan Prakash Naskar^a

^aDepartment of Chemistry, Jadavpur University, Kolkata, India; ^bDepartamento de Química Inorgánica, Universidad de Valencia, Burjassot, Valencia, Spain; ^cDepartment of Chemistry, Ramakrishna Mission Residential College, Kolkata, India

ABSTRACT

Two new one-dimensional (1-D) end-to-end azido and thiocyanato bridged Cu(II) coordination polymers, [Cu(L)(μ -1,3-N₃)]_n(ClO₄)_n (**1**) and [Cu(L)(μ -1,3-NCS)]_n(ClO₄)_n (**2**) with a morpholine-based tridentate *N,N,N*-donor Schiff base ligand (1-methyl-1*H*-imidazol-2-yl)-*N*-[2-(morpholin-4-yl)ethyl]methanimine, L) have been synthesized. Compounds **1** and **2** have been characterized by elemental analyses and spectroscopic techniques. The X-ray single crystal structures of **1** and **2** show the formation of regular zigzag chains with μ -1,3-azido and μ -1,3-thiocyanate bridges, respectively. Variable temperature (2–300 K) magnetic studies indicate that **1** shows a ferromagnetic intrachain exchange interaction with $g = 2.135(2)$ and $J = 2.13(2) \text{ cm}^{-1}$, while in **2** this interaction is antiferromagnetic with $g = 2.1412(3)$ and $J = -0.277(2) \text{ cm}^{-1}$. X-band EPR spectra of **1** and **2** in frozen (143 K) DMF solution corroborate our magnetic studies.

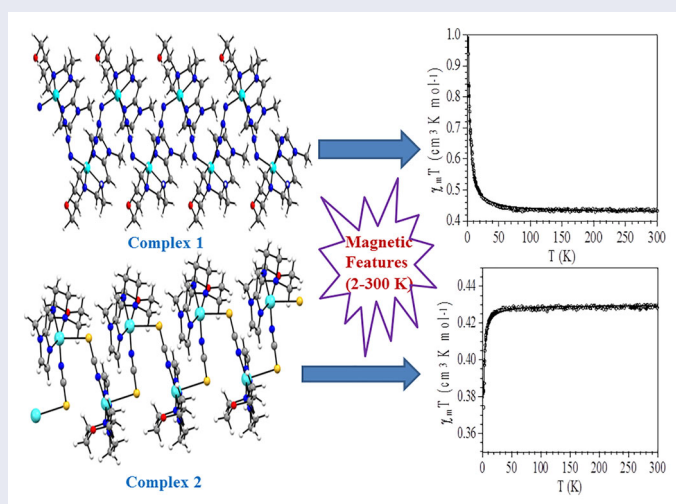
ARTICLE HISTORY

Received 23 December 2022

Accepted 30 March 2023

KEYWORDS

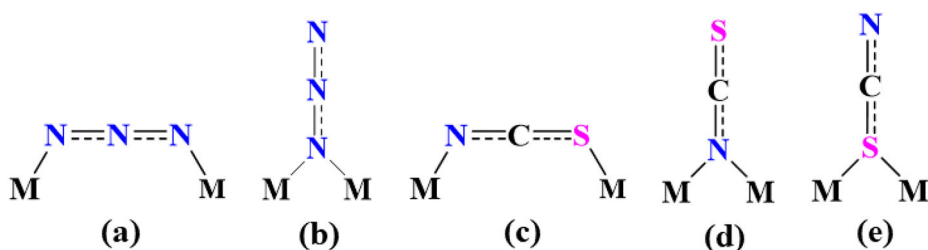
Copper; Schiff base; crystal structure; magnetic properties



CONTACT Jnan Prakash Naskar ✉ jpnaskar@rediffmail.com Department of Chemistry, Jadavpur University, Kolkata 700 032, India.

Supplemental data for this article can be accessed online at <https://doi.org/10.1080/00958972.2023.2203799>.

© 2023 Informa UK Limited, trading as Taylor & Francis Group



Scheme 1. μ -1,3 (a, c) and μ -1,1 (b, d, e) bridging modes of azido and thiocyanato ligands.

1. Introduction

Synthesis of discrete polynuclear molecules and/or coordination polymers with efficient mediators are of interest from the viewpoint of magnetochemistry [1, 2]. With diverse bridging modes, pseudo-halides are ubiquitous in mediating magnetic coupling [3]. Consequently, pseudo-halide bridged metal complexes are of interest for magnetic studies [4, 5]. Magneto-structural correlation on these systems is often sought. In this context, azido and thiocyanato-bridged complexes are noteworthy [6–9]. Two common bridging modes, μ -1,3 or end-to-end (EE) and μ -1,1 or end-on (EO), for azide and thiocyanate are shown in Scheme 1. Such complexes with structural diversities manifest magnetic behaviors [10–12]. A remarkable example, reported by Liu *et al.* in 2004, is a 1-D polymeric chain with azido linkers displaying spin-canted long range ferromagnetic exchange due to significant interchain magnetic interaction and strong axial magnetic anisotropy [13]. In addition, azido-based 1-D Cu(II) coordination polymers also show applications in opto-electronic devices [14]. Due to their different coordination modes, the azido ligand may give various structural topologies [15, 16]. Although there are some exceptions, magnetic coupling is generally ferromagnetic for the μ -1,1 mode and antiferromagnetic for the μ -1,3 mode [17–21]. The μ -1,3 thiocyanate bridges are generally found in binuclear compounds that show double μ -1,3 thiocyanate bridges. Copper(II) compounds with single thiocyanate bridges are quite scarce [22–24].

The goal of this present work is to synthesize new copper-based coordination assemblies with promising magnetic behavior mediated through pseudo-halides as co-ligands. Morpholine-based tridentate homoleptic Schiff base ligand has been found to be promising in this perspective [19]. The three nitrogen donors of this ligand may offer efficient binding to “hard” copper(II) centers simultaneously. The present Schiff base ligand has been selected as it can form a stable chelate ring through endo-cyclic N atom to bring about the desired degree of stability and plasticity around the copper(II) facilitating magnetic interaction. Here, we report the syntheses, X-ray structures, spectroscopic and magnetic properties of two new 1-D copper(II) coordination polymers formulated as $[Cu(L)(\mu$ -1,3- $N_3)]_n(ClO_4)_n$ (**1**) and $[Cu(L)(\mu$ -1,3-NCS)] $_n(ClO_4)_n$ (**2**), with the morpholine-based Schiff base ligand $L = (1\text{-methyl-}1H\text{-imidazol-}2\text{-yl})\text{-}N\text{-}[2\text{-(morpholin-4-yl)ethyl}]\text{methanimine}$. Compound **1** contains a single μ -1,3 azido auxiliary ligand, while single μ -1,3 ambidentate thiocyanate serves as the ancillary bridging ligand in **2**. Variable temperature magnetic studies have been performed on them. The observed magnetic behaviors have

been substantiated through low temperature Electron Paramagnetic Resonance (EPR) measurements.

2. Experimental

2.1. Reagents and instruments

Reagent grade 1-methyl-2-imidazolecarboxaldehyde and 4-(2-aminoethyl)morpholine were obtained from Sigma Aldrich, USA and used as received. Other chemicals, sodium azide and sodium thiocyanate, were also purchased from Sigma Aldrich and used as received. The solvents were of spectroscopic grade. Elemental analyses (C, H, and N) were performed on a Perkin Elmer 2400 II elemental analyzer. FT-Infrared spectra (KBr pellet) ($400\text{--}4000\text{ cm}^{-1}$) were recorded on a Shimadzu FTIR 8400 spectrophotometer. UV-vis spectra were recorded in acetonitrile solutions using a Shimadzu UV-1900I spectrophotometer. Solid-state electronic spectra of both **1** and **2** were recorded on a Perkin Elmer UV/VIS spectrophotometer (LAMBDA 35). Powder X-ray diffraction (PXRD) patterns of **1** and **2** were recorded on a Bruker D8 Advance X-ray diffractometer with Cu K α radiation ($\lambda = 1.548\text{ \AA}$) generated at 40 kV and 40 mA. ^1H and ^{13}C NMR spectra of **L** in CD_3OD solvent were measured on a Bruker NMR spectrometer. The ESI-MS (positive ion mode) spectra were measured on a Waters HRMS model XEVO-G2QTOF#YCA351 mass spectrometer. Room temperature electrical conductivity measurements of **1** and **2** in solution were measured on a calibrated direct reading conductivity meter (Systronics, India, model 304). Low temperature (143 K) EPR spectra of **1** and **2** were recorded with a Magnettech GmbH MiniScope MS400 spectrometer. The spectrometer was equipped with a temperature controller, TC H03. The spin resonance spectrometer was equipped with an FC400 frequency detector. Simulations of the EPR spectra were done using the EasySpin software package [25]. Variable temperature magnetic measurements were performed on polycrystalline samples of **1** and **2** (with masses of 25.043 and 28.912 mg, respectively) with a Quantum Design MPMS-XL-5 SQUID susceptometer from 2 to 300 K and with an applied magnetic field of 100 mT. The isothermal magnetization was measured with the same samples at 2 K with applied magnetic fields of 0 to 5 T. The susceptibility data were corrected for the sample holder previously measured using the same conditions and for the diamagnetic contribution of the samples as deduced by using Pascal's constant tables [26].

2.2. Synthesis of (1-methyl-1H-imidazol-2-yl)-N-[2-(morpholin-4-yl)ethyl]methanimine (**L**)

1-Methyl-2-imidazolecarboxaldehyde (55 mg, 0.5 mmol) was dissolved in 10 mL of methanol and 4-(2-aminoethyl) morpholine (65 mg, 0.5 mmol), dissolved in 10 mL of methanol, was added dropwise to the previous solution with continuous stirring. It was stirred for half an hour to obtain a colorless solution. The resulting solution was refluxed for 4 h in the presence of pre-activated molecular sieves ($4\text{ \AA} \times 5\text{ mm}$). After refluxing, the colorless reaction mixture was left in the air. After four days, the oily mass formed thereby was dried thoroughly keeping in a vacuum desiccator over anhydrous CaCl_2 .

Yield: 90 mg (81%). $C_{11}H_{18}N_4O$: (222.14). Anal. Calc. for $C_{11}H_{18}N_4O$: C, 59.42; H, 8.16; N, 25.20%. Found: C, 59.25; H, 8.35; N, 25.15%; 1H NMR (CD_3OD): δ (ppm): 8.28 (1H, s, azomethine proton), 7.19 (1H, d, for imidazole ring proton), 7.06 (1H, d, imidazole ring another proton), 4.00 (3H, s, N-methyl protons), 3.77 (2H, t, $-CH_2-$ protons close to morpholine ring N), 3.69 (4H, t, $-CH_2-$ proton of morpholine ring close to N), 2.71 (2H, t, $-CH_2-$ proton close to imine N), 2.56 (4H, t, $-CH_2-$ proton of morpholine ring close to O) (Figure S1); ^{13}C NMR (CD_3OD): δ (ppm): 154.28(C5), 144.17(C6), 129.22(C8), 126.61(C7), 67.66(C1), 60.27(C3), 59.76(C2), 55.01(C4), 35.75(C9) (Figure S2); FTIR (KBr pellet): (ν/cm^{-1}): 1648 (for $C=N$), 1440 (morpholine ring N) (Figure S3). UV-vis (CH_3CN): λ_{max} : 277 nm; ESI-MS (positive ion mode in CH_3OH) (m/z): (100%) ($L + Na^+$): 245.05 (Theo. 245.14) (Figure S4).

2.3. Synthesis of $[Cu(L)(\mu-1,3-N_3)]_n(ClO_4)_n$ (**1**)

The ligand **L** (22 mg, 0.1 mmol) was dissolved in 10 mL of methanol to have a colorless solution and was warmed at 40 °C for 5 min. $Cu(ClO_4)_2 \cdot 6H_2O$ (37 mg, 0.1 mmol), dissolved in 10 mL of methanol, was added dropwise to the warm solution of **L** with continuous stirring. After addition of metal solution, a light blue color appeared. The resulting reaction mixture was stirred for 30 min. After stirring, 5 mL aqueous solution of NaN_3 (6 mg, 0.1 mmol) was added dropwise to the resulting reaction mixture which turned deep blue. The resulting solution was further stirred for 30 min. Finally, the solution was left in open air for slow evaporation. After 3 days, a dark green crystalline precipitate separated, was filtered and washed thoroughly with chilled diethyl ether. The compound is soluble in CH_3CN , DMF, and DMSO and sparingly soluble in methanol but not in H_2O , THF, $CHCl_3$, DCM, and *n*-hexane.

Yield: 36 mg (85%); $C_{11}H_{18}N_7O_5ClCu$: (427.184), Anal. Calc. for $C_{11}H_{18}N_7O_5ClCu$: C, 30.90; H, 4.24; N, 22.94%; Found: C, 30.98; H, 4.18; N, 22.97%; FTIR (KBr pellet): (ν/cm^{-1}): 1639 (for $C=N$), 2082, 2054 and 2036 (for azide), 1088 and 623 (for perchlorate) (Figure S5); UV-vis (CH_3CN): λ_{max} (nm): 305, 385, and 669; Λ_M (CH_3CN): $119 \text{ Ohm}^{-1} \text{ cm}^2 \text{ mol}^{-1}$ (1:1 electrolyte).

2.4. Synthesis of $[Cu(L)(\mu-1,3-SCN)]_n(ClO_4)_n$ (**2**)

Compound **2** was synthesized following the same procedure and maintaining the same stoichiometric proportions as for **1**. Here, 5 mL of a methanolic solution of sodium thiocyanate (8 mg, 0.1 mmol) was employed in place of sodium azide. The compound is soluble in CH_3CN , $CHCl_3$, DMSO, THF, and DMF but insoluble in H_2O , MeOH, EtOH, DCM, *n*-hexane, and *n*-pentane.

Yield: 34 mg (77%); $C_{12}H_{18}N_5O_5SClCu$: (443.37), Anal. Calc. for $C_{12}H_{18}N_5O_5SClCu$: C, 32.48; H, 4.09; N, 15.79%; Found: C, 32.58; H, 4.05; N, 15.83%; FTIR (KBr pellet): (ν/cm^{-1}): 2089 and 2104 (for thiocyanate), 1094 and 625 (for perchlorate), 1641 (for $C=N$) (Figure S6); UV-vis (CH_3CN): λ_{max} (nm): 308 and 680; Λ_M (CH_3CN): $125 \text{ Ohm}^{-1} \text{ cm}^2 \text{ mol}^{-1}$ (1:1 electrolyte).

Dark green needle-shaped single crystals of **1** and **2**, suitable for X-ray diffraction, were harvested from their respective mother liquor.

CAUTION! The metal salts of perchlorate and azide with organic ligands are potentially explosive. They should be prepared and handled in small amounts with utmost care [27].

2.5. Crystallographic data collection and refinement

Dark green needle shaped crystals of **1** and **2** were examined under a microscope. Good diffraction quality single crystals of both complexes were hand-picked from their respective bulk material. High-resolution X-ray diffraction data for **1** at room temperature and for **2** at low temperature (104 K) were collected on a Bruker-Kappa APEX II CCD diffractometer. The instrument was equipped with a CCD detector. Graphite mono-chromated MoK α (0.71073 Å) radiation was used. The unit cell parameters were determined employing SMART software [28]. Empirical absorption corrections were made using SADABS [29]. The structures were solved using direct methods with the SHELXL-97 program package [30]. Subsequent difference Fourier syntheses and least-square refinements revealed the positions of the remaining non-hydrogen atoms that were refined anisotropically. Crystal data and structural refinement parameters for **1** and **2** are given in Table 1. Selected bond lengths and angles are listed in Table 2.

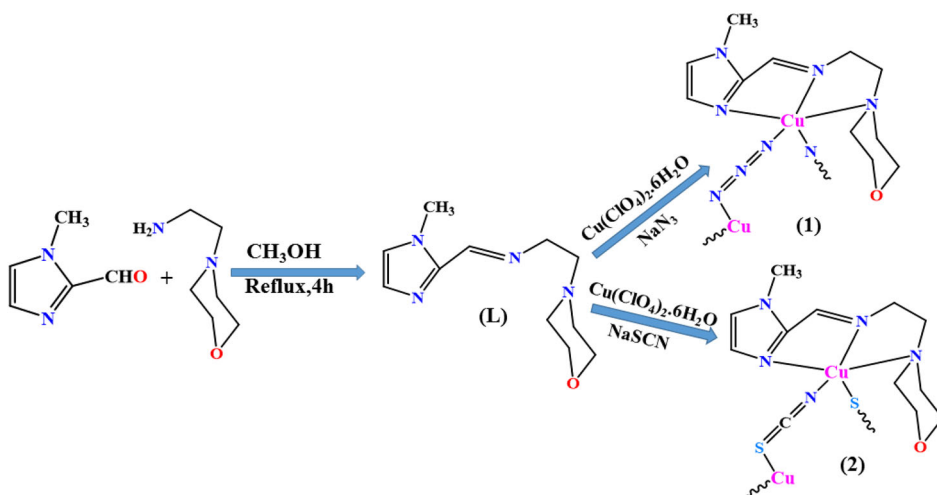
Table 1. Crystal data and structure refinement for **1** and **2**.

CCDC No.	2112634	2112635
Empirical formula	C ₁₁ H ₁₈ CuN ₇ O ₅ Cl	C ₁₂ H ₁₈ ClCuN ₅ O ₅ S
Formula weight	427.32	443.37
Temperature (K)	273	104
Wavelength (Å)	0.71073	0.71073
Crystal system	Orthorhombic	Monoclinic
Space group	<i>P</i> 2 ₁ 2 ₁ 2 ₁ (#19)	<i>P</i> 2 ₁ / <i>c</i> (#14)
<i>a</i> (Å)	6.9280(5)	10.8430(16)
<i>b</i> (Å)	13.5641(10)	6.2741(9)
<i>c</i> (Å)	18.6060(15)	24.823(4)
α (°)	90	90
β (°)	90	91.904(5)
γ (°)	90	90
Volume (Å ³)	1748.40(2)	1687.8(4)
<i>Z</i>	4	4
ρ_{calcd} (mg/cm ³)	1.62	3.59
Absorption coefficient (mm ⁻¹)	1.44	8.03
<i>F</i> (000)	876	1,764
θ Range for data collection (deg)	2.655–27.187	3.049–25.076
Limiting indices	–8 < <i>h</i> < 8 –17 < <i>k</i> < 16 –23 < <i>l</i> < 23	–12 < <i>h</i> < 12 –6 < <i>k</i> < 7 –29 < <i>l</i> < 29
Reflections collected/unique	15,725/3,857 [<i>R</i> _{int} = 0.0363]	11,744/2,949 [<i>R</i> _{int} = 0.0717]
Completeness of theta	99.4% (25.242)	98.5% (25.076)
Data/restraints/parameters	3,857/0/272	2,949/13/227
Goodness-of-fit on <i>F</i> ²	1.048	1.188
Final <i>R</i> indices [<i>I</i> > 2sigma (<i>I</i>)]	<i>R</i> ₁ = 0.0309 <i>wR</i> ₂ = 0.0686	<i>R</i> ₁ = 0.0960 <i>wR</i> ₂ = 0.2220
<i>R</i> indices (all data)	<i>R</i> ₁ = 0.0380 <i>wR</i> ₂ = 0.0723	<i>R</i> ₁ = 0.1066 <i>wR</i> ₂ = 0.2277
Largest diff. peak and hole	0.212 and –0.225 e Å ⁻³	1.912 and –1.126 e Å ⁻³

Table 2. Some selected bond lengths (Å) and angles (°) for **1** and **2**.

1			
Atoms	Distance (Å)	Atoms	Angle (°)
Cu1-N2	2.026(3)	N2-Cu1-N4	163.39(11)
Cu1-N3	1.963(3)	N2-Cu1-N7	90.06(13)
Cu1-N5	1.951(3)	N3-Cu1-N2	81.05(12)
Cu1-N4	2.075(3)	N3-Cu1-N4	82.34(12)
Cu1-N7	2.392(4)	N3-Cu1-N7	95.63(14)
		N5-Cu1-N2	100.53(13)
		N5-Cu1-N3	167.45(13)
		N5-Cu1-N4	95.68(12)
2			
Atoms	Distance (Å)	Atoms	Angle (°)
Cu1-S1	2.719(3)	N5-Cu1-S1	93.92(2)
Cu1-N5	2.092(8)	N3-Cu1-S1	93.62(2)
Cu1-N3	2.043(8)	N3-Cu1-N5	161.80(3)
Cu1-N4	1.965(8)	N4-Cu1-S1	95.70(3)
Cu1-N6	1.929(8)	N4-Cu1-N5	82.20(3)
		N4-Cu1-N3	80.50(3)
		N6-Cu1-S1	96.90(3)
		N6-Cu1-N4	167.30(4)

Symmetry code for **1**: $1/2 - x, -y, 1/2 + z$; for **2**: $1/2 - x, 1/2 + y, 1/2 + z$.

**Scheme 2.** Synthetic scheme of **L**, **1** and **2**.

3. Results and discussion

3.1. Syntheses of the complexes

Equimolar reaction of the morpholine-based Schiff base ligand (**L**) with copper(II) perchlorate hexahydrate in methanol followed by the addition of stoichiometric amount of sodium azide or sodium thiocyanate afforded, respectively, the polynuclear Cu(II) complexes, **1** and **2**, in satisfactory yield. The ligand and the complexes were characterized by elemental analysis, ESI-MS, FTIR, and UV-vis spectroscopy. In addition, formation of the ligand was confirmed by ^1H and ^{13}C NMR. Preparation of the ligand and complexes are depicted in Scheme 2.

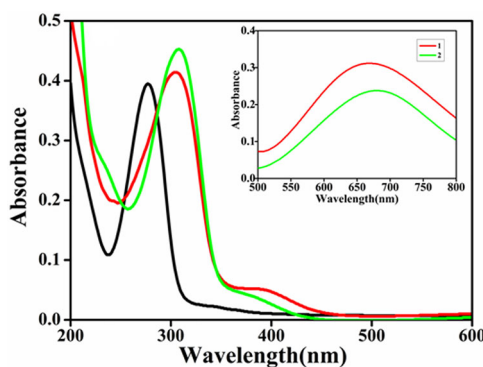


Figure 1. Electronic spectra of L (black), **1** (red), and **2** (green) in acetonitrile. Inset: d-d band of **1** and **2**.

3.2. Infrared spectra

The FTIR spectrum of the ligand shows a characteristic band at 1648 cm^{-1} , assigned to the imine ($\text{-C}=\text{N-}$) stretching vibration, that appears at 1639 cm^{-1} in **1** and 1641 cm^{-1} in **2**, suggesting coordination of the azomethine N atom to the copper(II) center [31]. The three bands at 2083 , 2054 , and 2037 cm^{-1} in **1** correspond to the μ -1,3 coordinated azido bridge [32]. Complex **2** shows two bands at 2089 and 2104 cm^{-1} , corresponding to N- and S-bonded thiocyanate bridge, respectively [9(d), 33–36]. Broad bands at 1088 cm^{-1} in **1** and 1094 cm^{-1} in **2** can be assigned to the asymmetric stretching vibration of non-coordinated perchlorate ion [37].

3.3. Electronic spectra

The electronic spectra of L, **1**, and **2** were recorded in acetonitrile solution (Figure 1). L shows a sharp absorption at 277 nm attributed to a $\pi\text{-}\pi^*$ transition [38]. In **1** and **2**, this transition is shifted, respectively, to 305 and 308 nm , indicating ligand binding. Much weaker but broad transition bands are observed at 669 and 680 nm , respectively, for **1** and **2**. These are assigned to d-d transition bands. Generally, broad d-d transition band appears at lower energy region below 700 nm . The position and the energetics of this band is characteristic of square-pyramidal copper(II) complexes [39].

3.4. Powder X-ray diffraction

To check the phase purity of the bulk materials with that of the simulated patterns (obtained from single-crystal structures), powder X-ray diffraction analyses of **1** and **2** at room temperature were recorded. In both compounds, the match between the experimental and simulated powder X-ray diffraction patterns confirms the phase purity of the samples (Figures S7 and S8).

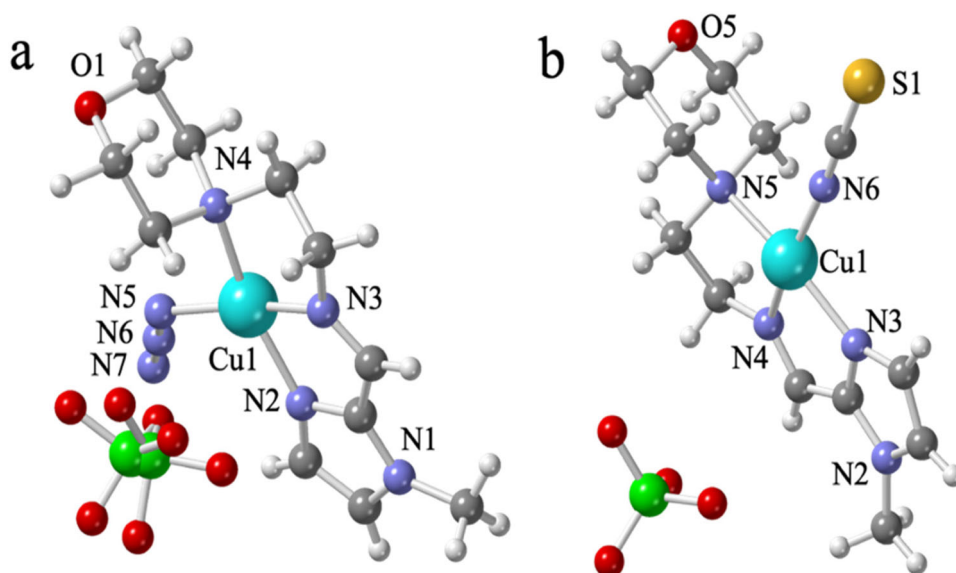


Figure 2. Asymmetric unit of **1** (a) and **2** (b) with the labeling of the main atoms.

3.5. Crystal structures of **1** and **2**

Single-crystal X-ray diffraction data show that **1** crystallizes in the orthorhombic space group $P2_12_12_1$ (#19), whereas **2** crystallizes in the monoclinic space group $P2_1/c$ (#14) (Table 1). The asymmetric unit of **1** contains one L, one N_3^- bridging ligand, one Cu(II) ion, and a free ClO_4^- anion, slightly disordered over two very close positions sharing one common oxygen atom (Figure 2(a)). The asymmetric unit of **2** is very similar: it contains one L, one SCN^- bridging ligand, one Cu(II) ion, and a free (ordered) ClO_4^- anion (Figure 2(b)).

In both compounds, the Cu(II) centers are chelated by the Schiff base ligand (L), acting as a tridentate chelating N_3 -donor. In **1** the Cu(II) ion is also coordinated to two azido anions that act as single μ -1,3 bridges, giving regular zigzag chains running along the a direction (Figure 3(a)). The disordered ClO_4^- is semi-coordinated to the Cu(II) ion with a long Cu-O distance of 2.971(4) Å. Compound **2** also presents zigzag regular chains (running along the b direction) where the μ -1,3- N_3^- bridges have been replaced by μ -1,3- SCN^- bridges (Figure 3(b)).

If we neglect the semi-coordinated ClO_4^- in **1**, we can consider that the Cu(II) ions in both compounds are five-coordinate with CuN_5 and CuN_4S chromophores in **1** and **2**, respectively. In both compounds the coordination geometry is a slightly distorted square pyramid, as indicated by their low Addison parameters (0.06 in **1** and 0.09 in **2**) [40]. In both compounds, the basal plane is formed by the three N atoms of L and by one N atom of a bridging azide (in **1**) or thiocyanate (in **2**). The axial position is occupied by a N atom of the other azide bridge in **1** or by the S atom of the other thiocyanate bridge in **2** (Figure 3). Packing diagram of **1** is shown in Figure S9.

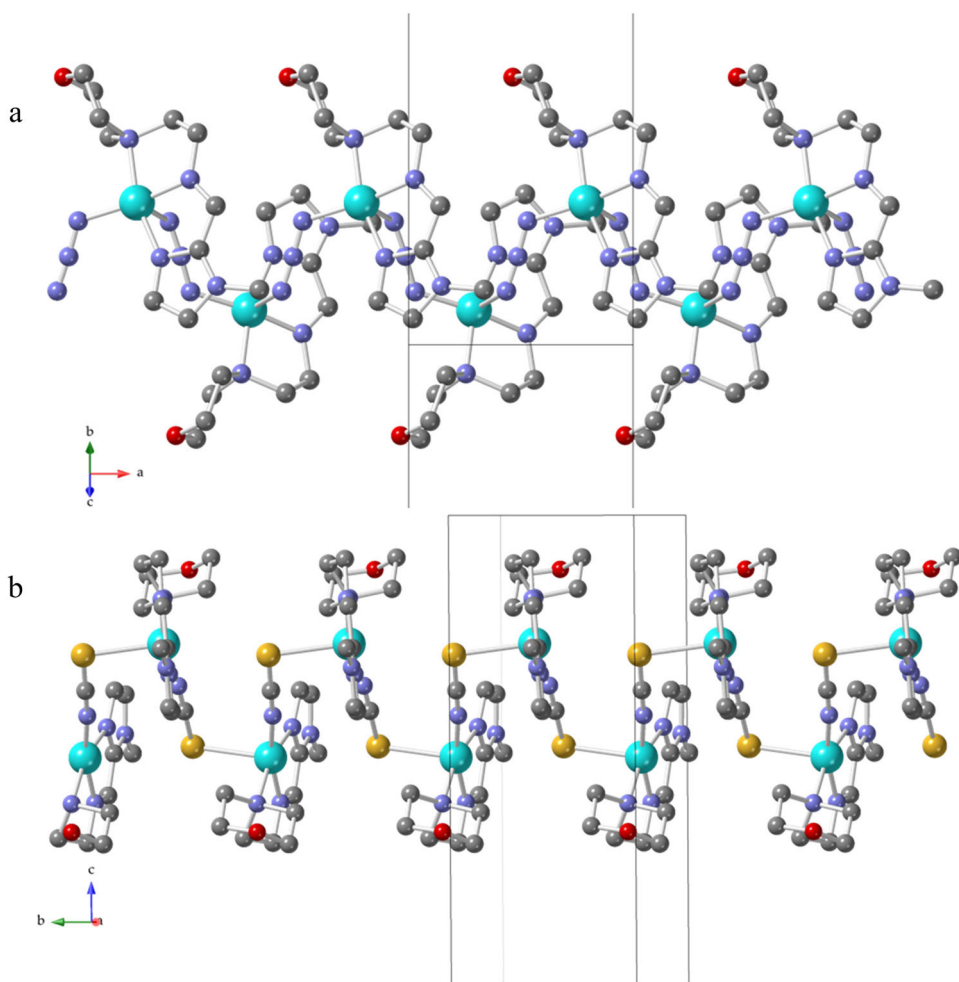


Figure 3. One-dimensional chain-like structures in **1** (a) (single end-to-end azido bridged) and in **2** (b) (single end-to-end thiocyanato bridged). ClO_4^- anions and H atoms are omitted for clarity. Color code: Cu = light blue, O = red, N = blue, S = yellow and C = gray.

As usually observed, in **1** the axial Cu1-N7 bond is significantly longer (2.392(4) Å) than the basal ones (Cu1-N2 = 2.026(3) Å, Cu1-N3 = 1.963(3) Å, Cu1-N4 = 2.075(3) Å and Cu1-N5 = 1.951(3) Å, Table 2) [41–43]. In **2**, the axial Cu1-S1 bond (2.719(3) Å) is also much longer than the basal Cu-N bonds (Cu1-N3 = 2.043(8) Å, Cu1-N4 = 1.965(8) Å, Cu1-N5 = 2.092(8) Å and Cu1-N6 = 1.929(8) Å). These values are consistent with those found in the literature [44]. The intrachain Cu...Cu distance in **1** is 5.7200(6) Å whereas in **2** this distance is 5.728(9) Å, both within the normal range (5.27–6.62 Å) observed in other similar Cu(II) single-bridged chain compounds [9(d), 24].

3.6. Magnetic properties

The thermal variation of the $\chi_m T$ product for **1** (χ_m is the molar magnetic susceptibility per Cu(II) ion) shows a room temperature value of ca. $0.42 \text{ cm}^3 \text{ K mol}^{-1}$, which is the

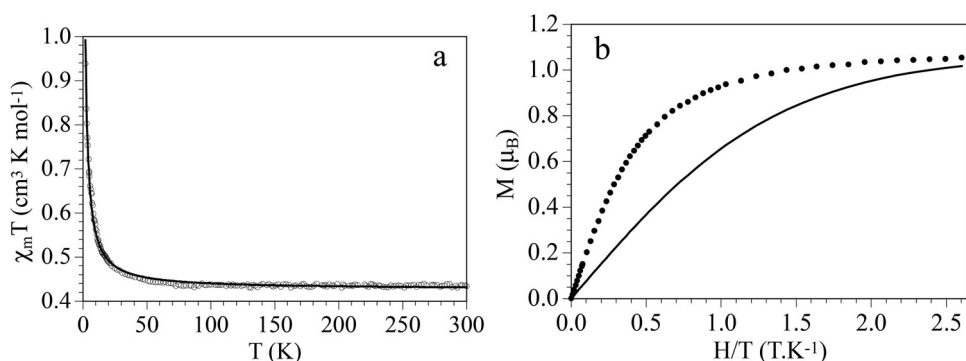


Figure 4. (a) Thermal variation of the $\chi_m T$ product for **1**. Solid line is the fit to the model (see text). (b) Isothermal magnetization at 2 K for **1**. Solid line is the Brillouin function for a $S = 1/2$ ion.

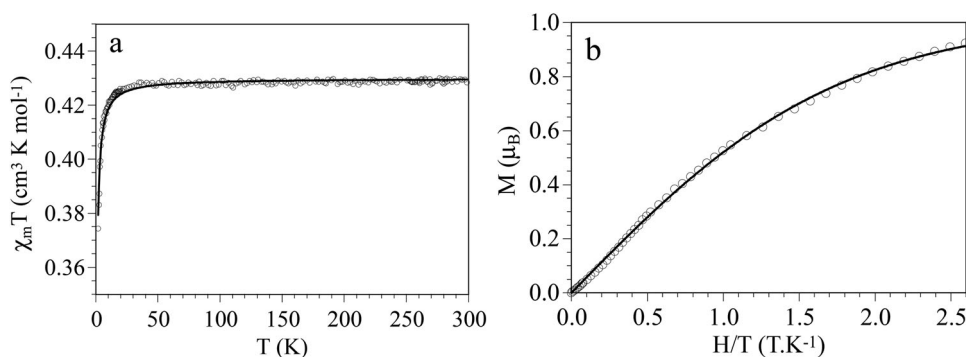


Figure 5. (a) Thermal variation of the $\chi_m T$ product for **2**. Solid line is the fit to the model (see text). (b) Isothermal magnetization at 2 K for **2**. Solid line is the Brillouin function for a $S = 1/2$ ion.

expected value for an isolated $S = 1/2$ Cu(II) ion. When the sample is cooled, $\chi_m T$ remains nearly constant to 50 K and it shows a progressive increase at lower temperatures, reaching a value of $0.95 \text{ cm}^3 \text{ K mol}^{-1}$ at 2 K (Figure 4(a)). This behavior indicates the presence of a weak intrachain Cu...Cu ferromagnetic interaction and, accordingly, we have fitted the magnetic data to a simple $S = 1/2$ regular ferromagnetic chain mode [1]. This model reproduces very satisfactorily the magnetic data in the whole temperature region with $g = 2.135(2)$ and $J = 2.13(2) \text{ cm}^{-1}$ (solid line in Figure 4(a); the Hamiltonian is written as $H = J \sum [S_i S_{i+1}]$).

The ferromagnetic coupling is further confirmed by the isothermal magnetization at 2 K that shows a rapid increase with increasing fields, well above the expected behavior for two independent $S = 1/2$ centers (solid line in Figure 4(b)).

As observed in **1**, the $\chi_m T$ product for **2** also shows a room temperature value close to $0.42 \text{ cm}^3 \text{ K mol}^{-1}$, the expected one for an isolated $S = 1/2$ Cu(II) ion (Figure 5(a)). This value remains constant down to ca. 10 K and below this temperature it shows a progressive decrease to reach a value of $0.38 \text{ cm}^3 \text{ K mol}^{-1}$ at 2 K. This behavior indicates that **2** presents a very weak antiferromagnetic intrachain Cu...Cu interaction.

Table 3. Structural and magnetic parameters for single or double (1,3) bridging azide ligand in Cu(II) complexes.

Compounds	Cu...Cu (Å)	Cu-N (Å)	Cu-N (Å)	Cu-N-N (°)	Geom	Mode	J (cm ⁻¹)	Ref.
[Cu(N ₃) ₂ (mtn)] _n	6.745	2.708	2.014	87.39	OC	EA	15.6/−2.6	47
[Cu(L1)(μ-1,3-N ₃) _n](ClO ₄) _n	—	2.266	1.991	136.7	SP	EA	2.69	48
[Cu(L2)(μ-1,3-N ₃) _n](ClO ₄) _n	—	2.398	1.946	122.5	SP	EA	2.02	48
[Cu ₂ (L2) ₂ (μ-1,3-N ₃) ₂](ClO ₄) ₂	5.746	2.950	2.037	123.0	OC	EA	2.4	49
[Cu(L1)(N ₃) _n](ClO ₄) _n	—	2.355	1.947	126.5	SP	EA	2.15	19
[Cu(L2)(N ₃) _n](ClO ₄) _n	5.630	2.311	1.965	131.2	SP	EA	3.61	19
1	5.720	2.392	1.951	124.2	SP	EA	2.14	This work

Abbreviations: mtn = N-methyl-1,3-propane diamine, OC = octahedral geometry, SP = square pyramidal geometry, EA = equatorial-axial bridge. [Cu(L1)(μ-1,3-N₃)_n](ClO₄)_n, L1 = *N,N*,2,2-tetramethyl-3-((pyridine-2-ylmethylene)amino)propan-1-amine; [Cu(L2)(μ-1,3-N₃)_n](ClO₄)_n, L2 = *N,N*-dimethyl-2-((pyridine-2-ylmethylene)amino)propan-1-amine; [Cu₂(L2)₂(μ-1,3-N₃)₂](ClO₄)₂, L2 = *N,N*-dimethyl-3-((pyridine-2-ylmethylene)amino)propan-1-amine; [Cu(L1)(N₃)_n](ClO₄)_n, L1 = *N,N*-dimethyl-2-((pyridine-2-ylmethylene)amino)ethan-1-amine; [Cu(L2)(N₃)_n](ClO₄)_n, L2 = *N,N*-diethyl-2-((pyridine-2-ylmethylene)amino)ethan-1-amine.

Accordingly, we have fitted the magnetic properties to a simple $S = 1/2$ antiferromagnetic regular chain [45]. This model reproduces satisfactorily the magnetic data in the whole temperature range with $g = 2.1412(3)$ and $J = -0.277(2)$ cm⁻¹ (solid line in Figure 5(a); the Hamiltonian is written as $H = -J \sum [S_i S_{i+1}]$). This very low J value confirms that the coupling is very weak and antiferromagnetic. A confirmation of the very weak antiferromagnetic coupling is provided by the isothermal magnetization at 2 K that can be well reproduced with the Brillouin function with $g = 2.03(1)$ and a very weak antiferromagnetic interaction of $-0.29(3)$ cm⁻¹ (solid line in Figure 5(b)).

3.7. Coupling mechanism

For d⁹ Cu(II) systems, the magnitude of the super-exchange phenomenon is strongly dependent on the bridging mode between the copper centers. Generally, μ-1,3 coordination mode of azido bridges gives antiferromagnetic coupling for different types of metals [1, 3, 46]. The e_g atomic orbitals are involved in this super-exchange mechanism. The coupling is strongly antiferromagnetic when the pseudo-halide ligand is bonded to equatorial coordination sites in both copper(II) ions (EE) since the d_{x²-y²} orbitals of both Cu(II) ions are involved in this exchange mechanism. In contrast when the azido bridge connects an axial position with an equatorial one (EA), the coupling is much weaker since the overlap between the d_{x²-y²} and d_{z²} atomic orbitals is very small.

In **1** and **2** the coordination geometry of the Cu(II) ions is square-pyramidal and the pseudohalide bridging ligand connects an axial with an equatorial coordination site (EA). So, we expect weak coupling between the copper(II) centers. The interaction may be ferro- or antiferromagnetic depending on their bond parameters in the bridging region. The maximum antiferromagnetic coupling occurs when the M-N-N bond angle is close to 110°. Accidental ferromagnetic coupling interaction may be found for larger bond angles. In **1**, the M-N-N bond angles are 124.2(3)° and 124.0(3)°. These values are similar to those found in other singly μ-1,3-N₃ bridged Cu(II) compounds, where very weak ferromagnetic couplings have been observed, as in **1** (Table 3). In **2**, the M-N-C and M-S-C angles are 175.0(9)° and 94.8(4)°, respectively. These values are

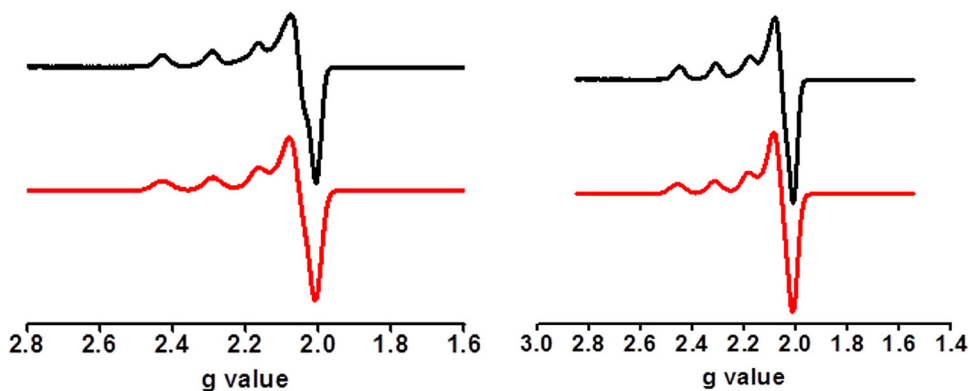
Table 4. Structural and magnetic parameters for the single or double (1,3) bridging thiocyanate ligand in Cu(II) complexes.

Compound	Cu...Cu (Å)	Cu-S (Å)	Cu-N (Å)	Cu-S-N (°)	Cu-N-C (°)	Geom	Mode	<i>J</i> (cm ⁻¹)	Ref.
[AsPh ₄][Cu(SCN) ₃]	5.549	2.775	1.966	98.2	163.8	SP	EE	-90	[50]
	5.559	2.409	1.930	104.1	165.9		EA		
[{Cu(L)(NCS) ₂ }] _n	5.599	2.770	1.960	97.6	146.5	SP	EA	0	[51]
[Cu(pyim)(NCS) ₂] _n	6.079	3.174	1.956	104.1	167.1	SP	EA	-0.03	[52]
[Cu ₂ (bpm)(NCS) ₂] _n	5.328	3.174	1.941	83.1	165.0	OC	EA	-0.6	[53]
[CuL(μ _{1,3} -NCS)] _n	6.628	2.806	1.954	111.3	173.2	SP	EA	-0.57	[54]
2	5.728	2.719	1.929	94.8	175	SP	EA	-0.28	This work

Abbreviations: pyim = 2-(2'-pyridyl)imidazole; bpm = 2,2'-bipyrimidine; OC = octahedral geometry, SP = square pyramidal geometry, EA = equatorial-axial bridge; EE = equatorial-equatorial bridge; [{Cu(L)(NCS)₂}]_n, L = 2-methylamino-5-pyridin-2-yl-1,3,4-oxadiazole; [CuL(μ_{1,3}-NCS)]_n, L = 3-((2-(dimethylamino)ethyl)imino)-1-phenylbutan-1-one.

Table 5. Magnetic parameters for **1** and **2**.

Complex	<i>g</i> values			<i>A</i> values (G)			Line width (G)
	<i>g</i> ₁	<i>g</i> ₂	<i>g</i> ₃	<i>A</i> ₁	<i>A</i> ₂	<i>A</i> ₃	
1	2.2284	2.0602	2.0519	172.29	17.85	1.77	5.8
2	2.2501	2.0573	177.32	14.85	6.4		

**Figure 6.** Experimental (black line) and simulated (red line) X-band EPR spectra of **1** (left) and **2** (right) obtained at 143 K in frozen DMF solution.

similar to those found in other Cu(II) compounds with a single μ-1,3 thiocyanato bridge, that show very weak antiferromagnetic couplings, as observed in **2** (Table 4).

3.8. EPR spectra

EPR spectra of **1** and **2** were recorded from frozen solution in DMF. The magnetic resonance parameters of **1** and **2** are shown in Table 5. Both EPR spectra obtained from frozen solution are characteristic of single μ-1,3 azido and thiocyanato bridged Cu(II) polymers, respectively, due to the d⁹ configuration of Cu(II) complexes with *S* = 1/2 spin state (Figure 6). Compound **1** shows a rhombic spectrum with *g*₁ > *g*₂ ≈ *g*₃ (Table 5), whereas **2** shows an axial spectrum with *g*₁ > *g*₂ = *g*₃ (Table 5). Both compounds show a hyperfine coupling of the unpaired electron with the *I* = 3/2 ⁶³Cu and ⁶⁵Cu nuclei, with much higher values for *A*₁ (Figure 6 and Table 5) [55]. The magnetic

resonance parameters obtained for **1** and **2** fully agree with the idea that the unpaired electron is located in the $d_{x^2-y^2}$ orbital [56–58].

4. Conclusion

The use of azide and thiocyanate as bridging ligands in combination with a morpholine-based tridentate N_3 -donor Schiff base ligand leads to the formation of two new 1-D copper(II) coordination polymers. Compound **1** contains single μ -1,3 azide bridges while **2** contains single μ -1,3 thiocyanate bridges. The magnetic susceptibility measurements reveal the presence of a weak ferromagnetic $Cu \cdots Cu$ intrachain interaction in **1** and a weak antiferromagnetic coupling in **2**, through the single μ -1,3 N_3^- and SCN^- bridges, respectively. Low temperature EPR spectra along with their simulation also corroborate the observed magnetic properties.

Disclosure statement

There is no conflict of interest to declare.

Acknowledgement

We are thankful to the reviewers for their valuable suggestions and comments to put the work into scientific context.

Funding

N.K.M. thankfully acknowledges the financial support received from the UGC, New Delhi, India in terms of senior research fellowship.

References

- [1] O. Kahn. *Molecular Magnetism*, Vch, Weinheim (1993).
- [2] (a) J.S. Miller, M. Drillon (Eds.), *Magnetism: Molecules to Materials*, Wiley-VCH, Weinheim (2007); (b) T.C. Stamatatos, G.S. Papaefstathiou, L.R. MacGillivray, A. Escuer, R. Vicente, E. Ruiz, S.P. Perlepes. *Inorg. Chem.*, **46**, 8843 (2007); (c) S. Sasmal, S. Sarkar, N. Aliaga-Alcalde, S. Mohanta. *Inorg. Chem.*, **50**, 5687 (2011); (d) E. Ruiz, P. Alemany, S. Alvarez, J. Cano. *J. Am. Chem. Soc.*, **119**, 1297 (1997); (d) A.C. Kathalikkattil, K.K. Bisht, N. Aliaga-Alcalde, E. Suresh. *Cryst. Growth Des.*, **11**, 1631 (2011).
- [3] (a) J. Ribas, A. Escuer, M. Monfort, R. Vicente, R. Cortés, L. Lezama, T. Rojo. *Coord. Chem. Rev.*, **193**, 1027 (1999); (b) H.Y. Zang, Y.Q. Lan, G.S. Yang, X.L. Wang, K.Z. Shao, G.J. Xu, Z.M. Su. *CrystEngComm*, **12**, 434 (2010); (c) M. Das, S. Chatterjee, S. Chattopadhyay. *Polyhedron*, **68**, 205 (2014); (d) A. Bacchi, M. Carcelli, T. Chiodo, P. Pelagatti. *CrystEngComm*, **12**, 4226 (2010).
- [4] (a) R. Lescouezec, J. Vaissermann, C. Ruiz-Perez, F. Lloret, R. Carrasco, M. Julve, M. Verdaguer, Y. Dromzee, D. Gatteschi, W. Wernsdorfer. *Angew. Chem. Int. Ed. Engl.*, **42**, 1483 (2003); (b) C. Biswas, S. Chattopadhyay, M.G.B. Drew, A. Ghosh. *Polyhedron*, **26**, 4411 (2007).
- [5] (a) L.M. Toma, R. Lescouezec, F. Lloret, M. Julve, J. Vaissermann, M. Verdaguer. *J. Chem. Soc. Chem. Commun.*, 1850 (2003); (b) Z.N. Chen, H.X. Zhang, K.B. Yu, K.C. Zheng, H. Cai, B.S. Kang. *J. Chem. Soc. Dalton Trans.*, 1133 (1998).

- [6] (a) E.-Q. Gao, S.-Q. Bai, C.-F. Wang, Y.-F. Yue, C.-H. Yan. *Inorg. Chem.*, **42**, 2933 (2010); (b) C. Adhikary, S. Koner. *Coord. Chem. Rev.*, **254**, 2933 (2010).
- [7] (a) L. Shen, Y.-Z. Xu. *J. Chem. Soc. Dalton Trans.*, 3413 (2001); (b) S. Mondal, P. Chakraborty, N. Aliaga-Alcalde, S. Mohanta. *Polyhedron*, **63**, 96 (2013).
- [8] (a) S. Khan, S. Sproules, L.S. Natrajan, K. Harms, S. Chattopadhyay. *New J. Chem.*, **42**, 1634 (2018); (b) C. Adhikary, R. Sen, G. Bocelli, A. Cantoni, S. Chaudhuri, S. Koner. *J. Coord. Chem.*, **62**, 3573 (2009); (c) S. Koner, S. Saha, T. Mallah, K.-I. Okamoto. *Inorg. Chem.*, **43**, 840 (2004).
- [9] (a) P. Cen, W. Yuan, S. Luo, X. Liu, G. Xie, S. Chen. *New J. Chem.*, **43**, 601 (2019); (b) S. Banerjee, M.G.B. Drew, C.-Z. Lu, J. Tercero, C. Diaz, A. Ghosh. *Eur. J. Inorg. Chem.*, 2376 (2005); (c) R.A. Bailey, S.L. Kozak, T.W. Michelsen, W.N. Mills. *Coord. Chem. Rev.*, **6**, 407 (1971); (d) Z.E. Serna, R. Cortes, M.K. Urtiaga, M.G. Barandika, L. Lezama, M.I. Arriortua, T. Rojo. *Eur. J. Inorg. Chem.*, 865 (2001).
- [10] F.R. Louka, S.S. Massoud, T.K. Haq, M. Koikawa, M. Mikuriya, M. Omote, R.C. Fischer, F.A. Mautner. *Polyhedron*, **138**, 177 (2017).
- [11] Z.-X. Miao, M.-X. Li, M. Shao, H.-J. Liu. *Inorg. Chem. Commun.*, **10**, 1117 (2007).
- [12] B. Machura, A. Świtlicka, J. Mroziński, B. Kalińska, R. Kruszynski. *Polyhedron*, **52**, 1276 (2013).
- [13] C.-M. Liu, S. Gao, D.-Q. Zhang, Y.-H. Huang, R.-G. Xiong, Z.-L. Liu, F.-C. Jiang, D.-B. Zhu. *Angew. Chem. Int. Ed. Engl.*, **43**, 990 (2004).
- [14] M. Mondal, S. Jana, M.G.B. Drew, A. Ghosh. *Polymer*, **204**, 122815 (2020).
- [15] I. Banerjee, J. Marek, R. Herchel, M. Ali. *Polyhedron*, **29**, 1201 (2010).
- [16] E.-Q. Gao, Y.-F. Yue, S.-Q. Bai, Z. He, C.-H. Yan. *Cryst. Growth Des.*, **5**, 1119 (2005).
- [17] A. Escuer, C.J. Harding, Y. Dussart, J. Nelson, V. McKee, R. Vicente. *J. Chem. Soc. Dalton Trans.*, 223 (1999).
- [18] Z. Shen, J.-L. Zuo, S. Gao, Y. Song, C.-M. Che, H.-K. Fun, X.-Z. You. *Angew. Chem. Int. Ed. Engl.*, **112**, 3779 (2000).
- [19] P.S. Mukherjee, T.K. Maji, A. Escuer, R. Vicente, J. Ribas, G. Rosair, F.A. Mautner, N.R. Chaudhuri. *Eur. J. Inorg. Chem.*, **2002**, 943 (2002).
- [20] C.S. Hong, Y. Do. *Angew. Chem. Int. Ed.*, **38**, 193 (1999).
- [21] C.S. Hong, J. Koo, S.-K. Son, Y.S. Lee, Y.-S. Kim, Y. Do. *Chem.—Eur. J.*, **7**, 4243 (2001).
- [22] J. Ribas, C. Diaz, X. Solans, M. Font-Bardía. *Inorg. Chim. Acta*, **231**, 229 (1995).
- [23] J. Cano, G. De Munno, F. Lloret, M. Julve. *Inorg. Chem.*, **39**, 1611 (2000).
- [24] N.K. Karan, S. Mitra, T. Matsushita, V. Gramlich, G. Rosair. *Inorg. Chim. Acta*, **332**, 87 (2002).
- [25] S. Stoll, A. Schweiger. *J. Magn. Reson.*, **178**, 42 (2006).
- [26] G.A. Bain, J.F. Berry. *J. Chem. Educ.*, **85**, 532 (2008).
- [27] (a) P.G. Urben (Ed.). *Bretherick's Handbook of Reactive Chemical Hazards*, 6th Edn., Butterworth-Heinemann, Oxford (1999); (b) W.C. Wolsey. *J. Chem. Educ.*, **50**, A335 (1973).
- [28] Bruker. *SMART (Version 5.0) and SAINT (Version 6.02)*, Bruker AXS inc., Madison, WI, USA (2000).
- [29] G.M. Sheldrick. *SADABS, Program for Empirical Correction of Area Detector Data*, University of Göttingen, Germany (2000).
- [30] G.M. Sheldrick. *SHELXS-97 and SHELXL-97, Program for Crystal Structure Refinement*, University of Göttingen, Germany (1997).
- [31] N.K. Mandal, B. Guhathakurta, P. Basu, A.B. Pradhan, C.S. Purohit, S. Chowdhury, J.P. Naskar. *J. Coord. Chem.*, **72**, 3625 (2019).
- [32] K. Nakamoto. *Infrared and Raman Spectra of Inorganic and Coordination Compounds*, 3rd Edn., Wiley, New York (1978).
- [33] J.S. Haynes, A. Kostikas, J.R. Sams, A. Simopoulos, R.C. Thompson. *Inorg. Chem.*, **26**, 2630 (1987).
- [34] B. Zurowska, J. Mroziński, M. Julve, F. Lloret, A. Maslejova, W. Sawka-Dobrowolska. *Inorg. Chem.*, **41**, 1771 (2002).
- [35] H. Grove, M. Julve, F. Lloret, P.E. Kruger, K.W. Törnroos, J. Sletten. *Inorg. Chim. Acta*, **325**, 115 (2001).

- [36] R. d. A. Farani, W.M. Teles, C.B. Pinheiro, K.J. Guedes, K. Krambrock, M.I. Yoshida, L.F.C. de Oliveira, F. C. Machado. *Inorg. Chim. Acta*, **361**, 2045 (2008).
- [37] (a) B.J. Hathaway, A.E. Underhill. *J. Chem. Soc.*, 3091(1961); (b) R.N. Patel, Y.P. Singh, Y. Singh, R.J. Butcher. *Polyhedron*, **104**, 116 (2016).
- [38] R. Li, B. Moubaraki, K.S. Murray, S. Brooker. *Eur. J. Inorg. Chem.*, **2009**, 2851 (2009).
- [39] A.B.P. Lever. *Inorganic Electronic Spectroscopy*, p. 553, Elsevier, Amsterdam (1984).
- [40] (a) A.W. Addison, T.N. Rao, J. Reedijk, J.V. Rijn, G.C. Verschoor. *J. Chem. Soc. Dalton Trans.*, 1349 (1984);(b) B. Guhathakurta, P. Basu, G.S. Kumar, L. Lu, M. Zhu, N. Bandyopadhyay, J.P. Naskar. *Polyhedron*, **110**, 227 (2016).
- [41] S. Banerjee, C. Adhikary, C. Rizzoli, R. Pal. *Inorg. Chim. Acta*, **409**, 202 (2014).
- [42] S. Sarkar, A. Mondal, J. Ribas, M.G.B. Drew, K. Pramanik, K.K. Rajak. *Inorg. Chim. Acta*, **358**, 641 (2005).
- [43] C. Adhikary, S. Koner. *Coord. Chem. Rev.*, **254**, 2933 (2010).
- [44] J. Lu, H.-T. Liu, D.-Q. Wang, X.-X. Zhang, D.-C. Li, J.-M. Dou. *J. Mol. Struct.*, **938**, 299 (2009).
- [45] D.B. Brown, J.A. Donner, J.W. Hall, S.R. Wilson, R.B. Wilson, D.J. Hodgson, W.E. Hatfield. *Inorg. Chem.*, **18**, 2635 (1979).
- [46] A. Escuer, R. Vicente, J. Ribas, M.S. El Fallah, X. Solans, M. Font-Bardia. *Inorg. Chem.*, **32**, 3727 (1993).
- [47] P. Bhowmik, S. Biswas, S. Chattopadhyay, C. Diaz, C.J. Gómez-García, A. Ghosh. *Dalton Trans.*, **43**, 12414 (2014).
- [48] S. Dalai, P.S. Mukherjee, M.G.B. Drew, T.-H. Lu, N.R. Chaudhuri. *Inorg. Chim. Acta*, **335**, 85 (2002).
- [49] P. Sarathi Mukherjee, S. Dalai, G. Mostafa, T.-H. Lu, E. Rentschler, N. Ray Chaudhuri. *New J. Chem.*, **25**, 1203 (2001).
- [50] C.A. White, G.P.A. Yap, N.P. Raju, J.E. Greedan, R.J. Crutchley. *Inorg. Chem.*, **38**, 2548 (1999).
- [51] P. Gómez-Saiz, J. García-Tojal, F.J. Arnáiz, M.A. Maestro, L. Lezama, T. Rojo. *Inorg. Chem. Commun.*, **6**, 558 (2003).
- [52] J. Carranza, J. Sletten, F. Lloret, M. Julve. *Polyhedron*, **28**, 2249 (2009).
- [53] M. Julve, M. Verdager, G.D. Munno, J.A. Real, G. Bruno. *Inorg. Chem.*, **32**, 795 (1993).
- [54] P. Talukder, A. Datta, S. Mitra, G. Rosair, M.S. El Fallah, J. Ribas. *Dalton Trans.*, 4161 (2004).
- [55] B.J. Pella, J. Niklas, O.G. Poluektov, A. Mukherjee. *Inorg. Chim. Acta*, **483**, 71 (2018).
- [56] L. Husarikova, Z. Repicka, J. Moncol, D. Valigura, M. Valko, M. Mazur. *Appl. Magn. Reson.*, **44**, 571 (2013).
- [57] B. Hathaway, D.E. Billing. *Coord. Chem. Rev.*, **5**, 143 (1970).
- [58] K. Das, S. Dolai, P. Vojtišek, S.C. Manna. *Polyhedron*, **149**, 7 (2018).

RESEARCH ARTICLE

Synthesis, characterization, crystal structure, thermal and redox behaviour and antiproliferative studies of morpholine-based two copper(II) compounds

Naba Kr Mandal¹  | Sudeshna Nandi²  | Krishnendu Acharya²  |
Jnan Prakash Naskar¹ 

¹Department of Chemistry, Jadavpur University, Kolkata, India

²Department of Botany, Molecular and Applied Mycology and Plant Pathology Laboratory, University of Calcutta, Kolkata, India

Correspondence

Jnan Prakash Naskar, Department of Chemistry, Jadavpur University, Kolkata 700 032, India.

Email: jpnaskar@rediffmail.com

Funding information

University Grants Commission; Jadavpur University

Two novel copper(II) complexes, $[\text{Cu}(\text{L})(\text{Cl})_2](\text{H}_2\text{O})$ (**1**) and $[\text{Cu}(\text{L})(\text{N}_3)_2]$ (**2**), have been synthesized from a morpholine-based *N,N,N* donor tridentate Schiff base ligand, (*E*)-*N*-(2-morpholinoethyl)-1-phenyl-1-(pyridin-2-yl)methanimine (**L**). Ligand (**L**) and its stabilized complexes, **1** and **2**, have been comprehensively characterized by different physical and spectroscopic techniques. Solid-state single-crystal X-ray structures of both **1** and **2** have been determined. Powder X-ray diffraction studies on the bulk samples of **1** and **2** have been executed to demonstrate that the synthesized bulk materials retain their solid-phase purity as that exists in the single crystals. Cyclic voltammetric experiments have been done to demonstrate the redox behaviour of **1** and **2**. UV-vis spectra of the copper(II) complexes with variation in time were accrued to probe that both **1** and **2** retain their stability in solution. Thermogravimetric analysis (TGA) has been performed to collate the thermal stability of **1** along with its possible thermal degradation behaviour. Room temperature magnetic moments of **1** and **2** have been determined. Cytotoxic activity of **1** and **2** has been screened against non-small human lung cancer cell, A549.

KEYWORDS

cancer and antiproliferation, copper, Schiff base, structure

1 | INTRODUCTION

Schiff bases, an important privileged class of organic compounds indeed, are deemed universal versatile ligands owing to their ubiquitous diverse anchoring propensities with different metal ions to foster a plethora of complexes with varied configurations.¹ These ligands and their complexes display promising catalytic, regulatory, antiradical, antibacterial, antiviral, antifungal, antioxidant and antiproliferative activities.² Morpholine-based assemblies are of contemporary interest for exhibiting excellent cytotoxic activity.³ In medicinal chemistry, morpholine acts as a good building block as well. The ring

oxygen atom in morpholine plays a big role for this manifested bioactivity.⁴ In our present work, we are concerned with a Schiff base ligand tethered with a morpholine moiety.

Cancer is the most leading cause of death worldwide.⁵ According to the World Health Organization (WHO), the year 2020 alone witnessed nearly 10 million fatalities globally out of this dreaded disease.⁶ Lung, liver, stomach, breast, colon and rectum cancers are quite common.⁷ By 2040, an estimated global fatality count will alarmingly reach 29.5 million. Thus, catastrophic disaster-like havoc is on the offing. Dreadful lung cancer (LC) is the most severe amongst all forms of cancer. The

5-year survival rate of LC patients is even lower than 20%.⁸ This malady is designated as the prime cause of anthropogenic fatality, morbidity and mortality. In the present study, we are concerned with human adenocarcinoma LC cell line, A549. To combat cancer, chemotherapy has still been focused as a prime clinical protocol. Owing to its anticancer efficacies, cis-platin and its suitable derivatives have clinically been used widely. Judged on their promising and remarkable success, platinum-based anticancer drugs seem to be indispensable in the management and therapy of cancer. However, platinum-based chemotherapy still suffers from some inherent therapeutic shortcomings. They pose non-negligible dose-limiting harsh side effects in terms of nephrotoxicity, liver toxicity, neurotoxicity, general toxicity and, most importantly, drug resistivity.⁹ Thus, development of new drugs with promising fruitfulness but with tolerable limit of marginalized side effects is the crying need of the day. In this perspective, a biocompatible coinage transition metal, copper, is proven to be the front runner. Copper is an essential microelement for most of the aerobic living organisms. Displaying untenable role in redox biology, it functions as a structural and catalytic cofactor in many crucial life-sustaining pathways.¹⁰ Contrary to platinum-based agents, copper-based systems principally bind DNA double helix in noncovalent mode. Copper complexes display electrostatic, groove and intercalative modes of protein binding propensities.¹¹ It has truly been demonstrated that copper and copper-anchoring proteins are interlinked with malignancy progression, propagation, angiogenesis and metastasis.¹² Consequently, copper-based coordination complexes may offer satisfactory antiproliferative, anticancer and antineoplastic efficacies.¹³ Again, the underlying viable mechanistic pathways of in vivo absorption, assimilation, propagation and excretion of copper have comprehensively been studied.¹⁴ All these aspects of copper chemistry rekindled unabated interest over the years to undertake sincere efforts to develop copper-based anticancer chemotherapeutic drugs. By this time, a good number of copper coordination complexes as artificial nucleases have successfully been demonstrated to show commendable cytotoxic effects on a variety of cancer cells.¹⁵ This can be reckoned readily that the noteworthy copper(II) compound of L. Ruiz-Azuara and co-workers, [Cu(II)(4,4'-dimethyl-2,2'-bipyridine)(acetylacetone)(NO₃)(H₂O)], has entered clinical trials (phase I).¹⁶ Copper complexes appear to be potential anticancer agents with limiting toxic and dose-limiting effects.¹⁷ This wonderful aspect of copper chemistry has aroused our interest as well to work along this line. Herein, we wish to report the syntheses, characterization and structures of two new mononuclear copper(II) complexes stabilized from a novel Schiff base

ligand. The ligand bears suitable disposition of pharmacologically crucial morpholine moiety. Redox and thermal behaviour of them has also been expounded. Our present study also encompasses the in vitro inhibitory cytotoxic activity of the ligand and its two mononuclear copper(II) complexes against non-small cell lung cancer (NSCLC) cell line, A549.

2 | EXPERIMENTAL SECTION

2.1 | Materials and methods/chemicals

High purity benzoyl pyridine ($\geq 99\%$) and 4-(2-aminoethyl)morpholine (99%) were procured from Sigma Aldrich. Other chemicals like CuCl₂·2H₂O and NaN₃ were of reagent grade and were used as such. Commercially available solvents of analytical grade reagent were used as received. For spectroscopic studies and cyclic voltammetric measurements, spectroscopic grade solvents were employed. Dulbecco's modified Eagle's medium (DMEM), 4',6-diamidino-2-phenylindole (DAPI), acridine orange (AO), ethidium bromide (EtBr) and propidium iodide (PI) were purchased from HiMedia (Mumbai, India). Antibiotic Pen-Strep and amphotericin B were procured from MP Biomedicals (USA). Fetal bovine serum (FBS) and water-soluble tetrazolium (WST) were purchased from Invitrogen (Carlsbad, CA, USA) and Takara Bio Inc (Japan), respectively. Copper(II) compounds, **1** and **2**, were dissolved in dimethylsulfoxide (DMSO), and a master concentration of 10 mM was prepared for performing all the cellular assays. At no point of our experiments did the concentration of DMSO exceed 0.8% (v/v) during treatment. All experiments were performed on cells treated with compounds and ligand for 24 h.^{17d,e}

Nuclear magnetic resonance (NMR) spectra (¹H, ¹³C and correlation spectroscopy [COSY]) of the ligand were recorded on a Bruker 400 MHz (ASCEND) spectrometer at room temperature in suitable deuterated solvents. Chemical shift was followed in parts per million with respect to internal standard reference, tetramethylsilane (TMS). Electronic absorption spectra of the ligand and its stabilized copper(II) complexes, **1** and **2**, were recorded on a SHIMADZU UV 1900i spectrophotometer in methanol. Mass spectra (positive ionization mode) were run on a Waters HRMS (XEVO-GTQTOF#YCA351) spectrometer. Magnetic susceptibilities of **1** and **2** were measured at room temperature on a PAR 155 magnetometer. The instrument was standardized with the standard calibrant, Hg[Co(SCN)₄]. The requisite diamagnetic corrections to the experimentally determined susceptibility values were made with the help of Pascal's constants.¹⁸ Fourier transform infrared (FT-IR) spectra were recorded by using a

SHIMADZU FT-IR-8400S spectrophotometer (4000–400 cm^{-1}). Powder X-ray diffraction (PXRD) patterns were acquired on a Bruker D8 Advance X-ray diffractometer (1D mode). The patterns were collected with $\text{CuK}\alpha$ ($\lambda = 1.548 \text{ \AA}$) radiation generated at 40 kV and 40 mA. Thermogravimetric analysis (TGA) of **1** was performed using a Diamond Pyris 480 (Perkin Elmer) thermal analyser. The data were accrued using $\alpha\text{-Al}_2\text{O}_3$ as a standard under dynamic nitrogen flow rate of 150 mL min^{-1} with a heating rate of $10^\circ\text{C min}^{-1}$. Electrical conductivities of the methanolic solutions of **1** and **2** were measured on a Systronics India (Model 304) direct reading conductivity cell. The conductivity metre was calibrated with aqueous KCl (0.1 M) solution prior use. Electrochemical cyclic voltammetric studies were conducted for **1** and **2** under the blanket of pure and dry N_2 gas in dehydrated and degassed methanol milieu on a CHI 600C (USA) electrochemical workstation at room temperature. The conventional three-electrode configuration was consisted of a BAS Glassy Carbon (GC) working electrode, a platinum wire counter electrode and a Ag/AgCl reference electrode. Tetra-*n*-butyl ammonium perchlorate (TBAP) in 0.1 M of concentration served the purpose of indifferent supporting electrolyte.

Caution: Azide salts are potentially explosive and, therefore, hazardous. Although we faced no difficulty, extreme care should be taken to handle this salt and must be used in small quantity.¹⁹

2.2 | Synthesis of the ligand (L)

A total of 0.130 g (1 mmol) of 4-(2-aminoethyl)morpholine was dissolved in 25 mL of methanol to have a colourless solution. A total of 0.183 g (1 mmol) of solid benzoyl pyridine was added all at a time to the morpholine solution at room temperature to obtain a colourless solution. The resulting reaction mixture was heated under reflux for 5 h. After refluxing, the faint yellow solution obtained thereby was kept in the air for slow aerial evaporation. A light yellow gummy product was imparted after 5 days of standing. This pasty mass so obtained was thoroughly dried in vacuo over fused anhydrous calcium chloride. The ligand is soluble in H_2O , MeOH, CH_3CN , dichloromethane (DCM) and DMSO.

Yield: 0.25 g (85%); Anal. Calcd for $\text{C}_{18}\text{H}_{21}\text{N}_3\text{O}$ (molecular weight [MW] 295.168): C, 73.17; H, 7.17; N, 14.22%; found: C, 73.13; H, 7.20; N, 14.25%; FT-IR (KBr pellet) (ν/cm^{-1}): 2940, 2855, 2810 (C—H); 1663 (C=N); 1115 (morpholine ring C—N) (Figure S1); electrospray ionization mass spectrometry (ESI-MS; positive ion mode in CH_3OH) (m/z): 318.157 $[(\text{L} + \text{Na})]^+$ (100%) (theo. value 318.168) (Figure S2). $^1\text{H-NMR}$ (CD_3OD): δ (ppm):

8.68 (1H, d, pyridine ring proton close to N), 7.98–8.00 (3H, m), 7.64–7.68 (2H, m), 7.51–7.62 (3H, m), 3.65–3.71 (6H, m), 2.75 (2H, t, CH_2 protons of morpholine ring N), 2.48 (4H, t, CH_2 protons of morpholine ring) (Figure S3); $^{13}\text{C-NMR}$ (CD_3OD): δ (ppm): 167.82 (C6), 154.84 (C5), 148.20 (C1), 138.24 (C7), 136.14 (C3), 132.93 (C10), 130.35 (C8), 127.98 (C9), 126.42 (C2), 124.26 (C4), 66.15 (C16), 58.89 (C14), 53.60 (C15), 50.54 (C13) (Figure S4); $^1\text{H-NMR}$ (CDCl_3): δ (ppm): 8.73 (1H, d, pyridine ring proton close to N), 8.07–8.03 (3H, m), 7.90 (1H, t), 7.60 (1H, d), 7.51–7.47 (3H, m), 3.70 (4H, t, $-\text{CH}_2$ protons close to morpholine O atom), 3.48 (2H, t, $-\text{CH}_2$ protons close to imine N), 2.49 (4H, t, CH_2 protons of morpholine ring), 1.22 (2H, t) (Figure S5); UV-vis (CH_3OH): λ_{max} ($\epsilon/\text{M}^{-1} \text{cm}^{-1}$): 261 nm (18,503).

In the 2D COSY NMR experiment, the spin-spin interaction through cross-contour peak has been determined for the adjacent protons. The ^1H – ^1H COSY NMR spectrum of **L** has been shown in Figure S6.

2.3 | Synthesis of $[\text{CuL}(\text{Cl})_2] \cdot \text{H}_2\text{O}$ (1)

A total of 0.030 g (0.1 mmol) of **L** was dissolved in 10 mL of methanol to have a faint yellow solution. This ligand solution was added dropwise to a 10-mL blue aqueous solution of $\text{CuCl}_2 \cdot 2\text{H}_2\text{O}$ (0.017 g, 0.1 mmol) with continuous stirring. Within a few minutes of stirring, the colour became green. This reaction mixture was further stirred for 3 h. Finally, the resulting dark green solution was left aside undisturbed at room temperature for slow evaporation. After 3 days, a crystalline compound was harvested by filtration followed by thorough washing with chilled diethyl ether. The compound is soluble in H_2O , MeOH, DMSO and CH_3CN . However, it is insoluble in tetrahydrofuran (THF), DCM and dimethylformamide (DMF).

Yield: 33 mg (76%); $\text{C}_{18}\text{H}_{23}\text{N}_3\text{O}_2\text{Cl}_2\text{Cu}$ (447.73); Anal. Calcd for $\text{C}_{18}\text{H}_{23}\text{N}_3\text{O}_2\text{Cl}_2\text{Cu}$: C, 48.26; H, 5.17; N, 9.38%; found: C, 48.22; H, 5.21; N, 9.35; FT-IR (KBr pellet) (ν/cm^{-1}): 3526 (ν O—H, H_2O), 1632 (C=N), 1441 (C—C), 1109 (C—N) (Figure S7); ESI-MS (positive ion mode in CH_3OH) (m/z): 393.216 for (Calcd 393.668) $[\text{Cu}^{63}\text{L}(\text{Cl} + \text{H}_2\text{O})]$ (100%) and 395.213 for (Calcd 395.668) $[\text{Cu}^{65}\text{L}(\text{Cl} + \text{H}_2\text{O})]$ (Figure S8); UV-vis (CH_3OH): λ_{max} ($\epsilon/\text{M}^{-1} \text{cm}^{-1}$): 274 nm (16,143), 695 nm (1 51); Λ_{M} (CH_3OH) (non-electrolyte); $\mu_{\text{eff.}} = 1.82 \mu_{\text{B}}$ at 298 K.

2.4 | Synthesis of $[\text{CuL}(\text{N}_3)_2]$ (2)

A total of 0.030 g (0.1 mmol) of **L** was dissolved in 10 mL of methanol to get a faint yellow solution. A 10-mL methanolic solution of $\text{CuCl}_2 \cdot 2\text{H}_2\text{O}$ (0.017 g, 0.1 mmol)

was added dropwise to the ligand solution with continuous stirring. Immediately, the colour of the solution turned green. After 15 min of stirring, a 5-mL aqueous solution of NaN_3 (0.007 g, 0.1 mmol) was added dropwise to the resulting green solution. The reaction mixture was further stirred for 30 min. A deep green solution obtained thereby was kept aside undisturbed in open air for slow evaporation. After 4 days, a dark green crystalline compound was obtained. The crystals were collected through filtration and were washed copiously with chilled diethyl ether.

Yield: 30 mg (66%); $\text{C}_{18}\text{H}_{21}\text{N}_9\text{OCu}$ (442.714); Anal. Calcd for $\text{C}_{18}\text{H}_{21}\text{N}_9\text{OCu}$: C, 48.78; H, 4.78; N, 28.46%; found: C, 48.74; H, 4.81; N, 28.49%; FT-IR (KBr pellet) (ν/cm^{-1}): 2062, 2015 (for azide), 1645 (for $\text{C}\equiv\text{N}$), 1444 ($\text{C}-\text{C}$), 1107 ($\text{C}-\text{N}$) (Figure S9); ESI-MS (positive ion mode in CH_3OH) (m/z): 393.054 for (Calcd 393.109) $[\text{Cu}^{63}\text{L} + \text{Li}]^+ \cdot (2\text{N}_2)$ and 395.050 for (Calcd 395.109) $[\text{Cu}^{65}\text{L} + \text{Li}]^+ \cdot (2\text{N}_2)$ (Figure S10); UV-vis (CH_3OH): λ_{max} ($\epsilon/\text{M}^{-1} \text{cm}^{-1}$): 272 nm (21,901), 396 nm (35 21) and 668 nm (268); Λ_{M} (CH_3OH) (non-electrolyte); $\mu_{\text{eff.}} = 1.80 \mu_{\text{B}}$ at 298 K.

2.5 | Cell culture

Human A549 NSCLC cells were purchased from the National Centre for Cell Science (Pune, India). Cells were maintained in complete DMEM supplemented with 1% antibiotic-antimycotic solution (Gibco; Thermo Fisher Scientific, Inc., Grand Island, NY, USA) and 10% FBS. The culture was maintained for 3–4 days so that cells get enough time to spread as a monolayer. Cells attaining a confluence of 80%–90% were then harvested for further analysis. The cells were maintained at 37°C in a humidified atmosphere containing 5% CO_2 for all the experiments.

2.6 | Cell proliferation assay

A standard WST-1 (WST salt) (Roche Applied Science, India) method was utilized to assess cellular viability assays. This method works on the basis of cleavage of tetrazolium into an insoluble purple formazan product by mitochondrial dehydrogenase of intact cells.²⁰ A total of 4×10^3 cells that were in the exponential growth phase were seeded into a 96-well culture plate along with negative untreated control set (only cells). Cells were further treated overnight with various concentrations (2.2–220 μM) of compounds **1** and **2** and ligand (**L**) along with a vehicle control set separately. Simultaneously, doxorubicin was taken as positive control and also subjected to

concentrations ranging from 0.1 to 10 μM . After incubating the cells for 24 h with compounds **1** and **2**, ligand (**L**) and doxorubicin, the WST-1 reagent was added to the medium and incubated for 2.5 h. The absorbance was measured at 450 nm using a Bio-Rad (Model 550) microplate reader. The percentage of cell viability was measured using WST-1 absorption percentage following the protocol of Nandi and co-workers.²¹

2.7 | Assay of cell viability with trypan blue exclusion assay

The cell viability was also evaluated following the protocol of trypan blue exclusion assay. A549 cells were cultured on 24-well plates until 70% confluence and then rinsed with phosphate-buffered saline (PBS) and exposed to various concentrations of compounds **1** and **2** and ligand (**L**) for 24 h. A negative control and a vehicle control were also taken. The adherent cells were trypsinized followed by centrifugation at 2500 rpm for 6 min to collect the cell pellet for three groups. In a fresh medium, the cell pellets were re-suspended from which a 10- μL aliquot was taken and an equal volume of 0.4% trypan blue dye was mixed with it. The absorbance of the samples was measured with a microplate reader at 590 nm of wavelength using a Multiskan GO microplate spectrophotometer. The percentage of viable cells was determined by calculating the number of cells able to exclude the dye based on the following formula:

$$\% \text{Inhibition} = (\text{Total dead cell count} / \text{Total cell count}) \times 100.$$

2.8 | Colony formation assay

A549 cells were trypsinized and plated into a 12-well culture plate at a density of 2×10^3 cells. Cells were treated with compounds **1** and **2** as indicated and cultured for 7–10 days to allow colony formation. After incubation, colonies were fixed with 4% paraformaldehyde (for 10 min) and stained with 0.1% crystal violet for 15 min. Later, extra crystal violet stains were washed out and images of stained colonies were scanned.

2.9 | Morphological evaluation

An inverted phase contrast microscope (CKX53; Olympus, Tokyo, Japan) was used to monitor morphological

changes in cancerous cells treated with our experimental drug. A total of 4×10^4 A549 cells were grown onto a 2-mm glass plate and were incubated at 37°C followed by conventional trypsinization. The alterations in morphological appearance of cells were imaged and considered in evaluation after 24 h post-treatment with various concentrations of compounds **1** and **2** and ligand (**L**). The untreated cells were served as negative control.

2.10 | Cell cycle assay

During each cell cycle, DNA content varied from one phase to another. Briefly, A549 cell pellets of both **1** and **2** were collected and rinsed thrice with buffer and fixed in ice-cold 70% ethanol overnight at -20°C prior to staining. The following day, cells were washed again with buffer and were stained with PI in the dark for 15 min at room temperature and were then examined for cell cycle distribution by Accuri C6 flow cytometer.²² Results were expressed as a percentage of cells accumulated in the G0/G1, S and G2/M phases on the basis of differential DNA content.

2.11 | Morphological observation of nuclear change

Cells were cultured in a six-well plate to a confluence of 70%–75% and then treated with two dosages of compounds **1** and **2** for 24 h. After incubation, A549 cells were rinsed and fixation was carried out with 4% paraformaldehyde. Subsequently, 0.1% Triton X was used to permeabilize the cells for better staining. The fixed cells were stained with 0.1 mg mL^{-1} DAPI solution, wrapped in aluminium foil and incubated in the dark for 10 min. The surplus stain was rinsed out from the plate and viewed under the fluorescence microscope (EVOS FL, Invitrogen).

2.12 | Assessment of apoptosis by AO/EtBr staining

To identify the different stages of apoptosis, comprising early, late and necrotic phases, 5×10^4 cells per well were treated with different concentrations of **1** and **2** and harvested after 24 h of treatment. The morphological features of apoptosis induced by both the compounds were evaluated using acridine orange–ethidium bromide dual (AO/EtBr) staining. The harvested cells were incubated for 10 min with AO/EtBr in a ratio of 1:1 at room temperature followed by rinsing the extra stain and images were

captured under an EVOS FL fluorescence microscope (Invitrogen).

2.13 | X-ray crystallography

Green needle-shaped single crystals of both **1** and **2**, obtained from respective mother liquor, were selected for data collection under observation through a polarizing microscope. Single-crystal X-ray diffraction (SC-XRD) data of both **1** and **2** were accrued employing a Bruker Smart Apex CCD diffractometer at room temperature. The instrument was equipped with graphite monochromated $\text{MoK}\alpha$ radiation ($\lambda = 0.71073 \text{ \AA}$). SAINTPLUS²³ and SADABS²⁴ programme packages were used respectively for data reduction and semi-empirical absorption correction. By using direct methods, the structures were solved and refined through SHELXS-97 programme package software.²⁵ All the hydrogen atoms were placed geometrically and non-hydrogen atoms were refined anisotropically. The crystal data along with structure refinement of both **1** and **2** are summarized in Table 1. Some important bond lengths and angles of **1** and **2** are presented in Table 2. Hydrogen bonding parameters of **1** along with symmetry code are given in Table 3. Other bonding parameters of **1** and **2** are presented in Tables 4 and 5.

3 | RESULTS AND DISCUSSION

3.1 | Synthesis and characterization

A morpholine-based Schiff base ligand (**L**) has been prepared by 1:1 Schiff base condensation of benzoyl pyridine and 4-(2-aminoethyl)morpholine. Mononuclear Cu(II) complexes in optimum yields were prepared by stirring a methanolic solution of $\text{CuCl}_2 \cdot 2\text{H}_2\text{O}$ with equimolar proportion of **L** for **1** and a methanolic $\text{CuCl}_2 \cdot 2\text{H}_2\text{O}$ solution followed by addition of sodium azide with equimolar proportion of the ligand for **2**. After a few days of slow evaporation of the respective mother liquor, green-coloured needle-shaped crystals, suitable for X-ray diffraction studies, were harvested at room temperature. The synthetic scheme of the ligand and its copper(II) complexes is depicted in Scheme 1. Both **1** and **2** were structurally characterized by single-crystal X-ray crystallography.

The FT-IR spectrum of bare **L** shows a characteristic vibrational stretching band at 1663 cm^{-1} . This evidences $\text{C}=\text{N}$ bond formation.²⁶ Upon complexation, this band shifted bathochromically to lower wavenumber values of 1632 and 1645 cm^{-1} for **1** and **2**, respectively. This owes

TABLE 1 Crystal data and structure refinement for **1** and **2**.

CCDC no.	2,218,689	2,218,688
Empirical formula	C ₁₈ H ₂₃ CuN ₃ O ₂ Cl ₂	C ₁₈ H ₂₁ CuN ₃ O
Formula weight	447.84	442.99
Temperature (K)	293(2)	273(2)
Wavelength (Å)	0.71073	0.71073
Crystal system	Orthorhombic	Monoclinic
Space group	Pbca	P21/c
a (Å)	11.046(2)	11.4787(10)
b (Å)	13.278(3)	16.0615(14)
c (Å)	25.871(5)	11.7291(11)
α (°)	90	90
β (°)	90	112.444(3)
γ (°)	90	90
Volume (Å ³)	3794.5(13)	1998.6(3)
Z	8	4
ρ _{calcd} (mg cm ⁻³)	1.568	1.472
Absorption coefficient (mm ⁻¹)	1.451	1.123
F (000)	1848.0	916
θ range for data collection (°)	2.423 to 27.163	1.920 to 27.769
Limiting indices	−14 < h < 14 −17 < k < 17 −33 < l < 33	−15 < h < 15 −20 < k < 20 −14 < l < 14
Reflections collected/unique	124,959/4210 (R _{int} = 0.0944)	66,940/4433 (R _{int} = 0.0573)
Completeness of theta	99.9% (25.242)	99.9% (25.242)
Data/restraints/parameters	4210/0/243	4693/0/262
Goodness of fit on F ²	1.033	1.050
Final R indices (I > 2 sigma [I])	R ₁ = 0.0309 wR ₂ = 0.0686	R ₁ = 0.0960 wR ₂ = 0.2220
R indices (all data)	R ₁ = 0.0594 wR ₂ = 0.1449	R ₁ = 0.0420 wR ₂ = 0.1021
Largest diff. peak and hole	0.446 and −0.585 e·Å ⁻³	0.617 and −0.718 e·Å ⁻³

to the coordination of azomethine N of free ligand to copper(II) centres.²⁷ The weakening of the free C=N bond during metallation results in this bathochromic shift.²⁸ **1** also shows a very broad infrared (IR) absorption band at 3526 cm⁻¹ for non-coordinating water molecule.²⁹

The electronic absorption spectra of the ligand (**L**) and its stabilized copper(II) complexes were recorded in methanol as depicted in Figure 1. Generally, intense electronic transition bands due to ligand moieties appear in

TABLE 2 Some selected bond lengths (Å) and bond angles (°) of **1** and **2**.

Complex 1			
Bond length		Bond angle	
Cu(1)—N(1)	2.067(2)	N(2)—Cu(1)—N(3)	79.39(10)
Cu(1)—N(2)	2.022(3)	N(2)—Cu(1)—N(1)	82.21(10)
Cu(1)—N(3)	1.975(2)	N(3)—Cu(1)—N(1)	160.73(9)
Cu(1)—Cl(1)	2.281(11)	N(2)—Cu(1)—Cl(1)	146.61(8)
Cu(1)—Cl(2)	2.456(12)	N(3)—Cu(1)—Cl(1)	96.31(8)
		N(1)—Cu(1)—Cl(1)	95.88(7)
		N(2)—Cu(1)—Cl(2)	105.76(8)
		N(3)—Cu(1)—Cl(2)	93.65(8)
		N(1)—Cu(1)—Cl(2)	96.82(7)
		Cl(1)—Cu(1)—Cl(2)	107.56(4)
Complex 2			
Bond length		Bond angle	
Cu(1)—N(4)	1.921(3)	N(4)—Cu(1)—N(2)	155.79(13)
Cu(1)—N(2)	1.924(2)	N(4)—Cu(1)—N(1)	96.79(13)
Cu(1)—N(1)	2.046(2)	N(2)—Cu(1)—N(1)	80.48(9)
Cu(1)—N(3)	2.076(3)	N(4)—Cu(1)—N(3)	96.52(13)
Cu(1)—N(7)	2.226(3)	N(2)—Cu(1)—N(3)	82.29(9)
		N(1)—Cu(1)—N(3)	161.81(10)
		N(4)—Cu(1)—N(7)	107.75(14)
		N(2)—Cu(1)—N(7)	96.46(12)
		N(1)—Cu(1)—N(7)	94.37(11)
		N(3)—Cu(1)—N(7)	93.33(11)

the UV region, whereas weak and forbidden d-d bands span the visible domain.³⁰ One-electron paramagnetic **1** (μ_{eff.} = 1.82 μ_B) and **2** (μ_{eff.} = 1.80 μ_B) displayed high-energy intense bands respectively at 274 and 272 nm due to π-π* intra-ligand charge transfer (ILCT) transition.³¹ The spectrum of **2** also shows an absorption band at 396 nm. This is ascribed to ligand-to-metal charge transfer (LMCT) transition.³² In the visible domain, a very weak but broad band appeared at 695 and 668 nm for **1** and **2**, respectively. These are characteristic d-d bands for the Jahn-Teller distorted mononuclear penta-coordinated copper(II) complexes.³³

3.2 | Description of the crystal structures of **1** and **2**

Both **1** and **2** are discrete mononuclear Cu(II) entities. The Oak Ridge thermal ellipsoid plots (ORTEPs) of both **1** and **2** with 30% probability ellipsoids along with atom

TABLE 3 Hydrogen bonding parameters of **1** (Å/°).

D—H...A	d(D—H)	d(H...A)	d(D...A)	∠D—H...A	Symmetry
O2—H19...Cl2	0.71(9)	2.62(9)	3.302(4)	160(8)	3/2 − x, −1/2 + y, z
O(2)—H(20)...Cl(2)	0.91(7)	2.44(7)	3.344(4)	172(5)	1/2 + x, 1/2 − y, 1 − z
C4—H4...O2	0.93	2.51	3.297(5)	143	x, 1 + y, z
C15—H15B...Cl1 (intra)	0.97	2.71	3.384(3)	127	
C17—H17B...Cl1	0.97	2.70	3.579(4)	150	1/2 − x, −1/2 + y, z

TABLE 4 X—H...Cg(n-ring) interactions for **1** (Å/°).

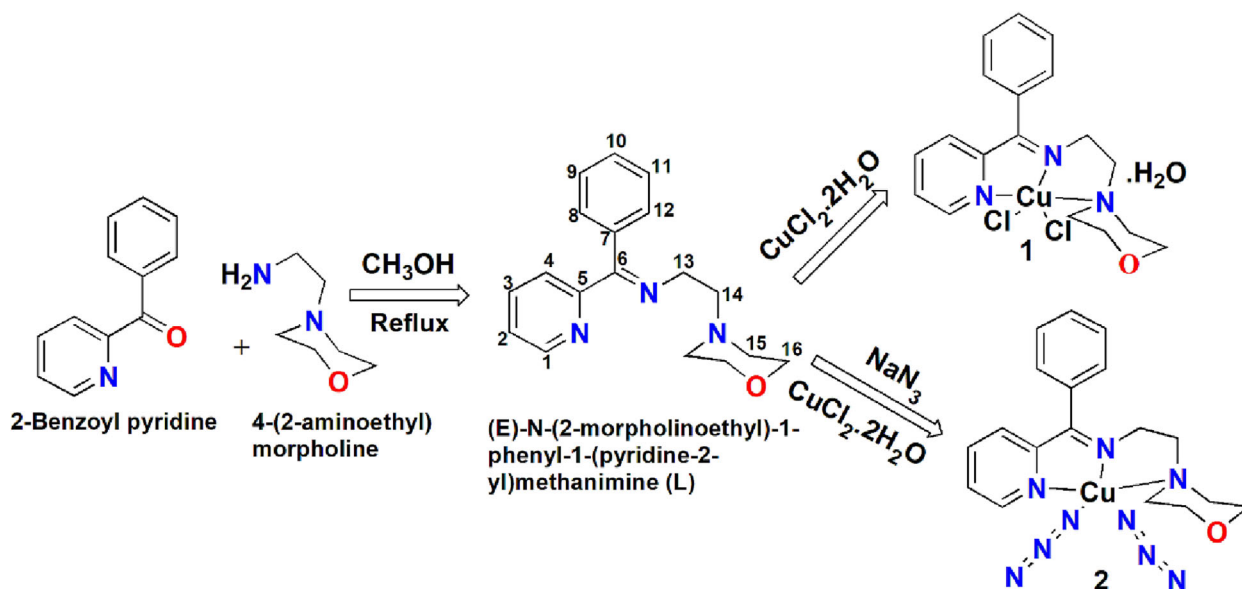
X—H(I)	Cg(J)	d(H...Cg)	∠X—H...Cg	d(X...Cg)	Symmetry
C3—H3	Cg(5)	2.99	131	3.665(3)	3/2 − X, 1/2 + Y, Z
C9—H9	Cg(4)	2.96	131	3.636(4)	1/2 + X, 3/2 − Y, Z

Note: Cg5 and Cg4 are the phenyl rings.

TABLE 5 Y—X...Cg(n-ring) interactions for **2** (Å/°).

Y—X(I)	Cg(J)	d(X...Cg)	∠Y—X...Cg	d(Y...Cg)	Symmetry
N8—N9	Cg(1)	3.742(5)	98.1(3)	4.063(3)	X, 1/2 − Y, 1/2 + Z

Note: Cg1 is the phenyl ring.

**SCHEME 1** Synthetic route of the ligand (**L**) and its copper(II) complexes, **1** and **2**.

labelling scheme are shown respectively in Figures 2 and 5. **1** and **2** crystallize respectively in the orthorhombic Pbc_a space group (*Z* = 8) and the monoclinic P2₁/c space group (*Z* = 4). The penta-coordination environment around the metal centres in **1** and **2** is respectively completed by 'N₃Cl₂' and 'N₅' donor sets. The copper(II) centre in **1** enjoys three nitrogen donation from the ligand moiety and two chlorides as counter anions, whereas the homoleptic donor environment in **2** is fulfilled by three nitrogen donors from **L** and two nitrogen donors from two terminally linked end-on azide ligands. In **1**, the

value of Addison's trigonality index parameter, τ_5 , comes out to be 0.23.³⁴ Accordingly, the disposed geometry around the metal centre in **1** is distorted square pyramidal. The basal plane around the metal centre in **1** is composed of Cu1—N1: 2.067(2), Cu1—N2: 2.022(3), Cu(1)—N(3): 1.975(2) and Cu1—Cl1: 2.281(11) Å bonds. The apical position is occupied by the Cl(2) atom at a distance of 2.456(12) Å from the metal centre. Analogous apical bond distances for chlorine donor atoms are, however, known for mononuclear copper(II) systems in similar geometric disposition.³⁵ Likewise, the copper(II) centre

in **2** also exhibits a square pyramidal geometric disposition. The calculated τ_5 value here is 0.10. As a result, the distortion in **2** is found to be comparatively less. The basal plane around copper(II) in **2** is composed of Cu1—N1: 2.046(2), Cu1—N2: 1.924(2), Cu1—N3: 2.076(3) and Cu1—N4: 1.921(3) Å bonds. The N(7) atom from a terminally disposed azide group occupies the apical position of the square-based pyramid. The apical Cu1—N7 bond is 2.226(3) Å. Two monodentate terminal

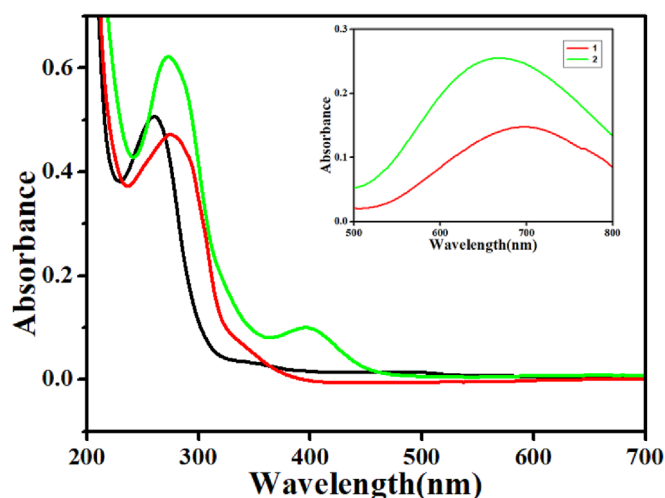


FIGURE 1 UV-vis spectra of **L** (black), **1** (red) and **2** (green). Concentrations of the ligand (**L**), **1** and **2** are respectively 2.74×10^{-5} , 2.93×10^{-5} and 2.84×10^{-5} M (inset: d-d band of **1** and **2**).

azide groups, N4—N5—N6 and N7—N8—N9, are found to be slightly asymmetric (N4—N5 = 1.068(4), N5—N6 = 1.154(5), N7—N8 = 1.149(4) and N8—N9 = 1.141(5) Å). The terminal azide group, N4—N5—N6, deviates more from linearity (N4—N5—N6 angle is $174.30(4)^\circ$) than the other terminally anchored azide group, N7—N8—N9 (N7—N8—N9 angle is $179.13(4)^\circ$). To the best of our knowledge, no mononuclear copper(II) complex in penta-coordination mode with two end-on azido ligands is known. However, only a mononuclear zinc(II) complex is known.³⁶ It is pertinent to note that Schiff base ligands offer diverse structurally interesting noteworthy coordination complexes.^{36b,c} The Z values for **1** and **2** are respectively 8 and 4 (Figures S11 and S12). In **1**, two molecular units are linked by Cl...H—C and O...H—C intermolecular hydrogen bonds (Figure 3). Figure 6 depicts the H-bonded packing diagram of **2**. The molecular packings of **1** and **2** are shown respectively in Figures 4 and 7. Figures 2–7 are shown as follows.

3.3 | In vitro cell growth inhibition

The cytotoxic effects of the compounds **1** and **2** and ligand (**L**) were evaluated using the WST-1 assay on lung adenocarcinoma cells of A549. The WST-1-based assay helped in exploring the metabolic activity of the mitochondria as a measure for the vital status of cells. The proliferation of cell and indirect cell demise can be estimated by this method on a large scale in microtiter

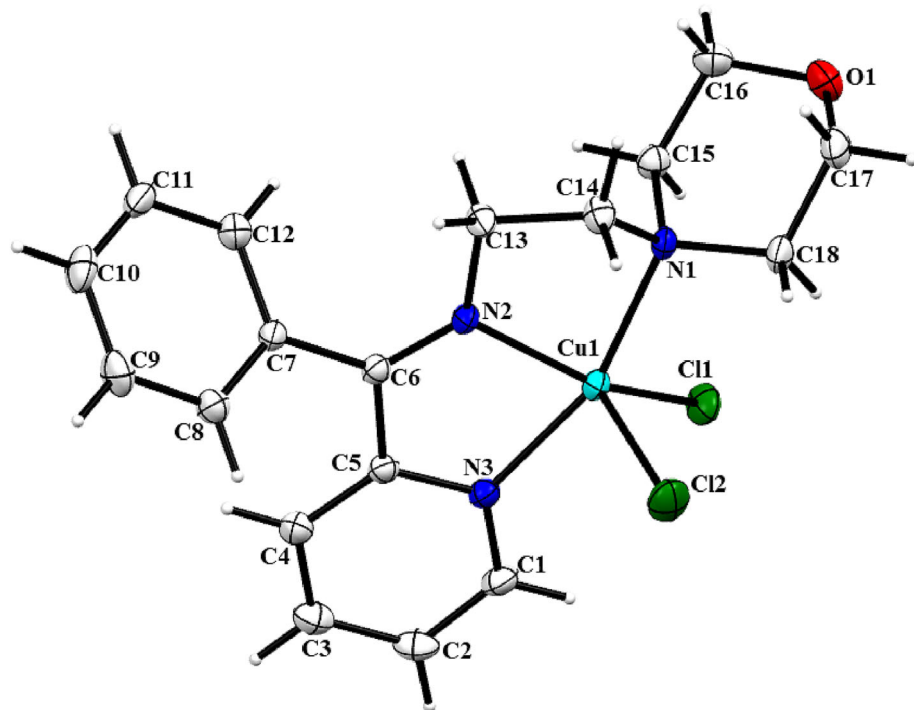
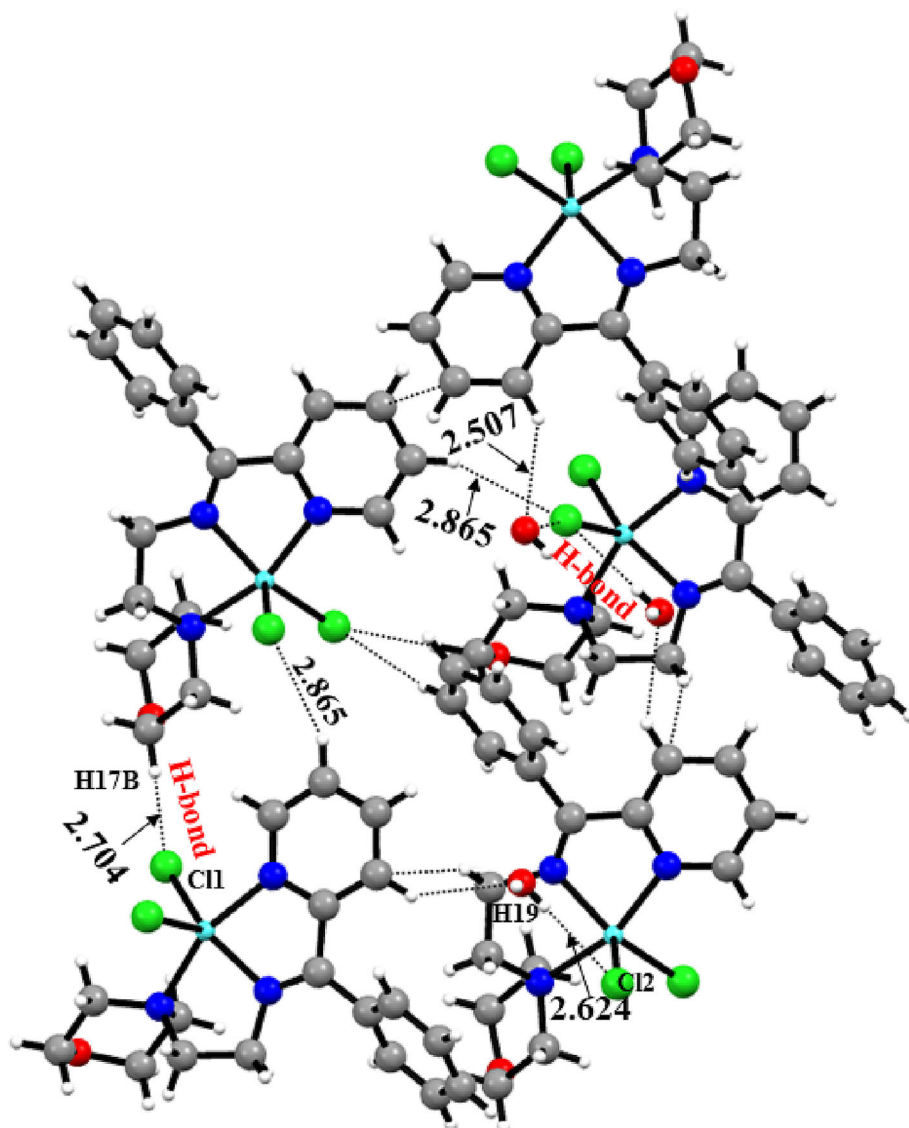


FIGURE 2 ORTEP of **1** with 30% probability ellipsoids. Solvent molecules are omitted for clarity.

FIGURE 3 Hydrogen-bonded, C—H...Cl, O—H...Cl, packing diagram of **1**.



plates.³⁷ In the presence of active dehydrogenase enzymes, the colorimetric salt WST-1 has permeated into the cytosol of a metabolically active cell and is reduced by cellular mitochondrial dehydrogenases producing an intracellular purple precipitate (formazan), suggesting that the higher the cell viability, the more the accumulation of dye. As shown in Figure 8a, compound **1** has strongly inhibited the growth and proliferation of cells in a dose-dependent manner followed by compound **2**, whereas the ligand displayed the least cytotoxicity towards the cancerous cell. Additionally, the WST-1 assay has helped us to calculate the IC_{50} value of compounds **1** and **2** and ligand (**L**) for A549 cells, which was noted to be 66, 88 and 200 μ M, respectively (Table 6). Compound **1** showed better cytotoxicity at a lower dose than compound **2**, whereas the ligand exhibited cytotoxicity at almost twice the concentration of compounds **1** and **2** and hence not taken for further experiments. The

concentration at which the inhibition was initiated for compounds **1** and **2** was 2.2 and 11 μ M, respectively.

The cytotoxicity of compounds **1** and **2** and ligand (**L**) was further asserted by trypan blue dye exclusion assay. Figure 8b summarizes the cytotoxic effect of both the compounds and ligand as determined by trypan blue dye exclusion assay. The expounded results were in accordance with WST-1 assay. A significant cytotoxic response was noted towards A549 cells by both the compounds **1** and **2**, whereas the ligand exhibited the least cytotoxicity. Thus, both the assays reaffirm the sensitivity of the lung adenocarcinoma cells on exposure to compounds **1** and **2**. Further experiments were carried out for both **1** and **2** with dose values lower than and equal to IC_{50} value. As the ligand did not exhibit any prominent cytotoxicity, so it was not employed in the following assays. Doxorubicin is a widely used chemotherapeutic drug, which is routinely used in the treatment of various

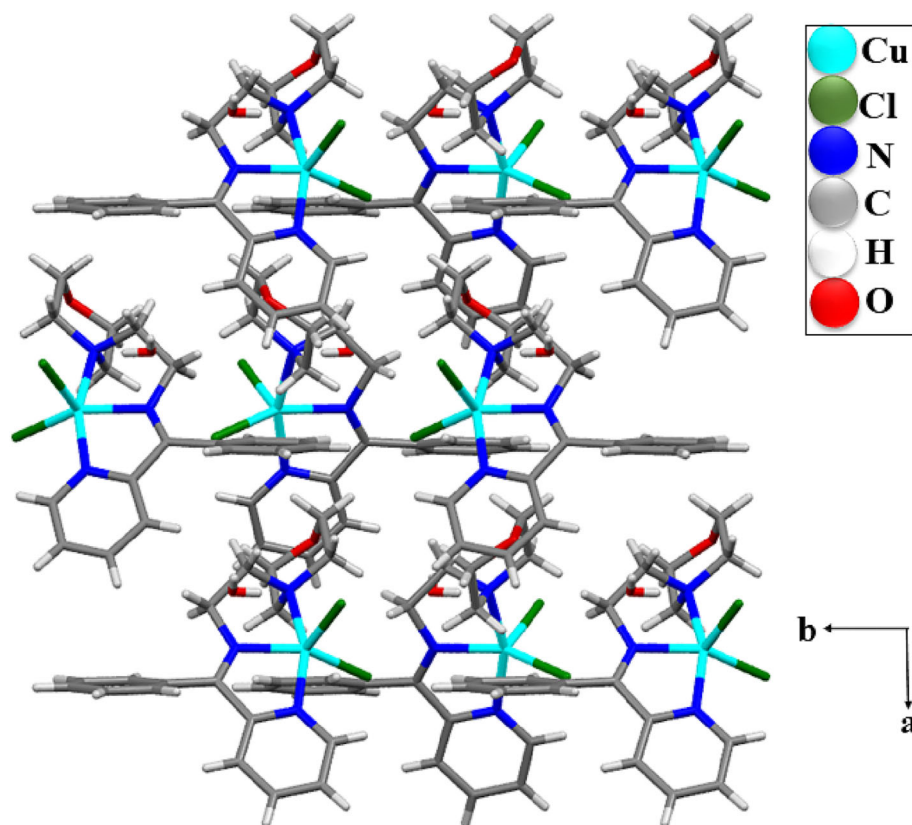


FIGURE 4 The molecular packing of **1** when viewed along crystallographic *c* axis.

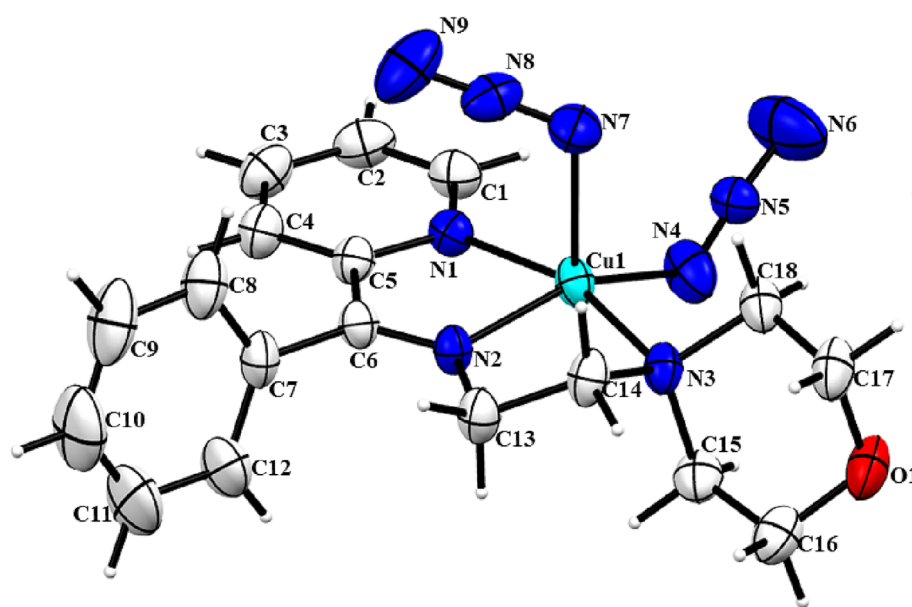


FIGURE 5 ORTEP of **2** with 30% probability ellipsoids.

cancers like breast, liver, lung, ovarian, thyroid, gastric, paediatric cancers, multiple myeloma and sarcoma.^{37b} During the course of this study, the susceptibility of LC cell line towards doxorubicin was investigated to compare the results of compounds **1** and **2** and ligand (**L**) with an established anticancer drug as positive control. The investigation showed that doxorubicin had an IC_{50} value of 1.1 μ M for A549 cells (Figure 8c), which is comparable with the published results.^{37c}

3.4 | Compounds **1** and **2** impede colony formation of A549 cells

To further validate the effect of compounds **1** and **2** on A549 cell growth and viability, clonogenic cell survival assay was performed. A total of 1×10^3 cancer cells were seeded with and without both the compounds and, after 7 days of incubation, the number of colonies formed was counted. As illustrated in Figure 9a–c, adequate

FIGURE 6 Hydrogen-bonded, C—H...O and C—H...N, packing diagram of **2**.

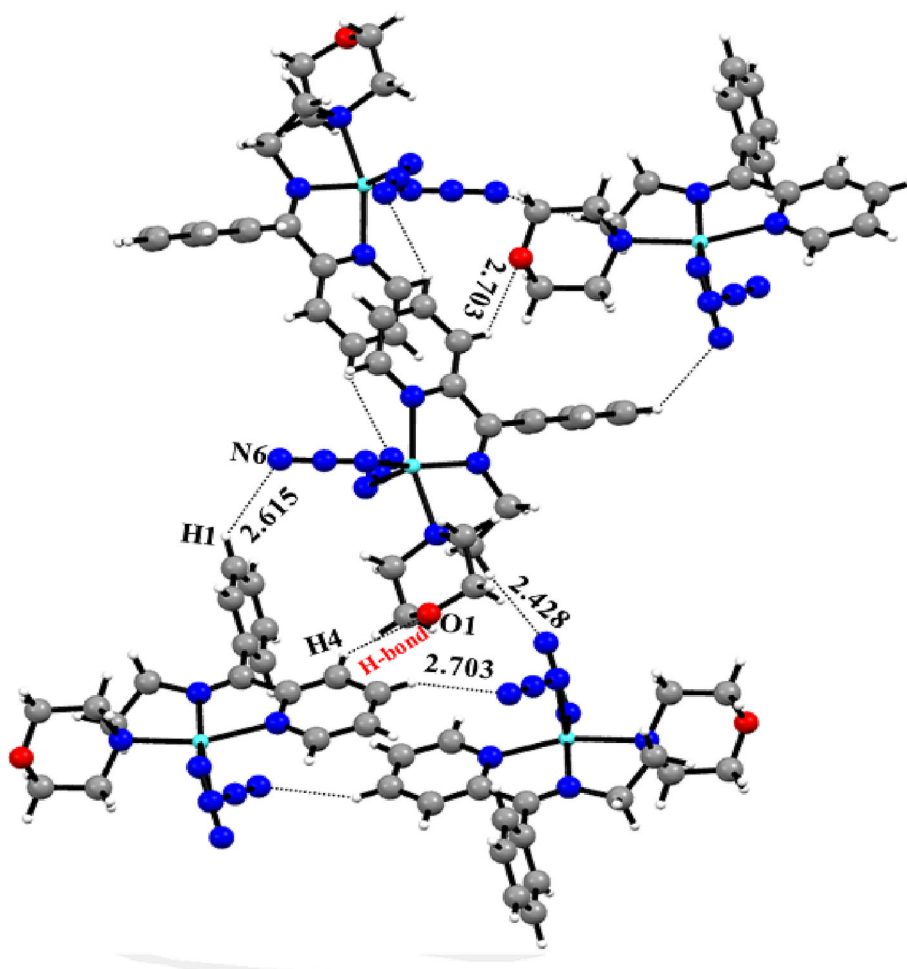
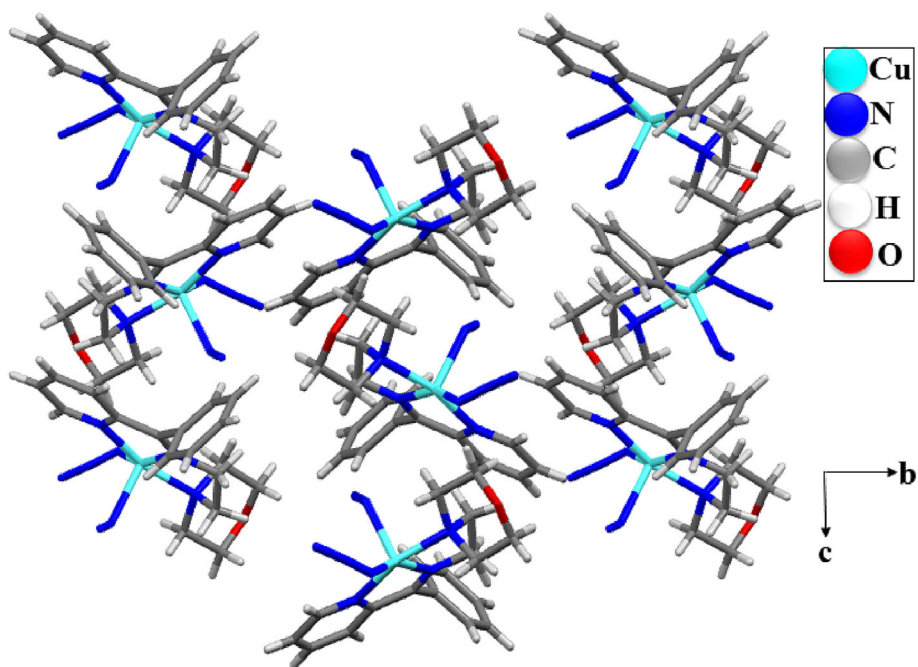


FIGURE 7 The molecular packing of **2** when viewed along crystallographic a axis.



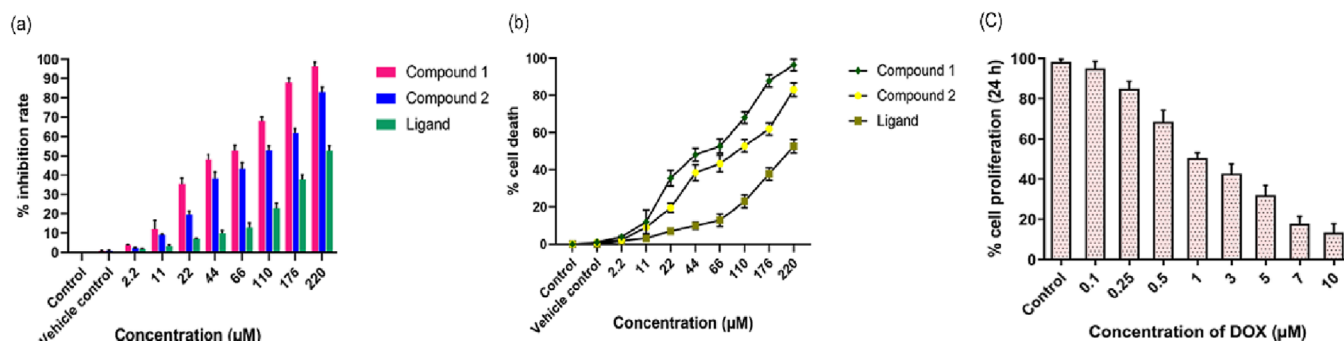


FIGURE 8 In vitro growth inhibition of lung adenocarcinoma cells of A549 following treatment with compounds for 24 h. The graphs, (a) WST-1 assay and (b) trypan blue assay, show the log dose cytotoxic effects of compounds **1** and **2** and ligand (**L**). (c) Dose–response effects of positive control, DOX, to A549 cell lines. The graphs were prepared as means \pm SD of three separate experiments using the GraphPad Prism 6 statistical software.

TABLE 6 IC₅₀ values obtained for the selected compounds and ligand.

	IC ₅₀ value (μM)
Compound 1	66
Compound 2	88
Ligand	200

Note: The IC₅₀ values represent the mean of at least three independent experiments.

inhibition of colony formation for compound **1** was observed on exposure to 33 and 66 μM and, on the other hand, inhibition in colony forming ability for compound **2** was noted for 44 and 88 μM (Figure 9d–f). Nonetheless, at IC₅₀ dose, the cell survivalist, adhesion and colony forming efficiency has further reduced and very few cells were found in well as compared with the full grown cells in the untreated set. This effect was not further altered even after cell grown in a drug-free condition for 1 week.

3.5 | Compounds 1 and 2 induce arrest in cell cycle progression

Most chemotherapeutic drugs target a physiological comprehending feature of cancerous cells as they inclined to proliferate more actively than normal cells. Most anticancer therapies restrict the growth and proliferation of cancerous cells by arresting the cell cycle progression at a particular phase.³⁸ In vitro assessment has already displayed that the compound has potent antiproliferative activity against A549 cells. Further inhibition of proliferation was examined by measuring cell cycle distribution using PI stain following treatment with different concentrations of **1** and **2** for 24 h as per the standardized protocol of Nandi and co-workers.³⁹ The DNA content of A549

cells in different phases of cell cycle was investigated. The histograms from flow cytometer demonstrated an increase in cell population at the sub-G0 phase with concomitant decrease in the proportion of cells in the G0/G1, S and G2/M phases of the cell cycle of treated cells in both the compounds when compared with the untreated control cells. In compound **1**, the proportion of cells in the S and G2/M phases decreased from 20.7% (control) to 12.2% and 7.2%, respectively (Figure 10a–c). Compound **2** exhibited a different pattern of reduction in cell number of the S and G2/M phases from 15.2% to 10.56% and 6.2%, respectively (Figure 10d–f). However, the untreated sets demonstrated a presumed pattern with no peak at the sub-G0 phase and a broad peak at the S and G2/M phases. The increase in the number of cells in the sub-G0 phase was further elevated to 35% and 25%, respectively, following exposure to 44 and 88 μM of compounds **1** and **2**. An increase in the cell population at the sub-G0 phase was a clear indication of apoptotic cells in a dose-dependent manner (Figure 10, right panel). Taken together, both compounds **1** and **2** caused growth arrest in the sub-G0 phase of the cell cycle.

3.6 | Compounds 1 and 2 induce morphological changes in cultured human adenocarcinoma cells of A549

Further, to validate the cytotoxic effect of the compounds on cancer cells, light microscopy observations were performed to observe the morphology alteration in A549 cells. After treatments with various concentrations for 24 h, Figure 11 shows bright-field micrographs of A549 cell lines. Dose-dependent morphological changes were visible upon exposure to **1** and **2** like reduced confluence, more bright-circular dead cells and debris were floating, cellular contraction and distorted longer to round shaped

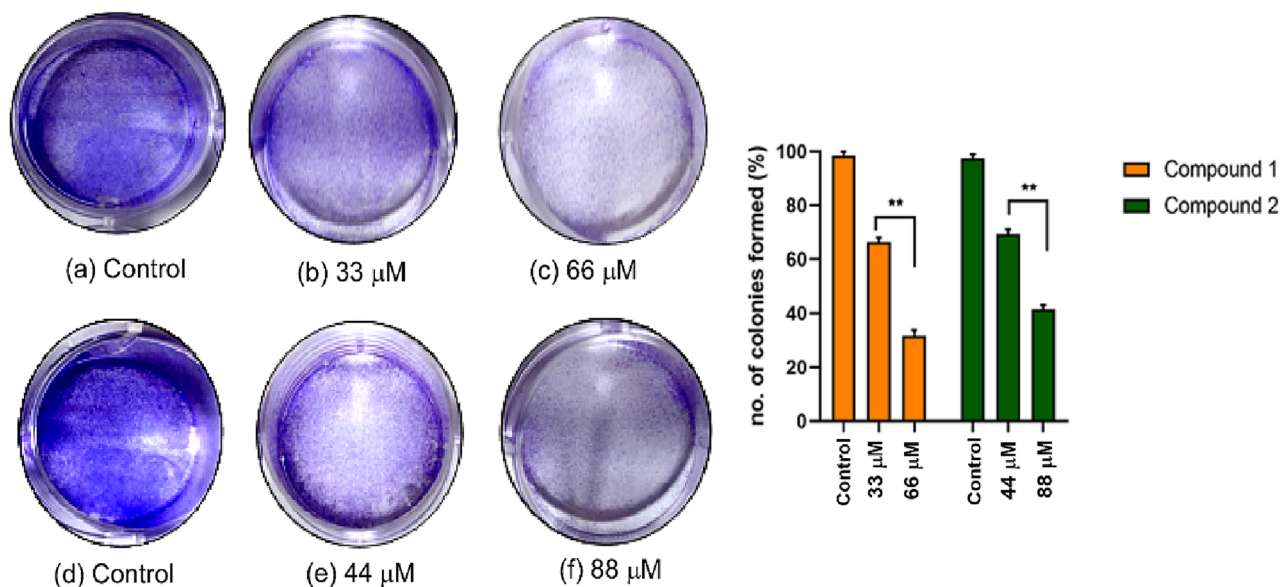


FIGURE 9 Colony forming ability of A549 cells cultured for a week, determined by a colony formation assay. (a–f) Influence of different concentrations of compounds **1** and **2** on colony forming ability of lung cancer cells. Quantitative analysis of the number of colonies formed in cells treated with various concentrations of compounds (right panel). Results are representative of at least three independent experiments. The graph represents mean \pm SEM using the GraphPad Prism 6 statistical software, whereas the asterisks *, ** and *** indicate significant difference at $p < 0.05$, $p < 0.001$ and $p < 0.0001$, respectively, from the untreated control cells.

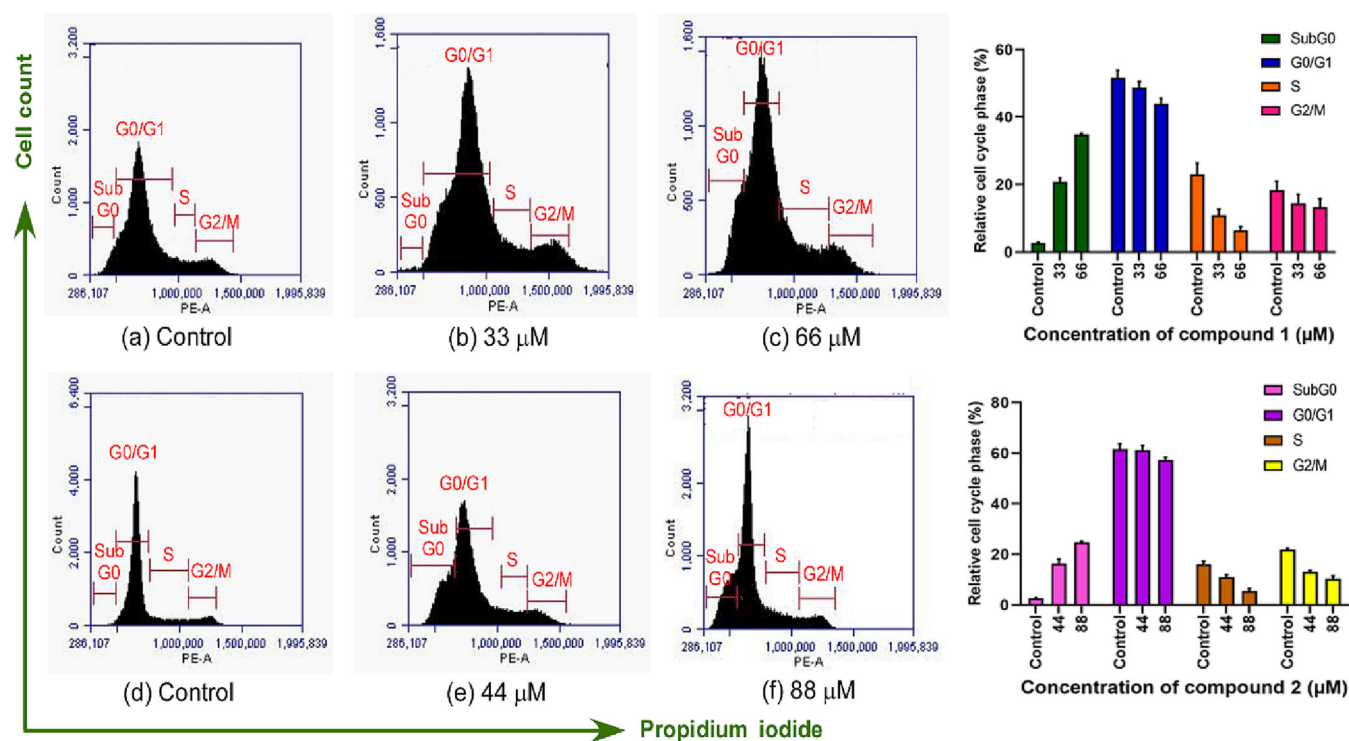


FIGURE 10 Compounds **1** and **2** induce cell cycle arrest in lung adenocarcinoma cells. Flow cytometry was used to represent cell cycle profiles of A549 cells treated with 33 and 66 μ M (compound **1**) and 44 and 88 μ M (compound **2**), respectively (a–f). X-axis represents the intensity of propidium iodide, and the Y-axis represents the cell counts. The graph shows the quantitative analysis of cell cycle distribution (right panel). Values are means \pm SD of three independent experiments, each conducted in triplicate.

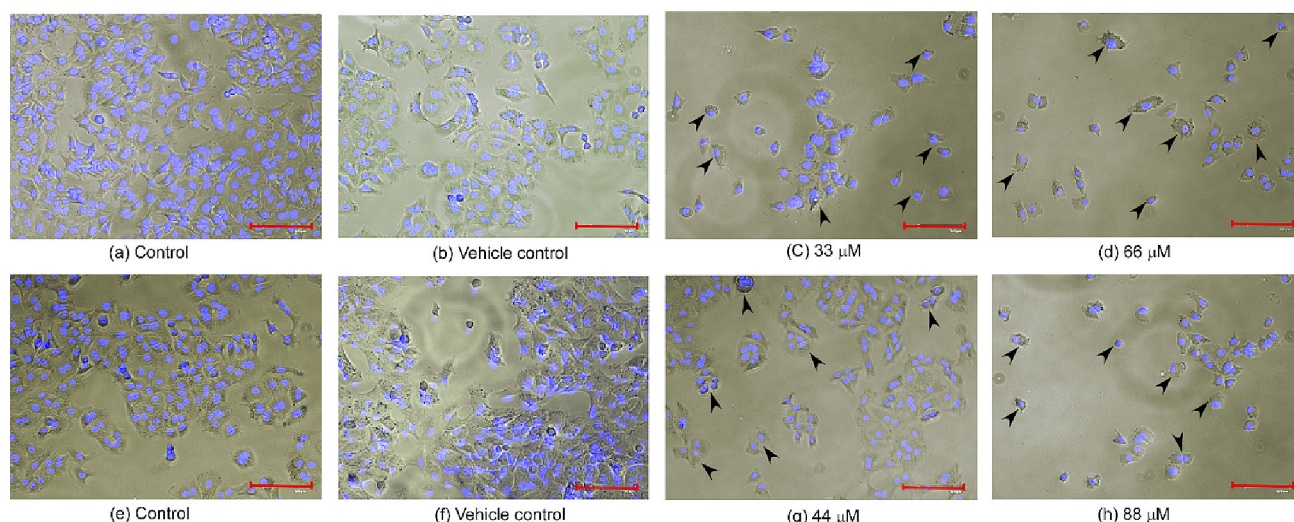


FIGURE 11 Effect of compounds **1** and **2** on cellular morphological alterations of A549 cancer cells observed under phase contrast light inverted microscope with 10 \times magnification. Cells were incubated for 24 h with different concentrations of both the compounds (a–h). Scale bar = 50 μ m. Black arrow signifies the morphological alteration after treatment with compounds **1** and **2**.

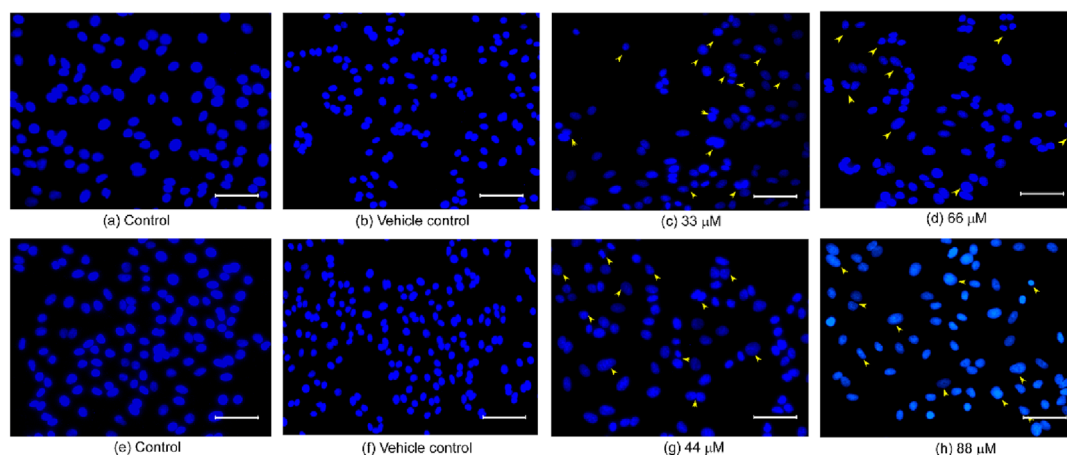


FIGURE 12 Compounds **1** and **2** induce apoptosis of A549 cells. Nuclear changes in apoptotic cells treated with both the compounds are shown by DAPI staining using fluorescence microscopy with 20 \times magnification (a–h). Scale bar = 100 μ m. Arrow indicates the deformed nuclei after exposure to compounds **1** and **2**.

acquired due to the loss of adhesion, suggesting a cytotoxic and antiproliferative effect (Figure 11c,d,g,h). Comparing these results with those of the untreated and vehicle controls, no such morphological alterations were observed. The untreated control cells exhibited an extended fusiform shape, well-adherent growth, clear cellular boundaries and higher cell density with lesser cytoplasmic granules (Figure 11a,b,e,f).

3.7 | Compounds **1** and **2** compelled apoptotic induction in A549 cells

Cell death by way of apoptosis is an essential factor for the anticancerous activity of any compound.⁴⁰ To

evaluate whether the cytotoxicity caused by compounds **1** and **2** towards lung adenocarcinoma cells was induced by apoptosis, various staining techniques have been performed. A fluorescent microscopic study was undertaken to analyse the changes induced by both the compounds in cellular and nuclear morphology of A549 cells and to understand their mode of cell death following staining with DAPI and AO/EtBr dyes. Staining the treated cells with DNA binding dye DAPI displayed typical morphological features of apoptosis including apoptotic nuclei with bright blue fluorescence, condensed chromatin and deformed and fragmented nuclei with membrane blebbing (indicated by arrow), whereas in the untreated and vehicle cells, nuclei were normal with no nuclear disruption, indicating healthy cells observed in both the

compounds (Figure 12a–h). It was also spotted that, at higher concentrations, that is, 66 and 88 μM , more cells had exhibited nuclear deformities (Figure 12d,h).

After 24 h of drug treatment, the morphological abnormalities were observed by double staining with AO/EtBr. The treated A549 cells exhibited nuclear margination and chromatin condensation, which were major consequences of the apoptotic trigger, after treatment of 24 h. In control, cells were intact, healthy with normal cytoplasm and morphology emitting green fluorescence (Figure 13a,d). Fluorescence microscopic images of cells treated with lower dose of compounds **1** and **2** distinctly revealed the yellowish green fluorescence, representing early apoptotic features (Figure 13b,e) like cellular shrinkage, membrane blebbing and chromatin condensation other deformities (indicated by arrow) and, in higher concentration of treatments, fewer cells fluoresced with yellowish orange along with yellowish green fluorescence, indicating the presence of both early and late apoptotic cells (Figure 13c,f). Late apoptotic cells displayed membrane loss and apoptotic bodies. These characteristic features detected on staining with DAPI and AO/EtBr were typical of apoptotic cells and were quite different

from the cells found in the untreated control set. Vehicle sets in both cases showed characteristic morphological features as the non-treated ones. This stipulated that exposure of compounds **1** and **2** was potentially competent to trigger apoptosis in most A549 cells.

The cytotoxicity assay was evaluated in solution. To check the stability of both **1** and **2** in solution, we have monitored them through UV–vis spectra with variation in time (Figures S13 and S14). **1** and **2** are found to be quite stable in solution.

3.8 | Cytotoxic mechanistic action and structure–activity relationship

To augment the cytotoxic potentiality of both **1** and **2** towards the NSCLC cell line, A549 under apoptosis, we employed PI staining. The DNA content of A549 cells in different phases of cell cycle was also monitored for cell apoptosis (cell death). The observed activity of **1** and **2** with the treated cells is plausibly due to an increase in cell population at the sub-G₀ phase with concomitant decrease in the proportion of cells at the G₀/G₁, S and

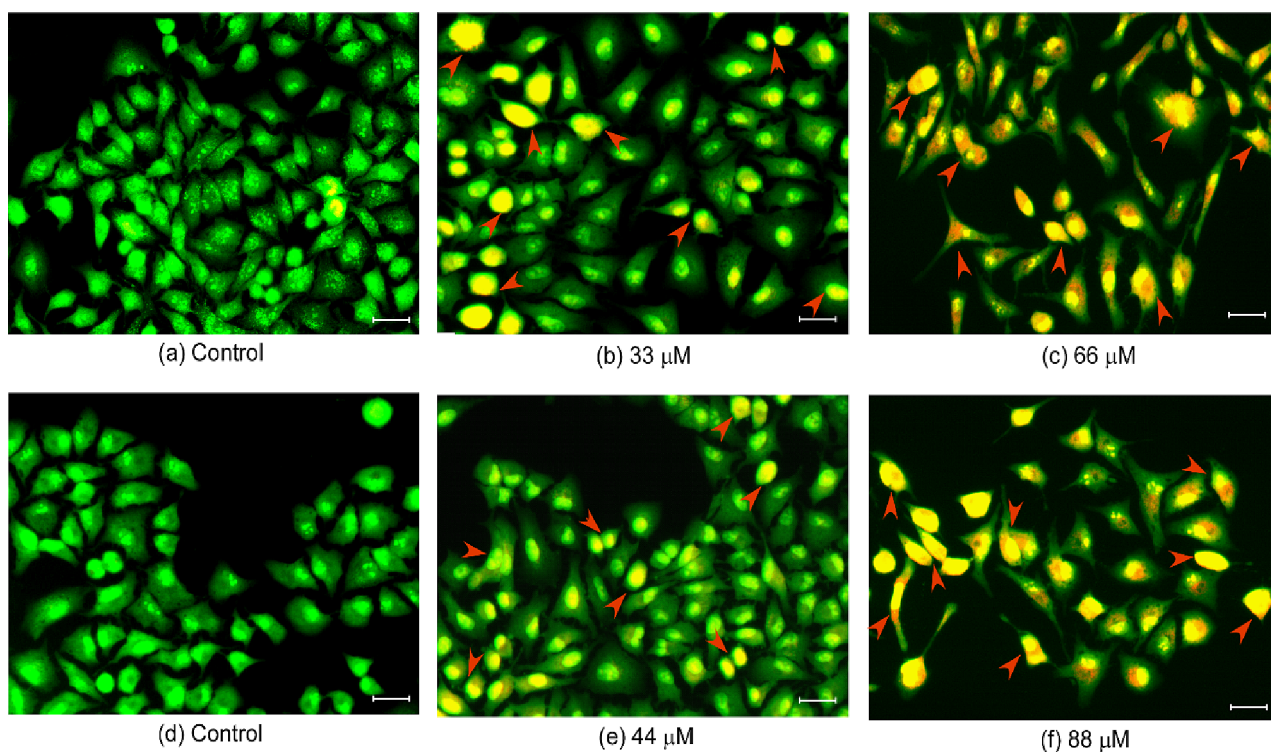


FIGURE 13 Induction of apoptosis with compounds **1** and **2** in lung adenocarcinoma cells after 24 h of incubation. Fluorescence microscopy images of acridine orange–ethidium bromide dual (AO/EtBr) stained A549 cells (a, d) untreated (control) and (b, c) compound **1** and (e, f) compound **2** treated at different concentrations. AO/EtBr images were recorded using excitation at 460 nm. Viable (light green), early apoptotic (bright green or yellowish green fluorescing) and late apoptosis (yellowish orange fluorescing) cells were observed. Magnification 20 \times . Scale bar = 100 μm . Arrow marks the treated cells showing typical characteristic of apoptosis.

G2/M phases of the cell cycle. Both **1** and **2** showed cell growth arrest in the sub-G0 phase of the cell cycle, leading to manifested cytotoxicity.⁴¹

Both **1** and **2** manifest promising activity in comparison with the complexing ligand towards A549. This significant enhancement of activity of **1** and **2** is due to the chelation of the ligand with Cu(II) centres. Extended square pyramidal structural disposition of the copper(II) centres, both in **1** and in **2**, accentuated by π - π^* conjugation due to metal ligand chelation is found to be contributing towards enhancement of activity.⁴² Inhibitory propensity of **1** against A549 cancer cell lines is observed to be higher than that observed for **2**. Most likely, this may be due to the presence of different co-ligand in the coordinating environment. Possibly, this ligand field effect also makes **1** more active towards WST-1 assay.

3.9 | Cyclic voltammetry

Electrochemical redox behaviour of **1** and **2** was studied at room temperature in dehydrated degassed methanol. The cyclic voltammetry (CV) experiments were conducted under dry and pure N₂ atmosphere using GC working electrode. Voltammograms of **1** and **2** are shown in Figure 14 and the pertinent data are tabulated in Table 7. On the positive side of Ag/AgCl reference electrode, **1** and **2** show oxidative response at 0.591 and 0.585 V, respectively. The corresponding reduction peaks for **1** and **2** are discernible respectively at -0.336 and -0.292 V versus Ag/AgCl. The ligand under similar electrochemical environment was found to be electrochemically inert. Accordingly, the manifested redox response can safely be attributed to copper centred. Comparing the observed redox response with that shown by the standard one-electron redox marker, ferrocene, the present response can be assigned to copper(II) to copper(I) reductions. The cathodic to anodic peak potential difference

(ΔE_p) for **1** and **2** was found respectively to be 255 and 297 mV at room temperature. The observed i_{pc}/i_{pa} value for **1** is 2.737, whereas that for **2** is 1.729. Accordingly, the observed redox response in both **1** and **2** is designated as irreversible.⁴³ The observed difference in redox behaviour between **1** and **2** is most likely due to ligand field effects.⁴⁴

3.10 | TGA

In order to assess the thermal behaviour of **1**, we have analysed it thermogravimetrically. A total of 6.54 mg of **1** was heated in the temperature range of 30–600°C in an aluminium crucible at the heating rate of 10°C min⁻¹ under dynamic nitrogen flow rate of 150 mL min⁻¹. The resulting TGA plot of **1** is shown in Figure S15. The thermogram indicates high thermal stability of **1**. It undergoes thermal decomposition in three consecutive steps. In the first step, loss of non-coordinated water molecule (thermal dehydration) occurs in between 100°C and 175°C.⁴⁵ The experimental mass loss of 3.93% for this thermal event is in concordance with the theoretical loss of 4.02%. The second step spans 200–260°C. The experimental mass loss of 16.86% fairly corresponds to the calculated loss of 16.52%. This is due to the liberation of two coordinated chlorine atoms. Beyond 400°C, a steady but sharp mass loss took place. This is due to complete combustion of the compound. The black residue is most

TABLE 7 Cyclic voltammetry data for **1** and **2**.

	E_{pa} (i_{pa})	E_{pc} (i_{pc})	$E_{1/2}$	i_{pc}/i_{pa}
Complex 1	0.591 (8.22)	-0.336 (-22.5)	0.463	2.737
Complex 2	0.589 (13.7)	-0.292 (-23.7)	0.440	1.729

Abbreviations: E_{pa} , anodic peak potential (V); E_{pc} , cathodic peak potential (V); i_{pa} , anodic peak current; i_{pc} , cathodic peak current.

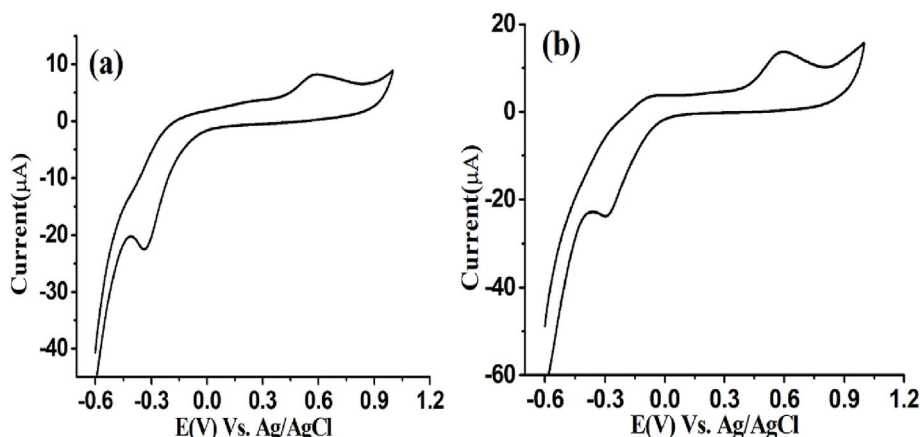


FIGURE 14 Cyclic voltammetry of the copper(II) complexes **1** (a) and **2** (b) in methanol at a scan rate of 100 mV s⁻¹.

likely cupric oxide along with little amount of carbon.^{27b} Compound **2** is explosive due to the presence of two azide groups. Owing to safety concerns, thermal analysis has not been realized for **2**. However, our literature survey on analogous copper(II) azide complexes reveals that such systems are thermally stable almost up to 160°C. Beyond this threshold critical temperature, azide-based copper(II) systems explode, rendering further thermogravimetric characterization non-realistic.⁴⁶

3.11 | PXRD

The PXRD analysis was performed at room temperature to test the bulk (phase) purity of the powdered crystalline sample of the two compounds, **1** and **2**. The patterns are shown in Figures S16 and S17. The major PXRD patterns of **1** and **2** (as obtained from the respective synthesized bulk powdered samples) are found to be consistent, both in position and in intensity, with those of the simulated pattern as obtained from SC-XRD data. This satisfactory concordance is indicative of the phase purity and consistency of the bulk of both **1** and **2**.

4 | CONCLUSIONS

Two mononuclear copper(II) complexes (**1** and **2**), based on a pharmacologically potential molecule, morpholine, dangled Schiff base ligand, were synthesized and thoroughly characterized. The X-ray crystal structures of both the complexes have been determined. PXRD studies were also undertaken to authenticate the bulk purity of the samples as that retained in the single crystals. Thermal analysis of **1** was also performed to show the thermal stability of the complex. Redox behaviour of the complexes was also monitored to validate the biocompatibility of the complexes. The observed redox response of the two complexes hint that the manifested potential values can even be achieved in vivo. The cytotoxic effects of both the complexes were screened against LC cell lines in a dose- and time-dependent manner. The ligand manifests no cytotoxic efficacies. On the contrary, low IC₅₀ value of **1** towards NSCLC shows better antiproliferative efficacies of it with low toxicity in comparison with **2**. Both **1** and **2** were induced towards lung adenocarcinoma cells by apoptosis. The expounded results show more cellular nuclear deformities at concentrations of 66 and 88 µM respectively for **1** and **2**. The morphological changes in NSCLC cells after treatment with **1** and **2**, monitored with AO/EtBr staining techniques, show annihilation of A549 cancer cell. Our present cytotoxic studies and the corroborated results obtained thereof clearly show that

1 and **2** bear potential prospect and possibility in chemotherapeutic cancer therapy and oncological management.

AUTHOR CONTRIBUTIONS

Naba Kr Mandal: Investigation; synthesis; data curation; methodology; software. **Sudeshna Nandi:** Data curation; methodology; bio studies; software. **Krishnendu Acharya:** Conceptualization; investigation; supervision. **Jnan Prakash Naskar:** Investigation; conceptualization; supervision; validation.

ACKNOWLEDGEMENTS

NKM gratefully thanks the University Grants Commission (UGC), New Delhi, Government of India, for senior research fellowship. JPN sincerely acknowledges the Jadavpur University for research grant.

CONFLICT OF INTEREST STATEMENT

The authors state no competing financial interest.

DATA AVAILABILITY STATEMENT

The supporting data pertaining to this present submission are available from the corresponding author on request.

ORCID

Naba Kr Mandal  <https://orcid.org/0009-0008-8669-7713>

Sudeshna Nandi  <https://orcid.org/0000-0002-1327-7258>

Krishnendu Acharya  <https://orcid.org/0000-0003-1193-1823>

Jnan Prakash Naskar  <https://orcid.org/0000-0001-6724-4892>

REFERENCES

- [1] a) H. Schiff, *Ann. Suppl.* **1864**, 3, 343; b) P. G. Cozzi, *Chem. Soc. Rev.* **2004**, 33, 410; c) M. H. Habibi, M. Montazerzohori, A. Lalegani, R. W. Harrington, W. Clegg, *J. Fluorine Chem.* **2006**, 127, 769; d) S. Shahraiki, A. Heidari, H. R. Mirzaei, M. Saeidifar, N. Ahmadasab, H. Mansouri-Torshizi, *J. Iran. Chem. Soc.* **2018**, 15(3), 697; e) H. Keypour, M. Rezaeivala, L. Valencia, P. Pérez-Lourido, H. R. Khavasi, *Polyhedron* **2009**, 28, 3755.
- [2] a) T. L. Yusuf, S. D. Oladipo, S. A. Olagboye, S. J. Zamisa, G. F. Tolufashe, *J. Mol. Struct.* **2020**, 1222, 128857; b) S. M. Wilkinson, T. M. Sheedy, E. J. New, *J. Chem. Educ.* **2016**, 93, 351; c) S. K. Tadavi, A. A. Yadav, R. S. Bendre, *J. Mol. Struct.* **2018**, 1152, 223; d) R. Chandrasekaran, S. A. Yadav, S. Sivaperumal, *J. Cluster Sci.* **2019**, 6, 1; e) K. S. Kumar, S. Ganguly, R. Veerasamy, E. De Clercq, *Eur. J. Med. Chem.* **2010**, 45, 5474.
- [3] a) K. Ohui, E. Afanasenko, F. Bacher, R. L. X. Ting, A. Zafar, N. Blanco-Cabra, E. Torrents, O. Domotor, N. V. May, D. Darvasiova, E. A. Enyedy, A. Popovic-Bijelic, J. Reynisson, P. Raptá, M. V. Babak, G. Pastorin, V. B. Arion, *J. Med. Chem.*

- 2019, 62, 512; b) K. Dhahagani, S. M. Kumar, G. Chakkaravarthi, K. Anitha, J. Rajesh, A. Ramu, G. Rajagopal, *Spectrochim. Acta Part A: Mol. Biomol. Spectrosc.* **2014**, 117, 87; c) P. A. Ajibade, F. P. Andrew, N. L. Botha, N. Solomane, *Molecules* **2020**, 25, 3584.
- [4] a) M. Hosseini-Kharat, R. Rahimi, D. Zargarian, Z. M. Lighvan, A. A. Momtazi-Borojeni, T. Sharifi, E. Abdollahi, H. Tavakol, T. Mohammadi, *J. Biomol. Struct. Dyn.* **2019**, 37, 3788; b) K. Rupak, S. R. Vulichi, K. Suman, *Int. J. Chem. Sci.* **2016**, 14, 1777; c) J. A. War, S. K. Srivastava, S. D. Srivastava, *Spectrochim. Acta Part A: Mol. Biomol. Spectrosc.* **2017**, 173, 270.
- [5] a) L. A. Torre, F. Bray, R. L. Siegel, J. Ferlay, J. Lortet-Tieulent, A. Jemal, *CA-Cancer J. Clin.* **2015**, 65, 87; b) J. Ferlay, I. Soerjomataram, R. Dikshit, S. Eser, C. Mathers, M. Rebelo, D. M. Parkin, D. Forman, F. Bray, *Int. J. Cancer* **2015**, 136, 359.
- [6] J. Ferlay, M. Ervik, F. Lam, M. Colombet, L. Mery, M. Piñeros, *Global Cancer Observatory: Cancer Today*, International Agency for Research on Cancer, Lyon **2020**.
- [7] a) Y. Xia, X. Liu, L. Zhang, J. Zhang, C. Li, N. Zhang, H. Xu, Y. Li, *Cancer Cell Int.* **2019**, 19, 81; b) B. Cvek, V. Milacic, J. Taraba, Q. P. Dou, *J. Med. Chem.* **2008**, 51, 6256; c) P. Baszuk, W. Marciniak, R. Derkacz, A. Jakubowska, C. Cybulski, J. Gronwald, T. Debniak, T. Huzarski, K. Białkowska, S. Pietrzak, M. Muszyńska, J. Kładny, S. A. Narod, J. Lubiński, M. R. Lener, *Biomedicines* **2021**, 9, 1628; d) M. Nurmamat, H. Yan, R. Wang, H. Zhao, Y. Li, X. Wang, K. Nurmaimaiti, T. Kurmanjiang, D. Luo, J. Baodi, G. Xu, J. Li, A. C. S. Med, *Chem. Lett.* **2021**, 12, 467; e) L. Quan, X. Luo, L. Xue, J. Li, Y. Ouyang, *J. Inorg. Organo. Polym. Mater.* **2020**, 30, 2744.
- [8] F. Bray, J. Ferlay, I. Soerjomataram, R. L. Siegel, L. A. Torre, A. Jemal, *CA: Cancer J. Clin.* **2018**, 68, 394.
- [9] a) S. Dilruba, G. V. Kalayda, *Cancer Chemo. Pharmacol.* **2016**, 77, 1103; b) E. Wong, C. M. Giandomenico, *Chem. Rev.* **1999**, 99, 2451; c) L. Kelland, *Nat. Rev. Cancer* **2007**, 7, 573; d) M. Galanski, B. K. Keppler, *Anti-Cancer Agent.* **2007**, 7, 55; e) T. C. Johnstone, K. Suntharalingam, S. J. Lippard, *Chem. Rev.* **2016**, 116, 3436.
- [10] a) V. Culotta, *J. Biol. Inorg. Chem.* **2010**, 15, 1; b) B. E. Kim, T. Nevitt, D. J. Thiele, *Nat. Chem. Biol.* **2008**, 4, 176.
- [11] a) M. Alagesan, N. S. P. Bhuvanesh, N. Dharmaraj, *Dalton Trans.* **2013**, 42, 7210; b) X. B. Fu, D. D. Liu, Y. Lin, W. Hu, Z. W. Mao, X. Y. Le, *Dalton Trans.* **2014**, 43, 8721.
- [12] a) L. M. Balsa, E. J. Baran, I. E. Leon, *Curr. Med. Chem.* **2021**, 16; b) Q. Pan, C. G. Kleer, K. L. van Golen, J. Irani, K. M. Bottema, C. Bias, M. de Carvalho, E. A. Mesri, D. M. Robins, R. D. Dick, G. J. Brewer, S. D. Merajver, *Cancer Res.* **2002**, 62, 4854; c) G. MacDonald, I. Nalvarte, T. Smirnova, M. Vecchi, N. Aceto, A. Dolemeyer, A. Frei, S. Lienhard, J. Wyckoff, D. Hess, J. Seebacher, J. J. Keusch, H. Gut, D. Salaun, G. Mazzarol, D. Disalvatore, M. Bentires-Alj, P. P. Di Fiore, A. Badache, N. E. Hynes, *Sci. Signaling* **2014**, 7, 1; d) L. M. Balsa, M. C. Ruitz, L. S. M. de la Parra, E. J. Baran, I. E. Leon, *J. Inorg. Biochem.* **2020**, 204, 110975.
- [13] a) C. Wittman, F. Bacher, E. A. Enyedy, O. Domotor, G. Spengler, C. Madejski, J. Reynisson, V. B. Arion, *J. Med. Chem.* **2022**, 65, 2238; b) L. M. Balsa, V. Ferraresi-Curotto, M. J. Lavecchia, G. A. Echeverría, O. E. Piro, J. García-Tojal, R. Pis-Diez, A. C. González-Baró, I. E. León, *Dalton Trans.* **2021**, 50, 9812; c) L. J. H. Borges, E. S. Bull, C. Fernandes, A. H. Jr, N. F. Azeredo, J. A. L. C. Resende, W. R. Freitas, E. C. Q. Carvalho, L. S. Lemos, H. Jerdy, M. M. Kanashiro, *Eur. J. Med. Chem.* **2016**, 123, 128; d) C. Santini, M. Pellei, V. Gandin, M. Porchia, F. Tisato, C. Marzano, *Chem. Rev.* **2014**, 114, 815.
- [14] a) T. Wang, Z. Guo, *J. Curr. Med. Chem.* **2006**, 13, 525; b) M. Valko, H. Morris, M. T. D. Cronin, *J. Curr. Med. Chem.* **2005**, 12, 1161; c) A. Gupte, R. J. Mumper, *Cancer Treat. Rev.* **2009**, 35, 32.
- [15] a) C. Marzano, M. Pellei, F. Tisato, C. Santini, *Anti-Cancer Agents Med. Chem.* **2009**, 9, 185; b) A. C. Hangan, G. Borodi, R. L. Stan, E. Pall, M. Cenariu, L. S. Oprean, B. Sevastre, *Inorg. Chim. Acta* **2018**, 482, 884; c) D. S. Raja, E. Ramachandran, N. S. P. Bhuvanesh, K. Natarajan, *Eur. J. Med. Chem.* **2013**, 64, 148; d) L. A. Alfonso-Herrera, S. Rosete-Luna, D. Hernandez-Romero, J. M. Rivera-Villanueva, J. L. Olivares-Romero, J. A. Cruz-Navarro, A. Soto-Contreras, A. Arenaza-Corona, D. Morales-Morales, R. Colorado-Peralta, *ChemMedChem* **2022**, 17, e2022003.
- [16] J. Serment-Guerrero, P. Cano-Sanchez, E. Reyes-Perez, F. Velazquez-Gracia, M. E. Bravo-Gomez, L. Ruiz-Azuara, *Toxicol. In Vitro* **2011**, 25, 1376.
- [17] a) K. H. Thompson, C. Orvig, *Dalton Trans.* **2006**, 761; b) D. Griffith, J. P. Parker, C. J. Marmion, *Anti-Cancer Agent Med. Chem.* **2010**, 10, 354; c) M. F. Primik, G. Muhlgassner, M. A. Jakupec, O. Zava, P. J. Dyson, V. B. Arion, B. K. Keppler, *Inorg. Chem.* **2010**, 49, 302; d) L. d. A. Costa, M. H. F. Ottoni, M. G. dos Santos, A. B. Meireles, V. G. de Almeida, W. d. F. Pereira, B. A. de Avelar-Freitas, G. E. A. Brito-Melo, *Molecules* **2017**, 22, 1789; e) C. Rodríguez-Burford, D. K. Oelschlager, L. I. Talley, M. N. Barnes, E. E. Partridge, W. E. Grizzle, *Bio-tech. Histochem.* **2003**, 78, 17.
- [18] G. A. Bain, J. F. Berry, *J. Chem. Educ.* **2008**, 85, 532.
- [19] a) P. G. Urben (Ed), *Bretherick's Handbook of Reactive Chemical Hazards*, Sixth ed., Butterworth-Heinemann, Oxford **1999**; b) W. C. Wolsey, *J. Chem. Educ.* **1973**, 50, A335.
- [20] T. W. Kim, D. W. Hong, C. M. Kang, S. H. Hong, *Exp. Mol. Med.* **2020**, 52, 1730.
- [21] S. Nandi, S. Chandra, R. Sikder, S. Bhattacharya, M. Ahir, D. Biswal, A. Adhikary, N. R. Pramanik, T. K. Lai, M. G. B. Drew, K. Acharya, *J. Agric. Food Chem.* **2019**, 67, 7660.
- [22] S. Nandi, S. Adhikary, K. Acharya, *J. Food Biochem.* **2022**, 46, e14021.
- [23] SMART (V 5.628), SAINT (V 6.45a), XPREP, SHELXTL, Bruker AXS Inc, Madison, USA **2004**.
- [24] G. M. Sheldrick, *Siemens Area Correction Absorption Correction Program*, University of Göttingen, Göttingen, Germany **1994**.
- [25] G. M. Sheldrick, *SHELXL-97 Program for Crystal Structure Solution and Refinement*, **1997**.
- [26] a) N. K. Mandal, N. Bandyopadhyay, P. Arya, S. Chowdhury, N. Raghav, J. P. Naskar, *Inorg. Chim. Acta* **2023**, 544, 121229; b) T. P. Dionízio, A. C. dos Santos, F. P. da Silva, F. d. S. Moura, E. D'Elia, F. M. d. S. Garrido, M. E. Medeiros, A. Casellato, *Electrocatalysis* **2021**, 12, 137.
- [27] a) M. Hazra, T. Dolai, A. Pandey, S. K. Dey, A. Patra, *Bioinorg. Chem. Appl.* **2014**, 2014, 104046; b) Y. Guo, X. Hu, X. Zhang, X. Pu, Y. Wang, *RSC Adv.* **2019**, 9, 41737.

- [28] C. Şenol, Z. Hayvali, H. Dal, T. Hökelek, *J. Mol. Struct.* **2011**, 997, 53.
- [29] B. Sreenivasulu, M. Vetrichelvan, F. Zhao, S. Gao, J. J. Vittal, *Eur. J. Inorg. Chem.* **2005**, 2005, 4635.
- [30] a) S. D. Oladipo, B. Omondi, C. Mocktar, *Appl. Organomet. Chem.* **2020**, 34, e5610; b) D. Lahiri, R. Majumdar, D. Mallick, T. K. Goswami, R. R. Dighe, A. R. Chakravarty, *J. Inorg. Biochem.* **2011**, 105, 1086.
- [31] a) S. Zolezzi, A. Decinti, E. Spodine, *Polyhedron* **1999**, 18, 897; b) C. E. Satheesh, P. R. Kumar, N. Shivakumar, K. Lingaraju, P. M. Krishna, H. Rajanaika, A. Hosamani, *Inorg. Chim. Acta* **2019**, 495, 118929; c) D. Tomczyk, L. Nowak, W. Bukowski, K. Bester, P. Urbaniak, G. Andrijewski, B. Olejniczak, *Electrochim. Acta* **2014**, 121, 64.
- [32] C. E. Satheesh, P. R. Kumar, P. Sharma, K. Lingaraju, B. S. Palakshamurthy, H. R. Raja Naika, *Inorg. Theor. Chim. Acta* **2016**, 442, 1.
- [33] T. L. Yusuf, S. D. Oladipo, S. Zamisa, H. M. Kumalo, I. A. Lawal, M. M. Lawal, N. Mabuba, *ACS Omega* **2021**, 6, 13704.
- [34] a) A. W. Addison, T. N. Rao, J. Reedijk, J. V. Rijn, G. C. Verschoor, *J. Chem. Soc., Dalton Trans.* **1984**, 1349; b) M. Li, A. Ellen, J. H. Espenson, *Inorg. Chem.* **2005**, 44, 3690; c) N. K. Mandal, B. Guhathakurta, P. Basu, A. B. Pradhan, C. S. Purohit, S. Chowdhury, J. P. Naskar, *J. Coord. Chem.* **2019**, 72, 3625.
- [35] A. K. Patel, R. N. Jadeja, H. Roy, R. N. Patel, S. K. Patel, R. J. Butcher, M. Cortijo, S. Herrero, *Polyhedron* **2020**, 186, 114624.
- [36] a) N. Stevanović, M. Zlatar, I. Novaković, A. Pevec, D. Radanović, I. Z. Matić, M. D. Crnogorac, T. Stanojković, M. Vujčić, M. Gruden, D. Sladić, K. Anđelković, I. Turel, B. Čobeljić, *Dalton Trans.* **2022**, 51, 185; b) D. Sutradhar, H. Chowdhury, S. Banerjee, N. C. Saha, B. K. Ghosh, *Inorg. Chim. Acta* **2019**, 485, 86; c) T. Chattopadhyay, M. Mukherjee, K. S. Banu, A. Banerjee, E. Suresh, E. Zangrando, D. Das, *J. Coord. Chem.* **2009**, 62, 967.
- [37] a) A. Guertler, A. Kraemer, U. Roessler, S. Hornhardt, U. Kulka, S. Moertl, A. A. Friedl, T. Illig, E. Wichmann, M. Gomolka, *Radiat. Prot. Dosim.* **2011**, 143, 487; b) C. F. Thorn, C. Oshiro, S. Marsh, T. Hernandez-Boussard, H. McLeod, T. E. Klein, R. B. Altman, *Pharmacogenet. Genomics* **2011**, 21, 440; c) R. Punia, K. Raina, R. Agarwal, R. P. Singh, *PLoS ONE* **2017**, 12, e0182870.
- [38] D. Alimbetov, S. Askarova, B. Umbayev, T. Davis, D. Kipling, *Int. J. Mol. Sci.* **2018**, 19, 1690.
- [39] S. Nandi, P. Upadhyay, A. Roy, A. Dasgupta, A. Sen, A. Adhikary, K. Acharya, *Environ. Toxicol.* **2022**, 37, 52.
- [40] A. Bansal, M. M. Saleh-E-In, P. Kar, A. Roy, N. R. Sharma, *Molecules* **2022**, 27, 4597.
- [41] D. S. Raja, N. S. P. Bhuvanesh, K. Natarajan, *J. Biol. Inorg. Chem.* **2012**, 17, 223.
- [42] G. Sharma, N. K. Rana, P. Singh, P. Dubey, D. S. Pandey, B. Koch, *Biomed. Pharmacother.* **2017**, 88, 218.
- [43] E. Tas, H. Kara, M. Durgun, A. Kilic, I. Yilmiz, *Synthesis and Reactivity in Inorganic, Metal-Organic, and Nano-Metal Chemistry*, Vol. 39 **2009** 379.
- [44] P. Mucha, P. Hikisz, K. Gwozdziński, U. Krajewska, A. Leniart, E. Budzisz, *RSC Adv.* **2019**, 9, 31943.
- [45] N. Kavitha, P. V. A. Lakshmi, *J. Saudi Chem. Soc.* **2017**, 21, 457.
- [46] a) M. Trivedi, G. Sing, A. Kumar, N. P. Rath, *RSC Adv.* **2014**, 4, 34110; b) A. Lehle, A. Beghidja, C. Beghidja, O. Mentre, R. Welter, *C. R. Chim.* **2011**, 14, 462.

SUPPORTING INFORMATION

Additional supporting information can be found online in the Supporting Information section at the end of this article.

How to cite this article: N. K. Mandal, S. Nandi, K. Acharya, J. P. Naskar, *Appl Organomet Chem* **2023**, 37(7), e7120. <https://doi.org/10.1002/aoc.7120>



Cite this: *New J. Chem.*, 2024, 48, 5782

Design, synthesis and structure of a trinuclear copper(II) complex having a Cu₃OH core with regard to aspects of antiproliferative activity and magnetic properties†

Naba Kr Mandal,^a Sudeshna Nandi,^{bc} Samia Benmansour,^d Carlos J. Gómez-García,^d Krishnendu Acharya^b and Jnan Prakash Naskar^{id}*^a

We report a novel triangular trinuclear copper(II) complex with a central μ_3 -OH bridge, [(CuL)₃(μ_3 -OH)(ClO₄)₂]-CH₃OH-H₂O (**1**), stabilised by the oxime-based Schiff base ligand, 3-(((5-bromothiophen-2-yl)methylene)hydrazineylidene)butan-2-one oxime (**HL**). Comprehensive characterization of **1** has been realised through different analytical and physical methods coupled with spectroscopic techniques. **1** has been structurally characterised by single crystal X-ray diffraction. The antiproliferative capacity of **HL** and **1** has been evaluated against human lung cancer cell line A549. Compound **1** shows promising efficacy in contrast to **HL**, which shows a limited cytotoxicity. Contrary to **HL**, **1** has distinctly impeded the proliferation of lung adenocarcinoma A549 cell lines in a dose-dependent way. Compound **1** has been employed as a potential therapeutic agent for promising cellular transformation of malevolent A549 cell lines. The programmed cell death mechanism of **1** reveals characteristic apoptotic changes in cellular morphology like chromatin condensation, fragmented nuclei, nuclear shrinkage along with blebbing, elevated number of nuclear body fragments and distorted nucleus, while round, clear edged, intact nucleus and uniformly stained round nuclei have been observed in the negative control. Variable-temperature magnetic studies show an antiferromagnetic Cu···Cu coupling of $-44.6(2) \text{ cm}^{-1}$. The *g* value as determined by EPR measurement of **1** in frozen *N,N*-dimethylformamide solution corroborates the experimental magnetic susceptibility values.

Received 19th October 2023,
Accepted 20th February 2024

DOI: 10.1039/d3nj04859d

rsc.li/njc

Introduction

Cancer, ranked as one of the most aggressive and lethal maladies, is due to pathophysiological changes in the inherent process of cell division. Worldwide, it is the second cause of human mortality. This disease alone kills an alarming number of people all over the world.¹ In the year 2021 alone, GLOBOCAN reported 9.6 million cancer death and an approximately 8.1 million new cancer cases. This puts a huge burden on the

health and economic well-being of millions of people.² Cancer persists as a challenge as well as a threat to anthropogenic morbidity, mortality and global health care.³ Breast, lung, liver, stomach, rectum, skin and colon are some common soft targets of this fatal ailment. Second only to breast cancer, lung cancer threatens humankind with the highest incidence and mortality rate globally.⁴ New cases of lung cancer and related mortality rate have roughly been increased respectively to 20% and 10% in 2012 and 2020.^{2a,5} By 2035, the projected number of fatality out of this malignancy will alarmingly touch 3 million worldwide and by around 2050, the predicted annual cases of infection will hover around 3.5 million.⁶ Clearly, a catastrophic disaster solely due to lung cancer is in the offing.

Lung cancer encompasses two major forms – non-small cell lung cancer (NSCLC) and small cell lung cancer (SCLC). Depending on the stage of detection, the therapeutic protocols of lung cancer also vary.⁷ Besides the classical approach like chemotherapy, some of the noted modern clinical protocols for the therapy and management of NSCLC are immunotherapy, targeted therapy, laser therapy, and photodynamic therapy. Chemotherapeutic protocols for NSCLC include usage of

^a Department of Chemistry, Jadavpur University, Kolkata 700 032, India.

E-mail: jpnaskar@rediffmail.com, jnanp.naskar@jadavpuruniversity.in;

Fax: +91 33 2414 6223

^b Department of Botany, Molecular and Applied Mycology and Plant Pathology Laboratory, University of Calcutta, 35 Ballygunge Circular Rd., Kolkata 700 019, India

^c Department of Botany, Vedanta College, Kadapara, Phoolbagan, Kolkata 700 054, India

^d Departamento de Química Inorgánica, Universidad de Valencia, Dr Moliner, 50, 46100 Burjassot, Valencia, Spain

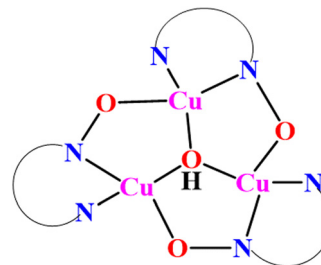
† Electronic supplementary information (ESI) available. CCDC 2270365. For ESI and crystallographic data in CIF or other electronic format see DOI: <https://doi.org/10.1039/d3nj04859d>

organic therapeutics like taxol and its derivatives, and inorganic platinum based cisplatin and carboplatin. As a therapeutic drug, the prospect and efficacy of cisplatin are commendable.⁸ However, cisplatin suffers from a copious number of adverse side effects that limit its applicability and viability. Non-negligible toxic side effects like nephrotoxicity, neurotoxicity, liver toxicity, general toxicity, ototoxicity, haemolysis and most importantly development of resistance to drugs restrict and marginalise the applicability of cisplatin.⁹

Over the past few decades, major research activities have been focused on developing novel transition metal based compounds to be used as promising anti-malignant agents. Accordingly, a plethora of transition metal based complexes have already been designed and synthesized to be optimally suitable for cytotoxic propensities and wound-recuperating abilities. The ruthenium based approach is noteworthy in this perspective.¹⁰ Palladium, gallium, titanium, gold, iron, osmium, rhenium, silver and cobalt compounds also show antiproliferative activities.¹¹

Being a biocompatible benign bio-element, coinage metal copper seems to be a prospective choice and prognostic marker in this regard. Copper based anticancer agents are so promising that some of them are in the preclinical and clinical trial phase.¹² It is worth emphasizing the key work of L. Ruiz-Azuara and co-workers that had reported a Cu(II) compound: [Cu(II)-(4,4'-dimethyl-2,2'-bipyridine)(acetylacetonate)(NO₃)(H₂O)]. This work is in clinical trials (Phase I) in Mexico.¹³ Recently, morpholine based mononuclear Cu(II) complexes have been screened by us against lung cancer cell lines A549.¹⁴ Copper(II) complexes with the Schiff base ligand manifest commendable biological activities due to high DNA binding affinity and biocompatible redox potential.¹⁵ The possible mechanisms of action of such complexes as anticancer agents are DNA interaction through non-covalent mode, generation of reactive oxygen species (ROS) and mitochondrial toxicity.¹⁶ Report on anticancer activity accentuated by trinuclear Cu(II) complexes is indeed very rare. Recently, linear trinuclear Cu(II) complexes with limited cytotoxicity (IC₅₀ > 100 μM) have been reported. The same were screened against human breast (MCF7) and liver cancer (HepG2) cells in a dose-dependent manner.¹⁷ To the best of our knowledge, the antiproliferative activity of the μ₃-oxido and/or μ₃-hydroxido bridged triangular trinuclear Cu(II) complex is unprecedented. Addressing this pertinent point, for the first time, herein we are concerned with such a system for its anticancer activity against lung cancer cell lines.

Polynuclear paramagnetic complexes are of contemporary interest owing to their significant applications as molecule-based magnetic materials. Spin coupling between paramagnetic metal centres of such type of exchange coupled systems is propagated through bridging atoms/groups.¹⁸ Oxime based ligands have been used in exchange coupled polynuclear systems. Diverse bridging modes of the oxime function can foster homo- and hetero-metallic (M–N–O–M') cores.¹⁹ In this context, triangular trinuclear copper(II) complexes having a central oxido/hydroxido bridge with peripheral oximato bridges are



Scheme 1 A μ₃-OH bridged triangular trinuclear Cu^{II} core with peripheral oximato bridges.

noteworthy from the viewpoint of magnetic aspect.²⁰ Accordingly, magnetic studies on trinuclear Cu(II) complexes with a central oxido/hydroxido bridge have become a fascinating area of interest in the last few decades.²¹ Such systems have drawn keen interest from the magnetic point of view due to their structural diversity and varying coordination environments around each copper centre.²² Triangular Cu(II) complexes have been studied as model systems since they represent the most basic spin triangle. This has made it possible to thoroughly analyse the magnetic characteristics of geometrically spin-frustrated systems.²³ A schematic representation of the μ₃-hydroxido bridged triangular trinuclear copper(II) core with peripheral oximato bridges, akin to our present work, is shown in Scheme 1.

The three unpaired electrons in this triangular core interact through Cu^{II}–O–Cu^{II} and Cu–O–N–Cu exchange pathways.²⁴ Such units may show antiferromagnetic (frustrated $S_{\text{total}} = 1/2$) or ferromagnetic ($S_{\text{total}} = 3/2$) coupling. Oxime based oxido-hydroxido bridged hexanuclear copper(II) systems with a Cu₃O···H···OCu₃ core have been reported along with their magneto-structural correlation.²⁵

Herein we report the synthesis, characterization and crystal structure of a new trinuclear copper(II) complex [(CuL)₃(μ₃-OH)(ClO₄)₂](CH₃OH)(H₂O) (**1**) having a central μ₃-OH bridge, stabilised by an oxime based NNO donor Schiff base ligand, 3-(((5-bromothiophen-2-yl)methylene)hydrazineylidene)butan-2-one oxime (**HL**). The antiproliferative activity of **1** has been screened against lung cancer cell line A549. We also perform the magnetic characterization of compound **1** with variable-temperature magnetic measurements and EPR spectroscopy.

Experimental

The details of materials and physical measurements are provided in the ESI.†

Solution preparation for spectroscopic studies

2 mM Tris–HCl buffer solution was prepared in millipore water of pH 6.8 to perform all the experiments. A 5 mL (1 mM) stock solution of **1** was prepared in DMSO.

DNA binding studies

The CT-DNA stock solution was prepared by following the standard procedure.²⁶ DNA solution was de-proteinized followed by ethanol precipitation.²⁷ It was then sonicated and further dialyzed several times at 5 °C under sterile conditions.²⁸ The purity of the CT-DNA solution was checked by monitoring the UV absorption spectrum at 260 and 280 nm. The (A₂₆₀/A₂₈₀) ratio was found to be between 1.88 and 1.92 and the (A₂₆₀/A₂₃₀) ratio was between 2.12 and 2.22. The concentration of the DNA stock solution was determined by considering the molar extinction coefficient (ϵ) of CT-DNA at 260 nm as 13 200 M⁻¹ cm⁻¹. CT-DNA was added each time to a fixed concentration (12.5 μ M) of complex solution in a cuvette and the spectra were recorded.

Cell culture

The human lung adenocarcinoma cancer cell line (A549) was obtained from the National Centre for Cell Science (Pune, India) and cultured in Dulbecco's modified Eagle's medium with 10% foetal bovine serum and 100 mg L⁻¹ antibiotics, namely, penicillin, streptomycin, and amphotericin B, in a humidified chamber containing 5% CO₂. Cells were allowed to reach 80–90% confluence before being trypsinized with trypsin-EDTA for use in experiments. All cell culture experiments were conducted in a biosafety cabinet under sterile conditions.

Cell viability assay using WST-1

The viability and proliferation of A549 cells were assessed using the WST-1 reagent (Takara Bio Inc., Japan) according to the manufacturer's protocol. In short, as described by Nandi *et al.*,²⁹ A549 cells were seeded and incubated for 24 h in a 96-well microtiter plate. The cells had been treated with varying concentrations (7.4–740 μ M) of compound **1**. Simultaneously cisplatin was used as a positive control drug and DMSO was used as a vehicle control set separately in triplicate and incubated at 37 °C for 24 h. The following day, 5 μ L of WST-1 reagent was added to each well and incubated in the dark for 3 h at 37 °C. Analysis was done at 450 nm through a Bio-Rad (model 550) microplate reader. The IC₅₀ value was determined with GraphPad Prism software (version 9.03).

Evaluation of A549 cell count and viability by trypan blue assay

Trypan blue dye exclusion assay was used to determine the effect of a drug on the viability of cancer cells. Briefly, the cells were seeded at a density of 1 \times 10⁵ cells per well in a 12-well culture plate and treated with different concentrations of **1** along with a negative control and vehicle control set separately in triplicate. The next day, cells were trypsinized and cell pellets were collected by centrifugation. Then the cell pellets were diluted in serum-free media and 10 μ L aliquot from the original

stock was mixed with an equal volume of 0.4% trypan blue dye. Detectable fluorescence of trypan blue was measured at 585 nm through a Bio-Rad (model 550) microplate reader. The readings were recorded and the percentage inhibition of cell viability was calculated based on the following formula:

$$\% \text{ Inhibition} = (\text{Total dead cell count} / \text{Total cell count}) \times 100$$

Colony formation assay

A549 cells were introduced into a 12-well plate at a density of 4 \times 10³ cells per well and they were treated with the vehicle as well as with compound **1** at 222 and 370 μ M the following day. After washing the cells with PBS, new medium was added. The cells were then grown for seven days at 37 °C in an incubator. On the eighth day, the cells were rinsed with PBS, fixed with 4% PFA, and stained for 0.5 h with 0.1% crystal violet. After that, colonies were rinsed with distilled water and photographs were taken.

Cytomorphological observation of A549 cells by bright field microscopy/fluorescence microscopy

A549 cells were cultured overnight in a 60-mm tissue culture dish for cell adhesion and treated with 222 and 370 μ M compound **1** for 24 h. The morphological changes of cells were observed using a phase contrast microscope. Further fluorescent staining with 1 μ g mL⁻¹ DAPI for 15 min in the dark was carried out for better visualisation of cells with nucleus under a fluorescence microscope (FLoid Imaging Station, Life Technologies, Waltham, MA, USA).

In vitro cell wound repair assay

The *in vitro* scratch wound repair assay was a modification of a previously described methodology of Nandi *et al.*³⁰ Briefly, 5 \times 10⁴ A549 cells per mL were cultured in 6-well plates to confluence as monolayers under standard conditions. Upon reaching a confluence of more than 75% for cultured cells, linear wounds were made with a 100 μ L pipette tip on cell monolayers followed by incubation with serum-free conditioned media for 24 h. Circumferential wound gaps were measured by ImageJ software and the percentage of wound repair was calculated.

Nuclear morphology by DAPI staining under fluorescent microscope

The DAPI staining technique was utilized to recognize the obvious signs of apoptosis in cancerous cells. A549 cells (5 \times 10⁴ cells per mL) were cultured in a 6-well culture plate overnight. Subsequently, cells were subjected to drug treatment at a concentration of 222 and 370 μ M. To examine alterations in

nuclear morphology, treated cells were rinsed with phosphate-buffered saline (PBS) and fixed with 4% paraformaldehyde for 10 min. More cells were washed with PBS and permeabilized with 0.1% Triton X-100. Finally, cells were exposed to DAPI ($1 \mu\text{g mL}^{-1}$ in PBS) for 15 min and were visualized under a fluorescence microscope (FLOID Imaging Station, Life Technologies, Waltham, MA, USA).

Direct fluorescence microscopic analysis for apoptosis induction

Dual staining with acridine orange/ethidium bromide (AO/EB) was performed to distinguish viable, apoptotic and necrotic cells with distinct morphological alterations in a cultured plate. 2×10^3 cells were grown in a 6-well plate and then the cells were treated with 222 and $370 \mu\text{M}$ compound **1** and kept overnight. The following day, the cells were stained with the acridine orange (AO, 5 mg mL^{-1}) and ethidium bromide (EB, 3 mg mL^{-1}) mixture. The extra unbound dye residues were rinsed with phosphate buffer saline prior to fluorescence microscopic visualisation.

Data analysis and statistics

Data are presented as the mean \pm standard deviation and SEM. All experiments were repeated at least three times. For paired comparisons, Student's *t*-test was used to determine the *P*-values. For multiple paired comparisons, analysis of variance and *post hoc* tests were used to determine the *P*-values. Prism9 software was used for all statistical analyses. Statistically, significance was defined as $P < 0.05$.

Synthesis of the ligand (HL)

Biacetyl monoxime monohydrazone (BMMH) (115 mg, 1 mmol) was dissolved in 30 mL of methanol to have a colourless solution. 5-Bromothiophene carboxaldehyde (90 μL , 1 mmol) was added to the above solution. The resulting solution turned light yellow. The reaction mixture was refluxed for 4 h in the presence of pre-activated molecular sieves ($4 \text{ \AA} \times 1.5 \text{ mm}$). The dark yellow solution obtained was left undisturbed in air for slow evaporation. After four days, a yellow crystalline solid was obtained. It was filtered and thoroughly washed with cold diethyl ether. The compound was dried *in vacuo* over CaCl_2 . The synthesized ligand is soluble in methanol, DCM, DMF, DMSO and THF. It is insoluble in *n*-hexane, *n*-pentane and H_2O .

Yield: 210 mg (72%); m.p.: 170°C ; anal. calc. for $\text{C}_9\text{H}_{10}\text{N}_3\text{OSBr}$: C, 37.48; H, 3.49; N, 14.57%; found: C, 37.44; H, 3.54; N, 14.53%; ^1H NMR ($\text{DMSO}-d_6$): δ (ppm): 11.69 (1H, s, -OH proton), 8.77 (1H, s, for azomethine proton), 7.45 (1H, d, ring proton of thiophene), 7.33 (1H, d, another ring proton of thiophene), 2.02 (s, 3H, -CH₃ proton), 1.92 (s, 3H, -CH₃ proton) (Fig. S1, ESI[†]); ^{13}C NMR ($\text{DMSO}-d_6$): δ (ppm): 156.04(C3), 155.35(C1), 154.91(C6), 140.51(C5), 135.10(C8), 132.30(C7), 117.87(C9), 13.10(C4), 9.73(C2) (Fig. S2, ESI[†]); FT-IR (KBr): (ν/cm^{-1}): 3229 (for -OH stretching), 1610 (for C=N), 1423 (C=N of oxime), 1360 (for -CH₃ asymmetric) (Fig. S3, ESI[†]); UV-Vis

(CH_3OH): λ_{max} ($\epsilon/\text{M}^{-1} \text{ cm}^{-1}$): 248 nm (26 288) and 351 nm (22 989); ESI-MS (CH_3OH) (*m/z*): (100%) (HL): 287.981 (theo. value: 288.080) (Fig. S4, ESI[†]).

Synthesis of complex $[(\text{CuL})_3(\mu_3\text{-OH})(\text{ClO}_4)_2] \cdot \text{CH}_3\text{OH} \cdot \text{H}_2\text{O}$ (**1**)

The ligand HL (57 mg, 0.2 mmol) was dissolved in 15 mL of methanol to obtain a light yellow solution. Anhydrous sodium acetate (17 mg, 0.2 mmol) was added to this solution, followed by $\text{Cu}(\text{ClO}_4)_2 \cdot 6\text{H}_2\text{O}$ (74 mg, 0.2 mmol) under stirring. Immediately, the colour of the solution turned dark green. The solution was stirred for 2 h and was filtered and kept undisturbed for slow evaporation at room temperature. A green crystalline compound was obtained after 2 days. It was filtered, washed thoroughly with cold diethyl ether and dried *in vacuo* at room temperature over calcium chloride. The green compound is soluble in methanol, acetonitrile, dichloromethane, DMF and DMSO.

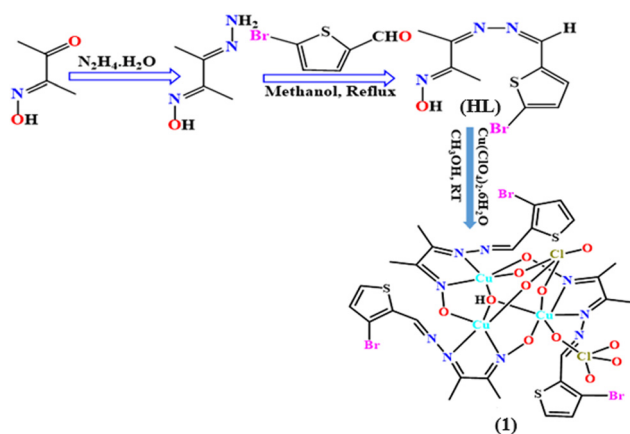
Yield: 30 mg (23%); anal. calc. for $\text{C}_{28}\text{H}_{34}\text{N}_9\text{O}_{14}\text{S}_3\text{Br}_3\text{Cl}_2\text{Cu}_3$: C, 25.49; H, 2.60; N, 9.56%; found: C, 25.45; H, 2.63; N, 9.53%; FT-IR (KBr): (ν/cm^{-1}): 3425 (for OH stretching), 1608, 1576 (for C=N), 1423 (C=N of oxime), 1144, 1113, 1088 and 627 (for ClO_4 stretching) (Fig. S5, ESI[†]); UV-Vis (CH_3OH): λ_{max} ($\epsilon/\text{M}^{-1} \text{ cm}^{-1}$): 277 nm (37 797), 356 nm (07 577) and 634 nm (2 61); $A_M(\text{CH}_3\text{OH})$: $165 \Omega^{-1} \text{ cm}^2 \text{ mol}^{-1}$ (1:2 electrolyte).

Shining needle shaped dark green crystals were grown by direct diffusion of *n*-hexane into a moderately concentrated DCM solution of compound **1**. The synthetic route to HL and **1** is shown in Scheme 2.

Caution! Perchlorate salts and their metal complexes with organic ligands are potentially explosive particularly during heating and shocking.³¹ Although we did not face any difficulty during our work, utmost care must be taken during their handling.

Crystallographic data collection and refinement

Crystallographic details and tables are provided in the ESI.[†]



Scheme 2 Synthetic route to HL and **1**.

Results and discussion

Synthesis and IR spectroscopy

The ligand **HL** was synthesized by equimolar Schiff base condensation of 5-bromo-2-thiophene carboxaldehyde and biacetyl monoxime monohydrazone (BMMH) with satisfactory yield. The trinuclear copper(II) complex was obtained by equimolar reaction of the synthesized ligand (**HL**) and copper(II) perchlorate hexahydrate in methanol at room temperature. In the FT-IR spectrum of **HL**, we have a characteristic sharp band at 1610 cm^{-1} which can be assigned to the imine stretching vibration. This band at 1610 cm^{-1} is slightly shifted to a lower wavenumber of 1604 cm^{-1} during complexation, indicative of the coordination of the nitrogen atom of the imine group to the metal center.³² The free OH group of the oxime fragment of **HL** shows a broad band around 3229 cm^{-1} . A sharp band also appears at 1423 cm^{-1} for the C=N stretching vibration of oxime. Compound **1** displays split bands at 1144, 1113 and 1088 cm^{-1} due to the asymmetric Cl–O stretching vibration and a single sharp band at 627 cm^{-1} attributed to the symmetric Cl–O stretching. These split bands are indicative of perchlorate ion coordination to the metal centre through oxygen, as confirmed by the X-ray structure.³³

Electronic spectra

The electronic absorption spectra of both **HL** and **1** were recorded in methanol (Fig. 1). The spectrum of free **HL** shows two intratransitions at 248 and 351 nm, whereas compound **1** shows bands at 277 and 356 nm. The bands at 351 nm in **HL** and 356 nm in **1** may be assigned to the $n\text{--}\pi^*$ charge transfer transitions.³⁴ The higher energy bands, in the range of 200–300 nm, are associated with the intra-ligand $\pi\text{--}\pi^*$ charge-transfer transitions.³⁵ A broad band has also been observed at 634 nm with a low molar extinction coefficient value for **1** ($261\text{ M}^{-1}\text{ cm}^{-1}$, inset in Fig. 1) that can be assigned to the d–d transition band in copper(II).³⁶

Following our literature survey, two dinuclear oxime based Cu(II) complexes having different non-coordinated counter anions exhibited broad absorption bands in the visible domain

at 636 and 635 nm. Additionally, sharp characteristic bands were also found at 427 and 426 nm owing to ligand to metal charge transfer transitions.²⁵ Moreover, an oxime based mononuclear Cu(II) complex shows characteristic bands at 402 and 624 nm, respectively, for the $\pi\text{--}\pi^*$ and d–d transitions.³⁷ All these reported d–d bands are similar to that obtained in the case of **1**. However, **1** manifests a low ligand to metal charge transfer band in contrast with the previously reported mono and dinuclear Cu(II) complexes under comparison. This may arise most likely due to different ligand environments.

Description of the crystal structure of $[(\text{CuL})_3(\mu_3\text{-OH})(\text{ClO}_4)_2]\cdot\text{CH}_3\text{OH}\cdot\text{H}_2\text{O}$ (**1**)

Compound **1** crystallizes in the triclinic $P\bar{1}$ space group. An ORTEP view with 50% probability ellipsoids of **1** is shown in Fig. 2. The asymmetric unit of **1** contains three L^- ligands, three Cu^{II} ions, a $\mu_3\text{-OH}$ group, and two coordinated ClO_4^- anions, with methanol and water molecules as solvents of crystallization. The molecular structure of **1** contains a discrete trinuclear copper(II) core, with a central $\mu_3\text{-hydroxido}$ bridge, surrounded by three L^- ligands and further stabilized by two coordinated perchlorate counter anions (Fig. 2). The Cu1–Cu2, Cu2–Cu3 and Cu3–Cu1 distances are very similar: 3.281, 3.297 and 3.326 \AA , respectively, with an average value of 3.301 \AA . As a result of the $\mu_3\text{-hydroxido}$ bridge, the three copper(II) centres adopt a near-equilateral triangular shape.³⁸ The Cu_3 triangle is capped on one side by the O1 atom of the central $\mu_3\text{-OH}^-$ ion and by a ClO_4^- anion (coordinated to the three Cu^{II} ions) on the other side. Cu1 and Cu2 centres show similar square pyramidal N_2O_3 coordination environments, whereas Cu3 shows an octahedral N_2O_4 environment.

Both Cu1 and Cu2 show a distorted square pyramidal environment with Addison's parameter, τ , of 0.29 for Cu1 and 0.15 for Cu2.³⁹ The basal positions are occupied by two N donor atoms from the L^- ligand, one O atom from an adjacent L^- ligand and the O atom of the central hydroxido bridge. The axial position is occupied by an O atom from a perchlorate ion. As usual, the axial bond distances (Cu1–O5 = 2.344 \AA and Cu2–O6 = 2.424 \AA) are longer than the basal ones (in the range of

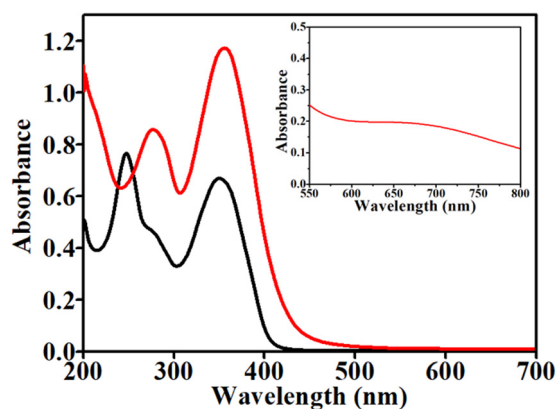


Fig. 1 UV-Vis spectra of **HL** (black) and **1** (red) in methanol. Inset: d–d band of **1**.

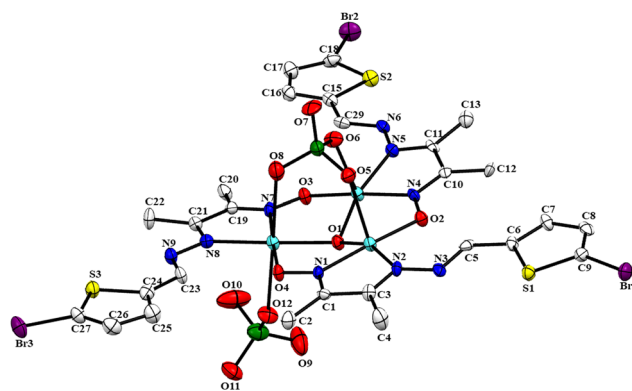


Fig. 2 Molecular structure of compound **1** with atomic displacement parameters shown with 30% probability ellipsoids. Hydrogen atoms and solvent molecules are omitted for clarity.

1.906–2.042 Å, Table 2). Cu3 shows a distorted N₂O₄ octahedral environment. The equatorial positions are occupied by two N atoms from the L[−] ligand, one O atom from an adjacent L[−] ligand and the O atom of the central hydroxido bridge (similar to the basal plane of Cu1 and Cu2). The axial positions are occupied by two O atoms from two ClO₄[−] coordinated anions, again with much longer Cu–O bond distances (2.449 and 2.639 Å) than the equatorial ones (in the range of 1.936–3.046 Å, Table 2). The Cu–N(oxime) and Cu–N(imine) bond lengths are in the range of 1.951–1.964 Å and 2.041–2.046 Å, respectively. These values are within the normal range observed in other similar trinuclear copper(II) complexes.⁴⁰ One of the two coordinated ClO₄[−] anions is connected through three O atoms (O5, O6 and O8) to the three Cu centres with Cu–O bond distances of Cu1–O5 = 2.344 Å, Cu2–O6 = 2.424 Å and Cu3–O8 = 2.639 Å. Consequently, this perchlorate acts as a μ₃-perchlorato-O,O',O'' capping ligand.⁴¹ The average Cu–O(perchlorate) bond distance is 2.464 Å. This rather long Cu–O(perchlorate) bond indicates that the perchlorate anions are weakly bound to the copper centres, as already observed in other similar trinuclear Cu3 complexes.⁴² This weak ligation has further been confirmed by the electrical conductivity measurements in solution. Compound **1** in methanol behaves as a 1:2 electrolyte. This is indicative of the total dissociation of the two ClO₄[−] anions in solution. As expected for a quasi-equilateral triangle, the intra-trimer Cu1–O1–Cu2, Cu2–O1–Cu3 and Cu3–O1–Cu1 bond angles are very similar: 112.4, 111.5 and 113.5°, respectively. The sum of these angles is less than 360° by 22.6°. This is due to the lack of planarity of the Cu₃O core (the O atom is located 0.538 Å away from the Cu₃ plane). Therefore, O1 shows a hybridization in between sp² and sp³.⁴³ In the domain of metalla-crown (MC) topology, the trinuclear copper core in **1** can be described as an *inverse*-9-metallacrown-3 (Fig. S6, ESI†).⁴⁴ As can be seen in Fig. 3, there is a weak C2–H2A⋯S2 and two O⋯Br interactions that connect the trimers to form a chain of trimers. Additionally, there are several intra-trimer C–H⋯O interactions that connect different L[−] ligands as well as H-bonds connecting the water molecule (O13) of crystallisation with the two perchlorate anions (O6, O9 and O12) and with the central μ₃-OH group (Table S5, ESI†).

DNA binding

To explore the interaction of a complex with DNA, UV-Visible spectroscopic analysis is one of the useful methods.⁴⁵

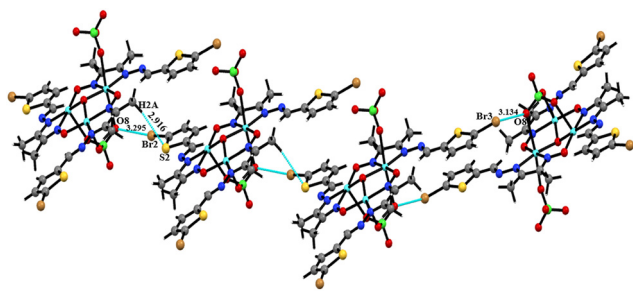


Fig. 3 H-bonded chain view of **1** through intermolecular interaction of C–Br⋯O and C–H⋯S. Solvent molecules are omitted for clarity. The H-bonds are indicated by the dashed line.

Electronic absorption titrations for **1** were carried out in the absence and presence of CT-DNA employing Tris buffer (pH = 6.8) at 20 °C (Fig. 4). In the absorption spectra, **1** displayed absorption maxima at 364 nm corresponding to metal-to-ligand charge-transfer (MLCT) bands. 12.5 μM complex **1** was titrated against increasing concentration of CT-DNA (0–135 μM). The absorption spectra with the concomitant change in intensity and wavelength were followed. Our expounded result clearly indicates that **1** shows 41.98% hypochromism with slight bathochromic shift as a result of the intercalation binding mode of the complex and DNA base pairs. The binding constant (*K*_b) for **1** was calculated from the Wolfe–Shimmer equation [eqn (1)]⁴⁶ in order to compare the interaction intensity with CT-DNA:

$$\frac{[\text{DNA}]}{\varepsilon_a - \varepsilon_f} = \frac{[\text{DNA}]}{\varepsilon_b - \varepsilon_f} + \frac{1}{k_b(\varepsilon_b - \varepsilon_f)} \quad (1)$$

where ε_a is the extinction coefficient at the given DNA concentration as determined by calculating Abs/[complex]. ε_f and ε_b correspond respectively to the extinction coefficient of the free complex and of the complex fully bound to DNA. The Wolfe–Shimmer binding constant (*k*_b) can be obtained from the ratio of the slope of the linear plots of [DNA]/($\varepsilon_a - \varepsilon_f$) vs. [DNA] and the intercept. The binding constant value for **1** was found to be $8.48 \times 10^4 \text{ M}^{-1}$.

CD spectra

The circular dichroism (CD) spectra of CT-DNA and its interaction with **1** are shown in Fig. 5. The CD signal peak, as the blank control, changed to a certain extent after the addition of **1**. As can be seen, the negative peak intensity decreased while the positive peak increased with certain degrees of red shift. Among them, the positive peak signal was enhanced in the CD spectrum due to the base stacking effect of DNA after the interaction of **1** with DNA base pair. As a result, the double helix was more compact. The decrease and red shift of the negative peaks indicate that **1** destroyed the right-hand helicity of DNA molecules.⁴⁷ This result shows that **1** interacts with CT-DNA in an intercalated manner. The change of the spectral pattern of the positive and negative peaks confirms the interaction of DNA with **1**.

Biological study

In order to investigate the potential cytotoxicity of compound **1** against cancer cells, we have used the human lung adenocarcinoma cell line (A549) as a model cell line to determine the effects of **1** on carcinoma cell proliferation.

Complex induced potent cytotoxic effects and inhibition of cell colony forming tendency

Water soluble tetrazolium 1 (WST-1) was utilised to investigate the cytotoxic activity against human lung adenocarcinoma cell line A549. The WST-1 assay is based on the amount of formazan dye formed directly through the metabolic activity of cells. To the best of our knowledge, this is the first report on the biological cytotoxic activity of any trinuclear copper(II) compound. The *in vitro* cytotoxicity of **HL** and **1**, along with

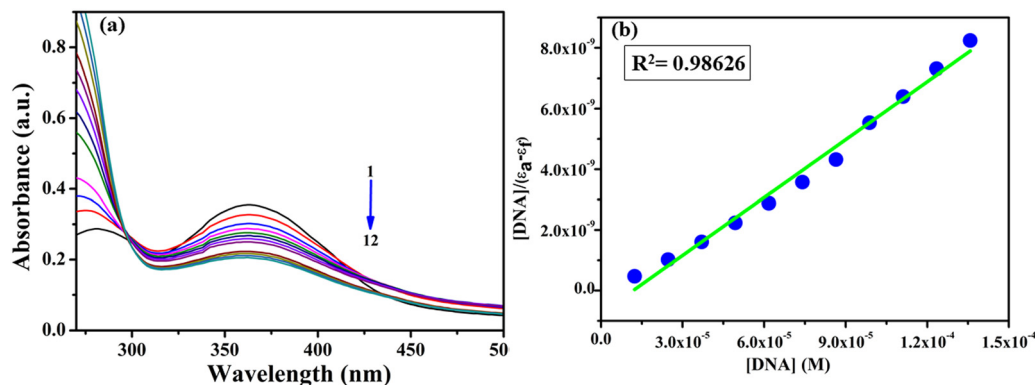


Fig. 4 (a) Absorption spectra of **1** (12.5 μ M) in Tris-HCl buffer (pH = 6.8) with increasing amount of DNA (135 μ M) at room temperature. (b) Linear plots of $[\text{DNA}]/(\epsilon_a - \epsilon_f)$ vs. $[\text{DNA}]$.

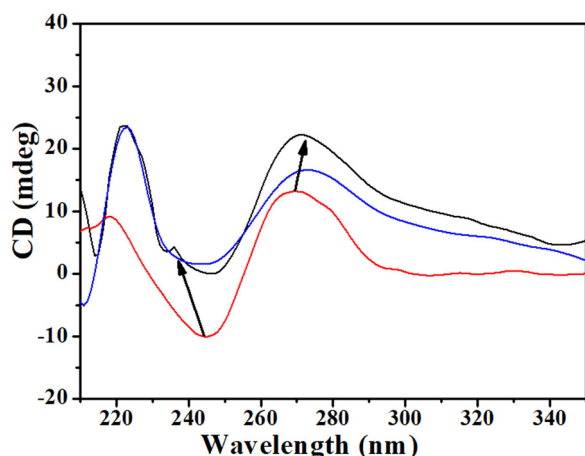


Fig. 5 CD spectra depicting interaction between **1** and CT-DNA. $C_{\text{DNA}} = 135 \mu\text{M}$.

standard drug cisplatin as a positive control and DMSO as a vehicle control, was studied using the WST-1 assay. The *in vitro* biological effects of **HL** and **1** on A549 cell proliferation are depicted in Fig. 6A. There was a dose-dependent activity; with an increase in the concentration of compound **1**, the percentage of cell viability decreased with moderate cytotoxicity when compared with **HL**. On the other hand, **HL** displayed almost negligible cytotoxicity even at the highest dose of 518 μM . The 50% inhibition of cell growth (IC_{50} value) for **1** and **HL** was calculated from the mean of three independent measurements by applying a non-linear regression curve fit analysis and was recorded as 222 and 592 μM respectively (Table 1).

Cisplatin was used as a positive control in A549 cell lines because it is considered as the most common and effective anticancer drug in lung cancer treatment regimens as mentioned in our introductory part. The lung cancer A549 cells were then subjected to cytotoxic studies with cisplatin as a standard drug for comparison, and the IC_{50} value of cisplatin was recorded to be 1.75 μM (Fig. 6B).

The apoptotic nature of the complex and ligand was also screened against breast cancer cell line MCF-7 by WST-1 assay

(Fig. 7). Complex **1** revealed an IC_{50} value of $224 \pm 0.25 \mu\text{M}$ against the breast cancer cell line (MCF-7).

It is pertinent to note that a similar high IC_{50} value $\geq 100 \mu\text{M}$ was also observed in human MCF-7 breast and HepG2 liver cancer cells by treatment with linear trinuclear Cu(II) complexes.¹⁷ Some mononuclear/dinuclear Cu(II) complexes show prominent cytotoxicity with lower IC_{50} values.⁴⁸ Triangular trinuclear Cu(II) complexes usually show lower cytotoxicity in comparison to mono/dinuclear Cu(II) complexes.

The cytotoxic effect of **1** was further confirmed by trypan blue dye exclusion assay. Corresponding to WST-1 results, close cytotoxic response was noted from A549 cells on treatment with **1**, demonstrating prominent changes in their ability to exclude trypan blue until 24 h (Fig. 6C). The expounded results have positively hinted that **1** exerts a potent cytotoxic effect than its stabilising ligand, **HL**, against human lung cancer cells. So, further studies were carried out on **1** taking two concentrations, *i.e.* 222 and 370 μM , which are IC_{50} and above IC_{50} values, respectively.

The inhibitory effect of **1** on the proliferation of A549 cells was determined with colony formation assay. Cultured A549 cells were treated with the complex at the two mentioned concentrations (222 and 370 μM) for a week, and then stained with crystal violet. As depicted in Fig. 8, compound **1** suppressed the colony formation tendency of A549 cells while the control and vehicle wells had almost fully grown cells. Cumulatively these results show that **1** has a dual effect: (i) decreases cell viability and (ii) inhibits the colony formation in a persistent way.

Morphological changes induced by complex **1**

Image analysis with phase contrast microscopy is a non-destructive cell imaging method, which allows one to visualise and analyse apoptosis without influencing the cell behaviour.⁴⁹ The results of microscopic image analyses established that **1** has a moderate toxic effect against A549 cells which led to alteration in the cell structure. In the negative control set, the cell appeared to be normal bearing usual morphology with strong adhesion, whereas in the treated set, changes in morphology such as cellular shrinkage accompanied by round cells,

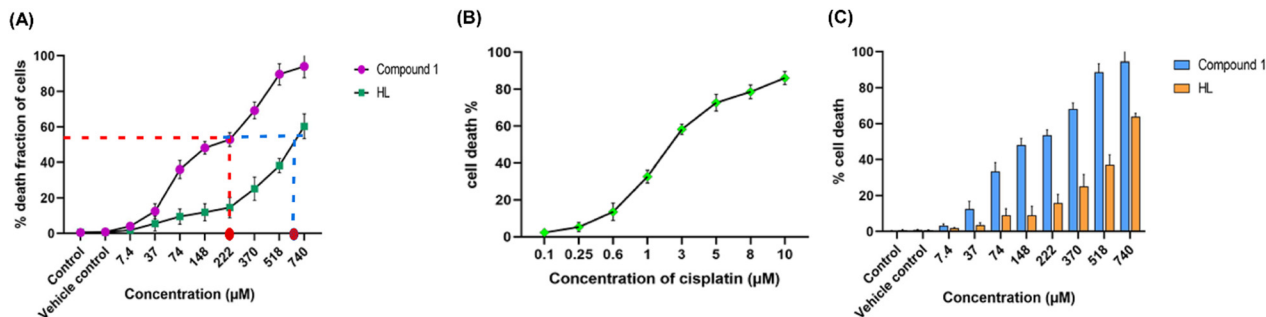


Fig. 6 Measurement of cytotoxic activity in A549 cells by (A) WST-1 assay with compound **1** and HL, (B) WST-1 assay performed with positive control cisplatin and (C) trypan blue viability assay. The results indicate the percentage of live or viable cells as compared to the total number of cells for each sample. Data were collected from two independent experiments with three replicates per sample and were analysed with two-way ANOVA. Error bars are standard deviations. Data are shown as the mean \pm SD of three independent experiments.

Table 1 IC_{50} values for **1** and HL

Compounds	IC_{50} value (μM)
1	222 ± 0.87
HL	592 ± 1.26

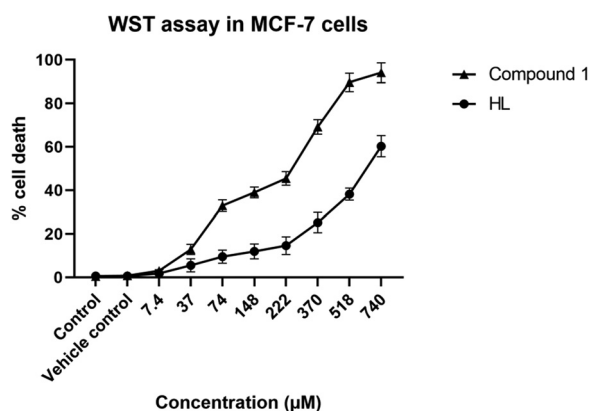


Fig. 7 Measurement of cytotoxic activity in MCF-7 cells by WST assay with compound **1** and HL.

elongated and distorted cells, poor cellular adhesion and reduced cell number with visible cellular debris were clearly observed (Fig. 9).

Apoptotic cell death in A549 cells induced by complex **1**

Studying apoptosis is a key point in cancer research since a dearth or a surplus of apoptosis is the sole cause of cancer. At present, several *in vitro* procedures are at hand to study apoptosis including various morphological staining methods like acridine orange and ethidium bromide (AO/EB), DAPI (4',6-diamidino-2-phenylindole), Hoechst staining, *etc.*⁵⁰ Hence, in order to decipher the cytotoxic mode of action of **1** against A549 cancer cells, staining experiments were conducted using DAPI and AO/EB. To determine the involvement of apoptosis in complex **1**-induced cytotoxicity in A549 cells, initial evaluation was carried out with fluorescent DNA binding dye DAPI. Fig. 8 shows how treatment with **1** causes characteristic apoptotic changes in cellular morphology such as chromatin condensation with irregular edges around the nucleus, fragmented nuclei, nuclear shrinkage as well as blebbing, elevated number of nuclear body fragments and distorted nucleus, whereas round, clear edged, intact nucleus and uniformly stained round nuclei were observed in the negative control.

Further fluorescence microscopic observations of the A549 cells stained with AO/EB validate the presence of early and late apoptotic stages of cells along with the prominent apoptotic features. Acridine orange (AO) being an important dye stains the nuclei green in both living and dead cells, while ethidium bromide (EB) stains only those cells that have lost their membrane integrity.⁵¹ When complex **1**-treated A549 cells were stained with the AO/EB dye mixture, a major proportion of cells showed cellular shrinkage, condensed or fragmented

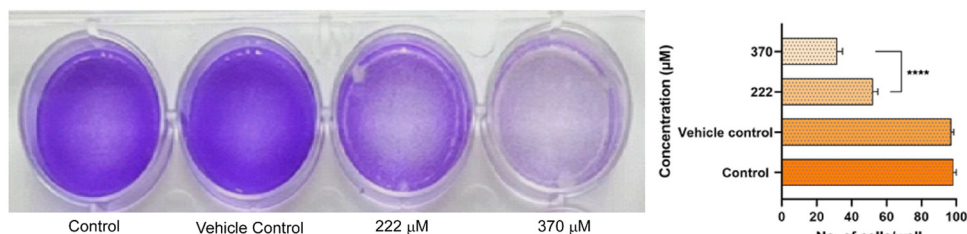


Fig. 8 Colony formation ability of lung adenocarcinoma cells treated with control, vehicle, and compound **1** at the indicated doses for appropriate time. The colony formation rate of cells was calculated and represented (right panel). The data are presented as the mean \pm SD of three separate experiments. * $P < 0.05$, ** $P < 0.01$, *** $P < 0.001$ indicate significant differences between treatment group and control group.

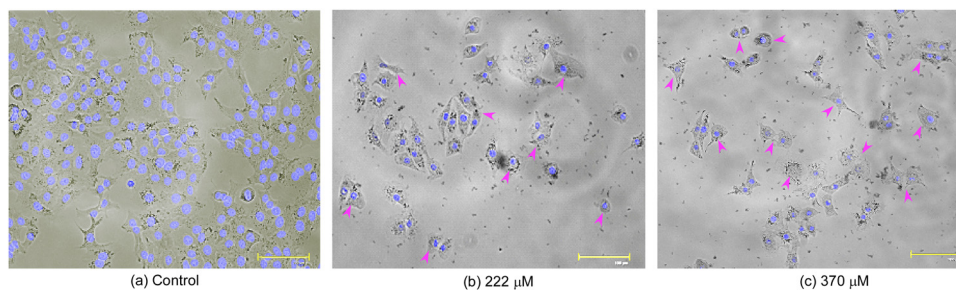


Fig. 9 Morphological alterations of lung adenocarcinoma A549 cells under inverted phase contrast microscopy. (a) Control, and (b) and (c) cells exposed to the complex. Magnification 40 \times .

chromatin, and membrane blebbing with distorted cellular morphology (Fig. 10B). Cells emitting yellowish green fluorescence were marked as early apoptotic as notably visible for 222 μ M concentration along with a few cells emitting yellowish orange indicating the presence of both early and late apoptotic cells. At the high concentration of 370 μ M, most of the cells fluoresced yellowish orange to bright orange indicating the late apoptotic stage. In contrast, non-apoptotic or live cells appeared wholly green in colour with no alternation in their morphology in the control. The results significantly reveal that cell death induced by **1** in A549 cells is due to apoptosis. By counting the number of yellowish orange, yellowish green and green cells, the apoptotic rate was calculated (Fig. 10B, right panel). Based on these results, complex **1** might be a possible choice for further test of the anticancer activity against human

lung adenocarcinoma cells for both *in vitro* and *in vivo* procedures.

Effect of complex **1** on the migration of A549 cells

Customarily, cells tend to migrate, which is essential for growth and to ensure proper tissue functions. In cancer cells, the migratory property leads to invasion and metastasis. This is the prime reason for the mortality of lung cancer patients.⁵² To study the effect of **1** on the migration of A549 cells, experiments were conducted for 24 h till the induced wound was completely closed in wound-healing assays. As can be seen in Fig. 11, the migration ability of A549 cells decreases as the amount of complex **1** covering the wound increases, whereas the negative control cells show almost 90% of wound closure after 24 h.

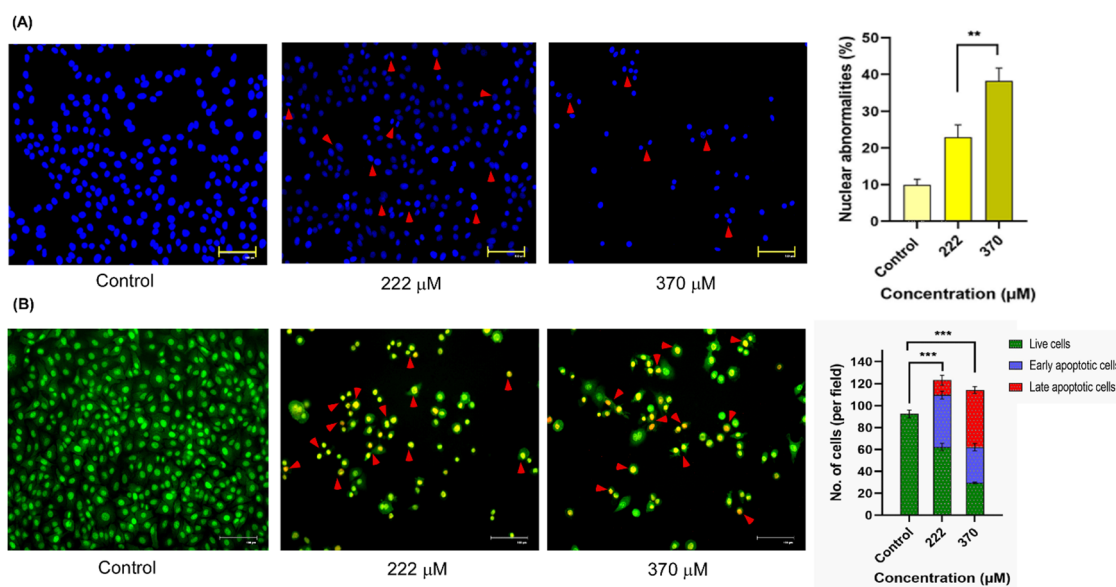


Fig. 10 Apoptosis induction studies of complex **1** in A549 cells. (A) DAPI staining. Arrows represent the nuclear anomalies which increased with the increasing dose of the complex. The percentage of nuclear abnormalities in the respective set of experiments is represented in a bar graph (right panel). (B) Acridine orange and ethidium bromide (AO/EB) staining by fluorescence microscopy. The arrow indicates early apoptotic (EA) and late apoptotic (LA) cells. The bar graph depicts the population of cells in different phases (right panel). Scale bar denotes 200 μ m. Magnification 45 \times . All the experiments were performed after 24 h incubation. Values represent the means \pm standard deviation (SD), and all samples were measured independently in triplicate. Differences among the groups were compared by one-way ANOVA, and the asterisks indicate significant differences between treatment group and control group (* P < 0.05, ** P < 0.01, *** P < 0.001).

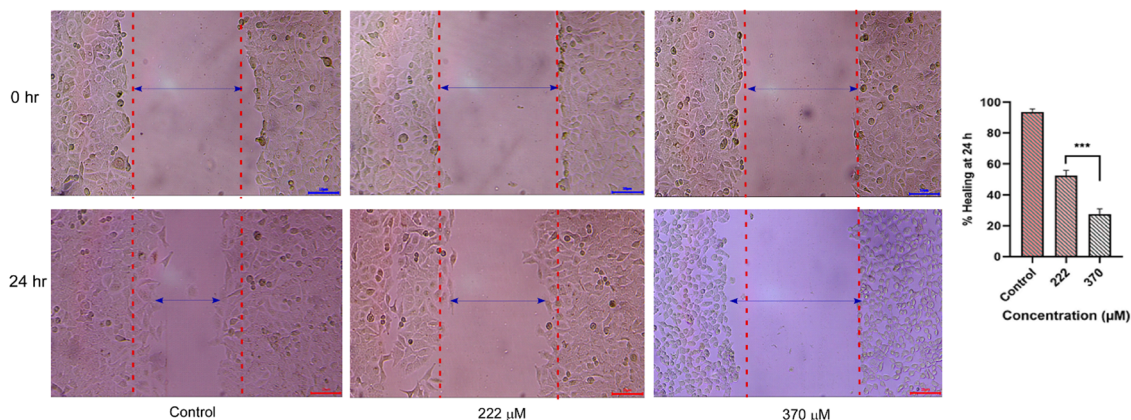


Fig. 11 Wound-healing assay of A549 cells after exposure to complex **1**. Representative wound-closure images taken at 0 h and 24 h with respective wound-closure ratios (left panel). Wound-closure analysis after the complex normalized to 0% at 0 h. Experiments were repeated three times. Bars represent standard deviation from one representative experiment (right panel). Magnification 100 \times .

Cell death mechanism

There are several comprehensive studies that focus on the diverse roles of inorganic compounds in cancer therapy.⁵³ Copper based complexes are favourable next-generation non-platinum anti-cancer agents and chemotherapeutics.⁵⁴ Our compound exhibits a regulated cell death against A549 lung cancer cells and in reference to other studies conducted previously, we infer that trinuclear copper(II) complexes induce cell death through diverse mechanisms, encompassing reactive oxygen species (ROS) responses, mitochondrial dysfunction and apoptosis through an intrinsic pathway. Gul *et al.* in 2020 reported two copper(II) complexes, Cu1 and Cu2, with isoquinoline derivatives as ligands that interacted *via* the mitochondrial-mediated pathway against A549 cells.⁵⁵ Yip *et al.* in 2011 found that disulfiram (DSF) can manifest strong copper-dependent toxicity *in vitro* against cultured breast cancer cells.⁵⁶ The combined application of disulfiram and Cu²⁺ inhibited breast cancer cell colony formation, induced ROS production and subsequently activated downstream apoptosis-related pathways, thereby induced breast cancer cell apoptosis. Again, *in vitro* antitumor effects of a Cu(II) complex, [Cu(4-fh)(phen)(ClO₄)₂], had been reported to act against melanoma B16F10 cells through DNA-damage, G0/G1 cell cycle arrest and triggered apoptosis.⁵⁷ Reports on promising *in vitro* anti-proliferative efficacy of copper(II) complexes against lung carcinoma cell NCI-H460 are also there. For ready reckoning, [Cu(L1)Cl]Cl·2H₂O induced cell death by apoptosis *via* cell cycle arrest in sub-G1 populations, plasma membrane blebbing, fragmentation and condensation of chromatin, alterations in mitochondria along with distinct changes on the cell surface.⁵⁸ Novel water-soluble ternary copper(II) mixed ligand complexes, [Cu(4-mphen)(tyr)(H₂O)]NO₃·2H₂O and [Cu(5mphen)(tyr)(H₂O)]NO₃·2H₂O, had been demonstrated to display apoptotic activity against adenocarcinomic human alveolar basal epithelial cell A549. These two complexes were also demonstrated to cause DNA damage possibly through significant induction of ROS-mediated oxidative damage in the cancer cell and varying degrees of cytotoxic and genotoxic damage in the cancer cell line.⁵⁹

To ascertain the stability of **1** during our antiproliferative assay, its UV-Vis spectra in 0.5% DMSO solution in time-variation mode were monitored (Fig. 12). **1** retained its unaltered identity in terms of structural rigidity in 0.5% DMSO solution. This prompted us to deploy 0.5% DMSO solution of **1** in our undertaken bio-assays.

Magnetic properties

The thermal variation of the product of the molar magnetic susceptibility per Cu₃ trimer times the temperature ($\chi_m T$) shows a value close to 0.9 cm³ K mol⁻¹ at room temperature (Fig. 13). When the sample is cooled, the $\chi_m T$ value shows a continuous decrease to reach a plateau at around 0.4 cm³ K mol⁻¹ below 50 K. At lower temperatures, $\chi_m T$ shows a further decrease to reach a value of 0.25 cm³ K mol⁻¹ at 2 K. This behaviour clearly indicates the presence of predominant anti-ferromagnetic Cu···Cu interactions inside the Cu₃ triangle, giving rise to spin frustration since in a triangular array of spins, it is not possible to simultaneously satisfy the three possible spin pairings in an antiferromagnetic way.¹⁸ Since complex **1** shows a quasi-equilateral triangle, we have fitted

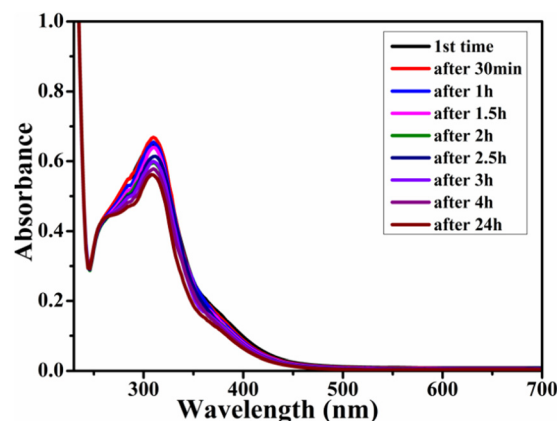


Fig. 12 UV-Vis spectra of **1** in 0.5% DMSO solution with variation in time mode.

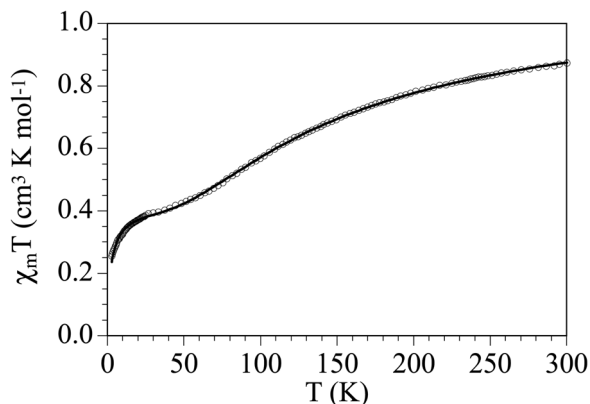


Fig. 13 Thermal variation of $\chi_m T$ per Cu_3 trimer in **1**. The solid line shows the best fit to the equilateral $S = \frac{1}{2}$ trimer model (see text).

the magnetic properties of **1** with a simple model of an equilateral $S = \frac{1}{2}$ triangle with the following Hamiltonian: $H = -2J[S_1S_2 + S_2S_3 + S_1S_3]$ including a weak inter-trimer coupling (zJ , to account for the decrease at very low temperatures) and a paramagnetic monomeric impurity, using the program PHI.⁶⁰ This model reproduces very satisfactorily the magnetic data in the whole temperature range with $g = 2.144(4)$, $J = -44.6(2) \text{ cm}^{-1}$, $zJ = -2.0(1) \text{ cm}^{-1}$ and a $S = \frac{1}{2}$ paramagnetic impurity of 2.2(1)% (solid line in Fig. 13).

Magneto-structural correlation

It is well established that in triangular Cu_3 complexes with a central O atom, the strength of the antiferromagnetic coupling mainly depends on the Cu–O–Cu bond angles since these angles are closely related to the planarity of the Cu_3O entity. The larger the angle, the larger the planarity and, accordingly, the stronger the antiferromagnetic coupling.⁶¹ Additionally, there are other factors that may affect the effective overlap of the magnetic orbitals and, therefore, the magnetic coupling such as (i) the deviation of the $\mu_3\text{-O}$ centre from the centroid of the Cu_3 triangle (the higher the deviation, the weaker the coupling), (ii) the Cu···Cu distance in the triangle and (iii) the co-planarity of the equatorial coordination plane around each copper centre (the greater the co-planarity, the stronger the magnetic coupling).

Since complex **1** contains (i) a central $\mu_3\text{-OH}$ bridge, (ii) a μ_3 -perchlorato-O,O',O'' capping ligand connecting the three Cu^{II} ions and (iii) a Cu_3 core surrounded by peripheral oximates, we have performed a search in the CCDC database (consulted in October 2023),^{42,62–66} to look for complexes similar to complex **1**. This search shows that there are only six trinuclear copper(II) complexes reported with these characteristics. Unfortunately, only three of them have been magnetically characterized (Table 2).^{62–64} In these three examples, the magnetic coupling is strong and antiferromagnetic, although the lack of more examples precludes a clear magneto-structural correlation. Furthermore, two of them have been fitted with an antisymmetric exchange and, therefore, the J values cannot be compared with the other case where a symmetric exchange model

Table 2 Comparison of structural and magnetic parameters of some oxime based $\mu_3\text{-OH}$ bridged trinuclear copper(II) complexes

Complex (CCDC)	Cu···Cu (Å)	α^a (°)	θ^b (°)	J^c (cm ^{−1})	zJ (cm ^{−1})	Ref.
1	3.281	112.40	9.37	−89.2	−2.0	This work
	3.297	111.46	20.34			
	3.326	113.45	0.77			
ACAFIW	3.203	111.06	8.70	−441(2) ^d		55
	3.225	112.47	8.17			
	3.217	111.89	11.44			
KUPRAP	3.198	114.92	6.37	−148	−7.65 ^e	56
	3.221	116.89	0.17			
	3.216	115.91	3.99			
	3.214	114.91	12.37			
	3.215	115.48	2.23			
	3.205	114.42	11.18			
YIZNOM	3.215	117.17	12.82	−636 ^d	−0.13 ^e	57
	3.215	116.12	4.85			
	3.227	114.99	3.74			

ACAFIW = $[\text{Cu}_3(\text{OH})(\text{ClO}_4)_2(\text{mpko})_3]\cdot\text{CH}_3\text{OH}$ (mpko = methyl(2-pyridyl)ketone oxime); KUPRAP = $[\{[\text{Cu}_3(\text{NHDEPO})_3(\mu_3\text{-O})(\text{ClO}_4)_2(\mu\text{-H})](\text{ClO}_4)_7\}\cdot 4\text{H}_2\text{O} (\text{NHDEPO} = 3\text{-}[3\text{-(diethylamino)propylimino]butan-2-one oxime})]$; YIZNOM = $[\{[\text{Cu}_3(\text{HL})_3(\text{ClO}_4)(\mu_3\text{-O})_2(\mu\text{-H})](\text{ClO}_4)_7 (\text{HL} = 3\text{-}[3\text{-(dimethylamino)propylimino]butan-2-one oxime})]\}$. ^a α = Cu–O–Cu angle. ^b θ = Cu–N–O–Cu torsion angle. ^c The Hamiltonian is $H = -J[S_1S_2 + S_2S_3 + S_3S_1]$. ^d Antisymmetric exchange. ^e θ value (Weiss correction of the temperature).

has been used. Nevertheless, we can compare compound **1** ($J = -89.2 \text{ cm}^{-1}$) with compound KUPRAP ($J = -148 \text{ cm}^{-1}$).⁶³ In compound KUPRAP the average Cu–O–Cu bond angle is larger compared to that in compound **1** (115.42° vs. 112.44°), the average dihedral Cu–N–O–Cu angle is lower (6.05° vs. 10.16°) and the average Cu···Cu distance is shorter (3.212 Å vs. 3.301 Å). All these structural parameters indicate that the magnetic coupling in KUPRAP must be stronger than that in **1**, in agreement with the experimental results (−148 cm^{−1} vs. −89.2 cm^{−1}) (Table 2).

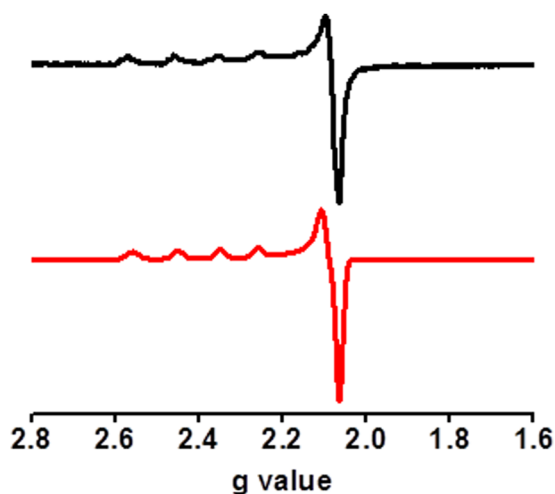


Fig. 14 X-band EPR spectrum of **1** in frozen DMF solution. Red (simulation) and black (experimental).

Table 3 Magnetic parameters of **1**

Complex	<i>g</i> value		<i>A</i> value (G)		Line width (G)
	<i>g</i> ₁	<i>g</i> ₂	<i>A</i> ₁	<i>A</i> ₂	
1	2.4000	2.0849	128.7	12.21	3

EPR spectroscopy

The EPR spectrum of **1**, recorded in a frozen *N,N*-dimethylformamide (DMF) solution at 143 K (Fig. 14), displays four hyperfine lines in the parallel (*g*_{||}) region, corresponding to the hyperfine coupling with the *I* = 3/2 nuclear spin of ⁶³Cu and ⁶⁵Cu nuclei (with natural abundances of 69.7% and 30.3%, respectively). Compound **1** shows a rhombic EPR spectrum with *g*_⊥ > 2.2 > *g*_{||} and *A*_⊥ > *A*_{||}. This spectrum can be very well simulated with a linewidth of 3 G, *g*_⊥ = 2.4000, *g*_{||} = 2.0849, *A*_⊥ = 128.7 G and *A*_{||} = 12.21 G (red line in Fig. 14). These values and the observed EPR spectrum agree with a Cu^{II} ion with an electronic ground state in which the unpaired electron mainly occupies the *d*_{x²-y² orbital.⁶⁷ The magnetic parameter values of **1** are shown in Table 3.}

Conclusions

In this work we have successfully synthesized and characterised a novel Schiff base ligand, 3-(((5-bromothiophen-2-yl)methylene)hydrazineylidene)butan-2-one oxime (**HL**), and a rare triangular trinuclear copper(II) complex (**1**) with a central μ₃-OH bridge and a capping ClO₄[−] anion connecting the three Cu^{II} ions. Both **HL** and **1** have been screened against lung adenocarcinoma cell lines A549. In contrast to the ligand **HL**, significant cell death has been induced by **1** in A549 cells. The IC₅₀ value for **1** is found to be much lower than that of **HL**. Cellular cell death induced by **1** is due to apoptosis. **1** displays elevated outstanding potency against A549 cells. Based on these results, compound **1** might be a possible choice of anticancer medication against human lung adenocarcinoma cells (A549) for both *in vitro* and *in vivo* experimental procedures. In addition, the magnetic properties of **1** show the presence of a moderate antiferromagnetic coupling that can be rationalized from the structural parameters.

Author contributions

Naba Kr Mandal: experimental work, methodology, investigation, data curation, formal analysis and writing original draft; Sudeshna Nandi: biological work, data curation, formal analysis and writing; Samia Benmansour: data curation, formal analysis and writing; Carlos J. Gómez-García: magnetic measurements, data curation, formal analysis, magnetic fitting and writing; Krishnendu Acharya: methodology, writing, review and editing; Jnan Prakash Naskar: conceptualization, supervision, project administration, methodology, funding acquisition, validation, writing, review and editing.

Conflicts of interest

There are no conflicts to declare.

Acknowledgements

N. K. M. sincerely acknowledges the University Grants Commission (UGC), New Delhi, India, with gratitude for a Senior Research Fellowship. J. P. N. humbly acknowledges Jadavpur University for infrastructural facilities and financial support. This study forms part of the Advanced Materials program and was supported by the Spanish MCIN with funding from European Union NextGeneration EU (PRTR-C17.I1) and the Generalitat Valenciana (project MFA-2022-057). We also acknowledge the project PID2021-125907NB-I00, financed by MCIN/AEI/10.13039/50110 0011033/FEDER, UE, and the project CIPROM-2022-060 from the Generalitat Valenciana, for financial support.

References

- (a) L. A. Torre, F. Bray, R. L. Siegel, J. Ferlay, J. Lortet-Tieulent and A. Jemal, *Ca-Cancer J. Clin.*, 2015, **65**, 87–108; (b) H. K. Matthews, C. Bertoli and R. A. M. de Bruin, *Nat. Rev. Mol. Cell Biol.*, 2022, **23**, 74–88; (c) D. Hanahan, *Cancer Discovery*, 2022, **12**, 31–46; (d) C. P. Wild, E. Weiderpass and B. W. Stewart, *Word cancer report: cancer report for cancer prevention*, IARC, Newyork, 2020.
- (a) H. Sung, J. Ferlay, R. L. Siegel, M. Laversanne, I. Soerjomataram, A. Jemal and F. Bray, *Ca-Cancer J. Clin.*, 2021, **71**, 209–249; (b) B. S. Chhikara and K. Parang, *Chem. Biol. Lett.*, 2023, **10**, 451; (c) J. Ferlay, M. Colombet and I. Soerjomataram, *Int. J. Cancer*, 2021, **149**, 778–789.
- The global challenge of cancer, *Nat. Cancer*, 2020, **1**, 1–2.
- (a) World Health Organization, Cancer facts sheets, lung cancer, <https://www.who.int/news-room/fact-sheets/detail/cancer>; (b) R. L. Siegel, K. D. Miller, H. E. Fuchs and A. Jemal, *Ca-Cancer J. Clin.*, 2022, **72**, 7–33.
- F. Bray, J. Ferlay, I. Soerjomataram, R. L. Siegel, L. A. Torre and A. Jemal, *Ca-Cancer J. Clin.*, 2018, **68**, 394–424.
- (a) J. Didkowska, U. Wojciechowska, M. Mańczuk and J. Lobaszewski, *Ann. Transl. Med.*, 2016, **4**, 1–11; (b) R. Sharma, *Int. J. Clin. Oncol.*, 2022, **27**, 665–675.
- (a) B. C. Bade and C. S. D. Cruz, *Clin. Chest Med.*, 2020, **41**, 1–24; (b) A. Wiczonek, A. R. Lewis, E. G. Boland, G. Avery, J. Kastelik, J. W. Boland, K. Moghissi, L. Cove-Smith, M. Loubani, M. Migliore, N. S. Tambe, P. Tcherveniakov, P. Barber, P. S. Nia, S. B. Knight and S. Heuts, *Perspectives in Lung Cancer*, Bentham Books, Singapore, 2020.
- (a) S. P. Fricker, *Dalton Trans.*, 2007, 4903–4917; (b) N. K. Singh, P. N. Yadav, A. A. Kumbhar, Y. R. Pokhrel and P. N. Yadav, *J. Inorg. Biochem.*, 2020, **210**, 111134; (c) American Cancer Society, Treating Non-Small Cell Lung Cancer, <https://www.cancer.org/cancer/lung-cancer/treating-non-small-cell.html>; (d) Y. Gao, P. Dorn, S. Liu, H. Deng, S. R. R. Hall, R. W. Peng, R. A. Schmid and T. M. Marti, *Cancer Cell Int.*, 2019, **19**, 1–14.
- (a) S. Dilruba and G. V. Kalayda, *Cancer Chemother. Pharmacol.*, 2016, **77**, 1103–1124; (b) T. C. Johnstone, K. Suntharalingam and S. J. Lippard, *Chem. Rev.*, 2016, **116**, 3436–3486; (c) M. S. Galanski and B. K. Keppler, *Anti-Cancer Agent.*

- 2007, **7**, 55–73; (d) L. Kelland, *Nat. Rev. Cancer*, 2007, **7**, 573–584; (e) E. Wong and C. M. Giandomenico, *Chem. Rev.*, 1999, **99**, 2451–2466; (f) A. M. Florea and D. Büsselberg, *Cancers*, 2011, **3**, 1351–1371; (g) Y. Jung and S. J. Lippard, *Chem. Rev.*, 2007, **107**, 1387–1407.
- 10 (a) Y. G. Gonçalves, A. B. Becceneri, A. E. Graminha, V. M. Miranda, R. R. Rios, F. Rinaldi-Neto, M. S. Costa, A. C. R. Gonçalves, V. M. Deflon, K. A. G. Yoneyama, P. I. S. Maia, E. F. Franca, M. R. Cominetti, R. S. Silva and G. V. Poelhsitz, *Dalton Trans.*, 2023, **52**, 9590–9606; (b) A. E. Graminha, J. Honorato, R. S. Correa, M. R. Cominetti, A. C. S. Menezes and A. A. Batista, *Dalton Trans.*, 2021, **50**, 323–335; (c) G. F. Grawe, K. M. Oliveira, C. M. Leite, T. D. de Oliveira, J. Honorato, A. G. Ferreira, E. E. Castellano, M. R. Cominetti, R. S. Correa and A. A. Batista, *J. Chem. Soc., Dalton Trans.*, 2022, **51**, 1489–1501; (d) J. Jiang, Q. Chen, T. Huan, Y. Nie, Z. Dai, D. Li, X. Xu, J. Lu, Z. Hua and H. Xu, *Dalton Trans.*, 2023, **52**, 14338–14349.
- 11 (a) T. J. Carneiro, A. S. Martins, M. P. M. Marques and A. M. Gil, *Front. Oncol.*, 2020, **10**, 590970; (b) M. N. Alam and F. Huq, *Coord. Chem. Rev.*, 2016, **316**, 36–67; (c) T. Lazarević, A. Rilak and Ž. D. Bugarčić, *Eur. J. Med. Chem.*, 2017, **142**, 8–31; (d) W. A. Wani, U. Baig, S. Shreaz, R. A. Shiekh, P. F. Iqbal, E. Jameel, A. Ahmad, S. H. Mohd-Setapar, M. Mushtaque and L. T. Hun, *New J. Chem.*, 2016, **40**, 1063–1090; (e) T. Nabyeva, C. Marschner and B. Blom, *Eur. J. Med. Chem.*, 2020, **201**, 112483; (f) C. R. Munteanu and K. Suntharalingam, *Dalton Trans.*, 2015, **44**, 13796–13808; (g) Y. Liu, Y. Wang, S. Song and H. Zhang, *Chem. Sci.*, 2021, **12**, 12234; (h) X. Li, Z. Shi, J. Wu, J. Wu, C. He, X. Hao and C. Duan, *Chem. Commun.*, 2020, **56**, 7537–7548; (i) M. Gallardo-Villagrán, L. Paulus, J. L. Charissoux, D. Y. Leger, P. Vergne-Salle, B. Therrien and B. Liagre, *Dalton Trans.*, 2022, **51**, 9673–9680; (j) R. Paprocka, M. Wiese-Szadkowska, S. Janciauskiene, T. Kosmalski, M. Kulik and A. Helmin-Basa, *Coord. Chem. Rev.*, 2022, **452**, 214307; (k) M. Kedia, S. Khatun, U. Phukon, B. Shankar, A. K. Rengan and M. Sathiyendiran, *Dalton Trans.*, 2023, **52**, 14314–14318.
- 12 (a) S. U. Parsekar, K. Paliwal, P. Haldar, P. K. S. Antharjanam and M. Kumar, *ACS Omega*, 2022, **7**, 2881–2896; (b) C. Santini, M. Pellei, V. Gandin, M. Porchia, F. Tisato and C. Marzano, *Chem. Rev.*, 2014, **114**, 815–862; (c) M. Das, S. Mukherjee, M. M. Islam, I. Choudhuri, N. Bhattacharyya, B. C. Samanta, B. Dutta and T. Maity, *ACS Omega*, 2022, **7**, 23276–23288; (d) N. Biswas, S. Khanra, A. Sarkar, S. Bhattacharjee, D. P. Mandal, A. Chaudhuri, S. Chakraborty and C. R. Choudhury, *New J. Chem.*, 2017, **41**, 12996–13011; (e) M. S. Galanski, V. B. Arion, M. A. Jakupcic and B. K. Keppler, *Curr. Pharm. Des.*, 2003, **9**, 2078–2089; (f) R. W.-Y. Sun, D.-L. Ma, E. L.-M. Wong and C.-M. Che, *Dalton Trans.*, 2007, 4884–4892; (g) Y. Li, K.-N. Wang, L. He, L.-N. Ji and Z.-W. Mao, *J. Inorg. Biochem.*, 2020, **205**, 110976; (h) M. N. Ahamad, K. Iman, M. K. Raza, M. Kumar, A. Ansari, M. Ahmad and M. Shahid, *Bioorg. Chem.*, 2020, **95**, 103561; (i) M. K. Gond, N. Rai, B. Chandra, V. Gautam, S. Garai, R. J. Butcher and M. K. Bharty, *Dalton Trans.*, 2023, **52**, 10213–10221; (j) Y. Chen, Z. Ke, L. Yuan, M. Liang and S. Zhang, *Dalton Trans.*, 2023, **52**, 12318–12331; (k) W. Lu, J. Tang, Z. Gu, L. Sun, H. Wei, Y. Wang, S. Yang, X. Chi and L. Xu, *J. Inorg. Biochem.*, 2023, **238**, 112030.
- 13 (a) J. Serment-Guerrero, P. Cano-Sanchez, E. Reyes-Perez, F. Velazquez-Gracia, M. E. Bravo-Gomez and L. Ruitz-Azuara, *Toxicol. In Vitro*, 2011, **25**, 1376–1384; (b) C. S. Novoa-Ramírez, A. Silva-Becerril, M. M. González-Ballesteros, V. Gomez-Vidal, M. Flores-Álamo, L. Ortiz-Frade, J. Garcia-Mora and L. Ruiz-Azuara, *J. Inorg. Biochem.*, 2023, **242**, 112097.
- 14 N. K. Mandal, S. Nandi, K. Acharya and J. P. Naskar, *Appl. Organomet. Chem.*, 2023, **37**, e7120.
- 15 (a) M. Anjomshoa, H. Hadadzadeh, M. Torkzadeh-Mahani, S. J. Fatemi, M. Adeli-Sardou, H. A. Rudbari and V. M. Nardo, *Eur. J. Med. Chem.*, 2015, **96**, 66–82; (b) P. Adak, B. Ghosh, A. Bauza, A. Frontera, A. J. Blake, M. Corbella, C. D. Mukhopadhyay and S. K. Chattopadhyay, *RSC Adv.*, 2016, **6**, 86851–86861.
- 16 (a) G.-Y. Li, K.-J. Du, J.-Q. Wang, J.-W. Liang, J.-F. Kou, X.-J. Hou, L.-N. Ji and H. Chao, *J. Inorg. Biochem.*, 2013, **119**, 43–53; (b) K. E. Prosser, S. W. Chang, F. Saraci, P. H. Le and C. J. Walsby, *J. Inorg. Biochem.*, 2017, **167**, 89–99; (c) G. Ramesh, S. Daravath, M. Swathi, V. Sumalatha, D. S. Shankar and S. Shivaraj, *Chem. Data Collect.*, 2020, **28**, 100434.
- 17 H. H. Nguyen, T. T. Pham, N. O. Pham-Thi, V. H. Tran, C. D. Le, B. V. Hoi, T. N. Trieu and C. T. Pham, *J. Mol. Struct.*, 2022, **1249**, 131680.
- 18 (a) O. Kahn, *Molecular Magnetism*, VCH, Weinheim, Germany, 1993; (b) J. K. McCusker, E. A. Schmitt and D. N. Hendrickson, *Magnetic Molecular Materials*, ed. D. Gatteschi, O. Kahn, J. S. Miller and F. Palacio, Kluwer, Dordrecht, 1991; (c) *Magnetism: Molecules to Materials*, ed. J. S. Miller and M. Brillon, Wiley-VCH, Weinheim, Germany, 2002.
- 19 (a) P. Chaudhuri, *Coord. Chem. Rev.*, 2003, **243**, 143–190; (b) M. E. Keeney, K. Osseo-Asare and K. A. Woode, *Coord. Chem. Rev.*, 1984, **59**, 141–201; (c) S. Khanra, B. Biswas, C. Golze, B. Buchner, V. Kataev, T. Weyhermüller and P. Chaudhuri, *Dalton Trans.*, 2007, 481–487; (d) P. Chaudhuri, T. Weyhermüller, R. Wagner, S. Khanra, B. Biswas, E. Bothe and E. Bill, *Inorg. Chem.*, 2007, **46**, 9003–9016; (e) C. J. Milios, C. P. Raptopoulou, A. Terzis, F. Lloret, R. Vicente, S. P. Perlepes and A. Escuer, *Angew. Chem., Int. Ed.*, 2004, **43**, 210–212.
- 20 (a) T. S. M. Abedin, L. K. Thompson, D. O. Miller and E. Krupicka, *Chem. Commun.*, 2003, 708–709; (b) N. F. Curtis, O. P. Gladkikh, S. L. Heath and K. R. Morgan, *Aust. J. Chem.*, 2000, **53**, 577–582; (c) Y. Agnus, R. Louis, B. Metz, C. Boudon, J. P. Gisselbrecht and M. Gross, *Inorg. Chem.*, 1991, **30**, 3155–3161; (d) T. Afrati, C. M. Zaleski, C. Dendrinou-Samara, G. Mezei, J. W. Kampf, V. L. Pecoraro and D. P. Kessissoglou, *Dalton Trans.*, 2007, 2658–2668.

- 21 (a) R. J. Butcher, C. J. O'Connor and E. Sinn, *Inorg. Chem.*, 1981, **20**, 537–545; (b) P. A. Angaridis, P. Baran, R. R. Boca, F. Cervantes-Lee, W. Haase, G. Mezei, R. G. Raptis and R. Werner, *Inorg. Chem.*, 2002, **41**, 2219–2228; (c) T. C. Stamatas, J. C. Vlahopoulou, Y. Sanakis, C. P. Raptopoulou, V. Psycharis, A. K. Boudalis and S. P. Perlepes, *Inorg. Chem. Commun.*, 2006, **9**, 814–818; (d) M. Angaroni, G. A. Ardizzio, T. Beringhelli, G. La Monica, D. Gatteschi, N. Masciocchi and M. Moret, *Dalton Trans.*, 1990, 3305–3309.
- 22 W. Cañon-Mancisidor, E. Spodine, V. Paredes-Garcia and D. Venegas-Yazigi, *J. Mol. Model.*, 2013, **19**, 2835–2844.
- 23 (a) S. Ferrer, J. G. Haasnoot, J. Reedijk, E. Müller, M. B. Cingi, M. Lanfranchi, A. M. Lanfredi and J. Ribas, *Inorg. Chem.*, 2000, **39**, 1859–1867; (b) J. E. Greedan, *J. Mater. Chem.*, 2001, **11**, 37–53.
- 24 (a) R. Beckett, R. Colton, B. F. Hoskins, R. L. Martin and D. G. Vince, *Aust. J. Chem.*, 1969, **22**, 2527–2533; (b) R. Beckett and B. F. Hoskins, *Dalton Trans.*, 1972, 291–295; (c) Y.-B. Jiang, H.-Z. Kou, R.-J. Wang, A.-L. Cui and J. Ribas, *Inorg. Chem.*, 2005, **44**, 709–715.
- 25 (a) L. K. Das, M. G. B. Drew, C. Diaz and A. Ghosh, *Dalton Trans.*, 2014, **43**, 7589–7598; (b) S. Karmakar, O. Das, S. Ghosh, E. Zangrando, M. Johann, E. Rentschler, T. Weyhermüller, S. Khanra and T. K. Paine, *Dalton Trans.*, 2010, **39**, 10920–10927.
- 26 R. Bhowmick, A. S. M. Islam, U. Saha, G. S. Kumar and M. Ali, *New J. Chem.*, 2018, **42**, 3435–3443.
- 27 G. H. Jeffery, J. Bassett, J. Mendham and R. C. D. Addison, *Vogel's Text Book of Quantative Chemical Analysis*, Wesley Longman Limited, United Kingdom, 5th ed., 1989.
- 28 G. M. Sheldrick, *Acta Crystallogr., Sect. A: Found. Adv.*, 2015, **78**, 3–8.
- 29 S. Nandi, S. Chandra, R. Sikder, S. Bhattacharya, M. Ahir, D. Biswal, A. Adhikary, N. R. Pramanik, T. K. Lai, M. G. B. Drew and K. Acharya, *J. Agric. Food Chem.*, 2019, **67**, 7660–7673.
- 30 S. Nandi, P. Upadhyay, A. Roy, A. Dasgupta, A. Sen, A. Adhikary and K. Acharya, *Environ. Toxicol.*, 2022, **37**, 52–68.
- 31 (a) *Bretherick's Handbook of Reactive Chemical Hazards*, ed. P. G. Urben, Butterworth-Heinemann, Oxford, 6th edn, 1999; (b) W. C. Wolsey, *J. Chem. Educ.*, 1973, **50**, A335.
- 32 N. K. Mandal, C. J. Gómez-García, P. Saha and J. P. Naskar, *J. Coord. Chem.*, 2023, **76**, 705–719.
- 33 (a) Y. Fukuda, A. Shimura, M. Mukaida, E. Fujita and K. Sone, *J. Inorg. Nucl. Chem.*, 1974, **36**, 1265–1270; (b) N. K. Mandal, N. Bandyopadhyay, P. Arya, S. Chowdhury, N. Raghav and J. P. Naskar, *Inorg. Chim. Acta*, 2023, **544**, 121229.
- 34 A. Golcu, M. Tumer, H. Demirelli and R. A. Wheatley, *Inorg. Chim. Acta*, 2005, **358**, 1785–1797.
- 35 (a) T. L. Yusuf, S. D. Oladipo, S. Zamisa, H. M. Kumalo, I. A. Lawal, M. M. Lawal and N. Mabuba, *ACS Omega*, 2021, **6**, 13704–13718; (b) C. E. Satheesh, P. R. Kumar, N. Shivakumar, K. Lingaraju, P. M. Krishna, H. Rajanaika and A. Hosamani, *Inorg. Chim. Acta*, 2019, **495**, 118929.
- 36 (a) M. Dieng, I. Thiam, M. Gaye, A. S. Sall and A. H. Barry, *Acta Chim. Slov.*, 2006, **53**, 417–423; (b) N. K. Mandal, B. Guhathakurta, P. Basu, A. B. Pradhan, C. S. Purohit, S. Chowdhury and J. P. Naskar, *J. Coord. Chem.*, 2019, **72**, 3625–3644.
- 37 A. Zengin, K. Karaoğlu, M. Emirik, E. Menteşe and K. Serbest, *J. Mol. Struct.*, 2019, **1193**, 444–449.
- 38 (a) J. P. Naskar, B. Guhathakurta, P. Basu, N. Bandyopadhyay, G. S. Kumar, M. Zhu and L. Lu, *Inorg. Chim. Acta*, 2017, **462**, 158–166; (b) S. Sengupta, S. Khan, S. K. Chattopadhyay, I. Banerjee, T. K. Panda and S. Naskar, *Polyhedron*, 2020, **182**, 114512.
- 39 (a) A. W. Addison, T. N. Rao, J. Reedijk, J. V. Rijn and G. C. Verschoor, *Dalton Trans.*, 1984, 1349–1356; (b) B. Guhathakurta, P. Basu, G. S. Kumar, L. Lu, M. Zhu, N. Bandyopadhyay and J. P. Naskar, *Polyhedron*, 2016, **110**, 227–234.
- 40 (a) F. Z. C. Fellah, J.-P. Costes, L. Vendier, C. Duhayon, S. Ladeira and J.-P. Tuchagues, *Eur. J. Inorg. Chem.*, 2012, 5729–5740; (b) M. Kwiatkowski, E. Kwiatkoski, A. Olechnowicz, D. M. Ho and E. Deutsch, *Inorg. Chim. Acta*, 1988, **150**, 65–73; (c) S. Naiya, B. Sarkar, Y. Song, S. Ianelli, M. G. B. Drew and A. Ghosh, *Inorg. Chim. Acta*, 2010, **363**, 2488–2495; (d) J.-P. Costes, F. Dahan and J. P. Laurent, *Inorg. Chem.*, 1986, **25**, 413–416.
- 41 D. Maity, P. Mukherjee, A. Ghosh, M. G. B. Drew, C. Diaz and G. Mukhopadhyay, *Eur. J. Inorg. Chem.*, 2010, 807–813.
- 42 P. Chakrabarti, V. G. Puranik, J. P. Naskar, S. Hati and D. Datta, *Ind. J. Chem.*, 2000, **39A**, 571–578.
- 43 H.-D. Bian, J.-Y. Xu, W. Gu, S.-P. Yan, P. Cheng, D.-Z. Liao and Z.-H. Jiang, *Polyhedron*, 2003, **22**, 2927–2932.
- 44 T. Afrati, C. Dendrinou-Samara, C. Raptopoulou, A. Terzis, V. Tangoulis, A. Tsiapis and D. P. Kessissoglou, *Inorg. Chem.*, 2008, **47**, 7545–7555.
- 45 L. Shivakumar, K. Shivaprasad and H. D. Revanasiddappa, *Spectrochim. Acta, A*, 2013, **107**, 203–212.
- 46 A. Wolfe, G. H. Shimer and T. Meehan, *Biochemistry*, 1987, **26**, 6392–6396.
- 47 X.-T. Song, Y. Zhou, G.-B. Liu, H.-C. Guan and S.-M. Yue, *J. Coord. Chem.*, 2023, **76**, 345–370.
- 48 (a) Y.-Q. Gu, Y.-J. Zhong, M.-Q. Hu, H.-Q. Li, K. Yang, Q. Dong, H. Liang and Z.-F. Chen, *Dalton Trans.*, 2022, **51**, 1968–1978; (b) Q. Peña, G. Sciortino, J.-D. Maréchal, S. Bertaina, A. J. Simaan, J. Lorenzo, M. Capdevila, P. Bayón, O. Iranzob and Ö. Palacios, *Inorg. Chem.*, 2021, **60**, 2939–2952; (c) H.-Q. Zhang, X. Lu, J.-L. Wu, M.-Q. Ou, N.-F. Chen, H. Liang and Z.-F. Chen, *Dalton Trans.*, 2024, **53**, 3244–3253.
- 49 R. Sakthivel, D. S. Malar and K. P. Devi, *Biomed. Pharmacol.*, 2018, **105**, 742–752.
- 50 D. Ribble, N. B. Goldstein, D. A. Norris and Y. G. Shellman, *BMC Biotechnol.*, 2005, **5**, 12.
- 51 A. Byczkowska, A. Kunikowska and A. Kaźmierczak, *Protoplasma*, 2013, **250**, 121–128.
- 52 R. Gomez-Casal, C. Bhattacharya, N. Ganesh, L. Bailey, P. Basse, M. Gibson, M. Epperly and V. Levina, *Mol. Cancer*, 2013, **12**, 94.
- 53 W. Zhang, W. C. Cho, S. H. Bloukh, Z. Edis, W. Du, Y. He, H. Y. Hu, T. L. M. T. Hagen and M. Falahati, *Int. J. Biol. Macromol.*, 2022, **212**, 358–369.

- 54 R. A. C. Souza, W. R. P. Costa, E. de, F. Faria, M. A. de, S. Bessa, R. de, P. Menezes, C. H. G. Martins, P. I. S. Maia, V. M. Defflon and C. G. Oliveira, *J. Inorg. Biochem.*, 2021, **223**, 111543.
- 55 N. S. Gul, T. M. Khan, M. Chen, K. B. Huang, C. Hou, M. I. Choudhary, H. Liang and Z. F. Chen, *J. Inorg. Biochem.*, 2020, **213**, 111260.
- 56 N. C. Yip, I. S. Fombon, P. Liu, S. Brown, V. Kannappan, A. L. Armesilla, B. Xu, J. Cassidy, J. L. Darling and W. Wang, *Br. J. Cancer*, 2011, **104**, 1564–1574.
- 57 P. H. A. Machado, D. A. Paixão, R. C. Lino, T. R. de Souza, N. J. de, S. Bontempo, L. M. Sousa, F. V. P. de, V. Azevedo, P. C. Orsolin, P. M. A. P. Lima, I. C. Martins, J. F. da, C. Guerra, S. C. Teixeira, T. G. Araújo, L. R. Goulart, S. Morelli, W. Guerra, R. J. de and O. Júnior, *Sci. Rep.*, 2021, **11**, 24450.
- 58 L. L. F. Maciel, W. R. de Freitas, E. S. Bull, C. Fernandes, A. Horn Jr, J. C. de, A. Almeida and M. M. Kanashiro, *J. Inorg. Biochem.*, 2020, **210**, 111166.
- 59 M. F. Abdullah, N. Cinkilic, O. Vatan, D. Inci and R. Aydin, *bioRxiv(biology)*, DOI: [10.1101/2022.08.12.503805](https://doi.org/10.1101/2022.08.12.503805).
- 60 N. F. Chilton, R. P. Anderson, L. D. Turner, A. Soncini and K. S. Murray, *J. Comput. Chem.*, 2013, **34**, 1164–1175.
- 61 S. Ferrer, F. Lloret, E. Pardo, J. M. Clemente-Juan, M. Liu-González and S. García-Granda, *Inorg. Chem.*, 2012, **51**, 985–1001.
- 62 L. Martínez, C. Bazzicalupi, A. Bianchi, F. Lloret, R. González, C. Kremer and R. Chiozzzone, *Polyhedron*, 2017, **138**, 125–132.
- 63 D. Maity, P. Mukherjee, A. Ghosh, M. G. B. Drew, C. Diaz and G. Mukhopadhyay, *Eur. J. Inorg. Chem.*, 2010, 807–813.
- 64 L. K. Das, M. G. B. Drew, C. Diaz and A. Ghosh, *Dalton Trans.*, 2014, **43**, 7589–7598.
- 65 B. D. Roach, R. S. Forgan, E. Kamenetzky, S. Parsons, P. G. Plieger, F. J. White, S. Woodhouse and P. A. Tasker, *Molecules*, 2022, **27**, 6421.
- 66 Y. Agnus, R. Louis, B. Metz, C. Boudon, J. P. Gisselbrecht and M. Gross, *Inorg. Chem.*, 1991, **30**, 3155–3161.
- 67 L. Husáriková, Z. Repická, J. Moncol, D. Valigura, M. Valko and M. Mazur, *Appl. Magn. Reson.*, 2013, **44**, 571–582.